

A
MITOCHONDRIAL PROFILE
in a
MOUSE MODEL
of
DOMINANT OPTIC ATROPHY

By

Caroline T Waters

School of Optometry and Vision Sciences

Cardiff University

Supervisors: Professor Marcela Votruba

Dr.Malgorzata Rózanowska.

Advisor: Professor James Morgan



Table of Contents

Chapter 1	Introduction	1
	1.1 Autosomal dominant optic atrophy	1
	1.1.1 Mitochondrial optic neuropathies	1
	1.1.2 Clinical features of ADOA	1
	1.1.3 Clinical features of ADOA plus	3
	1.1.4 Molecular genetics of ADOA	3
	1.2 OPA1 gene and protein.....	4
	1.2.1 OPA1 gene structure and function	4
	1.2.2 Opa1 protein structure and function	5
	1.2.3 Function of Opa1	5
	1.2.4 Opa1 and control of apoptosis	6
	1.2.5 Opa1 and stability of electron transport chain	7
	1.2.6 Opa1 mutations in ADOA	7
	1.3 Retinal ganglion cells	8
	1.3.1 Mammalian retinal ganglion cells	8
	1.3.2 RGC and stratification within the IPL	10
	1.3.3 The optic nerve	11
	1.4 Mitochondria	13
	1.4.1 Mitochondrial structure	13
	1.4.2 Mitochondrial function-the ATP powerhouse	14
	1.4.3 Mitochondrial control of cell signalling	15
	1.4.4 Mitochondrial dynamics: fusion and fission	17
	1.5 Animal models of Opa1 dysfunction.....	20
	1.5.1 Drosophila melanogaster	20
	1.5.2 C elegans	20
	1.5.3 Mouse	20
	1.5.4 Summary of pathophysiology of Opa1 dysfunction in animal models	24
	1.6 Reactive oxygen	25
	1.6.1 Function of ROS	25
	1.7 Reactive nitrogen species	26
	1.7.1 Function of RNS	26
	1.7.2 Relevance of ROS	26
	1.8 Endogenous antioxidants and defence.....	28

1.8.1	Superoxide dismutase	29
1.8.2	Catalase	29
1.8.3	Glutathione peroxidase	29
1.9	Emerging therapies for human ADOA	30
1.9.1	Co enzyme Q ₁₀ derivatives	30
1.10	Potential therapies for Opa1^{Q285STOP} mouse	31
1.10.1	Resveratrol	31
Chapter 2	Chapter 2 Materials and methods	34
2.1	Live mouse maintenance.....	34
2.1.1	Origins of Opa1 ^{Q285STOP} mouse	34
2.1.2	Breeding	35
2.1.3	Mouse genotyping	35
2.1.4	DNA extraction	35
2.1.5	Mouse Opa1 PCR	35
2.2	Mouse phenotyping	36
2.2.1	SHIRPA analysis	36
2.2.2	Rotarod	37
2.2.3	Tight rope test	38
2.2.4	Narrow beam testing	40
2.3	Cognitive function analysis in Opa1^{Q285STOP} mouse	41
2.3.1	T maze testing	41
2.3.2	Novel object testing (NOR)	43
2.4	Thermal imaging in Opa1^{Q285STOP} mouse	45
2.5	Tissue retrieval	45
2.6	Immunohistochemistry	46
2.6.1	Tissue fixation	46
2.6.2	Immunohistochemistry controls	47
2.6.3	IHC staining method	48
2.6.4	IHC Image analysis	49
2.7	Western blotting	50
2.7.1	Tissue homogenisation	50
2.7.2	Analysis of Western blot by densitometry	51
2.8	BCIP protein assay	52
2.9	Mitochondrial isolation.....	52
2.10	Mitochondrial staining.....	53
2.10.1	JC1 for $\Delta\Psi_m$	53
2.10.2	Mitotracker staining	54
2.11	Spectroscopy for electron transfer analysis	54
2.11.1	Fluorescence spectroscopy for complex I analysis	55
2.11.2	UV spectrophotometry for complex II analysis	56

2.11.3	UV spectrophotometry for complex IV analysis	57
2.12	ATP determination	59
2.13	Endogenous antioxidant assays	60
2.13.1	SOD assay	60
2.13.2	Catalase assay	62
2.14	Antioxidant therapy trial	64
2.14.1	Introduction	64
2.14.2	Experimental design of resveratrol study	64
2.15	Statistical analysis	65
2.16	Presentation of data	65
Chapter 3	Chapter 3 Neuromuscular & cognitive dysfunction in Opa1^{Q285STOP} mouse	66
3.1	Introduction	66
3.1.1	Osteoporosis in C57Bl/6 mouse population	66
3.2	Neuromuscular impairment in Opa1^{Q285STOP} mouse	67
3.2.1	Experimental design of SHIRPA analysis	67
3.2.2	In viewing jar:	68
3.2.3	In the arena:	70
3.2.4	Above the arena:	71
3.2.5	Rotarod analysis in Opa1 ^{Q285STOP} mouse	75
3.2.6	Tightrope testing in Opa1 ^{Q285STOP} mouse	78
3.2.7	Narrow beam testing in Opa1 ^{Q285STOP} mouse	79
3.2.8	Mouse learning in training trials	82
3.3	Thermal imaging of Opa1^{Q285STOP} mouse	83
3.3.1	Introduction	83
3.4	Cognitive impairment in Opa1^{Q285STOP} mouse	89
3.4.1	Introduction	89
3.4.2	T Maze analysis in WT and Het mouse	90
3.4.3	Novel object testing in Opa1 ^{Q285STOP} mouse	95
3.4.4	Discussion of cognitive decline in Opa1 ^{Q285STOP} mouse	100
3.4.5	Discussion of tissue weights at 15 months	104
3.4.6	Summary of Chapter 3: Neuromuscular and cognitive dysfunction in Opa1 ^{Q285STOP} mouse	105
Chapter 4	Bioenergetic impairment in Opa1^{Q285STOP} mouse	106
4.1	Introduction	106
4.1.1	Morphology of mitochondrial in Opa1 ^{Q285STOP} mouse	106
4.1.2	Mitochondrial membrane potential in Opa1 ^{Q285STOP} mouse	112
4.2	Determination of ATP in Opa1^{Q285STOP} mouse	114
4.2.1	Introduction	114
4.3	Electron transport analysis in Opa1^{Q285STOP} mouse	118
4.3.1	Introduction	118

4.4 Mitochondrial related proteins in Opa1^{Q285STOP} mouse	133
4.4.1 Introduction to mitochondrial related proteins	133
4.4.2 Experimental design of mitochondrial related proteins4	136
4.4.3 Results of mitochondrial related protein expression in the retina	136
4.4.4 Results of mitochondrial related protein expression in brain of WT and Het	147
4.4.5 Western blotting of brain homogenate in WT and Het	148
4.4.6 Discussion of mitochondrial related protein expression in WT and Het	155
4.4.7 Summary of Chapter 4: Bioenergetic impairment in Opa1 ^{Q285STOP} mouse	157
Chapter 5 Antioxidant deficit in Opa1^{Q285STOP} mouse	158
5.1 Introduction	158
5.1.1 Catalase assay in WT and Het mouse	159
5.1.2 SOD analysis in Opa1 ^{Q285STOP} mouse	162
5.1.3 Protein analysis of antioxidant SOD expression	167
5.1.4 Nitrated protein deposition in WT and Het	171
5.1.5 Discussion of antioxidant SOD expression in Het	175
5.1.6 Summary of Chapter 5: Antioxidant impairment in Opa1 ^{Q285STOP} mouse	176
Chapter 6 Trial of resveratrol in Opa1^{Q285STOP} mouse	177
6.1 Introduction	177
6.2 Other potential therapies.....	177
6.2.1 Coenzyme Q ₁₀ & synthetic derivative Idebenone	177
6.2.2 Minocyclin	178
6.2.3 Cyclosporine	179
6.2.4 Memantine	180
6.3 Resveratrol.....	181
6.3.1 Resveratrol treatment administration	181
6.3.2 Selection of product	181
6.3.3 Selection of dose	182
6.3.4 Route of administration	182
6.3.5 Vehicle treated controls	183
6.3.6 Daily water consumption in C57Bl/6	183
6.3.7 Efficacy, health and safety	183
6.3.8 Bioavailability of resveratrol	184
6.3.9 Solubility of resveratrol	185
6.4 Health monitoring of mice on resveratrol trial.....	187
6.4.1 Introduction	187
6.5 Neuromuscular dysfunction in res treated Opa1^{Q285STOP} mouse	189
6.5.1 Introduction	189
6.5.2 SHIRPA analysis in res treated Opa1 ^{Q285STOP} mouse	189
6.5.3 Rotarod analysis in res treated Opa1 ^{Q285STOP} mouse	191
6.5.4 Narrow beam testing in res treated Opa1 ^{Q285STOP} mouse	192

6.5.5	Tight rope test in res treated Opa1 ^{Q285STOP} mouse	193
6.5.6	Res Het mouse learning in training trials	195
6.6	Cognitive dysfunction in res treated Opa1^{Q285STOP} mouse	196
6.6.1	Introduction	196
6.6.2	T maze analysis in res treated Opa1 ^{Q285STOP} mouse	196
6.6.3	Novel object recognition in res treated Opa1 ^{Q285STOP} mouse	199
6.7	Bioenergetic impairment of res treated Opa1^{Q285STOP} mouse	201
6.7.1	Introduction	201
6.7.2	Analysis of electron transfer in Opa1 ^{Q285STOP} mouse	201
6.7.3	Introduction	201
6.7.4	Mitochondrial related protein expression in res treated Het	212
6.7.5	Results of mitochondrial related protein expression in res treated Het	212
6.7.6	Western blotting of retinal homogenate	218
6.7.7	Mitochondrial protein expression in brain of untreated and treated Het	226
6.7.8	Western blotting of untreated and res Het brain homogenate	227
6.7.9	Discussion of mitochondrial protein expression in res treated brain and retina	235
6.8	Endogenous antioxidants in res treated Opa1^{Q285STOP} mouse.....	238
6.8.1	Catalase activity in res treated Het	238
6.8.2	SOD activity in res treated Opa1 ^{Q285STOP} mouse	240
6.8.3	Antioxidant index in res treated Opa1 ^{Q285STOP} mouse	243
6.8.4	MnSOD protein expression in res treated Opa1 ^{Q285STOP} mouse	243
6.8.5	Results of MnSOD protein expression in untreated res and veh Het retina	244
6.8.6	3 Nitrotyrosine deposition in untreated res and veh Het retina	249
6.8.7	Summary of Chapter 6: Trial of resveratrol in Opa1 ^{Q285STOP} mouse	253
Chapter 7	Paradoxical effects of resveratrol in WT C57BL/6	255
7.1	Introduction.....	255
7.2	Health monitoring in res treated WT.....	255
7.2.1	Introduction	255
7.3	Neuromuscular impairment in res treated WT.....	257
7.3.1	SHIRPA analysis in res treated WT	257
7.4	Cognitive impairment in res treated WT	262
7.4.1	Introduction	262
7.4.2	T Maze testing in res treated WT	262
7.4.3	Novel object recognition testing in res treated WT	264
7.5	Bioenergetic dysfunction in res treated WT	267
7.5.1	Introduction	267
7.5.2	Results of mitochondrial related protein expression	273
7.5.3	Mitochondrial protein expression in brain of untreated and treated WT	285
7.5.4	Discussion of mitochondrial related protein expression in res WT	295
7.6	Endogenous antioxidants in res treated WT.....	296

7.6.1	Introduction to catalase activity in res treated WT	296
7.6.2	SOD analysis in res treated WT	298
7.6.3	Antioxidant profile for res treated WT	301
7.6.4	MnSOD protein expression in res treated WT	302
7.6.5	Results of MnSOD expression in res treated WT	302
7.6.6	3 Nitrotyrosine deposition in retina and brain of res treated WT	308
7.6.7	Discussion of 3 nitrotyrosine deposition in res treated WT	311
7.6.8	Summary of Chapter 7: Resveratrol administration in C57BL/6 mouse	312
Chapter 8	Discussion of Opa1^{Q285STOP} mouse model.....	314
8.1	Spectrum of phenotypic anomalies in Opa1^{Q285STOP} mouse	314
8.1.1	Spectrum of human phenotypic anomalies with ADOA Plus syndrome	316
8.2	Spectrum of bioenergetic anomalies in Opa1^{Q285STOP} mouse	317
8.2.1	Spectrum of human bioenergetic anomalies in ADOA Plus syndrome	320
8.3	Resveratrol therapy in Opa1^{Q285STOP} mouse.....	320
8.3.1	Spectrum of bioenergetic dysfunction in res treated Opa1 ^{Q285STOP} compared to WT	321
8.4	Spectrum of phenotypic anomalies in C57Bl/6 WT mouse	324
8.4.1	Spectrum of bioenergetic dysfunction in C57Bl/6 WT	324
8.5	Conclusions on resveratrol as a therapy for Opa1^{Q285STOP} mouse.....	327
8.6	Implications for novel therapy in Opa1^{Q285STOP} mouse	327
8.6.1	A novel therapy for Opa ^{Q285STOP} mouse	329
8.7	Conclusions on a mitochondrial profile of Opa1^{Q285STOP} mouse.....	330
Appendix A	Lux readings from Redwood animal house.....	331
Appendix B	Resveratrol Specification Sheet.....	332
Appendix C	Resveratrol Trial Design.....	333
Appendix D	Weight monitoring in untreated, res & veh WT and Het.....	334
Appendix E	SHIRPA Test Protocol	335
Appendix F	SHIRPA WT & Het 12 months	336
Appendix G	SHIRPA res treated WT & Het 12 months.....	337
Appendix H	Succinate content in complex 1 assay WT and Het	338
Appendix I	ETC substrate oxidation WT and Het.....	339
Appendix J	SOD inhibition of formazan formation WT and Het.	340
Appendix K	Succinate content in complex I assay Het res and veh Het.....	341
Appendix L	Kinetics of ET in isolated mitochondria of Het, res Het and veh Het	342
Appendix M	ETC substrate oxidation Het, res and veh Het	343

Appendix N	SOD kinetics in Het, res and veh Het tissue homogenate	344
Appendix O	SOD inhibition of formazan formation Het, res and veh Het	345
Appendix P	Succinate content in complex I assay of WT, res and veh WT.....	346
Appendix Q	Kinetics of ET in isolated mitochondria of WT, res and veh WT	347
Appendix R	ETC substrate oxidation WT, res and veh WT	348
Appendix S	SOD kinetics in WT, res and veh WT tissue homogenate	349
Appendix T	SOD inhibition of formazan formation in WT, res and veh WT	350
Appendix U	Positive Control sections for IHC	351
Appendix V	Retinal IHC counts Het res & veh Het	354
Appendix W	Statistical analysis of data presented	357
Appendix X	Copyright permission from Wiley	367
Appendix Y	Summary of mouse ID and numbers used in this study	368
Appendix Z	Reagents	369

Index of Figures

Figure 1.1 Opa1 isoforms in man and mouse	4
Figure 1.2 Opa1 isoform 4b stabilises mtDNA nucleoids	6
Figure 1.3 Opa1 maintains cristae structure	7
Figure 1.4 Mutations associated with ADOA	8
Figure 1.5 Mouse C57BL/6 RGC subsets.....	9
Figure 1.6 Organisation within the IPL	11
Figure 1.7 Mitochondrial function.....	17
Figure 1.8 Fusion and fission.....	19
Figure 1.9 Opa1 ^{Q285STOP} mouse model of ADOA	22
Figure 1.10 Reactive oxygen species	27
Figure 1.11 Resveratrol mode of action.....	32
Figure 2.1 Genotyping ID	35
Figure 2.2 Opa1 DNA PCR	36
Figure 2.3 Rotarod analysis in mouse.....	37
Figure 2.4 Mouse learning in training trials	38
Figure 2.5 Tight rope testing in mouse	39
Figure 2.6 Narrow beam testing in mouse	40
Figure 2.7 T Maze testing	42
Figure 2.8 Items for NOR testing.....	44
Figure 2.9 Cryostat sectioning.....	47
Figure 2.10 Determination of autofluorescence using control section.....	49
Figure 2.11 Western blot profile plots of an individual band.....	51
Figure 2.12 Standard curve NADH	55
Figure 2.13 DCPIP Standard curve	56
Figure 2.14 Spectra of 30µM cytochrome c	57
Figure 2.15 Absorbance of cytochrome c as a function of concentration.....	58
Figure 2.16 SOD assay analysis.....	62
Figure 3.1 C57Bl/6 at 6 months and 15 months following use of running saucer	67
Figure 3.2 SHIRPA analysis in WT & Het	74
Figure 3.3 Het mouse phenotype above the arena.....	75
Figure 3.4 Rotarod latency to fall analysis in WT & Het mouse	77
Figure 3.5 Tight rope and narrow beam testing in WT and Het mouse	80
Figure 3.6 Cage mates—and Opa1 ^{Q285STOP} and C57Bl/6 WT at 12 months	81
Figure 3.7 Learning in training trials.....	83
Figure 3.8 Thermal imaging in young & old WT & Het	85
Figure 3.9 Thermal analysis in WT and Het mouse.....	86

Figure 3.10 T maze testing parameters in WT and Het.....	91
Figure 3.11 T Maze IR and DR in WT and Het	92
Figure 3.12T maze learning trends and score in WT and Het	93
Figure 3.13Novel object testing parameters in WT and Het	96
Figure 3.14 NOR IR and DR in WT and Het	97
Figure 3.15 NOR learning trends in WT and Het	98
Figure 3.16 Summary of cognitive impairment in Opa1 ^{Q285STOP} mouse	100
Figure 4.1 Size variation in isolated mitochondria in WT and Het	109
Figure 4.2 Mitotracker staining of isolated mitochondria from WT and Het	109
Figure 4.3 Histogram of brain and retinal mitochondrial size in WT and Het	110
Figure 4.4 JC1 staining for $\Delta\Psi_m$ in WT and Het brain and retinal mitochondria.	113
Figure 4.5 ATP measurements in freshly isolated mitochondria of WT and Het	115
Figure 4.6 Representation of electron transport in the mitochondrial matrix	120
Figure 4.7 Kinetic activity of complex I in isolated mitochondria of WT and Het	125
Figure 4.8 Kinetic activity of complex II in isolated mitochondria of WT and Het.....	125
Figure 4.9 Kinetic activity of complex IV in isolated mitochondria of WT and Het.....	126
Figure 4.10 Bioenergetic assays in isolated mitochondria of WT and Het.....	126
Figure 4.11 ETC and tissue specific changes in Het mouse.....	128
Figure 4.12 Preli associated Opa1 maintenance of cristae structure.....	134
Figure 4.13 Mitochondrial related protein activity in mitochondria.....	135
Figure 4.14 Retinal mitochondrial related protein expression: Opa1, VDAC and Preli.....	137
Figure 4.15 Retinal mitochondrial related protein expression untreated WT and Het.....	138
Figure 4.16 Retinal profile of protein expression of WT and Het.....	139
Figure 4.17 Opa1 expression in retina of WT and Het	141
Figure 4.18 VDAC expression in retina of WT and Het	142
Figure 4.19 Preli expression in retina of WT and Het	143
Figure 4.20 Neuroglobin expression in retina of WT and Het	144
Figure 4.21 PSD95 expression in retina of WT and Het	145
Figure 4.22 NF L expression in retina of WT and Het.....	146
Figure 4.23 Mitochondrial protein expression in brain of WT and Het	147
Figure 4.24 Western blot of brain homogenate in WT and Het.....	148
Figure 4.25 Opa1 expression in brain of WT and Het	149
Figure 4.26 VDAC expression in brain of WT and Het.....	150
Figure 4.27 Preli expression in brain of WT and Het	151
Figure 4.28 Neuroglobin expression in brain of WT and Het	152
Figure 4.29 PSD95 expression in brain of WT and Het.....	153
Figure 4.30 Neurofilament Heavy chain expression in brain of WT and Het	154
Figure 4.31 Summary of protein profiles in retina and brain of WT and Het	155

Figure 5.1 Kinetics of H ₂ O ₂ decomposition in tissue homogenate of WT and Het.....	160
Figure 5.2 Catalase activity in WT and Het homogenate	160
Figure 5.3 Kinetics of formazan inhibition as a function of SOD in WT and Het	163
Figure 5.4 SOD units of activity in tissue homogenate of WT and Het.....	164
Figure 5.5 Percentage inhibition of formazan formation in WT and Het homogenate	165
Figure 5.6 MnSOD expression in retina and brain of WT and Het.....	167
Figure 5.7 Western blotting of brain homogenate in WT and Het	168
Figure 5.8 MnSOD expression in retinal sections of WT and Het.....	169
Figure 5.9 MnSOD expression in brain sections of WT and Het.....	170
Figure 5.10 3 Nitrotyrosine deposition in retinal layers and brain of WT and Het	172
Figure 5.11 3 Nitrotyrosine deposition in retina of WT and Het	173
Figure 5.12 3 Nitrotyrosine deposition in brain of WT and Het	174
Figure 5.13 The ratio of MnSOD to 3 nitrotyrosine in retinal layers of WT and Het	175
Figure 6.1 Absorbance spectra of resveratrol in ethanol and tap water	186
Figure 6.2 SHIRPA analysis in untreated and treated Opa1 ^{Q285STOP} mouse	190
Figure 6.3 Rotarod latency in untreated and treated Het mouse.....	192
Figure 6.4 Beam initiation and rope distance testing in untreated and treated Het mice	194
Figure 6.5 Parameters of T maze testing in untreated and treated Het mouse	197
Figure 6.6 T Maze <i>IR and DR</i> in untreated and treated Het mouse	198
Figure 6.7 T Maze Learning trend in Het, res and veh treated Het	198
Figure 6.8 Parameters of NOR testing in untreated and treated Het mouse.....	199
Figure 6.9 NOR <i>IR and DR</i> in resveratrol treated Het mouse.....	200
Figure 6.10 Complex I NADH oxidation in untreated and treated Het mitochondria	205
Figure 6.11 Complex II reduction of DCPIP in untreated and treated Het mitochondria.....	205
Figure 6.12 Complex IV oxidation of cyto c in untreated and treated Het mitochondria.....	206
Figure 6.13 Changes in specific complexes and tissue in res treated Het.....	211
Figure 6.14 Mitochondrial related AFU in untreated, res and veh Het retina	213
Figure 6.15 Mitochondrial related AFU in res treated Het.....	214
Figure 6.16 Protein profiles in untreated res and veh Het	217
Figure 6.17 Ratio of compensation to damage in untreated and treated Het	218
Figure 6.18 Western blotting of retinal homogenate in untreated and res Het.....	219
Figure 6.19 Opa1 protein expression in untreated res and veh treated Het retina	220
Figure 6.20 VDAC protein expression in untreated res and veh treated Het retina.....	221
Figure 6.21 Preli protein expression in untreated res and veh treated Het retina	222
Figure 6.22 Neuroglobin protein expression in untreated res and veh treated Het retina	223
Figure 6.23 PSD95 protein expression in untreated res and veh treated Het retina.....	224
Figure 6.24 NF I protein expression in untreated res and veh treated Het retina.....	225
Figure 6.25 Protein expression in brain of untreated res and veh Het.....	226

Figure 6.26 Western blotting of brain homogenate in untreated and res Het	228
Figure 6.27 Opa1 expression in brain of untreated res and veh Het	229
Figure 6.28 VDAC expression in brain of untreated res and veh Het	230
Figure 6.29 Preli expression in brain of untreated res and veh Het	231
Figure 6.30 Neuroglobin expression in brain of untreated res and veh Het	232
Figure 6.31 PSD95 expression in brain of untreated res and veh Het	233
Figure 6.32 NF h expression in brain of untreated res and veh Het	234
Figure 6.33 Protein profiles of untreated res and veh Het brain and retina	236
Figure 6.34 Kinetics of H ₂ O ₂ decomposition in Het, res and veh treated Het	239
Figure 6.35 Catalase activity in tissue homogenate of untreated and treated Het.	239
Figure 6.37 Non-SOD inhibition of formazan formation in Het homogenates	242
Figure 6.38 AO profile in res treated Het	243
Figure 6.39 MnSOD expression in untreated, res and veh Het retina and brain	244
Figure 6.40 MnSOD protein in brain and retinal homogenate of untreated and res Het	245
Figure 6.41 MnSOD expression in untreated res and veh treated retina	246
Figure 6.42 MnSOD expression in untreated res and veh treated brain	247
Figure 6.43 3 Nitrotyrosine deposition in untreated res and veh Het	249
Figure 6.44 3 Nitrotyrosine deposition in untreated res and veh Het retina	250
Figure 6.45 3 Nitrotyrosine deposition in untreated res and veh Het brain	251
Figure 6.46 Ratio of MnSOD to 3 Nitrotyrosine in res retina and brain	252
Figure 7.1 Latency to fall in untreated, res and veh WT	259
Figure 7.2 Beam initiation and tight rope distance in untreated res and veh WT	260
Figure 7.3 T Maze test parameters in untreated and treated WT	263
Figure 7.4 T maze IR and DR in untreated res and veh WT	264
Figure 7.5 NOR test parameters untreated and treated WT	265
Figure 7.6 NOR IR and DR in untreated, res and veh WT	266
Figure 7.7 Preference in NOR testing	267
Figure 7.8 Complex 1 activity in res WT mouse	269
Figure 7.9 Resveratrol specific bioenergetic effects in WT mouse	272
Figure 7.10 Mitochondrial related protein expression in untreated, res and veh WT retina	274
Figure 7.11 Mitochondrial related proteins expression in untreated and treated WT	275
Figure 7.12 Western blotting of untreated and res treated WT retinal homogenate	277
Figure 7.13 Opa1 expression in retina of untreated, res and veh treated WT	278
Figure 7.14 VDAC expression in retina of untreated, res and veh treated WT	279
Figure 7.15 Preli expression in retina of untreated, res and veh treated WT	280
Figure 7.16 Neuroglobin expression in retina of untreated, res and veh treated WT	281
Figure 7.17 PSD 95 expression in retina of untreated, res and veh treated WT	282
Figure 7.18 NF L expression in retina of untreated, res and veh treated WT	283

Figure 7.19 Protein profiles in untreated res and veh treated WT.....	284
Figure 7.20 Protein expression in brain of untreated res and veh WT	286
Figure 7.21 Western blotting of untreated and res treated WT brain homogenate.....	287
Figure 7.22 Opa1 expression in untreated res and veh WT brain.....	288
Figure 7.23 VDAC expression in untreated res and veh WT brain.....	289
Figure 7.24Preli expression in untreated res and veh WT brain.....	290
Figure 7.25 Neuroglobin expression in untreated res and veh WT brain.....	291
Figure 7.26 PSD95 expression in untreated res and veh WT brain.....	292
Figure 7.27 NF H expression in untreated res and veh WT brain.....	293
Figure 7.28 Protein profiles in retina and brain of untreated and treated WT.....	294
Figure 7.29 Effects of resveratrol on protein expression in retina and brain of WT	295
Figure 7.30 Kinetics of H₂O₂ decomposition in res treated WT mouse.....	297
Figure 7.31 Catalase activity in res treated WT	297
Figure 7.32 SOD activity in WT res and veh WT homogenate	299
Figure 7.33 Inhibition of formazan formation by non-SOD activity.....	301
Figure 7.34 AO profile in res treated WT	302
Figure 7.35 MnSOD expression in untreated and treated retinal layers and brain.....	303
Figure 7.36 MnSOD expression in brain and retinal homogenate of WT and res WT	304
Figure 7.37 MnSOD expression in retina of untreated, res and veh treated WT.....	305
Figure 7.38 MnSOD expression in untreated res and veh WT brain	306
Figure 7.39 3 Nitrotyrosine deposition in untreated res and veh WT	308
Figure 7.40 3 Nitrotyrosine deposition in retina of untreated, res and veh treated WT	309
Figure 7.41 3 Nitrotyrosine deposition in untreated res and veh WT brain.....	310
Figure 7.42 Ratio of MnSOD to 3 Nitrotyrosine expression in untreated res and veh WT.....	311
Figure 8.1 Opa1^{Q285STOP} mouse on the tight rope.....	314
Figure 8.2 Impaired cognitive function in Opa1^{Q285STOP} mouse	316
Figure 8.3 Mitochondria maintain function following cytochrome c release	318
Figure 8.4 Representative mouse age range in C57BL/6 with human age equivalents.....	319
Figure 8.5Schematic of the mitochondrial environment in WT and Het.....	322
Figure 8.6 Summary of Untreated, res and WT treated mitochondrial profiles.....	326
Figure 8.7 Opa1 Cardiolipin interaction.....	329

Index of Tables

Table 1.1 Mouse models of ADOA.....	24
Table 2.1 Antibodies for IHC and Western blotting.....	48
Table 2.2 Resveratrol three armed trial design.....	64
Table 3.1SHIRPA observational profiles for specific function	73
Table 3.2 Summary of test numbers for SHIRPA analysis in WT and Het.....	73
Table 3.3Summary of test numbers for rotarod analysis in WT and Het.....	76
Table 3.4 Summary of test numbers for rope and beam analysis in WT and Het	78
Table 3.5 Mouse learning in training trials.....	82
Table 3.6 Summary of test numbers for thermal imaging analysis in WT and Het	84
Table 3.7 Summary of thermal results WT and Het.....	86
Table 3.8 Summary of test numbers for T maze testing in WT and Het	90
Table 3.9 Summary of test numbers for NOR testing in WT and Het.....	95
Table 3.10 Body brain and cardiac weight ratio at 15 months in WT and Het.....	102
Table 3.11Effects of enrichment and housing on tissue weights in WT and Het.....	103
Table 4.1 Summary of mitochondrial properties in brain and retina of WT and Het	107
Table 4.2 Summary of sample numbers for analysis of ATP in WT and Het	114
Table 4.3Summary of sample numbers for complex I analysis in WT and Het.....	122
Table 4.4 Summary of sample numbers for complex II analysis in WT and Het	123
Table 4.5 Summary of samples numbers for complex IV analysis in WT and Het	124
Table 4.6 Ratio of complex activity in mitochondria of CNS in WT and Het	127
Table 4.7 Ratio of complex activity in skeletal muscle mitochondria in WT and Het	129
Table 4.8 Opa1,VDAC and Preli expression in retinal sections of WT and Het	137
Table 4.9 Neuroglobin, Neurofilament and PSD95 expression in WT and Het retina	138
Table 4.10 Targets in the Het retinal layer	139
Table 4.11 Ratio of compensation to damage protein expression in retina of WT and Het..	140
Table 4.12 Summary of mitochondrial related protein expression in brain of WT and Het	147
Table 5.1Summary of test samples for analysis of catalase activity in WT and Het.....	159
Table 5.2 Summary of sample numbers for SOD analysis in WT and Het	162
Table 5.3 Summary of SOD activity in tissue homogenate of WT and Het	163
Table 5.4 Fold changes of SOD activities in Het CNS.....	164
Table 5.5 Summary of SOD activity in Het spinal cord.....	166
Table 5.6 MnSOD expression in retinal layers of WT and Het.....	167
Table 5.7 Nitrotyrosine deposition in retina and brain of WT and Het.....	171
Table 6.1 Dose of resveratrol mg/kg.....	182
Table 6.2 Body brain and cardiac weight ratio in Het res & veh Het	188
Table 6.3 Summary of test numbers for SHIRPA analysis in untreated and res Het.....	190
Table 6.4 Summary of test numbers for rotarod analysis in untreated res and veh Het.....	191

Table 6.5 Summary of test numbers for rope and beam in untreated, res and veh Het.....	193
Table 6.6 Summary of test numbers for T maze analysis in Het res and veh Het	196
Table 6.7 Summary of test numbers for NOR in untreated, res and veh Het.	199
Table 6.8 Summary of test samples for complex I analysis in untreated ,res and veh Het ...	202
Table 6.9 Summary of test samples for complex II in untreated, res and veh Het	203
Table 6.10 Summary of test samples for complex IV analysis in untreated res and veh Het	204
Table 6.11 Ratio of complex activity in untreated res and veh Het mitochondria	207
Table 6.12 Percentage change of complex activity in res and veh Het mitochondria	208
Table 6.13 Ratio of complex activity compared to untreated WT	209
Table 6.14 Mitochondrial related proteins Opa1, VDAC and Preli in res treated Het	212
Table 6.15 Mitochondrial related Neuroglobin, PSD95 and NF in res treated Het	214
Table 6.16 Protein profiles in untreated res and veh Het retina.....	216
Table 6.17 Results of protein expression in brain of untreated res and veh Het.....	226
Table 6.18 Percentage change in retinal protein expression compared to WT	235
Table 6.19 Summary of test samples for catalase activity in untreated res and veh Het.....	238
Table 6.20 Summary of test samples for SOD analysis in untreated, res and veh Het	240
Table 6.21 Summary of SOD analysis in untreated, res and veh Het.....	240
Table 6.22 Summary of MnSOD protein expression in untreated and treated Het retina ...	244
Table 6.23 3Nitrotyrosine deposition in retinal layers of untreated res and veh Het	249
Table 7.1 Body brain and cardiac weight ratio in untreated, res and veh WT	256
Table 7.2 Summary of test numbers for rotarod in WT res and veh WT.....	258
Table 7.3 Summary of test numbers for beam and rope in WT	260
Table 7.4 Summary of test numbers for T maze in untreated res and veh WT	263
Table 7.5 Summary of test numbers for NOR testing in WT.....	264
Table 7.6 Bioenergetics of WT, res and veh WT	268
Table 7.7 Ratio of complex activity in untreated res and veh WT.....	270
Table 7.8 Percentage changes in res and veh treated WT mitochondria	271
Table 7.9 Mitochondrial protein expression in retina of untreated and treated WT	273
Table 7.10 Mitochondrial related proteins expression in untreated and treated WT	275
Table 7.11 Summary of retinal protein profile in untreated and treated WT.....	284
Table 7.12 Mitochondrial protein expression in brain of untreated and treated WT	286
Table 7.13 Summary of protein profile of retina and brain in untreated and treated WT... 	294
Table 7.14 Ratio compensation: damage protein expression in untreated and treated WT .	294
Table 7.15 Test numbers for catalase activity in untreated res and veh WT homogenate....	296
Table 7.16 Test numbers for SOD analysis in untreated res and veh WT homogenate	298
Table 7.17 Summary of analysis of SOD activity in untreated res and veh WT	298
Table 7.18 MnSOD expression in untreated and treated WT retina and brain.....	303

Table 7.19 3Nitrotyrosine deposition in res treated WT retina and brain..... 308

Table 8.1 Ratios of complex activity and tissue association 320

Abbreviations			
ADOA	Autosomal Dominant Optic Atrophy	NOR	Novel Object testing
ADP	Adenine Diphosphate	NOS	Nitric oxide synthase
AFU	Arbitrary Fluorescent Units	OMM	Outer Mitochondrial Membrane
ATP	Adenine Triphosphate	ONH	Optic Nerve Head
CI	Complex 1	ONL	Outer Nuclear Layer
CII	Complex 2	OPA1	Optic Atrophy 1
CIV	Complex 4	OPL	Outer Plexiform Layer
CoQ	Coenzyme Q	OXPHOS	Oxidative Phosphorylation
Cyto c	Cytochrome C	PRL	Photoreceptor Layer
CuZn	CopperZinc superoxide dismutase	PRL-IS	PRL inner segment
DNA	Deoxyribonucleic acid	rHet	Resveratrol treated Het
DOA	Dominant Optic Atrophy	rWT	Resveratrol treated WT
DR	Discrimination ratio	RD	Relative density
FWT	Female WT	RGC	Retinal Ganglion Cell
FHet	Female Heterozygous	RNA	Ribonucleic acid
GCL	Ganglion Cell Layer	RNS	Reactive Nitrogen Species
gWT	Group housed WT	ROS	Reactive Oxygen Species
gHet	Group housed Het	sWT	Solitary housed WT
Het	Heterozygous mutation	sHet	Solitary housed Het
H ₂ O ₂	Hydrogen peroxide	SHIRPA	SmithKlein Beecham, Harwell, Imperial Royal London, Phenotype Assessment
IMM	Inner Mitochondrial Membrane	SC	Spinal cord
INL	Inner Nuclear Layer	SOD	Super Oxidase Dismutase
IPL	Inner Plexiform Layer	UCP-1	Uncoupling protein 1
IR	Investigation ratio	vWT	Vehicle treated WT
LHON	Leber's Hereditary Optic Neuropathy	vHet	Vehicle treated Het
MWT	Male WT	VDAC	Voltage dependant anion channel
MHet	Male Heterozygous	WT	Wild type
Mfn1/2	Mitofusin 1/2		
MnSOD	Manganese Super Oxide Dismutase		
mRNA	messenger Ribonucleic acid	Radicals	
mtDNA	Mitochondrial DNA	NO ₂	Nitrogen oxide
NAD ⁺	Nicotinamide adenine Dinucleotide	O ₂ ^{-•}	Superoxide radical
NADH	Nicotinamide ADH	OH [•]	Hydroxyl
3'Nitro	3 Nitrotyrosine	ONOO ⁻	Peroxynitrite

Acknowledgements

I would like to express my deep gratitude to both my supervisors Professor Marcela Votruba and Dr. Małgorzata Rózanowska. To Professor Marcela Votruba for the opportunity to learn and as a reminder that ADOA is a human condition. To Dr. Małgorzata Rózanowska for continual feedback on all aspects of experimental design and execution. Both spent long laborious hours challenging me to see in this vision impaired environment.

I would also like to acknowledge all of my colleagues in room 2.11 for their companionship and tolerance of lateral thinking. They allowed for all things of an animal nature. They provided some logic to many random thought processes throughout the progress of this study.

I would also like to thank the administrative staff for their helpful advice on all matters that were outside the remit of science.

Finally I would like to acknowledge the mice who participated in this study. They are remembered individually with great fondness.

Dedication

I would like to dedicate this study to two individuals who could wait no more. To Susan, who was and will always be my older sister, and to Vincent who was my best friend.

Abstract

Autosomal dominant optic atrophy (ADOA) is a mitochondrial disorder caused by a nuclear DNA mutation. The mutation is within the OPA1 gene, which encodes a 120kDa protein product. The protein, *OPA1*, is a dynamin like GTPase, which is responsible for fusion of mitochondria. It is located in the inner mitochondrial membrane and functions in conjunction with outer membrane fission proteins to maintain mitochondrial integrity.

The OPA1 protein is expressed ubiquitously and heterozygous mutations cause atrophy of the optic nerve. The variability in human ADOA phenotype may suggest some level of susceptibility to vision loss whereas other individuals appear symptom free.

The Opa1^{Q285STOP} mouse model of ADOA provides a unique opportunity to examine the disease pathology with respect to mitochondrial haploinsufficiency. The tissue specificity of the disease suggests local control over the OXPHOS environment. The bioenergetic activity of Opa1^{Q285STOP} mouse is currently unestablished. The status of antioxidant activity supporting bioenergetic function may be vital in maintaining stability within fusion deficient mitochondria. Mitochondrial stability could influence the extent of reactive species, and ultimately, ATP production.

This thesis combined the study of mitochondrial haploinsufficiency with analysis of OXPHOS and antioxidant levels in Opa1^{Q285STOP} mouse where a bioenergetic deficit was identified in all mitochondria tested. The addition of a plant derived antioxidant and its potential effects within the retinal environment and surrounding central nervous system of Opa1^{Q285STOP} mouse did not appear to influence the extended phenotypic profile observed in this mouse model. The administration of resveratrol to the wild type population conferred disadvantages both *In Vivo* and *In Vitro*.

Chapter 1 Introduction

1.1 Autosomal dominant optic atrophy

Mitochondrial function is imperative to survival. Any anomaly in the performance of the respiratory chain will result in impaired cellular behaviour. Mitochondrial disorders can be due to mutations in the nuclear or mitochondrial DNA that encodes the structural proteins required for their correct function. Disorders of mitochondrial function can display multiple neurological features. This is due to the high energy demands of the central nervous system (CNS). Within the CNS, the retina exceeds the energy requirements of the brain (Ames 2000).

1.1.1 Mitochondrial optic neuropathies

Retinal disorders due to mitochondrial mutations were first realised in 1988 with the link between mitochondrial mutation and Leber's hereditary optic neuropathy (LHON) (Wallace et al. 1988). Since then, dominant optic atrophy has another significant genetically determined disease. Respiratory complex dysfunction resulting in reduced energy is also associated with other optic neuropathies.

Chronic progressive external ophthalmoplegia (CPEO) is associated with mutations in mitochondrial tRNA and can occur with systemic muscle weakness. Progressive external ophthalmoplegia (POLG) is associated with a multitude of phenotypic disorders and relies on the presence of one or more mutation in mitochondrial DNA (mtDNA) (Van Goethem et al. 2001; Horvath et al. 2006). Autosomal dominant optic atrophy (ADOA), is a mitochondrial disorder due to a mutation in nuclear DNA that encodes a mitochondrial specific protein. The spectrum of disease can include mitochondriopathies (Amati-Bonneau et al. 2005).

1.1.2 Clinical features of ADOA

The clinical features in ADOA are bilateral reduction of visual acuity, which is ascribed to loss of retinal ganglion cells and degeneration of the optic nerve. ADOA is characterised by a painless loss of visual acuity, tritanopia, loss of central visual field, and pallor of the optic,

Chapter 1 Introduction

nerve head (Votruba et al. 1998; Ferré et al. 2005). The resting energy reserves in mutant OPA1 muscle is reduced and a reduced oxidative capacity shows a mitochondrial ATP synthesis depletion of 36%. There are no reported mitochondrial myopathic hallmarks such as ragged red fibres or deletions in mtDNA to explain these deficits. Patients have a reduced optic nerve head size which may be congenital (Barboni et al. 2010). Reduction in the retinal nerve fibre thickness (RNFT) found in ADOA may also be associated with age related loss.

1.1.2.1 Epidemiology and demographics

The prevalence of ADOA is 3/100,000 in most populations in the world, but can reach 1/10,000 in Denmark where a founder effect was identified (Thiselton et al. 2002; Yu-Wai-Man P and *al* 2010; Yu-Wai-Man et al. 2010) The penetrance of ADOA is about 70% (Ferré et al. 2005)

1.1.2.2 Visual acuity and electrophysiology in ADOA

ADOA can be characterized by an insidious onset in early childhood. The wide spectrum of visual impairment may result in late diagnosis but visual acuity deteriorates slowly with age. Deterioration in visual acuity is a bilateral progressive deterioration with moderate irreversible loss of vision usually associated with central visual field deficit (Cohn et al. 2008). A reduction in the nerve fiber layer can be identified with Optical Coherence Tomography (OCT) Electrophysiology demonstrates visual evoked potentials (VEPs) are typically absent or delayed. In subclinical or mildly affected patients, no alternation of the VEPs can be found. Pattern electroretinogram (PERG) shows an abnormal N95:P50 ratio, with reduction in the amplitude of the N95 waveform suggesting alterations of the ganglion cells layer (Holder et al. 1998a, b)

1.1.2.3 ADOA is a ganglion cell disease

Mitochondrial distribution in the ganglion cell layer shows an uneven distribution between the unmyelinated axons and the myelinated optic nerve (Bristow et al. 2002). Haploinsufficiency within a high energy cellular field will result in impaired cellular function. As the function of the ganglion cell axon is to transport nerve impulses to the lateral geniculate nucleus in the thalamus, any interruption to the energy requirements will result in impaired visual processing.

Chapter 1 Introduction

Retinal ganglion cells are continually exposed to light which will result in an increase in reactive oxygen species (Osborne 2008; Wood et al. 2008). This, combined with impaired oxidative phosphorylation may precipitate ganglion cells to an apoptotic pathway.

In the case of ADOA, the selective targeting of retinal ganglion cells due to disruption in the normal physiological mitochondrial gradient at the optic nerve head is the first step in a compromised retina (Osborne 2010).

1.1.3 Clinical features of ADOA plus

Severe multisystemic disorder may be associated with specific *OPA1* GTPase mutations (Zeviani 2008). The disorder, called the ADOA ‘plus’ syndrome, associates optic atrophy with early onset in childhood, followed by chronic progressive external ophthalmoplegia, ataxia, sensorineural deafness, sensorimotor neuropathy, and myopathy in adult life. The energetic defect consists of reduced ATP synthesis and a decrease in respiratory function, observed in the patient’s fibroblasts compared with fibroblasts from other *OPA1* patients or controls.

Other atypical visual presentations in ADOA include sequential, acute visual loss, occurring late during life (Nochez et al. 2009). Some patients harbouring the pathogenic *OPA1* mutation can be asymptomatic; at the opposite end of the variability spectrum, mutations of the *OPA1* gene have been reported to enhance only multi systemic deficits, totally sparing the optic nerve (Milone et al. 2009).

1.1.4 Molecular genetics of ADOA

The gene for ADOA maps to chromosome 3q28-qter (Eiberg et al. 1994). Two independent research teams (Alexander et al. 2000; Delettre et al. 2000), identified the *OPA1* gene within the optic atrophy 1 candidate region that encodes a polypeptide with homology to a dynamin related GTPase. The presence of numerous loss-of function heterozygous mutations in affected individuals suggests that haploinsufficiency of *OPA1* is the pathogenic mechanism involved. Homozygous mutations in *OPA1* are lethal.

Chapter 1 Introduction

1.2 OPA1 gene and protein

1.2.1 OPA1 gene structure and function

Optic atrophy 1 (*OPA1*), exists as eight transcript variants encoding different isoforms with different chain lengths. The long (L) isoforms activate mitochondrial fusion by interacting with Mfns. Short isoforms (S) arrest fusion and generate mitochondrial fragments (Ishihara et al. 2006). Precursors from all eight mRNA are targeted to the mitochondria by the mitochondrial import signal (MIS) which is removed by mitochondrial processing peptidase (MMP) to resulting in L Opa1 (Satoh et al. 2003). Proteolysis on the long isoform generates either one or two short isoforms (Song et al. 2007). L-Opa1 anchors to the inner membrane while the s-isoform is attached peripherally to the IM.

Mouse *Opa1* shares 97% overall identity with the human sequence (Figure 1.1). Divergence within the first 200 N-terminal aminoacids results in an 87% homology with human *OPA1*. Sequence analysis of splice variants reveals that exon 4 is highly conserved across species. Optic Atrophy 1 (Opa1) is, to date, the only known dynamin related protein within the inner retina (Olichon et al. 2002)

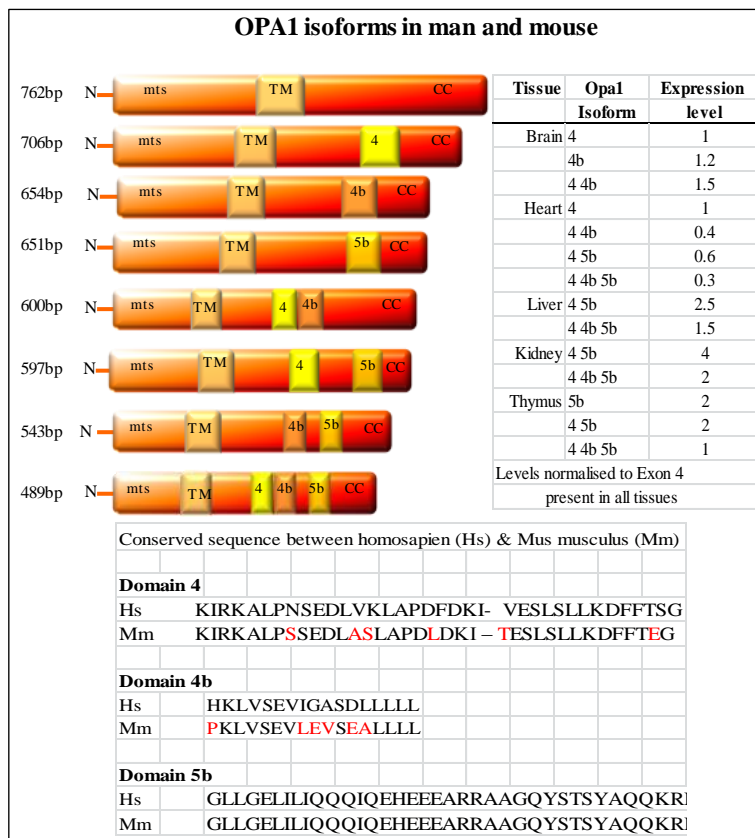


Figure 1.1 Opa1 isoforms in man and mouse

Opa1 isoforms in human and mouse are the products of post translational modification in the mitochondria with proteases *PARL* and *Yem11*. Tissue specificity for each isoform is shown

Chapter 1 Introduction

1.2.2 Opa1 protein structure and function

OPA1 is a dynamin like protein within the inner membrane and is associated with cristae modelling and inner mitochondrial fusion. Human OPA1 protein expression levels are highest in tissues with increased metabolic requirements that include the brain, retina, heart and skeletal muscle. Despite ubiquitous expression of OPA1 in mitochondria, the ocular presentation of ADOA may be due to the abundant expression in the retinal ganglion cells, nerve fibre layer, and both inner and outer plexiform layers. Autosomal dominant optic atrophy may be associated with other presentations including deafness or as a multisystemic disorder (ADOA Plus).

Opa1 isoforms are regulated by a variety of proteases that target Opa1 at specific locations under different cellular conditions including membrane potential, mitochondrial DNA loss and induction of apoptosis (Gripovic et al. 2007; Ehses et al. 2009). Opa1 is cleaved by protease presenilin associated rhomboid-like protease (PARL) at the first cleavage site S1 in exon 5 (Cipolat et al. 2006). Loss of PARL results in a reduction of soluble S-Opa1. Cristae junctions widen and accelerate the release of cytochrome c. Matrix localised m-AAA proteases AFG3L1 and paraplegin regulate the isoforms of Opa1 through peptidase OMA1 because of cellular stress.

Intermembrane space protease Yme1L also regulates Opa1 cleavage on the second transmembrane domain S2 at exon b.

Alternative splicing of exons 4, 4b and 5b result in eight differentially expressed isoforms with open reading frames for 960–1015 amino acids (Delettre et al. 2001). Conservation of exon 4 is reserved for vertebrate Gnathostomata. Exon 4 is primarily responsible for maintaining the mitochondrial membrane and upholding the required membrane potential.

1.2.3 Function of Opa1

Opa1 exon 4b is crucial for the maintenance of mtDNA. Figure 1.2 shows a possible way in which Opa1 supports mtDNA nucleoids. Mitochondrial nucleoids are anchored to the IMM on

Chapter 1 Introduction

the matrix side and replicate autonomously (Gilkerson et al. 2008). The peptide generated from the cleavage of OPA1 is a 10kDa hydrophobic 4b isoform (Elachouri et al. 2011)

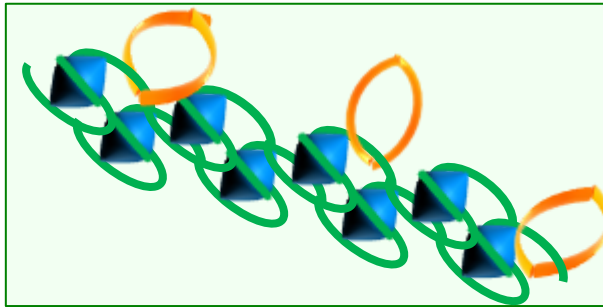


Figure 1.2 Opa1 isoform 4b stabilises mtDNA nucleoids

Exon 4b does not contain mtDNA binding sites but stabilises nucleoids to the inner membrane in an indirect method by supporting the nucleoid structure surrounding DNA.

Opa1 transcripts correlate with mtDNA copy number. Exon 4b has no DNA binding motif but it coimmunoprecipitates with nucleoids possibly through the intermediate loop (Elachouri et al. 2011). The DNA content of mitochondrial nucleoids could be dependent on the abundance of exon 4b without direct binding contact. Exon 4b may provide a membrane bound scaffold to anchor nucleoids thus permitting replication. An excess of mtDNA replication could potentially induce a bottleneck of nucleoids with negative impact on mitochondrial copy number (Khrapko 2008). Excessive processing of Opa1 increases the levels of soluble Opa1. Soluble Opa1 is also increased with the induction of apoptosis due to decreased membrane potential (Duvezin-Caubet et al. 2006; Duvezin-Caubet et al. 2007; Song et al. 2007). This fragmentation can be reversed with the addition of long isoform Opa1.

1.2.4 Opa1 and control of apoptosis

Opa1 isoforms 4 and 5b act as gatekeepers to cristae containing cytochrome c within the IMM. By maintaining the structural integrity of cristae, Opa1 controls the amount and duration of cytochrome c release in response to caspase dependent apoptotic events. Both exons 4b and 5b encode three transmembrane domains and a coiled coil domain predicted to homodimerise (Duvezin-Caubet et al. 2007; Wang et al. 2011). Prohibitins are essential for Opa1-dependent formation of mitochondrial cristae (Merkwirth et al. 2008). Deletion of Phb2 leads to a selective loss of long isoforms Opa1, resulting in aberrant cristae morphogenesis, impaired cellular

Chapter 1 Introduction

proliferation, and resistance to apoptosis. Figure 1.3 depicts both isoforms of Opa1 maintaining cristae structure.

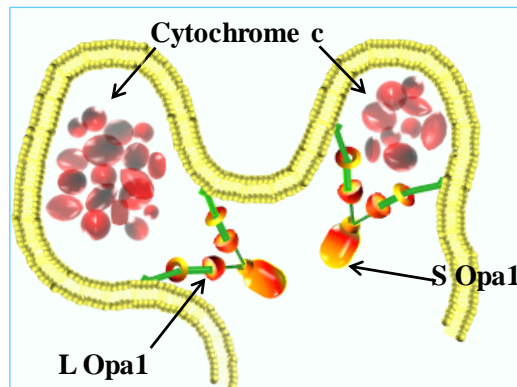


Figure 1.3 Opa1 maintains cristae structure

Cristae structure is maintained by docking two long isoforms and one short isoform. This prevents the release of cytochrome c and initiation of cell death through the apoptotic pathway

1.2.5 Opa1 and stability of electron transport chain

Opa1 maintains cristae shape and integrity. The electron transport chain is embedded in the cristae and relies on an equilibrium allowing fluidity of individual complexes according to requirements. The transfer of electrons requires the correct positioning of each complex to maintain a homogenous flow through the chain. By exerting a degree of stability in the mitochondrial matrix, Opa1 ensures a consistent flow of electrons in the generation of ATP. This in turn allows for paired electron transfer to molecular oxygen.

1.2.6 Opa1 mutations in ADOA

The mutations associated with *OPA1* include both missense and deletions (Alexander et al. 2000; Delettre et al. 2000). Truncation of *OPA1* protein resulting in loss of functional domains of GTPase within exons 8 – 15 have also been reported (Delettre et al. 2001). Figure 1.4 is a schematic representation of the spectrum of mutations found in the *OPA1* gene of ADOA. A coupling defect in the electron transport chain in LHON results in a reduction in ATP synthesis (Chevrollier et al. 2008). Similar analysis in mutant Opa1 fibroblasts fail to show complex I reduction but do demonstrate a complex IV deficit of 25% activity (Milone et al. 2009). *OPA1* is expressed in the inner ear (ADOAD), which may explain some rare cases of optic atrophy and deafness occurring in patients with a specific R445H mutation (Amati-Bonneau et al. 2005; Amati-Bonneau et al. 2009).

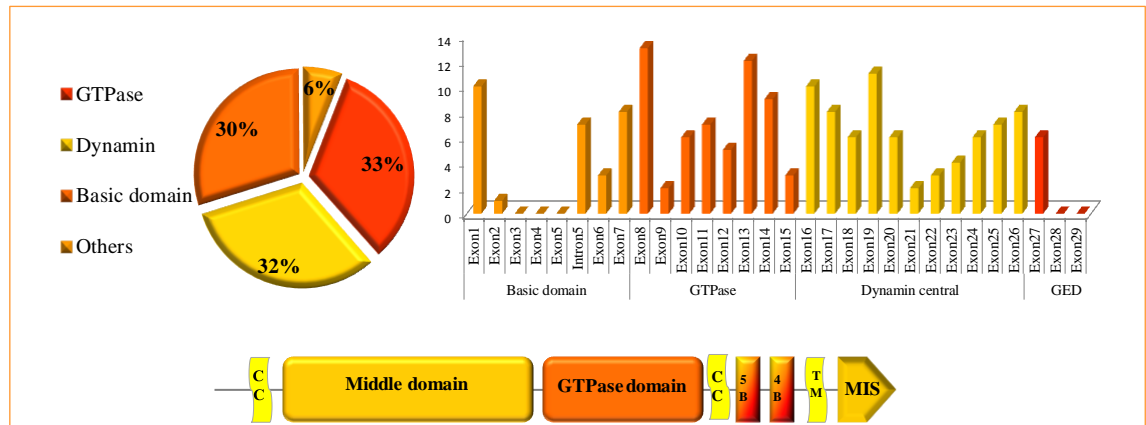


Figure 1.4 Mutations associated with ADOA

There are over 220 confirmed mutations associated with OPA1 in ADOA. Approximately 28% are deletions, 68% substitutions and 4% insertions. Frame shift mutations with one mutant OPA1 allele result in haploinsufficiency. Missense mutations cause loss of function with abnormal OPA1 replication. Mutations within specific functional regions include GTPase 32%, dynamin related 32%, basic domain 30% and others 6%

1.3 Retinal ganglion cells

Classification of retinal ganglion cells (RGC) includes the cell size parameters and the extent of its stratification within the inner plexiform layer.

1.3.1 Mammalian retinal ganglion cells

Human ganglion cell numbers vary from between 1,000,000 to 1,600,000 (Provis and van Driel 1985) The vertebrate retina has midget ganglion cells which project to the parvocellular layer of the lateral geniculate nucleus, which comprise 80% of the total ganglion cell population. They are responsible for spatial resolution, visual acuity colour vision, texture and contrast sensitivity.

Parasols which project to the magnocellular layer of the lateral geniculate nucleus, and provide low spatial frequency, depth perception and motion detection.

Bistratified ganglion cells also known as 'K' ganglion cells which project to the koniocellular layer of the lateral geniculate nucleus and are concerned with blue cone processing only.

Chapter 1 Introduction

Non-image forming melanopsin ganglion cells exist at 1% of the total ganglion cell population (Hattar et al. 2002) They are responsible for circadian clock preservation. Mouse RGC populations vary from 45,000-75,000 depending on the strain (Williams et al. 1996). The distribution of ganglion cells in mouse retina varies between dorsoventral and naso temporal. Peripheral nasal retina has higher densities than other peripheral regions (Jeon et al. 1998). Sub populations of RGC are divided into alpha large fast transient impulse fields, beta small stationary fine detailed fields and motion detection. Each cell type can be ON or OFF centre depending on the position of its dendrites within the inner plexiform layer. Even within a species as regulated as laboratory mouse, there remains some variation between strains. A study of synaptic circuitry in mouse strain C57/Bl6 retina identified twenty-two different retinal ganglion cell types (Völgyi et al. 2009). Camera lucida drawings are shown in Figure 1.5. Coupling of ganglion cells to neighbouring amacrine cells is found in most ON centre ganglion cells.

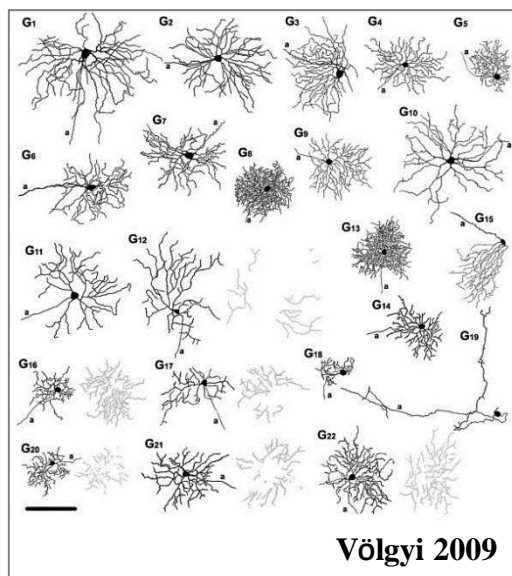


Figure 1.5 Mouse C57BL/6 RGC subsets

Camera lucida drawings of representative ganglion cells. G1–G22 labels on the top represent the name of each ganglion cell subtype. Proximally and distally stratifying dendrites of bistratified ganglion cells are shown in black and gray, respectively. a, axon. Scale bar = 100 μ m.

Coupling of ganglion cell to ganglion cell only occurs in cells whose dendrites partly stratify sub lamina A. This population comprises both ON and OFF centre cells. Ganglion cells with dendritic arbors that are restricted to sub lamina B never show homologous coupling. Homologous coupling only occurs in bistratified cells. In mouse, this comprises seven of the 22 ganglion cell types. In this population, both soma and proximal dendrite morphologies are identical. This demonstrates that mouse ganglion cells couple to nearby like-type ganglion cells.

Chapter 1 Introduction

1.3.2 RGC and stratification within the IPL

Precise synaptic connections are critical for visual processing. Retinal ganglion cells, amacrine and bipolar cells establish this stereotypic pattern within the inner plexiform layer (IPL) of the vertebrate retina. The IP is a laminar region divided into five parallel sub lamina layers (Wässle 2004). Direction of the cellular subsets to exact locations within the retina must account for the multiple morphologically distinct properties of these cells. The inner plexiform is divided into an upper sub lamina A (OFF) where S1 and S2 strata are located. The lower sub lamina B (ON) contains S3, S4 and S5 strata.

Each drives the ganglion cell dendritic tree response (Sanes and Zipursky 2010). Dopamine amacrine cells are restricted to the OFF strata of S1 near the inner nuclear/inner plexiform border. These cells synaptically couple to melanopsin ganglion cells in the S1 layer. This allows dopamine to generate a diffusible gradient throughout all layers of the IPL. Stratification provides a separation mechanism where each cell can respond to input stimuli without loss of signal or response from neighbouring cells. The ganglion midget cell pathway is organized into ON and OFF centre populations (Devries and Baylor 1997). Invaginating bipolar cells connect the cone photoreceptors to the dendrites of cone midget ganglion cells in the sub lamina B of the IPL. Flat midget bipolar cells in the OFF pathway connect dendrites of the OFF centre midget ganglion cells in the sub lamina A.

Multiple synapses are the basis and fundamental circuit connections of vision. Each stratum exacts a unique pair of excitatory and inhibitory patterns from a visual scene. In most cases, the excitatory is derived from the ON system while inhibitory pattern is derived from the OFF pathway (Müller and Holländer 1988). In other cases, inhibitory and excitatory patterns derive from the same cell (Figure 1.6)

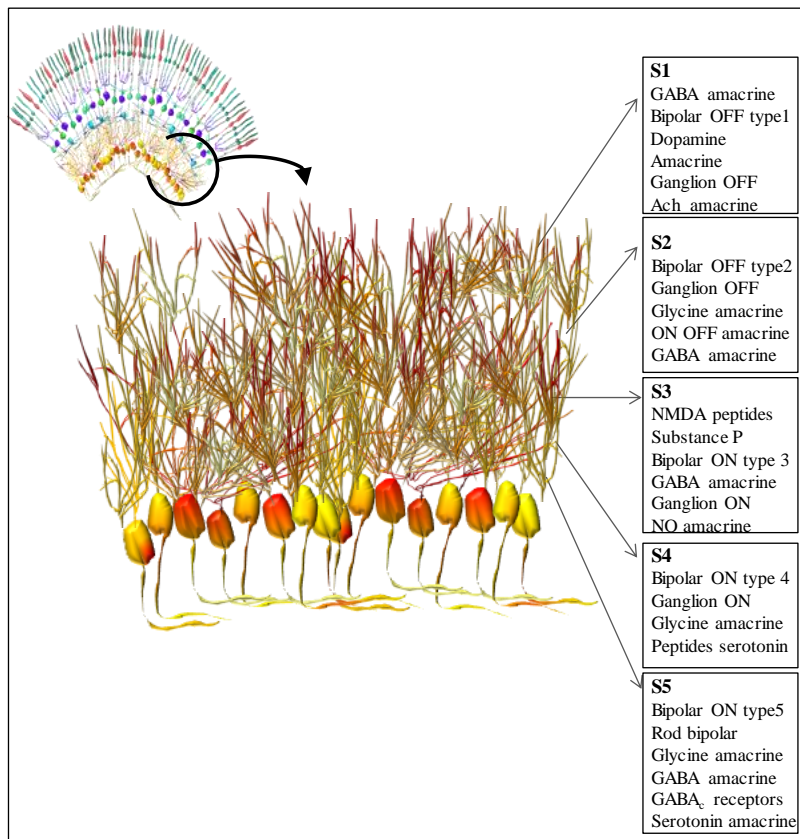


Figure 1.6
Organisation within the IPL

Stratification within the inner plexiform layer permits multiple synapses of unique inhibitory or excitatory patterns. S1–S2 contain mostly inhibitory OFF systems. S3–S5 contain excitatory ON systems. Dendrites from ganglion cells span the S2–S5 strata.

1.3.3 The optic nerve

Within the prelaminar zone, axons are held loosely by glial tissue. Astrocytes segregate the nerve fibre into fascicles of approximately 1000 axons. Astrocytes are the only glial cells in the prelaminar zone. They provide a nutritional function with stores of glycogen, regulate potassium and support axon function. Unmyelinated prelaminar and laminar regions display a high concentration of mitochondrial enzyme activity due to the dynamic functional requirements.

In mouse optic nerve (ON), the transition between unmyelinated and myelinated begins 0.6mm behind the globe. As the laminar cribrosa (LC), is absent in mouse, axons pass through an aperture in the sclera, which is surrounded by a ring of type three and type 1 collagen fibres (Hollyfield et al. 1997). Instead of connective tissue beams within the optic nerve, layers of elongated astrocytes transverse the ON. The arterial blood supply of the unmyelinated ON derives from the retinal artery. There are no choroid blood vessels. Mouse intraocular optic nerve is nonmyelinated and astrocytes surround the axon bundles. Oligodendrocyte cells occur in the retrobulbar portion where myelination of the nerve fibre begins. The transition zone is not

Chapter 1 Introduction

located at the level of the sclera but further posterior. Astrocyte processes transverse the non-myelinated nerve at the level of the sclera. Distribution of mitochondria actively reflects the functional requirements of such a highly specialised tissue as myelinated retro laminar axon and unmyelinated prelaminar axon have different bio energetic properties. In mouse, unmyelinated regions display a high concentration of mitochondrial enzyme activity due to the dynamic functional requirements. Mitochondria are typically about 0.4 μ M in diameter. RGC's must transport these mitochondria along their axons to distribute them along strategic, energy dependent locations within the optic nerve. Unmyelinated nerve by virtue of its unmyelinated state requires more energy to maintain its membrane potential against the plasma membrane. The optic nerve travels under considerable mechanical and hydrostatic force.

Recent findings on the influence of Opa1 mutations on the size of the optic nerve head suggest there is a role for Opa1 in the development of the optic nerve size and conformation (Barboni et al. 2010). Axon diameter is critical for normal physiological function. If a reduced axon diameter can impede the number of mitochondria permitted to travel the length of the axon, areas within the nerve will suffer stress. Given that approximately 50% of the mitochondria in heterozygous mutant Opa1 are functionally compromised, this could result in narrowed axons carrying a backlog of mitochondria only half of which can meet the ATP demands of the structure.

Other notable differences in mouse retinal structure include the lack of a macula. Mouse lens accounts for almost 80% of the vitreous cavity. Subsequently, the volume of vitreous is small compared to human. Mouse ciliary muscle is small and may have little function. The trabecular meshwork in mouse has smaller beams and termination in the anterior ciliary differs slightly to human.

Chapter 1 Introduction

1.4 Mitochondria

1.4.1 Mitochondrial structure

The primary function of mitochondria is the production of ATP. They also serve as storage depots for calcium required during signalling and apoptosis. Mitochondrial architecture determines structure-equating function. The three distinct mitochondrial compartments involved in specific function are the intermembrane space, intracristael space and the matrix. The size and shape of cristae and cristae number (Mannella 2006), combined with the ratio of ATP production part control events within the cell. The junction of cristae can control the movement of signalling molecules, enzyme substrates, and metabolites in or out of the inner boundary and cristae membranes (Frey et al. 2006).

1.4.1.1 Outer mitochondrial membrane (OMM)

The OMM encloses the entire mitochondrion and allows movement of molecules through a variety of channels to access the inter membrane space. The OMM is permeable to molecules of 5000 kDa and smaller (Sorgato et al. 1987). The presence of mitochondrial signal sequence translocase permits entry of proteins across the membrane conserved large GTPases, mitofusin 1 (Mfn1) and mitofusin 2 (Mfn2) are located on the OMM (Chen et al. 2003) et al., 2003). Both possess an N-terminal GTPase domain, two transmembrane domains and two coiled-coil motifs essential for protein interactions (Rojo et al. 2002) et al., 2002). Both mitofusins interlock the coiled coil domains with juxtaposed mitochondria to facilitate fusion. Mutations in the MFN2 gene are associated with Charcot-Marie-Tooth axonal disease (Cartoni and Martinou 2009), canine-fetal neuroaxonal dystrophy (Fyfe et al. 2011) et al., 2011ba), and degenerative axon disease in Tyrolean Grey cattle (Drögemüller et al. 2011).

Dynamamin related 1 protein (DRP1/DLP1/DNM1) is responsible for mitochondrial fission (Smirnova et al. 1998). Drp1 resides in the cytosol and is recruited to the site of fused mitochondria through outer membrane bound Fis1. Drp1 forms polymer rings around the fused structures and constricts until the two mitochondria are separated. Homozygous mutations in DRP1 gene cause microcephaly and metabolic alterations in glucose metabolism (Waterham et

Chapter 1 Introduction

al. 2007). It has significant implications in the progress of Alzheimer's disease and the presence of amyloid β huntingtin oligomers where Drp1 enhances its enzyme activity (Manczak et al. 2011; Song et al. 2011).

1.4.1.2 The intermembrane space

The intermembrane space is the region located between the OMM and inner mitochondrial membrane (IMM). Several proteins are located within the intermembrane space. TOM and TIM23 complexes (Chacinska et al. 2005) et al., 2005), apoptosis inducing factor (AIF),(Lindholm et al. 2004) and copper chaperone for superoxide dismutase (Reddehase et al. 2009).

The translocation of proteins from the cytosol to individual mitochondrial compartments requires presequences that act as a direct 'postcode' to the correct import channels. Nuclear encoded proteins destined for the mitochondria are imported through the TOM complex.

1.4.1.3 Inner mitochondrial membrane

The IMM contains proteins required for oxidative phosphorylation (OXPHOS) with ATP synthase, which generates ATP in the matrix. In addition, the inner membrane is rich in phospholipid cardiolipin. The IMM contains porins and is impermeable to all molecules. Almost all ions and molecules require special membrane transporters to enter or exit the matrix. The IMM is compartmentalised into numerous cristae, which expand the surface area of the inner mitochondrial membrane, enhancing its ability to produce ATP.

1.4.2 Mitochondrial function-the ATP powerhouse

1.4.2.1 Oxidative phosphorylation

All nutritionally derived substances are used to power the production of ATP within the mitochondria. The initial stage of digestion occurs within the gastrointestinal tract with the conversion of aminoacids and fatty acids to simple subunits. Polysaccharides are converted to simple sugars in the form of glucose. Within the cell cytoplasm, all subunits are converted from glucose to pyruvate through the glycolytic pathway. One molecule of glucose will hydrolyse 2 molecules of ATP. The conversion of pyruvate and fatty acids into acetyl CoA occurs in the

Chapter 1 Introduction

mitochondria. Acetyl groups linked to CoA are oxidised to CO₂ with the generation of NADH and FADH₂. The high energy electrons from NADH and FADH₂ are transported through the electron transport chain to molecular oxygen. This generates a proton gradient, which drives the ATP synthase proton pump. Oxidative phosphorylation drives ATP synthesis from the phosphorylation of adenine diphosphate (ADP).

1.4.3 Mitochondrial control of cell signalling

Mitochondria communicate with other organelles of the cell, such as the nucleus, through a process called retrograde signalling to maintain cellular homeostasis and adapt to changing metabolic requirements within the cell (El Zein et al. 2010; Passos et al. 2010; Shah and Iqbal 2010). Reactive oxygen species (ROS) contribute significantly to the regulation of activity of various signal transduction pathways and transcription factors. ROS activates members of the MAP kinase pathway. ROS play a role in growth factor receptor activation through oxidative deactivation of protein tyrosine phosphatases that maintain the growth factor receptors in an inactive state. Multiple transcription factors, including NF-κB (Foncea et al. 2000), AP-1 (Martínez-Salgado et al. 2005) TGF- (Lee et al. 2007) and p53 (Preta et al. 2010) are sensitive to ROS. Altered activation of these signalling pathways and transcription factors results in changes in gene expression and initiation of different cellular events, including cell proliferation, senescence, apoptosis, angiogenesis, and autophagy.

1.4.3.1 Mitochondrial control of apoptosis

The intrinsic pathway of apoptosis is sealed by mitochondrial membrane permeability (MMP) (Kroemer and Blomgren 2007). MMP leads to the loss of transmembrane potential, cession of ATP production and the release of several cytotoxic proteins into the cytosol (Green 2005). The presence of voltage gated anion channels (VDAC) is implicit in the pathway (Baines et al. 2007) but not ultimately as responsible as was previously thought (Adachi et al. 2004; Marin et al. 2007; Martin et al. 2011). VDAC isoforms may regulate Bax-Bak mediated MMP. Mitochondrial fission is an early trait of apoptosis, occurring simultaneously to BAX translocation from the cytosol and prior to caspase activation (Frank et al. 2001).

Chapter 1 Introduction

Within the intrinsic pathway of apoptosis, a normal cell has free anti apoptotic Bcl2, which binds to and sequesters proapoptotic Bax/Bak. When stressed, proapoptotic BH3 is up regulated and binds to anti apoptotic Bcl2 thus freeing proapoptotic Bax/Bak to promote cytochrome c release (Kim et al. 2009; Mérimo et al. 2009). Bax/Bak oligomerise and form pores on the outer mitochondrial membrane to facilitate cytochrome c release

The morphological changes associated with early stages of apoptosis include opening and widening of cristae junctions within the matrix. Mobilisation of cytochrome c from open cristae to the IMS promptly follows its release into the cytosol (Scorrano et al. 2002). Regulation of cristae opening and remodelling of cristae shape is specifically designated to particular exons within the Opa1 isoforms. The highly conserved exons 4 and 5b are paramount in restricting the extent of apoptosis by sequestering cytochrome c within the cristae under strict control of junctions within the cristae structures. Opa1 protein is the gatekeeper to imminent cell death. Once released into the cytosol, cytochrome c binds to apoptotic protease activating factor (APAF-1). This complex has high affinity for ATP, which forms apoptosome complexes of cytochrome c, APAF-1 and ATP. The apoptosome recruits executioner caspases via caspase 9 cysteine protease that cleaves intracellular substrates inducing chromatin condensation, DNA fragmentation, and reduction of the nuclear membrane and formation of apoptotic cell bodies. Figure 1.7 summarises the combined functions of mitochondria with respect to membrane potential of the matrix ultimately responsible for their survival.

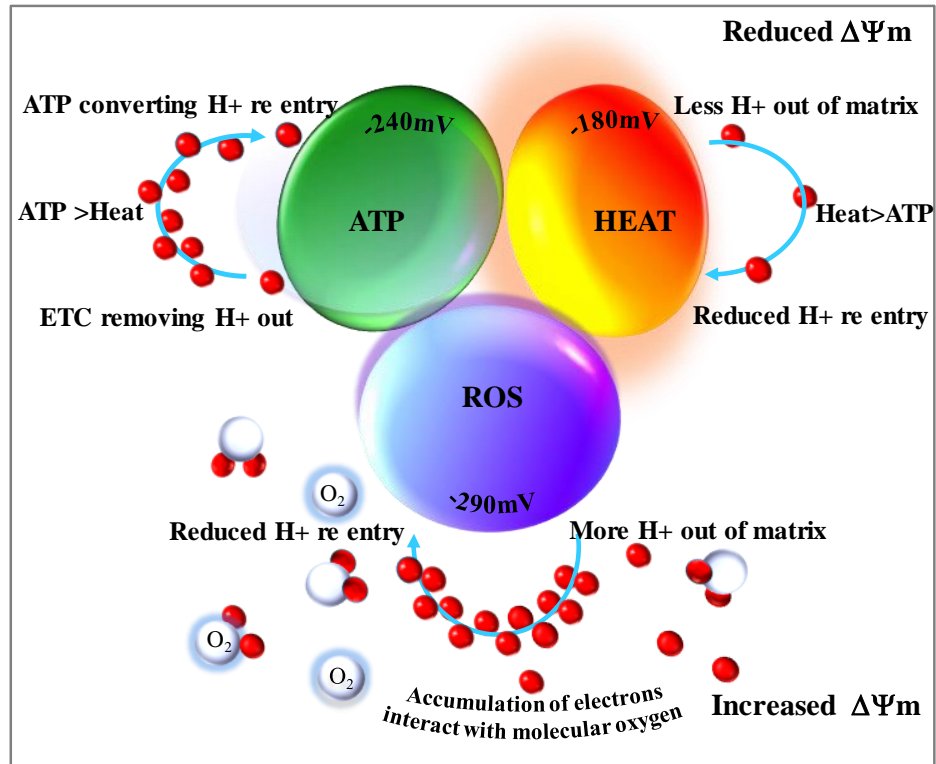


Figure 1.7 Mitochondrial function

Dietary conversion to ATP is determined by the coupling efficiency between respiration and OXPHOS. If ETC is efficient at pumping hydrogen out of the matrix, and ATP synthesis is converting hydrogen re-entry, then the negative membrane potential is maintained at -240mV and there is maximum ATP with minimum heat per calorie consumed. Uncoupled mitochondria generate heat rather than ATP due to a reduced membrane potential. Maintaining a core temperature despite environmental conditions is critical. Coupled mitochondria in the presence of excess calories and reduced cytoplasmic ADP have reduced hydrogen re-entry. The membrane potential increases until migration of electrons through the ETC is suspended. Accumulated non-oxidised electrons interact with molecular oxygen to generate reactive oxygen species. Maintaining a healthy mitochondrial membrane potential through calorific reduction and increasing OXPHOS through exercise thus ensuring adequate cytoplasmic ADP can alleviate stress in mitochondria.

1.4.4 Mitochondrial dynamics: fusion and fission

Mitochondria are responsible for the provision of ATP, which is a fundamental requirement of every cell. They are also regulators of thermogenesis, oxidative phosphorylation, apoptosis and

Chapter 1 Introduction

a storage depot for calcium. Mitochondrial dynamics ensure quality control through fusion, fission and mitophagy. They are semiautonomous structures, which depend on the expression of both nuclear and mitochondrial DNA. Fusion and fission dynamics ensure only healthy mitochondria fuse. Fission acts by separating out mitochondria that are not part of the mitochondrial network, but exist in separate fragmented isolation. Elimination of these functionally deficient structures by mitophagy ensures a healthy population in each cell.

Mitochondrial function is dependent on fission and fusion to affect change in shape according to their environment. Dynamin are ubiquitous enzymes that hydrolyse GTP to regulate fusion, fission, tubulation and elongation of cellular membranes (McNiven et al. 2000)

1.4.4.1 Mitochondrial fusion

Fusion is mediated by outer membrane Mfn1 and Mfn2 and inner membrane Opa1. Fusion facilitates the exchange of mtDNA and other vital components between mitochondria for the maintenance of functional mitochondria. Unbalanced fusion leads to elongation of mitochondria.

Two distinct forms of mitochondrial fusion exist-transient and complete (Liu et al. 2009b). Transient fusion is for exchange of mitochondrial contents while maintaining mitochondrial morphology describes this part fusion as 'Kiss and Run' whereby only the minimal requirements of fusion occur. In normally functional mitochondria, complete fusion is followed by fission. Transient fusion is Opa1 concentration dependent. When the levels of Opa1 are too low to support complete fusion, transient fusion occurs. The separation phase of transient fusion depends on Drp1. If fusion is not complete, Drp1 binds to the fusion site and initiates fission promptly. Mitochondria are operating under a force generated by motor proteins and mediated by the anchorage to microtubules. This tension may promote scission ring formation of Drp1 as is described in dynamin (Roux et al. 2006). Re separation of the mitochondrial membranes restores the original shape and prompts recovery of movement activity. Transient fusion provides an efficient recharging mechanism by allowing rapid equilibrium of soluble inner

Chapter 1 Introduction

mitochondrial matrix proteins. Transient fusion can operate with a compromised membrane potential (Mattenberger et al. 2003). A summary of fusion event is shown in Figure 1.8.

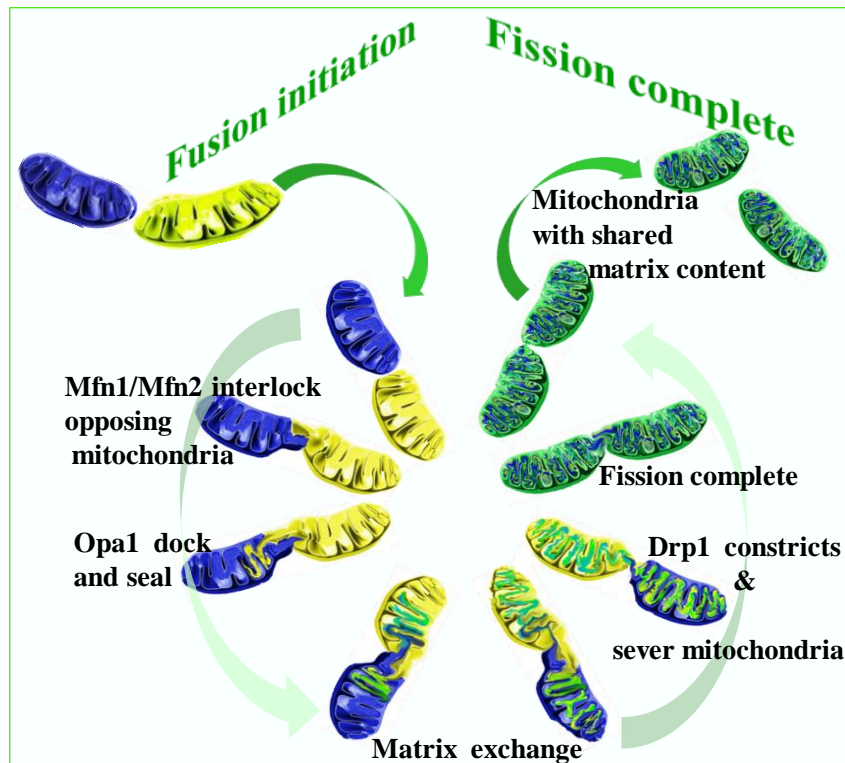


Figure 1.8 Fusion and fission

Mitochondrial fusion of both outer and inner mitochondrial membranes facilitated by Mfn1/Mfn2 and Opa1 is followed by Drp1 induced fission resulting in mitochondria with preserved essential component.

1.4.4.2 Mitochondrial fission

Fission is mediated by dynamin related protein Drp1, which is located in the cytosol. Drp1 translocates to the outer mitochondrial membrane by the surface receptor Fis1 (James et al. 2003). Drp1 acts by mechanically constricting and severing mitochondria. Mitochondrial fission factor (Mfi) may also recruit Drp1 (Otera et al. 2010). Mitochondrial fission contributes to the correct distribution of mitochondria in response to the local demand for ATP and the elimination of damaged mitochondrial fragments through mitophagy. Anterograde transport (kinesin) is responsible for the correct delivery of functional mitochondria to synapses of neurones (Chang and Blackstone 2007). Dysfunctional mitochondria return to the soma by retrograde transport (dynein) (Li et al. 2004; Russo et al. 2009).

Chapter 1 Introduction

1.5 Animal models of Opa1 dysfunction

1.5.1 Drosophila melanogaster

Homologues of human OPA1 are present in *Drosophila melanogaster* (Yarosh et al. 2008). Exploiting *Drosophila* genetics, an enhancer trap under Eyeless promoter permitted a viable homozygous mutant. The dOpa1 mutation results in a dual disease phenotype- ‘rough eye’ and ‘glossy eye’. Rough eye is the result of excess interommatidial cell apoptosis, which is unchecked due to reduced dOpa1. Glossy eye is due to lens depleted cone cells. Reversal of the phenotype was possible with the addition of ‘therapeutic’ SOD 1000units to the feed. The Mitosox staining signal was dramatically reduced. The addition of Vitamin E to the diet of *D. Melanogaster* enhanced the effect. These experiments demonstrated the dual pathogenic effect of homozygous dOpa1 mutation and the rescue of phenotype with the addition of antioxidant therapy.

1.5.2 C elegans

In *C.elegans*, the gene Eat-3 is homologous to human OPA1 (Kanazawa et al. 2008). Eat-3 mutations cause fusion defects in the inner mitochondrial membrane. The 964 amino acid protein plays a pivotal role in pharyngeal pumping hence the name Eat. Clearly because of the nature of the animal, Opa1 has no role in ophthalmic conditions, however the animal model does provide some significant detail on the role Opa1 has in other physiological systems. The importance of intestinal motility in ADOA recently identified in compound heterozygous offspring (Schaaf et al. 2011) might not have otherwise been associated as a function of Opa1.

1.5.3 Mouse

Currently there are four published mouse models of Opa1 dysfunction. Three models focus on ADOA. They are summarised in Table 1.1.

1.5.3.1 Mouse Opa1^{mBEWI}

Mouse model Opa1^{M1BEWI} is an ENU induced single point mutation with G→A transition in intron 10. These amino acids are an integral part of the GTPase domain. The mutation causes a 50% reduction in endogenous protein levels in heterozygous mice.

Chapter 1 Introduction

Heterozygous mutants are viable but exhibit an age-dependent loss of RGCs that eventually progresses to a severe degeneration of the ganglion cell and nerve fibre layer. The optic nerves of mutant mice showed a reduced number of axons, swelling and abnormal shape of the remaining axons. Mitochondria in these axons showed disorganized cristae structures (Alavi et al. 2007).

ERG responses in optic nerve of two-year-old mutant $Opa1^{mBewi}$ mice are normal. Visually evoked potentials (VEP), measurements reveal a significantly reduction in amplitudes indicating a reduction of RGC. Retrograde labelling demonstrates a significant reduction in the numbers of RGC in $Opa1^{mBewi}$ mice. Long-term experiments reveal the presence of microglial cells with ingested fluorescent dye (Heiduschka et al. 2010).

1.5.3.2 Mouse $Opa1^{Q285STOP}$

A truncated protein due to ENU induced C to T transition at 1051bp results in the Q285STOP substitution in exon 8, immediately before the central dynamin-GTPase. The heterozygous mutation B6; C3-OPA1Q285STOP leads to about a 50% reduction of protein in retina and all tissues. The mutation corresponds to several human OPA1 mutations including C→T at 868bp resulting in an arginine to tryptophan at 290, and G→T at 869bp causing arginine to glutamine at 290 mm (Ferré et al. 2005). Figure 1.9 shows a model of the $Opa1^{Q285STOP}$ mouse gene structure. The homozygous mutation is embryonic lethal by 13.5 dpc. Heterozygous mutants show a slow onset of degeneration in the optic nerve as determined by electron microscopy. There is evidence of mitochondrial dysfunction with $Opa1^{Q285STOP}$ mouse muscle fibroblast in culture, displaying punctuated mitochondria, with an abnormal ‘powdered’ appearance (Davies et al. 2007).

Ganglion cell populations remain intact in this $Opa1$ model with reported increase in the number of autophagosomes in the RGC layer in heterozygous mutants compared with wild type at 24 months (White et al. 2009). Axonal degeneration is observed in both wild type and mutant $Opa1$ at 24 months, which would suggest an age related reduction in myelin.

Chapter 1 Introduction

Ultra structure of the optic nerve in heterozygous mutants and wild-type littermate controls at six, nine, and 24 months using electron microscopy demonstrate increased autophagosomes in the RGC layer. Signs of optic nerve degeneration are confirmed as early as 9 months in $Opa1^{Q285STOP}$, with more severe degeneration by 24 months. The number of opaque mitochondria in the $Opa1^{Q285STOP}$ increase at 6 and 24 months (White et al. 2009). $Opa1^{Q285STOP}$ mouse shows late onset pruning in the dendritic branches of ON centre RGC (Williams, Morgan and Votruba, 2010). The ON centre ganglion cell population are specific to sub lamina B of the IPL. Glutamatergic ON centre ganglion cells are non-homologous coupling cells (Völgyi et al. 2009). As such, this may mean they can reduce the impact of impaired mitochondrial fusion by association with more competent dendrites.

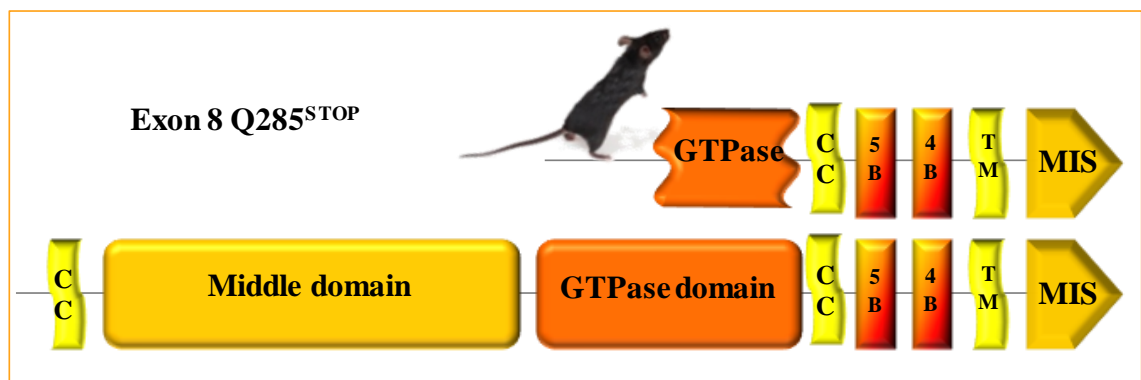


Figure 1.9 $Opa1^{Q285STOP}$ mouse model of ADOA

Exon 8 pre central dynamin GTPase domain C → T transition at 1051bp results in a premature STOP codon. Haploinsufficiency leads to 50% reduction of protein in retina and all tissues.

Electrophysiological deficits $Opa1^{Q285STOP}$ mouse model show no detectable difference in the major ERG components (α wave and β wave) from wild type in the amplitude or time of dark-adapted electroretinogram (ERG). Light-adapted ERG responses reveal a significant reduction in the photopic negative response (PhNR) amplitude in the mouse model when compared to wild types at the brighter intensities tested. Elements of the light-adapted VEP display functional deficits in electrophysiology that is consistent with ganglion cell dysfunction. The reduction of retinal nerve fibre layer thickness (RNFLT), combined with a PhNR below the

Chapter 1 Introduction

lower limits of normal does not necessarily mean visual abilities are impaired (Gowrisankaran et al. 2011). There are no obvious anomalies seen in 6-month Het organs when compared to wild type littermates (Davies et al. 2007). They demonstrate increased transfer arousal, when compared to wild type littermates of the same genetic background. Of equal significance, there is no clutch reflex anomaly in the *Opa1*^{Q285STOP} mouse model (personal observation). Clutch reflex is imperative if normal mating is to occur.

1.5.3.3 Mouse Opa^{lii}

The mouse model *Opa1*^{lii2} was generated by chemically induced (ENU) insertion mutation with nucleotide substitutions (Moore et al. 2010). The mutation leads to a A to G transition in intron 19 which results in a stable but mislocalized cytosolic protein. Homozygous *Opa1*^{lii3} survive through mid-gestation and die at E11.5. These mutants display growth retardation, encephalopathy, and abnormal patterning along the anterior-posterior axis, although the A-P axis itself remains intact. Mouse *Opa1*^{lii3} demonstrates mitochondrial retention of *Opa1* protein which is essential for normal embryogenesis (Moore et al. 2010).

1.5.3.4 Mouse Opa1^{delTTAG}

The most recent arrival to the ADOA mouse model array, mouse *Opa1*^{delTTAG} is a knock-in carrying the recurrent C.2708_2711delTTAG mutation (Sarzi et al. 2012). By deleting the four conserved base pairs in exon 27 and replacing them with a neomycin cassette. The subsequent recombinant stem cells were injected into 3.5 blastocysts of C57Bl6/J mice. By crossing the chimeras with a creatine expressing mouse line, thereby removing the neomycin cassette but resulting in a constitutive *Opa1* knock-in mouse. This mouse model would appear to demonstrate all the significant hallmarks of age related decline in mitochondrial function. Tissue specific haploinsufficiency results in visual and auditory loss, encephalomyopathy, ataxia, peripheral neuropathy and cardiomyopathy.

The authors refer to this mouse model as an accelerated aging mouse model of ADOA. Although the human version of ADOA may harbour multiple mitochondrial mutations as a direct result of impaired mitochondrial function, the vast spectrum of disorders presented in the

Chapter 1 Introduction

mouse model $Opa1^{\text{delTTAG}}$ is happily not necessarily present in Homo sapien. Electron complex destabilisation seen as a result of the aging process identified solitary sub complexes within the mitochondria.

	Opa1 ^{mBEWI}	Opa1 ^{Q285STOP}	Opa1 ^{delTTAG}	Opa1 ^{lil3}
Mutation	G → A Intron 10	C → T Intron 8	Del exons 29-31	A → G Intron 19
DNA	c1065+ 5G>A	c1051 C>T		c1616splice site
	GTPase domain	Central dynamin	Middel domain	GED domain
Hom	Lethal E8.5	Lethl E13.5	Lethal E10.5	Lethal E11.5
Het	50% reduction	50% reduction		Developmental defects
Retinal morphology	Age dep RGC loss periphery	RGC unaltered	RGC loss 11 months	Cell migration Cell organisation
Optic nerve	Axon loss by 8 months	No axon loss	Axon loss by 5 months	
ERG	Latency normal VEP normal	Latency normal VEP normal	Latency increase Reduced Amp	
		Reduced PNR response		
Neuro locomotion	Reduced Clutch reflex	Reduced Increased	Reduced Sensoneural	
	Reduced body fat	transfer	deafness	
	Reduced weight	arousal	Siatic nerve	
	COX RFF -ve		demyelination	
CNS			Dilated 4th ventricle	
Cardiac		Cardiomyopathy	Cardiac anomalies with myofibrils	

Ref: Moore et al., 2010, Alavi et al., 2007, Alavi et al., 2009, Heiduschka et al., 2010, Dav White et al 2009, Yu-Wai-Man et al., 2009, Barnard et al., 2011, Williams et al., 2011

Table 1.1 Mouse models of ADOA

A comparative summary of mouse models of ADOA with a summary of disease pathologies associated with each model

1.5.4 Summary of pathophysiology of Opa1 dysfunction in animal models

In summary, the availability of different species in the study of Opa1 has provided some significant information about the function of the mitochondrial GTPase in development and disease pathology. The generation of a viable homozygous mutant with *Drosophila* shows the dual pathologies due to a complete lack of Opa1 in the retina. The increase in ROS and response to exogenous addition of dietary antioxidants provides a potential therapeutic avenue. Based on these findings, it may be possible to reduce excess production of ROS, which may cause dendropathy of the IPL by the administration of antioxidant therapy.

C.elegans provides a significant link between the pathology of Opa1 mutation and a hitherto unrecognised gastrointestinal disorder. Reduced gastrointestinal motility in an adult human can

Chapter 1 Introduction

be relieved by dietary modification before it can develop into a pathological disorder. Presence of the condition in a very young child could ultimately prove fatal with severe electrolyte imbalance in a physiology that is too immature to cope. In the field of ophthalmology, *C.elegans* may have little input, but demonstrates that tissue specific ATP level maintenance requires the full quota of Opa1.

The wide variation in phenotypes as seen in both the Opa1^{M1BEWI} and in Opa1^{Q285STOP} models of disease would suggest there are some post translational modifications responsible for Opa1 function. Mouse Opa1^{Q285STOP} represents the GTPase domain where there are nine registered point mutations, which lead to ADOA, thus making Opa1^{Q285STOP} a significantly more relevant mouse model for the study of ADOA. This unique feature puts Opa1^{Q285STOP} at the pinnacle in the study of inherited dominant optic atrophy.

1.6 Reactive oxygen

The term reactive oxygen species (ROS) is used to describe both oxygen free and non-radical derivatives of molecular oxygen. The human brain is estimated to produce 10¹¹ free radicals a day (Perry et al. 2002). Any disturbance in the oxidant homeostasis can generate both radical and non-radical species that participate in the radical chain reactions. The reduction of oxygen by four one-electron steps progressively generate superoxide(O₂^{•-}), hydrogen peroxide(H₂O₂), and the hydroxyl radical OH[•] plus water. An excess of O₂^{•-} can damage nucleic acids and proteins. Reduction of this excess is by dismutation which is catalysed by superoxide dismutase (SOD), and produces H₂O₂ and water.

1.6.1 Function of ROS

Superoxide (O₂^{•-}) is a single electron oxidant and formed as a by-product within the electron transport chain (ETC) with one electron reduction of oxygen mediated by enzymes such as NAPH oxidase or circulating xanthine oxidase. The half-life of O₂^{•-} depends on pH and the availability of SOD within the different cellular compartments. A decrease in ROS production will deactivate the redox sensitive signalling pathways and have deleterious effects on cell cycle regulation.

Chapter 1 Introduction

The activity of ROS during embryological development is necessary for proliferation, differentiation and apoptosis. Embryological control over the specific activity of ROS is vital. The function of ROS in primary brain-derived neural progenitors maintains a high ROS status and is highly responsive to ROS stimulation.

1.7 Reactive nitrogen species

RNS are derived from nitric oxide (NO) with $O_2^{\bullet-}$ to form peroxynitrite (ONOO⁻) and nitrogen dioxide (NO_2^{\bullet}) (Castro et al. 2011). NO_2^{\bullet} can denature DNA, proteins and fats, and are potentially more damaging due to their non-selective targets.

Cellular sources of RNS are the enzyme catalysed formation of nitric oxide from arginine: NO^{\bullet} and $O_2^{\bullet-}$ combine to form the oxidizing agent ONOO⁻. Peroxynitrous acid breaks down to form additional ROS/RNS in the form OH^{\bullet} and NO_2^{\bullet} (Berski et al. 2011; Mòdol et al. 2011).

1.7.1 Function of RNS

There are tissue-specific NO synthases- neuronal (nNOS or NOS1) which are responsible for cell communication and are found within the central nervous system and skeletal muscle type II (Bradley et al. 2010; Hervera et al. 2010; Wisor et al. 2011). Inducible iNOS or NOS II is found within the immune system and cardiovascular system. It is induced on presentation of pathogenic lipopolysaccharide and certain cytokine subsets (Zheng and Kern 2009; Shin et al. 2010; Zhao et al. 2010).

1.7.2 Relevance of ROS

While ROS are important for normal cellular activities, aberrant production of ROS, or diminished capacity to scavenge excessive ROS, leads to an imbalance in the redox environment of the cell. ROS contributes to a wide field of disease states. (Lee et al. 2002; Duan et al. 2003; Yang and Hekimi 2010; Jiang et al. 2011; Lee et al. 2011). ROS-scavenging enzyme systems are in place to detoxify mitochondrial ROS. Manganese superoxide dismutase (MnSOD) (Yuyama et al. 2003) is the major ROS scavenger of the mitochondria catalyzing the dismutation of superoxide radicals.

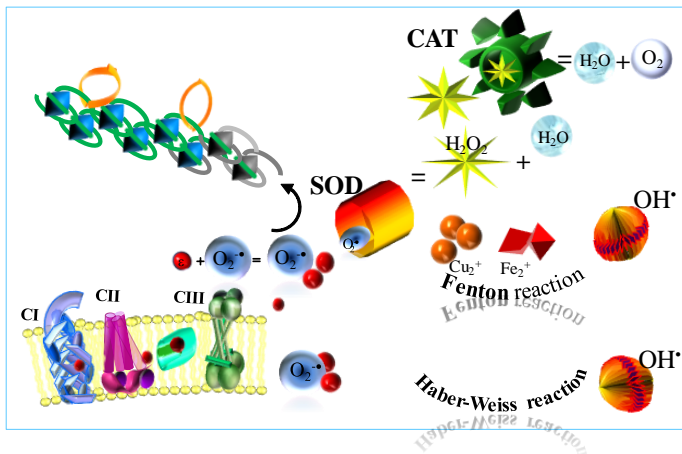
Chapter 1 Introduction

The target of ROS is of equal significance. ROS cause loss of essential cellular functions or gain of toxic functions. Essential targets during ROS stress include membrane lipid integrity (Colquhoun 2010), and activity of ROS-susceptible proteins, including proteins required for translation of mRNA (Jeong et al. 2010). Protein oxidation also triggers accumulation of toxic protein aggregates or apoptosis.

1.7.2.1 Superoxide anion

$O_2^{\bullet-}$ is highly reactive but due to its limited lipid solubility, cannot travel far. It can generate a more reactive hydroxyl and hydroperoxyl radical (HO^{\bullet}_2) by reacting with H_2O_2 in the Haber-Weiss reaction. This reaction is pH dependent at acidic environment within the lysosomes. H_2O_2 is a weak oxidiser but can generate OH^{\bullet} . Transition metals such as ferrous iron (Fe^{2+}) and copper (Cu^{2+}) catalyse the formation of OH^{\bullet} with H_2O_2 in the Fenton reaction as depicted in Figure 1.10. $O_2^{\bullet-}$ can oxidise iron sulphur (Fe-S) and release iron (Bhattacharya et al. 2011; Krätzer et al. 2011). $O_2^{\bullet-}$ can also react with thiols (in vitro) but due to its negative charge is unable to diffuse through the membrane making it a poor signalling molecule.

Figure 1.10 Reactive oxygen species



Superoxide anion ($O_2^{\bullet-}$) is dismutated to H_2O_2 and water. It can also react with H_2O_2 to form hydroxyl radicals (OH^{\bullet}) in the Haber Weiss reaction. In the presence of transition metals, H_2O_2 can generate OH^{\bullet} in the Fenton reaction. Catalase can reduce H_2O_2 and prevent hydroxyl formation.

1.7.2.2 Hydrogen peroxide

Hydrogen peroxide (H_2O_2) is formed from the spontaneous dismutation of $O_2^{\bullet-}$ or the action of SOD on $O_2^{\bullet-}$. H_2O_2 is a weak oxidant and can diffuse through membranes and lipid bilayer possibly via aquaporin (Conde et al. 2010). DNA is a highly charged anion capable of binding

Chapter 1 Introduction

both Cu^{2+} and Fe^{2+} ions (Zheng et al. 2009; Zheng et al. 2010a). The catalysis by metal ions of H_2O_2 reduces it to OH^\bullet . Scavengers cannot intercept OH^\bullet once it is formed directly on DNA.

1.7.2.3 Hydroxyl radicals

The hydroxyl radical, OH^\bullet , is the radical form of the hydroxide ion (OH^-). Hydroxyl radicals are highly reactive and consequently short-lived. OH^\bullet are produced from the decomposition of hydro peroxides (ROOH) (Kadiiska et al. 2005).

Hydroxyl radical scavengers cannot intercept OH^\bullet as it is formed directly on the DNA strand. Base pair mutations are increased with RNS (Chandor-Proust et al. 2008). Abasic sites are mutagenic and act to block DNA transcription and replication. The reaction of O_2^\bullet with hypochlorous acid (HOCl) and ONOOH results in further OH^\bullet production (Tretyakova et al. 2000).

1.8 Endogenous antioxidants and defence

Because of their potentially harmful effects, excessive ROS must be promptly eliminated from the cells by a variety of antioxidant defence mechanisms. Antioxidants include both hydrophilic and lipophilic molecules for metabolizing ROS (Pavlica and Gebhardt 2010; Rodrigo et al. 2011; Sun et al. 2011). There are several endogenous defence mechanisms, which normally act in synchronicity with ROS/RNS. The up regulation of a particular ROS may be due to a reduction of a particular antioxidant. An overload of ROS may deplete antioxidant levels, which can result in further increases in ROS. The balance between ROS/antioxidant once lost, can be detrimental not just to the cellular environment, but to whole organs. The antioxidant system consists of enzymes and small antioxidant molecules. The enzymes comprise of superoxide dismutase enzymes (CuZnSOD and MnSOD) catalase, glutathione peroxidases, the thioredoxin, thioredoxin reductase pair, haem oxygenase and heat shock proteins. Small antioxidant molecules are glutathione, uric acid, bilirubin, glucose, vitamins A, C, E, ubiquinone, carotenoids and flavonoids.

Chapter 1 Introduction

1.8.1 Superoxide dismutase

There are three mammalian isoforms of SOD. SOD 1 is located in the cytoplasm. The human form of CuZnSOD is a dimeric enzyme, which is negatively charged except for the copper binding site which directs $O_2^{\bullet -}$ by electrostatic facilitation. Copper ions mediate the dismutation. Zinc stabilises the enzyme. CuZnSOD is inhibited by cyanide. Extracellular CuZnSOD (SOD 3) is a tetrameric glycoprotein and exists in several forms. Most EC SOD is bound to cell surface proteins especially lung and blood vessel walls.

MnSOD Manganese SOD (SOD 2) is found primarily in the mitochondria and unlike CuZnSOD, is pH dependent with reduced activity at alkaline pH. MnSOD of neurons serves to detoxify the effects of ROS, which involve catabolizing glutamate and scavenging superoxide anions, respectively (St-Pierre et al. 2006). Both CuZnSOD and MnSOD enzymes catalyze one electron dismutation of superoxide anion to generate O_2 and H_2O_2 .

1.8.2 Catalase

All oxygen utilising organisms have catalase. The enzyme consists of four polypeptide chains each over 500 aminoacids long. It has four iron groups – porphyrin haem that allow interaction with H_2O_2 and decompose it to water and oxygen. Catalase activity is versatile at pH 6.8-7.5. Catalase is located in the peroxisomes of cell and the liver has the highest concentration.

1.8.3 Glutathione peroxidase

Glutathione peroxidase (GPx) is a selenium dependent scavenging enzyme that reduces lipid and hydrogen peroxides with concomitant oxidation of glutathione. Glutathione peroxidase (GSH-PO), is localised in both the mitochondria and cytosol (Utsunomiya et al. 1991). There are tissue specific glutathione peroxidases each performing individual antioxidant activities pertaining to their environment. GPx1 is located in the cytoplasm of virtually all cells of the body. It specifically targets H_2O_2 as its substrate. Gpx2 is found primarily in the gastrointestinal tract. Gpx4 is associated with lipid hydroperoxides. Mouse GPx1 knockouts are viable but develop cataracts early in life. Knockout for GPx4 are lethal indicating the importance of removal of lipid hydroperoxides (Ran et al. 2007).

Chapter 1 Introduction

1.9 Emerging therapies for human ADOA

In humans, the variability of phenotype with ADOA means that it is impossible to target pre-clinical mutant carriers before they develop symptoms. With age related disease onset, the use of antioxidants prior to pathology may have some application. The application of specific therapies targeted to individual complexes of the electron transport chain has been used in retinal disorders of mitochondrial origin.

1.9.1 Co enzyme Q₁₀ derivatives

The first randomized controlled trial in a mitochondrial disorder of Leber's hereditary optic neuropathy (LHON), used Idebenone as a therapy (Klopstock et al. 2011). Idebenone acts by increasing the complex I driven respiration by balancing electron fluxes between complex I and complex II. However not all individuals derive benefit from this. In a study of 9 LHON individuals, 16% showed an increase in complex I activity, whereas 42% showed a reduction (Angebault et al. 2011). More recently reports of a clinical trial with Idebenone in ADOA reported a positive outcome in 5 out of seven patients. Four of the five individuals, reported bilateral subjective improvement in visual function (Barboni et al. 2013).

EPI-743 is a third generation quinone with 1000 times greater activity compared to Idebenone. EPI-743 is a 'digital biochemical information transfer & sensing compound' (D-BITS), and acts by regulating metabolic control and replenishing glutathione pools. It has been used in a variety of mitochondrial disorders with overall improvement in skeletal/motor coordination and cognitive skills (Enns et al. 2012). Phase 2 of an on-going trial continues with four in five individuals with LHON were successfully treated as part of a clinical trial (Sadun et al. 2012).

Chapter 1 Introduction

1.10 Potential therapies for Opa1^{Q285STOP} mouse

1.10.1 Resveratrol

1.10.1.1 Introduction

Resveratrol is a polyphenolic phytoalexin and a derivative of stilbene. It is produced in plants as a defence mechanism against fungal pathogens. The substrate for stilbene is present in most plants however the enzyme stilbene synthase (STS) is only in a selected few. It is found in peanuts, red grape and pine nuts.

1.10.1.2 Pharmacological properties

Resveratrol displays several pharmacological actions including non-steroid anti-inflammatory (Song et al. 2013) antioxidant (Goldberg 1996; Bellaver et al. 2014; Liu et al. 2014) chemopreventive (Jang et al. 1997; Kma 2013) cardiovascular (Mokni et al. 2013) and platelet-inhibitory actions (Rotondo et al. 1996). The action of resveratrol in ophthalmic applications includes protection of the human lens from H₂O₂ induced oxidative stress (Zheng et al. 2010b) light induced damage on mouse retina (Kubota et al. 2010) inhibits diabetic induced activation of ganglion cell death (Kim et al. 2010) and inhibits endotoxin induced uveitis by inhibition of oxidation (Kubota et al. 2009)

1.10.1.3 Mode of action

Resveratrol is a competitive inhibitor of phosphodiesterases (PDE). PDE are a group of enzymes that regulate second messengers by controlling their degradation. PDE's are ubiquitously expressed with each tissue having a specific subtype. Glucagon stimulates the cAMP response through adenylate cyclase 1. In response to glucagon signalling, PDE-4 degrades cAMP. Inhibition of PDE4 results in the activation of Epac1, a cAMP effector protein which elevates calcium levels and triggers calcium/calmodulin dependent protein kinase AMPK pathway (CaMKK). This protein kinase activates peroxisome proliferator-activated receptor co activator PGC-1 α which acts as a transcriptional co activator regulating the genetic response to energy metabolism. PGC1 α is activated during cellular stress, hypothermia and stimulates mitochondrial biogenesis (Liang and Ward 2006). Resveratrol induces its antioxidant properties

Chapter 1 Introduction

through PGC1 α activation. PGC1 α is expressed in regions of high metabolic demand including heart, brain, retina, and brown adipose tissue (BAT). The tissue with highest gene expression is retina (Egger et al. 2012). PGC-1 α expression is up regulated in response to light induced retinal damage. Loss of function studies show increased apoptosis in PGC-1 α knockout mice.

In the retina, PDE6 is restricted to the PRL where it facilitates cGMP hydrolysis following light stimulation (Fung et al. 1981). PDE1 is activated by calmodulin found in the OPL photoreceptor terminals and the IPL synaptic terminals of bipolar cells and in the dendrites of ganglion cells (Cooper et al. 1985). PDE 4 is the most abundant PDE expressed in the CNS (Bolger et al. 1996). The presence of PDE4 in RGC may suggest a direct target for transcription factor CREB (cAMP response element binding protein) which is down regulated in axon damage (Fernandes et al. 2007). A schematic representation of resveratrol mode of action is shown in Figure 1.11.

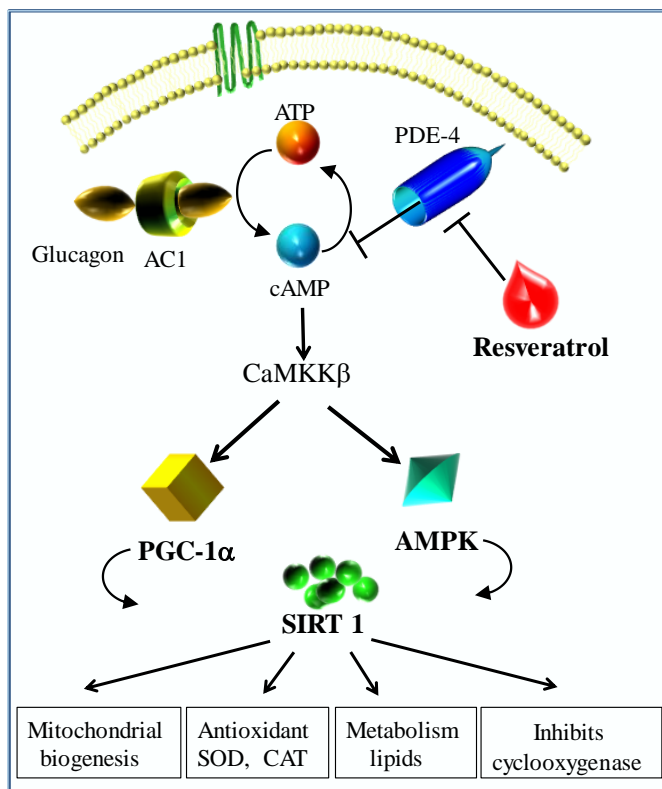


Figure 1.11 Resveratrol mode of action

Glucagon stimulates metabolic activity through adenylate cyclase 1. PDE-4 in the presence of glucagon degrades cAMP. Resveratrol competitively inhibits cAMP degradation through the inhibition of PDE-4. This activates the CaMKK β pathway. PGC-1 α is responsible for mitochondrial biogenesis and antioxidant properties associated with resveratrol

Hypothesis

The course of disease pathology may be due to impairment in one or several aspects of mitochondrial activity in Opa1^{Q285STOP} mouse. The precise nature of mitochondrial impairment in Opa1^{Q285STOP} mouse is unknown. Late onset ADOA may be due to a bioenergetic deficit. This may result in reduced tissue specific ATP quota.

The current available literature supports the presence of excess ROS in a fusion deficient environment. This excess ROS may result in a reduction of endogenous antioxidant thus a potential trigger for disease progression. To support this hypothesis, Opa1^{Q285STOP} mouse was administered the phytoalexin Resveratrol with the aim of exploiting its antioxidant properties and investigating its potential as a therapeutic agent in the treatment of late onset ADOA pathology.

By investigating several mitochondrial parameters the precise nature of disease onset may be determined. This study aims to compare Opa1^{Q285STOP} mouse model of ADOA with wild type C57BL/6 for the following investigation

- ▲ Explore to precise physiological effects that reduced mitochondrial fusion may have in the phenotypic function of Opa1^{Q285STOP} mouse
- ▲ Examine the functional activity of the electron transport chain and the presence of ATP.
- ▲ Review the endogenous antioxidant functions in mouse model Opa1^{Q285STOP} including enzyme assays for SOD and catalase activities.
- ▲ Consider other factors which may have a direct effect on OXPHOS including any compensatory mechanisms to overcome fusion deficits due to Opa1 haploinsufficiency

Chapter 2 Chapter 2 Materials and methods

2.1 Live mouse maintenance

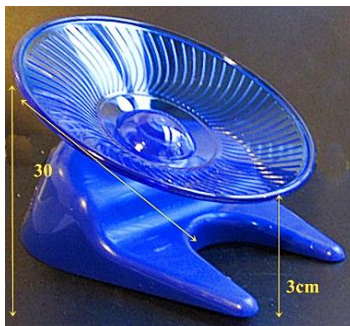
The implementation of the three ‘R’s’ (refinement reduction and replacement), is currently in practice and where possible an animal was culled only when necessary with forward planning of experimental procedures. Tissue retrieval of as many organs as possible at time of culling provided adequate supply of experimental material for most of the planned experiments.

2.1.1 Origins of *Opa1^{Q285STOP}* mouse

ENU mutagenized male C3H mouse donors were used for *in vitro* fertilization of female C57Bl/6J to generate ‘founder’ heterozygous hybrid (B6 : C3 *Opa1^{Q285STOP}* mouse line). Founder mice were crossed to C57Bl/6J (Charles River, East Lothian, UK) to generate a pure C57Bl/6J background.

The *Opa1* colony of mice was maintained by selective breeding and genotyping. With the assistance of the animal technicians, maintaining a healthy population of mice ensured continued high quality research data. Mice were maintained on a twelve-hour light cycle in average 10 lux intensity (max 9.3 minimum 2.66 Details of readings in Appendix A). Temperature and humidity were constant at 20 °C and 45% humidity.

Enrichment is an imperative part of animal maintenance (Cancedda et al. 2004; Sale et al. 2004; Landi et al. 2007; Sale et al. 2007; Maruoka et al. 2009; Baroncelli et al. 2010; Sparling et al. 2010). This study required that the mice were aged to at least 15 months. The provision of a running ‘saucer’ was also a preventative measure against osteoporosis.



Mouse saucer, which provided enrichment for animals housed in larger mouse boxes. It was also beneficial in the prevention and treatment of osteoporosis by increasing bone density and muscle mass. This wheel allowed up to three mice at any one time without any risk of spinning out or damaging their tails.

Chapter 2 Methods

2.1.2 Breeding

Female mice were introduced to a single male for a period of five days. Male mice with good ‘nest building’ abilities had a clear advantage over non-nest builders. Females were from the same litter, as this helped to synchronise their breeding cycles.

2.1.3 Mouse genotyping

2.1.3.1 Mouse ear punch protocol

Following sexing, females were ear punched in rotation (L1,R1 which corresponded to left 1, right 1 etc., (see Figure 2.1), by scruffing gently. Ear punch tissue samples were placed in sterile 1.5ml tubes with the corresponding mouse identity number and mouse was returned to its mother.

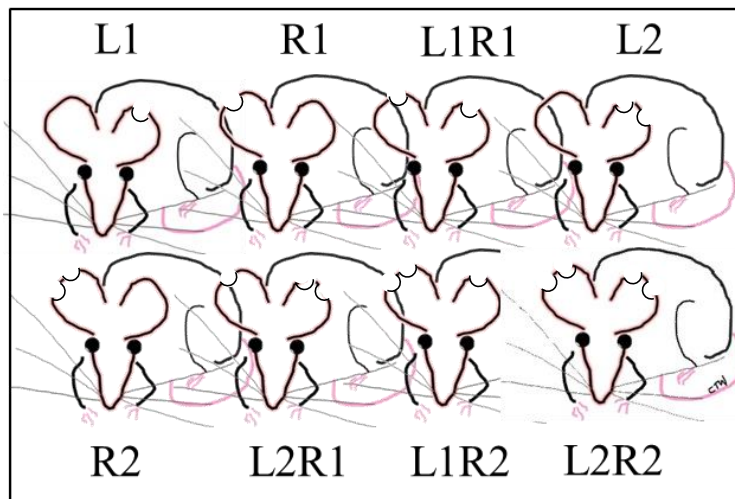


Figure 2.1 Genotyping ID

Mice were ear punched for identification purposes at day 16-20. L1, R1 corresponds to left 1 right 1 etc.

2.1.4 DNA extraction

Mouse ear punch samples were lysed with 50 μ l of 50mM sodium hydroxide ensuring the tissue was fully submerged in solution. Samples were transferred to a pre heated block at 95 $^{\circ}$ C, for five minutes. Following lysis, tissue was neutralised with 10 μ l of 1M Tris-HCl pH 6.0. Samples were centrifuged for 5 minutes and 1 μ l of solution was used to perform PCR reaction.

2.1.5 Mouse *Opal* PCR

Mouse genotyping was performed using custom primers targeting exon 8 of mouse *Opal* sequence (Sigma Genosys)

Chapter 2 Methods

Opa1 forward strand WT TCTCTTCATGTATCTGTGGTCTTTG and

Opa 1 reverse strand WT-TTACCCGTGGTAGGTGATCATG or

Opa 1 reverse strand Het-TTACCCGTGGTAGGTGATCATA.

The reaction was initiated with the addition of 12.5µl of Biomix to 1µl of mouse DNA. Denaturation at 92 °C was followed by annealing at 56 °C for 1 minute and extension at 72 oC for 1 minute. Final extension was 72 °C for five minutes and kept on 4 °C hold until run on a 1% agarose gel (TC512-PCR). Products were run with a 1kb molecular marker on ethidium gel at ~70v and bands with wild type forward and reverse primers at 180bp identified in all mice. Het DNA had bands with forward WT primer and reverse Het primer at the same 180bp location. Figure 2.2 shows a typical PCR product size following amplification with both primers.

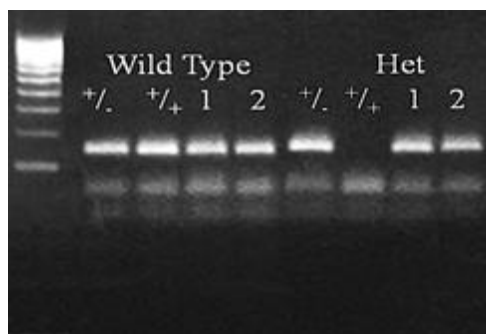


Figure 2.2 Opa1 DNA PCR

Mouse ear punch DNA amplified primers specific to Opa1. The WT primer produced bands of 180bp in both phenotypes. The Het primers, amplified a same size DNA band but in Het DNA only.

2.2 Mouse phenotyping

2.2.1 SHIRPA analysis

Phenotype screening procedure according to the MRC Harwell standard operating procedure, SHIRPA is an acronym for SmithKlein Beecham, Harwell, Imperial College, Royal London hospital Phenotype Assessment. It is an observational record of mouse in three stages: within a viewing jar, within and above the arena (Rogers et al. 1997).

The primary screen consisted of behavioural observation. Mice were transferred in their home cages to the procedure room where following a period of acclimatization, were transferred individually to a Perspex viewing tube measuring 14cm in diameter and 18cm in height. Here, the mouse was analysed for body position including activity on transfer, the presence of any tremor, general coat appearance and the presence of any piloerection, the presence of a full

Chapter 2 Methods

complement of whiskers, and whether defecation and urination occurred. The secondary screen assessed locomotor activity. Mouse was transferred to the arena and observed for transfer arousal, gait tail elevation and touch escape response. An IHR click box was used to record the startle response at 30cm above the arena. The final screen assessed sensory function. Above the arena, handling responses to tail and scruffing and supine positioning were recorded. The presence of trunk curl and limb grasping was recorded on tail hold. Reflexes were examined including corneal, pinna and contact righting inside a Perspex tube. Any attempt at biting and vocalization during the screen was noted and recorded. Data was recorded on a SHIRPA test sheet where results were scored from '0' to '2' depending on the result (Appendix E contains test procedure sheet).

2.2.2 Rotarod

The rotarod procedure was carried out according to the standard operation procedure (<http://empres.har.mrc.ac.uk/>). Rotarod is a test of balance and coordination. The rotarod is a rotating drum with a grooved rubber surface to facilitate grip. For training of the mice, the rotarod was set to 'run' mode with a maximum speed of 8 revolutions per minute (RPM) for a maximum duration of 1 minute. There were three training sessions with a fifteen-minute interval between each test. For the test, mice were placed on the drum in 'accelerate' mode where the speed of the drum increased from 8rpm to a maximum of 40rpm within 5 minutes. This was a fixed acceleration of 0.133 revolutions per second for 300 seconds. Each test lasted a maximum of one minute with a fifteen-minute rest session between tests.

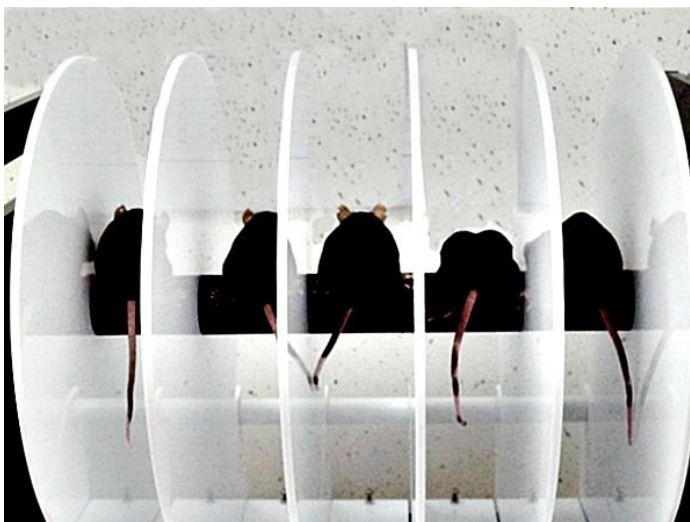


Figure 2.3 Rotarod analysis in mouse

Up to five mice were tested on rotarod simultaneously. The test recorded acceleration from 0-40rpm in 5 minutes with a 0.133 revolution per second increase.

Chapter 2 Methods

On three consecutive days, a total of three rotarod trials were performed each day. Any mouse that fell from the rod was returned to his cage for a fifteen minute rest period before the next trial. Mouse body weight was recorded prior to the test. During this test, no mouse completed a full passive rotation. Any aberrant behaviour was recorded on the test sheet. Figure 2.3 shows mice performing a rotarod test.

2.2.2.1 Mouse learning

As many of the phenotypic tests required some learning skills, the rotarod was taken as an example of increased learning ability. The mean score on day 1 was subtracted from the mean score on day 2 as described in the schematic Figure 2.4. It was anticipated that there may be a slight reduction in this value as seen in latency values in WT mice. The final score on day three represented the maximum trained latency a mouse can achieve and this was expected to show some level of improvement from day 1.

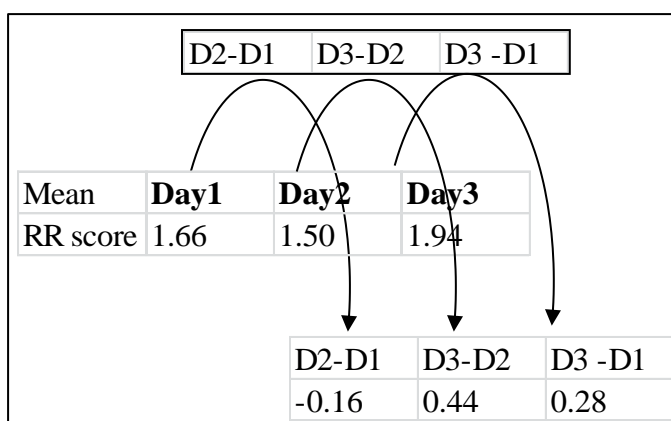


Figure 2.4 Mouse learning in training trials

Calculated from increased learning skills over a three day training period

2.2.3 Tight rope test

The rope grip test has been replaced by an instrumental analysis. (Bioseb or TSE grip strength meter apparatus). An automated grip strength meter measures the strength in hind and fore limbs. The measurements are a record of the force required in Newtons. The guidelines in the SOP for grip strength (<http://empress.har.mrc.ac.uk/>) were adhered to as far as appropriate. Mice were placed on a suspended rope 1cm in diameter. The tight rope was taut and not mobile. They were encouraged to either cling on with their front paws or to balance on both hind and fore paws with tester support until they gained balance. The tight rope test was placed over a

Chapter 2 Methods

large tank filled with cotton wool to avoid any injuries on falling. Mice were then encouraged to move along the tight rope by tilting it at a 15 degree incline. Mice will travel up rather than down in these circumstances. With the use of all four limbs and tail, balance and coordination are required before movement along the rope can be performed. The speed with which the task is performed depends on the ability of the animal to right itself on the rope thereby facilitating running. Analysis of the distance travelled and whether mice gained an upright position were analysed. Figure 2.5 shows sequential images from the rope test. The test has been applied to several mouse models of disease (Hall et al. 1987; Kashiwabuchi et al. 1995; Peled-Kamar et al. 1997; Heck et al. 2008).

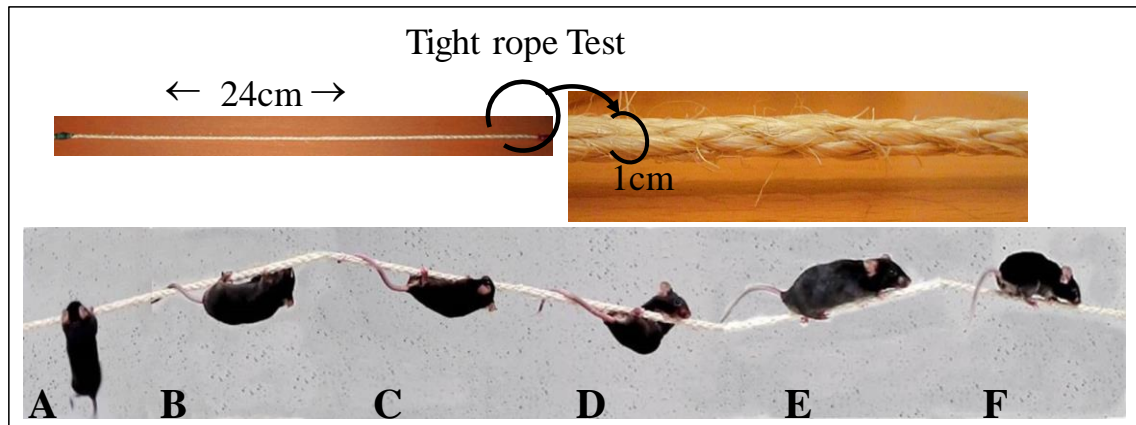


Figure 2.5 Tight rope testing in mouse

Rope 1cm in diameter secured between two weighted objects. There was no slack in the rope which provided a firm solid base for mouse to grip. It was suspended 30cm from the ground which was covered with cotton wool to reduce impact on falling (A) Mice suspended by two limbs were observed for incorporation of (B) 4 limbs and (C) distance travelled on the rope plus (D) a righting ability and (E) maintaining righting resulting in (F) a faster exit from the rope.

In order to optimise the tightrope test, it was observed in wild type mice that 60cm was too great a distance to travel on the tight rope. Mice were placed at a mid-point of the rope (at 30cm position), and they selected whether to move up or down hill from their position. Once they were confident of their balance, using all four limbs and tail, they began to travel.

Chapter 2 Methods

2.2.4 Narrow beam testing

Traversing an elevated narrow beam suspended between platforms is a method of assessing hind limb motor coordination. The use of the narrow beam test can help to distinguish the difference between an animal who is having difficulty performing a task due to weight, vision, balance or lethargy. There was no physical exertion involved. Mice with reduced vision were expected to require a longer time to initiate crossing (freeze). Analysis of the time taken to initiate crossing and distance travelled across the beam were recorded. Animals with balance and coordination issues could be observed clearly without any other immediate stress factor to consider, such as falling with the provision of a step. Figure 2.6 shows the beam and sequential images taken from a test.



Figure 2.6 Narrow beam testing in mouse

The beam was held in position at the widest end (2.5cm) where mouse was placed on. The beam narrowed at 10cm with gradual reduction of width to 1cm. The platform on either side of the beam provided a step to stabilize balance and a visual cue of beam width reduction.

The wooden beam was 60cm in length and 2.5cm wide at the nearest end tapering to 1cm width towards the farthest end. As the beam narrowed, provision was made for this adjustment with a 0.6cm step, which allowed a mouse to regain his balance but required a certain amount of dexterity. The furthest end of the beam rested on a platform where upon reaching it, mouse was returned to his home cage. The surface of the beam was scored diagonally at 1cm intervals to aid movement along the surface. A drop tank filled with cotton wool provided a soft landing for any casualties. Measurements of the distance travelled and the number of paw faults (using the platform) were used as a gauge of balance, gait and spatial awareness. (Carter et al. 2001).

Chapter 2 Methods

In order to permit all mice irrespective of weight to participate in the test, the platform was incorporated 10cm from the start of the beam. This permitted mouse to correct for speed his fall from the beam. It required that his peripheral senses were intact and that he could interpret the platform as a means of maintaining his position. The narrowing of the beam required the use of visual cues in order to realize that the space in which to walk was gradually reducing. The platform helped to provide these cues. At the furthest end, the beam tapered to a 1cm width. The test was performed once as this was adequate to provide the required information without learning association (Allbutt and Henderson 2007).

2.3 Cognitive function analysis in Opa1^{Q285STOP} mouse

2.3.1 T maze testing

Habituation of exploration can be induced by exposure to spatial location. The use of a T maze can demonstrate spontaneous alternation. Mice are started from the base of the maze and have free access to one of two arms of the maze. The repeat trial is carried out within one minute of the previous trial where the animal is given free access to both arms of the maze. Normal rodent behaviour suggests the animal will select the previously unvisited arm of the maze. This reflects an intact short term memory. The selection choice (novel/ unexplored) is called spontaneous alternation. The protocol was followed according to the Eumorphia Standard operating procedure method (www.euromorphia.org). (Youn et al. 2012).The walls of the T maze were clear Perspex which will induce anxiety in animals and affect their performance. The floor of the T maze was matt wood colored coating.

For T maze testing, mice were maintained in their home cages during acclimatisation to the location. Once testing began, mice were kept in a holding tank with one minute intervals between tests. Once the final test was complete, mouse was returned to his home cage and left undisturbed. In grouped cages, only the test mouse was transferred to the holding cage. The training period allowed the mouse to enter the T maze for a period of one minute to explore his surroundings. Once familiar with the surroundings, mouse was returned to his holding cage. Training sessions were extended over a five minute period so that when the tests began, mouse

Chapter 2 Methods

was familiar with the routine. Mice were started from the base of the maze and had free access to one of two arms of the maze. The repeat trial was carried out within one minute of the previous trial where the animal was given free access to both arms of the maze.

The time spent in the novel arm and time spent in the original arm were analyzed as functions of cognitive novelty recognition. A total of seven trials were performed. Figure 2.7 shows a T maze test in progress. Video recordings were made with a Canon Ixus 100IS 12MP 720p HD movie stabilized on a tripod and attached directly to a laptop to permit accurate analysis of each test and provide a record of analysis.

The investigation ratio (IR) was calculated by dividing the time in seconds spent in the novel arm by the time spent in both the novel and original arm.

The discrimination ratio (DR) was calculated by dividing the time in seconds spent in the novel arm minus time in original by time in novel arm plus original arm.



Figure 2.7 T Maze testing

He who hesitates... Mouse score based on the selection of the correct novel side, time spent in the novel arm and time spent in the original arm.

The only limit to the experiment was the time taken to acclimatise (10 minutes in the home cage), train (5 minutes), and test (20 minutes with a 1 minute interval between tests). The investigation ratio (IR) was calculated by dividing the time in seconds spent in the novel arm by the time spent in both the novel and original arm. The discrimination ratio (DR), was calculated by dividing the time in seconds spent in the novel arm minus time in original by time in novel arm plus original arm.

Chapter 2 Methods

2.3.2 Novel object testing (NOR)

The basis of the novel object recognition test was described by Ennaceur (Ennaceur and Delacour 1988), where they showed that in a familiar environment, rodents show an affinity towards new or novel objects. It assumes the rodent has a retention capacity for the familiar object. In the original experiments, rats were the subject animal. The protocol was performed with modifications (Akkerman et al. 2012a; Akkerman et al. 2012b).

Mice were given an acclimatisation period prior to the test, where they were free to explore the Perspex tray containing two identical novel objects. This 'training' period lasted 10 minutes. Following training, mouse was returned to his home cage for a period not exceeding 2 hours. Following the T maze data where C57BL/6 mice demonstrated laterality for the left side, novel objects were randomly placed in either left or right sides of the arena.

The test began with the return of the mouse to the arena following a one hour interval with the placement of an identical item seen during the training period and a new item previously unseen- the novel item. Each test was conducted from the time mouse was placed in the arena for a period of one minute. A total of seven novel objects were used in the experiment so at no time was mouse exposed to non-novelty item in any test.

Analysis of the raw data established the IR and DR for NOR. The time spent exploring the novel object divided by the time spent exploring either object yielded 'Investigation ratio'. The discrimination ratio was defined as the difference in exploration time for the objects divided by the total exploration time can be used for analysis of discrimination of normal exploration not necessarily associated with novelty.

Optimization of NOR testing included the provision of seven absolute novel duplicate items allowed for six individual tests of novelty recognition were performed at one session (Dere et al. 2007). One trial contained the selection of novel items suggested by Dere with variations in shape colour and texture. The duplicate item ensured the mouse initially approached the 'known' object with the same degree of curiosity as for the novel object. It was assumed that recognition of the 'known' object occurred with a combination of visual, tactile and olfactory

Chapter 2 Methods

contact. In the Het mice, it was considered that due to their impaired visual status, their olfactory memory may be enhanced. Also it was important to determine the difference in mouse ability to recognise based on visual cues and those of olfactory and tactile. To this end, duplicate identical items ensured the mouse did not ignore the ‘known’ object because he identified his own scent on the object and assumed he was familiar with it.

Novel object recognition was analysed according to the investigation ratio and discrimination ratio generated from the data collected during the test. The time to discover the novel object, the time spent with novel object and the time spent with the original object were measured in all 7 items in each mouse. Het mice who did not discover the novel object either because they did not leave the location they were placed in or did not move from the original familiar object were scored as 60 seconds in time to novel object. As each mouse had a specific time period of one minute (Dix and Aggleton 1999) to locate the item, or identify the original item before exploring the novel item, mice who didn’t explore obtained higher time scores. Figure 2.8 shows the items used for OR testing.

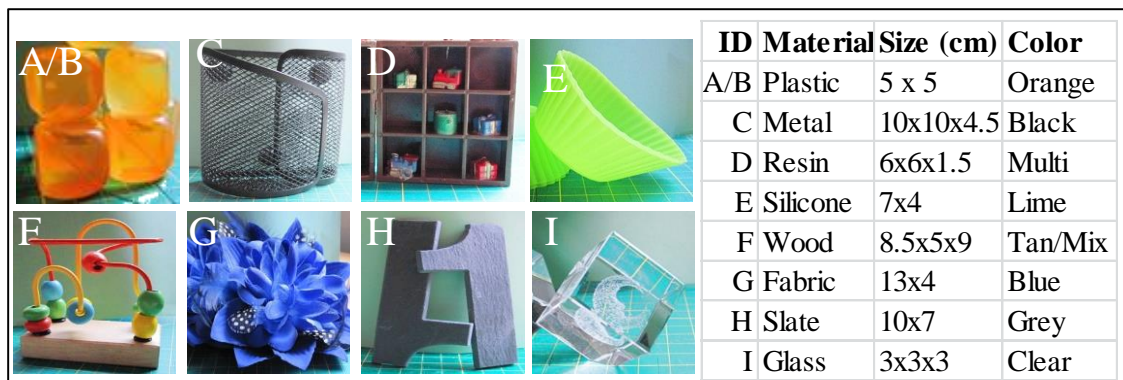


Figure 2.8 Items for NOR testing

The novelty items were made of plastic, metal, resin, silicone, wood, fabric, slate and glass. All objects were in duplicate. All items were cleaned with 70% alcohol prior to any testing, and evaporated with a bench top fan. All colour items were paint safe.

On the final test, mouse was returned to his home cage. The arena was cleaned with 70% ethanol, allowed to evaporate, and then wiped down with warm water. As each item was cleaned with 70% ethanol on removal from the arena and air dried with the use of a fan, the provision of ‘clean’ items for each mouse was ensured.

Chapter 2 Methods

2.4 Thermal imaging in Opa1^{Q285STOP} mouse

A thermal imaging camera was used to determine whether there was any difference in the core heat production in Opa1^{Q285STOP} mouse compared to his wild type littermates. A high resolution 320 x 320 pixel camera with thermal sensitivity of <0.05°C and temperature sensitivity from -20°C to +120°C was used to obtain images (FLIR E60). Measurements were corrected for reflected temperature, optic transmission and atmospheric transmission. Image processing was performed using FLIR Tools 2011 software. Measurement mode was in 'isotherm' and spot mode for precise temperature readings. Data was analysed from the same physical location in each animal. The head, tail base and flank region were selected to represent core, peripheral and central body temperatures. Mice were transferred to an arena as cage groups to reduce anxiety which may result in a rapid increase in temperature as an autonomic response to stress. Once acclimatised, the mice were identified by means of ear punch and isolated individually by means of a Perspex tube 20cm in diameter and 20cm in height. This allowed visual access to the mouse without the need to make physical contact. Because the mouse still had visual and olfactory cues to his surroundings, there were no immediate physiological alternations during the imaging process. Once an image was obtained, the Perspex tube was lifted, and mouse re-joined his cage mates in the arena.

2.5 Tissue retrieval

All procedures were performed in accordance with the Home Office Animals in Scientific Procedures Act. Mice were killed by cervical dislocation and tissue retrieval carried out as rapidly as tissue type permitted.

Mouse brain was removed by cutting along the coronal and sagittal suture. The parietal bones were folded back and the interparietal bone removed completely to gain access to the spinal canal. Using a broad ended forceps, the whole brain was scooped out of the cranial cavity as an intact organ. The tissue was placed in ice-cold 0.9% saline and any excess blood washed away. The brain was severed at the corpus callosum and both halves were placed on sterile gauze to

Chapter 2 Methods

absorb excess saline then transferred to a pre labelled cryo vial for immediate submersion in liquid nitrogen.

Mouse eye was removed with as much optic nerve intact as possible. Removal of the brain facilitates the complete removal of the orbit with intact optic nerve. If fixed retinal tissue was required, the orbit was washed in 0.9% saline and transferred to the appropriate fixative. Further resection of extra ocular muscle was performed following fixation.

The vertebrate column was resected at the lumbar region and vertebral muscles removed. The whole spinal column was washed in ice-cold 0.9% saline and using a blunt ended cannula, saline was introduced into the lumbar vertebrae to facilitate washing out the cord. This method worked well in young animals however, older mice with more tenacious spinal cords usually required further resection directly into saline. Tissue handling was kept to a minimum, and snap frozen immediately.

All internal organs were removed with an intact major blood vessel to facilitate blood washout in ice cold saline. Removal of blood was imperative for accurate analysis of SOD and other enzyme related assays. Larger organs were divided into two aliquots for storage at -80 °C.

Perfusion in normal saline was considered for complete removal of residual blood, but prolongs total tissue retrieval time by over twenty minutes. As it was imperative to remove tissue as expediently as possible, it was decided to continue with organ retrieval as described.

2.6 Immunohistochemistry

2.6.1 Tissue fixation

Whole mouse eye was removed and submerged in 4% paraformaldehyde (PFA), pH 7.4 for a minimum of four hours at room temperature. All but the superior rectus were removed. The rectus muscle was used to handle tissue and orientate prior to embedding. Tissue was cryopreserved in 30% sucrose and embedded in FSC 22 compound (Leica). Tissue sections were cut on a Leica CM1850 cryostat and left overnight to air dry. All sections were stored at -20 °C until required.

Chapter 2 Methods

Retina were cut as vertical 7 μ M serial sections on electrostatic charged slides. Where possible, sections pertaining to regions numbered 2-4 were used for analysis. See Figure 2.9 for details.

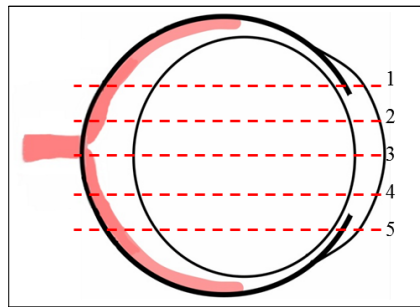


Figure 2.9 Cryostat sectioning

Numbered sections from vertical orientated block.

Whole brain from was divided at the corpus collusum, fixed, cryopreserved and 10 μ m sagittal sections placed on electrostatic microscope slides.

2.6.2 Immunohistochemistry controls

2.6.2.1 Antibody controls

Positive primary antibody controls were employed to determine the specificity of the primary antibody on a range of different tissue types known to express the antigen of interest. This also demonstrated the staining pattern of the epitope of interest. Titrations of the primary antibody were performed to determine the optimum concentration required to detect a positive signal. This was applied for each antibody as part of the experimental set up. Positive controls for each antibody are available in Appendix U.

Table 2.1 shows the primary antibodies used, the concentration and tissue specific positive control tissue used for this.

The secondary antibody control was determined by incubating the section in parallel with the test sections but in the absence of the primary antibody. This was performed to confirm that any fluorescence detected in the test sections was due to the binding of the conjugated antibody the Fc region of the primary antibody only. The presence of staining with the secondary fluorescence conjugated antibody in the absence of the primary antibody would indicate the availability of Fc receptors on the cell surface. This control was run in parallel with each experiment

Chapter 2 Methods

2.6.2.2 Tissue controls

Sections were examined by fluorescence microscopy following cutting prior to any antibody staining to detect the presence of any autofluorescence inherent to the tissue. Initial testing determined the presence of endogenous tissue background by incubating sections in all buffers but without primary and secondary antibodies. Any staining with detection reagents in the absence of primary antibody was considered to be non-specific. Each run included sections run in parallel without the primary antibody

Table 2.1 Antibodies for IHC and Western blotting

Antigen	Species	Iso	+ Con	Geno	Localisation	Company (cat no)	Dil IHC (cryo)	Dil WB	Band kDa
Opa1	Mouse	IgG ₁	Liver	C57Bl/6	Mitochondrial	BD 612607	1:500	1:1000	80-100
VDAC	Rabbit	IgG	Brain	C57Bl/6	Mitochondrial	Sigma V2139	1:500	1:1000	30
Neuroglobin	Goat	IgG	Cerebrum	C57Bl/6	Mitochondrial	Santa Cruz 22001	1:500	1:4000	17
MnSOD	Rabbit	IgG	Liver	C57Bl/6	Mitochondrial	Abcam 13533	1:500	1:5000	25
PSD95	Goat	IgG	Brain	C57Bl/6	Cell membrane	Abcam 12093	1:500	1:5000	105
Preli	Mouse	IgG _{1k}	Cardiac	C57Bl/6	Mitochondrial	SigmaWH0027166M	1:500	1:5000	25
NF H	Goat	IgG	Brain	Python	Cytoplasmic	Santa Cruz 22909	1:500	1:1000	200
NF L	Goat	IgG	Brain	Python	Cytoplasmic	Santa Cruz 12966	1:500	1:4000	80
3'Nitro	Rabbit	IgG	Kidney	C57Bl/6		Sigma N0409	1:250	1:4000	
Actin	Mouse	IgG				Sigma A1978	NA	1:5000	42

Primary antibodies used for IHC. Specificity was confirmed on tissue specific substrates. Antigen localisation is shown. Dilutions are shown for IHC and Western blotting (WB). Secondary antibodies for Western blotting were HRP conjugated. Secondary antibodies for IHC were conjugated to green fluorophore 488

2.6.3 IHC staining method

Slides from -20°C were allowed to equilibrate to room temperature and were immersed in phosphate buffered saline (PBS), pH 7.4, blocked with 10% heat inactivated normal goat serum for 30 minutes at room temperature and endogenous peroxidases removed with freshly prepared 3% hydrogen peroxide. Primary antibodies were incubated at stated dilutions at room temperature (21°C) for 4 hours. Secondary antibody was applied for 2 hours. Sections were counterstained with Hoechst 33342 nuclear stain applied for 4 minutes at a dilution of 1:1000. Sections were mounted using ProLong Gold (Life Technologies).

Chapter 2 Methods

2.6.4 IHC Image analysis

Sections were viewed with a fluorescent microscope (Leica Wetzlar DM6000) using 10x and 20x objectives and a 10x eyepiece which provided a total magnification of 100x and 200x, using filters for Hoechst (excitation/emission maxima 352/461nm) and Alexafluor 488 (excitation/emission maxima 495/519nm). Fluorophore saturation was avoided by setting the threshold, gains and exposure to the same setting in both channels for all images within the density histogram. The image acquisition parameters were set so that no detection channel showed pixels reading zero or saturated levels. This was visualized in histogram settings for each image.

The quantification of fluorescence was calculated using Image-J software. Figure 2.10 summarizes the method used for subtraction the background fluorescence from the test section. Briefly, the control section (with no primary antibody) was converted to 8-bit TIFF to preserve the linear relationship between photons and image intensity values (Staal et al. 2004). Using the threshold tool the autofluorescence was determined. This threshold was applied to the layers that were analyzed: PRL-IS,ONL,OPL,INL,IPL and GCL and applied to the test section.

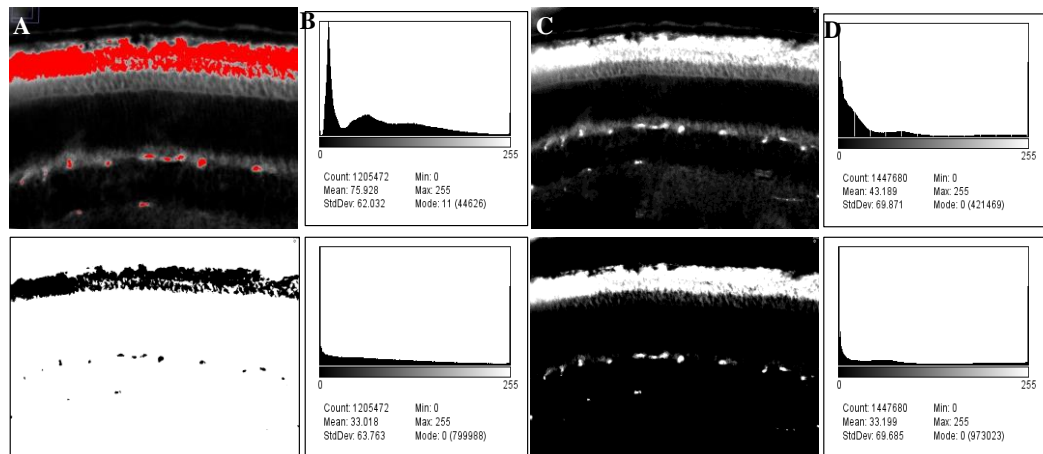


Figure 2.10 Determination of autofluorescence using control section

(A) Control section with no primary threshold was set which (B) identified autofluorescence in the PRL OS and OPL. (C) The test section before background correction (D) After background correction.

Pixel density was measured for threshold intensity within the selected areas (PRL, ONL, INL etc.). Measurements of area, mean and integrated density were obtained. Specifically for the analysis of PRL-IS, the inner segment only was used to calculate the fluorescence intensity as

Chapter 2 Methods

the outer segments frequently autofluoresces resulting in inaccurate reporting. Each genotype included control sections for each test run.

Using Image J, the regions of interest were selected using polygon tool and area, mean and integrated density values selected. The corrected cell fluorescence was calculated by subtracting the mean fluorescence background multiplied by the area selected (Abramoff et al. 2010; Rasband 2014).

Retinal images reported AFU of each layer from the photoreceptor inner segment layer (PRL IS) to ganglion cell layer (GCL). Brain sections were orientated to permit maximum exposure to the hypothalamic region. In the absence of a tissue specific marker, brain sections were analysed as total RGB count minus background staining. IHC are reported as arbitrary fluorescent units (AFU).

2.7 Western blotting

2.7.1 Tissue homogenisation

Tissue was defrosted on ice and washed briefly in ice-cold 0.9% saline to remove any remaining blood. Wet weights were recorded and tissue divided into equal aliquots. Aliquots were suspended in ice-cold homogenisation buffer at a ratio of 1:4 W/V in 1.5 ml tube. The tissue was homogenised using a Teflon pestle on ice to reduce degradation of contents. Balanced homogenates were centrifuged at 4°C at 500 x g for 20 minutes and the pellet was resuspended in buffer with protease inhibitor cocktail (Sigma protease inhibitor cocktail), at manufacturers recommended dilution. The supernatant was transferred to a fresh pre chilled tube. Protein was measured by bicinchoninic acid (BCIP), mitochondrial extractions were diluted in 2% TritonX-100 and assays were performed in triplicate with the results recorded as the average of three results.

Approximately 20µg protein supernatant was applied to each well. Protein samples were resolved on 14% SDS–polyacrylamide gels and transferred to nitrocellulose membranes (Biorad). The membranes were blocked for 1 hour at room temperature with blocking solution

Chapter 2 Methods

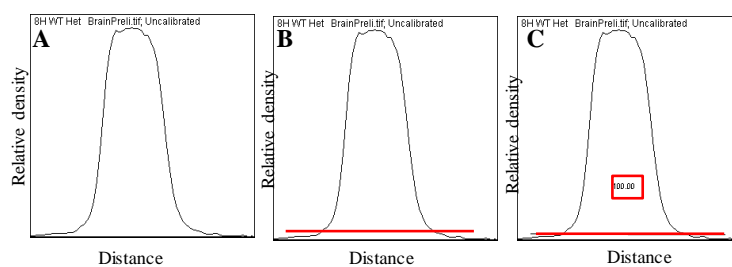
(5% skimmed milk). Primary antibodies were incubated overnight at 4° C on a rocking platform with the antibodies shown in Table 2.1.

Following washing, the membrane was incubated with HRP conjugated secondary antibody. Further washing was followed by incubation with enhanced chemiluminescent (ECL) substrate and exposure to clear blue X-ray film for development.

2.7.2 Analysis of Western blot by densitometry

X Ray film of blotted proteins were acquired as .tiff files by flatbed scanner (Canon) and imported into Image J 1.47v software where they were converted to 8 bit image and processed for densitometry using the Gel Analysis according to established methods (Abramoff and Magalhaes 2004; Gassmann et al. 2009; Taylor et al. 2013). Briefly, each lane was selected individually and a plot of the profile obtained (See Figure 2.11). The plots represented the relative density of the contents of the selected lane. Background noise was eliminated using the straight line tool to close off the end of each plot. The ‘area’ measurement represented the pixel density value of the band and the percentage value was relative to the total size and density of bands for any given image. Each blot had β actin as a loading control. For each blot, one sample was selected to be the standard e.g.: WT was selected in blots of WT and Het, untreated Het was selected in blots of Het and res treated Het. The percentage value was divided by the percentage value in the standard. This gave a measure of the relative density of each peak.

Figure 2.11 Western blot profile plots of an individual band



Images show the two-dimensional graph of pixel intensity along a line within the selected band. The x axis represents the distance along the line and the y axis represents the intensity. (A) profile plot (B) plot minus the background (C) and the percentage.

Chapter 2 Methods

This process was repeated for the loading controls. The relative density of the loading control represented the total protein loaded for each sample. The value obtained for the relative density of each test band was divided by the relative density of its corresponding β -actin loading control. This gave the adjusted relative density value relative to the total amount of protein examined. Western blot are reported as relative density (RD). Results are presented according to the primary antibody used.

2.8 BCIP protein assay

Protein concentrations of both mitochondria and tissue homogenates were measured using a commercial protein assay kit (Thermo Scientific BCA protein assay kit (cat# 23225))

BSA standards were plated in triplicate in a flat bottomed 96-well plate and incubated for 30 minutes at room temperature. The plate was read at 540nm wavelength. The average of each absorbance reading was plotted on the y axis against the known protein concentration of the standard on the x axis. The BCA method is compatible with up to 5% Triton X-100 in protein samples (Thermo Scientific Tech Tip #68)

2.9 Mitochondrial isolation

Mitochondria were isolated from tissue stored at -80 °C using a commercial mitochondrial isolation kit (Sigma Mitochondrial Isolation Kit (cat# MITOISO1)). The kit was designed for the isolation of viable mitochondria in animal tissue of 10-20g wet weight. Isolation of mitochondria was by differential centrifugation in sucrose. The mitochondria were re suspended in an OXPHOS support storage buffer which contained 10mM HEPES pH 7.5, 250mM sucrose, 1mM ATP, 0.08mM ADP, 5mM sodium succinate and 2mM phosphate. The kit also included a JC-1 stain for measurement of electrochemical proton gradient ($\Delta\Psi$) of the inner mitochondrial membrane.

For each assay, tissue was defrosted on ice and washed in extraction buffer. The average of three weights was used as wet weight of tissue. Tissue was chopped into fragments on a glass dish. Tissue was homogenised using a Teflon pestle. The homogenate was transferred to a fresh pre chilled 2ml tube and centrifuged at 600xg at 4 °C for 5 minutes. (Sigma 1-15pk). The

Chapter 2 Methods

supernatant was transferred to a fresh pre chilled tube and centrifuged at 11,000xg for 10 minutes at 4°C. The supernatant was removed and the pellet was resuspended in extraction buffer followed by further centrifugation at 600xg and 11,000xg as before with final pellet resuspended in storage buffer at 40µl per 100mg of the original tissue weight. Mitochondria were resuspended in storage buffer which supports OXPHOS and diluted in phosphate buffer to 1mg/ml in preparation for analysis following protein assay. The mitochondrial populations in the Het tissues were considered to have potentially more lysozyme activity however the isolation of lysosomes requires centrifugation at speeds in excess of 20,000 x g. The population of isolated Het mitochondria was considered to be as close to *In vivo* environmental conditions as possible. Mitochondria were maintained at 4°C in storage buffer containing 5mM sodium succinate for a period not extending 30 minutes prior to spectrophotometric analysis which did not impact on the analysis performed. It was considered important to provide support to mitochondria prior to dilution in the appropriate phosphate buffer.

2.10 Mitochondrial staining

2.10.1 JC1 for $\Delta\Psi_m$

JC-1 (5,5,6,6'-tetrachloro-1,1',3,3'-tetraethylbenz-imidazolcarbocyanine iodide) is a cationic carbocyanine dye. The stain stock (1mg/ml) in DMSO was vortexed vigorously prior to use. The stock solution was diluted to 0.2mg/ml in DMSO and kept at room temperature in a dark amber tube to protect it from light according to the manufacturers instructions. Mitochondria were diluted to a final protein concentration of 0.020mg/ml with storage buffer. The suspension was gently pipetted to resuspend mitochondria. JC1 stain was added at 40µg/ml to the diluted mitochondria and mixed thoroughly but gently. The mitochondrial suspension was incubated with JC1 at room temperature in the dark for 7 minutes and analysed immediately using a disposable haemocytometer. Chambers were visualised using a 20x objective with a 10x eyepiece giving a 200 times magnification with a 470nm +/- 40 nm excitation and 525 nm +/-50 nm emission wide band pass filter and 546 nm +/-12 nm excitation and 600 +/- 40 nm emission band pass filter using a Leica Wetzlar DM6000 microscope equipped with a DFC 350 FX digital camera. Fluorescence was pseudocolored and third channel merge was a combined dual

Chapter 2 Methods

immunofluorescence from both filter cubes. Counts were performed using Image J plug-in for tricolour cell count with split channel analysis of individual fluorescence. The ratio of viable red and reducing potential green is an indicator of membrane potential. For simultaneous visualisation, excitation at 488 nm and 568 nm were used. The reduction of membrane potential is associated with H₂O₂ production and subsequent mitochondrial death.

2.10.2 Mitotracker staining

Mitotracker stain (Mitotracker Red CMXRos MW 531.53 (M7512 Life Technologies) was resuspended in 940.6µl anhydrous dimethylsulfoxide (DMSO) to give a stock concentration of 100µM. DMSO. For mitochondrial staining, mitochondria were diluted to 1mg/ml in storage buffer containing Mitotracker Red at a concentration of 20nM. Stock Mitotracker was diluted to 20nM by adding 1µl of stock to 5ml of storage buffer containing 10mM HEPES pH 7.5, 250mM sucrose, 1mM ATP, 0.08mM ADP, 5mM sodium succinate and 2mM phosphate

Mitochondria from WT and Het tissues were incubated with Mitotracker Red in 1.5ml tubes and protected from light. Tubes were incubated at 37°C in a rotating incubator to ensure adequate mixing of contents. Following incubation, tubes were kept in the original dark container and the contents analysed on PTFE well plates at 5µl/well. Wells were visualised using a x100 objective under oil immersion with a x10 eyepiece (x1000 magnification) and visualised with 580nm excitation and 600 +/- 40nm emission on a Leica Wetzlar DM6000 microscope with a DFC Fx digital camera.

2.11 Spectroscopy for electron transfer analysis

Age matched wild type and Het mice were killed by cervical dislocation according to approved schedule one UK Home Office guidelines (Scientific Procedures Act, 1986). Tissues of the central nervous system (brain, spinal cord and retina), were rapidly snap frozen and stored at -80°C until processed for mitochondrial extraction. Mitochondrial preparations were kept on ice throughout analysis. Statistical analysis was performed using SPSS. A normality test for distribution using Shapiro-Wilk was used and univariate ANOVA with post hoc Tukey HSD where a value of <0.05 was considered significant.

Chapter 2 Methods

2.11.1 Fluorescence spectroscopy for complex I analysis

The specific activity of NADH ubiquinone oxidoreductase - complex I was investigated by the oxidation of NADH. NADH passes electrons to complex I that are then passed to the synthetic ubiquinone Coenzyme Q₁ (CoQ₁) as the electron acceptor. Using a fluorometric assay, with excitation of 340nm and emission 460nm, complex I activity was monitored by the decrease in absorbance of NADH at 460nm as a function of time (Starkov et al. 2004). The assay was performed in 20mM phosphate buffer pH7.4 at room temperature (21-23°C) in a final volume of 1ml. Buffer contained 100µM NADH, 1mM KCN and 40µM CoQ₁. Specificity of the assay was conformed using rotenone at a concentration of 2µM. Mitochondria were diluted to 1mg/ml and added at a concentration of 30µg/ml. The expected absorbance of 100µM NADH was calculated from the absorption coefficient of NADH at 340nm $6200 \text{ M}^{-1} \times \text{cm}^{-1}$ (McComb et al. 1976). A standard curve was used to calculate NADH concentration from 30-160 µM at 340nm and repeated using fluorescence at 460nm. The equation for the line from the fluorescence standard was used to calculate NADH concentration in the kinetic assay. Figure 2.12 shows the fluorescence spectrum of NADH from 350-700nm at 30-160µM and the standard curve generated from fluorescence spectrophotometry.

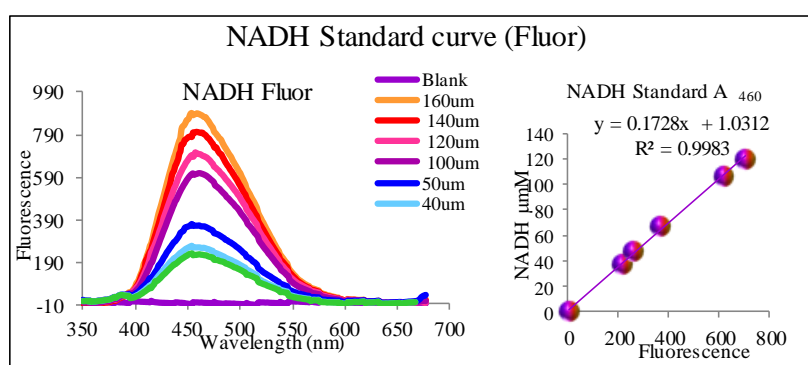


Figure 2.12 Standard curve NADH

Fluorescence spectrum of 30-160µM NADH from wavelengths 350-700nm and standard curve from fluorescence absorbance at 460nm used to calculate the oxidation of NADH for complex I.

The data was expressed as µmol/mg mitochondrial protein/ml. Magnetic stir bars were included in the cuvette to ensure adequate mixing of reagents. All reagents were supplied by Sigma. All buffers were treated with Chelex overnight to eliminate transition metals.

Chapter 2 Methods

2.11.2 UV spectrophotometry for complex II analysis

Complex II activity was analysed using the oxidation of succinate with an artificial electron acceptor 2,6 dichlorophenol indophenols (DCPIP) resulting in a reduction of DCPIP turning it from blue to colourless. This resulted in an increase in light transmittance, which was measured spectrophotometrically. The assay was performed at 30°C in 20mM phosphate buffer pH 7.8 containing 10mM succinate, 100µM decylubiquinone and 2mM potassium cyanide (KCN). DCPIP was prepared fresh at a concentration of 16mM. This was diluted to 16µM (1:10), with the addition of buffer containing 100µM decylubiquinone and 2mM KCN. The expected absorbance of 16mM DCPIP at 600nm was calculated from the extinction coefficient of DCPIP $22 \times 10^3 \text{ M}^{-1} \cdot \text{cm}^{-1}$ (Arrigoni and Singer 1962). This was calculated to be 0.352. A standard curve was generated with concentrations from 0.6-20mm (Figure 2.13).

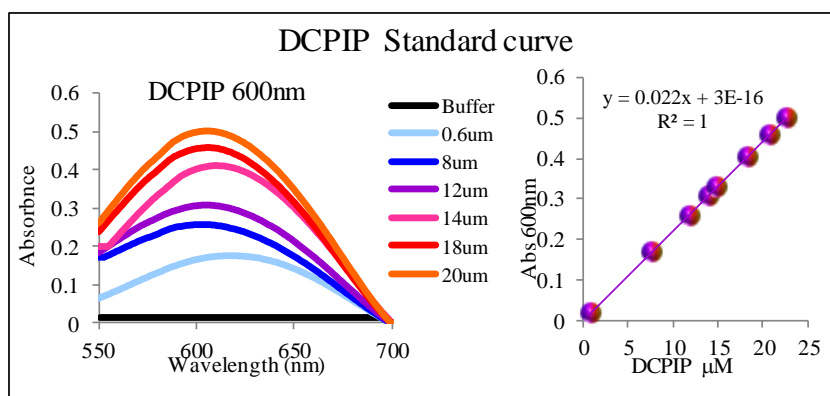


Figure 2.13 DCPIP Standard curve

Absorbance spectrum of 0.6-20µM DCPIP from wavelengths 550-700nm and standard curve from absorbance at 600nm.

Mitochondria were diluted to

1mg/ml and 50µg used for each assay of brain and spinal cord. Retinal mitochondria were used at a concentration of 30µg/ml. Buffer containing 100µM decylubiquinone, 2mM KCN and 16µM DCPIP was followed with the addition of 30µg mitochondria. The rate of reduction of DCPIP was expressed in µmol/mg/ml.

Chapter 2 Methods

2.11.3 UV spectrophotometry for complex IV analysis

Complex IV activity was analysed by measuring the change in absorbance at 550nm of reduced cytochrome c. 2mm cytochrome c was reduced with the addition of 1ml of 100mM ascorbate and was purified by Sephadex G-25 chromatography. In order to determine the concentration of reduced cytochrome c in each preparation, the isosbestic point of equine cytochrome c was determined.

2.11.3.1 Isosbestic point of equine cytochrome c

The isosbestic point of equine cytochrome c was determined using 30 μ M oxidised cytochrome c incubated with 30 μ M ascorbate. The spectrum was read from 500-730nm at 1 minute intervals for 24 minutes. The reduction of 30 μ M cytochrome c in the presence of 30 μ M ascorbate was followed for 24 minutes. The reduction plateaued at 7 minutes without further addition of ascorbate (Figure 2.14).

The wavelength which showed the least difference in absorbance between oxidised and reduced cytochrome c was determined. This was identified at 542nm which agreed with the published isosbestic point at 541.75 nm (Margoliash and Frohwirt 1959).

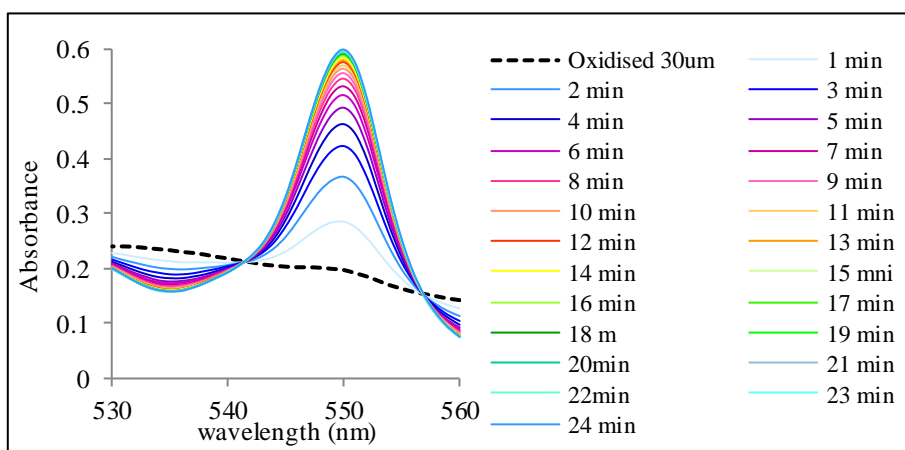


Figure 2.14 Spectra of 30 μ M cytochrome c

during incubation with 30 μ M ascorbate

The absorption coefficient at the wavelength corresponding to the isosbestic point was obtained from three independent preparations of 1.99mM oxidised cytochrome c from which seven concentrations of 100 μ M, 80 μ M, 60 μ M, 40 μ M, 20 μ M, 10 μ M and 5 μ M were prepared. The absorption coefficient at 542nm which corresponded to the isosbestic point ϵ^{iso} was calculated using the formula 1:

Chapter 2 Methods

Formula 1: $\epsilon^{iso} = A_{iso} / cL$

where A^{iso} was the absorbance at the isosbestic point of 542nm, c was the concentration of cytochrome c and L was the optical pathlength of 1cm. The ϵ^{iso} was $9.056 \pm 0.010 \times 10^3 \times M^{-1} \times cm^{-1}$. Figure 2.15 A shows the absorbance of oxidised cytochrome c from 450-700nm and B shows a graph of absorbance at 542nm with corresponding concentrations of cytochrome c

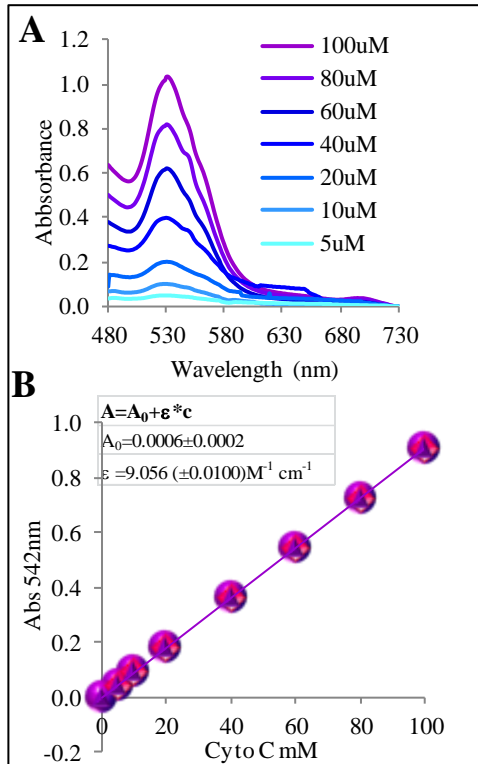


Figure 2.15 Absorbance of cytochrome c as a function of concentration

(A) Representative absorbance spectra of cytochrome c at indicated concentrations (B) Absorbance of cytochrome c at 542nm as a function of concentration. The absorbance was calculated from A_0 of 0.0006 ± 0.0002 and the extinction from $9.030, 9.050$ and $9.053 \times 10^3 M^{-1} cm^{-1}$.

For complex IV assays, the spectrum of reduced cytochrome c was recorded prior to the assay. The

concentration of total cytochrome c was calculated from the absorbance of reduced cytochrome c at 542nm using Formula 1: $\epsilon^{iso} = A^{iso} / cL$

The concentration of reduced cytochrome c was calculated using the following formula 2:

Formula 2: $C_{red} = (A^{550} - \epsilon_{ox}^{550} A^{iso} / \epsilon^{iso}) / ((\epsilon_{red}^{550} - \epsilon_{ox}^{550})L)$

Where A^{550} was the absorbance at 550nm

ϵ_{ox}^{550} was the extinction coefficient of oxidised cytochrome at 550nm which was $8.4 \times 10^3 M^{-1} \times cm^{-1}$ (Van Gelder and Slater 1962).

A^{iso} was the absorbance at isosbestic point of 542nm and

Chapter 2 Methods

ϵ^{iso} was the absorption coefficient at the wavelength corresponding to the isosbestic point at 542nm equal to $9.056 \times 10^3 \times M^{-1} \times cm^{-1}$.

ϵ_{red}^{550} was the absorption coefficient of reduced cytochrome c at 550nm equal to $29.5 \times 10^3 \times M^{-1} \times cm^{-1}$ (Van Gelder and Slater 1962) and L was the optical pathlength of 1cm.

The absorbance corresponding to the lowest concentration of reduced cytochrome c used in the analysis of complex IV was calculated using the formula 3:

$$\text{Formula 3: } A^{550} = (\epsilon_{red}^{550} - \epsilon_{ox}^{550}) C_{red} L + \epsilon_{ox}^{550} A^{iso} / \epsilon^{iso}$$

Where $\epsilon_{red}^{550} - \epsilon_{ox}^{550}$ was the absorption coefficient of reduced cytochrome c at 550nm (equal to $29.5 \times 10^3 \times M^{-1} \times cm^{-1}$) minus the absorption coefficient of oxidised cytochrome at 550nm ($8.4 \times 10^3 M^{-1} \times cm^{-1}$) which was $21.1 \times 10^3 M^{-1} cm^{-1}$.

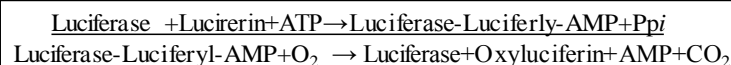
The absorbance calculated using formula 3 was used to determine the absorbance at 550nm which was the start of exponential decay fittings at the same initial concentration of reduced cytochrome c

For the assay of complex 4 activity, reduced cytochrome c was aliquoted under Argon gas and stored at $-80^{\circ}C$. The assay was performed at $30^{\circ}C$ using a water bath to control temperature in 10mM phosphate buffer pH 7.4 a final volume of 600 μ l containing 100 μ M cytochrome c and 0.025% *n*-Dodecyl β -D-maltoside. Mitochondria were added at a tissue specific concentration of 50 μ g/ml for brain, spinal cord and muscle and 30 μ g/ml for retina.

Mitochondria were mixed well with stir sticks (Fisher #NCO116097), before the lid was closed. The reaction was recorded by measuring the absorbance at 550nm as a function of time. The linear slope of the kinetic reaction was obtained.

2.12 ATP determination

Recombinant firefly luciferase and its substrate D-luciferin was used to determine ATP in isolated mitochondria. Luciferase requires ATP to produce light (emission at maximum 560nm at pH 7.8) from the reaction



Chapter 2 Methods

Measurement of the light produced in the reaction was monitored with a BMG Labtech FLUOstar Omega plate reader using a black clear bottomed 96 well microtitre plate (Costar). Background luminescence intensity was accounted for.

Due to the extreme sensitivity of the assay, all exogenous sources of ATP were eliminated by the application of GLP. This included the use of sterile tubes and pipette tips and MilliQ water. For each assay, a standard curve of ATP from 1nM to 1 μ M was prepared. The final volume of standard and mitochondria was no more than 10% of the total assay volume (of 100 μ l). Plate loading was the same as directional analysis of the plate reader to ensure the same luminance development in all wells. Initial analysis using a 5 μ l volume of both standards and mitochondria yielded low luminescence levels. The optimum temperature for analysis was 25°C.

Mitochondria were isolated from fresh tissue. In cryopreserved tissue, ATP production can be enhanced and may reflect an inaccurate base level (Barksdale et al. 2010). Each reaction was performed in triplicate and contained 0.5mM D-luciferin, 1.25 μ g/ml firefly luciferase, 25mM tricine buffer pH 7.8, 5mM MgSO₄, 100 μ M EDTA and 1mM DTT. All products were protected from direct light source. Firefly luciferase was mixed by gently inversion due to the easily denatured structure of the product. The light intensity of the assay and its effective linear range was proportional to the luciferase concentration from 10⁻²⁰ to 10⁻¹³ moles of ATP. Dilution of mitochondria in storage buffers yielded increased background signals. For the purpose of these assays, an aliquot of mitochondria was diluted in isolation buffer which reduced background levels of luminance. Owing to the speed of the reaction, it was necessary to load mitochondria with the plate on the plate carriage to ensure a rapid read.

2.13 Endogenous antioxidant assays

2.13.1 SOD assay

SOD assay was performed using a commercial kit (Sigma SOD Assay Kit (cat# 19160-1KT-F). Bovine superoxide dismutase was obtained from Sigma (cat# S9697). One unit of enzyme activity was defined as the amount required to inhibit the reduction of cytochrome c by 50% in a coupled system with xanthine and xanthine oxidase at pH 7.8 at 25°C. A 96 well plate assay

Chapter 2 Methods

(Fisher-Scientific), was used to measure superoxide dismutase activity by colorimetric assay. Reagents were diluted according to the manufacturer guidelines. The absorbance at 450nm was proportional to the amount of $O_2^{\bullet-}$. Superoxide dismutase (SOD) catalyzes the dismutation of $O_2^{\bullet-}$ into hydrogen peroxide (H_2O_2) and molecular oxygen (O_2). Indirect measurement using Dojindo's water soluble tetrazolium salts was performed. WST-1 produces a water-soluble formazan dye absorbing at 450nm on reduction with $O_2^{\bullet-}$. SOD scavenges the $O_2^{\bullet-}$ and inhibits the formation of formazan. IC_{50} refers to 50% inhibition of the rate of formazan formation. SOD activity as an inhibitor was quantified by measuring the rates of colour development at 450nm. Tissue homogenate was diluted to 1mg/ml in SOD dilution buffer.

The inhibition of formazan formation due to SOD activity (inhibition rate %) was calculated using the following equation: Inhibition $\left(\frac{(S1-S3) - (SS - S2)}{(S1-S3)} \right) \times 100$ where S1 contained enzyme, WST, and no homogenate which acted as an uninhibited formation of formazan in the absence of SOD. S2 contained homogenate, WST dilution buffer and no enzyme which acted as test blank for homogenate without the presence of enzyme and S3 contained WST, dilution buffer no enzyme and no homogenate which was the background absorbance as detected at 450nm. Figure 2.16 shows a summary of the test controls run with each assay.

For MnSOD inhibition in tissue homogenates samples were resuspended in SOD buffer containing 2% SDS. For CuZnSOD inhibition in tissue homogenates, samples were incubated in a final concentration of 5mM of potassium cyanide for 45 minutes at room temperature (Geller and Winge 1983). Results for SOD activity are presented as units of SOD activity per mg tissue in total SOD, CuZnSOD and MnSOD. Statistical analysis was performed using SPSS ANOVA multivariate analysis with significance of <0.05 followed by Post hoc Tukey.

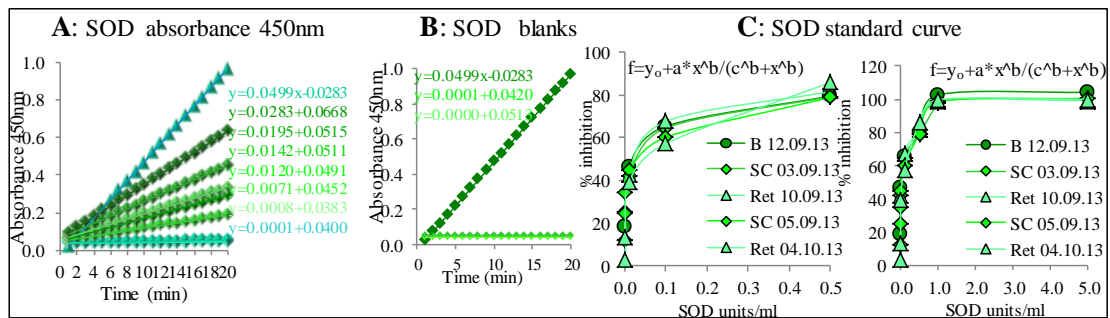


Figure 2.16 SOD assay analysis

(A) SOD inhibition of formazan formation as a function of concentration in units/ml. Formazan produced a yellow colour which absorbed light at 450nm causing an increase in absorbance. Increased SOD units inhibited the formation resulting in reduced absorbance. (B) Blanks included were uninhibited formazan formation in the absence of SOD, homogenate without the presence of enzyme and background absorbance from dilution buffer. (C) Standard curve of SOD units/ml against percentage inhibition of formazan showing the formula used to determine SOD units in tissue homogenate.

2.13.2 Catalase assay

The application of Amplex red for the measurement of catalase activity was considered for this assay however, Amplex red is unstable in the presence of instrumental excitation light and can generate the fluorescent resorufin in the absence of H₂O₂ and HRP. The generation of the superoxide radical and H₂O₂ are artefacts of photooxidation (Zhao et al. 2012), Therefore, the method of Aebi (Aebi 1984), and Beers (Beers and Sizer 1952) was employed to calculate the catalytic activity of tissue homogenates. The method measured the decomposition of a known concentration of H₂O₂ using the change in absorption at 240nm. The assay employed 10.3mM H₂O₂ which was critical because there is direct proportionality between the substrate concentration and the rate of decomposition. A concentration of 10.3mM H₂O₂ also prevents inactivation of catalase and reduces the formation of air bubbles due to the liberation of O₂. H₂O₂ at concentrations in excess of 0.1M results in rapid inactivation of catalase (Aebi).

Age matched WT and Het mice were killed by cervical dislocation according to approved schedule one UK Home Office guidelines (Scientific Procedures Act, 1986). Tissue samples stored at -80°C were defrosted on ice and homogenised in 50mM phosphate buffer pH 7.0 using a hand held homogeniser with Teflon pestle. Tissue homogenates were centrifuged at 600g at

Chapter 2 Methods

4°C for five minutes. This yields a pellet consisting of unbroken tissue, whole cells, cell nuclei, and large debris. The supernatant was used to quantify protein concentration by BCIP. Supernatants were diluted to 1mg/ml and following optimisation, a concentration of 80µg/ml was used to assay the catalytic activity of brain, spinal cord and retina in WT and Opa1^{Q285STOP} mouse tissue. As the optical density of tissue homogenate was expected to be considerably higher than the absorption of hydrogen peroxide, (absorbance values up to 0.727) the UV spectrophotometer was blanked with 50mM phosphate buffer containing tissue homogenate. The assay was followed as a kinetic reaction over 600 seconds. All buffers were treated with Chelex to remove transition metals.

As the assays were performed in a quartz cuvette, this was rinsed twice with MQ water between samples. As the kinetic assay followed H₂O₂ prior to addition of catalase, any alternation in absorption could be detected indicating extraneous catalytic activity. To validate each assay, a positive control was incorporated in each test run. The positive control was 1 unit of bovine catalase (Sigma #C1345) in phosphate buffer pH 7.0. One unit of catalase will decompose 1µMole of H₂O₂/min at pH7.0. The application of a standard curve was not employed as the rate of H₂O₂ decomposition reaction using pure catalase was not comparable to the rates obtained using tissue homogenate. Thus the slope of a standard reaction obtained within 120 seconds of addition to a known concentration of H₂O₂ was not comparable to the same slope generated over a ten minute period using tissue samples.

The catalase assay was performed using UV spectrophotometer measuring the change in absorbance of the substrate H₂O₂ in the presence of catalase. The kinetics of H₂O₂ decomposition was followed for 600 seconds. The reaction is first-order in both enzyme and substrate therefore the amount of peroxide decomposition is directionally proportional to the concentration of catalase. The concentration of H₂O₂ was determined from absorbance at 240nm using a quartz cuvette with the absorption coefficient $\epsilon_{240\text{mM}} = 0.0436\text{mM}^{-1} \times \text{cm}^{-1}$ (Beers and Sizer, 1952). The reaction was performed in 1ml of 50mM phosphate buffer pH 7.0 with 10.3mM H₂O₂ and 80µg tissue homogenate protein. Straight line fitting was applied to kinetic

Chapter 2 Methods

reaction to calculate catalase activity in units/mg tissue homogenate. The difference in extinction $\Delta\epsilon_{240}$ per unit of time is a direct measure of catalase activity.

Statistical analysis was performed using SPSS with multivariate analysis ANOVA. Statistically significant values are given with the F value followed by the p value where $p < 0.05$ was considered significant.

2.14 Antioxidant therapy trial

2.14.1 Introduction

2.14.2 Experimental design of resveratrol study

The resveratrol study was performed as a three armed trial. Each arm consisted of age matched WT and Het mice. Arm one consisted of untreated WT and Het mice. There were a total of 34 untreated WT and 47 untreated Het mice. The resveratrol arm had 26 WT and 27 Het mice. The vehicle arm had 12 WT and 19 Het mice. Table 2.2 summarises these participants. A detailed trial design is shown in Appendix C.

3 Armed trial					
No Treatment		Resveratrol 13.5mg/Kg (219.06 μ M)		Vehicle Ethanol 0.1% (17mM)	
WT	34	WT	26	WT	12
F WT	24	F WT	14	F WT	6
M WT	10	M WT	12	M WT	6
Het	47	Het	33	Het	19
F Het	24	F Het	22	F Het	11
M Het	23	M Het	11	M Het	8

Table 2.2 Resveratrol three armed trial design

The table shows a summary of the design of a 3 armed trial of resveratrol administration to both WT and Het mice over a 15 month period. Arm 1 consisted of no treatment in WT and Het, arm 2 was resveratrol treated and arm 3 was vehicle treated.

In order to increase the number of participating animals, a cohort of 3 month old WT and Het mice were commenced on resveratrol for 1 month. Following intensive health screening, these mice were crossed to produce the first round of off spring for treatment beginning in utero. This cohort consisted of 3 WT and 6 Het for resveratrol therapy and 4 mice for vehicle treatment.

The inclusion criteria for the initial set up was that the females were of breeding age and that they had not been crossed before. The male mice were all housed as solitary animals none of

Chapter 2 Methods

whom had been crossed. The subsequent crosses were performed at six, fourteen and twenty six weeks from starting the trial. The inclusion criteria for these mice were that they were matched WT for Het. There was a concerted effort to sex match the babies so that both male and female WT and Het mice could be studied.

2.15 Statistical analysis

Results are expressed as a mean \pm SD. Statistical analysis was performed with SPSS software (V20). Data was analyzed for distribution using Shapiro-Wilk where all data above 0.05 was considered normally distributed. Parametric t test were performed where Levene's test for equality of variance was observed. Parametric data demonstrating a significant difference was further analyzed using multivariate analysis of variance with post hoc Tukey or Dunnett for unequal sample numbers. Where data was not normally distributed, Mann –Whitney U test or Kruskal –Wallis H test for multiple groups was performed with Bonferroni adjustment. Data where the null hypothesis was rejected are indicated with asterisks where * $p < 0.05$, ** $p < 0.010$ and *** $p < 0.001$. The F value in ANOVA is the between group variability divided by the within group variability.

2.16 Presentation of data

Unless otherwise described, bar graphs show the mean with error bars showing \pm SD. Box plot graphs show all data with the upper and lower boxes representing the first and third quartile. The dividing line between the two boxes is the median. The upper whisker represents the maximum range and the lower whisker represents the minimum range. Graphs of IHC show the mean \pm SEM. Line graphs showing mean \pm SD include the WT value for reference. Kinetic graphs are explained in the text.

Chapter 3 Chapter 3 Neuromuscular & cognitive dysfunction in Opa1^{Q285STOP} mouse

3.1 Introduction

As Opa1 is ubiquitously expressed in all tissues, it was considered that tissues exerting a high demand on available ATP may be influenced by impaired mitochondrial fusion. The skeletal and cardiovascular system of Opa1^{Q285STOP} mouse was analyzed for endurance performance in a selection of tests designed to demonstrate any impairment in gait, balance and coordination. Peripheral neuropathy is associated with impaired oxidative phosphorylation.

3.1.1 Osteoporosis in C57Bl/6 mouse population

Bone density is maintained through the balanced activity of osteoblast and osteoclasts. Osteoblasts synthesize bone and regulate osteoclast number and activity. Osteoclast cells reabsorb bone tissue and are responsible for bone remodelling. In C57Bl/6 mouse, bone density peaks at 4-8 months followed by a gradual decline (Perkins et al. 1994; Cao et al. 2003; Ferguson et al. 2004). The loss of balanced blast clast activity results in expanded bone reabsorbing osteoclasts. Age related osteoporosis can be associated with reduced levels of circulation oestrogen which enhances bone reabsorption (Silberberg and Silberberg 1970; Ambrus et al. 1984). Diet can influence bone mass including proanabolic supplements (Halloran et al. 2010). Vertebrate osteoporosis responds well to moderate physical exercise (Wu et al. 2003; Kesavan and Mohan 2010; Thongchote et al. 2014; Yamada et al. 2014). The provision of a running wheel was designed to alleviate the discomfort and potential effects of reduced bone density in aged inactive mice.

C57Bl/6 mouse is predisposed to develop osteoporosis (Ambrus et al. 1978; Massie et al. 1989; Akhter et al. 1998; Judex et al. 2002). The provision of a running saucer (Small & Furry) was considered appropriate in the alleviation of this age related onset. As Opa1^{Q285STOP} mouse was required to reach the minimum age of 15 months, saucers were provided for at least the last eight months of life. The speed of learning in Het mouse was dependant on whether they shared a mixed genotype cage. In one particular Het cage, the skill was mastered in aged 18 month old

Chapter 3 Neuromuscular and cognitive dysfunction in $Opa1^{Q285STOP}$ mouse

Het males who continued to use their saucer until 28 months of age. Figure 3.1 shows a female mouse at 6 months and at 12 months following use of a running saucer, which demonstrates a reduction in vertebrate scoliosis.

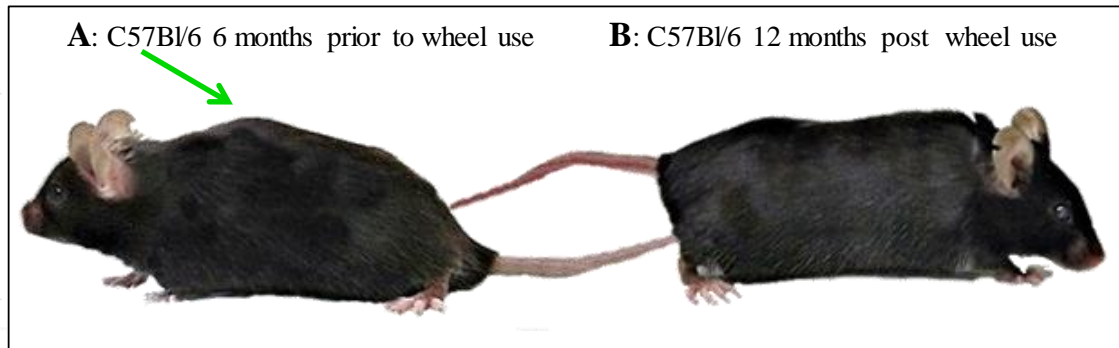


Figure 3.1 C57Bl/6 at 6 months and 15 months following use of running saucer

(A) Male C57Bl/6 mouse at 6 months was living in a shared cage without a running wheel. Mouse spinal vertebrae are pronounced with scoliosis (green arrow). (B) Male 6 months following use of wheel showing less curvature in vertebrate.

Owing to the somewhat sedentary lifestyle of the average laboratory mouse, the presence of osteoporosis can reduce physical performance of exertion based exercises. As the $Opa1$ mice were observed to have a degree of osteoporosis, the provision of running saucers provided them with an adequate means of daily exercise and a means of improving their bone density. By the completion of this thesis, there was a significant improvement in the bone density with a reduced incidence in osteoporosis. As it was considered to be a cage induced lack of exercise, the provision of saucers improved the overall skeletal frame of all mice.

3.2 Neuromuscular impairment in $Opa1^{Q285STOP}$ mouse

3.2.1 Experimental design of SHIRPA analysis

SHIRPA testing was performed as described in Chapter 2 Methods section 2.2.

There were some limitations of the SHIRPA protocol. Mice that were accustomed to handling produced a more accurate representation of the phenotype that was not influenced further by fear or intimidation. Spontaneous activity in mice was preserved due to familiarity with the handler. Many of the observations noted during SHIRPA testing were originally observed during routine testing with rotarod, tight rope and narrow beam testing. Vigilance and an

Chapter 3 Neuromuscular and cognitive dysfunction in $Opal^{Q285STOP}$ mouse

accurate record of all activities in all animals can help to detect the more significantly affected mice in the Het population. Interpretation of SHIRPA results were examined by dividing each behavioral or physical trait into one of five categories: lower motor function, cerebrospinal function, sensory function, neuropsychiatric function and autonomic function. As several of the observations belonged to more than one category, there was more than one test to determine the extent of anomalous behavior. Detailed below are the observations of SHIRPA

The SHIRPA protocol is a three staged measurement of physical and neurological health body condition sensory and motor function. The purpose of SHIRPA is to identify any anomalies in neurological motor sensory and autonomic function.

The primary test incorporates measurements of body and coat condition, gait, posture and motor function. The secondary tests include motor function, spontaneous locomotion and open field observations. The tertiary assessment includes tests of neuropsychiatric and cognitive function, grip strength, trunk curl and limb clasping. Automatic responses including pinna pinch and self righting. Environmental induced variations must be accounted for. Mouse maintenance, noise, housing conditions light intensity and the time of testing (light cycle) can all influence the observed phenotype. The individual observations of SHIRPA are detailed. Before removal from the cage, a healthy mouse should respond to open cage with curiosity. This is normal mouse behaviour. Familiarity with the handler eases this process and reduced stress induced aberrant behaviours.

3.2.2 In viewing jar:

Observations were made over a minimum of five minutes and maximum of 15 minutes. Prolonged testing time can influence the results.

- Body: General physical condition including mouse stance. Use of all four paws flat on the surface is normal mouse stance. Mouse body weight recorded.
- Body position: On transfer to the viewing jar, mouse normally maintains a flat position with all four paws in position for rapid movement. Any prone position where legs are

Chapter 3 Neuromuscular and cognitive dysfunction in $Opal^{Q285STOP}$ mouse

visible is abnormal. Stereotypic behaviours observed include mouse rearing on hind legs with or without repeated vertical leaping or continuous circling (Waltzer).

- Coat: Includes coat colour and condition. The mouse coat should be well groomed. Colour density may depend on the age of the mouse. Regions of discolouration or ‘damp’ looking regions require further examination. Matted fur is unusual in short haired rodents but is indicative of reduced grooming. Coat can appear ‘spiky’ as though standing on end. This is piloerection and indicative of prolonged stress. Regions of alopecia may be indicative of in cage fighting, underlying injury or wound, allergies or excessive grooming. Whiskers should be symmetrical straight and twitching in response to their environment. Mouse with whiskers that have been chewed by another cage mate should be transferred to another cage as barbering including whiskers is an aggressive behaviour. Whiskers are required for texture discrimination balance and orientation.
- Defecation: Mouse response to transfer to the viewing jar should be done in a calm efficient manner. Mice that are used to handling will not exhibit aberrant behaviour associated with fear. The presence of defecation and the amount produced correlates directly to anxiety in mouse (Kalueff and Tuohimaa 2004; Savignac et al. 2011; Muñoz-Castañeda et al. 2014)
- Urination: Mouse urination in a strange environment is normal behaviour. Mouse will intentionally lift the tail and not allow it to become wet. Incontinence is abnormal behaviour suggesting neurological motor or autonomic disturbances.
- Tremor: Any involuntary repetitive cyclical movements of the mouse or mouse parts when at rest or which manifests in response to movement is abnormal. Very fine tremor can be observed in mouse ears. The environmental temperature and mouse room temperatures should not differ more than 2 degrees.
- Palperbral closure: Mouse eyes should be wide open giving a round appearance. The inability to maintain an open eyed position may indicate impaired motor control, neurological disorder, injury, infection. Microphthalmia can be associated with hydrocephalus.

Chapter 3 Neuromuscular and cognitive dysfunction in $Opal^{Q285STOP}$ mouse

- Lacrimation: Mouse eye is large globe structure slightly protruding on side profile. It should appear shiny and moist without discharge or excess tearing. Excessive tearing in mouse eye is abnormal. It may be indicative of excessive tear production or a blockage in the tear duct.

3.2.3 In the arena:

Observations over a period of five minutes not exceeding 15 minutes comprised of body positions, touch escape and startle response.

- Transfer arousal: On transfer to the viewing jar, latency to move is observed. Normal mouse behaviour on transfer to the viewing jar is to remain inactive for several seconds and then move into the central space to begin investigating. Abnormal transfer arousal include inactivity or hyperactivity. Thigmotaxis and digging in response to transfer are considered abnormal behaviours.
- Gait: Mouse normal gait is sleek and smooth with no variation in body height as movement progresses. Mouse uses the front pad of the paw when walking. At least two mouse paws are in contact with the surface at all times. Impaired mobility and abnormal gaits can be indicative of impaired lower motor function, cerebrospinal function sensory dysfunction or autonomic function. Unbalanced gait due to physical injury because of in cage fighting should be investigated. Mouse paw pads should be examined for condition colour and sensitivity (toe pinch). Mouse toes should be bent at a soft angle of 5 degrees. All nails should be visible on examination but not excessively long.
- Tail elevation: Normal mouse tail is straight and held parallel to the ground. An elevated or straub tail is rigid dorsiflexed and is abnormal. Tail dragging is also abnormal and may be indicative of impaired sensory cerebrospinal function.
- Pelvic elevation: Normal pelvic elevation in mouse is approximately 2mm from the floor (dependant on age and sex of mouse). Normal elevation is less than 5mm. Elevation more than 5mm is abnormal and may indicate pain or distress because this position is anatomically difficult to maintain.

Chapter 3 Neuromuscular and cognitive dysfunction in $Opa1^{Q285STOP}$ mouse

- Startle response: The startle response is a stereotyped motor response to sudden intense stimulus. Using a IHR click box held above the arena which elicits the Preyer reflex. The Preyer reflex is the backwards flick of the ears in response to the noise. On repeat testing, the Preyer reflex is absent. This is a normal conditioned response.
- Touch escape: Mouse response to increased stroke pressure is to escape. As well handled mice are responsive to stroking, a gradual increase in the pressure will elicit alarm and they will try to flee. The extent to which mouse attempts to flee is measured as mild struggle to increased pressure (normal), moderate struggle to escape a light stroke and a vigorous struggle to escape the approach of the handler.

3.2.4 Above the arena:

Tests comprised of manual handling, reflexes biting and vocalisation

- Trunk curl: When suspended by the base of the tail a healthy mouse will position the hind legs in a 'V' shape and stretch the front limbs towards the floor. After several seconds, mouse will then attempt to right himself and grip onto the handlers hand. Mice with impaired vestibular function will curl their hind limbs towards their abdomen in a trunk curl.
- Limb grasping: A test of grip strength measures the muscle strength of the forelimbs and coordination of fore and hind limbs. Mouse is suspended above a grid and allowed to grip with the front paws. When they make contact with the grid, the handler attempts to dislodge the grip by pulling back with sustained gently pressure. How easily the mouse lets go of the grip depends on the amount of exertion required to dislodge him.
- Corneal reflex: When the cornea is touched gently with a cotton bud mouse reaction is to blink. This is a normal autonomic response to a foreign object in the cornea. Impaired autonomic function may reduce this blink reflex.
- Pinna reflex: Mouse is gently restrained and the auditory meatus is touched lightly with the tip of a cotton bud minus the cotton. This elicits a rapid ear retraction or head

Chapter 3 Neuromuscular and cognitive dysfunction in $Opal^{Q285STOP}$ mouse

movement. Impaired autonomic function may result in an impaired or absent pinna reflex response.

- **Contact righting:** Mouse is placed in a Perspex tube which is slowly inverted. Intact proprioceptors on the mouse paw with normal vestibular function sense body position and rotate back to their original position. Impaired vestibular apparatus in mouse rely on paw pressure only and remain inverted in the Perspex tube.
- **Evidence of biting:** Provoked biting is a normal response in mouse. A wooden dowel is placed to one side of mouse mouth between the teeth. Mouse response will be to withdraw his head back slightly and grip the dowel between his teeth. This is normal mouse behaviour. Mouse attempting to bite the handler when picked up is a fear response and can be eliminated with regular careful gentle handling.
- **Vocalisation:** Mouse normally vocalises when he is highly anxious or in pain. Vocal mice are usually frightened but with practice will soon adapt to handling especially when there are no procedures carried out. Mouse in pain must be carefully examined for the site of damage. Chronic pain is usually identified in mouse sitting hunched and alone in their shared cage.. Vocalisation in mouse with chronic pain should be dealt with as humanly and quickly as possible.

Table 3.1 summaries the observational data recorded and the number of specific functional observations made pertaining to function.

Table 3.1 SHIRPA observational profiles for specific function

Location	Measure		Function						
Viewing Jar	Body position	A B	lower motor cerebrosplinal						
	Coat	D E	neuropsychiatric autonomic						
	Defecation	B D E	cerebrosplinal neuropsychiatric autonomic						
	Urination	B D E	cerebrosplinal neuropsychiatric autonomic						
	Tremor	AD E	lower motor neuropsychiatric autonomic						
	Palpebral closure	C E	sensory autonomic						
	Lacrimation	C E	sensory autonomic						
In Arena	Transfer Arousal	A B D	lower motor cerebrosplinal neuropsychiatric						
	Gait	A B	lower motor cerebrosplinal						
	Tail elevation	A B E	lower motor cerebrosplinal autonomic						
	Pelvic elevation	A B E	lower motor cerebrosplinal autonomic						
	Startle response	C D E	sensory neuropsychiatric autonomic						
	Touch escape	C D E	sensory neuropsychiatric autonomic	Viewing jar	2	3	2	4	6
	Position	A B E	lower motor cerebrosplinal autonomic	Arena	4	5	2	3	4
Above Arena	Trunk curl	A B E	lower motor cerebrosplinal autonomic	Above Arena	5	5	3	1	7
	Limb grasping	A B E	lower motor cerebrosplinal autonomic		11	13	7	8	17
	Pinna reflex	A B E	lower motor cerebrosplinal autonomic	A	lower motor function				
	Corneal reflex	C E	sensory autonomic	B	cerebrosplinal function				
	Contact righting	A B E	lower motor cerebrosplinal autonomic	C	sensory function				
	Evidence biting	C E	sensory autonomic	D	neuropsychiatric function				
	Vocalisation	C D	sensory neuropsychiatric	E	autonomic function				

Multiple observations of mouse from in the viewing jar to above the arena were used to compile a functional assessment of specific systems with graded data from zero (normal) to 3 (impaired/reduced/abnormal). The number of observations for each function is shown in the insert

3.2.4.1 Results of SHIRPA

	SHIRPA		
F WT	3	M WT	3
F Het	5	M Het	3

Table 3.2 Summary of test numbers for SHIRPA analysis in WT and Het

As previously described, SHIRPA categories of mouse behavior were divided into 5 main functions. Figure 3.2 shows a summary of the values obtained and the statistical difference between both male and female WT and Het.

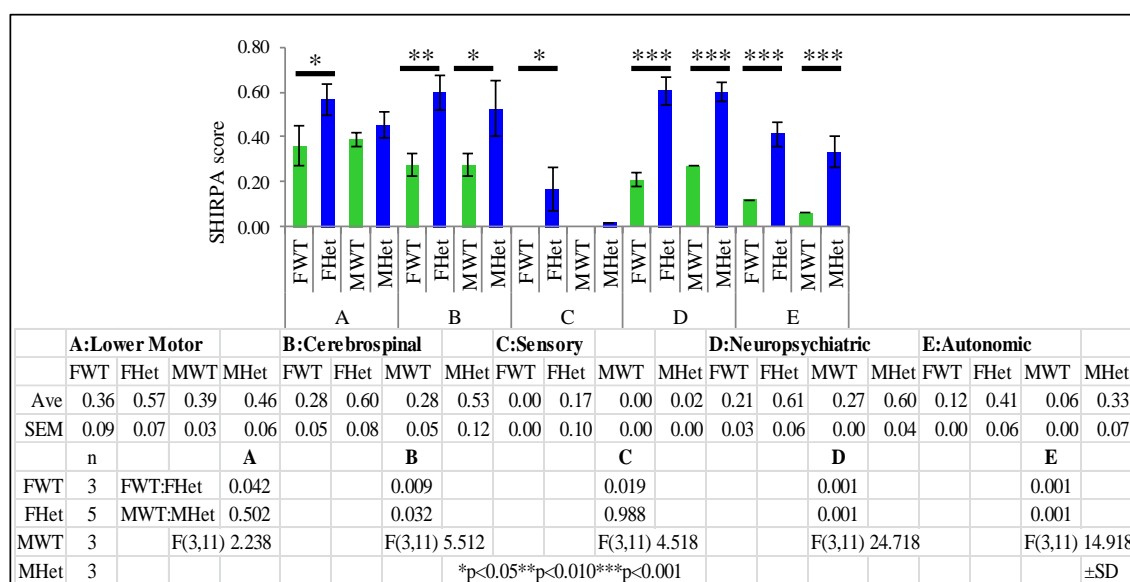


Figure 3.2 SHIRPA analysis in WT & Het

Graph showing the average SHIRPA observational values for all functions in female and male WT (n6) and Het(n8) at 12 months.

3.2.4.2 Discussion of SHIRPA analysis in WT and Het mouse

The phenotype analysis using SHIRPA was designed to test several functions: Muscle and lower motor function, cerebrospinal function, sensory, neuropsychiatric and autonomic function through a combination of test parameters. Body position which was a test of lower motor function cerebrospinal and neuropsychiatric function was present in all Het mice and absent in all but one WT mouse suggested Het mice had some impairment involving all three functions. Tremor was present in eight of nine Het mice tested and absent in all wild type mice. Gait anomalies were identified as ‘other’ on the score sheet and were described as ‘jerky’ or ‘tip-toe’ which suggested lower motor sensory and cerebrospinal function impairment. Figure 3.3 shows typical Het stance where foot placement is asymmetrical.

Autonomic function in tail elevation was observed in all Het mice. Vocalization was another factor present in Het mice that was absent in WT mice. Although sensory function was within normal limits in the Het mice, this demonstrates the application of visual cues to mouse in bright light (47.8 lux compared to an average 10.4 lux in the mouse room). Mice rely primarily on their olfactory senses especially in an unfamiliar territory where all visual cues are unknown.



Figure 3.3 Het mouse phenotype above the arena

Female Het grooming required balancing on two hind paws but the right paw does not make contact with the floor. ($Opa1^{Q285STOP}$ mouse was previously back crossed into CH3 strain and occasional CH3 coat colour occurred.)

3.2.5 Rotarod analysis in $Opa1^{Q285STOP}$ mouse

3.2.5.1 Experimental design of rotarod testing

Mice remained in their original cages and were transferred to the test room for a period of fifteen minutes to acclimatise. Each test required that mouse began with the rod rotating at 8rpm. Once the mice were balanced, the ‘acceleration’ mode was selected. This was 0-40 rpm in 5 minutes. This was achieved by an increase of 0.133 revolutions per second for 300 seconds. Individual floor sections were elevated to initiate the built in timer device which recorded the time in seconds that individual mice remained on the rod. When the mouse fell onto the floor panel, the timing device stopped recording and a record was made of the latency. Mouse was returned to his cage for a 15-minute rest period before repeat testing. Three tests were performed. During this test, no mouse completed a full passive rotation. Any aberrant behaviour was recorded on the test sheet.

Housing conditions were considered where 12 month old mice had been housed for at least nine consecutive months as a group where the minimum number of mice was three or housed as solitary. Some male mice were housed as solitary for breeding purposes or for in cage fighting. No female mice were caged solitary.

Chapter 3 Neuromuscular and cognitive dysfunction in $Opa1^{Q285STOP}$ mouse

In order to optimise rotarod analysis, a test run was performed to give the mice an opportunity to familiarise themselves with the slowly rotating rubber grip rod. This test was carried out on 'run' setting, which maintains the rate and speed of acceleration. Mice demonstrated a preference for an 8rpm speed. Mice were retained in a holding cage between tests so that they were prepared for the next stage of testing. Mouse weight can have a limiting effect on their ability to perform this procedure. Male WT mice who weighed in excess of 34g appeared to have more difficulty with synchronised hind limb movement compared to their lighter cage mates

3.2.5.2 Results of rotarod testing

Rotarod Analysis			
F WT	11	M WT	8
F Het	13	M Het	15
sMWT	4	gMWT	5
sMHet	5	gMHet	10
s:solitary g:group			

Table 3.3 Summary of test numbers for rotarod analysis in WT and Het

's' denotes solitary housed and 'g' denotes group housed as explained in the text

Female WT had a latency of 114±4 seconds. Female Het latency was 82±4 seconds /sec which was significantly reduced compared to female WT (F (3,42) 3.897 p=0.004).

Male WT latency was 70±5 seconds. Male Het latency was 71±5 seconds which was not significantly different compared to male WT (p=0.744). Figure 3.4 A shows this data.

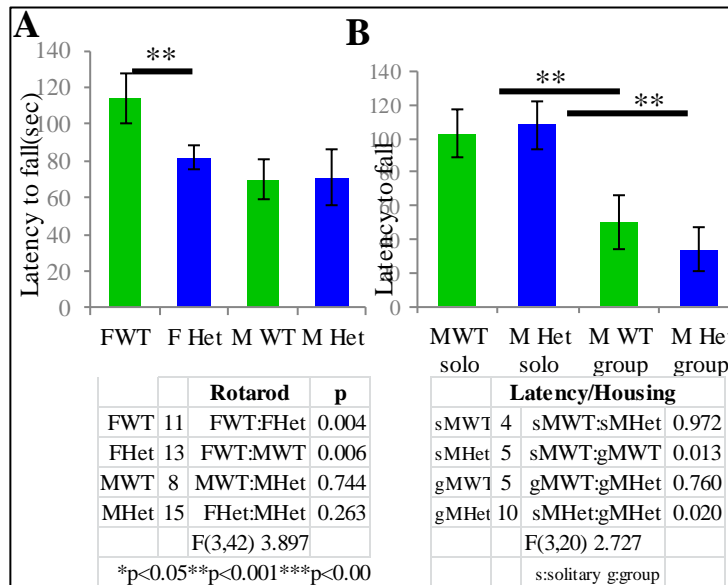
As one of the conditions that differed between male and female mice was housing, latency in solitary and paired male mice was examined. Housing conditions can influence rotarod performance (Abramov et al. 2008). As there were no solitary housed females, the analysis was performed in male mice only.

Solitary housed male mice had significantly increased latencies compared to group housed males regardless of phenotype. Solitary male WT had a latency of 103±6 seconds. Group housed male WT latency was 50±5 seconds which was significantly reduced compared to solitary housed WT males (F(3,20) 2.727 p=0.013).

Chapter 3 Neuromuscular and cognitive dysfunction in *Opal*^{Q285STOP} mouse

Solitary Het male latency was 108±3 seconds and group housed latency was 34±7 seconds which was also significantly reduced compared to solitary housed Het males (F(3,20) 2.727 p=0.020). Solitary housed male WT and Het mouse latencies were not significantly different (p=0.934). Group housed male WT and Het latencies were not significantly different (p=0.898).

Figure 3.4 B shows a graph of these findings.



The possible effects of weight were considered. As 34g was the maximum weight at which no difficulties in synchronising hind leg movement was observed, this was selected as the value at which to examine latencies. No female WT or Het mice weighed in excess of 34g. Two male Het mice weighed in excess of 34g and so were excluded from the analysis. Male WT weight versus latencies was examined. Male WT weighing less than 34g had a latency of 76±5/sec and male WT who weighed more than 34g had a latency of 61±6/sec which was not significantly different to male WT who weighed less than 34g (p=0.076).

3.2.5.3 Discussion of rotarod test in WT and Het mouse

Female WT mice had significantly increased latency to fall compared to female Het mice (p=0.001). This represented a 28% reduction in latency in the female Het mice. In the male population, the Het mice had a 2% increase in latency compared to WT males. On further investigation, it was considered that many of the Het males were housed in solitary conditions for breeding purposes. WT males were usually housed in groups. Further rotarod analysis

Chapter 3 Neuromuscular and cognitive dysfunction in $Opal^{Q285STOP}$ mouse

revealed the statistical difference seen in rotarod performance which directly correlated to housing conditions. The solitary housed WT males had a significant 107% increase in latency compared to group housed male WT ($F(7,205) 21.433 p=0.001$). Solitary housed Het males had a 221% increase in latency compared to group housed male Het ($p=0.001$). Latency to fall in solitary housed male WT and male Het was not significantly different ($p=0.134$). Latency to fall in group housed WT and Het was not significantly different ($p=0.480$).

WT male group housed latency was 52% less than solitary housed WT. In the Het population, the group housed latency was 69% less than solitary housed male Het. As there were no solitary housed female mice and it was considered more stressful to separate a group of cohabitating mice the investigations on housing completed here.

3.2.6 Tightrope testing in $Opal^{Q285STOP}$ mouse

3.2.6.1 Experimental design of tight rope testing

The object of the tight rope test was to observe symmetrical coordination and balance. There were some limitations to the tightrope test. Individual testing on the tight rope test required mice to be observed carefully for signs of exhaustion. Any mouse seen to be distressed at any time during the test was carefully given a platform by way of an open palm on which to drop. Mice frequently wire hang from their cage roofs and were familiar with this method of collection. Analysis of the tightrope test included latency to fall from the rope with a maximum time of 60 second duration.

3.2.6.2 Results of tight rope testing

Rope/Beam			
WT	10	Het	15
F WT	5	M WT	5
F Het	7	M Het	8

Table 3.4 Summary of test numbers for rope and beam analysis in WT and Het

The total distance travelled down the rope was the first parameter analysed. The total distance travelled was calculated from the maximum time (1 minute) that mouse was suspended from the rope in either direction. Female WT mice travelled 7.4 ± 1.7 cm. Female Het travelled 4.7 ± 1.2 cm

Chapter 3 Neuromuscular and cognitive dysfunction in $Opa1^{Q285STOP}$ mouse

which was not significantly different compared to female WT ($p=0.082$). Male WT travelled $9.9\text{cm}\pm 0.4$ and Het males 3.6 ± 0.6 which was significantly reduced compared to male WT ($F(3,21) 1.498 p=0.026$). These results are shown in Figure 3.5A.

3.2.6.3 Discussion of tight rope testing in WT and Het mouse

Other observations included in this test were the ability to obtain and maintain an upright position on the rope. As this was dependent on weight, female Het mice performed well, however as this was also considered an extremely stressful test, it was decided not to pursue it. As the lifestyle of the Het mouse does not involve any gross exertion, it was considered that their cardiac function may not have coped well with the challenge (Chen et al. 2012). Instead, a less physical test was employed using the narrow beam.

3.2.7 Narrow beam testing in $Opa1^{Q285STOP}$ mouse

3.2.7.1 Experimental design of narrow beam testing

The narrow beam test was a measure of mouse balance, gait and spatial awareness while walking a wooden beam towards a platform.

The limits of the narrow beam experiment were that visually impaired mice may not see the platform or realize its intention. It was anticipated that mice would require the platform at least once during the trial and avail of it again as the beam narrows. Mice whose gait was not synchronized were encouraged to continue uphill by tilting the beam at a 150 angle against gravity. Measurements analyzed were the time to initiate movement along the beam and distance travelled along the beam measured in cm.

3.2.7.2 Results of narrow beam testing

The time to initiate movement along the beam was analyzed. In female WT the time to initiate movement along the beam was 2.0 ± 0.5 seconds. In the female Het mice, this was 45 ± 8 seconds which was significantly increased compared to female WT ($F(3,21) 5.725 p=0.003$). In the male WT initiation was 7.4 ± 2 seconds. In the Het males, initiation was 39.2 ± 8.0 seconds which was significantly increased compared to male WT ($p=0.007$). The second parameter measured was the distance travelled down the beam. It was observed that once Het mouse moved, he ran the

Chapter 3 Neuromuscular and cognitive dysfunction in *Opa1^{Q285STOP}* mouse

length of the beam to return to his home cage. WT mice travelled an average distance of 42 ± 20 cm. However, wild type mice stopped on route to investigate the beam and their surroundings, including walking back the way they had travelled. As a result the distance travelled by both genotypes was not comparable. While the Het mice were clearly looking for an escape from the beam, the WT were busy investigating the experimental design. Figure 3.5 B shows a summary of these findings.

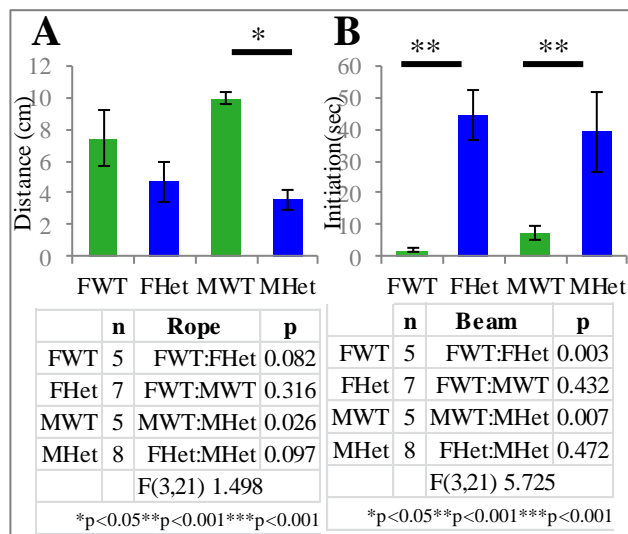


Figure 3.5 Tight rope and narrow beam testing in WT and Het mouse

Graph showing means \pm SD (A) Tightrope distance travelled in cm in WT and Het and (B) Narrow beam initiation time in seconds in WT and Het

3.2.7.3 Discussion of narrow beam testing in WT and Het mouse

The narrow beam test was used to identify imbalance and uncoordinated behavior in mice who manage to perform the rotarod test successfully. The sensitivity of the rotarod can be reduced through training and practice. The aim of the narrow beam was to give mouse a novel environment without any immediate threat, and a means of escaping. Time to initiate travel down the beam showed a significant difference between WT and Het mice with Het mice taking an average 550% more time to initiate travel.

Female Het mice showed a 42 fold increase in time to initiate compared to female WT. Male Het showed a 32 fold increase compared to male WT.

In the WT population, female mice were 265% quicker to initiate travel and travelled 21% further compared to male WT. This may indicate that the female WT were more anxious to return to their home cage. Male WT explored their surroundings.

Chapter 3 Neuromuscular and cognitive dysfunction in $Opa1^{Q285STOP}$ mouse

In the Het population, females were 13% slower to initiate travel and travelled 16% less compared to male Het.

The innate curiosity of healthy mice may have led to some curious data but for the observations of what constitutes normal behavior in mouse behavior. The extended freeze seen in the Het mouse was also observed on placement into the arena during SHIRPA analysis resulted in increased initiation times which were not present in WT mice thus significant observations seen. The ability to complete the task in WT males resulted in a reduced distance in the WT population. Again, some individual mice performed the task with the skill and dexterity of practiced animals while others seemed disorientated and hesitant once the travel was initiated. Figure 3.6 shows an image of female WT and Het on completion of the narrow beam test. Female WT appears bright eyed and curious. The Het mouse is demonstrating poor spatial awareness (right rear toes are overhanging the beam). Unlike female WT, the Het fur is spiky and appears to be standing on end. She appears nervous and not paying attention to her surroundings. On returning to their home cage these physical appearances were less obvious.



Figure 3.6 Cage mates—and $Opa1^{Q285STOP}$ and C57Bl/6 WT at 12 months

$Opa1^{Q285STOP}$ mouse sitting beside WT on the narrow beam awaiting return to home cage. Note Het rear right paw overhanging the beam. Lack of eye contact and slightly ruffed fur (piloerection) indicative of distress.

3.2.8 Mouse learning in training trials

3.2.8.1 Introduction

Rotarod was a learning trial where the mean latency from three individual tests were compared over three consecutive days. The final score on day three represented the maximum trained latency a mouse can achieve and was expected to show some level of improvement from day 1.

3.2.8.2 Results of mouse learning

Table 3.5 shows a summary of learning scores from three consecutive days testing in female and male WT and Het. There was no statistical difference in learning between solitary and group housed male WT (p=0.099). Solitary housed male Het learning was significantly different compared to group housed Het males (p=0.036). Figure 3.7 shows line graphs of learning in WT and Het

Table 3.5 Mouse learning in training trials

Table shows (A) the mean score from learned training trial from three consecutive days with the statistical difference between groups. (B) Housing associated learning in solitary and group housed male WT and Het.

A	D1	D2	D2-D1	D3	D3-D2	D3-D1	B	D1	D2	D2-D1	D3	D3-D2	D3-D1
FWT	1.72	1.70	-0.02	2.28	0.58	0.56	sMWT	1.42	1.80	0.38	1.99	0.18	0.56
SEM	0.13	0.12		0.10			SEM	0.04	0.13		0.06		
FHet	1.01	1.16	0.16	1.34	0.18	0.34	sMHet	1.53	1.82	0.29	1.54	-0.28	0.01
SEM	0.17	0.29		0.02			SEM	0.16	0.21		0.19		
FWT:FHet			F(3,41)	4.725	0.088		sMWT:sMHet			F(3,20)	4.747	0.151	
MWT	1.30	1.31	0.01	1.52	0.21	0.22	gMWT	0.75	0.77	0.02	0.95	0.18	0.20
SEM	0.09	0.09		0.01			SEM	0.21	0.35		0.33		
MHet	1.35	1.22	-0.13	1.15	-0.07	-0.20	gMHet	1.26	0.92	-0.34	0.96	0.04	-0.30
SEM	0.20	0.16		0.01			SEM	0.28	0.14		0.14		
MWT:MHet			F(3,41)	4.725	0.018		gMWT:gMHet			F(3,20)	4.747	0.071	

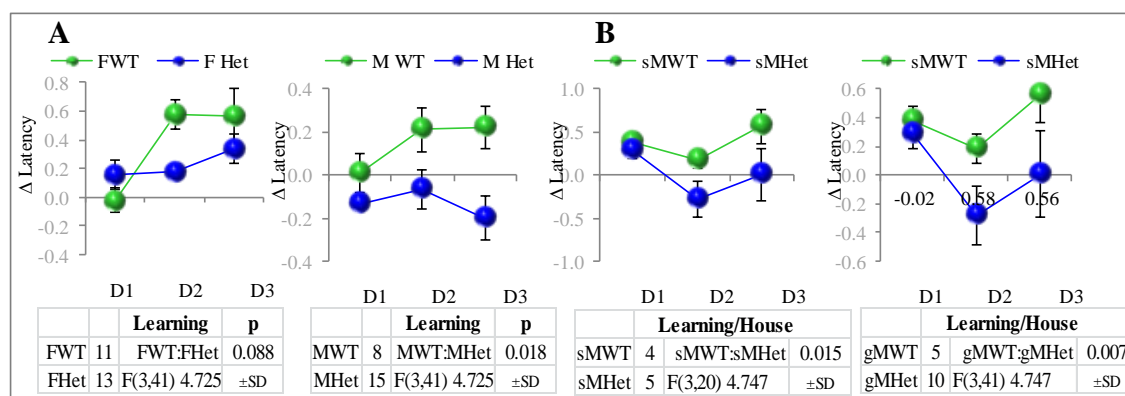


Figure 3.7 Learning in training trials

Line graphs showing mean learning trends over three sequential days in (A) female and male WT and Het. (B) Male solitary housed and group housed learning.

3.2.8.3 Discussion of mouse learning in training trials

There was no significant difference in female Het learning compared to female WT ($p=0.088$). Male Het learning was significantly reduced compared to male WT ($F(9,70) 2.554 p=0.018$). This was examined with respect to housing conditions Solitary housed male Het learning was not significantly different to solitary housed male WT ($p=0.151$). Group housed male Het learning was significantly reduced compared to group housed male WT ($F(3,17) 4.747 p=0.007$) showing a 2.5 fold reduction.

3.3 Thermal imaging of *Opa1^{Q285STOP}* mouse

3.3.1 Introduction

A thermal imaging camera was used to determine whether there was any difference in the core heat production in *Opa1^{Q285STOP}* mouse compared to his wild type littermates. The metabolic rate is influenced by core body temperature. Oxidative stress can be influenced by temperature, and cooling of core temperature can reduce the accumulation of reactive species through the reduction of energy expenditure (Lane et al. 1996). Caloric restriction which has been established as a means of reducing oxidative stress (Alemany 2012; Jang et al. 2012; Lee and Wei 2012) has the secondary effect of reducing the body core temperature (Weindruch et al. 1988). This reduction in core temperature can have beneficial effects in controlling the effects

Chapter 3 Neuromuscular and cognitive dysfunction in $Opal^{Q285STOP}$ mouse

of oxidative stress and increased oxygen demand. By reducing the tissue oxygen requirements, fusion deficient mouse may be demonstrating an adaptive mechanism through reduced thermal conductance.

3.3.1.1 Experimental design of thermal imaging

Thermal imaging data was designed to be a provisional experiment to support the hire of a thermal camera. As this did not come to fruition, it was decided to present this provisional data as it shows a significant finding in younger Het mice which does not extend into aged Het when compared to WT. Mice were divided according to age into two groups. Young mice were between 2-6 months of age. Old mice were between 12-15 months of age. All wild type and Het mice were analysed within 1 hour of the start of a dark phase of the 12 hour light-dark cycle.

A limiting factor of thermal imaging experiment was the spatial resolution of the camera which was 1.36mrad with an image frequency of 60Hz and a minimum focussing distance of 0.4 meters. As a result, the time delay from shutter activation and image acquisition was increased. This resulted in several ‘missed’ shots as mice were not manually restrained at any point. Although the camera was sensitive, it was unable to detect the heat transferred from mouse paw to the floor of the arena, and thermal imaging of potential gait anomalies were not realised.

3.3.1.2 Data analysis of thermal imaging in WT and Het mouse

Thermal			
yWT	9	yHet	4
oWT	8	oHet	9

Table 3.6 Summary of test numbers for thermal imaging analysis in WT and Het

‘y’ denotes young and ‘o’ denotes old

Following image acquisition, three regions of the mouse were used for interpretation of data. Mouse head was targeted between the frontal and occipital region. This represented mouse central temperature. As this region is located directly between the cooling influence of the ears, it was considered an appropriate location in which to analyse core brain temperature measurement. For the sake of clarity, this reading was called the head temperature. Tail base readings were taken from the base of the tail where residual heat was visible in the first third. This represented peripheral temperature. Flank readings were taken from both left and right side

where possible. This represented a mean central temperature readings in the mouse. Figure 3.8 shows representative images taken with the thermal camera and Figure 3.9 shows graphs of head, flank and tail reading in young and older WT and Het mice.

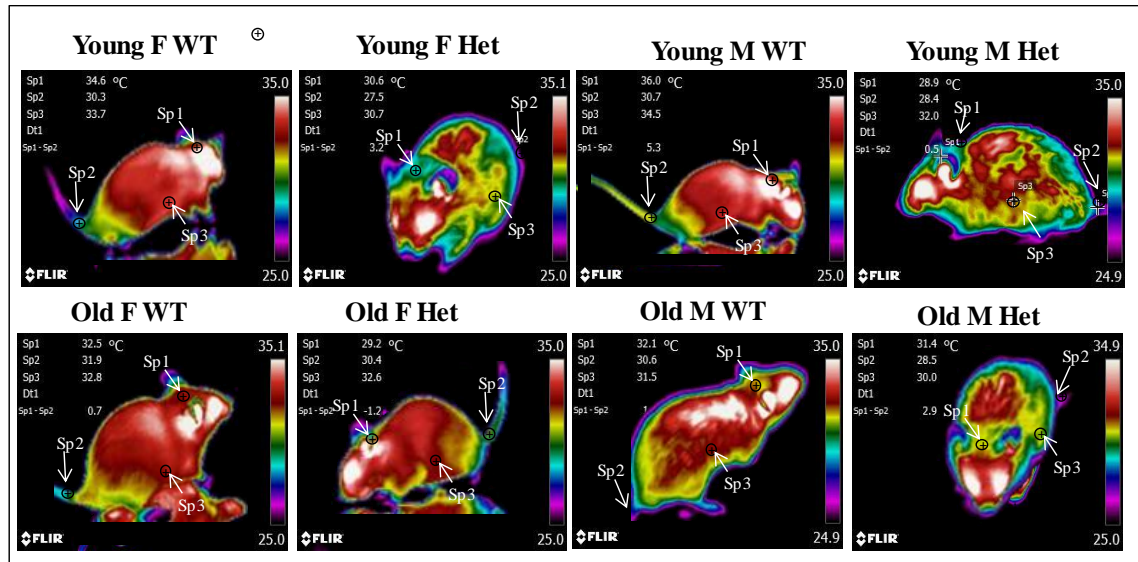


Figure 3.8 Thermal imaging in young & old WT & Het

Thermal images of young (2-6 months) and older (12-15 month) WT and Het mice in the arena. The thermal camera was set to detect temperatures within the range of 25°C-35°C. No manual handling or restriction of mouse movement was done. In each image, the ‘Sp’ denotes spot metering where temperature measurement was analysed. SP1 Head, SP 2 tail end, SP3 flank

3.3.1.3 Results of thermal imaging in WT and Het

The results were analysed as groups of ‘young’ (2-6 months), ‘old’ (12-15 months) head, flank and tail. Table 3.7 shows a summary of these data.

Table 3.7 Summary of thermal results WT and Het

Table shows the mean \pm SEM of thermal readings taken from head, tail and flank regions of young and old WT and Het. The statistical difference between groups is shown.

Young						Old					
n	Age(m)	Head	Tail	Flank		n	Age(m)	Head	Tail	Flank	
yWT	8	4	32.8	29.4	33	oWT	8	12	32.2	27.7	32.5
SEM		2	0.9	1.6	1.1	SEM		2	1.4	1.4	1
yHet	4	4	30	26.9	31.4	oHet	9	12	30.2	28.3	31.9
SEM		2	1.2	0.8	0.4	SEM		1	1.6	2.4	11.4
yWT:yHet			0.001	0.024	0.006	oWT:oHet			0.004	0.287	0.130
F		F(3,26)	38.542			F		F(3,26)	2.077		

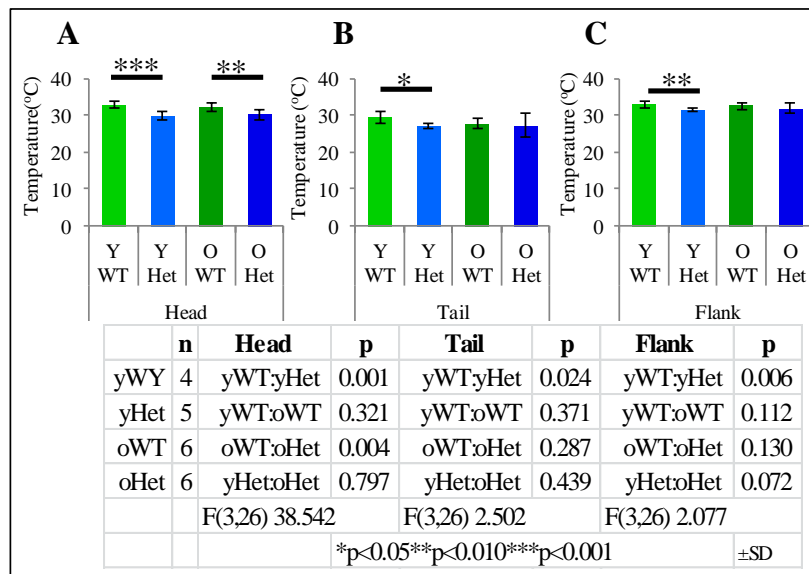


Figure 3.9 Thermal analysis in WT and Het mouse

Graphs showing the mean \pm SD temperature in degrees Celsius in (A) Head, (B) Tail and (C) flank in young and old WT and Het. 'y' denotes young and 'o' denotes old.

3.3.1.4 Discussion of thermal imaging in WT and Het mouse

Heat preservation in the mouse presents a challenge because of the high surface to volume ratio. The large surface area presents a source of heat loss and requires an increased metabolic rate to maintain core body temperatures. In *Opal^{Q285STOP}* mouse, the average body temperature was reduced in both young and older aged mice.

3.3.1.4.1 Young WT and Het mice thermal analysis

In the young Het mice, there was a significant reduction in body temperatures compared to young WT. The head reading was a significant 9% less than WT (F(3,26) 38.542 p=0.001). Tail temperature was also reduced by 9% which was significantly different to WT (F(3,26) 2.502 p=0.024). Flank temperature in Het mouse was 5% less than WT which was also statistically different to WT (F(3,26) 2.077 p=0.006).

Chapter 3 Neuromuscular and cognitive dysfunction in $Opa1^{Q285STOP}$ mouse

3.3.1.4.2 Older WT and Het thermal analysis

In the older aged mice, the Het head temperature was reduced by a mean 2%. This temperature reduction was significantly different in Het head recording which had a 6% reduction compared to WT ($F(3,26) 2.077 p=0.004$). Tail and flank temperatures in older Het were not significantly different to older WT.

As mice aged, the differences between WT and Het mice with respect thermal readings was less pronounced possibly due to age related decline in core temperatures.

The reduction in temperature with age observed in the WT population demonstrated a reduction of 3% compared to young WT. There was a 2% reduction in head temperature with a 6% reduction in tail and 2% reduction in flank region. In the Het population, the age related reduction in temperature was not observed. The head temperature showed an increase of 0.6%, the tail temperature showed a 5% increase and the flank region showed a 2% increase compared to young Het temperatures. This represented a mean 2.4% increase in temperature in old Het mouse compared to young Het mouse. In summary, young Het mice had a 7% reduction in thermal readings compared to young WT. In older mice, the percentage difference in Het was a 2% reduction compared to older WT mice.

A variety of causal factors may result in a reduced surface body temperature including social housing and dietary input. Calorific restriction reducing oxidative damage also reduces body core temperatures (Merry 2004). The reduction in core temperature associated with uncoupling protein 2 results in an elevated hypothalamic temperature causing a reset of the internal thermostat (Conti et al. 2006). The heat generation observed in older Het may a by-product of inefficient mitochondrial ATP production. Might the reduced temperatures seen in the young Het mice be a compensatory mechanism for reduced OXPHOS function?

Findings of thermal imaging and the role of *Opa1* as a fusion protein in mitochondrial dynamics may be interpreted as a functional maintenance role in mitochondrial activity. The generation of heat in WT mice was considered a response to the environmental temperature of the procedure room (23°C) compared to the mouse stock room (20°C). WT mice demonstrated a healthy

Chapter 3 Neuromuscular and cognitive dysfunction in Opa1^{Q285STOP} mouse

response to a transient increase in environmental temperature. In the Het population, the increase in ambient temperature was not sufficient to alter the body surface temperature seen in these mice. A recent paper discussing the obliteration of a mitochondrial protease OMA results in a reduction of short isoform Opa1. These mice demonstrated increased body weight and defective thermogenesis due to defective brown adipose fat (BAT) oxidation (Quirós et al. 2012). In Opa1^{Q285STOP} mouse, it was not the reduction of short isoform but the reduction of Opa1 that may result in reduced BAT oxidation. An age related reduction in thermoregulation may also signify the replacement of BAT for adipose fat (Sellayah and Sikder 2014). At 15 months of age, the core temperature of mice can be reduced regardless of pathology (Gonzales and Rikke 2010) .

Both WT and Het mice were caged in groups of 4 where they had free access to the same diet (Teklad Global 14% protein maintenance diet). Mouse thermo neutral zone is between 26°C and 34°C. Studies in C57BL/6 mice demonstrate a preference for warmer ambient temperatures (Gaskill et al. 2012) in order to maintain optimum health. Mice whose mitochondria are compromised have even greater need for basic provision of heat. If these provisions are not met, might this inadvertently prolong the mitochondrial life span of these mice?

Temperature homeostasis is regulated by neurones of the preoptic area (POA) of the anterior hypothalamus. The core body temperature is set within narrow range and is dependent on feedback from both the local and peripheral temperatures. The presence of mitochondrial uncoupling protein 2 (UCP-2) expression in the preoptic area (Horvath et al. 1999) can alter the core thermostat. UCP-2 is an inner mitochondrial membrane protein that uncouples oxidative phosphorylation from respiration by leaking hydrogen ions from the intermembrane space to the matrix, thereby dissipating the proton gradient energy in the form of heat. This will produce an increase in the local preoptic area temperature and result in a thermostat reset of the core temperature. Reduced mitochondrial fusion in the POA could initiate UCP-2 resulting in reduced core temperatures observed in Opa1^{Q285STOP} mouse.

Chapter 3 Neuromuscular and cognitive dysfunction in Opa1^{Q285STOP} mouse

Temperature governs the metabolic rate. A cold defence reaction will result in increased metabolic rate to generate heat in place of ATP or a cold induced reduction of metabolism (induced hypothermia). The reduction in core temperature confers protection by reducing the requirements for ATP while maintaining the membrane potential in high energy demand tissues (Zeevalk and Nicklas 1996). The loss of electrons and concomitant ROS production depend maintenance of the inner membrane potential.

Adaptive thermogenesis has been identified in *C. elegans* (Zhao and Wang 2012) where the hypothermic induced longevity conferred increased lifespan while reducing resistance to oxidative stress. This suggests that ROS play a positive role in survival.

3.4 Cognitive impairment in Opa1^{Q285STOP} mouse

3.4.1 Introduction

The ability to investigate cognitive function in mammals employs the use of particular tests designed to highlight specific retentive functions of the hypothalamus. A test of spontaneous alternation employs the T maze. Habituation of exploration can be induced by exposure to spatial location. The use of a T maze can demonstrate spontaneous alternation. Normal rodent behaviour suggests the animal will select the previously unvisited arm of the maze. This reflects an intact short term memory. The selection choice (novel/ unexplored) is called spontaneous alternation.

The basis of the novel object recognition test was described by Ennaceur (Ennaceur et al. 1997) where they showed that in a familiar environment, rodents show an affinity towards new or novel objects. It assumes the rodent has a retention capacity for the familiar object. In the original experiments, rats were the subject animal. The method has been modified for mouse with variations on the procedure and the parameters analysed including repeat testing within a 24 hour period (Ferguson et al. 2004; Arqué et al. 2008). Studies in sleep deprivation in mice (Palchykova et al. 2006) and the effects of housing can alter the outcome of the performance (Võikar et al. 2005) A recent study on the effects of reactive oxygen species (ROS), in the

Chapter 3 Neuromuscular and cognitive dysfunction in $Opa1^{Q285STOP}$ mouse

brains of aged mice determined the impaired novel object recognition seen in some aged mice was due to NOX induced synaptic ROS (Ali et al. 2011).

3.4.2 T Maze analysis in WT and Het mouse

3.4.2.1 Experimental design of T maze testing

Rewards in the form of food treats were not included in this trial. Mice showed spontaneous alternation pattern as an intrinsic behaviour and not as a food motivated response. Treat and reward trials can produce reverse results if the anticipated reward was less than expected. This can result in contrast reward where the mouse loses motivation to continue the test (Youn et al. 2012).

Habituated mice who performed the test under stress less conditions learned the routine quickly. Their ability to recall events from one minute previous can be adversely affected if the animal is removed from the maze in a hurried fashion. Allowing the mouse to climb onto the testers hand will ensure a rapid turn round of repeat tests. Therefore, the only limit to the experiment was the time taken to acclimatise (10 minutes in the home cage), train (5 minutes), and test (20 minutes with a 0.5 minute interval between tests).

3.4.2.2 Results of T maze testing in WT and Het mouse

T Maze			
WT	13	Het	16
F WT	6	F Het	7
M WT	7	M Het	9

Table 3.8 Summary of test numbers for T maze testing in WT and Het

Mice were analysed according to shared cages. Alternate female/male grouped cages were tested to eliminate any confounder effect initiated by the stress of new location. Mice were analysed alternately WT and Het. The T maze was cleaned with 70% ethanol followed by warm water between each mouse regardless of their phenotype. The data collected from the time in seconds before the novel arm was located, the time in seconds spent in the novel arm and the time in seconds spent in the original familiar arm was used to generate the investigation ratio and discrimination ratio for the test. The mean time to novel arm was in female WT was 10.2 ± 2.4 seconds. Female Het time to novel was 31 ± 3.9 seconds which was significantly increased

Chapter 3 Neuromuscular and cognitive dysfunction in *Opal*^{Q285STOP} mouse

compared to WT (F(3,25)6.675 p=0.001). Time to novel in male WT was 11.9±2.6 seconds and 33.1±3.2 seconds in male Het which was significantly increased compared to male WT(p=0.005). Time in novel arm in female WT was 33.1±3.2 seconds and in female Het 16±2.8 seconds which was significant reduced compared to WT (F(3,25) 4.455 p=0.001). Time in novel arm in male WT was 23.8±2.2 seconds and 21.4±1 seconds in male Het which was not significantly different to WT (p=0.530). Time in the original arm in female WT was 11.5±2.6 seconds and 11.5±2.6 seconds in female Het which was not significantly different to WT (p=0.741). Time in original arm in male WT was 11±1.5 seconds and 15.1±1.4 seconds in male Het which was significantly increased compared to WT (F(3,25) 6.675 p=0.021). Figure 3.10 shows a summary of these data.

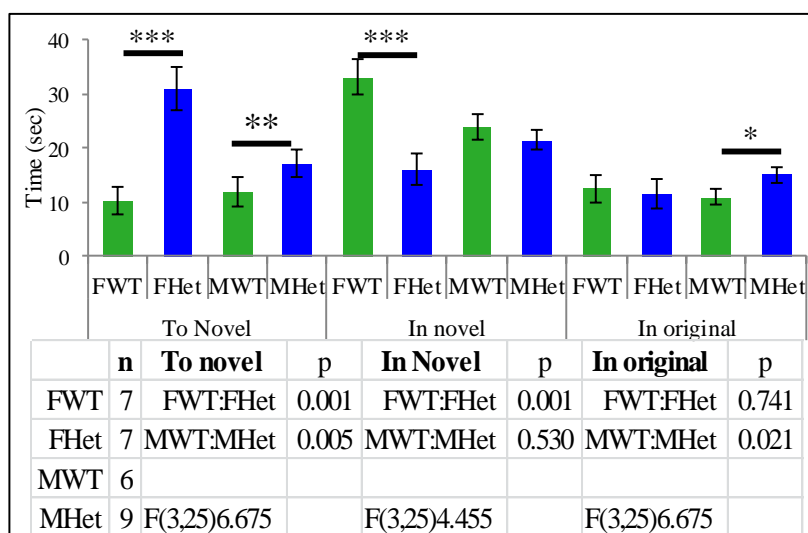


Figure 3.10 T maze testing parameters in WT and Het

Graph showing mean ±SD of T maze spontaneous alternation testing parameters in female and male WT and Het.

The investigation ratio (IR) female WT was 0.66 ±0.06 and in female Het was 0.41±0.07 which was significantly reduced compared to WT (F(3,25)10.619 p=0.006). The IR in male WT was 0.68±0.04 and in male Het was 0.56±0.04 which was not significantly different compared to male WT (p=0.144). The discrimination ratio (DR) in female WT was 0.40±0.10 and in female Het was 0.12±0.01 which was significantly reduced compared to WT (F(3,25) 11.741 p=0.002). The DR in male WT was 0.66±0.08 and in male Het was 0.51±0.05 which was not significantly different compared to male WT (p=0.096). Figure 3.11 shows a summary of these ratios.

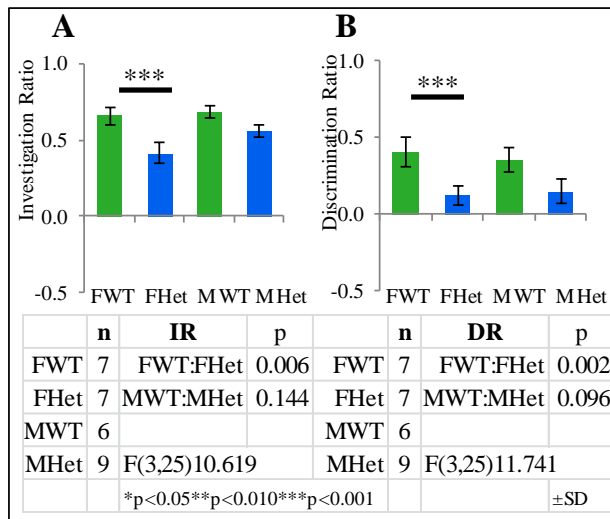


Figure 3.11 T Maze IR and DR in WT and Het

Graph of mean \pm SD of the investigation ratio and discrimination ratio for T maze spontaneous alternation in WT and Het at 15 months

The selection of the correct novel arm in repeat tests reflects a degree of recall and learning. The average correct selection of the novel arm provides an indication of participation in the population (Whishaw and Tomie 1996; Wolfer et al. 1998). For example, selection in test number 10 often resulted in mouse remaining between both arms and selecting neither. This was interpreted as inertia due to lack of motivation. The novel arm was exactly the same as the original arm except that it was on the opposite side. As far as structure and lighting levels were concerned there was very little novelty. Spontaneous alternation testing did not include reward and so it was important to discover what the boredom threshold for WT mouse was and apply it across the range of animals tested. The number of repeat tests was 7. Female WT scored the correct selection in 74% of tests. Female Het scored 40% correct which was significantly reduced compared to WT ($F(3,25) 10.832p=0.001$). Male WT scored 66% correct selections and male Het scored 51% correct which was not statistically different compared to male WT ($p=0.454$). Figure 3.12 shows a summary of these findings and shows details of test participation.

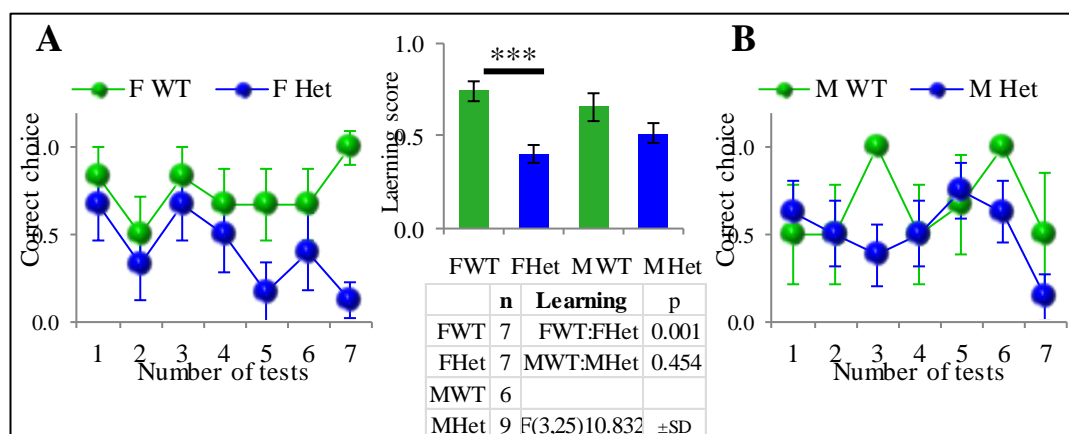


Figure 3.12 T maze learning trends and score in WT and Het

Line graphs show the mean \pm SD participation of female and male WT and Het in the total repeat tests. Graph (A) shows female WT and Het repeat test and (B) male WT and Het repeat tests showing participation was reduced by test number 7. The bar graph represents the mean \pm SD correct choice selection across all the repeat tests performed.

The learning pattern of the T maze in WT and Het mice was examined. The combined correct choice selection and time spent in the novel arm was used to calculate a learning score for each test. The mean of 53 independent experiments in WT showed an initial reduction in motivation in both male and female WT on the second test. The trend in learning continued until the 6th test where motivation began a slow decline. In the Het population, the average of 85 independent tests again showed a decline in the second test. The trend in learning was erratic in female Het mice compared to male Het. By test number 5, the female Het population appear to have reduced participation unlike male Het who were still actively participating in the test. Enthusiasm for the test began to evaporate at test 6 indicating that the number of repeat tests of 7 was the correct choice.

3.4.2.3 Discussion of T maze in WT and Het mouse

This protocol was based on timed investigations where mouse had one minute to ‘discover’ the novel arm and score further points by remaining in the novel arm, Het mice who were reluctant to explore the environment may not have accessed both sides of the T maze. If Het mouse did not ‘discover’ the previous arm then both arms represented a novel arm and he should have been awarded accordingly. This discrepancy remains unresolved.

Chapter 3 Neuromuscular and cognitive dysfunction in $Opa1^{Q285STOP}$ mouse

Time spent in the novel arm was statistically different in male and female WT and Het mice. Male WT took 17% longer time to investigate the novel arm compared to female WT and spent 28% less time in it. Male WT spent 12% less time in the original arm compared to female WT. Male Het were 45% quicker to explore and spent 34% more time compared to female Het. They spent 32% more time in the original arm compared to female Het indicating their discrimination for novel over original was impaired.

The investigation ratio in male WT was 4% higher compared to female WT and their discrimination ratio was 13% less than female WT. Male Het IR was increased 35% compared to female Het and the DR was 20% higher compared to female Het suggesting that the reduced investigation ratio in female Het may have been due to an enhanced fear response. Female Het had a 200% increase in time to novel compared to female WT which suggests that this was an exaggerated response to novel. The enhanced discrimination ratio in male Het reflected the reduced exploratory activity of female Het.

The DR revealed that female Het mice showed 69% less discrimination in novel arm identification compared to female WT. DR required investigation of both sides and the selection of one arm over the other. The Het mice that did explore the novel arm were unlikely to select the novel arm for its novel properties but selected it based on which side it was on. Het mice appeared to have a preference for right sided (personal observation). Despite attempts to demonstrate this, moving the direction the T maze altered the amount of light flooding the maze thus altering the investigational parameters of the experiment. Reduced visual cues appeared not to influence the results obtained with the T maze. As mice are primarily olfactory driven in bright light, and their tactile senses were intact, both of these functions were in evidence in the wild type population.

In conclusion, the spatial testing of $Opa1^{Q285STOP}$ mouse by T maze showed that female Het mice were very reluctant to explore a territory that should have been familiar after thirty minutes of testing. When they did locate the novel arm, the female Het mice spent significantly less time in it compared to female wild type mice. Male Het reluctance to explore was not as profound as

Chapter 3 Neuromuscular and cognitive dysfunction in $Opal^{Q285STOP}$ mouse

female Het, but discrimination of novel was reduced. Laterality in C57BL/6 mouse is an already established finding (Watanabe et al. 2004; Goto et al. 2010; Apostolova et al. 2012), however it would appear to be reduced in $Opal^{Q285STOP}$ mouse.

3.4.3 Novel object testing in $Opal^{Q285STOP}$ mouse

3.4.3.1 Optimization of NOR testing

The handling and training of animals is imperative if accurate analysis is to be performed (Powell et al. 2004). The technique is based on normal behaviour in mouse and conditions must be as 'normalised' as possible. Other factors that require consideration are sex of the mice. Male C57BL/6 mice were identified as having an enhanced NOR score compared to female animals (Frick and Gresack 2003). However it has been established that co-learning in females can enhance their NOR skills (Lipina and Roder 2012). In rats, single housed animals have better object recognition skills compared to group housed (van Goethem et al. 2012).

Other factors which required attention included the precise nature of the test and testing parameters including training period, data collection and analysis, and repeat testing interval. A factor of trial retention intervals can affect performance. As the delay between training and test increases, so performance can deteriorate. A short retention interval is considered to be less than three hours (Obinu et al. 2002; Schiapparelli et al. 2006). All mice were tested within the short retention maximum of three hours

3.4.3.2 Results of NOR testing in WT and Het mouse

NOR			
WT	11	Het	17
F WT	6	M WT	5
F Het	8	M Het	9

Table 3.9 Summary of test numbers for NOR testing in WT and Het

Novel object recognition was analysed according to the investigation ratio and discrimination ratio generated from the data collected during the test.

The time to novel object in female WT was 9.7 ± 2.4 seconds Female Het took 25.7 ± 4.4 seconds /sec which was significantly increased compared to female WT (F(3,24) 10.129 p=0.001). Male

Chapter 3 Neuromuscular and cognitive dysfunction in *Opal*^{Q285STOP} mouse

WT time to novel was 11±0.9 seconds and male Het 29.9±4.4 seconds which was significantly increased compared to male WT (p=0.001). Time with novel object in female WT was 26.4±3.9 seconds and female Het was 12.4±3.9 seconds which was significantly reduced compared to female WT (F(3,24) 8.188 p=0.004). Male WT time with novel object was 26.2±1.1 seconds and Het male was 13.5±2.2 seconds which was significantly reduced compared to male WT (p=0.001). Time with original object in female WT was 4.72±1.1 seconds and female Het 6.6±2.5 seconds (p=0.823). Male time with original object was 6.5±0.45 seconds and male Het was 14.2±2.5 seconds which was significantly increased compared to male WT (F(3,24) 1.880 p=0.021). Figure 3.13 shows a summary of the raw data used to generate the IR and DR of novel object recognition.

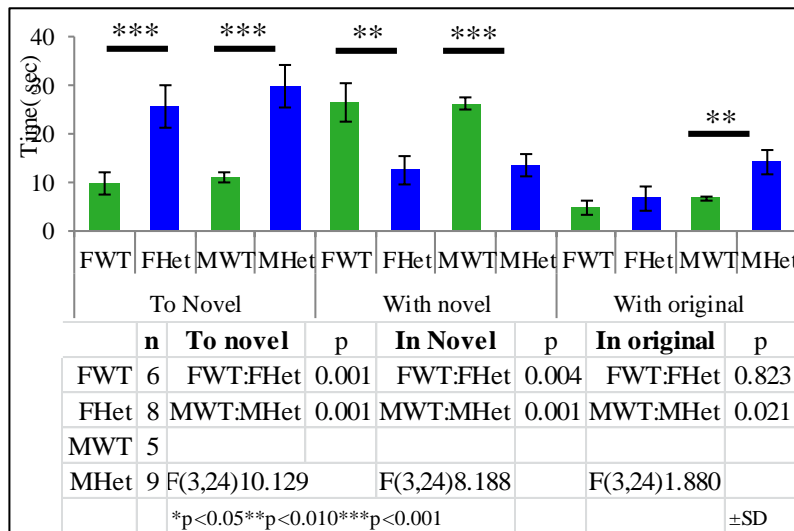


Figure 3.13 Novel object testing parameters in WT and Het

Graph showing the mean ±SD testing parameters of novel object recognition in WT and Het

The IR in female WT was 0.65±0.04 and female Het was 0.52 ±0.06 which was significantly reduced compared to female WT (F(3,24) 6.926 p=0.005). The IR in male WT was 0.81 ±0.02 and 0.45±0.05 in the male Het which was significantly reduced compared to male WT (p=0.004). The DR in female WT was 0.46±0.05 and in female Het was 0.28±0.05 which was significantly reduced compared to female WT (F(3,24) 7.634 p=0.004). The DR in male WT was 0.59±0.04 and male Het was -0.01 ±0.18 which was significantly reduced compared to male WT (p=0.002). Figure 3.14 shows these data.

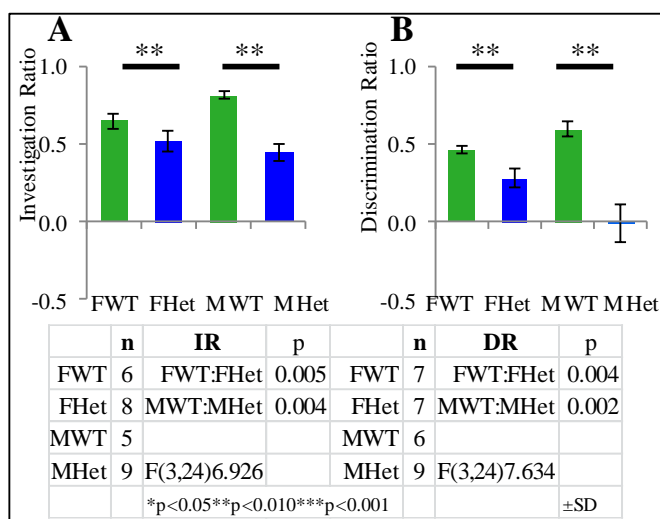


Figure 3.14 NOR IR and DR in WT and Het

Graphs showing the mean \pm SD of (A) IR and (B)DR as calculated from the observations of NOR in male and female WT and Het.

The learning trend in NOR between WT and Het mice was examined.

Unlike T maze where there was no

diversity in each arm, the novel object recognition test provided a novel item to examine. In the series of seven novel items, the mean score for each item was placed on a scale of correct or incorrect. As it was presumed that *Opal*^{Q285STOP} mouse had no olfactory deficit, the objects were anticipated to generate some curiosity in both WT and Het mice. The female WT score was 0.66 ± 0.06 and female Het score was 0.50 ± 0.11 which was not significantly different compared to female WT ($p=0.144$). The learning score for male WT was 0.57 ± 0.13 and for male Het was 0.43 ± 0.06 which was not significantly different compared to male WT ($p=0.200$). The identification of preference in WT and Het was examined. Female Het spent significantly less time with resin compared to female WT ($F(3,23) 1.807 p=0.032$) and male Het spent significantly less time with glass compared to male WT ($F(3,23) 2.071 p=0.025$). The learning trend observed in both female and male Het was reduced but not significantly different compared to WT.

As seen in Figure 3.15, both WT and Het demonstrated a reduction in time with novel on the second test. This was mice displaying an acclimatization period where the time spent doing anything appropriate was lost. This is possibly a part of learning where the test parameters are being processed by mouse brain. In both T maze and NOR, both WT and Het mouse sit between novel and original for longer periods than at any other time in the assays. The response seen in the Het mice demonstrated that they appeared not to have impaired vibrissae activity. Mice use single whiskers to investigate the texture which results in a characteristic whisker vibration or

kinetic signature. This allows sensory discrimination (Hutson and Masterton 1986; Diamond et al. 2008) . The single item to illicit avoidance in WT and Het mice was slate. The composition and texture of slate was cold and hard. As the exploratory mode of activity (whiskering without contact) (Ferezou et al. 2006), was clearly in use by both WT and Het mice they both elected to avoid slate. Observation of the trend in Het mice showed that they spent a greater time before becoming accustomed to the test and by test 5 had begun to demonstrate some interest in their environment. The ability to make an informed choice with preference in some Het mice indicated that their innate curiosity was depressed compared to WT. Figure 3.15 shows the learning trend and correct choice selection of NOR testing.

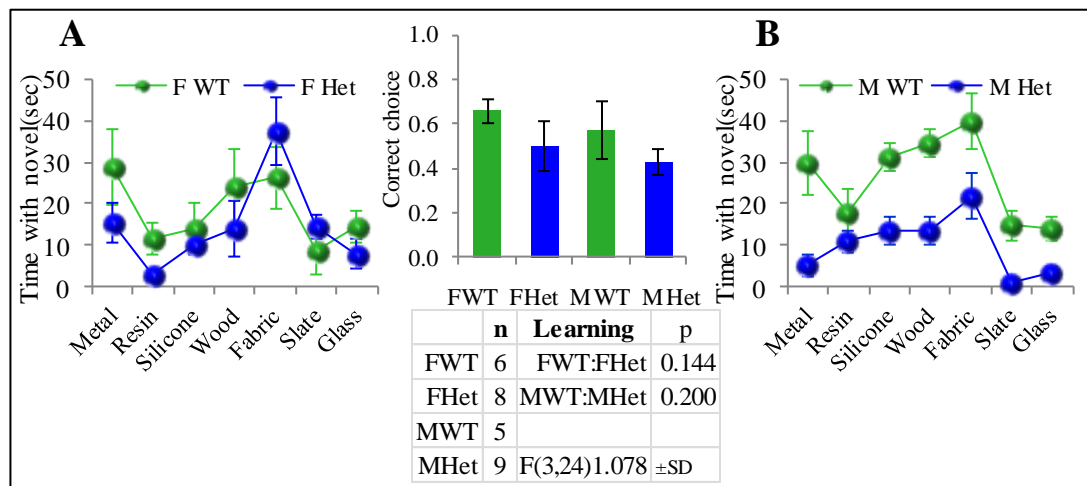


Figure 3.15 NOR learning trends in WT and Het

Line graphs show the mean ±SD participation of female and male WT and Het in NOR testing. Graph (A) shows female WT and Het time with novel and (B) male WT and Het time with novel showing full participation in all tests. The bar graph represents the mean ±SD correct choice selection across all the repeat tests performed.

Finally, the response to one particular item (fabric) suggested that Het mice were preserving their energy. The response towards this item that was not just novelty but usefulness suggested that the issue of nesting material might be addressed. As previously shown, the core temperature of Het mice was reduced by a mean 7%. Any opportunity to preserve and maintain body temperature was evidently worth investigating.

3.4.3.3 Discussion of NOR in WT and Het mouse

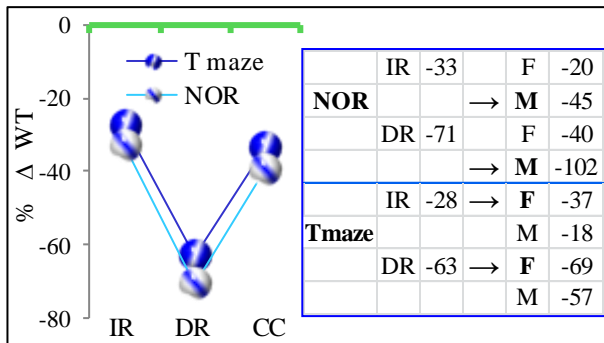
The time taken to explore the novel items in female Het mice was 165% longer than female WT and 173% percent longer in male Het compared to male WT. Once the novel item was located, female Het mice spent an average 51% less time compared to wild type females. The time spent with the original object was increased by 42% in female Het compared to female WT and increased by 116% in male Het compared to male WT. The selection of items for this test was expected to generate the natural curiosity of mice. In the wild type population, on investigating the original item, many mice returned more than once for a very brief time as though to confirm they had investigated it before returning to the novel item. Both WT and the Het mice, who did explore, climbed onto objects and approached from different directions in the course of their explorations, both investigating initially by mystacial vibrissae. It demonstrated an intact whisker mediated texture discrimination. Further investigation was usually followed by both forepaw investigations. Recent discrimination task development has incorporated this testing parameter into novel screening methods(Wu et al. 2013). Detection of impaired somatosensory systems may be indicative of axonal damage. A sub population of individual axons representing whisker movement in the brain stem trigeminal nuclear complex is responsible for interpretation of this sensory information in mouse (Wu et al. 2011). Any sensory or motor system that has a high demand for ATP may be impaired in the Opa1^{Q285STOP} mouse model and tactile investigation using all senses was therefore considered noteworthy. The male Het mice who spent extensive time with the original item were not doing so because it was familiar to them as it was a replacement item, but the tactile sensation or shape was known. The reluctance to explore may have been associated with fear; however the female Het mice demonstrated that they were able to overcome their initial trepidation. Some male Het mice appeared to be disorientated and sat in the middle of the arena.

The investigation ratio showed the male Het mice investigated 13% less compared to female Het mice and 45% less compared to male wild type mice. The discrimination ratio (DR) demonstrated that some of the male Het mice were unable to discriminate between novel and original objects; the mean reduction in DR score was 102% in male Het mice and a 40%

Chapter 3 Neuromuscular and cognitive dysfunction in *Opa1*^{Q285STOP} mouse

reduction in Het females. However this may also be due to some Het mice not investigating either object, thus not contributing any valid information to the test. The analysis suggests that *Opa1*^{Q285STOP} mice were memory impaired, with male Het mice more impaired compared to female Het mice. These are summarized in Figure 3.16.

Figure 3.16 Summary of cognitive impairment in *Opa1*^{Q285STOP} mouse



Different cognitive tests reveal the same cognitive defects. The graph shows the reduction in IR, DR and correct choice selection in T maze and NOR testing compared to WT (represented by green line). The box shows the percentage reduction for IR and DR in NOR and T maze.

A further observation of the experiment was confirmed where it was shown that male C57BL/6 mice demonstrate enhanced NOR performance (Frick and Gresack 2003). Male WT C57BL/6 had enhanced IR compared to WT females with a 26% increase. The male WT DR also showed a 28% increase compared to female WT. This was clearly not so in the male Het mice.

Housing conditions in solitary, paired and group housed mice was examined for evidence of enhanced performance in solitary housed animals (van Goethem et al. 2012). As there were no solitary housed female mice, analysis was restricted to male mice only. In wild type mice, there was no significant difference observed between solitary (n3) and paired (n2) mice. With Het male mice, there was no significant difference identified in solitary (n6) compared to paired male (n3) or grouped male (n3) mice for IR (p=0.759) or DR (p=0.255).

Co learning in female C57BL/6 mice was examined in group housed female mice. There were 12 wild type females and sixteen Het females sharing a collective six cages. It may explain how the Het females outperformed the Het males.

3.4.4 Discussion of cognitive decline in *Opa1*^{Q285STOP} mouse

Both the T maze and novel object recognition imparted valuable information about the impact fusion deficiency had on memory recall and spatial habituation. The T maze test showed a 45%

Chapter 3 Neuromuscular and cognitive dysfunction in $Opa1^{Q285STOP}$ mouse

deficit of function in Het. T maze identified that female Het mouse had significant impairment of IR and DR that was greater than male Het compared to WT female and male respectively. Because the investigation ratio was reduced, the ability to discriminate between novel and original was impaired. Observations of WT mouse showed that for both T maze and NOR tests, male WT IR and DR exceeded female WT by 15% and 7 % respectively. If the reference sample was WT then it was expected that Het male scores would exceed female Het. For IR, male Het scores exceeded female Het by 11%. The DR score in male Het was 20% higher than female Het for T maze only. The discrimination required in novel object recognition was reduced by 95% compared to female Het.

The NOR test revealed a 52% deficit of function in Het compared to WT. NOR revealed that male Het demonstrated a significant reduction in IR and DR Male Het deficit was 66% greater than female Het when compared to WT counterparts. As the novel object recognition test included many aspects of the T maze including initiation of investigation and identity of the novel, NOR offered an increased opportunity to succeed because unlike T maze, there was a novelty to be discovered. Female Het mice appeared to grasp the concept but Het males scored a negative DR. Their inability to tell novel from original was demonstrated by the time spent with novel and original.

T maze required self-motivation without any clear advantage in locating the novel arm. In this respect the female Het mice conserved their ATP levels with many remaining in the arm of the maze not venturing down either arm of the maze. As these experiments were performed on the same cohort of mice, direct comparisons with respect to T maze and NOR was possible. Het females spent 5% less time with the original item compared to WT females demonstrating ability to learn and remember.

At 15 months of age, these mice were mature but not elderly; therefore the results were not due to age related deterioration. This phenotype variation is seen in humans with dominant optic atrophy where the same mutation in different individuals can produce different severity of

Chapter 3 Neuromuscular and cognitive dysfunction in *Opal*^{Q285STOP} mouse

disease. Although the *Opal*^{Q285STOP} mouse originates from the same original stock and this might be expected to reduce the variability in their extra ocular phenotype.

3.4.4.1 Tissue weights at 15 months

At 15 months, full tissue retrieval was performed in order to continue with the analysis of Het mouse. Body weight, brain weight and cardiac weight ratio was obtained for all animals. There was no significant difference observed between the body weights of female WT (n=25) and female Het (n=25) (p=0.427 or between male WT (n10) and male Het (n23) (p=0.272). Female Het (n25) brain weight was 0.53±0.04g was significantly reduced compared to female WT (n=25) 0.59±0.02g (F(3,79) 2.647p=0.013). There was no significant difference observed between male WT and male Het brain weight (p=0.839).

Housing conditions and enrichment can affect brain weight (Mazarakis et al. 2014). There were no solitary housed female mice. Analysis was confined to male WT and Het only. Table 3.10 summarises the body brain and cardiac weight ratio in WT and Het at 15 months. Enrichment

		n	Body weight(g)	Brain weight(g)	Cardiac Ratio
	eFWT	25	28.2 ±1.7	0.58 ± 0.18	0.62 ± 0.14
	eF Het	17	28.2±1.3	0.48 ± 0.03	0.63 ± 0.03
E	F Het	4	23.0±1.7	0.57 ± 0.06	0.74 ± 0.05
N	eFWT:eFHet		0.833	0.013	0.96
R	eFHet:FHet		0.009	0.020	0.009
I	F(3,79)		14.03	2.647	1.164
C	eMWT	4	28.2 ±1.3	0.47 ± 0.06	0.68 ± 0.05
H	eM Het	7	29.0±1.3	0.44 ± 0.04	0.70 ± 0.04
M	eMWT:eMHet		0.729	0.688	0.781
E	eMWT:MWT		0.001	0.846	0.287
N	eMHet:MHet		0.008	0.534	0.004
T	F(3,79)		10.469	1.369	1.681
	M WT	6	35.4 ±1.3	0.49 ± 0.03	0.61 ± 0.04
	M Het	16	33.1±0.8	0.47 ± 0.03	0.60 ± 0.03
H	S M WT:M Het		0.154	0.839	0.866
O	O F(5,37)		5.372	1.65	1.186
U	L sMWT	4	34.0 ±2.6	0.49±0.08	0.52±0.08
S	O sMHet	14	32.6 ±1.0	0.49±0.03	0.60±0.03
I			0.634	0.963	0.343
N	G sMWT:gMWT		0.624	0.009	0.012
G	R sMHet:gMHet		0.247	0.015	0.129
	P F(5,37)		5.372	1.65	1.186
	gMWT	7	32.5±1.2	0.48±0.04	0.66±0.03
	gMHet	9	30.7±1.25	0.42±0.04	0.68±0.09
	gMWT:gMHet		0.317	0.288	0.779
	F(5,37)		5.372	1.65	1.186
	e enrichment-s=solitary housed g-group housed				

was provided with a running saucer (Small n Furry) in all multiple occupancy cages. Mice housed in smaller cages were prevented from having saucer enrichment due to cage size limitations.

Table 3.10 Body brain and cardiac weight ratio at 15 months in WT and Het

Table showing a summary of weight in WT and Het body, brain and cardiac weight ratios at 15 months. The effect of enrichment (e) on body weight was significant in all phenotypes examined. Enrichment had a significant effect on Het cardiac ratios. Housing conditions had a significant impact on both WT and Het male WT brain weight.

Chapter 3 Neuromuscular and cognitive dysfunction in *Opal*^{Q285STOP} mouse

Enrichment had a positive effect on body weight in male WT. Compared to no saucer male WT there was a significant 20% reduction in enriched male WT weight (F(5,50) 10.469 p=0.001). Body weight in enriched male Het was also significantly reduced by 12% (p=0.008) compared to male Het without saucer. Body weight in enriched female Het increased by a significant 23% (F(3,79) 14.03 p=0.009) compared to female Het without saucer.

Brain weight in enriched male WT weighed 4% less than non-enrichment male WT (p=0.846). Enriched male Het brain weight was 6% less than non-enrichment male Het (p=0.534). Enriched female Het brain weight was significantly reduced by 16% (F(3,79) 2.647 p=0.020) compared to non-enriched female Het.

Cardiac weight ratio in enriched male WT was increased by 12% (p=0.287) compared to non-enriched male WT. Cardiac weight ratio in enriched male Het was significantly increased by 17% (F(5,79) 1.681 p=0.004) compared to non-enriched male Het. Enriched female Het cardiac weight ratio was reduced by a significant 15% (p=0.009) compared to non-enriched female Het.

Housing conditions in male mice showed that solitary housed male WT body weighed 5% (p=0.624) more than group housed male WT. Solitary housed male WT brain weighed 2% (p=0.909) more than group housed and cardiac weight ratio was significantly reduced by 21% (F(5,37) 1.186 p=0.012) compared to group housed male WT.

		n	Body weight (g)	Brain weight (g)	Cardiac ratio
E	M WT	10	↓20%	↓4%	↑12%
N	eMWT:MT		0.001	0.846	0.287
R	M Het	23	↓12%	↓6%	↑17%
I	eMHet:MHet		0.008	0.534	0.004
C	F Het	21	↑23%	↓16%	↓15%
H	eFHet:FHet		0.009	0.020	0.009
	F(5,50)		10.469	0.408	2.467
H	sMWT	4	↑5%	↑2%	↓21%
O	sMWT:gMWT		0.624	0.909	0.012
U	sMHet	14	↑6%	↑18%	↓12%
S	sMHet:gMHet		0.247	0.015	0.129
E	F(5,37)		1.202	1.323	3.534
e-enrichment e=no enrichment s=solitary g=group					

Table 3.11 Effects of enrichment and housing on tissue weights in WT and Het

Table summarising the effects of enrichment in male WT and Het showing a significant reduction in body weight and in male Het an increase in cardiac weight ratio. Female Het showed a significant increase in body weight with a significant reduction in both brain and cardiac weight ratio. Compared to group housed, solitary housed male WT had a significant reduction in cardiac weight ratio. Solitary housed male Het had a significant reduction in brain weight.

3.4.5 Discussion of tissue weights at 15 months

Solitary housed male Het weighed 6% more ($p=0.247$) than group housed male Het. Solitary housed male Het brain weight was a significant 18% ($F(5,37) 1.65$ $p=0.015$) more than group housed and cardiac weight ratio was 12% ($p=0.129$) less than group housed male Het. Table 3.11 summarises these data.

The advantages of physical exercise on brain function are well documented (Kohman et al. 2012; Nishijima et al. 2013; Waters et al. 2013; Meek et al. 2014). A change in regional specific brain activity due to a reduction in tissue mass may result in subtle behavioural alternations (Burke and Barnes, 2006) but is unlikely to cause an alternation in weight. The increase in cardiac weight in the enriched population has been documented (Stones et al. 2009; Sultanova 2010; Aufradet et al. 2012). It is associated with the altered morphological and mechanical properties of cardiac myocytes (Allen et al. 2001; Natali et al. 2002).

Chapter 3 Neuromuscular and cognitive dysfunction in Opa1^{Q285STOP} mouse

3.4.6 Summary of Chapter 3: Neuromuscular and cognitive dysfunction in Opa1^{Q285STOP} mouse

3.4.6.1 Significant neuromuscular dysfunction in Opa1^{Q285STOP} mouse

Opa1^{Q285STOP} mouse showed significant physiological impairment of lower motor function with impaired gait, balance, and coordination as tested by rotarod, rope, and narrow beam. Autonomic dysfunctions were also observed. Het mice showed a reduction in core temperature which was more significant in younger aged mice. SHIRPA revealed neuropsychiatric disturbances with increased extended freeze and initiation. Other phenotypic findings included reduced learning skills in the Het population. Some of these findings were influenced by the housing conditions of both WT and Het mice.

3.4.6.2 Significant reduction in cognitive function in Opa1^{Q285STOP} mouse

Opa1^{Q285STOP} mouse showed a significant reduction in short term retentive memory as observed in spontaneous alternation testing. Regional impairment of specific functions associated with prefrontal cortex were observed with increased initiation times in Het mice. The specific object recognition function of the perirhinal cortex was especially reduced in male Het mice as determined by NOR testing. Co learning in Het females was more evident than in male Het mice.

3.4.6.3 Post mortem body organ weight

Enrichment had a significant effect on body weight in WT and Het. Male WT and Het showed a significant reduction in weight and female Het showed a significant increase. Brain weight was significantly reduced in female Het and cardiac weight ratio was increased in male Het but reduced in female Het. Housing conditions affected brain weight in male Het but not male WT.

The extended phenotype found in Opa1^{Q285STOP} mouse would suggest that the Opa1 mutation resulted in functional impairment that extended beyond the retina. Because of these data, it was decided to extend the tissue range of mitochondrial assays to include the spinal cord and skeletal muscle. This was anticipated to provide a broader picture of the effects of Opa1 haploinsufficiency on the mitochondrial environment.

Chapter 4 Bioenergetic impairment in Opa1^{Q285STOP} mouse

4.1 Introduction

In the previous chapter the extended phenotype of Opa1^{Q285STOP} mouse was investigated using several phenotypic techniques which highlighted the extent of impairment in this mouse model. Despite this, the overall health of mouse at 15 months was intact. His appetite was healthy and he appeared to enjoy the use of a running saucer for a few hours each day. At 15 months, it was not considered that this was an especially aged animal but in order to investigate the mitochondrial profile it was important to eliminate age as a confounder from the analysis. Opa1^{Q285STOP} mouse was culled at 15 months for full tissue retrieval. WT cage mates were culled at the same time to permit age matched analysis. All central nervous system tissue was employed in the following investigations

4.1.1 Morphology of mitochondrial in Opa1^{Q285STOP} mouse

4.1.1.1 Experimental design of mitochondrial morphology

Mitochondrial staining with Mitotracker Red CMXRos was performed as discussed in Chapter 2 Methods (2.10.2). Mitochondria were freshly isolated from three WT and Het brain and four WT and Het retina and diluted to 1mg/ml. A volume of 5µl was used for analysis of Mitotracker staining.

4.1.1.2 Results of mitochondrial morphology in WT and Het

Mitochondria were isolated from brain of three WT and three Het mice and were stained with Mitotracker red. Mitochondria were also isolated from retina of four WT and four Het mice. The purpose was to measure a range of parameters using Image J. Table 4.1 shows a summary of the number of mitochondria analyzed from both WT and Het brain and retina. In the interest of studying the complete mitochondrial profile of Het mice, it was considered that the isolated mitochondria included an accurate representation of all populations and sizes. If this population did contain structures other than mitochondria, then this was the environment that Het

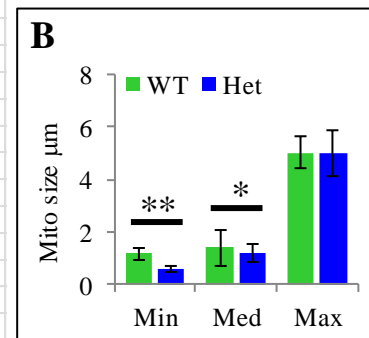
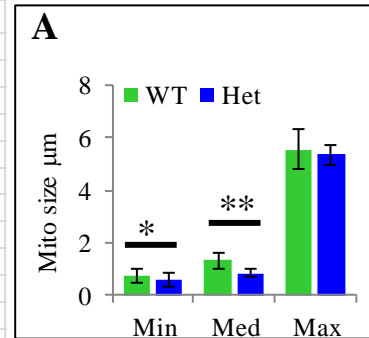
Chapter 4 Bioenergetic impairment in *Opa1*^{Q285STOP} mouse

mitochondria survived in. However as previously addressed, isolation of lysosomes would require more intensive centrifugation at greater speeds.

Data analysis was performed in SPSS by ANOVA followed by Tukey's post hoc test where $p < 0.05$ was considered statistically significant and as non-parametric Mann-Whitney U test followed by Kruskal -Wallis H test.

Table 4.1 Summary of mitochondrial properties in brain and retina of WT and Het

A									Total		Brain	
WT	n	Brain	Min	Med	Max			n	WT:Het	p		
	1	684	1.032	1.325	6.051							
	2	756	0.587	1.326	4.045	WT	Min	727	WT:Het	0.007		
	3	725	0.587	1.321	6.625	Het	Min	4757	F(5,12)	26.391		
		Ave $\mu\text{M}/5\mu\text{g}$	0.735	1.324	5.573							
		STDEV	0.257	0.302	0.742	WT	Med	495	WT:Het	0.007		
Het	1	1489	0.587	0.981	4.602	Het	Med	1095	F(5,12)	26.391		
	2	3783	0.587	0.660	6.960							
	3	1181	0.580	0.917	4.558	WT	Max	764	WT:Het	0.855		
		Ave $\mu\text{M}/5\mu\text{g}$	0.585	0.853	5.373	Het	Max	1947	F(5,12)	26.391		
		STDEV	0.254	0.170	0.375							
B									Total		Retina	
WT	n	Retina	Min	Med	Max			n	WT:Het	p		
	1	664	1.165	1.486	7.491							
	2	755	1.174	1.394	4.193	WT	Min	2794	WT:Het	0.009		
	3	735	1.173	1.321	4.193	Het	Min	2394	F(5,18)	23.307		
	4	742	1.174	1.380	4.300							
		Ave $\mu\text{M}/5\mu\text{g}$	1.172	1.395	5.044	WT	Med	454	WT:Het	0.048		
		STDEV	0.244	0.682	0.623	Het	Med	168	F(5,18)	23.307		
Het	1	754	0.567	1.394	3.061							
	2	698	0.587	1.321	4.548	WT	Max	343	WT:Het	0.971		
	3	704	0.587	1.380	7.472	Het	Max	307	F(5,18)	23.307		
	4	717	0.587	0.660	5.045							
		Ave $\mu\text{M}/5\mu\text{g}$	0.582	1.189	5.031							
		STDEV	0.100	0.354	0.880							
			* $p < 0.05$ ** $p < 0.010$ *** $p < 0.001$									\pm SD



The table shows the total number of events from each (A)brain and (B)retina and the mean size of each category. The p value indicates the statistical difference between groups. (A)Brain mitochondrial size: A total of 2165 mitochondria (events) were recorded from WT brain. In the Het brain, 6453 were recorded. There was a significant difference in the minimum size of mitochondria between WT and Het ($p=0.045$) and the medium sized mitochondria ($p=0.006$) but not the maximum sized ($p=0.855$). (B) Retinal mitochondrial size: WT (n2896) events and Het (n2873) events. There was a significant difference between the minimum sized mitochondria ($p=0.009$)and the medium sized ($p=0.048$) but not the maximum ($p=0.971$).

Chapter 4 Bioenergetic impairment in $Opa1^{Q285STOP}$ mouse

Measurements of mitochondria included area and perimeter. Both the perimeter and area measurements were dependent on image magnification. The aspect ratio reports the change in length but using a formula based on both area and perimeter which was Formfactor. The Formfactor was $(Pm^2)/4\pi Am$ (Koopman et al. 2006; Koopman et al. 2010) where Pm^2 is the perimeter squared, Am is area and π (3.1415) is the ratio between the circumference and the diameter of a circle which has a minimal value of 1 corresponding to a circular mitochondria. This allowed the Formfactor to report the length of individual mitochondria.

Brain mitochondrial size was calculated using the equation $(Pm^2)/4\pi Am$. The median size in WT (n=2165) brain mitochondria was $1.321\mu m \pm 0.324$ with the minimum size $0.735\mu m \pm 0.257$ and the maximum size $5.57\mu m \pm 0.742$. In Het (n=6453) brain mitochondria the median size was $0.853\mu m \pm 0.170$ which was significantly reduced compared to WT (F(5,12) 26.391 p=0.007). The minimum size was $0.585\mu m \pm 0.254$ which was significantly smaller than WT (F(5,12) 26.391 p=0.007). The maximum size in Het brain was $5.37\mu m \pm 0.375$ which was not statistically different compared to WT (p=0.855).

Isolated retinal mitochondria were analysed from WT (n=2896) which showed a range from the minimum $1.171\mu m \pm 0.244$, median $1.395\mu m \pm 0.682$ to the maximum $5.044\mu m \pm 0.623$. Het (n=2873) retinal mitochondrial measured from the minimum $0.582\mu m \pm 0.100$ which was significantly smaller compared to WT (F(5,18) 23.307 p=0.009). The median size was $1.189\mu m \pm 0.354$ which was statistically different compared to WT (F(5,18) 23.307 p=0.048). The maximum size was $5.031\mu m \pm 0.880$ which was not statistically different to WT (p=0.971). Table 4.1 shows the range sizes in brain and retina for WT and Het with the statistical difference between groups and a graphical representation of these findings showing the range of sizes in WT and Het brain and retina and a table. Figure 4.1 shows a bar and whisker plot demonstrating the range of size in WT and Het brain and retina. Figure 4.2 are representative images of mitochondria from both WT and Het brain and retina.

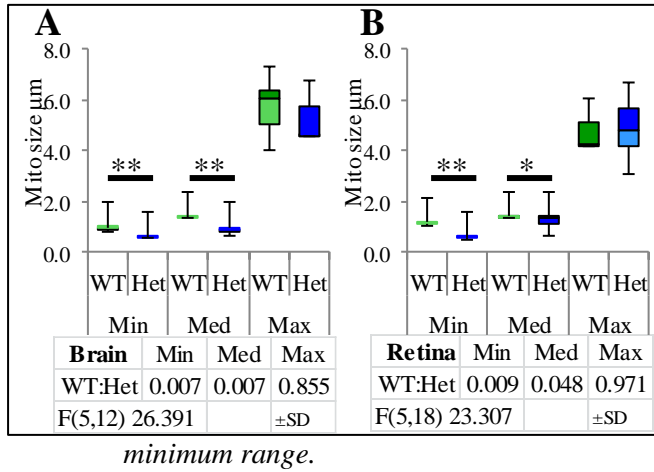


Figure 4.1 Size variation in isolated mitochondria in WT and Het

Box graphs show all the range of size of mitochondria in brain (A) and retina (B) in WT and Het with the upper and lower boxes representing the first and third quartile. The dividing line between the two boxes is the median. The upper whisker represents the maximum range and the lower whisker represents the

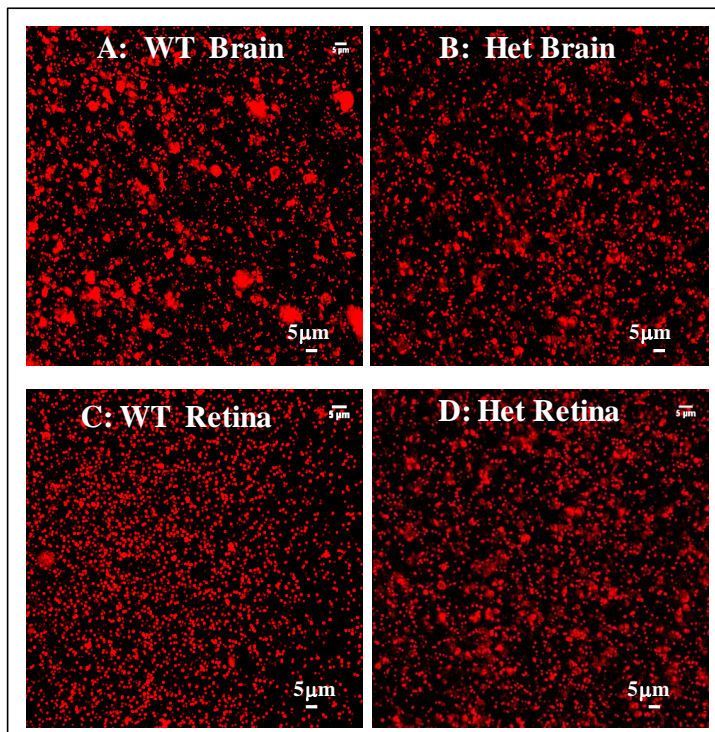


Figure 4.2 Mitotracker staining of isolated mitochondria from WT and Het

Mitotracker Red CMXRos staining of isolated mitochondrial from brain of WT brain (A) and Het (B), and retina of WT (C) and Het (D). Scale bar $5\mu\text{m}$

The range of mitochondrial sizes was plotted in a histogram and sorted according to size. This allowed a direct overlay of both histograms from WT and Het. Figure 4.3 shows double plotted Mann-Whitney histograms and the results for statistical test (Mann-Whitney U test, Kruskal-Wallis H test).

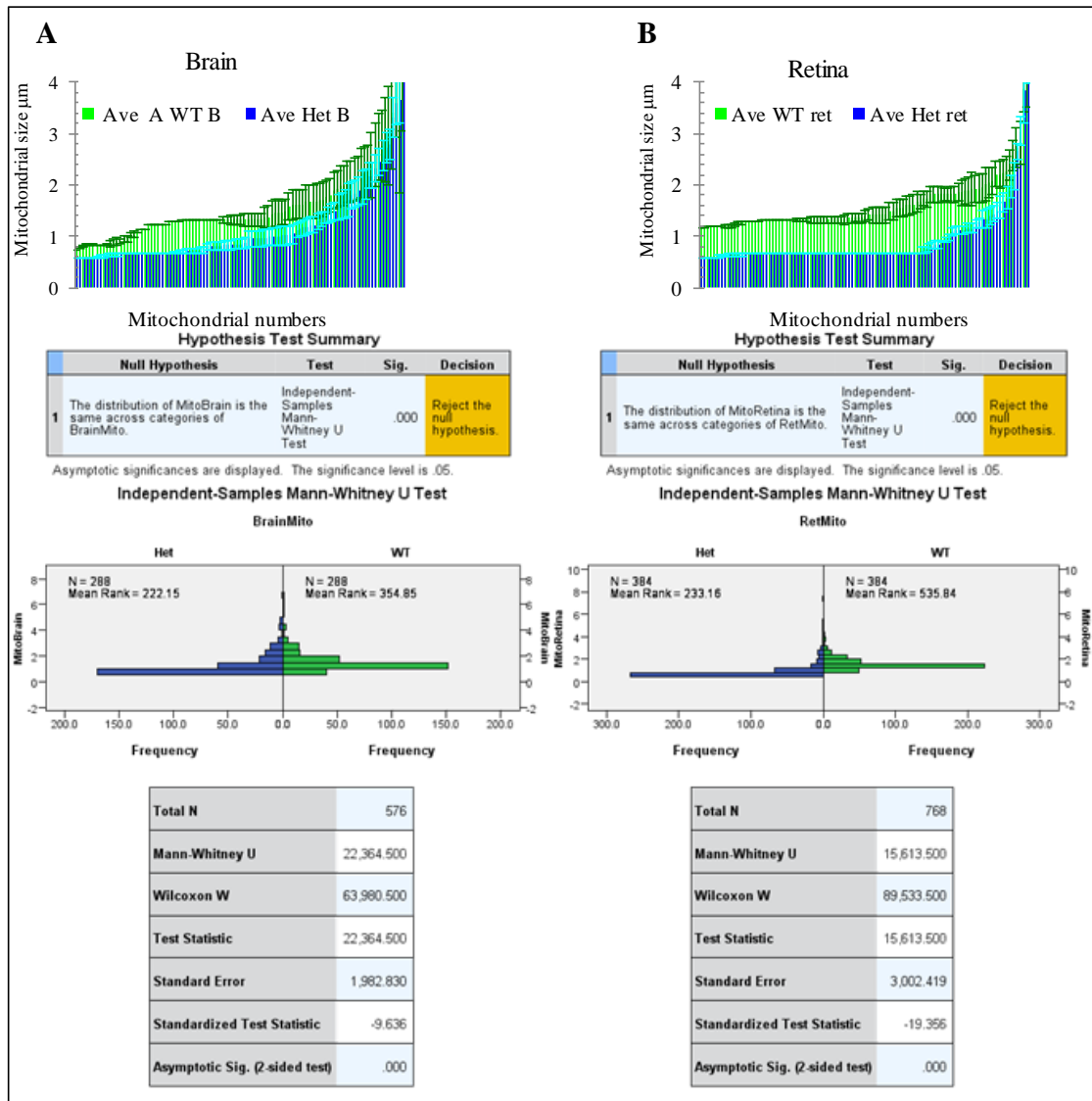


Figure 4.3 Histogram of brain and retinal mitochondrial size in WT and Het

Graphs show non parametric analysis of mitochondrial size in WT and Het. Histogram of mitochondrial size as calculated by area and perimeter readings and plotted according to size. (A) Brain mitochondria in WT (green) and Het (blue) plotted as a function of size. WT size range from $0.735\mu\text{m}$ to $5.573\mu\text{m}$ Het size range from $0.580\mu\text{m}$ to $5.373\mu\text{m}$ which was significantly different ($U 22.3 p=0.001$)

(B) Retinal mitochondria in WT and Het plotted as a function of size. WT size range from $1.172\mu\text{m}$ to $5.044\mu\text{m}$. Het retinal mitochondrial size range from $0.582\mu\text{m}$ to $5.031\mu\text{m}$ which was significantly different to WT ($U 15.6 p=0.001$).

4.1.1.3 Discussion of mitochondrial morphology in WT and Het

The aim of these experiments was to confirm that the whole range of available mitochondria were being isolated. A range of sizes from $0.5\mu\text{m}$ to $5.3\mu\text{m}$ is in agreement with previous

Chapter 4 Bioenergetic impairment in $Opa1^{Q285STOP}$ mouse

findings (Munn 1974; Schwerzmann et al. 1986; Cereghetti and Scorrano 2006; Scheffler 2007; Youle and van der Bliek 2012). However as the aim of isolating mitochondria was to perform functional studies, it was important to include the whole available range. The mitochondria in brain of Het mouse showed that there were higher proportions of smaller sized mitochondria. The mean reduction in size was 20% compared to WT. The larger sized mitochondria in WT were $5.573\mu\text{m}$ In Het brain they were $5.37\mu\text{m}$. This represented a 4% reduction in larger size. The median range in WT brain was $1.321\mu\text{m}$ and in Het brain was $0.853\mu\text{m}$ which represented a reduction of 36% in mitochondrial size. The smallest sized mitochondria in WT brain were 20% bigger than the smallest size in Het brain.

In the retina, there was a significant difference in the smaller sized mitochondria. WT retinal mitochondria were $1.17\mu\text{m}$. Het smallest sized retinal mitochondria were $0.587\mu\text{m}$ which was 50% smaller than WT. In contrast, the larger sized mitochondria in WT and Het showed less than 1% difference in size.

This might suggest that to compensate for such a high population of possible inadequate mitochondria, Het mouse retinal mitochondria that have fused with adjoining mitochondria remain in this fused state, thus avoiding mitophagy and elimination. The mean of median size in WT retina was $1.380\mu\text{m}$ and in Het retina was $1.189\mu\text{m}$ which represented a 15% reduction in mitochondrial size throughout the retina. The 50% reduction in smaller sized brain mitochondria is possibly below the threshold for pathological effects, however with much physical phenotyping, the threshold may be approaching in several animals. The retina of Het mouse would appear to be home to a very large population of very small mitochondria. If these mitochondria have a reduced membrane potential then it would seem advisable to eliminate them as this will ultimately result in ROS mediated damage. The size threshold for mitophagy induced elimination may be adjusted in Het mouse to incorporate smaller sized mitochondria but the function threshold must remain the same. The presence of larger sized mitochondria would suggest there was some damage limitation in the retina, however it must be reminded that most mitochondria reside in the photoreceptor layer and what percentage of isolated

Chapter 4 Bioenergetic impairment in $Opa1^{Q285STOP}$ mouse

mitochondria originate from the ganglion cell layer would require more sophisticated methods for examination.

Mitochondrial fragmentation due to fusion imbalance results in bioenergetic impairment. The initiation of mitochondrial fragmentation is due to reduced membrane potential. A reduction in membrane potential will trigger mitophagy (McBride et al. 2006; Carlucci et al. 2008). Reduced transport of electrons (Ishihara et al. 2004) with subsequent reduction in ATP (Legros et al. 2002).are insufficient to trigger mitophagy (Westermann 2003)

Mitophagy serves to eliminate non-functional mitochondria and is important in the prevention of excessive ROS generation and the reduction of potential mtDNA mutations.

4.1.2 Mitochondrial membrane potential in $Opa1^{Q285STOP}$ mouse

4.1.2.1 Experimental design of JC1 staining

JC-1 is a cationic dye that accumulates in energised mitochondria. JC-1 remains as a monomer within the cytoplasm and fluoresce green. When in the mitochondria, the dye aggregates into red fluorescent molecules provided the membrane potential of the mitochondria remains hyperpolarised.

On at least three separate occasions, JC1 staining was performed on freshly isolated mitochondria from WT and Het brain and retina to determine if the membrane potential differed between the two populations. Mitochondria were diluted to a final protein concentration of 0.20µg/ml with storage buffer. The mitochondrial suspension was incubated with JC-1at room temperature for 7 minutes and analysed immediately using a disposable haemocytometer. Viable healthy mitochondria with intact membrane potential fluoresced red, mitochondria with reduced membrane potential were green and mitochondria that were in the process of losing membrane potential termed ‘transition’ were fluorescent yellow.

4.1.2.2 Results of JC1 staining

In WT brain (n5), a total of 60122 mitochondria were analysed. The percentage of red fluorescence representing intact membrane potential was 89%±4%. Green fluorescent

Chapter 4 Bioenergetic impairment in *Opa1*^{Q285STOP} mouse

representing reduced membrane potential was 4%±3% and mitochondria in transition (yellow) was 7%±2%. In Het brain (n5), a total of 45930 mitochondria were analysed. Mitochondria with intact membrane potential was 85%±2% which was not significantly different to WT (p=0.011), reduced membrane potential was 5%±3% which was not significantly different to WT (p=0.226) and in transition was 9%±2% which was not statistically significant (p=0.254)

In WT(n5) retina, a total 69388 mitochondria were analysed. The intact population was 80% ±3%, and the reduced was 12%±2% with 8%±3% in transition. The total number of retinal mitochondria from Het (n5) was 61311 which had 82%±4% intact membrane potential which was not significantly different to WT (p=0.120), 5%±5% reduced potential which was not statistically different to WT (p=0.560) and 12%±4% in transition which was not statistically different to WT (p=0.329). Figure 4.4 shows a representation of JC-1 stained mitochondria in WT and Het brain and retina.

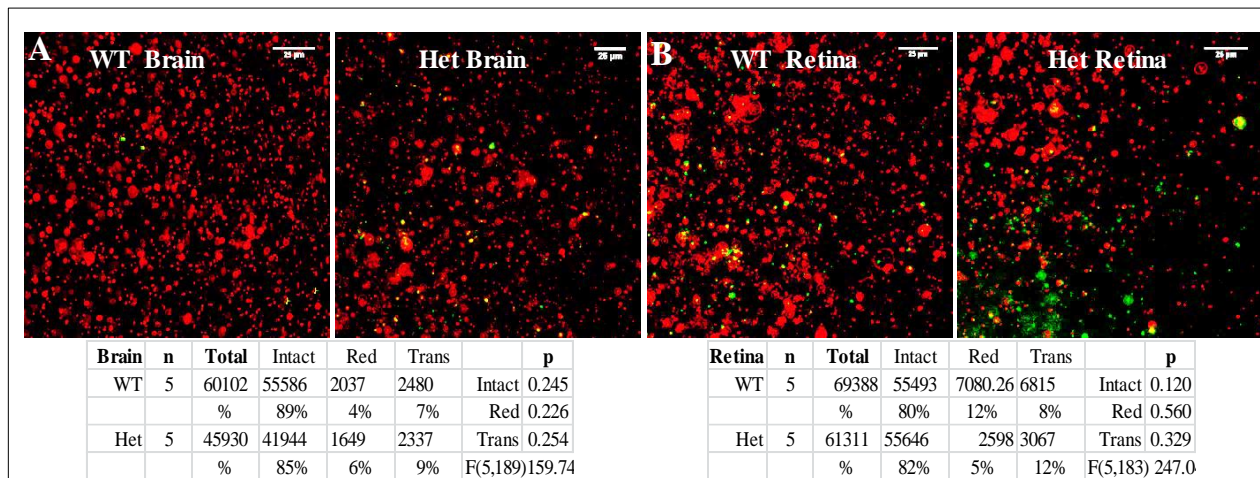


Figure 4.4 JC1 staining for $\Delta\Psi_m$ in WT and Het brain and retinal mitochondria.

Representative images of freshly isolated mitochondria which were stained with JC-1 to determine the membrane potential in brain and retina of WT and Het. (A) In WT brain (n5), a total of 60102 mitochondria were analysed. In Het brain (n5), in a total of 45930 mitochondria were analysed., where there was no statistical difference in any population observed between WT and Het brain mitochondria. (B) In the WT retina (n5) a total of 69388 mitochondria were analysed. In Het retina (n5) a total of 138309 mitochondria showed no statistical difference in any population observed between WT and Het retinal mitochondria.

Chapter 4 Bioenergetic impairment in *Opa1*^{Q285STOP} mouse

4.1.2.3 Discussion of membrane potential in WT and Het brain and retina

There was no statistical difference observed between WT and Het brain or retina in intact, reduced or mitochondria in transition.

4.2 Determination of ATP in *Opa1*^{Q285STOP} mouse

4.2.1 Introduction

The central nervous system consumes about 20% of inspired oxygen at rest, thus has vast metabolic demand. This demand is met by oxidative phosphorylation within mitochondria. Any impairment in the mitochondrial population serving the tissue specific requirements will result in dysregulation of function. Maintenance of ionic gradients ensuring excitability of neuronal cells requires 60-80% of ATP consumption (Ames 2000). Mitochondria with impaired fusion may harbour damaged matrix content but owing to the *Opa1* mutation, cannot exchange their content. This results in reduced oxidative phosphorylation and available ATP (Kanazawa et al. 2008; Van Bergen et al. 2011; MacVicar and Lane 2014). Recombinant firefly luciferase and its substrate D-luciferin was used to determine ATP in freshly isolated mitochondria.

4.2.1.1 Experimental design of ATP measurements

For the measurement of ATP in the central nervous system of *Opa1*^{Q285STOP} mouse, brain, spinal cord and retinal mitochondria were examined. Mitochondria were isolated from fresh tissue. In cryopreserved tissue, ATP production can be enhanced and may reflect an inaccurate base level (Barksdale et al. 2010). Each reaction was performed in triplicate and were protected from direct light source.

4.2.1.2 Results of ATP measurement in WT and Het

Brain	n	SC	n	Retina	n
F WT	3	F WT	3	F WT	3
M WT	4	M WT	4	M WT	3
F Het	6	F Het	6	F Het	5
M Het	4	M Het	4	M Het	4

Table 4.2 Summary of sample numbers for analysis of ATP in WT and Het

ATP in brain of female WT was 6.25 ± 0.18 nmol/mg. Female Het brain had 6.26 ± 0.50 nmol/mg which was not significantly different to F WT ($p=0.859$). Male WT had 6.76 ± 0.64 nmol/mg

Chapter 4 Bioenergetic impairment in *Opa1*^{Q285STOP} mouse

and male Het had 7.97±1.05 nmol/mg which was not significantly different compared to male WT (p=0.349).

ATP in spinal cord of female WT was 7.78±0.92nmol/mg. Female Het had 8.48 ±0.69 nmol/mg which was not statistically different to female WT (p=0.218). Male WT spinal cord ATP was 8.42±0.73 nmol/mg and male Het SC was 8.01±1.05 nmol/mg which was not statistically different to male WT (p=0.737).

Retinal ATP in female WT was 8.41±1.08 nmol/mg and 7.40±0.90 nmol/mg in female Het which was not significantly different to female WT (p=0.171). Retinal ATP in male WT had 9.34±0.26 nmol/mg and male Het had 9.28±0.19 nmol/mg which was not significantly different to M WT (p=0.969). Figure 4.5 shows a summary of these findings.

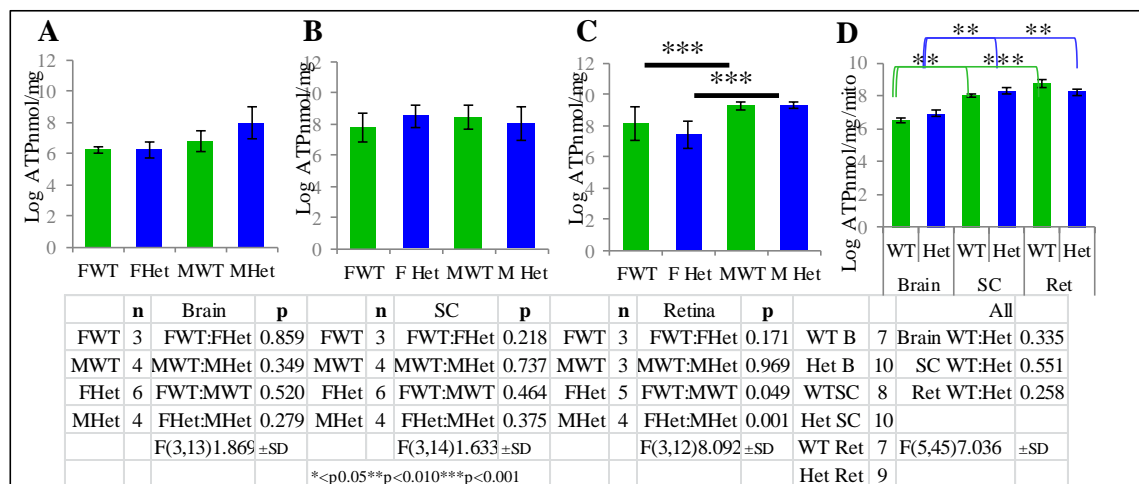


Figure 4.5 ATP measurements in freshly isolated mitochondria of WT and Het

Graph of mean ±SD ATP in isolated mitochondria of WT and Het (A) ATP in brain (B) Spinal cord (SC) and (C)ATP in retina (D) ATP in all WT and Het brain, SC and retina.

The ATP in male Het brain was 18% higher than in male WT brain which was significantly increased (p=0.023). Female Het had less than 1% more compared to female WT. Spinal cord ATP in female Het was 9% higher than in female WT (p=0.029). Male Het spinal cord ATP was reduced by 5% compared to male WT.

Retinal ATP was reduced in female Het who showed 12% reduction although not statistically significant compared to female WT (p=0.118), it was significantly different to male Het

Chapter 4 Bioenergetic impairment in Opa1^{Q285STOP} mouse

(p=0.006) which might suggest that female Opa1 mutation carriers may be more susceptible to impaired ATP production.

The total ATP in female WT was 7.44±1.21 nmol/mg and 7.53±1.15 nmol/mg in female Het which was not significantly different (p=0.860). Total ATP in Male WT was 8.16±1.22 nmol/mg and 8.17 ±1.37 nmol/mg in male Het which was not significantly different (p=0.897). In WT, the male mice had an average 9% more ATP compared to female. In the Het population, the male mice had an average 25% more ATP compared to female Het. The exception in Het tissue was spinal cord where male Het had 6% less ATP compared to female Het spinal cord mitochondria.

4.2.1.3 Discussion of ATP determination in WT and Het mouse

ATP determination in specific tissues of the central nervous system of both wild type and Opa1^{Q285STOP} mouse demonstrated several potentially important findings.

The enhanced ATP in the retina of male Het would suggest that the presence of oestrogen may modulate ATP synthase activity in a tissue specific manner (Moreno et al. 2013). In a WT environment, the presence of oestrogen in retinal specific cell types confers protection (Onishi et al. 2010; Prokai-Tatrai et al. 2013; Wang et al. 2014), however it may offer less advantage in a fusion deficient environment.

Compensatory mechanisms may also influence the effects of fusion deficiency. Up regulation of neuroglobin may confer protection in Opa1 deficient retinal ganglion cells, this may result in increased ATP production within the retina as a direct response to oxidative stress (Lechauve et al. 2012). The association of neuroglobin with cytochrome c in the mitochondrial matrix prevents the apoptotic cascade associated with cytochrome c release into the cytosol (Fiocchetti et al. 2013). Compensatory mechanisms can override ATP reduction by altering specific cellular expression. As previously discussed, Opa1^{Q285STOP} mouse had reduced core temperature. This can initiate uncoupling protein 4 (UCP4) transcription (Yu et al. 2000). As UCP4 is found almost exclusively in mitochondria of neuronal cells (Smorodchenko et al. 2009) and can enhance ATP levels (Ho et al. 2012; Ramsden et al. 2012).

Chapter 4 Bioenergetic impairment in $Opa1^{Q285STOP}$ mouse

The ATP synthase enzyme consists of F₀-F₁ ATP synthase subunits. Oestrogen can bind to a subunit of the F₀-F₁ subunit and modulate its activity (Zheng and Ramirez 1999; Massart et al. 2002). This binding results in the uncoupling of the ATP synthase (Moreno et al. 2013). The presence of oestrogen can confer protection to cerebrovascular mitochondria by increasing their capacity for ATP production (Kemper et al. 2013). The presence of oestrogen receptors on the surface of retinal ganglion cells (Munaut et al. 2001; Kumar et al. 2005; Real et al. 2008) can confer a protective role (Giordano et al. 2011; Hao et al. 2015). Specific oestrogen receptor activity is associated with different functions. The presence of estrogen receptor α (ERG- α) impairs exercise induced skeletal muscle repair (LaBarge et al. 2014). The reduction of ERG- α can promote metabolic and inflammatory responses in hepatic tissue (Hong et al. 2013). Activation of ERG- β is associated with impaired OXPHOS (Manente et al. 2013) and a variety of malignancies (Thomas et al. 2011).

4.3 Electron transport analysis in Opa1^{Q285STOP} mouse

4.3.1 Introduction

Electron transport is the final step in cellular respiration. In the presence of oxygen, electrons are passed by redox reaction along a series of protein units in the lipid membrane of mitochondria. Redox reactions are coupled with the transfer of protons across the membrane which generate a proton gradient in the intermembrane space. The proton gradient provides the proton motive force that drives ADP and inorganic phosphates to ATP via ATP synthase.

Complex I or NADH-Coenzyme Q reductase is the first point of entry of electrons into the electron transport chain. Complex I is made up by 45 different subunits (Lazarou et al. 2007). A total of seven of the subunits of the complex are encoded by mitochondrial DNA, while the remainder subunits are nuclear encoded (Carroll et al. 2006) Complex I oxidises NADH to NAD⁺ by using flavin mononucleotide (FMN) which is an absolute requirement for activity. FMN accepts two electrons and donates them to CoQ. Each electron is passed to coenzyme Q which acts as an electron acceptor. The process allows 4 hydrogen atoms to pass across the membrane into the inter membrane space where they accumulate generating a proton motive force due to the positive charge.

Complex II or succinate dehydrogenase complex is composed of four nuclear encoded subunits containing flavin. Complex II binds FAD to generate FADH₂ which acts as the electron donor passing two electrons individually to coenzyme Q. No protons are transported across the membrane during complex 2 oxidation because the change in energy of the whole reaction is too small to drive protons across the inner membrane.

Complex III is also known as coenzyme Q- cytochrome c oxidoreductase. The complex contains 11 different subunits, one of which is cytochrome c1. Electrons from complex I or complex II are passed to the mobile iron-sulphur protein in complex III called the Rieske protein. This mobile carrier transfers electrons to cytochrome c1. Cytochrome c1 donates these electrons to the mobile carrier cytochrome c. This generates energy for the production of 1

Chapter 4 Bioenergetic impairment in $Opa1^{Q285STOP}$ mouse

molecule of ATP from ADP plus Pi. Four protons are released into the intermembrane space in this reaction.

Cytochrome c is a mobile electron carrier that shuffles between complexes III and IV carrying electrons from complex III and depositing them to the copper binding sites of complex 4.

Complex IV or cytochrome c oxidase is the electron acceptor for cytochrome c. Cytochrome c contains two haem groups (cytochrome a and cytochrome a₃) and two copper proteins (CuA and CuB). The copper sites act as the electron acceptor and carry electrons one at a time to cytochrome a and a₃ respectively. Cytochrome a and a₃ reduce molecular oxygen to water by the addition of electrons. Two protons transverse from the matrix to the inter membrane space and four protons move from the intermembranes space into the matrix

Complex V – ATP synthase catalyses the phosphorylation of ADP in a reaction driven by proton movement across the inner membrane. This causes the synthase motor to spin releasing ATP in exchange for ADP and Pi. Generation of a proton motive force is maintained by the continual transfer of negatively charged hydrogen atoms into the positively charged intermembrane space. The result is an electrochemical gradient of both membrane potential and pH (Mitchell 1974). The pH of the mitochondrial matrix is pH8 and the intermembrane space is pH 7.2. The pH gradient provides the gradient to drive pyruvate import. The voltage gradient drives ADP-ATP exchange and permits the release of ATP. Figure 4.6 shows a schematic version of the electron transport chain.

From a functional aspect the electron chain is organised into supercomplexes where the relevant components reside in close proximity of each other which serves to enhance activity and conserve energy (Hochman et al. 1982; Schäfer et al. 2006; Althoff et al. 2011). The presence of an assembly protein SCAFI (SC) in supercomplex formation of complexes I,III and IV where all three complexes are bound (Lapiente-Brun et al. 2013) is not present in C57Bl/6 mouse strain. ATP production in SC- phenotypes is higher than in SC+. This suggests that by allowing complex IV to act in free form would allow for more diverse functional control in tissues of different metabolic rates (Genova and Lenaz 2013).

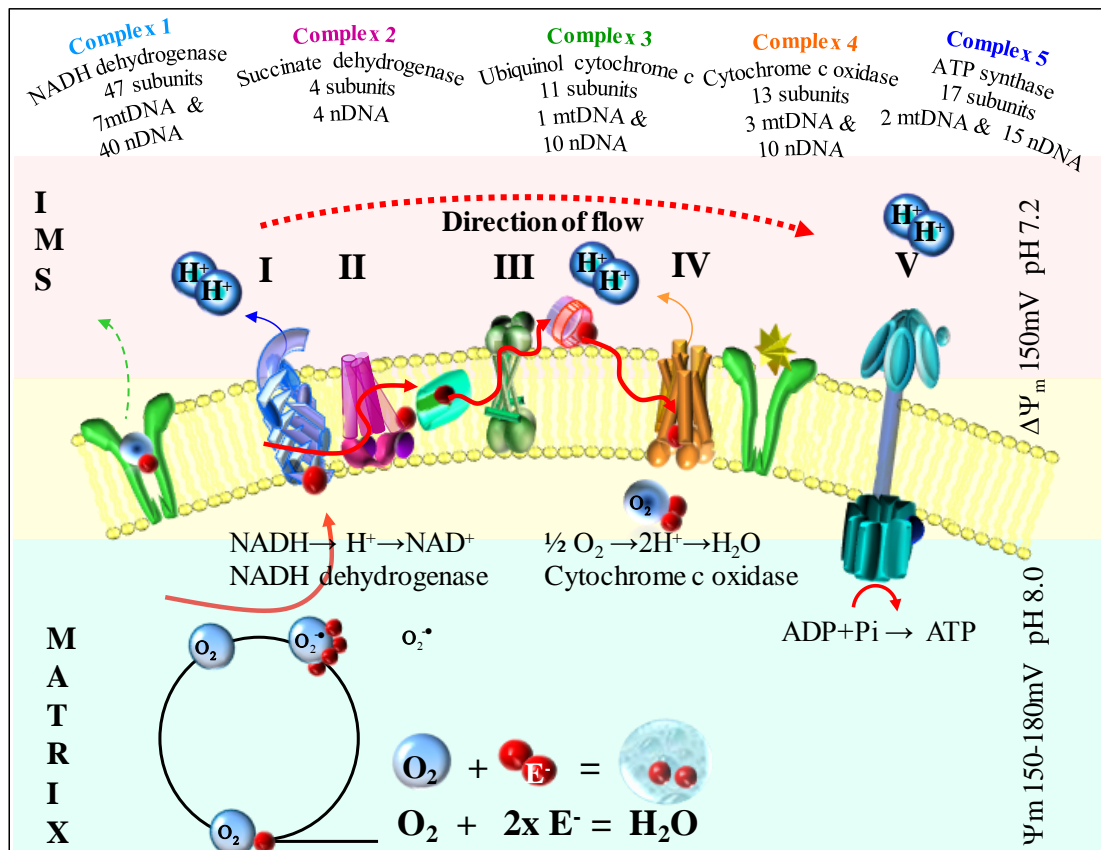


Figure 4.6 Representation of electron transport in the mitochondrial matrix

Schematic of electron flow through the electron transport chain. Complex 1 NADH initiates the reaction by donating two electrons to NADH dehydrogenase. Simultaneously, two protons are pumped out from the matrix to the intermembrane space (IMS). The electrons are passed via coenzyme Q to complex III which transfers them one by one to cytochrome c. Complex III also transfers protons out to the IMS. Complex II donates electrons from FADH_2^+ and passes them to cytochrome c. Cytochrome c is fully mobile and occupies the space between CII and CIII. It passes single electrons to copper sites of complex IV which reduces molecular oxygen to water. A further 4 protons are pumped to the IMS. Complex V F1F0-ATP synthase transfers protons from the IMS which initiates the conversion of $\text{ADP} + \text{P}_i$ to ATP. The red line denotes the path travelled by electrons as they pass through the chain.

Determining the functional ability of individual complexes in *Opa1^{Q285STOP}* mouse was considered vital to the relevance of potential therapy.

4.3.1.1 Experimental design of ETC assays

As analysis of each electron complex required a specific buffer in order to enhance the kinetic performance, mitochondrial were resuspended in a minimum volume of storage buffer (see methods section 2.8), and diluted to the required concentration in the required buffer according

*Chapter 4 Bioenergetic impairment in *Opa1*^{Q285STOP} mouse*

to the assay. In order to perform assays for complex I, II and IV on the same samples, a maximum of eight animals were analysed in any one session. This may have prolonged the final analysis, however it was determined that mitochondria analysed within 14 hours of isolation demonstrated little variation in kinetic performance.

The decision to select complex's I, II and IV and not complex III were two fold. One considered the availability of mitochondria to include in a test run where possible all complex activity would be included. Secondly, the function of complex III is to transfer electrons from ubiquinol to complex IV. Therefore the activity of complex III relies on the functional ability of complex I and complex II. If both complexes I and II were fully functional, complex III might have been considered.

Abbreviations: ETC: electron transport chain, CI, CII, CIV: complex I, complex II complex IV.

Data is shown according to the individual complex presenting brain, spinal cord retina and skeletal muscle from aged matched wild type and Het mice. Each assay is shown with a table of sample sizes, mouse numbers and observations obtained, as one mouse contributed multiple observations in more than two tissue types.

Isolated mitochondria were maintained in storage buffer from the time of isolation throughout the duration of protein analysis which did not exceed 30 minutes. However storage buffer contained 5mM succinate which may have had an adverse effect on complex I activity. Individual rates of activity were plotted against succinate concentrations which did not exceed 0.08028mM in any one sample. There was no significant difference observed for succinate concentration and rate of complex I activity in any samples. Graphs and statistical analysis are in Appendix H. Calculations of substrate oxidation are shown in Appendix H.

4.3.1.2 Results of ETC activity in WT and Het

4.3.1.2.1 Complex I activity in WT and Het

C1 Brain		C1 Retina	
WT	8	WT	9
Het	11	Het	9
C1 SC		C1 Muscle	
WT	10	WT	5
Het	10	Het	5

Table 4.3 Summary of sample numbers for complex I analysis in WT and Het

In order to confirm that the assay was specifically testing the function of NADH oxidation, mitochondria from brain of WT and Het were first analysed for oxidation activity and then the activity of complex I in the presence of 2µM rotenone which was a specific inhibitor of complex I (Horgan et al. 1968) and the assay repeated.

Complex I activity in brain of WT (n=3) mouse oxidised 357±30 nmol/mg. When inhibited with 2µM rotenone WT brain oxidised 32.1±1.5nmol/mg which meant that 91% of the activity was specific to complex 1 and 9% was mediated by other complexes. Het mouse brain (n=3) oxidised 139±6 nMol/mg and when inhibited with rotenone, oxidised 36±2nmol/mg which meant that 74% of the activity observed was specific to complex 1 and 26% was due to other ETC activity.

WT brain oxidised 263±33 nmol/mg. Het brain oxidised 108±6 nmol/mg which was statistically reduced compared to WT (F(7,55) 25.123 p=0.001).

WT spinal cord oxidised 341±54 nmol/mg. Het spinal cord oxidised 83±9nmol/mg which was significantly reduced compared to WT (F (7,55) 89.435, p=0.001). WT retinal mitochondria oxidised 289±14nmol/mg Het retinal mitochondria oxidised 52±17nmol/mg which was significantly reduced compared to WT (F (7,55) 60.655 p=0.001). WT Muscle oxidation of NADH was 155 ±36 nmol/mg.. Het muscle oxidised 95±10nmol/mg which was significantly reduced compared to WT (F (7,55) 66.350 p=0.011).

4.3.1.2.2 Complex II activity in WT and Het

C2 Brain		C2 Retina	
WT	9	WT	9
Het	8	Het	9
C2 SC		C2 Muscle	
WT	7	WT	5
Het	7	Het	5

Table 4.4 Summary of sample numbers for complex II analysis in WT and Het

In order to confirm that the assay was testing the function of succinate dehydrogenase, repeat assays including the complex II inhibitor TTFA (Tapel 1960) at a concentration of 100µM was included in the assay. Complex II activity was analysed for the reduction of DCPIP which acted as an electron acceptor in the presence of succinate. The reaction was followed at 600nm using a UV spectrophotometer. Table 4.4 shows a summary of sample sizes used for the complex II assay.

WT brain (n=3) reduced 47±9µmol/mg. When inhibited with 100µM TTFA, WT brain reduced 0.084±0.036µmol/mg. This meant that 99.8% of the activity observed was specific to succinate dehydrogenase activity and 0.18% was due to other ETC activity. Het brain (n=3) reduced 20±2.5µmol/mg In the presence of TTFA, Het reduced 0.0836±0.014µmol/mg. which meant that 99.6% of the activity was succinate dehydrogenase specific and the remaining 0.42% due to other activity.

Brain mitochondria in WT reduced 50±13µmol/mg. Het brain mitochondria reduced 21 ±6µmol/mg. which was statistically different compared to WT (F(7,48) 55.804, p=0.001). WT spinal cord mitochondria reduced 54±3µmol/mg. Het spinal cord mitochondria reduced 19±7µmol/mg. which was statistically reduced compared to WT (F (7,48) 54.260 p=0.001).

WT retinal mitochondria reduced 128±27µmol/mg. Het reduced 58.3±14µmol/mg was considered significantly reduced compared to WT (F(7,48) 45.570 p=0.001). Muscle mitochondria in WT reduced 39±13 µmol/mg and Het muscle reduced 25±6 µmol/mg which was significantly different compared to WT (F (7,48) 4.374 p=0.025)

4.3.1.2.3 *Complex IV activity in WT and Het*

C4 Brain		C4 Retina	
WT	10	WT	8
Het	11	Het	8
C4 SC		C4Muscle	
WT	9	WT	4
Het	10	Het	5

Table 4.5 Summary of samples numbers for complex IV analysis in WT and Het

Reduced cytochrome c was followed at 550nm and the change in absorbance was observed from reduced to oxidized cytochrome c. Reduced cytochrome c was prepared in batches on at least five separate occasions concurrent with tissue availability. All efforts were made to prevent re-oxidation of reduced cytochrome c by treating buffers with Chelex and saturating solutions with argon gas. Batches of reduced cytochrome c showed variation in the ratio between the oxidized and reduced form. The analysis of kinetics was performed starting from the same concentration of reduced cytochrome c. The initial rate of cytochrome c oxidation by complex IV was used in the analysis.

To confirm that the assay was examining the activity of cytochrome oxidase, inhibition of the complex with 20mM potassium cyanide was performed in each assay.

WT brain (n=3) oxidised $689 \pm 174 \mu\text{mol}/\text{mg}$ of reduced cytochrome c. When inhibited with 20mM KCN, oxidised $0.0506 \pm 0.0109 \mu\text{mol}/\text{mg}$ which meant that 99.9% of the activity observed was specific to cytochrome oxidase. Het brain (n=3) oxidised $926 \pm 36 \mu\text{mol}/\text{mg}$ and in the presence of KCN oxidised 0.0569 ± 0.0001 which meant that less than 0.007% was due to activity other than cytochrome oxidase.

WT brain mitochondria oxidized cytochrome c at $3.26 \pm 0.17 \mu\text{mol}/\text{mg}$. Het brain mitochondria oxidized $2.80 \pm 0.13 \mu\text{mol}/\text{mg}$ which was significantly different to WT (F(7,53) 27.562 p=0.017).

Spinal cord mitochondria in WT oxidised $2.50 \pm 0.11 \mu\text{mol}/\text{mg}$. Het spinal cord mitochondria oxidized $2.68 \pm 0.18 \mu\text{mol}/\text{mg}$ which was not significantly different compared to WT (p=0.203).

Retinal mitochondrial oxidation of cytochrome c in WT was $2.39 \pm 0.09 \mu\text{mol}/\text{mg}$ and Het retinal mitochondria oxidised $0.968 \pm 0.06 \mu\text{mol}/\text{mg}$ which was considered statistically different to WT

Chapter 4 Bioenergetic impairment in *Opa1*^{Q285STOP} mouse

(F(5,34) 8.631 p=0.001). Muscle oxidation of cytochrome c in WT was 2.56 ± 0.06 $\mu\text{mol}/\text{mg}$. Het muscle oxidised 1.63 ± 0.34 $\mu\text{mol}/\text{mg}$ which was statistically different compared to WT (F 7, 53) 13.864 p=0.001). Figures 4.7-4.9 show the kinetics of these reactions. Figure 4.10 shows a graphical representation of the results.

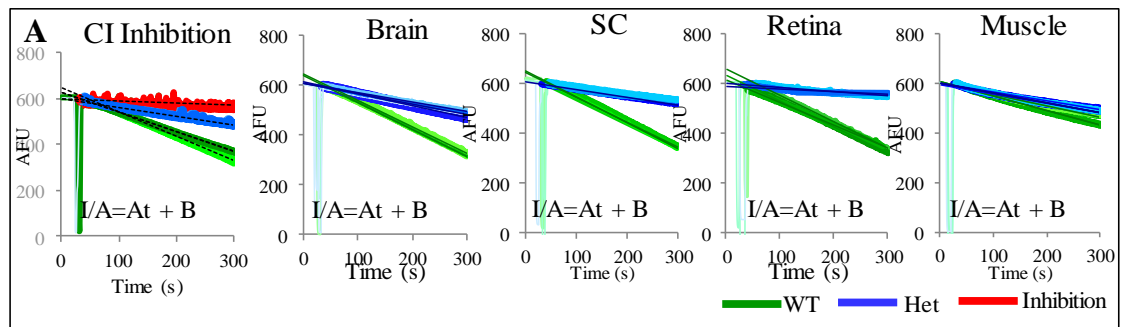


Figure 4.7 Kinetic activity of complex I in isolated mitochondria of WT and Het

Representative kinetics of complex I activity in isolated mitochondria of WT and Het

(A) Complex I activity was followed at 460nm using fluorescence spectrophotometry. Inhibition of complex I in the presence of 30 $\mu\text{g}/\text{ml}$ mitochondria with 100 μM NADH, 1mM KCN, 40 μM CoQ₁ and 20mM rotenone confirmed the specificity of the assay for NADH dehydrogenase activity. In the presence of 100 μM NADH, 1mM KCN, and 40 μM CoQ₁ and 30 $\mu\text{g}/\text{ml}$ of mitochondrial proteins, the reduction in NADH fluorescence from brain, SC, retina and skeletal muscle in WT and Het was fitted with a straight line.

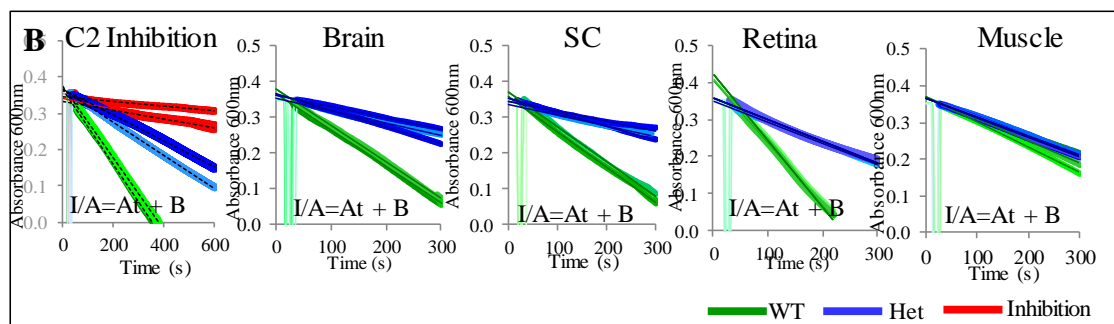


Figure 4.8 Kinetic activity of complex II in isolated mitochondria of WT and Het

Representative kinetics of complex II succinate dehydrogenase activity in WT and Het

(B) Complex II reduction of DCPIP: complex II in the presence of 100 μM TTFA confirmed that 99.8% of the reaction was specific to the activity of succinate dehydrogenase. Complex II was followed at 600nm in the presence of 10mM succinate, 100 μM decylubiquinone, 2mM KCN and 16 μM DCPIP. The reduction in absorbance in the presence of mitochondrial protein from 50 $\mu\text{g}/\text{ml}$ brain, SC, retina and skeletal muscle in WT and Het. was fitted with a straight line.

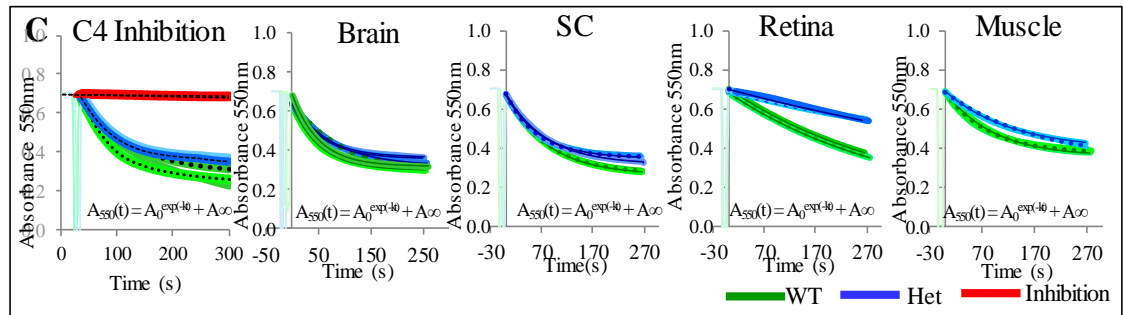


Figure 4.9 Kinetic activity of complex IV in isolated mitochondria of WT and Het

Representative kinetics of complex IV cytochrome oxidase activity in WT and Het

(C) Complex IV oxidation of reduced cytochrome *c*: complex IV in the presence of 20mM KCN confirmed that 99.9% of the reaction was specific to the activity of cytochrome oxidase. Complex IV activity was followed in samples equilibrated with air at room temperature (21-23°C) by monitoring absorbance at 550nm in the presence of reduced cytochrome *c* at concentrations close to 100 μM. The rate of absorbance decay in the presence of mitochondrial protein from 50μg/ml brain, SC, retina and skeletal muscle in WT and Het was fitted by an exponential decay starting from 29.9-31.9mM concentration of the reduced form of cytochrome *c*. The initial rate of oxidation was used in the analysis of complex IV.

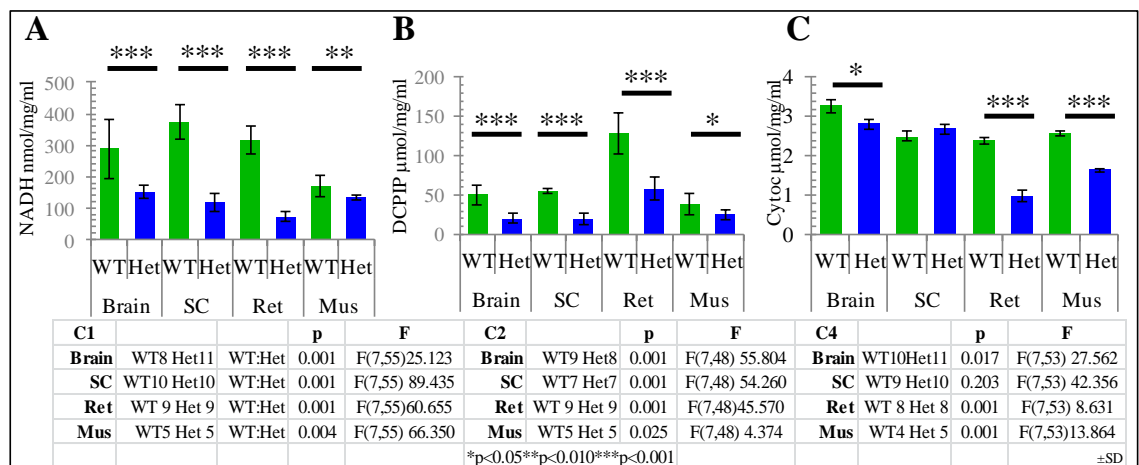


Figure 4.10 Bioenergetic assays in isolated mitochondria of WT and Het

*Graphs showing the mean ±SD of bioenergetic assays performed in isolated mitochondria of 15 month WT and Het brain, spinal cord (SC), retina(Ret) and skeletal muscle(Mus) showing (A) Complex I activity using 30μg mitochondria/ml compared the oxidation of NADH in WT and Het. (B) Complex II activity in 50μg/ml of isolated mitochondria compared the rate of reduction of DCPIP. (C) Complex IV activity compared the rate of oxidation of reduced cytochrome *c* in 50μg/ml of isolated mitochondria from WT and Het.*

Chapter 4 Bioenergetic impairment in *Opa1^{Q285STOP}* mouse

As the Het population demonstrated a reduction in activity across the range, the ratio of complex activity between tissues was examined in brain spinal cord and retina. The total oxidation for each complex was calculated and the ratio of each according to tissue type calculated. Table 4.2 summarises these findings.

Table 4.6 Ratio of complex activity in mitochondria of CNS in WT and Het

	Brain		SC		Ret	
CI	WT8	Het11	WT10	Het10	WT9	Het9
Ave	29±8	45±5	38±7	33±6	33±7	22±6
WT:Het		0.017		0.685		0.597
	F(5,48)2.144					
CII	WT9	Het8	WT9	Het9	WT9	Het9
Ave	21±3	21±5	23±5	19±6	56±10	60±1
WT:Het		0.675		0.626		0.779
	F(4,40)45.389					
CIV	WT10	Het11	WT9	Het10	WT8	Het8
Ave	41±6	43±4	30±5	42±6	29±2	15±2
WT:Het		0.278		0.001		0.001
	F(5,46)38.685					

The table shows the ratio of the percentage of total activity for each complex in the CNS of WT and Het. The p value represents the statistical significance between pairs.

In mitochondria from the CNS, the ratio of complex I activity in WT was highest in the spinal cord at 38%. Het complex I ratio in spinal cord mitochondria did not differ significantly compared to WT with 33% (p=0.578). The ratio of complex II activity was highest in both WT with 56% and Het with 60% in retinal mitochondria. The ratio of complex IV activity in WT was highest in brain with 41% and in Het was 43% which was not significantly different (p=0.822).

4.3.1.3 Discussion of ETC activity in WT and Het

In Het mouse, there was a 54% reduction of mitochondrial complex I activity compared to WT. Het brain mitochondria had a 48% reduction, spinal cord mitochondria 69%, and retinal mitochondria 77% and skeletal muscle mitochondria 22%.

Compared to WT, complex II activity in Het mitochondria was reduced by 53%. Brain showed a reduction of 54%, spinal cord of 65%, and retina of 55% and skeletal muscle of 35%.

Compared to WT, complex IV activity in Het CNS mitochondria was reduced by 26%. Het brain mitochondria had a 14% reduction, retina had 60% and skeletal muscle 36% reduction. Spinal cord showed a 7% increase.

Chapter 4 Bioenergetic impairment in *Opa1^{Q285STOP}* mouse

Mitochondrial tissue specific changes were observed for ETC activity compared to WT where brain had a 40% reduction; spinal cord showed a 42% reduction, retina a 64% reduction and skeletal muscle a 31% reduction. These findings are summarised in Figure 4.11 with a summary of percent reductions in each complex.

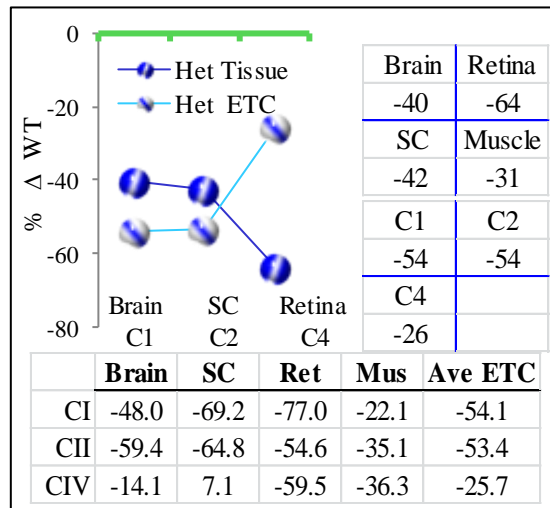


Figure 4.11 ETC and tissue specific changes in Het mouse

Line graph showing Het percent changes of electron transport in individual complex's and in specific tissues. The green line represents WT values. All complex's showed a significant reduction in activity. All three CNS tissues showed reduced ETC activity with retina showing the biggest loss. The lower box shows the percentage reduction in each complex for each tissue type.

The net function of electron transfer is to generate sufficient ATP to maintain cellular function. How this is maintained will depend on the requirements of the cell and the environment it survives in. The mitochondrial threshold effect suggests that cells have the ability to challenge a reduction in ETC activity up to their threshold. When this is reached, the viability of the cell is compromised (Letellier et al. 1994; Rossignol et al. 1999). The value of the threshold for any given complex depends on the tissue type and the metabolic demand. For example, the threshold value in rat brain for complex I activity is 50.3 ± 7 . The skeletal muscle of rat for complex I is 74.5 ± 5 . Complex IV threshold in rat brain is 87.8 ± 4 and 66.8 ± 4 in skeletal muscle (Rossignol et al. 1999). Considering the physical activity of the average laboratory rat, the threshold values in skeletal muscle appear high. This might suggest a genetic component is responsible for setting the threshold value during development (Faustin et al. 2004). The threshold values in specific cell types may be adjusted to circumvent the bioenergetic deficits before they become established (Rocher et al. 2008).

The ratio of complex specific activity in skeletal muscle for WT and Het showed that WT had the same ratio of complex I, complex II and complex IV. Het skeletal muscle maintained this

Chapter 4 Bioenergetic impairment in *Opa1^{Q285STOP}* mouse

same ratio albeit at a reduced percentage. Table 4.7 shows a summary of the ratio of complex activity in skeletal muscle mitochondria

Table 4.7 Ratio of complex activity in skeletal muscle mitochondria in WT and Het

Skeletal muscle Ratio					
CI		CII		CIV	
WT 5	Het5	WT 5	Het5	WT 4	Het5
25±1	20±2	25±4	20±3	25±2	20±1
	0.022		0.036		0.255
F(5,17) 11.87		F(5,17) 1.87		F(5,16) 13.55	

The table shows the ratio of the percentage of total complex activity for isolated skeletal muscle mitochondria in WT and Het. The same ratio of activity was present in both WT and Het except the ratio of complex I and complex IV was significantly reduced in Het muscle

The bioenergetic activity of Het cardiac muscle was shown to have a significant reduction in complex I and complex IV activity with complex II not demonstrating any significant difference (Chen et al. 2012). Considering the bioenergetic threshold for both cardiac and skeletal muscle the difference in complex II mediated activity can be explained.

Both cardiac and skeletal muscle are striated however cardiac muscle is involuntary and under the control of the medulla. Cardiac mitochondria fill about 25% of the cell and use aerobic respiration exclusively. The metabolic by-products are CO₂ and water which do not adversely affect function.

Skeletal muscle is under voluntary control and the bioenergetic demands will depend on the amount of physical activity. Skeletal muscle mitochondria reside between sarcomeres fill about 2% of the cell. As skeletal muscle contains different myosin isoforms, and each has its own oxidative potential, both high and low oxidative potentials exist in the same tissue. They utilise a combination of oxidative phosphorylation and anaerobic oxidation resulting in an accumulation of lactic acid which imposes restrictions on function. Finally, the examination of cardiac mitochondrial function in *Opa1^{Q285STOP}* mouse may have been influenced by the use of inhalation anaesthetic. Het mouse underwent a surgical procedure (thoracotomy for haemodynamic measurement) requiring general anaesthetic. Inhalation anaesthetics commonly used in mouse surgery are ketamine/xylazine and isoflurane. The activity of these anaesthetics has been shown to cause reduced complex I activity (Yan and Sohal 1998; Schenkman and Yan 2000; Hanley et al. 2002). Post anaesthetic mitochondrial recovery is delayed due to alternations

Chapter 4 Bioenergetic impairment in Opa1^{Q285STOP} mouse

of the biosensor function in mitochondria. Alternations in calcium flux can occur (Branca et al. 1988). This can be induced by altered lipid composition (Dekutovich and Kargapolov 1986).

Tissue retrieval in both WT and Het did not employ any anaesthetic agents and the activities of all mitochondria were considered to reflect an accurate analysis of true function at 15 months.

Opa1^{Q285STOP} mouse demonstrated a 54% reduction in complex I activity. Tissue specific reduction was observed in retina, spinal cord, brain and skeletal muscle in order of ascending reduction. Because complex I is central to energy production in the cell, its malfunction results in a wide range of disorders in cells with increased ATP requirements. Both neurological and neuromuscular impairment were observed during phenotyping. It would appear Het mouse had reached a critical threshold for complex I activity.

Acquired complex I dysfunctions are associated with many disorders. Unlike inherited disorders of complex I where particular mutations result in specific disease, acquired complex I dysfunction can be the cause or the result of a host of disorders. The mitochondrial threshold effect possibly determines whether symptoms arise from such impairment.

Aging can contribute to reduced activity. In aged rats, reduced complex I activity was associated with poor neuromuscular performance. This in turn was associated with changes in mitochondrial size where the percentage of small mitochondria in brain was higher in young than in old animals, whereas the opposite occurred for large mitochondria (Sastre et al. 1998).

Mitochondrial morphology helps to support the requirements of threshold maintenance. Impaired mitochondrial dynamics lead to defects in oxidative phosphorylation (Parone et al. 2008). In an Opa1 knockout, brain mitochondria exhibited a dose-dependent reduction in oligomeric OPA1 which was accompanied by parallel increases in non-oligomeric OPA1 isoforms. There were morphological alternations in mitochondrial sizes where increased mitochondria with a length of >3µM considered as elongated were identified and no change in mitochondria smaller than 0.5 µM considered as fragmented (Ramonet et al. 2013).

Reduced electron transport function may initiate a pro survival response to stress in impaired mitochondria resulting in hyperfusion (Gomes et al. 2011; Rolland et al. 2013). If the fusion machinery is impaired, then other mechanism may intervene.

Chapter 4 Bioenergetic impairment in *Opa1*^{Q285STOP} mouse

The formation of supercomplexes within healthy mitochondria may help to support the necessary requirements in fusion deficient mice. A form of mitochondrial hypertrophy has recently been suggested as a compensatory mechanism (Sgarbi et al. 2014). In a different mouse model of ADOA, *Opa1*^{del Δ g} mouse, it was observed at 5 months that an accumulation of complex III and IV monomers coincided with a reduction in supercomplexes (Sarzi et al. 2012). As the absence of SCAF1 protein in C57Bl/6 has already been established, the 'loss' of supercomplexes would not be associated with disease pathology in this mouse model.

The bioenergetic deficits observed in *Opa1*^{Q285STOP} mouse were compared to the previous literature on *Opa1* reduction. Lymphocytes isolated from human ADOA showed reductions in complex I and complex II (Van Bergen et al. 2011). In mouse models of ADOA, skeletal muscle mitochondria showed a combined reduction in both complexes I and IV. (Sarzi et al. 2012). However this is an accelerated age onset disorder. Complex I deficiencies were also observed in fibroblast cultures of ADOA patients (Chevrollier et al. 2008).

A significant finding was that despite the reduction in Het bioenergetic activity, the ratio of electron transfer within complexes was preserved for all tissue of the CNS. Considering that individual complexes are part of a chain, maintaining the correct ratio of activity between complexes may be more important than the preservation of individual complex activity. As C57Bl/6 mouse has the versatility of SCAF- mitochondrial environment it may confer the advantage of mobility (Lapunte-Brun et al. 2013).

Dietary intake may influence electron transport. Polyunsaturated n-3 fatty acids are prone to oxidative damage. Investigating a mouse model that can synthesize its own n-3 fatty acid revealed impaired complex 1 activity with reduced H₂O₂ production which was due to a decrease in ROS production from ETC complex I (Hagopian et al. 2010). As *Opa1*^{Q285STOP} mouse received a daily intake of 2.1% polyunsaturated (Ω 3: Ω 6 ratio of 1:5) this could potentially put them at risk of oxidative damage.

In a type II diabetic mouse model *ob/ob* mouse, both the activity and gene expression of mtDNA complex I components are reduced. Peroxynitrite induced degradation of complex I

Chapter 4 Bioenergetic impairment in *Opa1*^{Q285STOP} mouse

subunits or reduced synthesis of complex I subunits was ascribed to be the cause (García-Ruiz et al. 2010).

In Parkinson Disease (PD) there is a profound reduction of complex I activity (Schapira et al. 1990) which has been linked to the kinase domain Pink 1 which is responsible for the phosphorylation status of the complex (Morais et al. 2009).

The role of electron transfer in the neuropsychiatric disorder autism has demonstrated reduced complex I activity by 31% (Gu et al. 2013). Stress can also influence complex I activity (Madrigal et al. 2001).

Reactive nitrogen species (RNS) may also have a significant impact on complex I activity. The conversion of nitric oxide (NO) to a more reactive derivative (RNS) can have major implications on electron transfer function. NO can cause reversible inhibition of cytochrome oxidase by competing with oxygen (Brown and Borutaite 2001). Peroxynitrite can inhibit complex I, (Brown and Borutaite 1999), complex II, and complex IV and MnSOD (Cassina and Radi 1996).

ATP production depends on the efficiency of OXPHOS energy conservation (Cocco et al. 2009). How efficient the ETC chain is depends on the permeability of the inner membrane and the pumping efficiency of complexes. Peroxynitrite can also induce the mitochondrial permeability transition pore (Packer and Murphy 1994; Borutaite et al. 1999). The precise mechanism for complex I inhibition could be nitration of tyrosine residues, modification of NADH or FMN (Gadelha et al. 1997).

The compensatory mechanisms that may override a complex mediated deficiency would by nature of the electron transfer chain be limited to the extent of the deficiency. As complex IV requires electron donations from either complex I or II, a reduction in one or both will eventually impact complex IV activity. Cellular compensation may attempt to reduce the ATP requirement by minimising function. The inability to adapt would ultimately result in cell death.

4.4 Mitochondrial related proteins in Opa1^{Q285STOP} mouse

4.4.1 Introduction to mitochondrial related proteins

The data from extracted mitochondria may only be considered a version of the events that are occurring within the cell. Tissue handling and processing although kept to minimum will alter the final result. Homogenization of tissues results in the release of proteases and apoptotic caspases, with the final event yielding reduced protein content. Immunohistochemistry is a method designed to avoid excess structural alternation and maintain the integrity of cellular content. Tissue sections of retina and brain can be probed using a variety of established antibodies which can then be quantified according to immunofluorescence intensity. This also permits the localization of proteins of interest within the tissue architecture. The antibodies that were used in this study are detailed.

4.4.1.1.1 VDAC expression

Voltage gated anion channel 1 (VDAC) is a global regulator of mitochondrial function (Lemasters and Holmuhamedov 2006). It provides permeability between the inner membrane space and the cytoplasm and permits the transport of small hydrophilic molecules including substrates for respiration (Maldonado and Lemasters 2014). At reduced $\Delta\Psi_m$ VDAC remains in an open state (Mannella and Kinnally 2008). VDAC can also participate to mitochondrial membrane permeabilization, an apoptotic checkpoint in stress and pathological conditions. By altering its conductance, VDAC can inhibit apoptosis (Duan et al. 2003; Shoshan-Barmatz et al. 2010) It is an important regulator of mitochondrial calcium.

4.4.1.1.2 Neuroglobin expression

Neuroglobin is a member of the oxygen carrying globin family that has a higher affinity for oxygen than haemoglobin (Kiger et al. 2011). It is found throughout the CNS including the CSF (Casado et al. 2005) and retina (Schmidt et al. 2003; Lechaue et al. 2012). Complex I impaired Harlequin mouse recently were shown to have a twofold reduction in neuroglobin expression with optic atrophy and RGC loss. Intravitreal injections of a Neuroglobin construct returned complex I activity and prevented RGC and axon loss (Lechaue et al. 2014).

Neuroglobin can inhibit apoptosis by interacting with cytochrome c preventing its release to the cytoplasm (Fiocchetti et al. 2013).

4.4.1.1.3 *Preli expression*

The Preli gene encodes a member of the late embryogenesis abundant (Lea) motif-containing protein family. The encoded protein is localized to mitochondria (Sesaki et al. 2006). Preli ensures the accumulation of cardiolipin by acting as a transporter of phosphatidic acid (PA) which is a requirement for cardiolipin synthesis (Hall et al. 1987; Potting et al. 2010). The cellular adaptive response through cristae remodelling is due to the interaction of preli with Opa1 (McKeller et al. 2010). This interaction is responsible for maintaining the negative curvature of the membrane especially at sites of membrane fusion (Renner and Weibel 2011; Chan and McQuibban 2012) (See Figure 4.12). Opa1 regulation of cristae is independent of fusion function. Substrate availability determines the mitochondrial architecture which is determined by Opa1 (Patten et al. 2014).

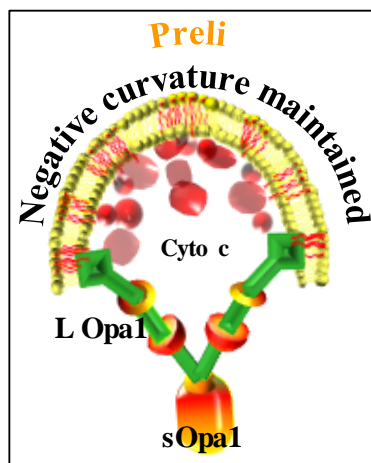


Figure 4.12 Preli associated Opa1 maintenance of cristae structure

Preli enhances Opa1 sequestration of cytochrome c by allowing tight curvature in the membrane. This also enhances fusion.

The interaction of Preli with Opa1 upholds mitochondrial $\Delta\Psi$ and enhances respiratory chain function. The increased cardiolipin content increases the fluidity of the inner mitochondrial membrane (Verstraeten et al. 2005; Unsay et al. 2013). This permits respiratory complexes to move into closer proximity to each other enhancing function (Mileykovskaya and Dowhan 2014; Paradies et al. 2014). Figure 4.13 summarises some of the known functions of these proteins.

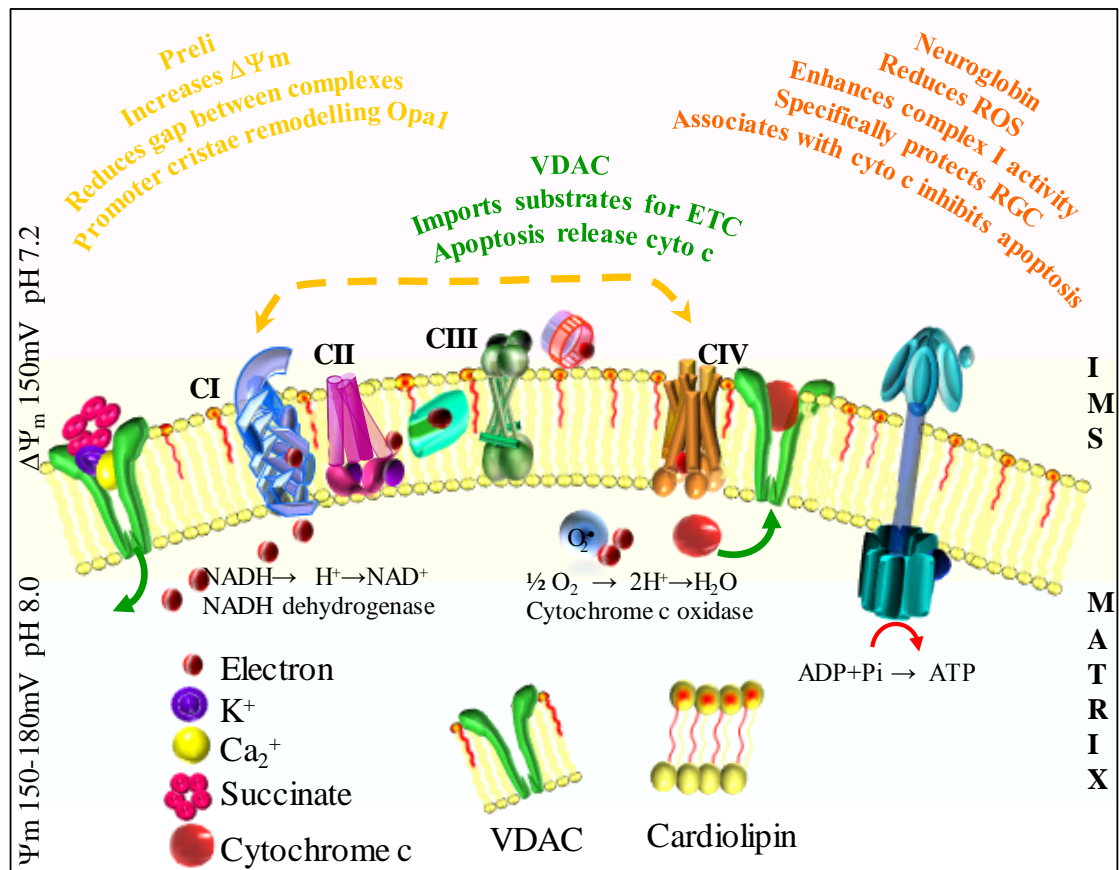


Figure 4.13 Mitochondrial related protein activity in mitochondria

Schematic summarises some of the known functions of VDAC, Neuroglobin and Preli proteins and the impact of expression on mitochondrial size shape function bioenergetics and control of apoptosis.

4.4.1.1.4 PSD95 expression

PSD95 is a scaffold protein found at post synaptic glutamate receptors where it provides anchorage and support to the vertical filaments at the post synaptic domain. PSD95 interacts with the cytoplasmic tail of NMDA receptor subunits and shaker-type potassium channels (Eldstrom et al. 2002). PSD95 is involved in synaptic plasticity (Meyer et al. 2014). Overexpression or depletion of PSD95 changes the ratio of excitatory to inhibitory synapses in neurons. The pruning of dendritic branches is paralleled by a significant elevation in synaptic expression of PSD95 (Bustos et al. 2014). This inverse correlation has also been seen in RGC of both rabbit and mouse (Jakobs et al. 2008; Chen and Chiao 2014).

Chapter 4 Bioenergetic impairment in Opa1^{Q285STOP} mouse

4.4.1.1.5 Neurofilament expression

Neurofilaments (NF) are a neuronal cytoskeleton proteins with a diameter of 10nm and are abundant in the axons of neurons. They are essential for the maintenance of axon calibre and the transmission of electrical impulses along axons (Eyer and Peterson 1994; Yum et al. 2009). NF-H is present in brain but not in all retinal ganglion cell axons (Ruiz-Ederra et al. 2004).

An excess of NF-H can result in a reduction of dendritic branching (Sánchez et al. 1996). A pathological accumulation of neurofilament has been implicated in several diseases including Charcot-Marie-Tooth (CMT) (Abe et al. 2009), Spinal muscle atrophy (SMA) (Perrot and Eyer 2009; Liu et al. 2011), Alzheimer and Parkinson's disease (Szaro and Strong 2010).

4.4.2 Experimental design of mitochondrial related proteins4

Using a variety of antibodies, mitochondrial proteins were investigated. In order to evaluate the significance of staining intensity, profiles were established where specific functions were considered- mitochondrial specific, compensation, and damage mediated. Mitochondrial specific antibodies were Opa1 and VDAC; compensatory proteins were Preli and Neuroglobin. Damage mediated proteins were PSD95 and neurofilament.

4.4.3 Results of mitochondrial related protein expression in the retina

Table 4.8 shows a summary of AFU in retinal layers for Opa1, VDAC and Preli. Table 4.9 shows a summary for Neuroglobin, PSD95 and NF L expression in WT and Het. Figure 5.6 and Figure 5.7 shows graphs representing AFU in retinal layers of WT and Het.

Table 4.8 Opa1,VDAC and Preli expression in retinal sections of WT and Het

A	Opa1	PRL		ONL		OPL		INL		IPL		GCL	
		WT5	Het6	WT5	Het6	WT5	Het6	WT5	Het6	WT5	Het6	WT5	Het6
Ave		192	96.4	256	98.8	258	130	224	71.1	281	89	187	77.7
SEM		39.3	26.8	52.6	37.6	73	26.3	79.2	11.9	41.8	29.2	30.5	10.3
WT:Het		0.241		0.024		0.006		0.177		0.022		0.008	
		F (5,15) 3.865		F (5,15) 4.390		F (5,15) 2.751		F (5,15) 5.463		F (5,15) 9.729		F (5,15) 3.971	
B	VDAC	PRL		ONL		OPL		INL		IPL		GCL	
		WT5	Het6	WT5	Het6	WT5	Het6	WT5	Het6	WT5	Het6	WT5	Het6
Ave		91.9	555	273	944	184	526	215	890	181	747	404	798
SEM		15.9	88	25.1	23.5	19.6	81.9	26.5	66.1	25.7	67.6	30.6	65.8
WT:Het		0.005		0.769		0.023		0.008		0.010		0.031	
		F (5,15) 10.47		F (5,15) 1.380		F (5,15) 6.747		F (5,15) 1.028		F (5,15) 1.146		F (5,15) 0.441	
C	Preli	PRL		ONL		OPL		INL		IPL		GCL	
		WT5	Het6	WT5	Het6	WT5	Het6	WT5	Het6	WT5	Het6	WT5	Het6
Ave		366	255	17	186	194	144	110	120	122	215	213	99
SEM		120	71	4	113	63	58	16	43	37	106	61	30
WT:Het		0.386		0.520		0.004		0.898		0.027		0.003	
		F (5,21) 21.466		F (5,21) 1.843		F (5,15) 5.851		F (5,15) 4.645		F (5,15) 1.132		F (5,15) 3.626	

Table shows the mean (\pm SEM) of (A) *Opa1*, (B) *VDAC* and (C) *Preli*, expression in retinal layers of WT and Het. Statistical difference between groups is represented by the p value

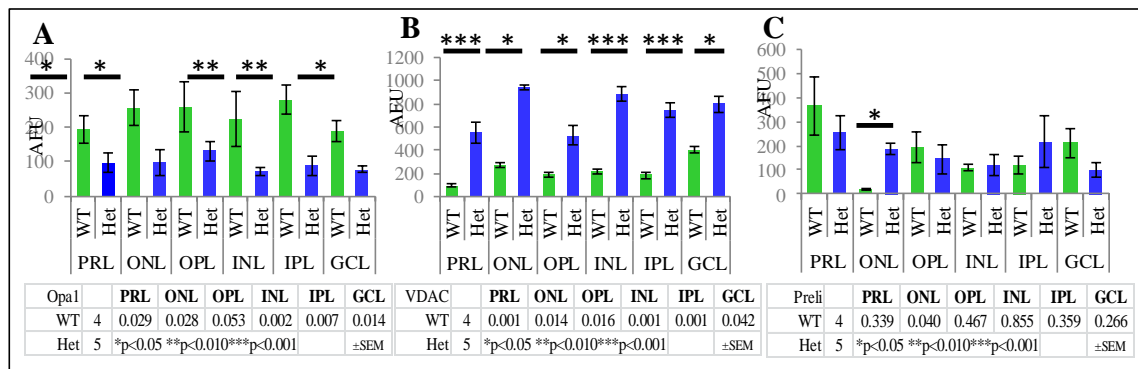


Figure 4.14 Retinal mitochondrial related protein expression: Opa1, VDAC and Preli

Graphs show the mean \pm SEM AFU of (A) *Opa1*, (B) *VDAC* and (C) *Preli* expression in retinal sections of WT and Het.

Retinal protein expression in Het was compared to WT. Het *Opa1* protein expression was reduced by 59% compared to WT. The INL showed the highest reduction of protein expression with a 68% reduction which was statistically different compared to WT (F(5,13) 1.191 p=0.002). *VDAC* expression was increased by 277% in Het retina. The PRL had the highest percentage increase with 504% which was statistically increased compared to WT (F(5,12) 6.623 p=0.001).

Table 4.9 Neuroglobin, Neurofilament and PSD95 expression in WT and Het retina

	PRL		ONL		OPL		INL		IPL		GCL	
D Neuro	WT5	Het6	WT5	Het6	WT5	Het6	WT5	Het6	WT5	Het6	WT5	Het6
Ave	228.1	250.5	218.1	349.2	170.2	129.8	163.3	259.3	180.9	90.4	71.3	64.8
SEM	52.3	38.1	99.9	39.0	54.2	20.8	81.3	21.3	80.6	35.0	36.4	23.2
WT:Het	0.384		0.722		0.701		0.634		0.846		0.503	
	F (5,20) 1.530		F (5,20) 0.784		F (5,20) 0.969		F (5,20) 0.896		F (5,20) 1.654		F (5,20) 0.838	
	PRL		ONL		OPL		INL		IPL		GCL	
E PSD95	WT5	Het6	WT5	Het6	WT5	Het6	WT5	Het6	WT5	Het6	WT5	Het6
Ave	90.5	267.0	37.8	162.0	84.4	239.0	24.5	82.8	40.3	211.0	34.0	92.9
SEM	10.2	24.2	10.3	32.0	24.6	2.3	11.3	11.2	18.1	15.8	26.4	15.6
WT:Het	0.314		0.292		0.75		0.272		0.122		0.346	
	F (5,28) 1.900		F (5,28) 1.176		F (5,28) 4.913		F (5,28) 2.091		F (5,28) 2.78		F (5,28) 1.762	
	PRL		ONL		OPL		INL		IPL		GCL	
F NF L	WT5	Het6	WT5	Het6	WT5	Het6	WT5	Het6	WT5	Het6	WT5	Het6
Ave	112.0	128.0	165.0	168.0	99.2	182.0	57.1	140.0	195.0	173.0	443.0	405.0
SEM	13.2	56.5	87.1	54.8	3.6	70.4	11.7	42.0	28.3	54.7	37.6	105.0
WT:Het	0.020		0.536		0.059		0.452		0.740		0.038	
	F (5,23) 8.530		F (5,23) 1.280		F (5,23) 4.219		F (5,23) 3.493		F (5,23) 7.706		F (5,23) 2.512	

Table shows the mean (\pm SEM) of (D) Neuroglobin, (E) PSD95 and (F) Neurofilament expression in retinal layers of WT and Het. Statistical difference between groups is represented by the p value.

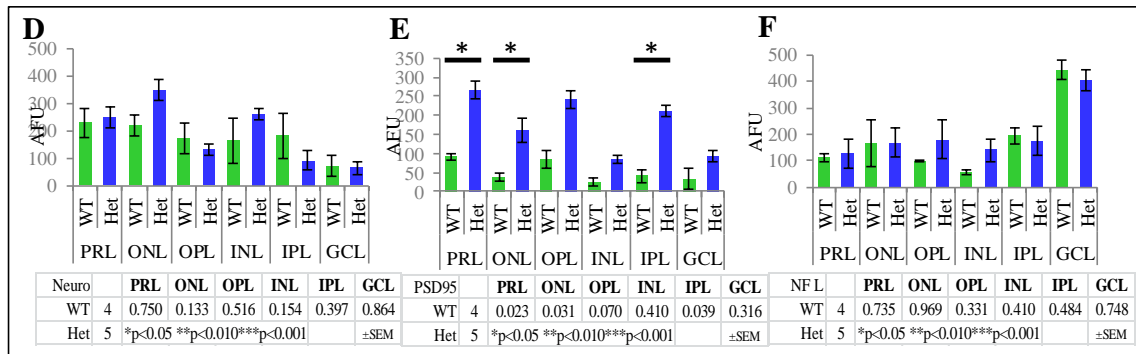


Figure 4.15 Retinal mitochondrial related protein expression untreated WT and Het

Graphs show the mean \pm SEM AFU of (D) Neuroglobin (E) PSD95 and (F) NF L expression in retinal sections of WT and Het.

Het retina showed Preli expression was reduced by 3% compared to WT. The GCL had a significant 54% reduction which was statistically reduced compared to WT (F(5,14) 0.561 p=0.026). Neuroglobin expression in Het retina was increased by 8%. The ONL had the highest percentage increase with 59 % (p=0.133).

PSD95 expression in Het retina was increased by 257% compared to WT. The IPL showed a significant 423% increase (F(5,12) 2.052 p=0.039) compared to WT. Neurofilament light chain expression was increased by 37% compared to WT. The OPL had a significant increase with 83% more than WT (F(5,12) 5.578 p=0.031).

Chapter 4 Bioenergetic impairment in *Opa1^{Q285STOP}* mouse

In order to identify which retinal layers were specifically targeted for the activities examined, the combined AFU were re-examined. Table 4.10 shows a summary of these data and Figure 4.16 shows graphs representing the AFU from all mitochondrial, compensatory and damage related proteins in WT and Het retinal layers.

Table 4.10 Targets in the Het retinal layer

A	Mito	PRL		ONL		OPL		INL		IPL		GCL	
		WT5	Het6	WT5	Het6	WT5	Het6	WT5	Het6	WT5	Het6	WT5	Het6
	Ave	637	985	556	383	498	379	411	355	691	663	702	458
	SEM	85.3	140	97.9	67.8	63	54.8	65.7	63.2	124	148	118	87.4
	p		0.366		0.044		0.531		0.090		0.067		0.683
		F(5,69) 5.364		F(5,69) 3.036		F(5,69) 2.201		F(5,69) 1.791		F(5,69) 3.187		F(5,69) 3.187	
B	Comp	PRL		ONL		OPL		INL		IPL		GCL	
		WT	Het	WT	Het	WT	Het	WT	Het	WT	Het	WT	Het
	Ave	414	500	344	403	333	391	198	378	288	395	298	362
	SEM	57.6	58.1	62.9	53.8	58.2	54.3	33.7	55.1	63.4	69.8	55.8	73.7
	p		0.074		0.002		0.250		0.005		0.014		0.376
		F(5,78) 2.133		F(5,78) 0.851		F(5,78) 0.705		F(5,78) 2.759		F(5,78) 1.570		F(5,78) 0.961	
C	Dam	PRL		ONL		OPL		INL		IPL		GCL	
		WT	Het	WT	Het	WT	Het	WT	Het	WT	Het	WT	Het
	Ave	342	571	253	232	307	378	160	203	264	313	278	392
	SEM	47.4	50.7	24.9	45.4	34.9	45.2	28.6	51.8	34.5	58.6	37.6	56.2
	p		0.046		0.370		0.006		0.001		0.110		0.485
		F(5,81) 0.741		F(5,81) 2.097		F(5,81) 0.948		F(5,81) 1.660		F(5,81) 1.198		F(5,81) 1.321	

The table shows the mean \pm SEM of AFU for all (A) mitochondrial (B) compensatory and (C) damage mediated protein activities in retina of WT and Het. The statistical difference between groups is represented by the p value.

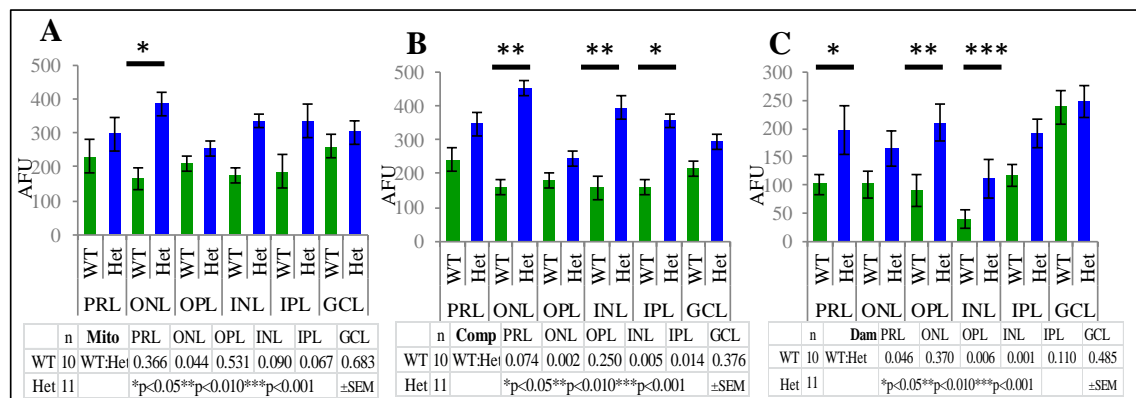


Figure 4.16 Retinal profile of protein expression of WT and Het

Graphs show the mean \pm SEM AFU of (A) mitochondrial, (B) compensatory and (C) damage mediated protein expression in the retinal layers of WT and Het.

Mitochondrial related protein expression was increased by a mean 62% in Het retina. The ONL showed a significant 135% increase (F(5,54) 1.909 p=0.044) compared to WT. No other retinal layers were significantly different compared to WT. Compensation protein expression in Het retina showed a mean 96% increase compared to WT. All retinal layers showed an increase in

Chapter 4 Bioenergetic impairment in *Opa1*^{Q285STOP} mouse

protein expression compared to WT. Het ONL showed a significant 185% increase compared to WT (F(5,52)1.883 p=0.002). The INL had a significant 150% increase (F(5,52) 2.253 p=0.005). The IPL had 39% increase (F(5,52) 2.695 p=0.014). Damage mediated protein expression in Het retinal layers was increased by 89%. The specific layers targeted were the INL with a 178% increase (F(5,48) 2.548 p=0.001), the OPL with a 131% increase (F(5,48) 3.380 p=0.006).

Considering that compensatory protein expression was significantly increased in both the outer and inner nuclear layer and that damage mediated protein expression was significantly increased in the corresponding plexiform layers might suggest that the compensation effects were insufficient, however, the activity of compensatory proteins within the inner plexiform layer were 92% higher than that of WT.

The ratio of compensatory to damage protein (C:D) expression was examined. Table 4.11 shows a summary of these findings.

Table 4.11 Ratio of compensation to damage protein expression in retina of WT and Het

C:D 1:	PRL	ONL	OPL	INL	IPL	GCL
WT	0.42	0.64	0.50	0.25	0.74	1.12
Het	0.57	0.36	0.86	0.28	0.54	0.84
% WT	36	-44	72	12	-27	-25

Table shows the ratio of compensation to damage mediated protein expression in WT and Het retinal layers. A ratio of less than 1 suggested that the activity of compensation was exerting a positive effect on damage mediated protein expression. In WT retinal layers, there was a positive compensation to damage ratio in all layers. In Het retinal layers all but the RGC layer showed a positive compensation to damage mediated ratio. The percentage difference between groups is shown.

Figures 4.17- 4.21 show representative images of these protein expression in retinal sections of WT and Het.

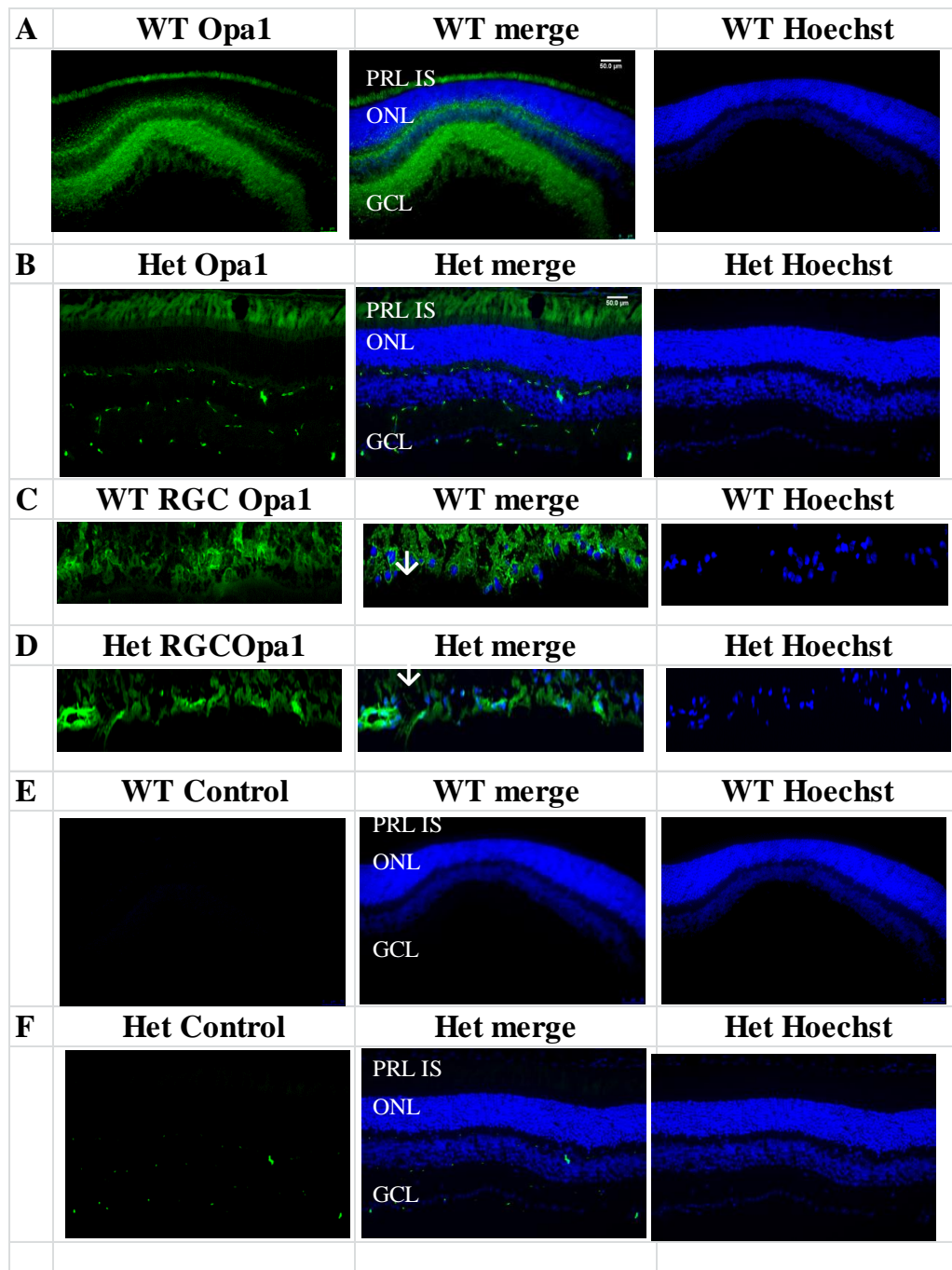


Figure 4.17 *Opa1* expression in retina of WT and Het

Representative images of Opa1 expression in WT and Het retina (A-B) with RGC regions for (C) WT and (D) Het (indicated by arrows). (E) Control sections for WT and (F) Het were processed without the primary antibody.

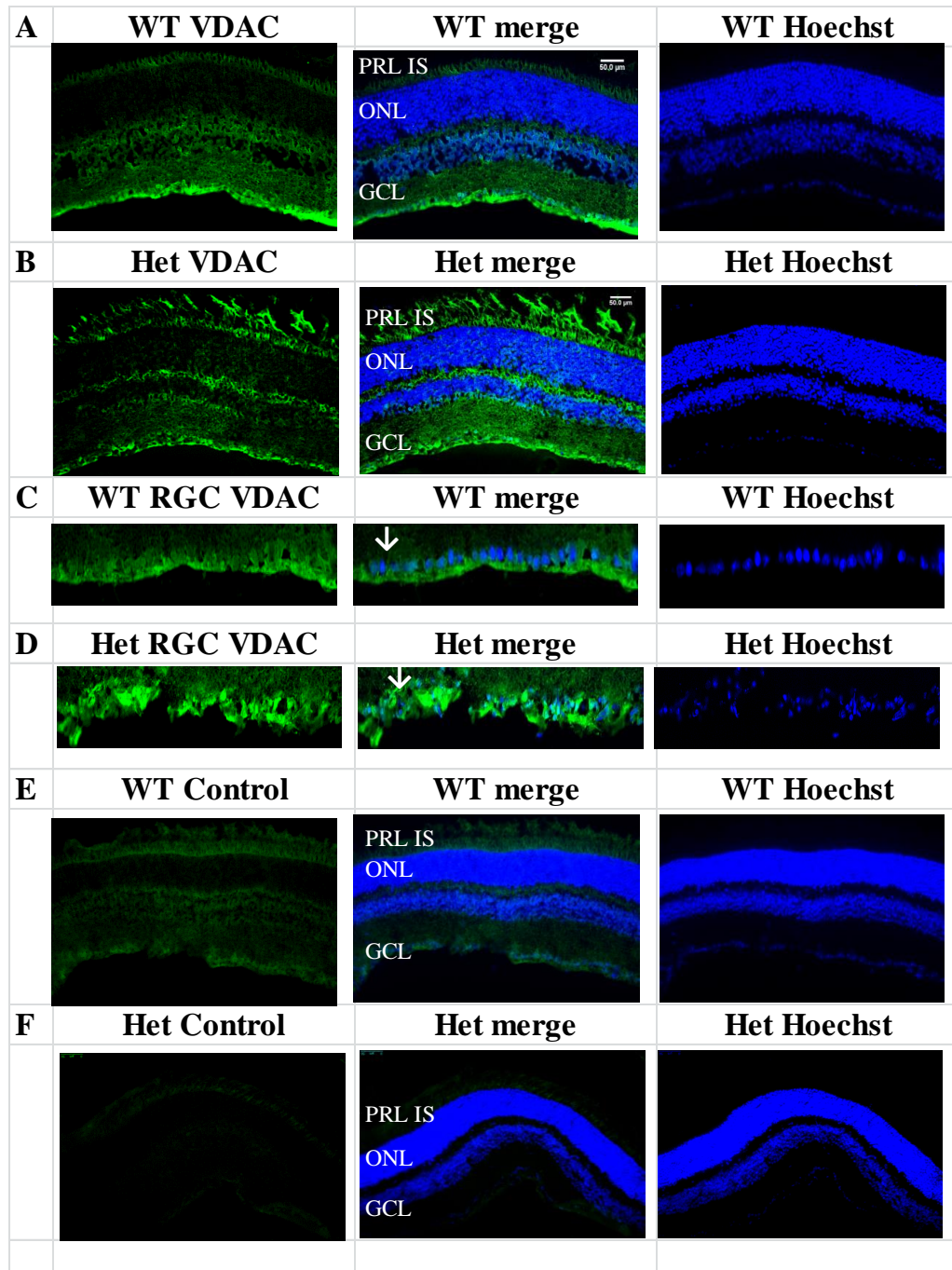


Figure 4.18 VDAC expression in retina of WT and Het

Representative images of VDAC expression in WT and Het retina (A-B) showing RGC regions for (C) WT and (D) Het (indicated by arrows). (E) Control sections for WT and (F) Het were processed without the primary antibody.

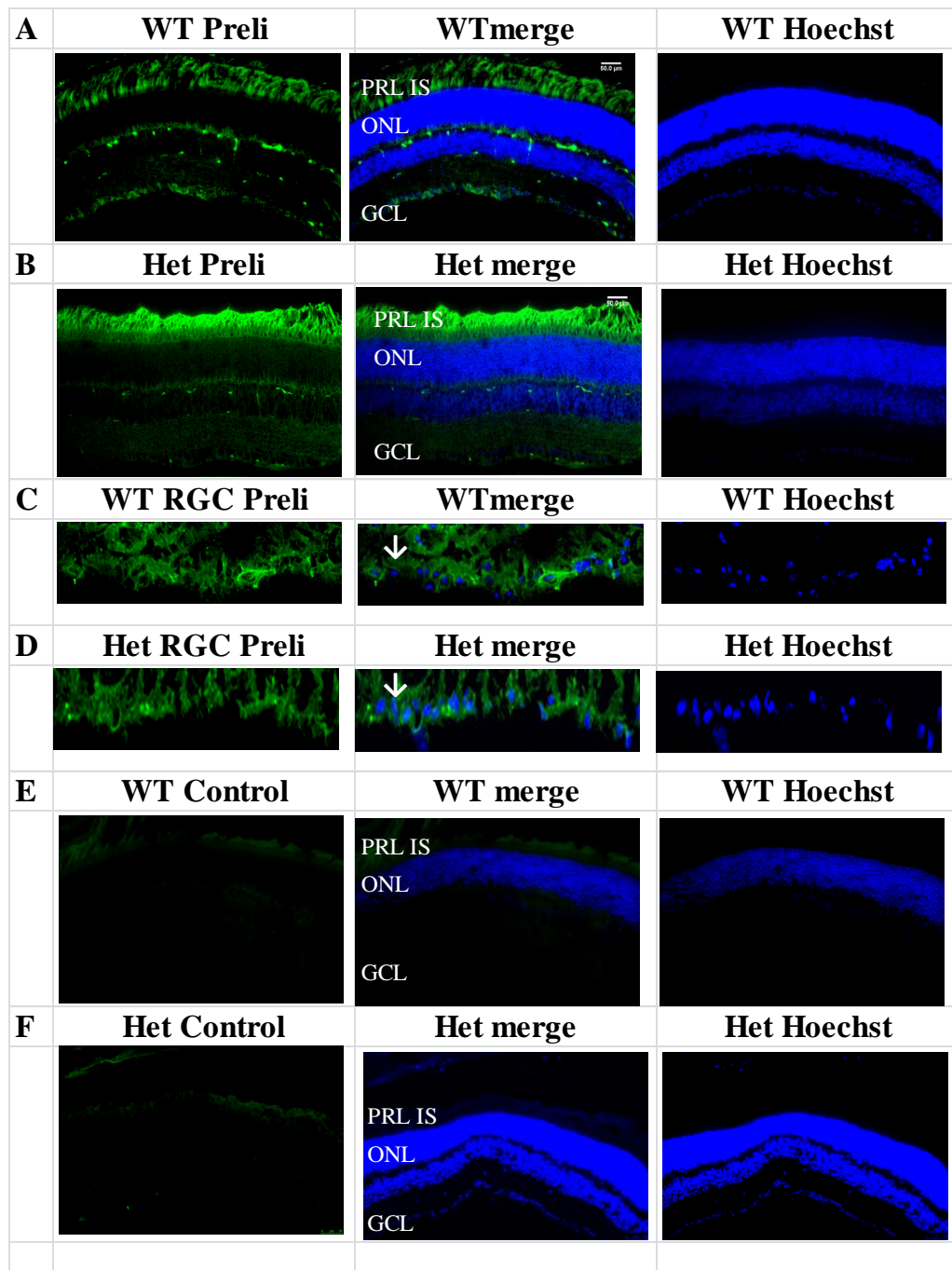


Figure 4.19 Preli expression in retina of WT and Het

Representative images of *Preli* expression in WT and Het retina (A-B) showing RGC regions for (C) WT and (D) Het (indicated by arrows). (E) Control sections for WT and (F) Het were processed without the primary antibody.

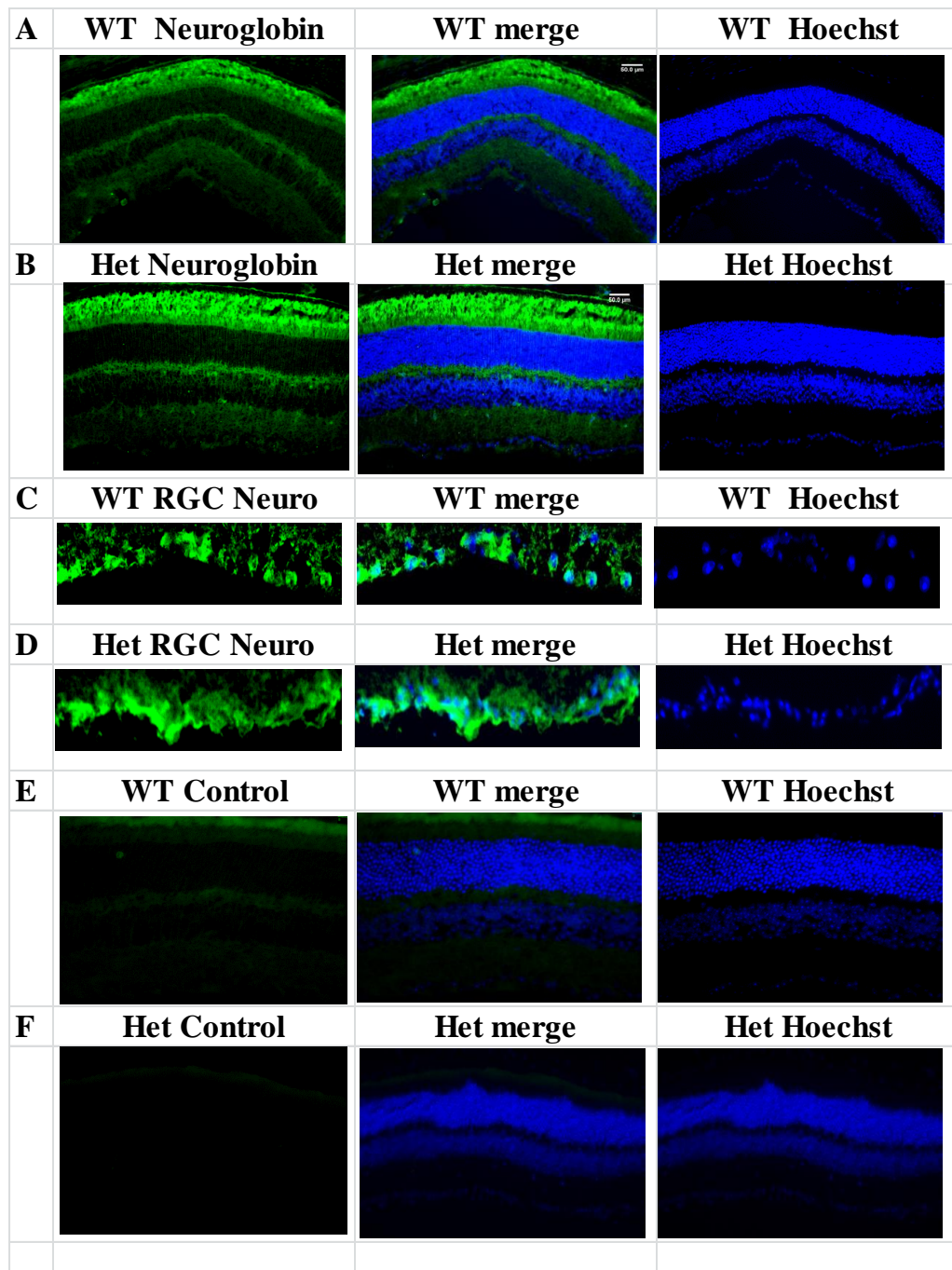


Figure 4.20 Neuroglobin expression in retina of WT and Het

Representative images of Neuroglobin expression in WT and Het retina (A-B) showing RGC regions for (C) WT and (D) Het (indicated by arrows). (E) Control sections for WT and (F) Het were processed without the primary antibody.

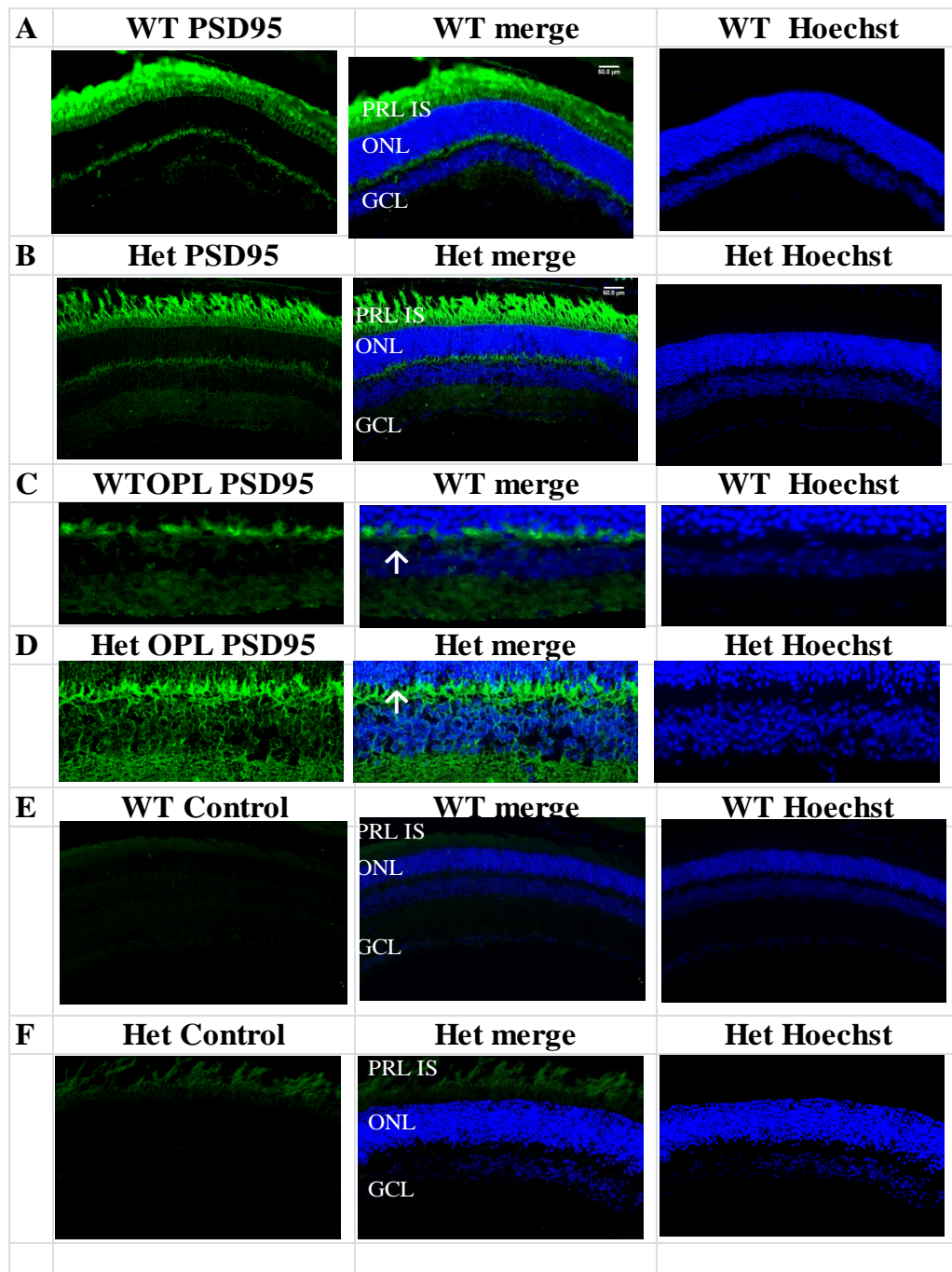


Figure 4.21 PSD95 expression in retina of WT and Het

Representative images of PSD95 expression in WT and Het retina (A-B) showing OPL regions for (C) WT and (D) Het (indicated by arrows). (E) Control sections for WT and (F) Het were processed without the primary antibody.

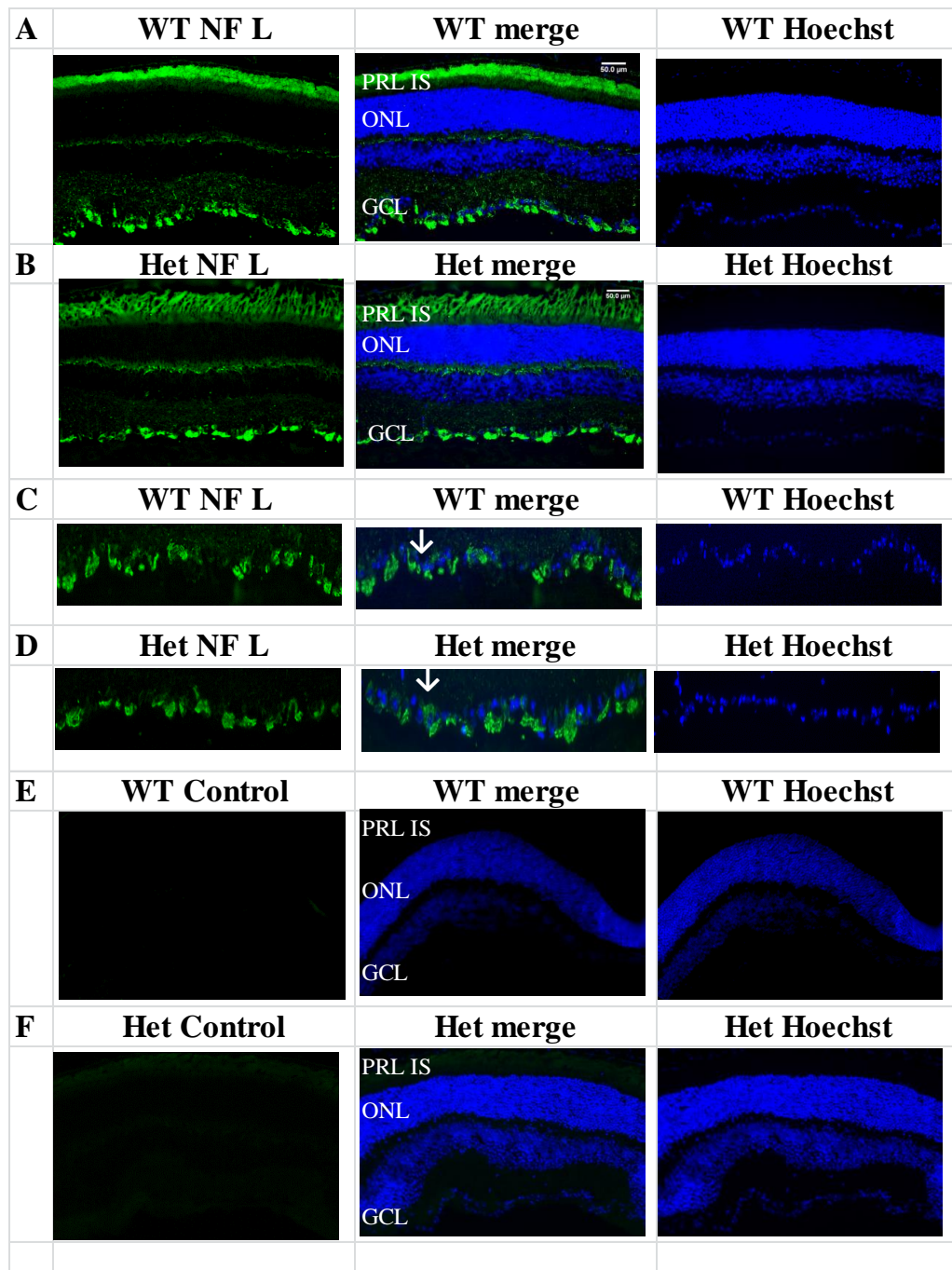


Figure 4.22 NF L expression in retina of WT and Het

Representative images of NF L expression in WT and Het retina (A-B) showing RGC regions for (C) WT and (D) Het (indicated by arrows). (E) Control sections for WT and (F) Het were processed without the primary antibody.

Chapter 4 Bioenergetic impairment in *Opa1^{Q285STOP}* mouse

4.4.4 Results of mitochondrial related protein expression in brain of WT and Het

Table shows a summary of AFU in brain for mitochondrial *Opa1* VDAC, Neuroglobin, Preli, PSD95 and NF H expression in brain of WT and Het. Figure 5.9 shows graphs representing AFU in protein expression of WT and Het brain.

Table 4.12 Summary of mitochondrial related protein expression in brain of WT and Het

A	Opa1	WT(n5)	Het(n5)	D	Preli	WT(n5)	Het(n5)
	Ave	619.9	419.1		Ave	542.4	1016
	SEM	119.6	80.2		SEM	107.6	299.8
	WT:Het		0.008		WT:Het		0.008
		F(5,30) 4.527			F(5,30) 4.627		
B	VDAC	WT(n5)	Het(n5)	E	PSD95	WT(n5)	Het(n5)
	Ave	542.4	1016		Ave	623	164.44
	SEM	107.6	299.8		SEM	93.35	36.664
	WT:Het		0.005		WT:Het		0.112
		F(5,18) 2.870			F(5,39) 2.983		
C	Neuro	WT(n5)	Het(n5)	F	NF H	WT(n5)	Het(n5)
	Ave	390	969		Ave	524.5	1469
	SEM	128.7	195		SEM	176	305.9
	WT:Het		0.003		WT:Het		0.001
		F(5,17) 2.454			F(5,17) 7.832		

Table shows the mean (\pm SEM) of brain mitochondrial (A) *Opa1*, (B) *VDAC* (C) *Neuroglobin*, (D) *Preli* (E) *PSD95* and (F) *NF H* proteins expression in brain of WT and Het. difference between groups is represented by p value.

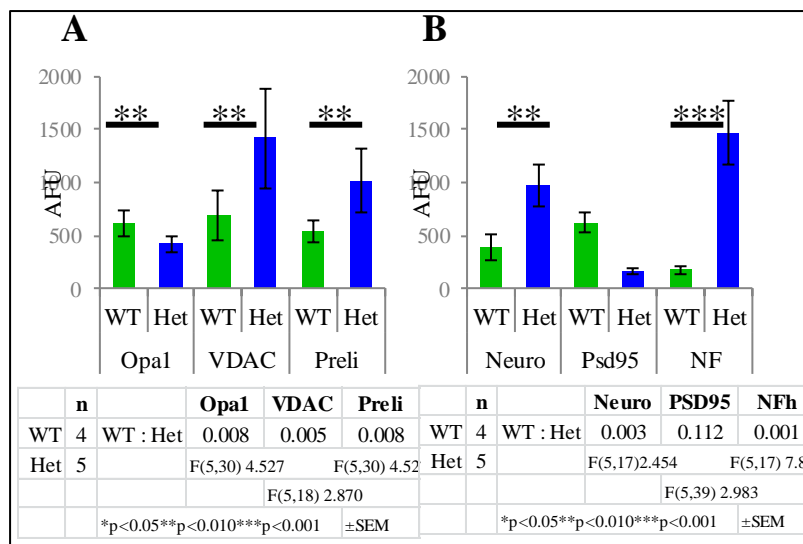


Figure 4.23 Mitochondrial protein expression in brain of WT and Het

Graphs show the mean \pm SEM of AFU for (A) *Opa1*, *VDAC* and *Preli* proteins (B) *Neuroglobin*, *PSD95* and *NF H* protein expression in brain of WT and Het.

Mitochondrial related protein expression in Het brain showed a 32% reduction in *Opa1* protein expression ($p=0.492$) compared to WT. *VDAC* expression was increased by 105% which was significantly increased compared to WT ($F(5,24) 2.223 p=0.005$).

Chapter 4 Bioenergetic impairment in *Opa1*^{Q285STOP} mouse

Het brain had a significant 87% increase in preli expression compared to WT (F(5,26) 1.615 p=0.008). Neuroglobin expression was increased by 148% which was statistically significant compared to WT (F(5,19) 5.086 p=0.003).

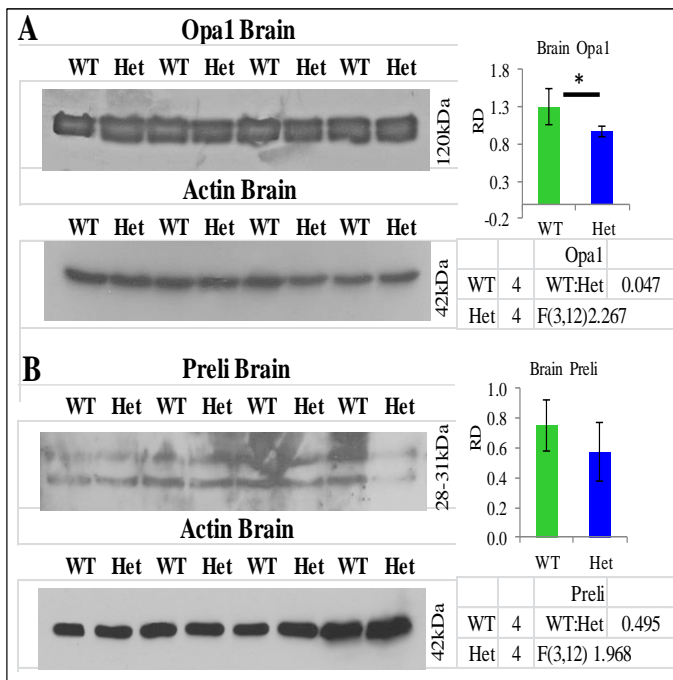
Het brain showed a 74% reduction in PSD 95 expression compared to WT which was not statistically different to WT (p=0.112). Neurofilament expression in Het brain was increased by 725% which was significantly increased compared to WT (F(5,25) 6.683 p=0.001). p=0.001).

4.4.5 Western blotting of brain homogenate in WT and Het

Western blotting of WT and Het brain homogenate *Opa1* expression in WT brain homogenate had 1.30±0.24 RD and Het had 0.97±0.07 which was significantly reduced compared to WT (F(3,12) 2.267 p=0.047). Preli expression in WT brain homogenate had 0.75±0.17 RD and Het had 0.58±0.20 RD which was not significantly different compared to WT (p=0.495). Figure 4.23 shows a summary of these findings.

Figure 4.24 Western blot of brain homogenate in WT and Het

Western blot of brain homogenate from WT (n4) and Het (n4) for (A) Opa1 (B)Preli expression with corresponding β actin beneath.



Figures 4.24- 4. Show representative images of brain sections expressing the above proteins.

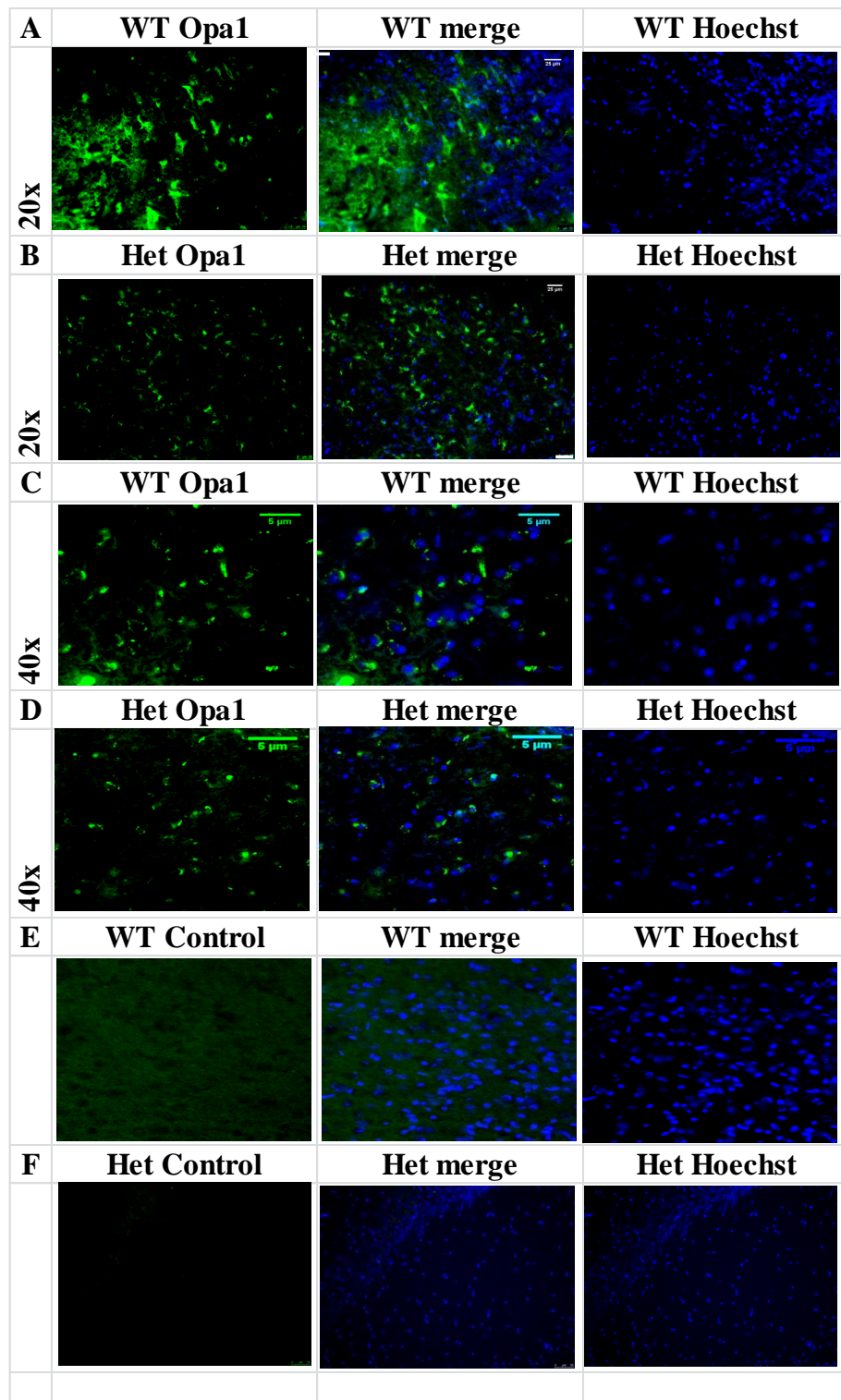


Figure 4.25 *Opa1* expression in brain of WT and Het

Representative images of Opa1 expression in WT and Het brain (A-B) with 40x magnified regions (C-D). Control sections for WT and Het (E-F) were processed without primary antibody.

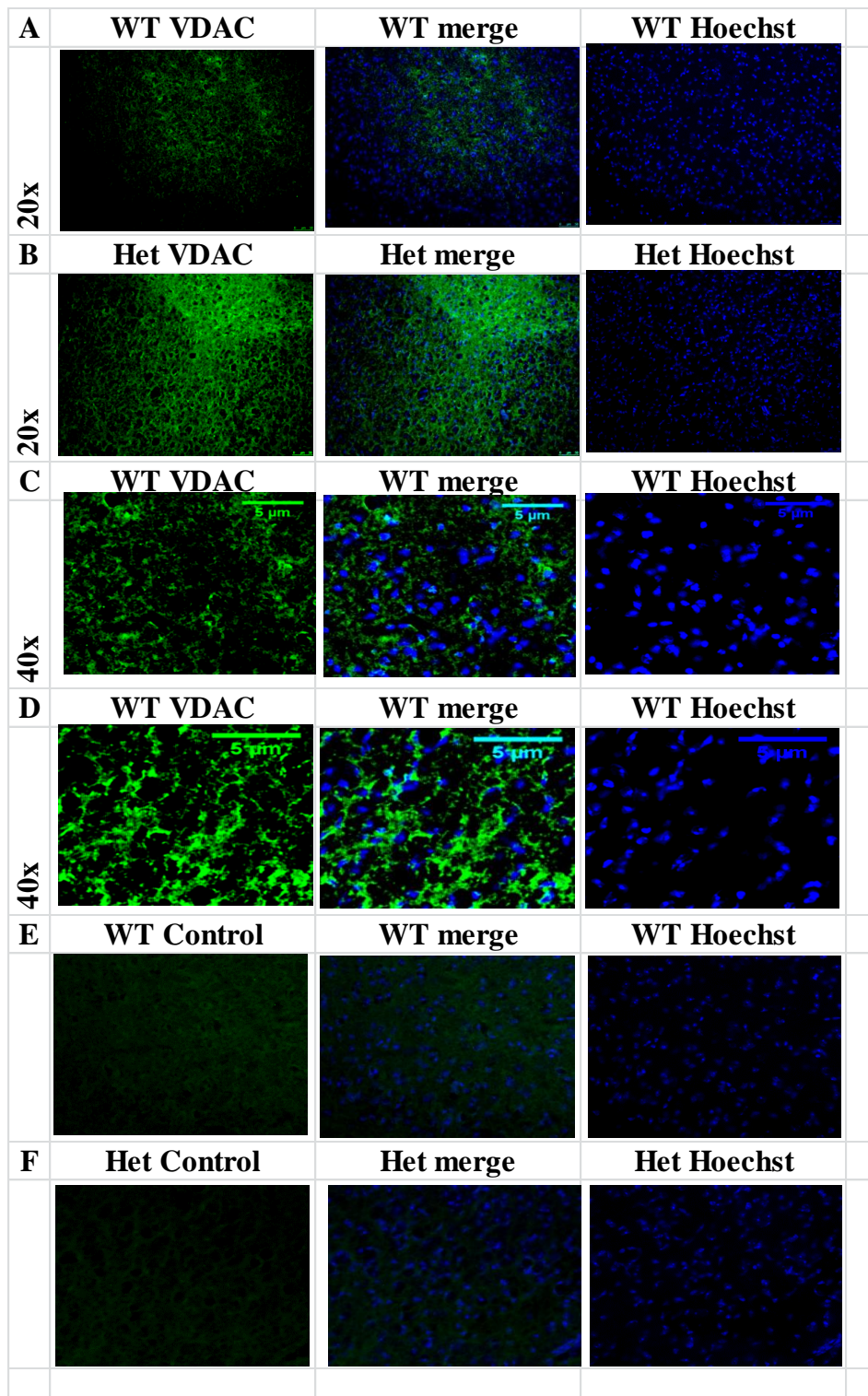


Figure 4.26 VDAC expression in brain of WT and Het

Representative images of VDAC expression in WT and Het brain (A-B) with 40x magnified regions (C-D). Control sections for WT and Het (E-F) were processed without primary antibody.

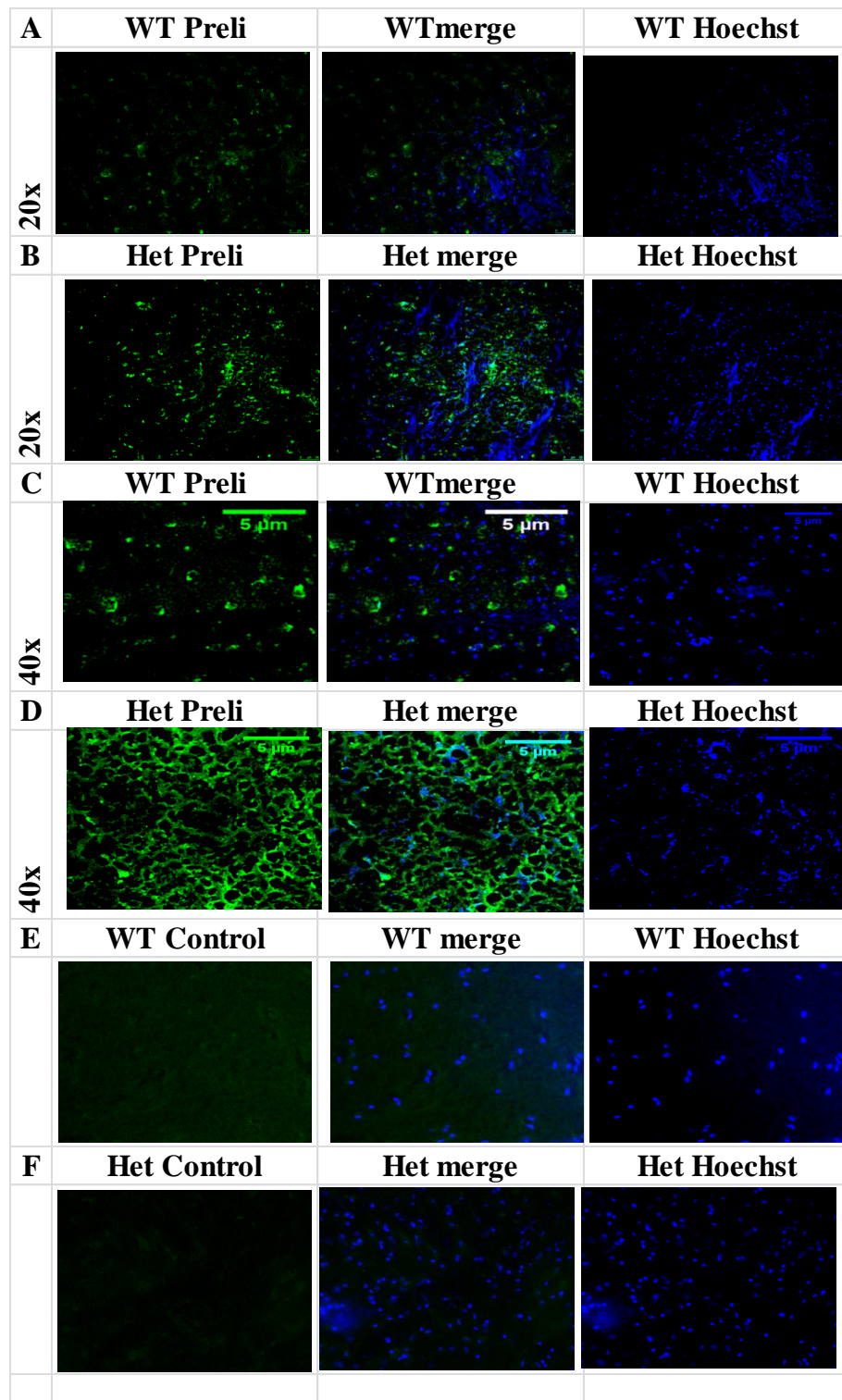


Figure 4.27 Preli expression in brain of WT and Het

Representative images of Preli expression in WT and Het brain (A-B) with 40x magnified regions (C-D). Control sections for WT and Het (E-F) were processed without primary antibody.

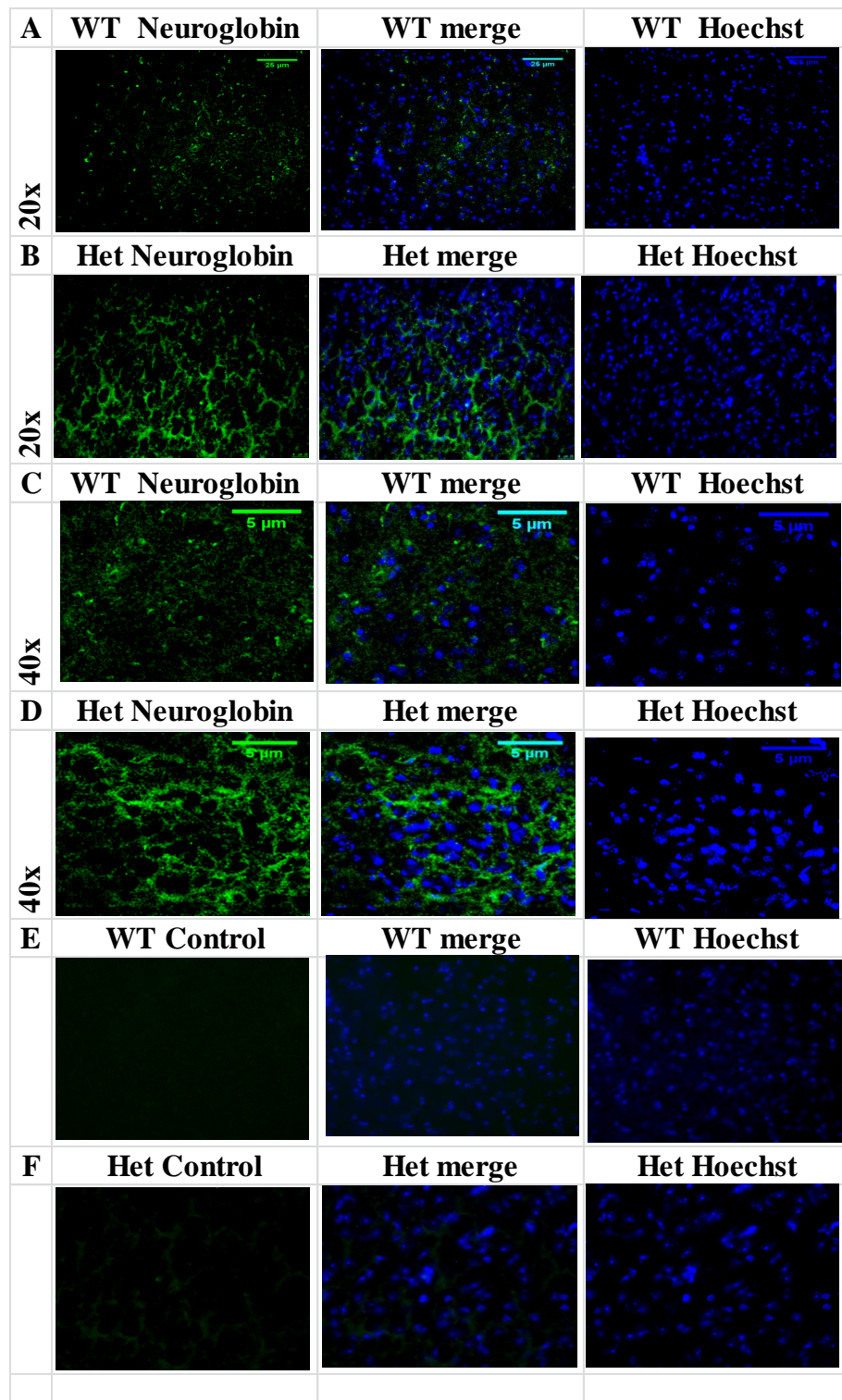


Figure 4.28 Neuroglobin expression in brain of WT and Het

Representative images of Neuroglobin expression in WT and Het brain (A-B) with 40x magnified regions (C-D). Control sections for WT and Het (E-F) were processed without primary antibody.

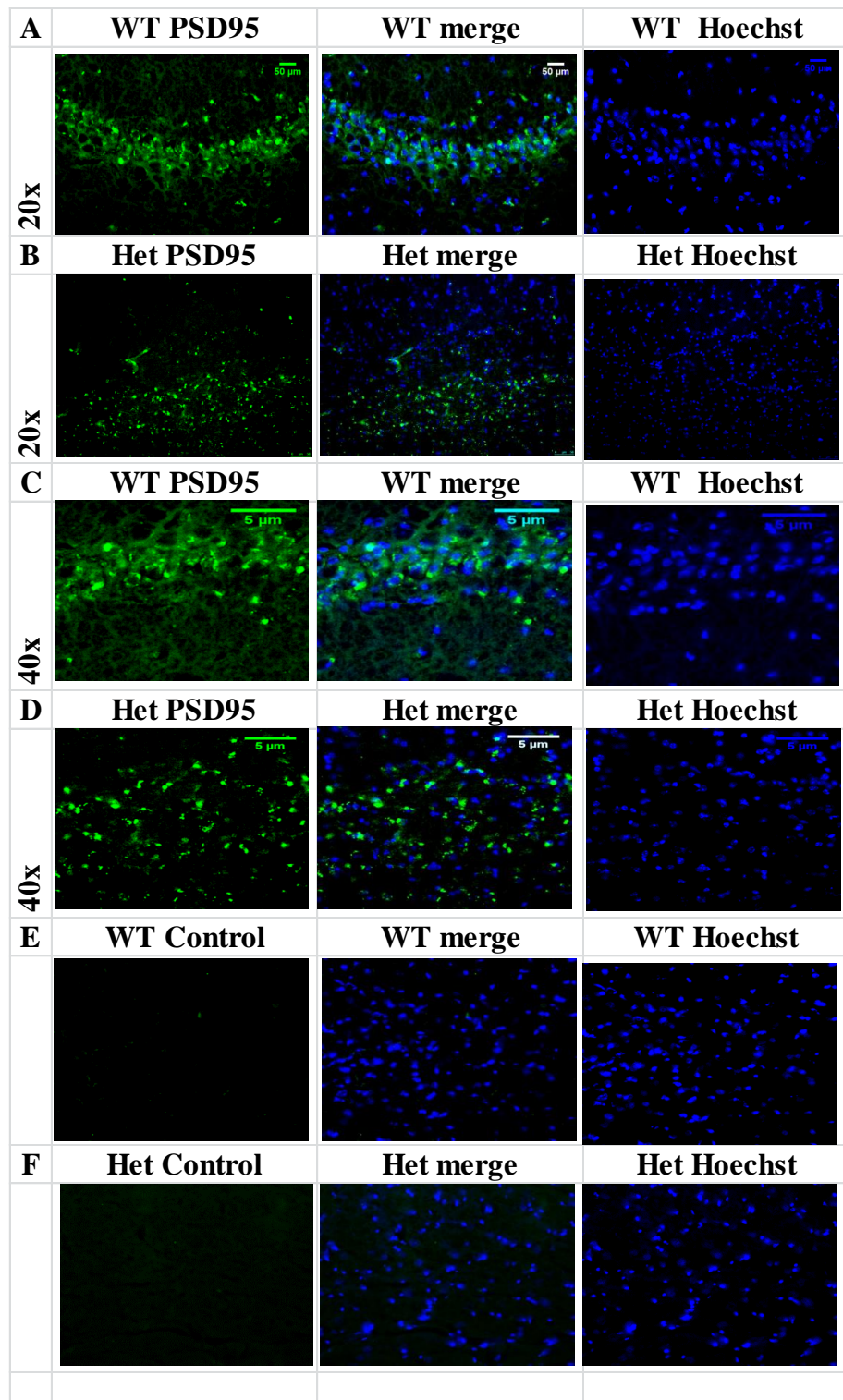


Figure 4.29 PSD95 expression in brain of WT and Het

Representative images of PSD95 expression in WT and Het brain (A-B) with 40x magnified regions (C-D). Control sections for WT and Het (E-F) were processed without primary antibody.

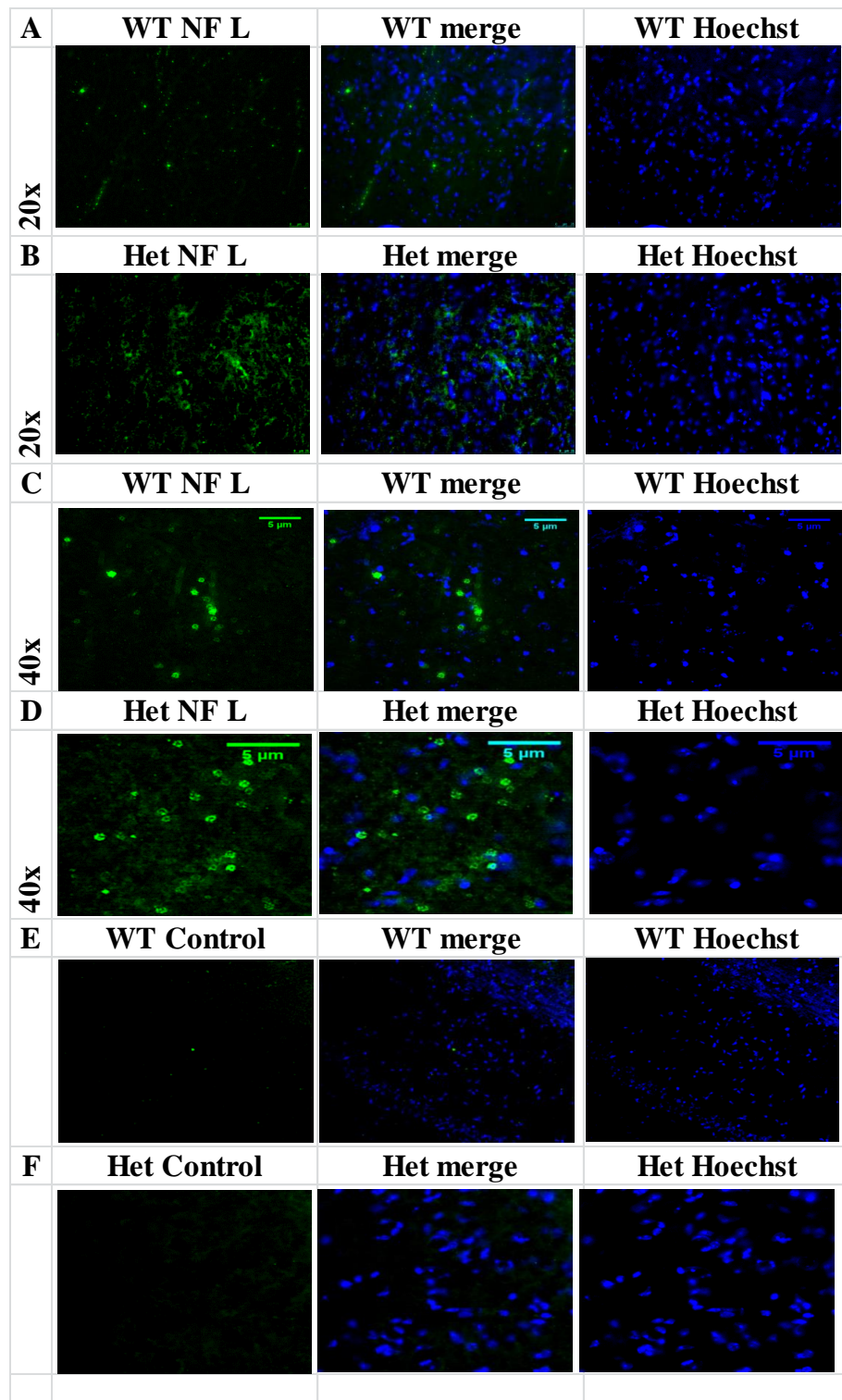


Figure 4.30 Neurofilament Heavy chain expression in brain of WT and Het

Representative images of NF H expression in WT and Het brain (A-B) with 40x magnified regions (C-D). Control sections for WT and Het (E-F) were processed without primary antibody.

Chapter 4 Bioenergetic impairment in *Opa1^{Q285STOP}* mouse

The protein profile for Het brain showed that there was 46% increase in mitochondrial related protein expression compared to WT (p=0.134). Compensatory protein expression was increased by 118% which was significantly increased compares to WT (F(5,81) 3.029 p=0.001). Damage mediated protein expression was increased by 119% which was also significantly increased compared to WT (F(5,58) 7.739 p=0.007). The ratio of compensatory to damage mediated in WT brain was 0.76 and 0.77 in Het brain. Figure 4.31 shows a summary of protein profiles for both retina and brain.

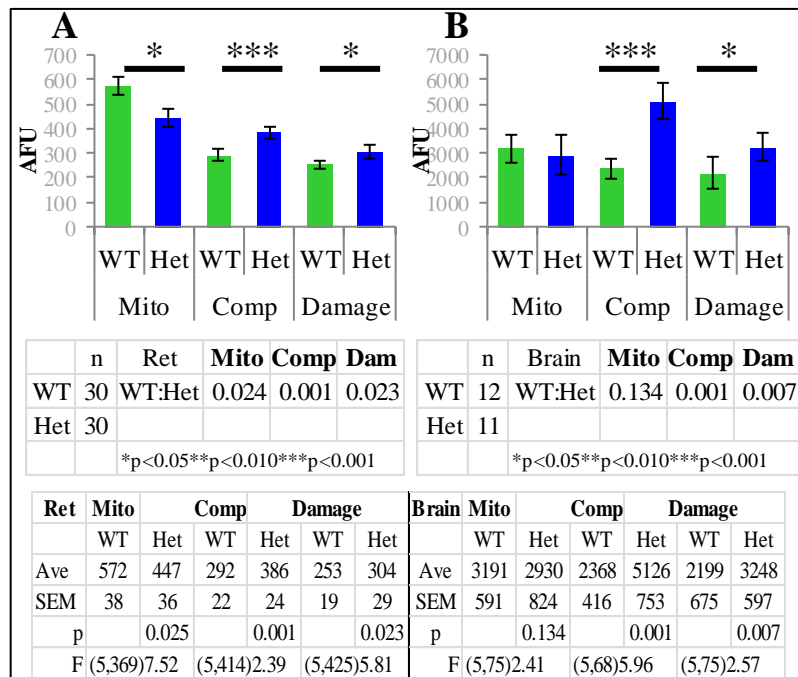


Figure 4.31 Summary of protein profiles in retina and brain of WT and Het

Graphs show a summary of mitochondrial, compensatory and damage mediated protein expression in (A)retina and (B) brain of WT and Het.

4.4.6 Discussion of mitochondrial related protein expression in WT and Het

Immunohistochemical analysis of mitochondrial function in intact tissue provided an accurate investigation platform for a variety of proteins. As ADOA is primarily a retinal disease, the laminated structures of the retina provided an excellent substrate for protein localisation. By combining retinal and brain histology, a particular profile emerges that lends support to the physical phenotypes seen in this mouse model of disease.

From the analysis it was observed that the mitochondrial profile in the specific layers of Het retina showed enhanced activity with the ONL showing a significant 135% increase in activity compared to WT. The Het RGC showed the least change with 15% increase compared to WT.

Chapter 4 Bioenergetic impairment in $Opa1^{Q285STOP}$ mouse

The compensation profile of retinal layers in Het showed the ONL had a significant 185% increase in protein expression compared to WT. The Het RGC layer had the least increase of 38% in compensation proteins.

The damage profile in the retina of Het showed all layers had increased damage mediated protein expression. The highest was the INL which had a significant 178% increase compared to WT. The RGC showed the least damage with 4% more than WT.

The expression of PSD95 is negatively correlated with dendritic branching (Levinson and El-Husseini 2005; Marshak et al. 2012; Bustos et al. 2014).

Increased PSD95 expression is considered a compensatory mechanism for reduced pre synaptic scaffold proteins (Weisenhaus et al. 2010; Plowey et al. 2014; Li et al. 2015). Neurofilament expression is associated with damage mediated cellular response. Enhanced expression of both PSD95 and NF-L have been identified in the substantia nigra of schizophrenia (Mueller et al. 2004; Kristiansen et al. 2006). This was also observed in dyskinetic marmoset (Hurley et al. 2005.)

The comparative analysis of Het brain and retina with respect to protein expression showed that despite its size the retinal tissue exerted a significant increase in compensatory proteins with compensation: damage ratio of 0.54. Het brain also had a positive ratio of 0.77. In summary, Het retina had 22% less damage mediated protein expression and subsequently had 25% less compensatory protein expression.

Chapter 4 Bioenergetic impairment in Opa1^{Q285STOP} mouse

4.4.7 Summary of Chapter 4: Bioenergetic impairment in Opa1^{Q285STOP} mouse

4.4.7.1 Significant reduction of mitochondrial size in brain and retina

Opa1^{Q285STOP} mouse showed a significant increase in the proportion of smaller sized mitochondria and a significant reduction in median sized mitochondria compared to WT brain and retina.

4.4.7.2 Enhanced ATP levels

ATP levels in brain (male Het) and spinal cord (female Het) were significantly increased compared to WT. Compared to WT, retinal ATP was not significantly different in Het mice.

4.4.7.3 Bioenergetic impairment in all CNS tissues examined

Electron transfer in complex I, II and IV were significantly reduced in brain, spinal cord, retinal and skeletal muscle mitochondria of Het mouse. Complex IV activity in Het spinal cord was the single tissue that exhibited a 7% increase in complex IV activity which may suggest it was the final tissue to preserve electron transport function.

4.4.7.4 Preservation of electron complex ratios in CNS of Het

Despite the reduction in bioenergetic activity, the ratio of complex activity was preserved in all Het tissue examined.

4.4.7.5 Compensation for damage mediated protein expression

Both the retina and brain of Het showed a positive ratio of compensation to damage mediated protein expression. There was a significant amount of damage associated to the INL but not to the RGC layer.

The significant increase in smaller fragmented mitochondria in brain and retina of Het mouse suggested that despite maintaining ATP values in excess of WT, the bioenergetic deficit was resulting in the physiological phenotypes observed. The preservation of electron complex ratios was considered to be vitally important. This preservation may have been aided by the increase in compensatory protein expression observed in brain and retina of Het mouse.

Chapter 5 Antioxidant deficit in Opa1^{Q285STOP} mouse

5.1 Introduction

ROS normally exist in balance with antioxidants. A disturbance in the oxidant-antioxidant homeostasis can result in the generation of reactive non-radical and radical species that may participate in the chain reaction. The essential trigger of the endogenous antioxidant system will vary according to the sensitivity of the tissue to ROS. The cellular components that are susceptible to ROS damage are unsaturated fatty acids in cell membranes, (Bicknell et al. 2002; Tanito et al. 2009; van den Elsen et al. 2013), proteins which can be denatured (Kortuem et al. 2000; Tezel 2006; Saccà et al. 2013) and nucleic acids (Organisciak et al. 1996; Betzen et al. 2009; Witte et al. 2013).

Defence mechanisms against excessive ROS are vital in maintaining normal tissue function in healthy cells. In tissue with an existing mitochondrial dysfunction, the presence of excessive unregulated ROS may be due to an insufficient response to the amount of ROS or due to a direct attack on the antioxidant system itself.

The need for antioxidants arises from normal cellular respiration. Superoxide anion (O_2^-) is the product of a one electron reduction of molecular oxygen. Superoxide ($O_2^{\bullet-}$) is the precursor of many reactive species. It can generate a more reactive hydroxyl radical (OH^{\bullet}) by reacting with transition metals (Fe_2^+) in the Fenton reaction. $O_2^{\bullet-}$ and H_2O_2 can produce OH^{\bullet} in the Haber-Weiss reaction but the reaction is pH dependant at acidic environment within the lysosomes.

Hydrogen peroxide (H_2O_2) is formed from the spontaneous dismutation of $O_2^{\bullet-}$ or the action of superoxide dismutase (SOD) on $O_2^{\bullet-}$. Mitochondria can contribute 40% hydrogen peroxide to the cellular environment (Boveris et al. 1972; Chance et al. 1979; Zager and Burkhart 1997; Kaminsky and Kosenko 2008; Grivennikova et al. 2010). The catalase enzyme is found within the peroxisomes of most cells. Catalase performs a functional role in signal transduction (Suzuki et al. 1997), and development (Pierce et al. 1991). Catalase eliminates excess H_2O_2 thereby breaking the chain of ROS generation.

Chapter 5 Antioxidant deficit in *Opal*^{Q285STOP} mouse

A reduction in antioxidant activity can result in a cumulative ROS production. The late onset ADOA disease profile may be associated with ROS production. (Shahrestani et al. 2009; Tang et al. 2009; Chen et al. 2012). The aim of this section was to establish if the presence of impaired antioxidant response was present in the *Opal*^{Q285STOP} mouse model.

5.1.1 Catalase assay in WT and Het mouse

5.1.1.1 Experimental design of catalase assay

The method of Aebi (Aebi 1984) and Beers (Beers and Sizer 1952) was employed to calculate the catalytic activity of tissue homogenates (as detailed in Chapter 2 section 2.13). The method measured the decomposition of a known concentration of H₂O₂ using the change in absorption at 240nm. A concentration of 10.3mM H₂O₂ prevents inactivation of catalase and reduces the formation of air bubbles due to the liberation of O₂ (Beers and Sizer 1952). H₂O₂ at concentrations in excess of 0.1M results in rapid inactivation of catalase (Altomare et al. 1974; Claiborne et al. 1979; Arnao et al. 1990; Lardinois 1995). The concentration of H₂O₂ at 0.3% in tissue homogenate is insufficient to significantly alter the function of peroxidase activity (Vetrano et al. 2005). Details of test samples are shown in Table 5.1.

5.1.1.2 Results of catalase assay in WT and Het

Brain		Retina	
WT	6	WT	4
Het	8	Het	4
SC			
WT	7		
Het	7		

Table 5.1 Summary of test samples for analysis of catalase activity in WT and Het

In WT brain, the catalase activity was 4.30±0.38 units/mg and Het brain was 3.50±0.31 units/mg which was not considered statistically different to WT (p=0.099).

The catalase activity in spinal cord homogenate of WT was 3.90±0.54 units/mg and Het spinal cord was 1.70±0.25 units/mg which was significantly reduced compared to WT (F(5,18) 10.902 p=0.001).

Catalase activity in WT retinal homogenate was 3.70±0.51 units/mg and 2.10±0.35 units/mg in Het retina which was significantly reduced compared to WT retina (F(3,10) 9.156 p=0.007)

The kinetics of the catalase reactions are presented in Figure 5.1 and a graph representing the results is shown in Figure 5.2.

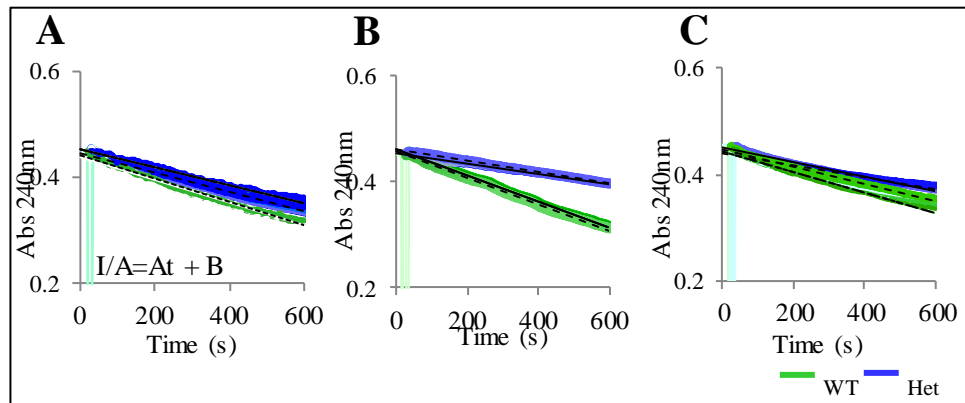


Figure 5.1 Kinetics of H_2O_2 decomposition in tissue homogenate of WT and Het

Representative kinetics of the decomposition of H_2O_2 in the presence of $80\mu g$ homogenate from both WT and Het brain (A), spinal cord (B) and retina (C).

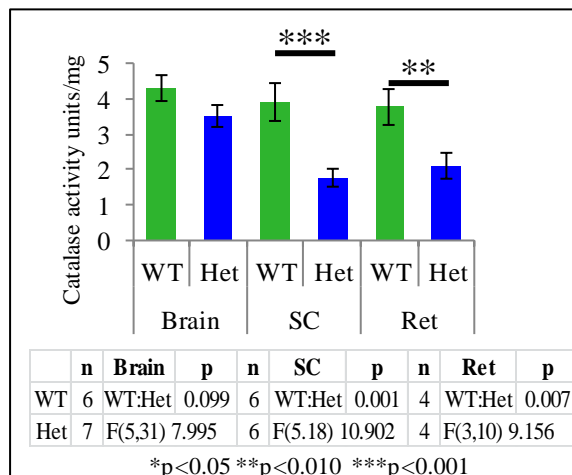


Figure 5.2 Catalase activity in WT and Het homogenate

Graph showing the mean \pm SD of catalase activity per mg of protein in tissue homogenate from WT and Het brain, spinal cord (SC) and retina (Ret).

5.1.1.3 Discussion of catalase activity in WT and Het mouse

Brain homogenate of Het showed no significant difference in catalase activity compared to WT brain. Het spinal cord had a 56% reduction in catalase activity compared to WT which was significantly different ($p=0.001$). There was a 43% reduction in retinal catalase activity which was significantly reduced when compared to WT retinal homogenate ($p=0.007$).

This suggested that Het spinal cord had the least protection against H_2O_2 damage, and that Het retinal tissue was also more vulnerable to H_2O_2 mediated damage.

Chapter 5 Antioxidant deficit in $Opa1^{Q285STOP}$ mouse

The significance of this reduction in tissues which both require myelin in order to function might suggest that reduction of catalase may induce demyelination in susceptible tissues (Guy et al. 1989; Spanevello et al. 2009; Goecks et al. 2012).

Genetic factors that control the amount of catalase production do so by altering the rate of catalase degradation and not the rate of synthesis (Rehceigl and Heston 1967). The activity of glutathione peroxidase has a higher affinity for H_2O_2 than that of catalase (Hirrlinger et al. 2002). With respect to the tissue specific activity of catalase in spinal cord homogenate, the combined activities of both glutathione peroxidase and catalase are required in the control of spinal cord oxidative damage (Baud et al. 2004).

The spinal cord is highly susceptible to oxidative stress (Uttara et al. 2009; Jia et al. 2012). The intrinsic difference in the mitochondria of spinal cord compared to brain is a reduced threshold for Ca^{2+} -induced mitochondrial permeability transition (mPT) (Brown et al. 2006; Morota et al. 2007). The mPT is a disruption in the proton motive force. The mPT pore acts as a voltage and calcium sensor between the inner and outer mitochondrial membrane (Martin et al. 2011; Bernardi 2013). Disruption to the mPT alters Ca^{2+} within the mitochondrial matrix resulting in mitochondrial depolarisation. The mPT is under the influence of complex I derived reactive oxygen species (Batandier et al. 2004). As the bioenergetic activity of complex I was significantly reduced in Het spinal cord mitochondria this will result in a reduction of ROS mediated signalling and altered spinal cord mPT. Increased cytoplasmic Ca^{2+} initiates excitotoxicity (Ankarcrona et al. 1995; Dutta and Trapp 2011) which triggers a cascade of mitophagic signals (Celsi et al. 2009; Perez-Pinzon et al. 2012).

Chapter 5 Antioxidant deficit in $Opa1^{Q285STOP}$ mouse

5.1.2 SOD analysis in $Opa1^{Q285STOP}$ mouse

5.1.2.1 Experimental design of SOD analysis

The antioxidant activity of SOD was analysed in tissue homogenate of WT and Het at 15 months. The tissues analysed were brain, spinal cord and retina. The total SOD activity was determined and with the use of specific inhibitors of MnSOD and CuZnSOD, the activity of mitochondrial and cytoplasmic SOD examined by the percentage inhibition of formazan formation.

Tissue homogenates from brain, spinal cord and retina were processed as described in Chapter 2 (Methods). Protein assays were performed and homogenate diluted to 1mg/ml. Each sample was run in triplicate with a standard curve for each run. For specific analysis of MnSOD, CuZnSOD was inhibited with potassium cyanide (1mM). For analysis of CuZnSOD activity, MnSOD was inhibited with 2% SDS.

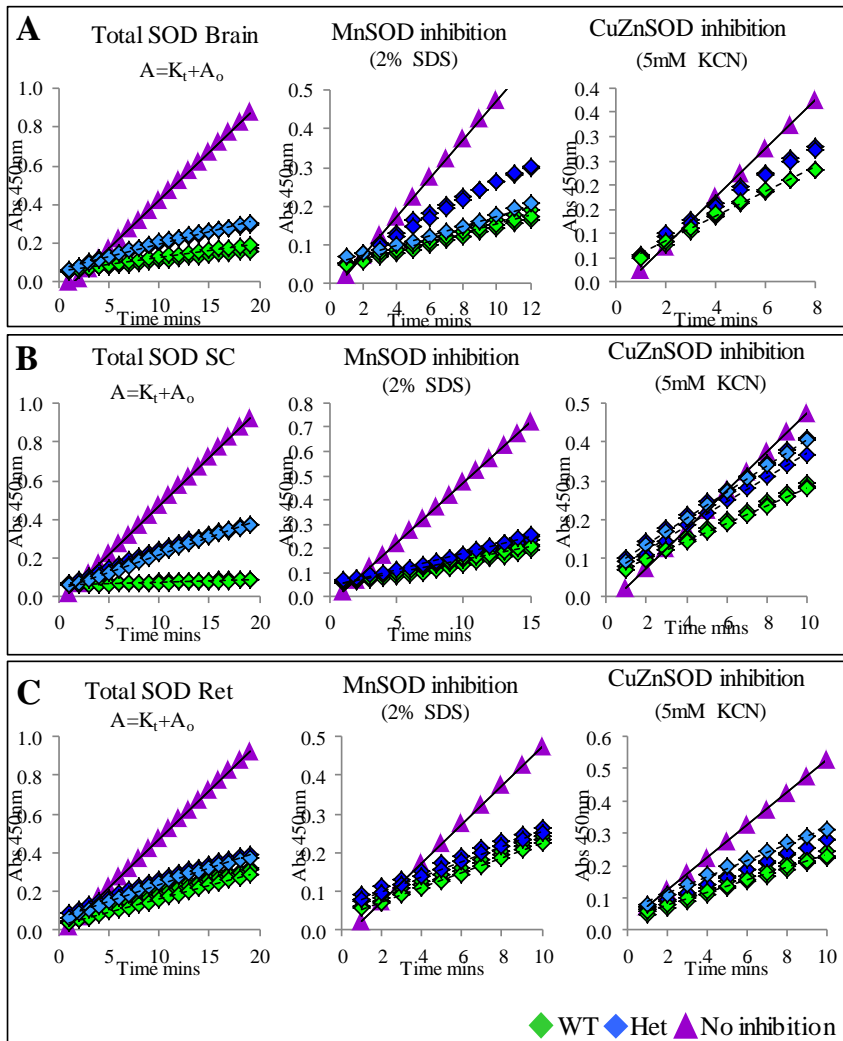
5.1.2.2 Results of SOD analysis in WT and Het

Brain		Retina	
WT	6	WT	6
Het	7	Het	6
SC			
WT	4		
Het	4		

Table 5.2 Summary of sample numbers for SOD analysis in WT and Het

Figure 5.3 shows the kinetic assays. Table 5.3 shows a summary of SOD analysis in WT and Het. and Figure 5.4 shows a representative graph of these findings. Calculation of line fittings for SOD activity is shown in Appendix J.

Figure 5.3 Kinetics of formazan inhibition as a function of SOD in WT and Het



Representative kinetics of formazan formation in the absence of SOD and the inhibition of formazan formation in the presence of WT and Het homogenate from brain, spinal cord (SC) and retina (Ret). Total SOD activity was measured without any inhibitors. CuZnSOD activity was determined by inhibition of MnSOD with 2% SDS. MnSOD activity was determined by inhibition of CuZnSOD with 1mM KCN.

	Brain		SC		Ret	
Total SOD	WT(6)	Het(6)	WT(7)	Het(7)	WT(6)	Het(6)
Ave	25.0	10.3	32.9	0.6	2.9	1.6
SEM	3.0	0.1	0.6	0.1	1.0	0.5
WT:Het		0.001		0.001		0.003
	F(5,12)32.43		F(5,12) 105.3		F(5,12)8.8	
CuZnSOD	WT	Het	WT	Het	WT	Het
Ave	7.10	1.60	1.30	0.08	0.33	0.24
SEM	0.03	0.02	0.06	0.04	0.07	0.08
WT:Het		0.004		0.001		0.299
	F(5,12)257.8		F(5,12)15.4		F(5,12)10.8	
MnSOD	WT	Het	WT	Het	WT	Het
Ave	1.60	0.40	0.15	0.00	0.38	0.16
SEM	0.06	0.04	0.07	0.00	0.02	0.09
WT:Het		0.001		0.001		0.029
	F(5,12)48.7		F(5,12)22.6		F(5,12)3.74	

Table 5.3 Summary of SOD activity in tissue homogenate of WT and Het

Table shows a summary of total SOD, MnSOD and CuZnSOD activity in WT and Het brain, spinal cord (SC) and retinal (Ret) homogenate. The statistical difference (*p* value) between groups is shown.

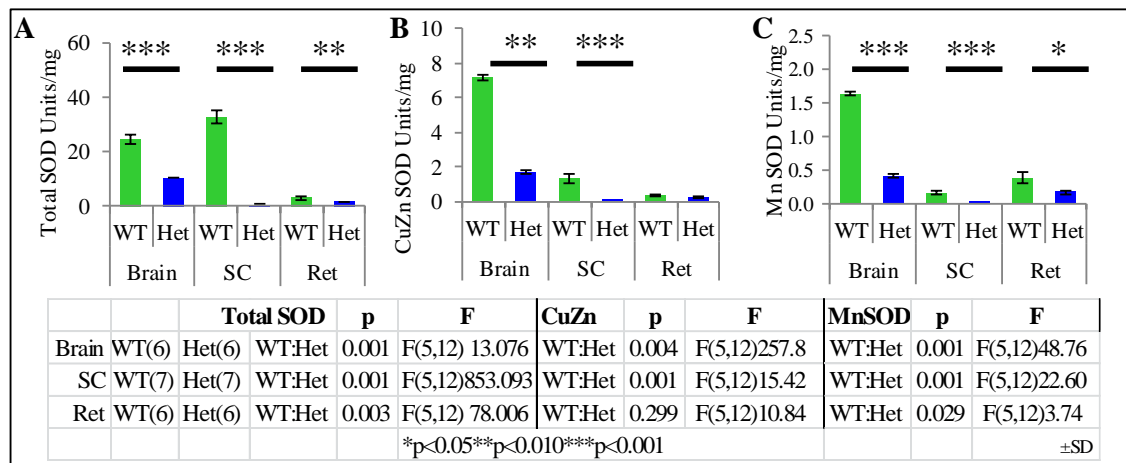


Figure 5.4 SOD units of activity in tissue homogenate of WT and Het

Graphs showing the mean \pm SD SOD activity in tissue homogenate of 15 month WT and Het Brain, spinal cord (SC) and retina(Ret) showing (A) Total SOD activity (B)CuZnSOD activity (C)MnSOD activity.

The mean fold reduction of SOD activity in Het brain homogenate was 2.6 compared to WT brain. CuZnSOD activity was reduced 3.3 fold and MnSOD activity reduced 3.0 fold.

Het spinal cord homogenate had the highest fold reduction of 33 compared to WT. CuZnSOD activity was reduced 14 fold and MnSOD activity reduced 34 fold.

Het retinal homogenate had 0.8 fold reduction in SOD activity compared to WT. CuZnSOD activity was reduced 0.4 fold and MnSOD activity reduced 1.3 fold. Table 5.4 summarises these findings.

Table 5.4 Fold changes of SOD activities in Het CNS

fold	SOD	CuZn	MnSOD	Non-SOD	Ave
Brain	1.4	3.3	3.0	405.0	103.2
SC	51.0	14.0	33.7	1.4	25.0
Ret	0.8	0.4	1.3	0.3	0.7
Ave	17.7	5.9	12.7	135.6	

Tissue specific fold changes in Het homogenate compared to WT showed spinal cord had the highest reduction of all tissues tested.

Chapter 5 Antioxidant deficit in *Opa1*^{Q285STOP} mouse

The percentage inhibition of formazan formation in tissue homogenate represented the total SOD activity in WT and Het. The combined percentage inhibition of CuZnSOD and MnSOD should have equalled the total SOD activity. In WT brain, there was less than 1%±1 non-SOD activity, Het brain homogenate had 23%±3 non-SOD activity which was significantly increased compared to WT (F(5,30) 25.624 p=0.001). WT spinal cord homogenate had 14%±4 non-SOD and Het had 35%±1 which was significantly increased compared to WT (F(5,20) 19.228 p=0.001). There was no statistical difference in non-SOD activity between WT 15%±3 and Het 21%±2 (p=0.109). Figure 5.5 summarises these findings.

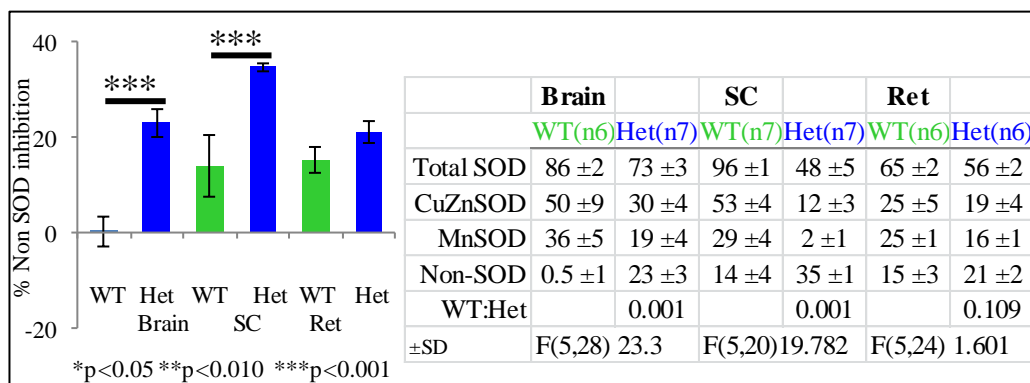


Figure 5.5 Percentage inhibition of formazan formation in WT and Het homogenate

Graph shows the mean± SD of percentage inhibition of formazan formation due to non-SOD activity in WT and Het brain spinal cord (SC) and retina (Ret). The table shows the percentage inhibition of formazan formation due to total SOD, CuZn SOD and MnSOD in brain, SC and retina and the non-SOD activity calculated from these data.

Het spinal cord homogenate had significantly greater reduction in total SOD activity compared to Het brain (F(8,39) 853.864 p=0.001) and to Het retinal homogenate (p=0.001). CuZnSOD activity in Het spinal cord homogenate was significantly reduced compared to CuZnSOD activity in Het brain homogenate (F(8,39) 85.864 p=0.001) but not compared to Het retinal homogenate (p=0.313). Het MnSOD activity in spinal cord homogenate was significantly reduced compared to brain homogenate (F(8,39) 853.864 p=0.007) but not compared to Het retinal homogenate (p=0.167). Non SOD activity in Het spinal cord homogenate was

Chapter 5 Antioxidant deficit in *Opa1*^{Q285STOP} mouse

significantly greater compared to Het brain homogenate (F(2,17)8.763 p=0.006) and compared to Het retinal homogenate (p=0.001). Table 5.5 summarises these findings.

Table 5.5 Summary of SOD activity in Het spinal cord

	SOD	CuZn	MnSOD	Non-SOD
SC>B	94%	95%	99%	51%
SC:B	0.001	0.001	0.007	0.006
SC>R	60%	65%	98%	66%
SC:R	0.001	0.313	0.167	0.001

Table shows a summary of SOD activity in Het spinal cord homogenate compared to Het brain and retinal homogenate. The statistical difference between groups is shown.

5.1.2.3 Discussion of SOD analysis in WT and Het

Het tissue homogenate demonstrated a significant reduction in SOD activity compared to WT homogenate. Within the tissues tested Het spinal cord activity was significantly reduced compared to Het brain and Het retina. Although all tissues of the Het CNS showed impaired antioxidant activity, spinal cord appeared to have significantly more dysfunction. The combined reduction in threshold for Ca²⁺ induced mPT opening in spinal cord mitochondria with reduced mitochondrial fusion renders the spinal cord more susceptible to oxidative stress. Reduced SOD activity permits the accumulation of O₂[•] which results in oxidative stress. Lipid peroxidation of polyunsaturated fats (PUFA) in the mitochondrial membrane reduces fluidity and function. This further impairs electron transport. The influx of calcium into the mitochondrial matrix initiates a cardiolipin Ca²⁺ dependant dissociation of complex II resulting in apoptotic induction (Hwang et al. 2014). Mitochondria with reduced membrane potential cannot restore or maintain sufficient proton motive force to generate ATP. In sufficient numbers, they will trigger mitophagy which will ultimately result in cell death.

Het mouse was observed to have gait anomalies which are associated with spinal cord neuropathy (Gupta et al. 2012; Guo et al. 2013). The reduction of cytoplasmic CuZnSOD has been associated with impaired neurotransmitter release and reduced skeletal muscle strength (Shi et al. 2014). This was observed in rotarod testing, wire hang, and tight rope testing.

5.1.3 Protein analysis of antioxidant SOD expression

IHC was performed as previously described.

5.1.3.1 IHC of retina and brain for MnSOD expression

IHC was performed on retinal and brain sections of WT and Het to determine the protein expression of MnSOD. Table 5.6 shows a summary of SOD expression in the retinal layers of WT and Het. Figure shows a graph of representative AFU in retinal layers.

Table 5.6 MnSOD expression in retinal layers of WT and Het

	PRL		ONL		OPL		INL		IPL		GCL	
MnSOD	WT5	Het6	WT5	Het6	WT5	Het6	WT5	Het6	WT5	Het6	WT5	Het6
Ave	228.1	250.5	218.1	349.2	170.2	129.8	163.3	259.3	180.9	90.41	71.34	64.78
SEM	52.27	38.15	99.93	38.98	54.2	20.76	81.32	21.29	80.56	34.99	36.4	23.16
WT:Het		0.651		0.653		0.020		0.606		0.886		0.002
	F F (5,16) 8.912		F (5,16)11.416		F (5,16) 10.44		F (5,16)4.028		F (5,16) 2.850		F (5,16) 8.476	

Table shows the mean \pm SEM of MnSOD expression in retinal layers and brain of WT and Het

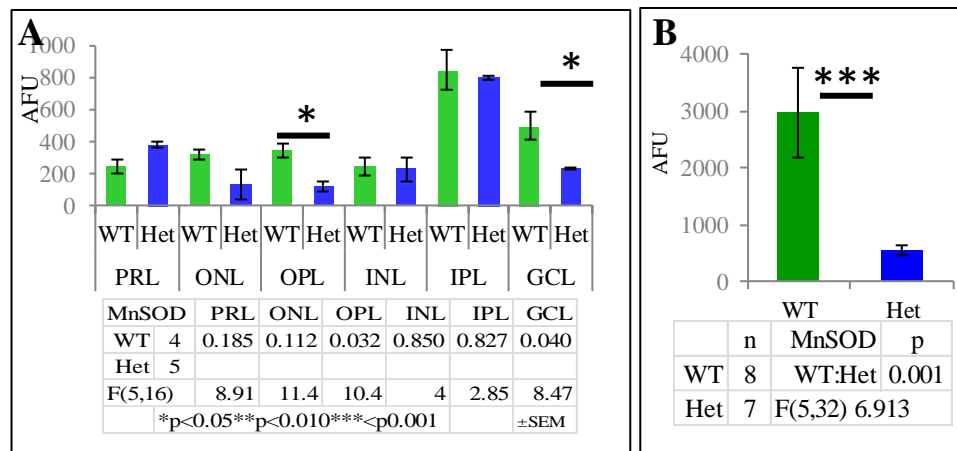


Figure 5.6 MnSOD expression in retina and brain of WT and Het

Graph show the mean \pm SEM AFU of MnSOD expression in (A)retina and (B) Brain of WT and Het.

Het retinal layers showed a significant 68% reduction of MnSOD expression in the OPL (F(5,17) 1.889 p=0.032) and 54% reduction in the RGC layer (F(5,17) 1.582 p=0.040). Het brain had 81% reduction which was significant compared to WT (F(5,32) 6.913 p=0.001).

Chapter 5 Antioxidant deficit in Opa1^{Q285STOP} mouse

5.1.3.2 Western blotting of brain homogenate in WT and Het

Western blotting of WT and Het brain homogenate for MnSOD showed WT had an RD of 1.0 ± 0.21 and Het had 0.73 ± 0.02 which was significantly reduced compared to WT (F(3,36) 6.199 p= 0.021). Figure 5.7 shows a summary of these data.

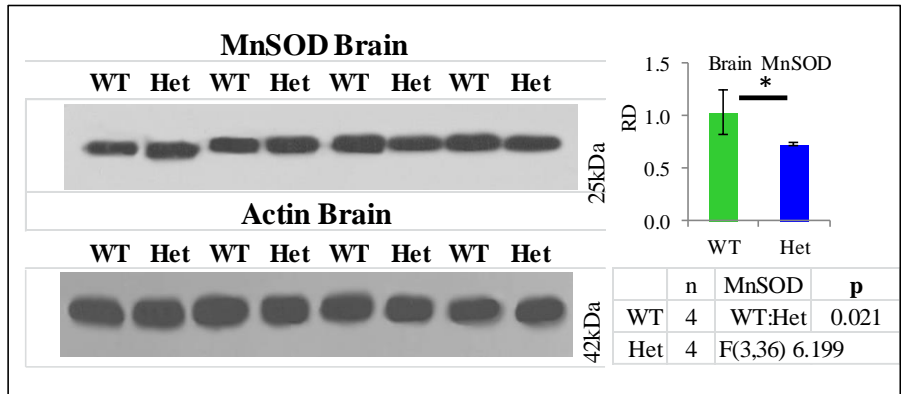


Figure 5.7 Western blotting of brain homogenate in WT and Het

Western blot of brain homogenate from WT (n4) and Het (n4) for MnSOD.

Figure 5.8 shows representative images of retinal expression of MnSOD and Figure 5.9 shows MnSOD expression in brain of WT and Het.

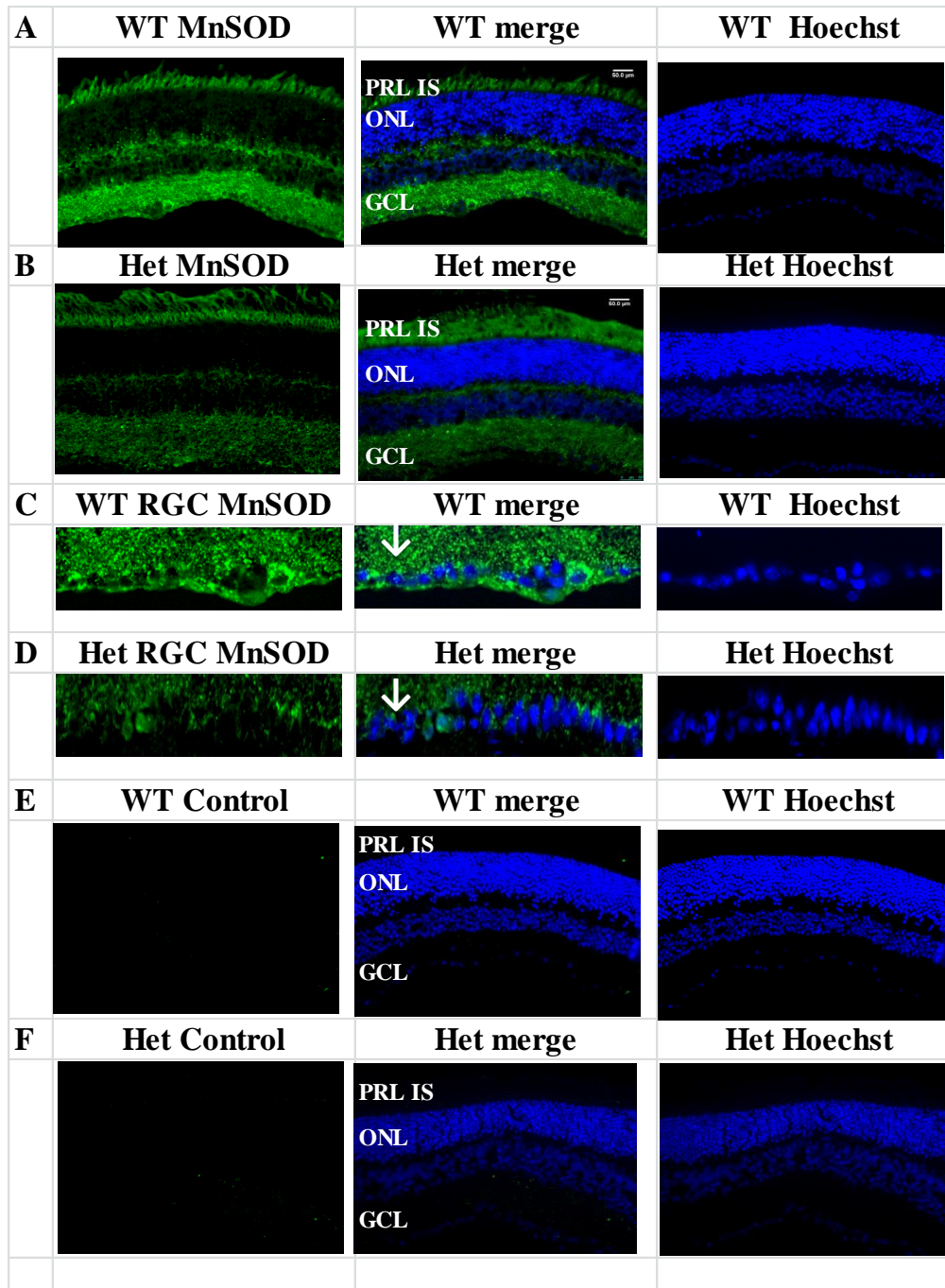


Figure 5.8 MnSOD expression in retinal sections of WT and Het

Representative images of MnSOD expression in WT and Het retina (A-B) showing RGC regions for (C) WT and (D) Het (indicated by arrows). (E) Control sections for WT and (F) Het were processed without the primary antibody.

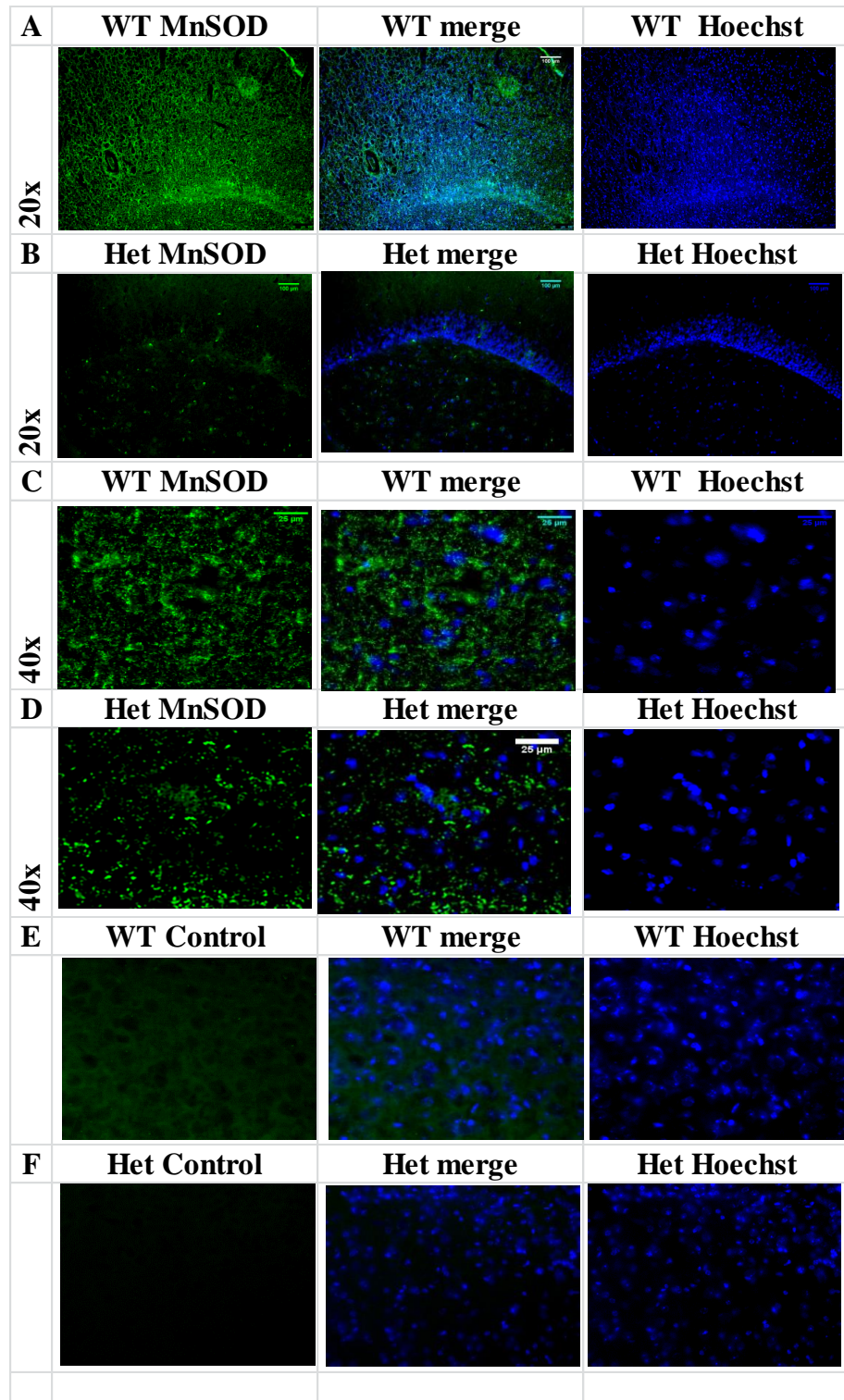


Figure 5.9 MnSOD expression in brain sections of WT and Het

Representative images of MnSOD expression in WT and Het brain (A-B) with 40x magnified regions (C-D). Control sections for WT and Het (E-F) were processed without primary antibody.

Chapter 5 Antioxidant deficit in *Opa1*^{Q285STOP} mouse

5.1.4 Nitrate protein deposition in WT and Het

5.1.4.1 Introduction to nitrated protein deposition

Protein nitration results from the interaction of secondary oxidants derived from peroxynitrite (ONOO⁻) with tyrosine containing proteins. Peroxynitrite anion protonation to ONOOH gives rise to tyrosine nitrating agents. This reaction is initiated by a one electron oxidation of tyrosine to tyrosyl radical. The susceptibility of tyrosine to nitration depends on the accessibility of the residue. Nitrated proteins are associated with other retinal disorders including glaucoma (Feilchenfeld et al. 2008), diabetic retinopathy (Kowluru 2003; Beauchamp et al. 2004; Kanwar et al. 2007) and age related macular degeneration (AMD) (Zhou et al. 2010). The incidence of increased protein nitration in the presence of reduced SOD activity has been established (Sasaki et al. 2000; Moreno et al. 2011; Miyamoto et al. 2014).

Clearance of nitrated proteins with denitrase has been demonstrated as an inducible factor in eliminating nitrated proteins (Kamisaki et al. 1998; Irie et al. 2003; Deeb et al. 2013). If denitration was initiated before nitration was extensive, the denitration of proteins could permit the restoration of their function. (Sadowska-Bartosz et al. 2014).

3^oNitrotyrosine antibody was used for the detection of nitration (Franze et al. 2004; Khan et al. 2006) in brain and retinal sections.

5.1.4.2 Results of 3 nitrotyrosine deposition in retina and brain of WT and Het

Table 5.7 shows a summary of 3 nitrotyrosine deposition in retinal layers of WT and Het.

Figure 5.10 shows a graph of this data.

Table 5.7 Nitrotyrosine deposition in retina and brain of WT and Het

3Nitro	PRL		ONL		OPL		INL		IPL		GCL	
	WT5	Het6	WT5	Het6	WT5	Het6	WT5	Het6	WT5	Het6	WT5	Het6
Ave	245.4	381.3	318	131.8	344.9	119.1	244.9	227.2	847.5	800	497.7	228.8
SEM	47.57	20.21	31.72	90.69	41.43	32.28	56.74	75.88	224.9	14.84	85.14	4.403
WT:Het		0.048		0.001		0.84		0.032		0.547		0.023
	F (5,20)	2.732	F (5,20)	10.78	F (5,20)	0.774	F (5,20)	1.842	F (5,20)	1.040	F (5,20)	3.443

Table shows the mean ±SEM of 3 nitrotyrosine deposition in retinal layers and in brain of WT and Het. Statistical difference between groups is represented by p value.

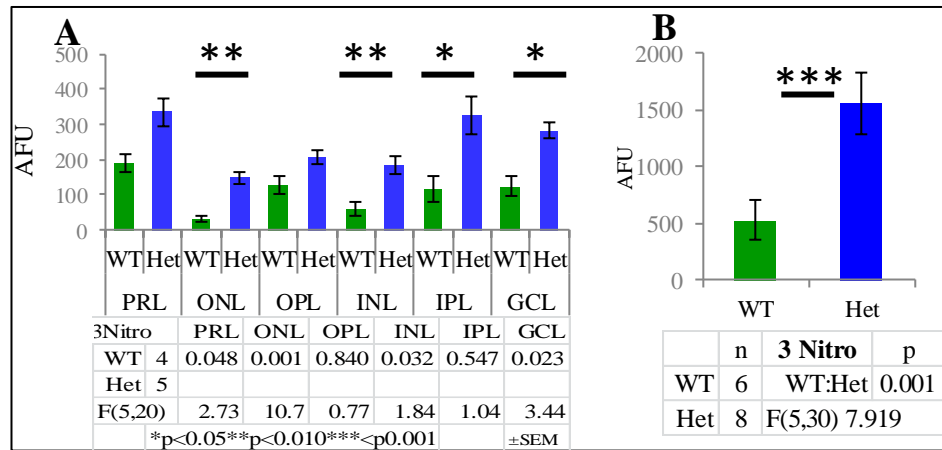


Figure 5.10 3 Nitrotyrosine deposition in retinal layers and brain of WT and Het

Graphs show the mean ±SEM of AFU for nitrotyrosine deposition in (A) retinal layers (B) brain of WT and Het.

There was a mean 74% increase in 3 nitrotyrosine in the retinal layers of Het. The ONL showed a significant 348% increase (F(5,12) 2.548 p=0.009) compared to WT. There was a 210% increase in the INL (F(5,12) 1.415 p=0.010), 177% in the IPL (F(5,12) 1.402 p=0.014) and 126% in the GCL (F(5,12) 4.201 p=0.019). The brain of Het had a 197% increase compared to WT (F(5,25) 7.919 p=0.001).

Figures 5.11 show representative images of 3 nitrotyrosine deposition in retina of WT and Het and Figure 5.12 show representative images of 3 nitrotyrosine deposition in brain.

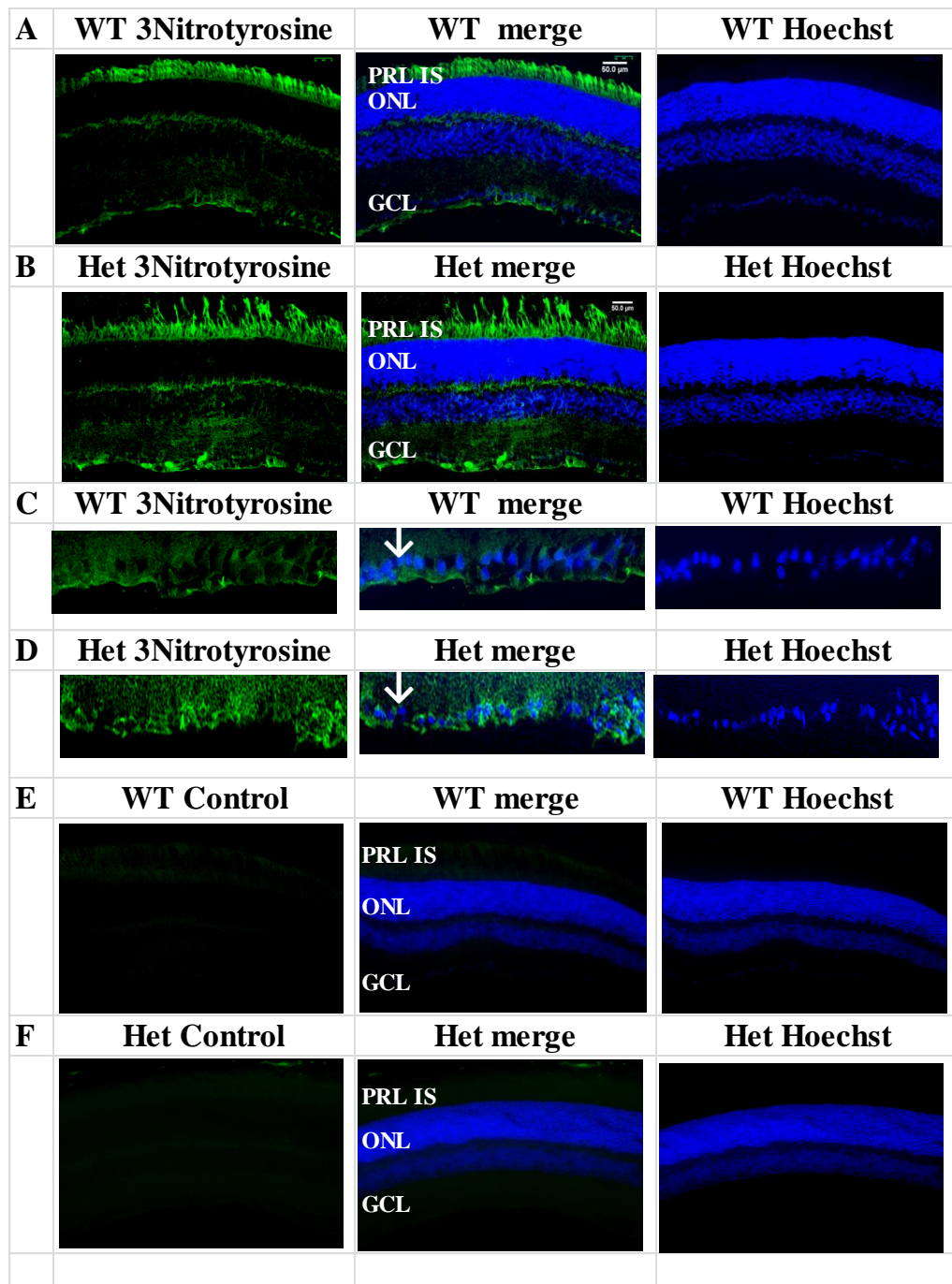


Figure 5.11 3Nitrotyrosine deposition in retina of WT and Het

Representative images of 3 nitrotyrosine deposition in WT and Het retina (A-B) showing RGC regions for (C) WT and (D) Het (indicated by arrows). (E) Control sections for WT and (F) Het were processed without the primary antibody.

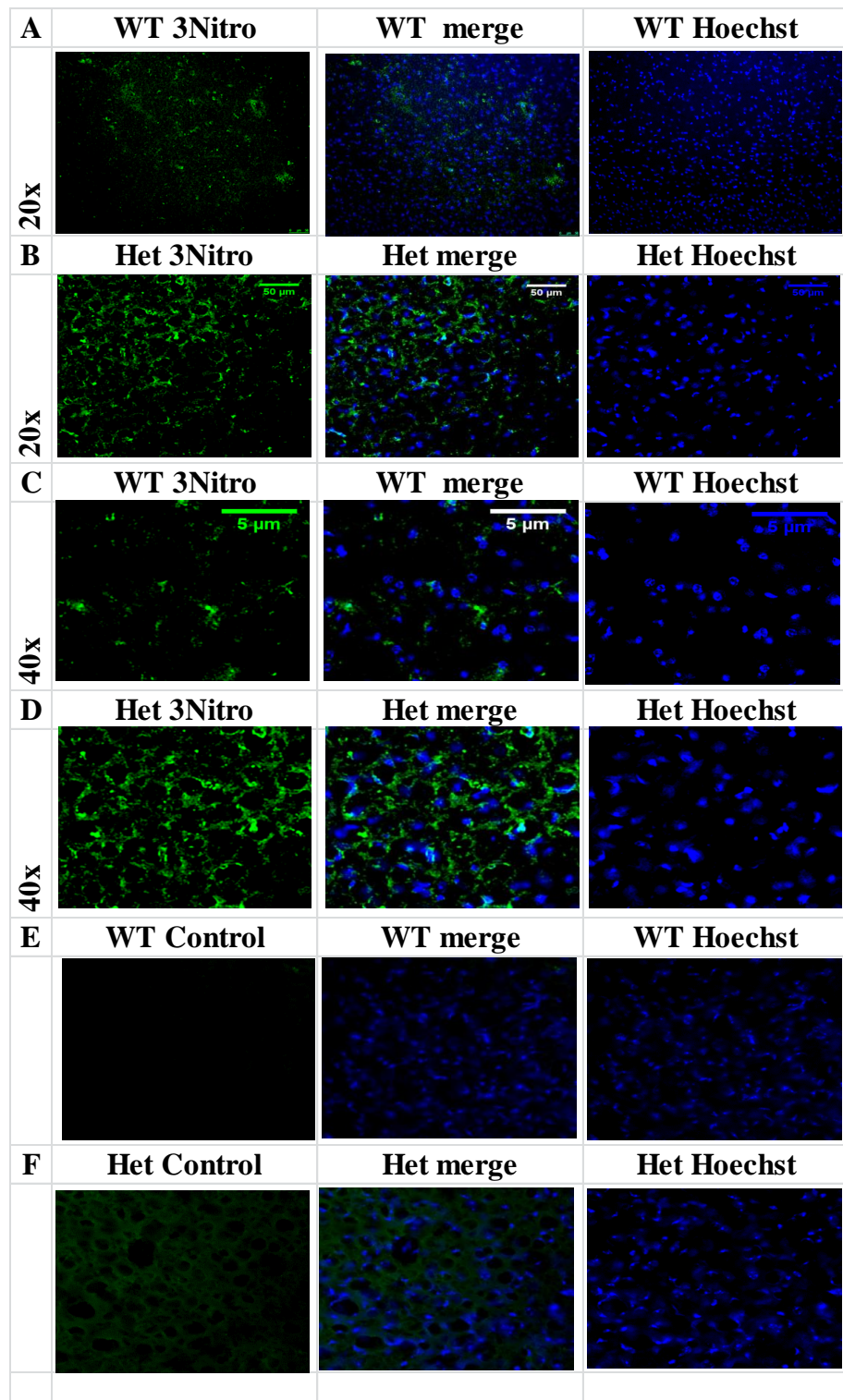


Figure 5.12 3 Nitrotyrosine deposition in brain of WT and Het

Representative images of 3Nitrotyrosine deposition in WT and Het brain (A-B) with 40x magnified regions (C-D). Control sections for WT and Het (E-F) were processed without primary antibody.

5.1.5 Discussion of antioxidant SOD expression in *Het*

The combined percentage reduction of MnSOD expression in *Het* retina was 38%. The retinal MnSOD assay demonstrated a 58% reduction in functional activity. This suggested that 20% of the expressed MnSOD was not functionally active. The percentage reduction of MnSOD expression in *Het* brain was 81%. This correlated with the 75% reduction in MnSOD activity in *Het* brain.

The percentage difference in the deposition of 3 nitrotyrosine between WT and *Het* was compared to the percentage difference in MnSOD expression in retinal layers. This was then used to generate the ratio of MnSOD compensation against 3 nitrotyrosine deposition. As before, a ratio of less than a value of 1 suggested that control factors against nitrotyrosine were successfully combatting the damage mediated effects. Figure 5.13 shows this finding.

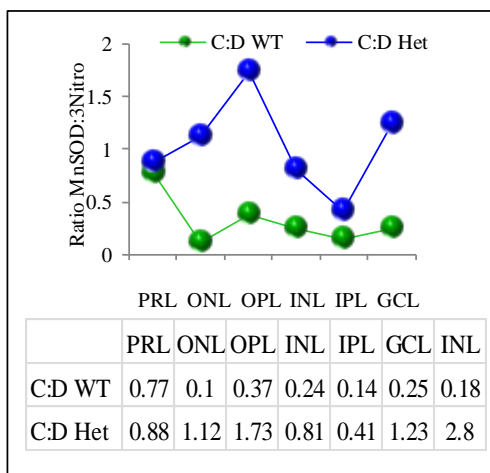


Figure 5.13 The ratio of MnSOD to 3 nitrotyrosine in retinal layers of WT and *Het*

*Graph shows the ratio of MnSOD expression to 3 nitrotyrosine deposition in WT and *Het* retina where a value of less than 1 was considered beneficial in the control of damage mediated activity.*

MnSOD competes with nitric oxide for the reaction with O_2^- and prevents the generation of peroxynitrite. MnSOD can be the target of nitration leading to a reduction in its enzymatic activity. (MacMillan-Crow and Thompson 1999; Bayir et al. 2007; Surmeli et al. 2010). Of the seven tyrosine residues two are potential targets due to their surface location (Perry et al. 2009; Porta et al. 2010). Nitration of Tyr34 results in MnSOD inactivation (Demicheli et al. 2007).

Chapter 5 Antioxidant deficit in $Opa1^{Q285STOP}$ mouse

5.1.6 Summary of Chapter 5: Antioxidant impairment in $Opa1^{Q285STOP}$ mouse

There was a significant reduction in antioxidant activity of $Opa1^{Q285STOP}$ mouse tissue homogenates compared to WT.

5.1.6.1 Significant reduction of catalase activity in $Opa1^{Q285STOP}$ mouse

The antioxidant activity of catalase was significantly reduced in both spinal cord and retina of Het mouse homogenate. Catalase activity in Het brain homogenate was not significantly different to WT.

5.1.6.2 Significant reduction of SOD activity in $Opa1^{Q285STOP}$ mouse

Compared to WT, the total SOD activity was reduced in Het brain, spinal cord and retina. Spinal cord homogenate showed the highest tissue specific reduction of all SOD activity. MnSOD activity was reduced by greater than 75%. CuZnSOD activity was reduced by more than 60%.

The reduction of antioxidant activity observed in all tissues of Het mouse was considered secondary to the bioenergetic deficit as observed in the previous chapter. The reduction in catalase activity in the spinal cord and retinal tissue homogenate and not brain suggested that there was tissue specific preservation of catalase activity. The reduction of MnSOD in all tissues tested suggested several possible scenarios: that either there was a reduction in the requirement for MnSOD due to the bioenergetic reduction especially in complex I. Or that there was insufficient production of MnSOD although it would appear unlikely as the phenotype changes which occur at a late stage (more than 10 months) would more likely manifest at an earlier age. Or possibly MnSOD activity was specifically reduced possibly due to the presence of nitration to the susceptible tyrosine residues present on the surface of the MnSOD molecule.

Chapter 6 Trial of resveratrol in Opa1^{Q285STOP} mouse

6.1 Introduction

The objective of the trial was to determine if the administration of resveratrol as an antioxidant could alleviate potential ROS induced optic atrophy. The retinal pathology in Opa1^{Q285STOP} mouse was considered late on-set beginning at 12 months. The efficacy of resveratrol administration in other ophthalmic conditions (Kubota et al. 2009; Zheng and Kern 2009; Zheng et al. 2009; Zheng et al. 2010a), indicated that resveratrol could gain access through the retinal-brain barrier. The second objective of the trial was the safety aspect of resveratrol administration over a prolonged period of time where the female recipients would be crossed to generate the next cohort of study subjects.

6.2 Other potential therapies

A range of potential antioxidant therapies were considered. Endogenous antioxidant activity is finely balanced with ROS/RNS production in healthy tissue with an ongoing damage limitation by repair [DNA] or replacement (oxidised proteins). In 1991, (Sies 1991) defined the term oxidative stress as ‘a disturbance in the prooxidant-antioxidant balance in favour of the former leading to potential damage’. Summarised are a selection of antioxidant therapies with relevant clinical trial results.

6.2.1 Coenzyme Q₁₀ & synthetic derivative Idebenone

Coenzyme Q₁₀ (CoQ₁₀) or ubiquinone is a biologically active quinone found in the membranes of the endoplasmic reticulum (ER) peroxisomes and the inner mitochondrial membrane. Within the electron transport chain, (ETC) electrons pass from complex I NADH and complex II succinate to CoQ₁₀ where it functions as an electron carrier from both complexes to complex III. CoQ on the inner mitochondrial membrane accepts electrons from reducing equivalents generated during fatty acid and glucose metabolism and transfers them to electron acceptors. The reduced form of CoQ₁₀H₂ in the cell membrane inhibits lipid peroxidation when low-

Chapter 6 Trial of resveratrol in Opa1^{Q285STOP} mouse

density proteins (LDL) and cell membranes are exposed to oxidising conditions *ex vivo*. The formation of oxidised lipids and consumption of α tocopherol are suppressed when CoQ₁₀H₂ is present.

The biopharmaceutical kinetics of Idebenone inhibits lipid peroxidation and prevents oxidative damage by preserving ATP formation. It is rapidly absorbed with a peak plasma level within 15 minutes after oral administration and a half-life of between 2.2 0 15 hours. The highest concentrations are found in the GI tract, liver and kidney. It is excreted via the renal system within 18 hours of administration with no cumulative effects.

The mode of action of Idebenone can function in either an oxidised or a reduced state. Its effects on astroglial cells demonstrate an inhibition of enzymatic metabolism of arachidonic acid by cyclooxygenase and lipoxygenase. In its reduced form, Idebenone has a powerful anti-inflammatory effect within the CNS (Paolino et al. 2004). *In vitro* experiments in cell culture show synaptosomes of rat brain cortex under oxidative injury are protected from ROS within the cytosol and mitochondria. (Rauchová et al. 2008) et al., 2006) Oxidative lipid peroxidation is reduced and it may confer some protection to mitochondrial cell membranes (Becker et al 2010).

6.2.1.1 Reasons for non-selection

Idebenone although marketed as a substitute for CoQ₁₀ has activities that CoQ₁₀ clearly does not possess. It has some antioxidant properties against the products of lipid peroxidation but despite extensive clinical trials in various disorders (Friedrich's ataxia, MELAS, Parkinson's disease) the overall primary outcome –gross motor function, lowering of cerebral lactate and increasing plasma CoQ₁₀ levels remains dependant on several factors including age, stage of disease process and quantity of does administration.

6.2.2 Minocyclin

A tetracycline analogue lacking methyl and hydroxyl groups' minocyclin is a highly lipid soluble long acting protein inhibitor and inhibitor of 5 lipoxygenase. Minocyclin binds to the

Chapter 6 Trial of resveratrol in Opa1^{Q285STOP} mouse

30S ribosomal subunit preventing the binding of tRNA to mRNA ribosome complex. Metabolised in the liver minocyclin is prescribed in cases of acne.

The documented toxicity studies include increased I¹²⁵ uptake and thyroid tumour incidence (Doerge et al. 1997) retinal pigment epithelial apoptosis via p38 MAPK pathway and p38 phosphorylation (Hollborn et al. 2010) neurotoxicity including induction of proapoptotic GADD 45 γ , IFN1 and cytokine induced growth factor (Krügel et al. 2011)

6.2.2.1 Reasons for non-selection

Opa1^{Q285STOP} mouse general health is good. They are mobile well developed and reproduce albeit with slightly reduced brood size. The average lifespan exceeds 24 months. Given the option of antioxidant treatment with minocyclin and no treatment, the literature provides compelling evidence that no treatment would be the healthier option. These mice have an extensive mitochondrial haploinsufficiency that puts them in a high-risk category. It is not the intention of this therapy to risk their health with an agent that carries an inordinate number of documented and potential toxic side effects.

6.2.3 Cyclosporine

The use of cyclosporine in the prevention of graft versus host disease exerts specific T helper cell immunosuppression.. Cyclosporin binds to cyclophilin which forms a calcineurin inhibiting complex normally responsible for transcription of interleukin 2 (IL2).Repeated topical application of cyclosporine for the treatment of keratoconjunctivitis at 0.1% concentrations has been reported to induce acute inflammatory reaction on rabbit eye resulting in a breakdown of the blood retinal barrier and increased aqueous protein concentration (Toshida 1998).

6.2.3.1 Reasons for non-selection

The toxicity of cyclosporine includes nephrotoxicity, hypertension, and diabetes and haemolytic uraemia. There is also evidence of its potential carcinogenic properties (Weischer et al. 2007) et al. 2007). Documented reports of oxidative and nitrosative stress with elevated

Chapter 6 Trial of resveratrol in *Opa1^{Q285STOP}* mouse

expression of inducible nitric oxide are reported in a variety of organs including renal (Josephine et al. 2007) hepatic (Lee 2010) and neurological (Schröter et al. 2005).

6.2.4 Memantine

Memantine is an amantadine derivative with a moderate-affinity for NMDA receptors. It is a non-competitive NMDA receptor antagonist that binds preferentially to NMDA receptor-operated cation channels. It blocks the effects of excessive levels of glutamate that may lead to neuronal dysfunction by acting on glutamatergic neurotransmission. There is some evidence that dysfunction of glutamatergic neurotransmission, manifested as neuronal excitotoxicity, is involved in the aetiology of Alzheimer's disease (Cacabelos et al. 1999). Memantine undergoes partial hepatic metabolism. About 48% of administered drug is excreted unchanged in urine. Side effects include pain, leg pain, fever, increased appetite, dizziness, confusion, headache, hallucinations, and tiredness. Less common side effects include vomiting, anxiety, and hypertonia.

Memantine has the ability to block only the excessive pathological inducing NMDA receptors with an uncompetitive mechanism and a fast off rate. With neurodegenerative conditions, the existence of extra synaptic NMDA's causes an increased Ca^{+2} influx. NADPH oxidase (NOX) in the presence of increased Ca^{+2} levels activates neuronal NO synthase (nNOS) to generate nitric oxide (NO). Recently Nakamura (Nakamura and Lipton 2011) published a report on the role of s-nitrosylation which he states is responsible for protein misfolding in many neurodegenerative diseases including Parkinson's α synuclein protein and Alzheimer's amyloid β and Tau proteins.

6.2.4.1 Reasons for non-selection

The safety review by the NDA (pharmaceutical marketing: report location at [:www.fda.gov/ohrms/dockets/ac/03/briefing/3979B1_04_FDA-Safety%20Review.pdf](http://www.fda.gov/ohrms/dockets/ac/03/briefing/3979B1_04_FDA-Safety%20Review.pdf)) published an extensive safety report on this agent. The manufacturers (Forest Laboratories Inc.) reported the following effects on rodents (both rat and mouse populations) 'Corneal opacities, obscured retinal blood vessels and corneal endothelial vacuolization'. The cause of these clearly

Chapter 6 Trial of resveratrol in $Opa1^{Q285STOP}$ mouse

damaging effects was due to ‘abnormal local drug storage due to saturated excretion and not clinically relative’! Further rodent exposure to the product reveals cortical neuron vacuolization lesions on brains of rat and mouse’ Forest laboratories concluded that these were ‘Olney lesions’. Rodent populations being susceptible to increased cortical ablation through necrotic cell death on administration of NMDA antagonists. This toxic effect is reported to be the result of increased metabolism and is associated with older animals. To date no Olney’s lesions have been proven or unproven to occur in human brain primarily because no one is looking for them

6.3 Resveratrol

Resveratrol was administered to mice over a 15-month period from time of conception. Resveratrol was added to drinking water at a concentration of 219.06 μ M, which was calculated as 13.5mg/kg. Concurrent treatment of mice with vehicle was given 0.1% ethanol administered in drinking water. In order to mimic the normal housing conditions of these mice, both WT and Het mice remained in shared cages. As the long term effects of resveratrol administration over a prolonged period were unknown, it was considered imperative to include an age matched WT cohort.

6.3.1 Resveratrol treatment administration

6.3.2 Selection of product

The isolation of resveratrol from established plant sources including Japanese knotweed requires extensive extraction steps to remove impurities. One impurity is emodin which is a naturally occurring product within Japanese knotweed and is known for inducing unwanted side effects relating to gastro intestinal disturbances. The specification of any resveratrol product required the reporting of emodin content. A most generous gift of resveratrol from Interpharma-Praha (a subsidiary of the Japanese Otsuka pharmaceutical company]) was made. The product included the specification sheet which stated resveratrol at a purity of 98.8% with an emodin content of less than 0.01% (Resveratrol specification sheet Appendix B).

6.3.3 Selection of dose

The dose of resveratrol administered was selected on the established NOAEL (No-observed-adverse-effects-level) which was reported as 22.4mg/kg (Crowell et al. 2004; Horn et al. 2007; Edwards et al. 2011). As the mice were to receive resveratrol for a 15 month period and during gestation, it was decided to reduce the prescribed dose to 13.56g/kg. This would provide 219.06µm a day. The administration of resveratrol during gestation required embryo-fetal toxicity studies. The dose of resveratrol from 20mg/kg up to 100 mg/kg were reported in a diversity of animals including rat (Breinholt et al. 2003; Williams et al. 2009) chick (Hancock and Miller 2006; Dias et al. 2008) bovine (Klinge et al. 2008) and mouse (Huang et al. 2009; Singh et al. 2011). There were no reports of adverse effects on either mother or embryos. Table 6.1 shows the calculations used to obtain the dose of mg/kg.

Table 6.1 Dose of resveratrol mg/kg

	MW	Stock	mM/ml	mg/L	µM/L	Vol/	Dose	Weight	mg/kg
		mg/ml				/ml	mg/ml	/kg	
Res	228.2	50	219.07	50	219.07	5.7	0.05	0.021	13.57
Etoh	46.07	0.789	17.13	789	17.13	5.7	0.789	0.021	214.16

Table shows the molecular weight and the dose per kg weight calculated by multiplying the volume by the dose and dividing by weight in kg

6.3.4 Route of administration

The route of administration was considered an imperative part of this trial. Reports of administration by intraperitoneal injection were considered inappropriate for a prolonged study. Treatment by gavage was also considered inexpedient as the effects of daily handling for the purposes of gavage were likely to traumatize the mouse. The administration of resveratrol in water was the most appropriate route. Stock resveratrol was prepared in 1 ml aliquots. The molecular weight of resveratrol was 228.24. Stock resveratrol was prepared by adding 2.5g/50ml ethanol. This gave 0.05g at a concentration of 219.06mM per ml. One 1ml aliquot was added to 1 litre of drinking water which gave 49.99mg of resveratrol containing 219.06µM. Mice were given resveratrol in drinking water at a dose of 13.57mg/kg calculated as volume of water ingested (5.7ml) multiplied by the dose in mg/ml 0.0499 divided by weight of an average

Chapter 6 Trial of resveratrol in $Opa1^{Q285STOP}$ mouse

mouse in kg (0.021). Resveratrol was sensitive to light at 366nm so mouse water bottles were covered in blue filter, which blocked this wavelength (Lee filters 355). The presence of blue filter cover did not alter water consumption in resveratrol treated mice.

6.3.5 Vehicle treated controls

For vehicle treated animals, 1ml of 100% ethanol (0.789mg/l) was added to 1 litre of drinking water which provided 17mM ethanol. Drinking bottles were covered in green Lee filter to maintain consistency in the trial and allow immediate identification of the bottle contents.

6.3.6 Daily water consumption in C57Bl/6

The daily consumption of water was measured over a 1 week period using a commercial mouse water bottle with a ball bearing which prevented leakage when the cage was moved. The daily content of the water bottle was measured using a syringe for accurate analysis. The mean daily water intake in both WT and Het mice was 5.7 ± 0.4 ml. These findings were in agreement with previously published data on water consumption in C57BL/6 mice (Bachmanov et al. 2002).

Resveratrol could be dissolved in ethanol or DMSO. Ethanol was used as DMSO can impart antioxidant properties (Santos et al. 2003; Colucci et al. 2008) which would confound the effects of resveratrol. The density of ethanol was 789g/l with a molecular weight of 46.07. The alcoholic content of the vehicle was examined. In the UK a unit of alcohol is defined as 10ml of pure ethanol or 7.9g/ml. The percentage alcohol by volume (%AbV) of 0.1% in an end volume of 5.7ml was 1.75%AbV (Tapson 2004).

The calorific content of vehicle treatment was considered. There is 230kJoule (55 calories) in 1 unit of alcohol. Vehicle and res treated mice received 0.131kJ(0.03cal) daily from a volume of 5.7ml.

6.3.7 Efficacy, health and safety

In order for resveratrol to be effective, it was imperative to refresh the contents within 24 hours of dispensing. This provided an excellent opportunity to observe the mice for any signs of adverse effects. Daily weigh recordings were changed to weekly when it was considered mouse

Chapter 6 Trial of resveratrol in $Opa1^{Q285STOP}$ mouse

weight was maintaining stability. In the subsequent mice, weekly weighing was continued for 16 weeks following weaning and continued throughout the duration of the trial at monthly intervals from month 4. The reason for selection of 16 weeks was with the female pups, this was the age at which they were ready for mating and would be separated from the mum (Appendix D contains weekly and monthly growth rates). The efficacy of resveratrol treatment was tested in vivo at 12 months of age with SHIRPA, rotarod, narrow beam and tight rope testing. At 15 months, cognitive function testing was performed. At 15 months of age, mice were culled for full tissue retrieval. Growth rates were calculated using the weekly and monthly weight recordings. The rate was calculated as the difference between the initial weight at weaning and the weight at day 28 which is when mouse reaches his maximum post natal growth (Eisen 1976).

6.3.8 Bioavailability of resveratrol

In order to determine the bioavailability of resveratrol in mice treated over a 15-month period, whole blood analysis was analysed by HPLC-UV.

Measurement of resveratrol was performed with modifications according to Biasutto (Biasutto et al. 2010). Whole blood from both resveratrol and control treated mice was collected at time of tissue retrieval. Whole blood was collected in pediatric EDTA vials and inverted to permit mixing. Blood was stabilized with the addition of freshly prepared ascorbic acid (10mM at 0.1 vol), and acidified with 0.6M acetic acid at 0.1 vol. Following mixing, 4 volumes of acetone was added followed by sonication (or vortexing) for 2 minutes. Blood was centrifuged at 4°C for 8 minutes at 10,000g. Supernatants were transferred to a fresh tube where acetone was evaporated by vacuum centrifugation at room temperature. Samples were precipitated with methanol and 20µl was applied to a Gemini C18 reverse phase column. Untreated blood samples were spiked with known quantities of resveratrol to determine the yield of recovered product.

Chapter 6 Trial of resveratrol in *Opa1^{Q285STOP}* mouse

6.3.8.1 Reasons for selection

Resveratrol has an excellent safety record with no documented side effects. The dose required to exert any toxicological effect was a staggering 3000mg/kg (13.14mMol/kg) –over 3.5 thousand times the recommended dose. The side effects produced nephrotoxicity as resveratrol is eliminated via urine, dehydration, dyspnoea, rough coat, diarrhoea, anaemia and in male rat leukocytosis. Mice were given resveratrol at a concentration of 219.06mM in their drinking water. Vehicle treated mice were given ethanol at a concentration of 17mM. Mice were examined thoroughly for any adverse effects including gastro intestinal disturbances that might indicate the presence of emodin at greater than acceptable concentration. The bottled water containing resveratrol required replacement at 24 hour intervals which also provided an opportunity to examine the mice for signs of stress. The trial design is available in Appendix C.

6.3.9 Solubility of resveratrol

The solubility of resveratrol in water was less than 3% (Kristl et al. 2009). Stock resveratrol was prepared in 1ml aliquots in 100% ethanol. This was added to one litre of tap water and used to fill mouse drinking bottles. The addition of the ethanol base product to tap water could potentially cause precipitation. This potential precipitation was investigated.

6.3.9.1 Spectrophotometric analysis of resveratrol

Stock resveratrol at 50mg/ml was diluted to 0.05mg/ml in either 100% ethanol which represented complete dissolution or cold tap water. This was mixed by inversion. *Trans* resveratrol can photoisomerise to *Cis* resveratrol when exposed to UV. The absorption coefficient of *Trans* resveratrol at 304nm is 33400 M⁻¹ cm⁻¹ (Pinto et al. 1999). The expected absorbance of 219.06µM of resveratrol at 304nm wavelength was calculated from the absorption coefficient of 33400 M⁻¹ cm⁻¹ was 7.316. The product was further diluted to permit spectroscopy analysis at 200-450nm.

6.3.9.2 Results of resveratrol solubility

The absorbance of resveratrol at 304nm wavelength in 100% ethanol was 0.918. The absorbance of resveratrol in 0.1% ethanol was 0.903. The concentration of resveratrol in 100%

Chapter 6 Trial of resveratrol in *Opa1^{Q285STOP}* mouse

ethanol was calculated as 27.48 μ M and with the dilution factor (times 8) gave a final concentration of 219.8 μ M. The concentration of resveratrol in 0.1% ethanol was calculated as 27.03 μ M and adjusted with the dilution factor was 216.28 μ M. The presence of *Cis* resveratrol was observed at 286nm wavelength. Resveratrol in 100% ethanol had an absorbance of 0.031 which was 7.425 μ M. Resveratrol in 0.1% ethanol contained 4.311 μ M *Cis* resveratrol with an absorbance of 0.018 at 286nm. In order to reduce precipitation, the tap water was allowed to reach room temperature (RT) and the readings repeated. *Trans* resveratrol in 0.1% ethanol and water at RT had an absorbance of 0.912 at 304nm which was 218.44 μ M. *Cis* resveratrol absorbance at 286nm was 0.022 which was 5.26 μ M. Figure 6.1 shows the absorbance spectra of resveratrol.

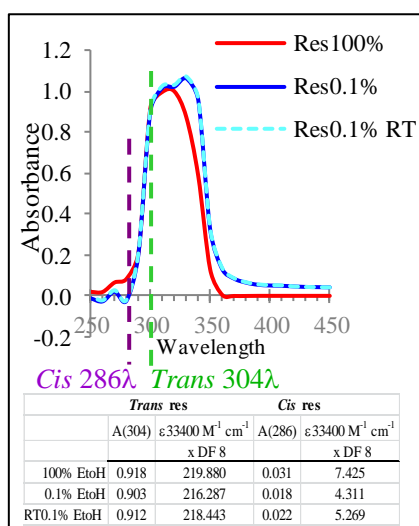


Figure 6.1 Absorbance spectra of resveratrol in ethanol and tap water

Absorbance of Trans resveratrol in 100% ethanol at wavelength of 304nm was 0.918. In 0.1% ethanol the absorbance was 0.903. In 0.1% ethanol (RT) the absorbance was 0.912. The absorbance of Cis resveratrol in 100% ethanol at wavelength of 286nm was 0.031. In 0.1% ethanol the absorbance was 0.018. In 0.1% ethanol (RT) the absorbance was 0.022.

6.3.9.3 Discussion of resveratrol solubility

The addition of resveratrol to cold tap water caused 1.6% precipitation. By allowing the tap water to reach room temperature there was a reduction to 0.65%. Stock drinking water was allowed to stand at room temperature prior to dispensing.

6.4 Health monitoring of mice on resveratrol trial

6.4.1 Introduction

Throughout the trial, the health and safety of the mice was paramount. The general health of Opa1^{Q285STOP} mouse was good with a satisfactory breeding record. As this therapy was designed to improve their mitochondrial health, any deviation from normal mouse behaviour while receiving resveratrol or vehicle may have required withdrawal from the trial. In the original cohort, one mouse was removed from the trial due to gastro intestinal disturbance. As it transpired, this was not due to resveratrol as he continued to have occasional upsets throughout without any change in body weight. A second female mouse was lost to trauma at seven months. Shredded nesting material became wrapped around her hind limb resulting in extensive ischemia. This mouse would have required limb amputation under general anaesthetic. Due to her immediate distress she was culled.

6.4.1.1 Weight monitoring

The weight of the mice was recorded throughout the trial. With all participants, weight was recorded weekly for a minimum of sixteen weeks. Thereafter weights were recorded monthly. Mouse reaches its maximum post natal growth rate at about half its mature asymptotic weight (Eisen 1976). There is an increase from birth to 28 days followed by an eventual stabilization which is dependent on sex, diet and environment (Cheek and Holt 1963).

As mouse weights were recorded weekly for the first 16 weeks post weaning, the growth rate was calculated for the first 4 weeks following weaning. Weight monitoring continued throughout the trial at monthly intervals to 15 months.

Any variation in monthly weight would indicate that the chronic administration of resveratrol or vehicle was having an adverse effect (Appendix D contains weekly and monthly weight rates for all animals tested). Body weight and brain weight are reported in grams (g). Cardiac weight is reported as a ratio of body weight.

6.4.1.2 Results of weight monitoring

Res treated female WT (n13) growth rate was 1.57±0.35. Vehicle treated female WT (n6) growth rate was 1.08±0.37 which was not significantly different to res WT female (p=0.747). Res treated Het female (n16) growth rate was 1.28±0.49. Vehicle treated Het female (n11) growth rate was 1.16±0.54 which was not significantly different to female res Het(p=0.801). Resveratrol treated male WT (n9) rate was 1.70±0.68/g. Vehicle treated male WT (n6) rate was 1.75±0.61 which was not significantly different to res WT male (p=0.182). Male res Het (n8) growth rate was 1.77±0.61. Veh treated male Het (n7) growth rate was 2.0±0.55 which was not significantly different compared to res male Het (p=0.135).

At 15 months, full tissue retrieval was performed and mouse body, brain and cardiac weight was documented. Table 6.2 shows the mean weight ±SD in all untreated, res and veh treated male and female Het. Male Het populations have been analysed according to housing conditions as was previously seen solitary housed mouse brain weight was increased and cardiac weight ratio reduced. There were no solitary housed veh treated male Het mice. The statistical significance between groups is shown with the percentage difference between untreated and treated Het.

		n	Body weight(g)	Brain weight(g)	Cardiac Ratio
	F Het	25	26.9 ± 4.0	0.48 ± 0.05	0.64 ± 0.10
	rFHet	22	28.8 ± 2.8	0.42 ± 0.07	0.62 ± 0.10
	vFHet	11	28.2 ± 3.3	0.45 ± 0.02	0.55 ± 0.09
	FHet:rFHet		0.135	0.025	0.505
	FHet:vFHet		0.401	0.263	0.035
	rFHet:vFHet		0.656	0.458	0.112
	F(11,191)		9.866	2.725	1.935
S	sMHet	14	32.6±1.0	0.49±0.03	0.60±0.03
O	srMHet	4	34.5±1.5	0.42±0.06	0.62±0.04
H L	sMHet:srMH		0.385	0.385	0.820
O O	sMHet:gmH		0.247	0.015	0.129
U	srMHet:grMH		0.450	0.829	0.962
S G	F(9,57)		1.043	1.037	2.565
I R	gmH	9	30.7±1.2	0.42±0.04	0.68±0.04
N O	grMHet	7	32.7±1.4	0.44±0.04	0.61±0.05
G U	gvMHet	7	32.7±1.4	0.45±0.05	0.72±0.05
	P gmH:grMH		0.308	0.672	0.275
	gmH:gvMH		0.308	0.653	0.452
	grMH:gvMH		0.998	0.981	0.083
	F(9,57)		1.043	1.037	2.565
	r=resveratrol v=vehicle s=solitary housed g=group housed				

Table 6.2 Body brain & Cardiac weight ratio in Het res & veh Het

Body, brain and cardiac weight ratio in untreated female and male Het compared to res treated Het showing a significant difference in female res treated brain weight compared to untreated (p=0.025). Compared to untreated male Het, res treated male Het was not significantly different in any weight measures. Compared to untreated males, veh treated Het male was not significantly different in any weight measures.

Chapter 6 Trial of resveratrol in $Opal^{Q285STOP}$ mouse

6.4.1.3 Discussion of weight in res treated Het at 15 months

The brain weight in res treated female Het population weighed 17% less than untreated female Het. Veh female Het brain weight was 10% less than untreated female Het which suggested that resveratrol was responsible for at least 7% reduction in brain weight. Solitary housed res treated male Het Male brain weight was reduced by 14% compared to solitary housed male Het. Group housed res treated male Het brain weighed 6% more than group housed male Het. Veh treated group housed male Het brain weight was increased by 7% compared to untreated male Het.

The cardiac weight ratio in res treated females was reduced by 4%. Veh treated female cardiac weight ratio was significantly reduced by 13% compared to untreated female Het ($p=0.035$). Cardiac weight ratio in solitary housed male res treated Het had a 3% increase compared to solitary housed untreated male Het. Group housed res treated males had a 10% reduction in cardiac weight ratio compared to group housed male Het. Veh treated group housed male Het had a 7% increase in cardiac weight ratio compared to untreated group housed male Het.

6.5 Neuromuscular dysfunction in res treated $Opal^{Q285STOP}$ mouse

6.5.1 Introduction

Studies of the neuromuscular and cognitive function in the untreated Het mouse at 12 months clearly demonstrated impaired musculoskeletal function. SHIRPA analysis revealed extensive aberrations in all but the sensory function. As many of these tests were observational in method, the reduced visual acuity of Het mouse did not bias findings.

It was the intention to repeat these phenotypic analyses to determine the effect of resveratrol after a 12 month administration period.

6.5.2 SHIRPA analysis in res treated $Opal^{Q285STOP}$ mouse

For SHIRPA analysis eight resveratrol treated Het mice were analysed with 10 untreated Het mice. The test was performed as described in Chapter 3.2. Essentially, different functional abilities were scored depending on whether the animal was in the arena under observation or

Chapter 6 Trial of resveratrol in *Opal*^{Q285STOP} mouse

whether performing physical tasks. The raw data from SHIRPA analysis of res treated Het mouse is shown in Appendix G.

For lower motor function there were a total of eleven independent tests, for cerebrospinal function, a total of 12 tests, sensory function had 7 tests, neuropsychiatric had eight tests and autonomic had 17 independent tests. Results are shown as the mean direct score (SD±1).

6.5.2.1 Results of SHIRPA analysis in res treated Het mouse

SHIRPA	
Het	8
rHet	6
FHet	5
rFHet	3
MHet	3
rMHet	3

Table 6.3 Summary of test numbers for SHIRPA analysis in untreated and res Het

The results for SHIRPA analysis are shown in Figure 6.2 where untreated WT has been included on the graph for comparison only. Appendix G contains the raw data for SHIRPA.

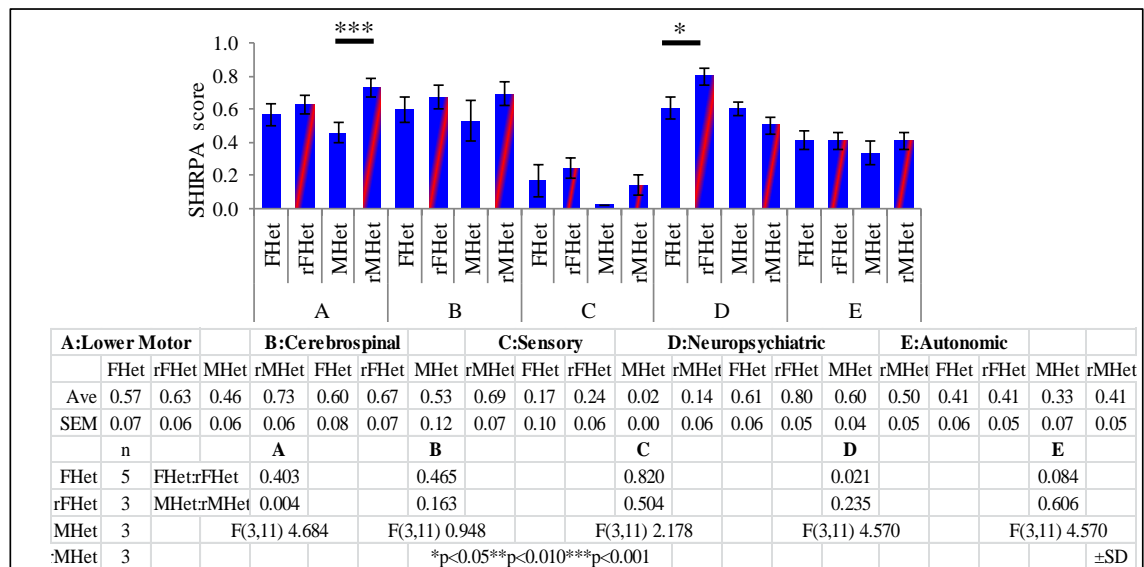


Figure 6.2 SHIRPA analysis in untreated and treated *Opal*^{Q285STOP} mouse

Graphs showing Observational SHIRPA analysis in untreated (n8) and res treated (n6) Het mice.

6.5.2.2 Discussion of SHIRPA in res treated Het

The functional impairment of untreated Het mouse was established at an earlier time. Any improvement in the five functional activities tested was not observed in resveratrol treated Het. In res Het mouse, lower motor function was significantly reduced by 60% in male res Het (F(3,11)4.684 p=0.004) compared to untreated male Het.

Chapter 6 Trial of resveratrol in *Opal*^{Q285STOP} mouse

Neuropsychiatric function in res Het female showed a significant 32% increase (F3,11) 4.570 p=0.021) compared to untreated female Het.

The results of SHIRPA indicated that resveratrol was exerting an adverse effect in the lower motor function of male res Het and in the neuropsychiatric function of female res Het. These findings would be confirmed using other phenotypic testing.

6.5.3 Rotarod analysis in res treated *Opal*^{Q285STOP} mouse

Rotarod Analysis			
F Het	13	M Het	15
rFHet	7	rMHet	6
vFHet	5	vMHet	0
sMHet	5	gMHet	10
srMHet	3	grMHet	3
s:solitary	g:group	r:res	v:veh

Table 6.4 Summary of test numbers for rotarod analysis in untreated res and veh Het

Untreated female Het latency was 84±4 seconds. Latency in resveratrol treated Het females was 62±6 seconds which was significantly reduced when compared to female Het (F (4,41) 1.867 p=0.021). Vehicle treated female Het latency was 62±2 seconds which was significantly reduced compared to untreated female Het (F (4,41) 1.867 p=0.040). Untreated male Het latency was 71±5 seconds Latency in male res Het mouse was 72±5 seconds which did not differ significantly to untreated male Het (p=0.848). Figure 6.3 A shows a summary of rotarod latency to fall in res treated Het mouse.

As previously examined, housing conditions influenced the latency to fall in male mice. Latency to fall in untreated solitary housed male Het mice was 109±14 seconds Latency in res treated solitary housed male Het mice was 64±13 seconds which was significantly reduced compared to untreated solitary housed male Het (F (3,17) 1.992 p=0.001). Latency in untreated group housed Het males was 35±7 seconds. Res treated group housed Het male latency was 72±6 seconds which was significantly increased compared to untreated (F (3,17) 1.992 p=0.001). Figure 6.3 B shows a summary of these findings.

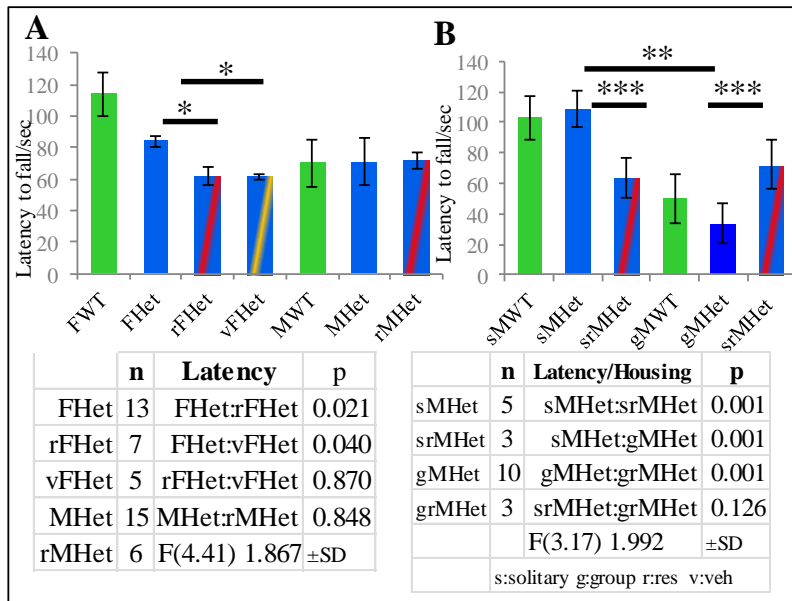


Figure 6.3 Rotarod latency in untreated and treated Het mouse

Graph shows mean ±SD (A) Latency to fall in untreated and treated female and male Het mice. (B) Housing conditions in solitary and group housed untreated and treated male Het.

6.5.3.1 Discussion of rotarod in res treated Het mouse

There was a reduction in latency to fall in the resveratrol treated Het mice. Female Het mice showed a reduction of 18% compared to untreated female Het mice. Male res treated Het mice had less than 4% reduction compared to untreated Het males. Housing conditions did not appear to have a significant effect on resveratrol treated males unlike untreated males who performed significantly better as solitary housed animals. Vehicle treated female Het mice had a significant 23% reduction in latency compared to untreated female Het mice. There was no significant difference between the res and vehicle treated female Het mice. Whether the reduction in latencies was due to the ethanol content was investigated further.

The effects of body weight were considered; Untreated female Het who weighed less than 28g had a latency of 87±5 seconds. Res treated female Het weighing less than 28g had a latency of 63±5 seconds which was significantly reduced compared to untreated female Het (F7,370) 5.716 p=0.002). Latency in untreated Het males who weighed less than 34g was 80±3 seconds and latency in res Het males weighing less than 34g was 67±6 seconds which was not significantly different to untreated Het (p=0.077).

6.5.4 Narrow beam testing in res treated *Opal^{Q285STOP}* mouse

The narrow beam test was performed as previously described in Chapter 3.2. Mice were placed at one end of an elevated gradually narrowing beam and on completing the distance of 60cm

Chapter 6 Trial of resveratrol in *Opa1^{Q285STOP}* mouse

returned to their home cage. The test measured mouse gait and spatial awareness. The initial test was designed to measure the distance travelled on the beam, however as previously identified, Het mice had initiation issues where no travel down the beam was observed. It was decided to continue with this test measure as any improvement could be rapidly detected.

6.5.4.1 Results of narrow beam test in res treated Het mouse

Beam/Rope			
F WT	5	M WT	5
F Het	7	M Het	8
rFHet	4	rMHet	4
vFHet	3	vMHet	0

Table 6.5 Summary of test numbers for rope and beam in untreated, res and veh Het

Figure 6.4 A shows a summary of the initiation time on the narrow beam in untreated, res and veh treated female and male Het mice.

6.5.5 Tight rope test in res treated *Opa1^{Q285STOP}* mouse

The tight rope test was performed as described in Chapter 3.2.3. Mice were placed at the mid-point of an extended rope and supported until they had obtained purchase. The distance travelled from the mid-point was not in excess of 30cm. The test was designed to test symmetrical coordination and balance. The test measured the distance travelled on the rope.

6.5.5.1 Results of tight rope test in res treated Het mouse

Figure 6.4 B shows of the distance travelled on the tight rope in untreated, res and veh treated female and male Het mice.

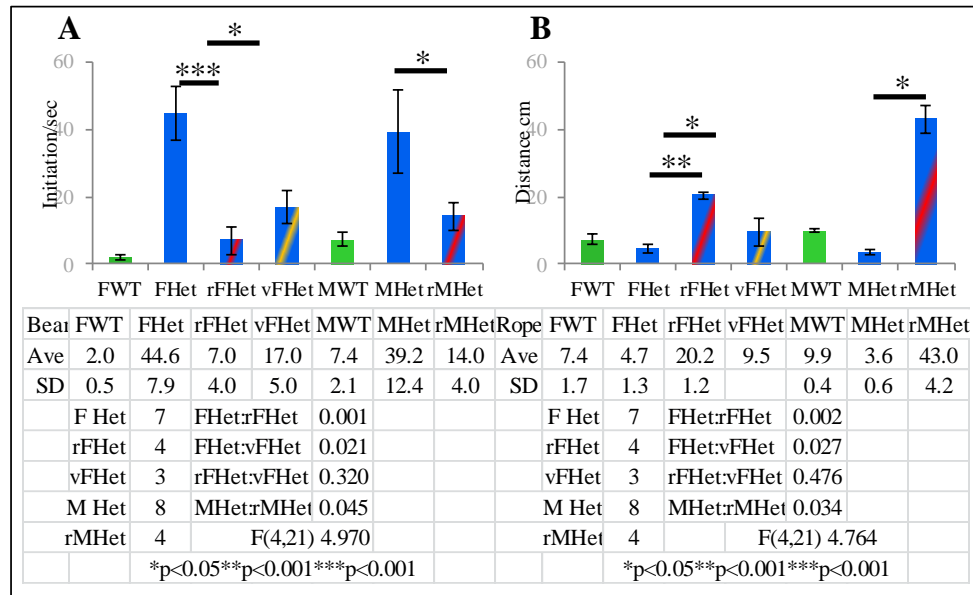


Figure 6.4 Beam initiation and rope distance testing in untreated and treated Het mice

Graph of means \pm SD (A) narrow beam time to initiation travel in seconds which was significantly reduced in both res and veh Het compared to untreated and (B) distance travelled in cm on tight rope in untreated, res and veh treated Het.

6.5.5.2 Discussion of narrow beam and tight rope in res treated Het mouse

Resveratrol treated Het mice appeared to excel at tests where the usual Het trepidation resulted in reduced performance scores. In the narrow beam test, the time to initiate travel on the narrow beam was reduced by 79% compared to untreated Het. Initiation time in veh Het had was reduced by 53% compared to untreated Het. The distance travelled along the beam in both res and veh Het was also significantly increased compared to untreated Het.

In the tight rope test, the distance travelled by the resveratrol treated Het mice was 4.1 fold further compared to untreated Het. Veh treated female Het were also significantly different compared to untreated Het (p=0.027).

The narrow beam test was designed as a spontaneous response to escape requiring spatial awareness and some coordination as the beam narrowed the result reflected the true nature of the problems inherent in the Het population. These difficulties appeared to have been overcome in the resveratrol treated Het mice because there appeared to be little hesitation at performing

Chapter 6 Trial of resveratrol in $Opa1^{Q285STOP}$ mouse

the task. Res treated Het mouse fear response appeared to be reduced thus permitting a quicker response to the task.

The tight rope test differed from the narrow beam test in that the ability to move along the rope in order to return to the home cage required skill and stamina. It also required an ability to determine the logic of travel along a rope 1cm in diameter. The untreated Het population travelled for 24 ± 2.2 seconds on top of the rope yet only covered 4.2 ± 1.0 cm in distance. The untreated Het population failed to cover more distance because their ability to gain balance was impaired. In most instances, once on top of the rope several Het mice simply froze in position anticipating their rescue within the test time of one minute.

The resveratrol treated Het mice spent 17.3 ± 5.3 seconds travelling on top of the rope and covered a significant 21.8 ± 2.5 cm ($F(4,21) 4.764$ $p=0.001$). Although they were curious about their environment, the test procedure did not lend itself to hesitation. More significant was the distance of 21.8 ± 2.5 cm given that the full length of the rope was 30cm. The reduced fear response in res treated Het resulted in a significant distance travelled in a shorter period of time.

6.5.6 Res Het mouse learning in training trials

The ability to learn from previous tests was shown to be impaired in the Het population. This was demonstrated by the use of improved rotarod latency over a three day period where the skills learnt on the first day of testing are applied on the second day, and those of the second day are applied on the third day of testing. The gradual increase or decrease in latency can be seen over the three day test period where the initial value changes incrementally. Negative values denote a reduction in score from the initial to the final value.

6.5.6.1 Results of mouse learning in res treated Het mouse

Female Het mice ($n=12$) had a learning score of 0.20 ± 0.12 . Female res Het ($n=7$) mice scored -0.160 ± 0.03 which was not significantly different compared to untreated female Het ($p=0.124$). Female vehicle treated Het ($n=5$) mice had a learning score of -0.160 ± 0.010 which was not significantly different to untreated female Het ($p=0.177$). Male Het mice ($n=14$) scored -0.195

Chapter 6 Trial of resveratrol in Opa1^{Q285STOP} mouse

± 0.021 and res Het males (n=6) scored -0.210 ± 0.030 which when compared to untreated Het males was not statistically significant (p=0.968).

Housing conditions did not influence learning ability in untreated and treated Het. There was no significant difference in learning skills between solitary housed (p=0.572) and group housed (p=0.761) in both untreated and res treated mice.

6.6 Cognitive dysfunction in res treated Opa1^{Q285STOP} mouse

6.6.1 Introduction

Concerns with the findings of reduced SHIRPA scores for neuropsychiatric and autonomic function combined with poor rotarod performance in the resveratrol treated Het population suggested that resveratrol appeared to be having a detrimental effect in the Het population. The cognitive function tests performed were the T maze test and novel object recognition as described in Chapter 3 section 2.2.

6.6.2 T maze analysis in res treated Opa1^{Q285STOP} mouse

As before, the investigation ratio and discrimination ratio were calculated from the combination of time spent in the novel arm divided by the time in both the original and novel arm (investigation ratio) and the time spent in the novel arm minus time in original arm divided by time in both novel and original arm (discrimination ratio).

A summary of mouse test numbers is shown in Table 6.6. All mice were within 14 days of their 15 month date of birth.

6.6.2.1 Results of T maze testing in res treated Het mouse

T Maze			
Het	16	rHet	9
F Het	8	rFHet	5
M Het	8	rMHet	4
vFHet	4	vMHet	3

Table 6.6 Summary of test numbers for T maze analysis in Het res and veh Het

The time taken to locate the novel arm was 23 ± 4 seconds in untreated Het mice. This was reduced to 15 ± 2 seconds in res Het mice which was significantly reduced compared to untreated

Chapter 6 Trial of resveratrol in *Opal^{Q285STOP}* mouse

Het (F (2,29) 4.639 p=0.021). Vehicle treated Het mice time to the novel arm was 12±1 seconds which was statistically different to untreated Het (p=0.008). The time spent exploring the novel arm was 20±2 seconds in Het mice and 27±2 seconds in res treated Het mice which was significantly more than untreated Het (F(2,29) 3.939 p=0.030). Veh Het spent 25 ±2 seconds in the novel arm which was not significantly different to untreated Het (p=0.137). The time spent in the original arm was 14±2/sec in untreated Het, 12 ±2 seconds in res treated and 14±2 seconds in vehicle treated Het mice. Res treated Het time in original arm was statistically reduced compared to untreated Het mice (F(2,29) 1.864 p=0.028). The time spent by veh Het was not statistically different to untreated Het (p=0.987). Figure 6.5 shows a summary of this data.

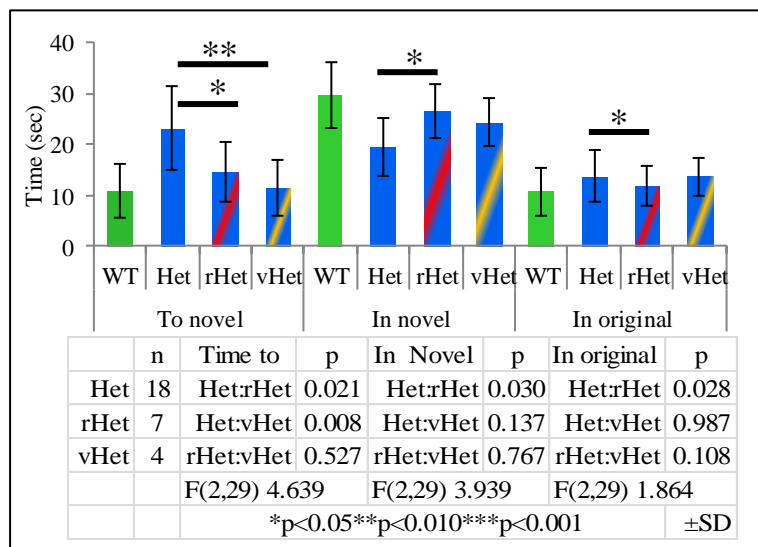


Figure 6.5 Parameters of T maze testing in untreated and treated Het mouse

Graph showing the mean ±SD of T maze testing parameters in untreated, res treated and veh treated Het was analysed by measuring: Het time to locate novel arm, Time spent in novel arm and Time spent in original arm in a series of seven consecutive tests.

From the above data, the investigation ratio (IR) was determined. In untreated Het mice the IR was 0.49 ±0.04. Res Het IR was 0.65 ±0.03 and in vehicle treated Het was 0.63 ±0.02. There was a statistical difference between untreated and res treated Het IR (F (2,29) 2.418 p=0.006). There was no statistical difference between untreated and veh treated Het mice (p=0.144).

The discrimination ratio (DR) in untreated Het was 0.14±0.06. In res treated Het the DR was 0.34 ±0.06 and in veh treated Het the DR was 0.26±0.05. There was a statistical difference between untreated and res treated Het (F(2,29) 6.708 p=0.002). There was no significant difference between untreated and veh treated Het (p=0.096). Figure 6.6 shows a summary of this.

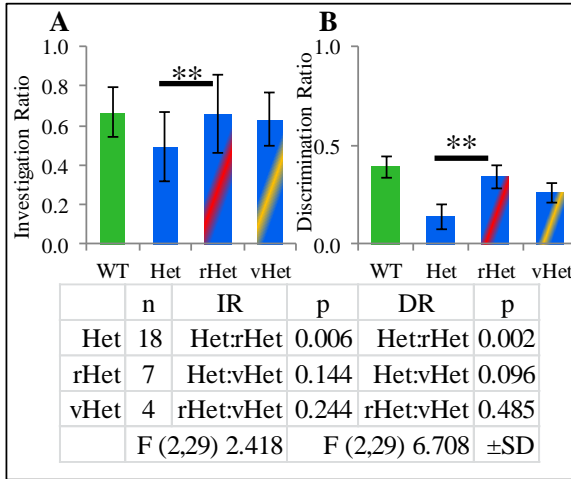


Figure 6.6 T Maze IR and DR in untreated and treated Het mouse

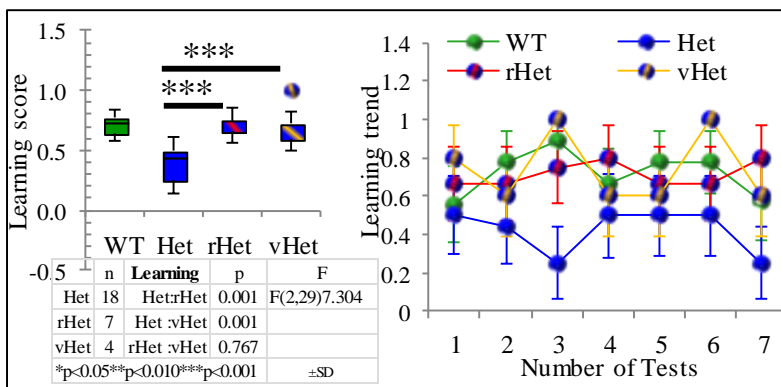
Graph showing the (A) IR and (B) DR in T maze testing of untreated Het, res and veh Het.

6.6.2.2 Discussion of T maze testing in res treated Het mouse

The IR in res treated Het was increased by 55% compared to untreated Het and veh treated IR was increased by 63%. This suggested that res and veh treated Het were less anxious and prepared to investigate their surroundings. The DR in res Het mice was significantly increased compared to untreated Het by 36%. The increase in veh treated Het DR was not statistically significant but represented a 30% increase compared to untreated Het.

The learning trend in res treated Het mouse was examined with respect to serial repeat testing. The mean score in untreated Het mouse was 0.14 ± 0.09 . Res Het score was 0.34 ± 0.13 which was significantly increased compared to untreated Het mouse ($F(2,29) 7.304$ $p=0.001$). Veh Het score was 0.26 ± 0.14 which was also significantly increased compared to untreated Het ($F(2,29) 7.304$ $p=0.001$). Figure 6.7 shows a summary of these findings.

Figure 6.7 T Maze Learning trend in Het, res and veh treated Het



The learning score for T maze in untreated Het was significantly reduced compared to both res and veh treated Het.

The trend showed untreated Het slow decline with recovery for no more than three consecutive tests. Both res and veh treated Het showed no decline in trend.

Chapter 6 Trial of resveratrol in *Opa1^{Q285STOP}* mouse

6.6.3 Novel object recognition in res treated *Opa1^{Q285STOP}* mouse

Novel object recognition (NOR) testing was performed as previously described in Chapter 3 section 3.3. A summary of test numbers is shown in Table 6.7.

6.6.3.1 Results of NOR in res treated Het mouse

NOR			
Het	17	rHet	9
F Het	8	M Het	9
rFHet	5	rMHet	4
vFHet	4	vMHet	3

Table 6.7 Summary of test numbers for NOR in untreated, res and veh Het.

The time spent with the novel item in the Het group was 13 ± 2 seconds. In the res Het group this was 12 ± 2 seconds and 15 ± 4 seconds in the vehicle group. There was no statistical difference between untreated Het and res Het ($p=0.588$) or untreated Het and vehicle treated Het mice ($p=0.583$). The time spent with the original item in untreated Het mice was 10 ± 2 seconds and 7 ± 2 seconds in res Het mice which was not significantly different compared to untreated Het ($p=0.085$) Vehicle treated Het mice spent 5 ± 2 seconds with the original object which was not significantly different compared to untreated Het ($p=0.112$). These data are presented in Figure 6.8.

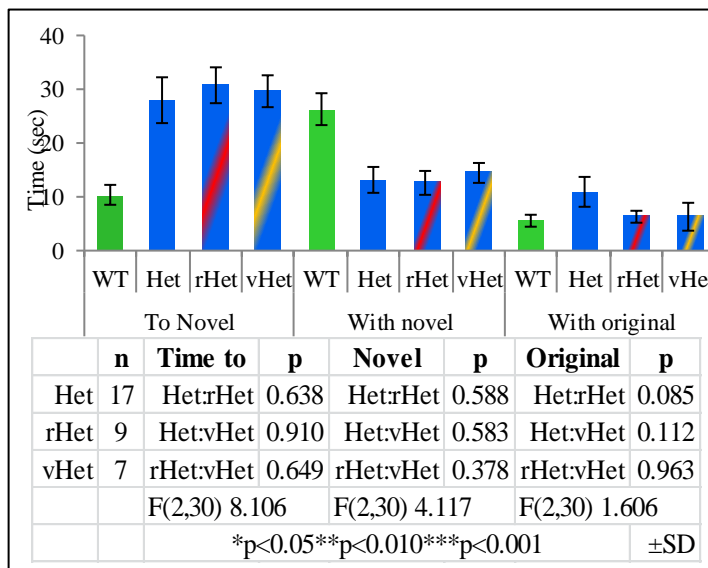


Figure 6.8 Parameters of NOR testing in untreated and treated Het mouse

Graph showing mean \pm SD of the parameters used to investigate novel object recognition. Time to locate novel object, time spent with novel object and time spent with the original object in Het, res and veh Het treated mice.

The IR in untreated Het mice was 0.49 ± 0.05 . The res treated Het mice had an IR score of 0.58 ± 0.09 which was not statistically significant compared to untreated Het ($p=0.067$). The IR in vehicle treated Het mice was 0.67 ± 0.12 which was also not statistically significant ($p=0.069$)

Chapter 6 Trial of resveratrol in *Opal^{Q285STOP}* mouse

The DR in untreated Het mice was 0.13 ± 0.09 . The res Het mice scored 0.29 ± 0.16 which was not statistically significant compared to untreated Het ($p=0.078$). The DR in vehicle treated Het mice was 0.50 ± 0.15 which was statistically significant compared to untreated Het ($F(2,30) 2.254 p=0.024$). This is shown in Figure 6.9.

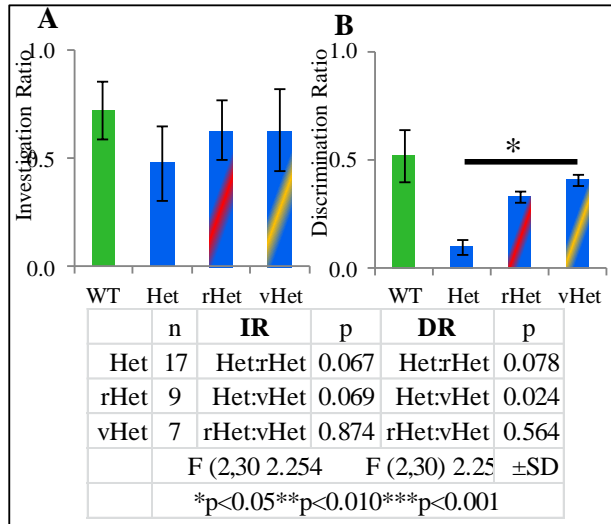


Figure 6.9 NOR IR and DR in resveratrol treated Het mouse

Graph showing (A) investigation and (B) discrimination ratio of NOR in untreated, res treated and veh Het treated Het

6.6.3.2 Discussion of NOR in res treated Het mouse

There was very little variation between the untreated Het mice and resveratrol treated Het mice. There was a 18% increase in IR seen in res Het and veh Het showed a 37% increase compared to untreated Het. The DR in res treated Het mice showed a 123% increase compared to untreated Het DR. The vehicle treated Het mice showed an increased DR of 285% compared to untreated Het mice. However, despite this improvement, it did not alter the learning pattern in res Het mice. There was no statistical difference in the correct choice between untreated and res treated Het mice. The average correct score in untreated Het mouse was 0.46 ± 0.08 . This was 0.441 ± 0.65 in res Het. ($p=0.475$) and 38 ± 0.11 in vehicle treated ($p=0.419$). Finally, the objects used in NOR testing did not demonstrate any statistical significant difference in the time spent with each item. This suggested that there was no preferential treatment towards any objects or no specific influence discrimination of particular items used in novel object recognition.

6.7 Bioenergetic impairment of res treated Opa1^{Q285STOP} mouse

6.7.1 Introduction

Resveratrol enhances mitochondrial biogenesis via the activation of the energy sensor AMP-activated kinase (AMPK) (Baur and Sinclair 2006; Lagouge et al. 2006; Chung et al. 2010; Um et al. 2010). As a result, increased AMPK activation increases fatty acid oxidation and mitochondrial biogenesis. Whether mitochondrial biogenesis is mediated by indirect activation of sirtuins or whether AMPK is a direct target of resveratrol remains to be clarified (Chung et al. 2010; Pacholec et al. 2010). Increased biogenesis may result in increased ATP production and it was intended to measure endogenous ATP in brain and retinal homogenate, however following some very ambiguous results it was discovered that resveratrol inhibits the activity of luciferase firefly (Bakhtiarova et al. 2006). As previous analysis demonstrated that the Het mouse appeared not to have compromised levels of ATP, it was decided to continue to electron transport analysis.

6.7.1.1 Bioavailability of resveratrol

Whole blood samples were prepared as described in Chapter 2 section 20.2. HPLC UV was performed on whole blood samples from mice who had been treated with resveratrol or vehicle for a total of 15 months. The level of back ground was reported to be too high to estimate the presence of resveratrol. This was possibly due to the quality of reagents used in the preparation process.

6.7.2 Analysis of electron transfer in Opa1^{Q285STOP} mouse

6.7.3 Introduction

Electron transfer assays were performed as described in Chapter 4 section 4.3. Briefly, a series of experiments were performed where a minimum of three individual WT, Het, res WT, res Het, veh WT and veh Het tissues were tested simultaneously. In order to maximise the number of experimental tests, each mouse contributed several organs for combined analysis. The tests performed were on the activity of complex I oxidation of NADH by mitochondria which was

Chapter 6 Trial of resveratrol in *Opa1^{Q285STOP}* mouse

analysed by fluorescence spectrophotometer, complex II succinate dehydrogenase (SDH) analysed by the reduction of DCPIP in the presence of succinate at 600nm using a UV spectrophotometer and complex IV oxidation of reduced cytochrome c followed at 550nm. The presence of residual succinate from storage buffer had no significant effect in complex I analysis which is shown in Appendix K. The kinetic reactions for electron complex analysis are in Appendix L and the calculations for line fitting are in Appendix M. Summaries for sample numbers in each analysis are shown in the table preceding results.

6.7.3.1 Results of complex I oxidation of NADH

Complex I activity was measured in brain, spinal cord, retina and muscle mitochondria.

CI Brain		CI Retina	
Het	9	Het	9
rHet	8	rHet	6
vHet	5	vHet	6
CI SC		CI Mus	
Het	10	Het	5
rHet	9	rHet	4
vHet	8	vHet	3

Table 6.8 Summary of test samples for complex I analysis in untreated, res and veh Het

Isolated mitochondria from Het brain oxidised 108 ± 6 nmol/mg Res treated Het brain oxidised 166 ± 7 nmol/mg which was significantly increased compared to untreated Het ($F(2,21) 25.123$ $p=0.002$). Vehicle treated Het brain oxidised 43 ± 4 nmol/mg which was significantly reduced compared to untreated Het ($F(2,21) 197.42$ $p=0.001$).

Complex I activity in untreated Het spinal cord oxidised 82 ± 9 nmol/mg and res Het spinal cord mitochondria oxidised 48 ± 9 nmol/mg which was significantly reduced compared to untreated Het ($F(2,24) 18.191$ $p=0.008$). Veh Het spinal cord oxidised 78 ± 19 nmol/mg which was not significantly different to untreated Het ($p=0.548$).

Het retinal mitochondrial oxidised 52 ± 17 nmol/mg Res Het retina oxidised 94 ± 38 nmol/mg which was not statistically different compared to untreated Het ($p=0.057$). Veh Het oxidised 59 ± 28 nmol/mg NADH which was not significantly different to untreated Het ($p=0.828$).

Complex I activity in Het muscle oxidised 95 ± 10 nmol/mg res Het muscle oxidised 63 ± 11 nmol/mg which was significantly reduced compared to untreated Het ($F(2,9) 16.72$ $p=0.014$).

Chapter 6 Trial of resveratrol in *Opa1^{Q285STOP}* mouse

Veh Het oxidised 56 ± 2 nmol/mg which was significantly reduced ($p=0.001$) compared to untreated Het.

6.7.3.2 Results of complex II succinate dehydrogenase

CII B		CII SC	
Het	11	Het	9
rHet	6	rHet	6
vHet	6	vHet	6
CII Ret		CII Mus	
Het	9	Het	5
rHet	6	rHet	4
vHet	6	vHet	3

Table 6.9 Summary of test samples for complex II in untreated, res and veh Het

Complex II activity in untreated Het brain mitochondria reduced 20 ± 6 $\mu\text{mol/mg}$. Res Het brain reduced 31 ± 6 $\mu\text{mol/mg}$. which was significantly reduced compared to untreated Het ($F(2,17)$ 185.152 $p=0.012$). Veh Het brain reduced 77 ± 2 $\mu\text{mol/mg}$ which was significantly increased compared to untreated Het ($p=0.001$).

Spinal cord in untreated Het reduced 19 ± 2 $\mu\text{mol/mg}$. per mg, res Het reduced 26 ± 7 $\mu\text{mol/mg}$. which was significantly increased compared to untreated Het ($F(2,17)$ 5.032 $p=0.023$). Veh Het SC reduced 17 ± 11 $\mu\text{mol/mg}$. which was not significantly different ($p=0.527$) compared to untreated Het.

Retinal complex II activity in untreated Het reduced 58 ± 14 $\mu\text{mol/mg}$. Res treated retinal mitochondrial reduced 21 ± 6 $\mu\text{mol/mg}$. which was significantly reduced compared to untreated Het ($F(2,18)$ 47.199 $p=0.001$). Veh treated Het retinal mitochondria reduced 102 ± 5 $\mu\text{mol/mg}$. which was significantly increased compared to untreated Het ($p=0.001$).

Complex II in untreated Het muscle mitochondria reduced 25 ± 6 $\mu\text{mol/mg}$., res Het reduced 17 ± 5 $\mu\text{mol/mg}$ which was not significantly different compared to untreated Het ($p=0.146$) and veh Het reduced 16 ± 4 $\mu\text{mol/mg}$ which was not statistically different compared to untreated Het ($p=0.148$).

6.7.3.3 Results of complex IV oxidation of cytochrome c

CIV B		CIV SC	
Het	9	Het	9
rHet	8	rHet	8
vHet	5	vHet	6
CIV Ret		CIV Mus	
Het	8	Het	4
rHet	6	rHet	4
vHet	4	vHet	3

Table 6.10 Summary of test samples for complex IV analysis in untreated res and veh Het

Untreated Het brain mitochondria oxidised 2.80 ± 0.13 $\mu\text{mol/mg}$ Res Het oxidised 1.45 ± 0.51 $\mu\text{mol/mg}$ which was significantly reduced compared to untreated Het ($F(2,18)$ 40.212 $p=0.001$). Veh Het oxidised 1.30 ± 0.01 $\mu\text{mol/mg}$ which was also significantly reduced compared to untreated Het ($p=0.001$).

Het spinal cord mitochondria oxidised 2.68 ± 0.11 $\mu\text{mol/mg}$ Res Het spinal cord mitochondria oxidised 1.48 ± 0.08 $\mu\text{mol/mg}$ which was significantly reduced compared to untreated Het ($F(2,21)$ 4.7478 $p=0.001$), and veh Het oxidised 1.50 ± 0.05 $\mu\text{mol/mg}$ which was also significantly reduced compared to untreated Het ($p=0.001$).

Retinal oxidation in untreated Het was 0.96 ± 0.14 $\mu\text{mol/mg}$. Res Het retinal mitochondria oxidised 2.52 ± 0.43 $\mu\text{mol/mg}$ which was significantly increased compared to untreated Het ($F(2,17)$ 15.120 $p=0.001$), and veh Het oxidised 1.92 ± 0.98 $\mu\text{mol/mg}$ which was also significantly increased compared to untreated Het ($p=0.010$).

Muscle mitochondria oxidation in untreated Het was 1.63 ± 0.04 $\mu\text{mol/mg}$ Res Het oxidised 1.89 ± 0.16 $\mu\text{mol/mg}$ which was not significantly different to untreated Het ($p=0.172$), and veh Het muscle oxidised 1.01 ± 0.62 $\mu\text{mol/mg}$ which was significantly reduced compared to untreated Het ($F(2,9)$ 13.572 $p=0.007$).

Figure 6.10 - 6.12 shows a graphical representation of the data.

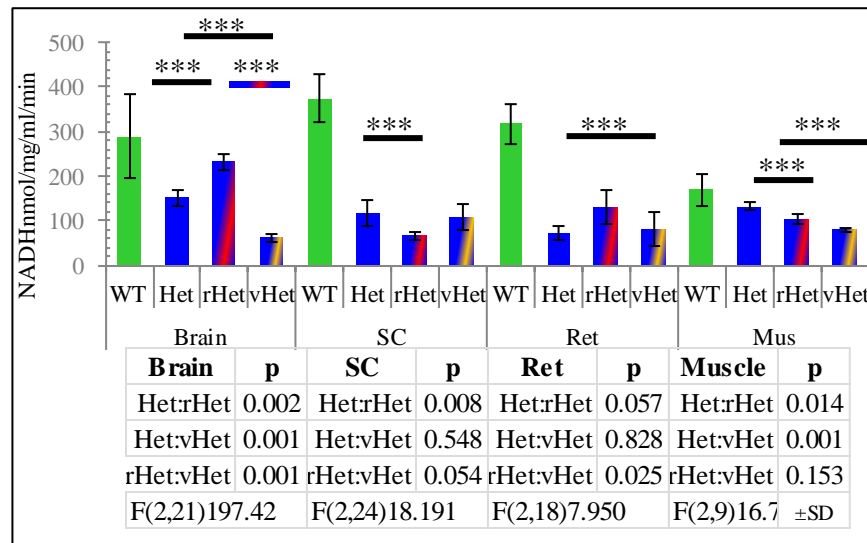


Figure 6.10 Complex I NADH oxidation in untreated and treated Het mitochondria

Graphs of mean \pm SD of complex I oxidation of NADH in untreated, res and veh treated Het brain, spinal cord (SC) retina (Ret) and skeletal muscle (Mus) mitochondria. The graph shows complex I oxidation of NADH nmol/mg in 30 μ g mitochondria/ml

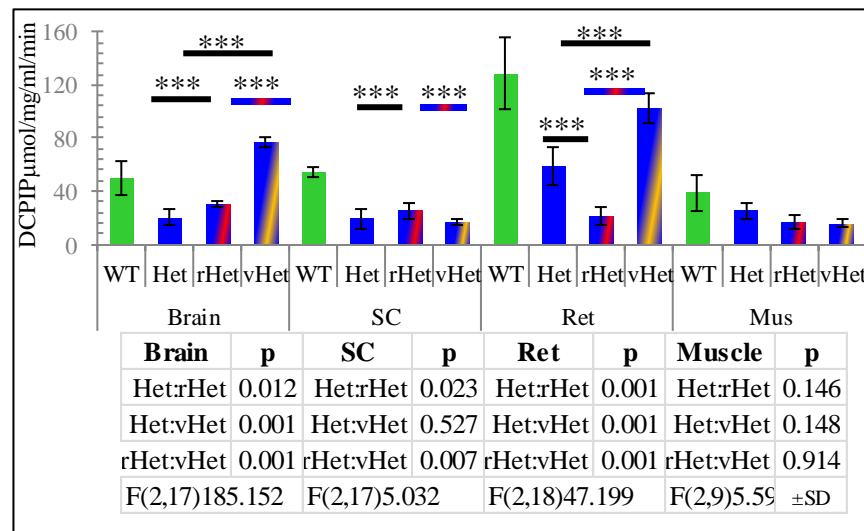


Figure 6.11 Complex II reduction of DCPIP in untreated and treated Het mitochondria

Graphs of mean \pm SD complex II reduction of DCPIP in untreated, res and veh Het mitochondria from brain, spinal cord (SC) retina (Ret) and skeletal muscle (Mus) mitochondria. The graph shows the reduction of DCPIP μ mol/mg in 50 μ g mitochondrial protein.

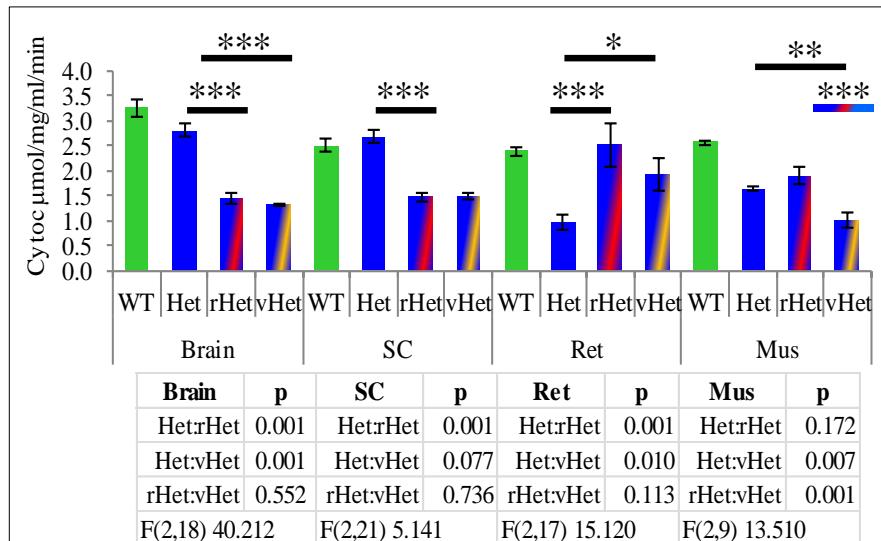


Figure 6.12 Complex IV oxidation of cyto c in untreated and treated Het mitochondria

Graphs of mean \pm SD complex IV oxidation of reduced cytochrome c in untreated, res and veh treated Het mitochondria from brain, spinal cord (SC) retina (Ret) and skeletal muscle (Mus) mitochondria. The graph shows reduced cytochrome c μ mol/mg in 50 μ g of mitochondrial protein.

The ratio of complex activity in each tissue was examined. Previous examination of complex ratios in the CNS of untreated WT demonstrated that the ratio of complex I was highest in spinal cord mitochondria. The ratio of complex II was highest in retinal mitochondria and the ratio of complex IV was highest in brain mitochondria. Untreated Het maintained these ratios. Table 6.11 shows a summary of the ratio of each complex for brain, spinal cord and retinal mitochondria with the statistical difference between groups.

Table 6.11 Ratio of complex activity in untreated res and veh Het mitochondria

	Brain			Spinal cord			Retina		
	Het	rHet	vHet	Het	rHet	vHet	Het	rHet	vHet
CI	45±5	54±4	25±3	33±6	16±1	44±10	22±6	30±4	31±8
Het:rHet		0.909			0.001			0.781	
Het:vHet			0.001			0.775			0.736
rHet:vHet		0.002			0.003			0.946	
F(2,68)4.432									
CII	21±5	39±5	39±2	19±6	33±5	9±1	60±1	28±7	52±2
Het:rHet		0.001			0.001			0.001	
Het:vHet			0.001			0.004			0.011
rHet:vHet		0.816			0.001			0.001	
F(2,48) 45.389									
CIV	43±4	30±3	30±0.9	42±6	33±6	34±4	15±2	37±19	36±5
Het:rHet		0.001			0.001			0.001	
Het:vHet			0.001			0.052			0.001
rHet:vHet		0.531			0.126			0.268	
F(2, 46) 38.685									

Table shows the ratio of complex activity according to tissue type. Compared to untreated Het the ratio of complex I activity was reduced in res Het spinal cord. The ratio of Complex II activity was increased in all res Het tissues. Complex IV ratio was reduced in res Het brain and spinal cord mitochondria and increased in retinal mitochondria. Compared to untreated Het, veh Het had a reduction in complex I ratio in brain. The ratio of Complex II activity was reduced in spinal cord and enhanced in retinal mitochondria. Compared to untreated Het, veh Het ratio of complex IV was reduced in brain and increased in retinal mitochondria.

In res Het spinal cord, the ratio of complex I activity was significantly reduced by 52% (F(2,68)4.432 p=0.001) compared to untreated Het. The ratio of complex II activity in res Het retina was significantly reduced by 53% compared to untreated Het (F(2,48) 45.389 p=0.001). Compared to untreated Het, the ratio of complex IV activity was significantly reduced in res Het brain by 30% (F(2,46) 38.685 p=0.001) and in spinal cord by 33% (p=0.001).

Compared to untreated Het, veh Het complex I ratio was increased by 33% in spinal cord mitochondria and the correct ratio was maintained (p=0.775). The ratio of complex II activity in veh Het retina was reduced by 13% (F(2,48) 45.389 p=0.011) but the correct ratio was maintained. The ratio of complex IV activity in veh Het brain was reduced by 30% F(2,46) 38.685 p=0.001).

6.7.3.4 Discussion of ETC activity in res treated *Opa1^{Q285STOP}* mouse

The percentage change in res and veh treated Het were compared to untreated Het mice. Table 6.12 shows a summary of the percentage changes compared to untreated Het.

Table 6.12 Percentage change of complex activity in res and veh Het mitochondria

rHet	Brain	SC	Ret	Mus	Ave ETC
CI	46	-45	71	-26	11
CII	49	34	-64	-34	-4
CIV	-48	-45	161	16	21
Ave	16	-19	56	-15	
vHet	Brain	SC	Ret	Mus	Ave ETC
CI	-62	-10	7	-44	-27
CII	276	-10	75	-921	-145
CIV	-53	-44	99	-38	-9
Ave	54	-21	60	-334	

The table shows the percentage change in individual complex activity in brain, spinal cord, retinal and skeletal muscle mitochondria compared to untreated Het mitochondria. The average percent change in bioenergetic activity for tissue types is also shown.

Tissue specific alternations in mitochondrial electron transport activity were calculated from the total change in complexes I, II and IV compared to untreated Het. In res Het treated mitochondria, both brain and retina showed an increase in ETC activity compared to untreated Het. Both spinal cord and skeletal muscle mitochondria showed a reduction in bioenergetic activity. Veh Het showed enhanced activity in brain and retinal mitochondria and reduced activity in spinal cord and skeletal muscle mitochondria compared to untreated Het.

If the ratio of individual complex activity in untreated Het was established as a means of mitohormesis (Tapia 2006; Ristow and Zarse 2010; Bouitbir et al. 2012; Ristow 2014), then by comparing the ratio of bioenergetic activity in res and veh treated Het to untreated WT would demonstrate any improvement in tissue specific activity.

The ratio of complex I activity was highest in untreated WT spinal cord mitochondria. Compared to untreated WT, the difference in ratio of complex I activity in spinal cord mitochondria of untreated Het was 13% which was not significantly different to untreated WT (p=0.578). Res Het had 58% reduction in the ratio of complex I activity in spinal cord

Chapter 6 Trial of resveratrol in *Opa1^{Q285STOP}* mouse

mitochondria which was significantly reduced (F(2,68) 2.144 p=0.009). Veh Het had a 16% increase in the ratio of complex I activity in spinal cord mitochondria compared to untreated WT which was not significantly different (p=0.462).

The ratio of complex II activity was highest in untreated WT retinal mitochondria. Compared to WT, the difference in ratio of complex II activity in Het retinal mitochondria was enhanced by 7% and was not significantly different to WT (p=0.706). The ratio of complex II activity in res Het retinal mitochondria was reduced by 50% compared to WT which was statistically significant (F(2,48) 45.389 p=0.001). Veh Het ratio of complex II activity in retinal mitochondria was reduced by 7% which was not significantly different compared to WT (p=0.260).

The ratio of complex IV activity was highest in untreated WT brain mitochondria. Compared to WT, complex IV ratio in untreated Het brain mitochondria was enhanced by 5% which was not significantly different to WT (p=0.822). Res Het brain mitochondrial ratio of complex IV activity was significantly reduced by 27% compared to WT (F(2,46) 38.685 p=0.001). Veh Het ratio of complex IV activity in brain mitochondria was also significantly reduced by 27% which was significantly different to WT brain (p=0.001). Table 6.13 shows a summary of the ratio of complex activity compared to untreated WT.

		Het	rHet	vHet
CI(SC)	% Δ	-13	-58	16
: WT	p=	0.578	0.009	0.462
F(2,68)2.144				
CII(Ret)	% Δ	7	-50	-7
: WT	p=	0.706	0.001	0.260
F(2,48) 45.389				
CIV(B)	% Δ	5	-27	-27
: WT	p=	0.822	0.001	0.001
F(2, 46) 38.685				

Table 6.13 Ratio of complex activity compared to untreated WT

The table shows the percentage difference in the ratio of complex I activity in spinal cord mitochondria, complex II activity in retinal mitochondria and complex IV activity in brain mitochondria compared to untreated WT. The statistical significance between groups is represented by the p value.

Untreated Het mitochondria maintained the correct tissue specific ratios of activity in complex I, II and IV. Veh Het maintained the correct tissue specific ratios of activity for complex I and

Chapter 6 Trial of resveratrol in $Opa1^{Q285STOP}$ mouse

complex II but showed a significant reduction in complex IV activity for brain. Res Het mitochondria showed the tissue specific ratios of all complex activities were not preserved.

If the ratio of individual complex activity for specific tissues reflects the functional ability to maintain a healthy mitochondrial environment, then resveratrol conferred no advantages to Het function. The possibility of correcting the ratio of complexes by mixing of the mitochondrial matrix content is reduced in Het but not absent. As Het CNS mitochondria maintained the correct ratios of complexes and veh Het maintained both complex I and II suggests the presence of ethanol was responsible for the reduction of complex IV in treated Het brain mitochondria. Resveratrol alone was responsible for the altered complex I and complex II ratios.

The effects of 0.1% ethanol were not anticipated to yield effects but vehicle treated Het demonstrated significant differences compared to untreated Het. The administration of a low dose over a prolonged period clearly produced effects that were either eliminated or exaggerated by the combined administration of resveratrol with 0.1% ethanol. Figure 6.13 shows the effects of resveratrol minus the ethanol effect for both tissue specific and ETC supercomplex activity. For example, complex I activity in veh Het brain mitochondria showed a 61% reduction in activity compared to untreated Het. Res Het brain mitochondria showed a 45% increase in activity. The effects of ethanol (61% reduction) were subtracted from 45% increase to get the actual effects of resveratrol minus the effect of ethanol. This was applied to all ETC activity to determine a more exact tissue specific effect of resveratrol.

Res Het complex I activity was enhanced by 39% compared to untreated Het. Complex II was reduced by 80% and complex IV was enhanced by 30%. Tissue specific mitochondrial changes were seen in brain with 39% reduction in activity, spinal cord had 3% increase, retina had 4% reduction and skeletal muscle showed a 25% increase compared to untreated Het.

The effects of resveratrol have been reported to cause a reduction in complex I and complex II activity at a concentration of 10mg/kg in rats (Sassi et al. 2014), which was not as a result of Ca^{2+} dysregulation but the accumulation of ‘compounds’ in mitochondria. These ‘compounds’ are most likely H_2O_2 generated by the dismutation of superoxide by the enhanced presence of

MnSOD. *OPA1* regulation of calcium Mitochondria act as store houses for calcium and the presence of a fusion mutation renders mitochondria more susceptible to mitophagy.

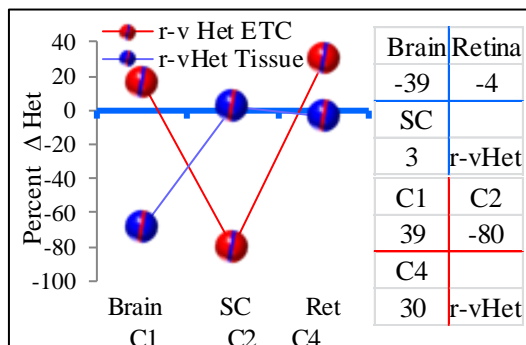


Figure 6.13 Changes in specific complexes and tissue in res treated Het

Graph showing the tissue specific and complex specific effects of resveratrol in Het mouse. The tissue specific bioenergetics in res Het brain were reduced by 39%, spinal cord and retinal mitochondria were unchanged. Skeletal muscle were increased by 25%. Complex I activity was increased by 39%, complex IV by 30% and complex II reduced by 80%.

Loss of mitochondria results in a local cellular increase in calcium. This progressive rise in local calcium concentration can induce autophagy (Pinton et al. 2008). Retinal ganglion cells are dependent on calcium clearance during development . (Dayanithi et al. 2010). Calcium dysregulation has been associated with Dominant optic atrophy (Lenaers et al. 2009; Fülöp et al. 2011; Kushnareva et al. 2013) and other neurological disorders including Parkinson’s disease (Büeler 2010; Chu 2010; Zhu and Chu 2010; Buhlman et al. 2014) .

The dose specific activity of resveratrol has been reported in cell culture (Guo et al. 2011; Carpéné et al. 2014; Martins et al. 2014; Meira Martins et al. 2014). Because of the variability in bioavailability of resveratrol, it is not always possible to determine what concentration is available to specific cell populations. There are reports that female recipients derive less benefit from resveratrol administration (Liesa et al. 2009; Yao et al. 2011). This is possibly due to the presence of estrogen receptors which compete for binding with resveratrol (Araújo et al. 2008; Chakraborty et al. 2013). Astrocytes respond to estrogen with enhanced expression of both fusion and fission genes (Liesa et al. 2009). If resveratrol was capable of reducing the already limited availability of *OPA1* in Het mice, it was anticipated that this would have produced serious side effects and possible loss of animals.

6.7.4 Mitochondrial related protein expression in res treated Het

6.7.4.1 Introduction

As described in Chapter 4 section 4.4, localization of protein in specific tissue can support some of the previous findings. Western blotting of retinal homogenates was performed on untreated Het (n5) and resveratrol treated Het (n6) tissues. Immunohistology was performed using a range of antibodies as previously described on untreated Het (n4), res Het (n4) and veh Het (n4) retinal sections. Western blotting was performed on untreated Het (n4) and res Het (n4) brain homogenate and sections of brain were analysed using the same panel of antibodies used for retinal sections.

6.7.5 Results of mitochondrial related protein expression in res treated Het

Table 6.14 shows a summary of the mitochondrial related protein expression of Opa1, VDAC and Preli in the retina of untreated Het res and veh Het. Figure 6.14 shows the mean AFU for (A)Opa1, (B) VDAC and (C) Preli expression in untreated, res and veh Het retina.

Table 6.14 Mitochondrial related proteins Opa1, VDAC and Preli in res treated Het

A	PRL			ONL			OPL			INL			IPL			GCL		
	Opal	Het	rHet	vHet	Het	rHet	vHet	Het	rHet	vHet	Het	rHet	vHet	Het	rHet	vHet	Het	rHet
Ave	96.4	235	188	98.8	131	164	130	185	217	71.1	93.4	160	89	101	162	77.7	52.6	146
SEM	26.8	72.3	84.6	37.6	24.7	53.6	26.3	61.6	75.8	11.9	36.1	50.3	29.2	23.7	72.1	10.3	12.4	23.5
Het:rHet		0.603			0.959			0.539			0.818			0.877				0.557
Het:vHet			0.691			0.524			0.030			0.004			0.014			0.017
F	F (5,16) 2.285			F (5,15) 4.390			F (5,15) 2.751			F (5,15)5.463			F (5,15) 9.729			F (5,15) 15.05		
B	PRL			ONL			OPL			INL			IPL			GCL		
	VDAC	Het	rHet	vHet	Het	rHet	vHet	Het	rHet	vHet	Het	rHet	vHet	Het	rHet	vHet	Het	rHet
Ave	555	422	269	944	403	311	526	221	250	890	351	339	747	244	268	798	390	349
SEM	88	72.8	70.7	23.5	116	76	81.9	72.3	84.4	66.1	61.4	66.4	67.6	34.7	89.8	65.8	44.1	79.6
Het:rHet		0.374			0.012			0.698			0.004			0.665				0.228
Het:vHet			0.008			0.952			0.016			0.001			0.074			0.461
F	F (5,15) 10.470			F (5,15) 1.380			F (5,15) 6.747			F (5,15)1.028			F (5,15)1.146			F (5,15)0.441		
C	PRL			ONL			OPL			INL			IPL			GCL		
	Preli	Het	rHet	vHet	Het	rHet	vHet	Het	rHet	vHet	Het	rHet	vHet	Het	rHet	vHet	Het	rHet
Ave	255	380	368	186	88	109	144	182	196	120	96	162	215	178	284	99	171	236
SEM	71	52	73	113	85	66	58	34	53	43	33	94	106	31	131	30	16	104
Het:rHet		0.252			0.780			0.723			0.228			0.342				0.591
Het:vHet			0.447			0.075			0.875			0.152			0.461			0.943
F	F (5,21) 21.466			F (5,21) 1.843			F (5,15) 5.851			F (5,15)4.645			F (5,15) 1.132			F (5,15) 3.622		

Table shows the mean (\pm SEM) of retinal mitochondrial expression of (A) Opa1 (B) VDAC (C) Preli in untreated, res and veh treated Het. The statistical difference between groups is represented by p value.

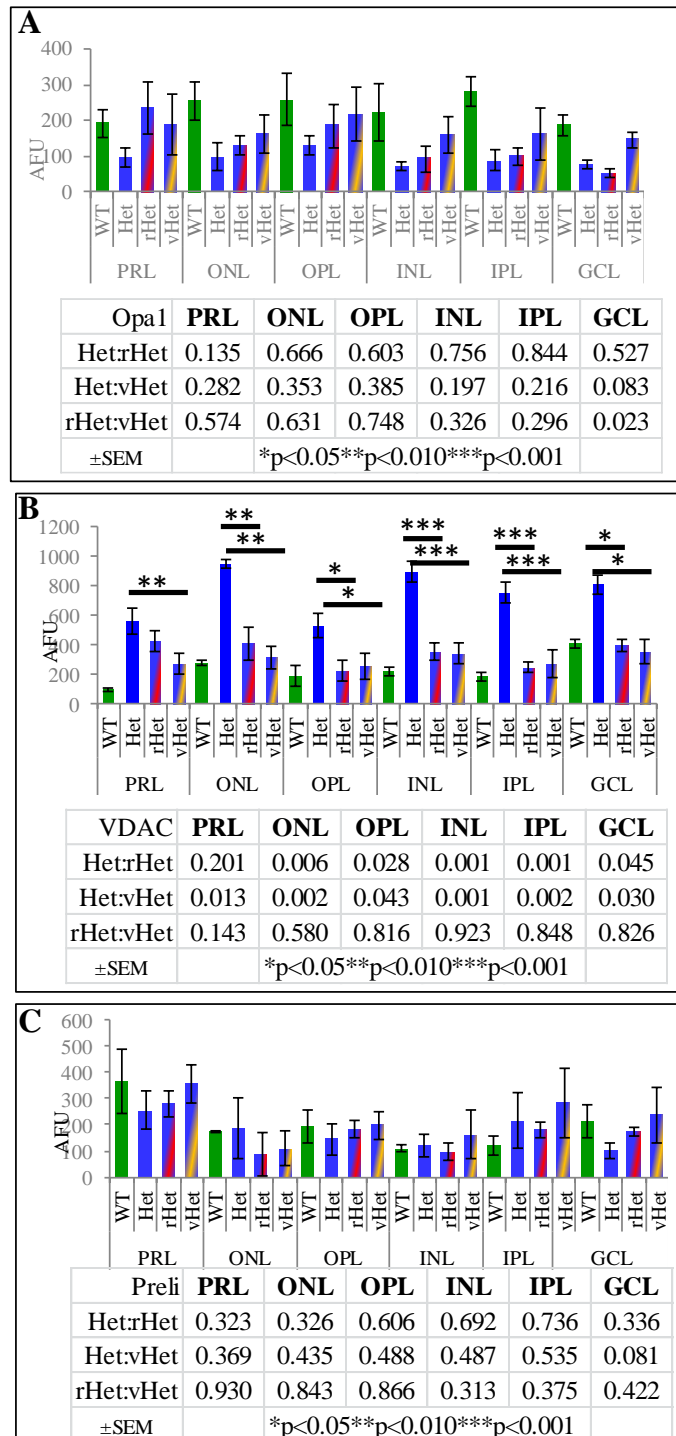


Figure 6.14 Mitochondrial related AFU in untreated, res and veh Het retina

Graph shows the mean \pm SEM of (A) *Opa1* expression (B) VDAC and (C) *Preli* in Het, res Het and veh Het retinal layers.

Table 6.15 shows a summary of the Neuroglobin, PSD95 and NF L expression in *Preli* in the retina of untreated Het res and veh Het. Figure 6.15 shows the mean AFU for (D) Neuroglobin, (E) PSD95 and (F) Neurofilament expression in untreated, res and veh Het retina.

Table 6.15 Mitochondrial related Neuroglobin, PSD95 and NF in res treated Het

D	PRL			ONL			OPL			INL			IPL			GCL		
	Neuro	Het	rHet	vHet	Het	rHet	vHet	Het	rHet	vHet	Het	rHet	vHet	Het	rHet	vHet	Het	rHet
Ave	250.5	214.3	176.4	349.2	181.4	267.1	129.8	85.71	134.2	259.3	94.48	151.1	90.41	95.08	223.1	64.78	66.7	129.3
SEM	38.15	30.29	97.47	38.98	5.215	69.44	20.76	13.97	70.63	21.29	27.37	29.79	34.99	42.04	150.6	23.16	10.76	40.57
Het:rHet	0.454			0.457			0.508			0.781			0.537			0.410		
Het:vHet	0.776			0.102			0.341			0.223			0.090			0.928		
F	F (5,20) 1.530			F (5,20) 0.784			F (5,20) 0.969			F (5,20)0.896			F (5,20) 1.654			F (5,20) 0.838		
E	PRL			ONL			OPL			INL			IPL			GCL		
	PSD95	Het	rHet	vHet	Het	rHet	vHet	Het	rHet	vHet	Het	rHet	vHet	Het	rHet	vHet	Het	rHet
Ave	267	252	250	162	352	256	239	230	215	82.8	174	131	211	125	167	92.9	75.7	63.9
SEM	24.2	58.5	62	32	115	18.7	2.26	71.5	13.7	11.2	70.7	42.5	15.8	75.4	38.8	15.6	36.5	11.7
Het:rHet	0.654			0.347			0.347			0.850			0.293			0.446		
Het:vHet	0.041			0.050			0.049			0.113			0.028			0.115		
F	F (5,28) 1.900			F (5,28) 1.176			F (5,28) 4.913			F (5,28)2.091			F (5,28)2.78			F (5,28) 1.768		
F	PRL			ONL			OPL			INL			IPL			GCL		
	NF L	Het	rHet	vHet	Het	rHet	vHet	Het	rHet	vHet	Het	rHet	vHet	Het	rHet	vHet	Het	rHet
Ave	128	291	143	168	281	121	182	506	185	140	242	291	173	318	124	405	602	341
SEM	56.5	39.5	25.8	54.8	89	48.3	70.4	76.5	81.6	42	81.1	173	54.7	24.9	55.8	105	28.5	97.5
Het:rHet	0.029			0.023			0.011			0.002			0.001			0.890		
Het:vHet	0.938			0.369			0.556			0.040			0.820			0.263		
F	F (5,23) 8.530			F (5,23) 1.280			F (5,23) 4.219			F (5,23)3.493			F (5,23) 7.706			F (5,23) 2.511		

Table shows the mean (\pm SEM) of retinal mitochondrial expression of (D) Neuroglobin (E) PSD95(F)Neurofilament L in untreated, res and veh treated Het. The statistical difference between groups is represented by p value.

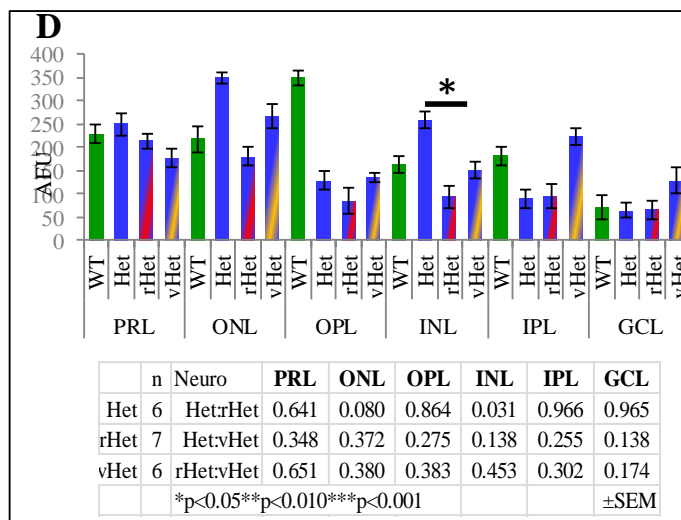
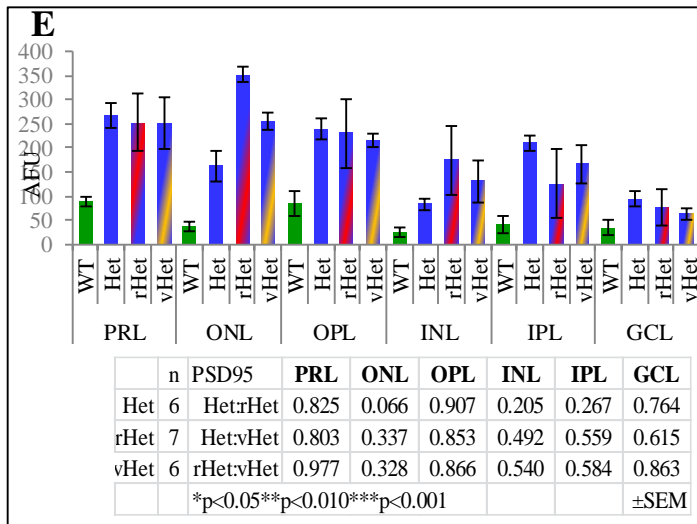


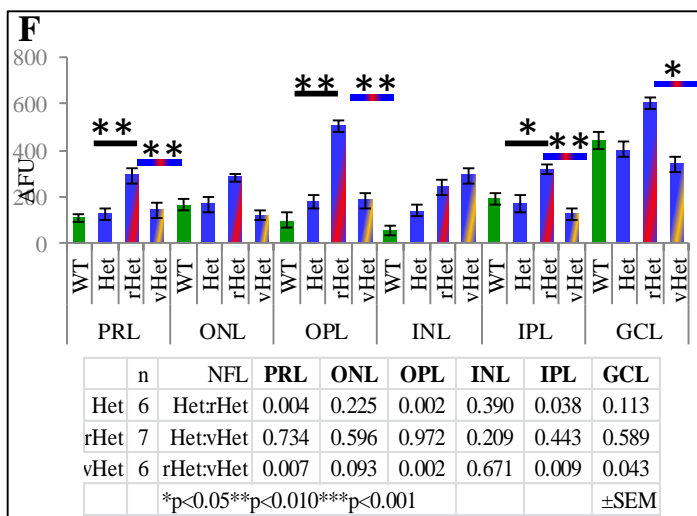
Figure 6.15 Mitochondrial related AFU in res treated Het

Graphs show the mean \pm SEM AFU of (D)Neuroglobin in Het, res Het and veh Het retinal layers.



...Figure 6.15

Graphs show the mean \pm SEM AFU of (E) PSD95 and (F) NFL in Het, res Het and veh Het retinal layers.



There was no significant difference observed in *Opal* expression between untreated and res treated Het. There was a significant difference observed in VDAC expression between untreated and res treated Het. Res Het had a significant 54% reduction in VDAC expression in the ONL (F(5,12) 5.9998 p=0.006), OPL (F(5,12) 2.784 p=0.028), INL (F(5,12) 9.494 p=0.001), IPL (F(5,12) 7.013 p=0.001) and GCL (F(5,12) 2.250 p=0.045). This reduction in VDAC expression was also observed in veh Het who had a 60% reduction compared to untreated Het. Compensatory protein expression of preli and neuroglobin were not statistically different in res and veh Het compared to untreated Het.

Damage mediated protein expression of PSD95 was not significantly different in res and veh Het compared to untreated Het. Neurofilament light chain expression was increased by 87% in

Chapter 6 Trial of resveratrol in Opa1^{Q285STOP} mouse

res Het retina. Res Het PRL has a significant 127% increase (F(5,12) 1.246 p=0.004). There was a 178% increase in NFl in the OPL (F(5,12)6.922 p=0.002) and 83% increase in the IPL (F(5,12) 5.823 p=0.038).

By combining the AFU of Opa1, VDAC and Preli a mitochondrial specific profile was obtained. The combined Preli, Neuroglobin and VDAC expression were combined to obtain compensatory proteins and PSD95 and neurofilament combined to obtain a damage mediated profile. The purposes of this was to determine if there was a particular region within the retinal layers that showed enhanced activity compared to untreated Het retina. Table 6.16 summarises these results. Figure 6.16 summarises these findings.

Table 6.16 Protein profiles in untreated res and veh Het retina

A	PRL			ONL			OPL			INL			IPL			GCL		
	Het	rHet	vHet	Het	rHet	vHet	Het	rHet	vHet	Het	rHet	vHet	Het	rHet	vHet	Het	rHet	vHet
Ave	297	345	275	387	207	194	254	196	220	336	179	220	336	174	237	302	204	243
SEM	26.8	72.3	84.6	37.6	24.7	53.6	26.3	61.6	75.8	11.9	36.1	50.3	29.2	23.7	72.1	10.3	12.4	23.5
HetrHet	0.514			0.108			0.423			0.109			0.054			0.331		
Het:vHet	0.765			0.086			0.461			0.232			0.233			0.556		
rHet:vHet	0.355			0.910			0.741			0.382			0.457			0.706		
F	F (5,16) 2.285			F (5,15) 4.390			F (5,15) 2.751			F (5,15)5.463			F (5,15) 9.729			F (5,15) 15.05		
B	PRL			ONL			OPL			INL			IPL			GCL		
	Het	rHet	vHet	Het	rHet	vHet	Het	rHet	vHet	Het	rHet	vHet	Het	rHet	vHet	Het	rHet	vHet
Ave	348	338	271	453	224	245	245	163	193	395	180	217	357	172	258	294	209	237
SEM	88	72.8	70.7	23.5	116	76	81.9	72.3	84.4	66.1	61.4	66.4	67.6	34.7	89.8	65.8	44.1	79.6
HetrHet	0.881			0.023			0.156			0.015			0.030			0.380		
Het:vHet	0.222			0.026			0.337			0.043			0.236			0.559		
rHet:vHet	0.329			0.965			0.364			0.697			0.355			0.789		
F	F (5,15) 10.470			F (5,15) 1.380			F (5,15) 6.747			F (5,15)1.028			F (5,15)1.146			F (5,15)0.441		
C	PRL			ONL			OPL			INL			IPL			GCL		
	Het	rHet	vHet	Het	rHet	vHet	Het	rHet	vHet	Het	rHet	vHet	Het	rHet	vHet	Het	rHet	vHet
Ave	197	271	196	164	316	188	210	367	199	111	207	211	192	221	145	248	338	202
SEM	71	52	73	113	85	66	58	34	53	43	33	94	106	31	131	30	16	104
HetrHet	0.117			0.038			0.027			0.166			0.375			0.489		
Het:vHet	0.987			0.741			0.877			0.152			0.501			0.717		
rHet:vHet	####			0.076			0.019			0.960			0.278			0.293		
F	F (5,21) 21.466			F (5,21) 1.843			F (5,15) 5.851			F (5,15)4.645			F (5,15) 1.132			F (5,15) 3.620		

Table shows the mean (\pm SEM) of (A) mitochondrial (B) compensation and (C) damage mediated protein expression in retinal layers of untreated res and veh Het. Statistical difference between groups is represented by the p value.

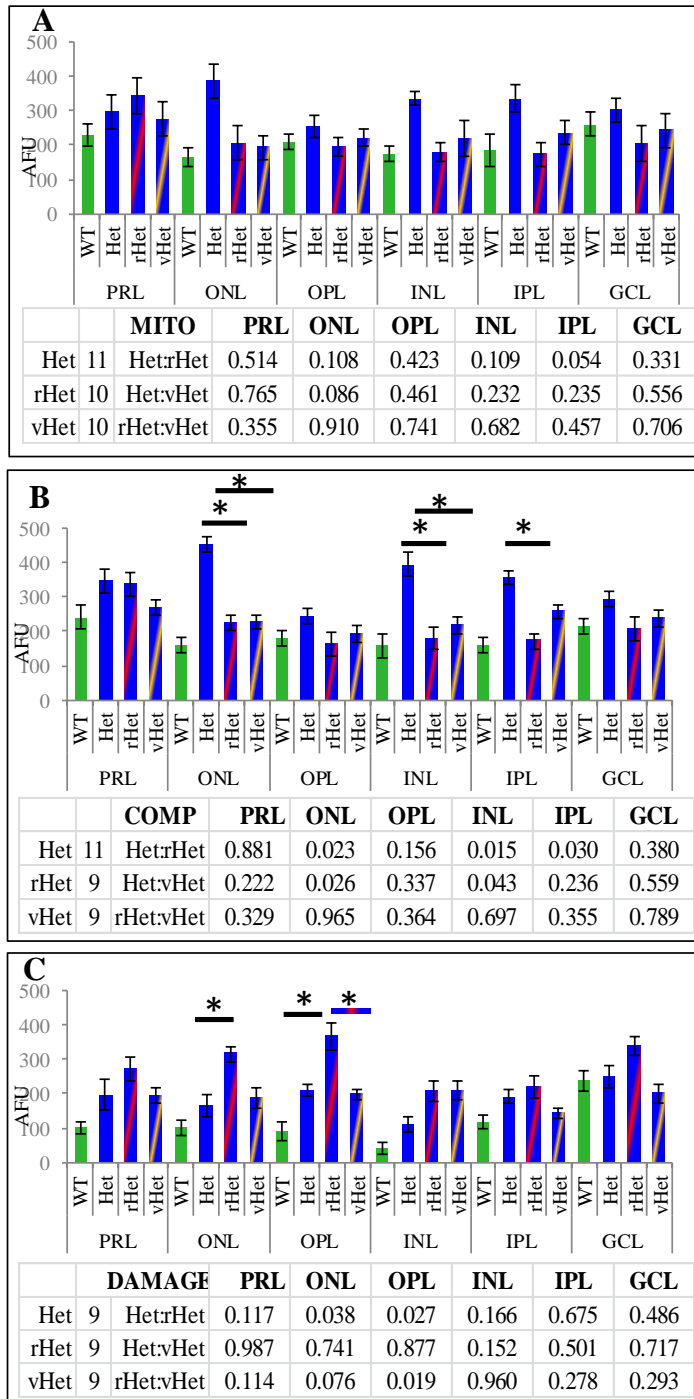


Figure 6.16 Protein profiles in untreated res and veh Het

Graphs showing the mean \pm SEM AFU of (A) mitochondrial (B) compensatory and (C) damage mediated expression in retinal sections of untreated res and veh Het.

There was no significant difference in any retinal layer for mitochondrial specific proteins in untreated res and veh Het. Compensatory protein expression in res Het was significantly reduced in the ONL ($p=0.023$) and INL ($p=0.015$). Veh Het also had a significant reduction of compensatory proteins in the ONL ($p=0.026$) and INL ($p=0.043$). Damage mediated protein expression was significantly increased in res Het ONL ($p=0.038$) and OPL ($p=0.027$). Veh Het damage mediated protein profile was not significantly different compared to untreated Het.

Chapter 6 Trial of resveratrol in *Opa1^{Q285STOP}* mouse

The ratio of compensatory to damage mediated protein expression was examined as before. A value of less than 1 was considered a positive measure in controlling damage mediated protein expression. Figure 6.17 summarises these findings.

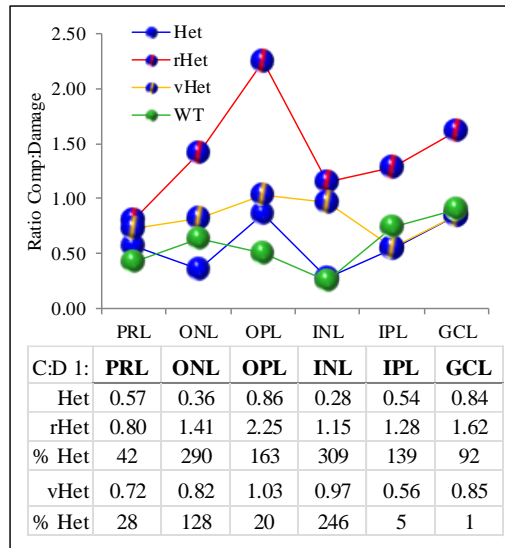


Figure 6.17 Ratio of compensation to damage in untreated and treated Het

Line graph shows the ratio of compensatory protein expression to damage mediated protein expression in retinal layers of untreated res and veh Het. Untreated WT is included for reference.

Res treated Het ONL and OPL appeared to be more compromised with respect to increased damage mediated protein expression. Both res and veh showed reduced compensatory protein expression. Res Het only showed enhanced damage mediated protein expression.

6.7.6 Western blotting of retinal homogenate

Western blotting of Het and res Het retinal homogenate was analysed for Opa1, neuroglobin and preli expression. Western blotting for Opa1 expression in retinal protein homogenate in untreated Het had 0.92 ± 0.11 and res treated Het retina had 0.54 ± 0.1 which was significantly reduced compared to untreated Het ($F(3,12) 7.895 p=0.005$). Neuroglobin expression of retinal homogenate from untreated Het had 0.82 ± 0.19 and res Het retina had 0.92 ± 0.18 which was not significantly different to untreated Het ($p=0.484$). Western blotting for preli expression in retinal homogenate of untreated Het was 0.57 ± 0.16 . Res treated Het retina had 0.42 ± 0.02 which was significantly reduced compared to untreated Het ($F(3,12) 5.115 p=0.032$). Figure 6.18 (A-D) shows representative bands from Western blot gels.

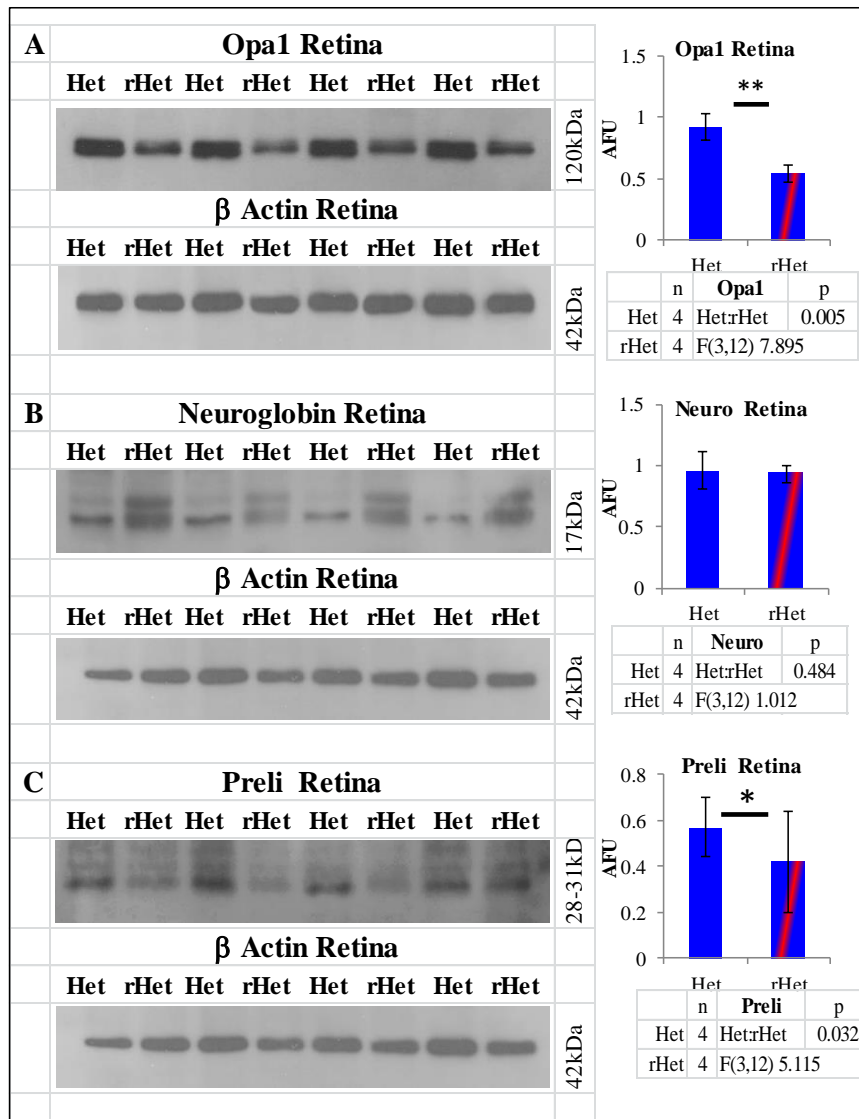


Figure 6.18 Western blotting of retinal homogenate in untreated and res Het

Images show representative bands from Western blotting of retinal homogenate from untreated Het (n4) and res treated Het (n4) for (A) Opa1 (B), neuroglobin (C) preli. Lower bands show β actin as a loading control.

Western blot results demonstrated that preli had two isoforms 28kDa and 31kDa in untreated Het retina. Res Het retina appeared to have reduced 31kDa sized band. Neuroglobin had two isoforms 17kDa and 20kDa. Res Het retina appeared to have both isoforms in equal proportion. Untreated Het had a higher proportion of 17kDa only.

Figures 6.19- 6.24. Show representative images of retinal protein expression in untreated, res and veh Het.

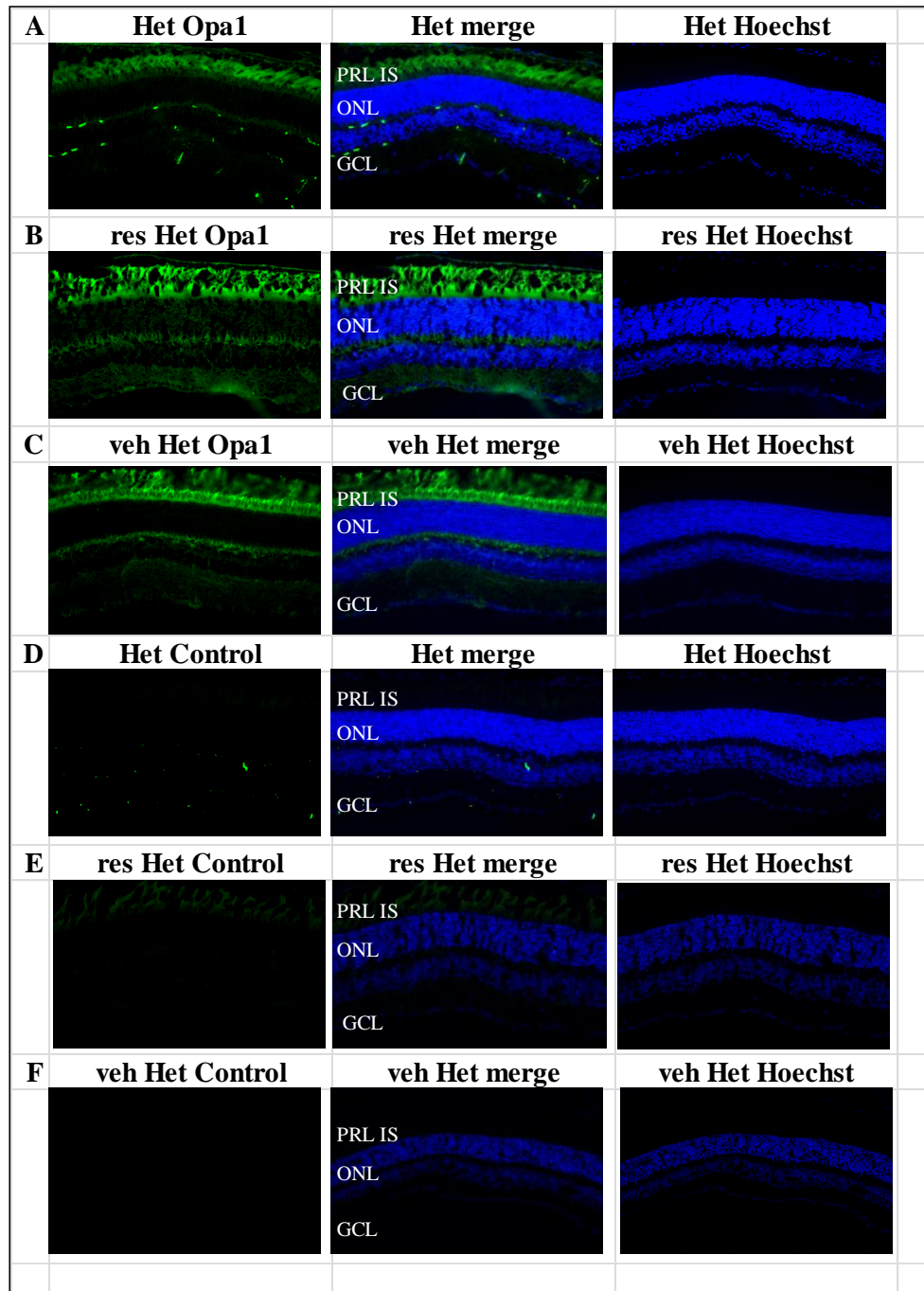


Figure 6.19 *Opa1* protein expression in untreated res and veh treated Het retina

Representative images of Opa1 expression in Het (A), res Het (B) and veh Het (C) retinal sections. Negative control sections (omission of primary antibody) for Het (D), res Het (E) and veh Het (F) are shown.

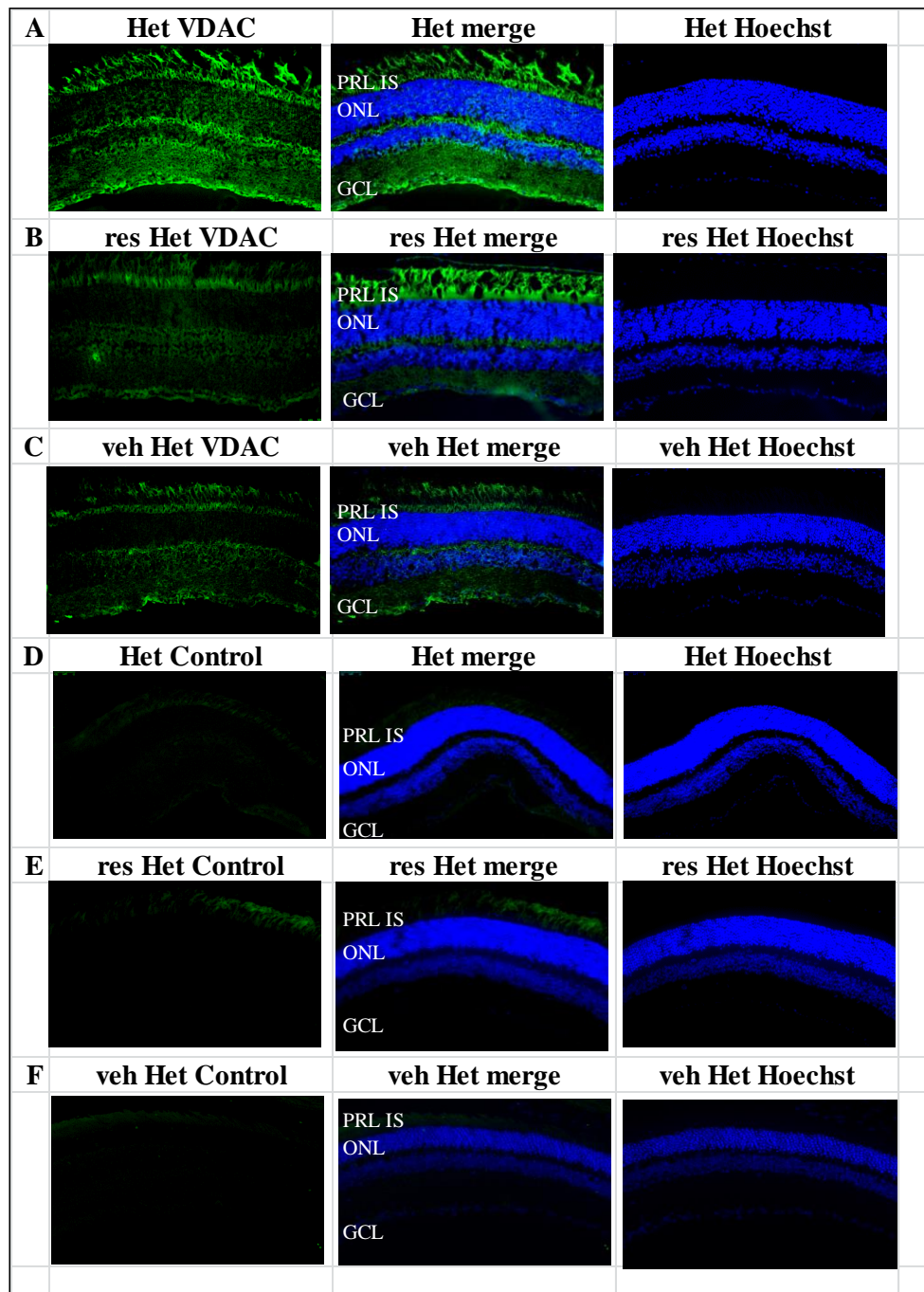


Figure 6.20 VDAC protein expression in untreated res and veh treated Het retina

Representative images of VDAC expression in Het (A), res Het (B) and veh Het (C) retinal sections. Negative control sections (omission of primary antibody) for Het (D), res Het (E) and veh Het (F) are shown.

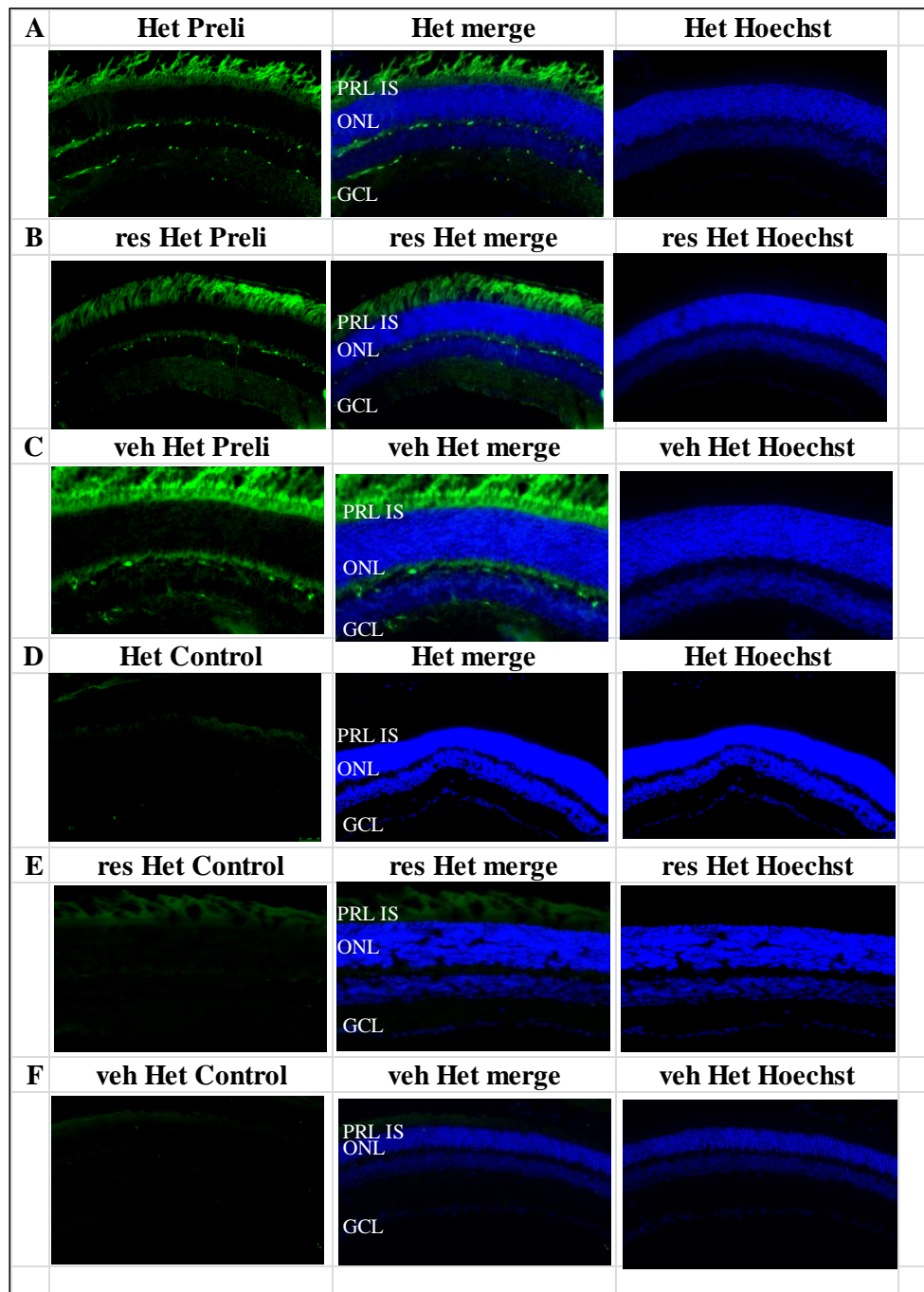


Figure 6.21 Preli protein expression in untreated res and veh treated Het retina

Representative images of Preli expression in Het (A), res Het (B) and veh Het (C) retinal sections. Negative control sections (omission of primary antibody) for Het (D), res Het (E) and veh Het (F) are shown.

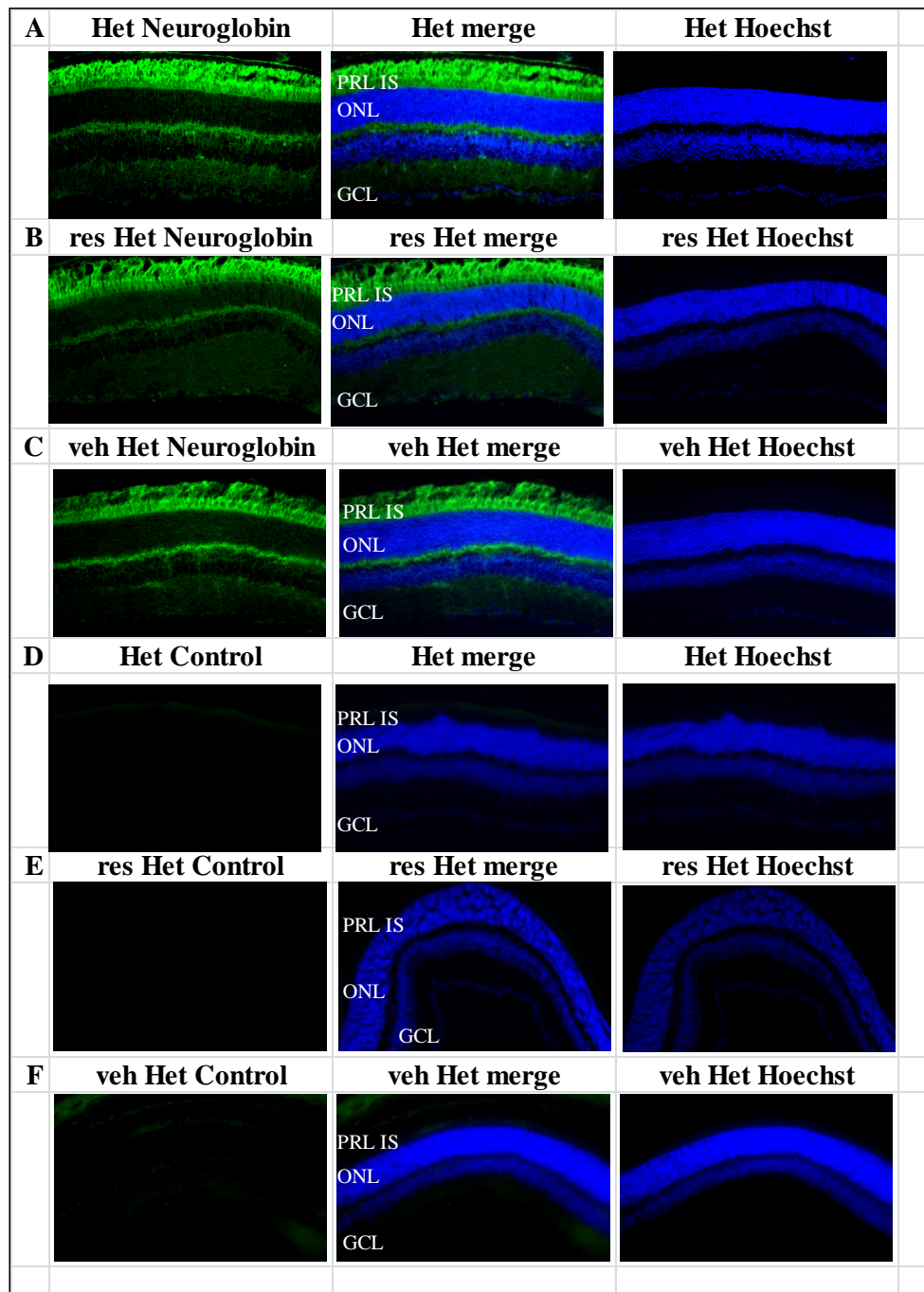


Figure 6.22 Neuroglobin protein expression in untreated res and veh treated Het retina

Representative images of Neuroglobin expression in Het (A), res Het (B) and veh Het (C) retinal sections. Negative control sections (omission of primary antibody) for Het (D), res Het (E) and veh Het (F) are shown.

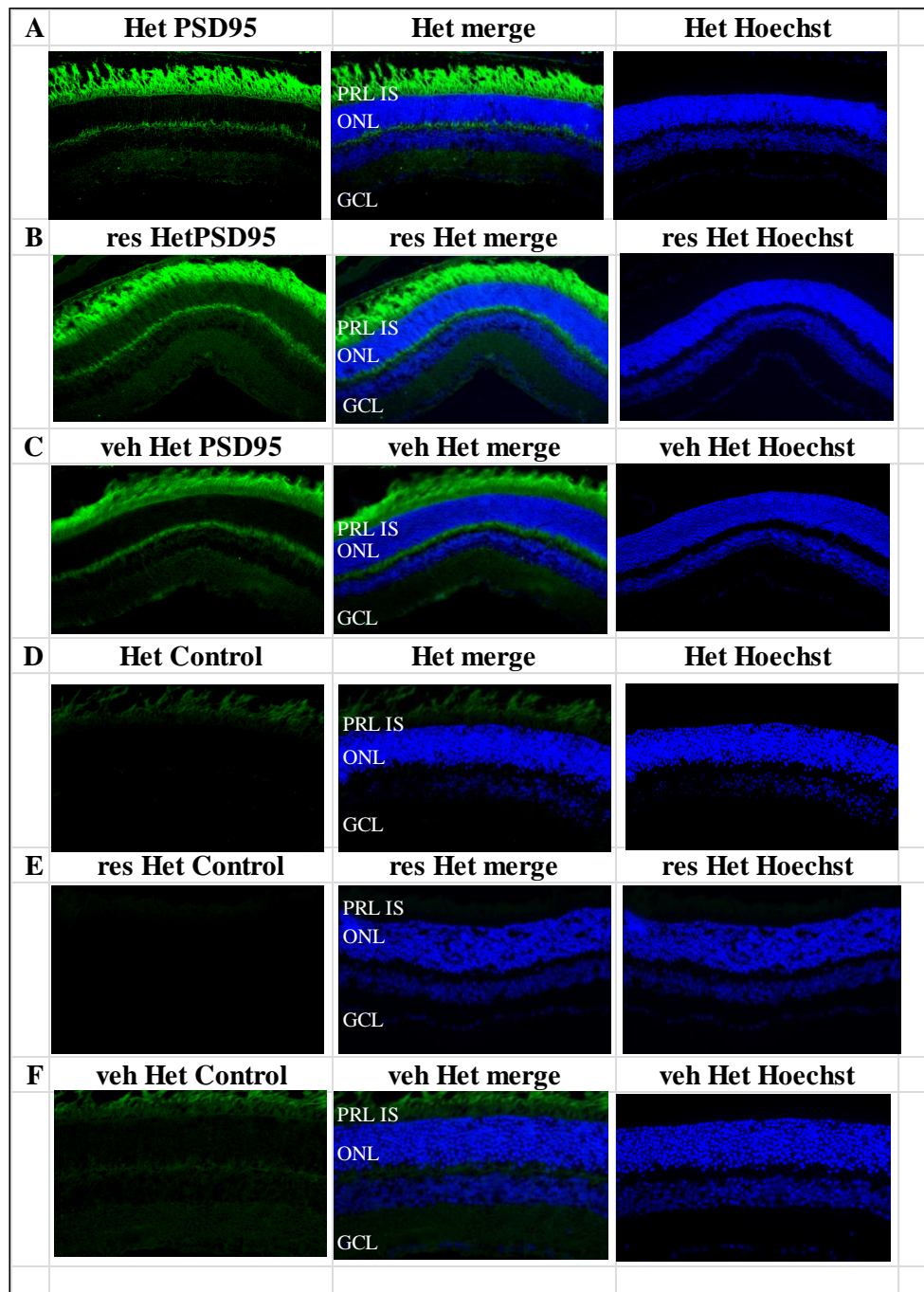


Figure 6.23 PSD95 protein expression in untreated res and veh treated Het retina

Representative images of PSD95 expression in Het (A), res Het (B) and veh Het (C) retinal sections. Negative control sections (omission of primary antibody) for Het (D), res Het (E) and veh Het (F) are shown.

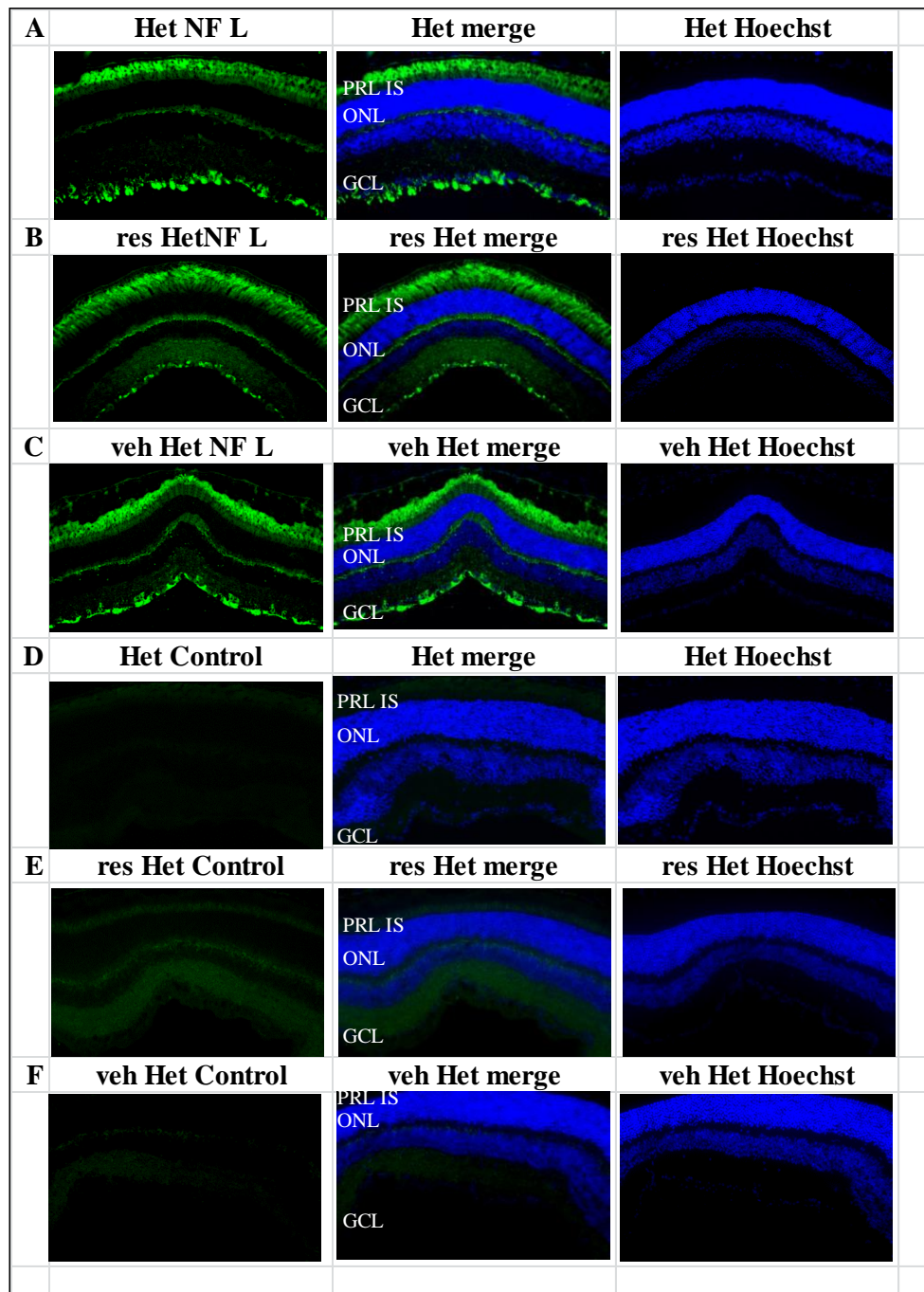


Figure 6.24 NF L protein expression in untreated res and veh treated Het retina

Representative images of NFL expression in Het (A), res Het (B) and veh Het (C) retinal sections. Negative control sections (omission of primary antibody) for Het (D), res Het (E) and veh Het (F) are shown.

6.7.7 Mitochondrial protein expression in brain of untreated and treated Het

Table 6.17 shows a summary of the results of brain IHC for all antibodies tested in tissue sections from untreated, res and veh Het. Figure 6.25 shows graphs representing the mean \pm SEM AFU of these data.

Table 6.17 Results of protein expression in brain of untreated res and veh Het

A	Opal	Het(n5)	rHet(n4)	vHet(n3)	D	Preli	Het(n5)	rHet(n4)	vHet(n3)
	Ave	419.1	589.4	471.4		Ave	1016	939.7	901.4
	SEM	80.2	211.4	126.7		SEM	299.8	220	40.36
	Het:rHet		0.582			Het:rHet		0.813	
	Het:vHet			0.159		Het:vHet			0.723
	rHet:vHet		0.462			rHet:vHet		0.914	
	F(5,30)	4.527				F(5,30)	4.627		
B	VDAC	Het(n5)	rHet(n4)	vHet(n3)	E	PSD95	Het(n5)	rHet(n4)	vHet(n3)
	Ave	1016	939.7	901.4		Ave	164.44	1660.01	259.23
	SEM	299.8	220	40.36		SEM	36.664	52.4783	88.3637
	Het:rHet		0.005			Het:rHet		0.001	
	Het:vHet			0.017		Het:vHet			0.761
	rHet:vHet		0.589			rHet:vHet		0.001	
	F(5,18)	2.870				F(5,39)	2.983		
C	Neuro	Het(n5)	rHet(n4)	vHet(n3)	F	NF H	Het(n5)	rHet(n4)	vHet(n3)
	Ave	969	159.9	542.5		Ave	1469	1135	265.5
	SEM	195	51.9	177.8		SEM	305.9	295.2	126.9
	Het:rHet		0.001			Het:rHet		0.635	
	Het:vHet			0.054		Het:vHet			0.001
	rHet:vHet		0.117			rHet:vHet		0.002	
	F(5,17)	2.454				F(5,17)	7.832		

Table shows the mean (\pm SEM) of mitochondrial (A) *Opal* (B) *VDAC* (C)*Neuroglobin* (D)*Preli* *PSD95* and (F) *NF H* in brain of untreated, res and veh Het. The statistical difference between groups is represented by the *p* value.

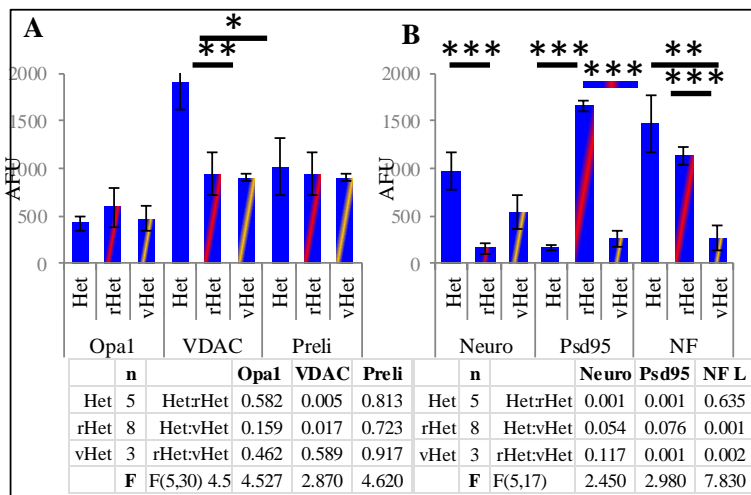


Figure 6.25 Protein expression in brain of untreated res and veh Het.

Graphs show the mean \pm SEM AFU of (A) *Opal*, *VDAC*, *Preli* (B) *neuroglobin*, *PSD95*, *NF H* in brain sections of untreated res and veh Het.

Compared to untreated Het, *Opal* expression was unchanged in res Het ($p=0.582$) and in veh Het ($p=0.159$). *VDAC* expression was reduced by 41% in res Het which was significantly different compared to untreated Het ($F(5,24)$ 2.223 $p=0.005$). Veh Het had a 32% reduction

Chapter 6 Trial of resveratrol in Opa1^{Q285STOP} mouse

which was also significantly different compared to untreated Het (p=0.017). Preli expression in untreated Het was not significantly different in res Het (p=0.813) or veh Het (p=0.723). Compared to untreated Het, Neuroglobin expression was significantly reduced by 86% in res Het brain (F(5,19) 5.086 p=0.001), and was not statistically different to untreated Het in veh Het brain (p=0.054). Compared to untreated Het, PSD95 expression in res Het had a significant 909% increase (F(5,27) 15.381 p=0.001). Veh Het was not significantly different to untreated Het (p=0.761). Neurofilament expression was unchanged in res Het brain (p=0.635), but veh Het showed a significant 88% reduction (F(5,25) 6.683 p=0.001).

6.7.8 Western blotting of untreated and res Het brain homogenate

Western blotting of Het and res Het brain homogenate was analysed for Opa1, neuroglobin and VDAC expression. Western blotting of brain homogenate for Opa1 protein showed untreated Het had 0.983±0.105 RD and res treated Het brain had 0.930±0.10 RD which was not significantly different to untreated Het (p=0.446). Western blotting in untreated Het brain for neuroglobin had 0.95±0.15 RD. Res treated Het brain had 0.93±0.07 which was not statistically different compared to untreated Het (p=0.076). Western blot of brain homogenate for VDAC expression in untreated Het brain was 0.836±0.070 RD. Res treated Het brain had 0.735±0.082 which was not significantly different compared to untreated Het (p=0.372). Figure 6.26 shows representative bands from Western blot gels.

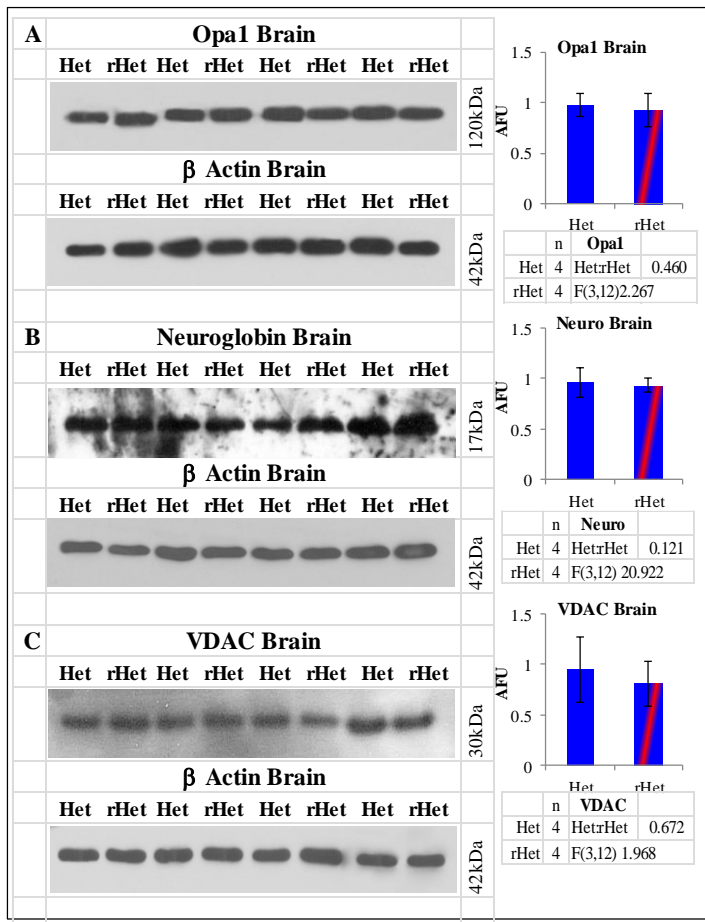


Figure 6.26 Western blotting of brain homogenate in untreated and res Het

Western blots show representative bands from brain homogenate of untreated Het (n4) and res treated Het (n4) for (A) *Opa1*, (B) neuroglobin and (C) VDAC. Lower bands show β actin as a loading control.

The ratio of compensation to damage

mediated protein expression in brain was examined. In untreated Het the ratio was 0.77. In res treated Het the ratio was 2.26. Veh Het ratio was 0.40. This suggested that res Het was not compensating for an excess of damage mediated protein expression.

Figures 6.27- 6.6.32 show representative images of IHC in brain for all the antibody staining reported.

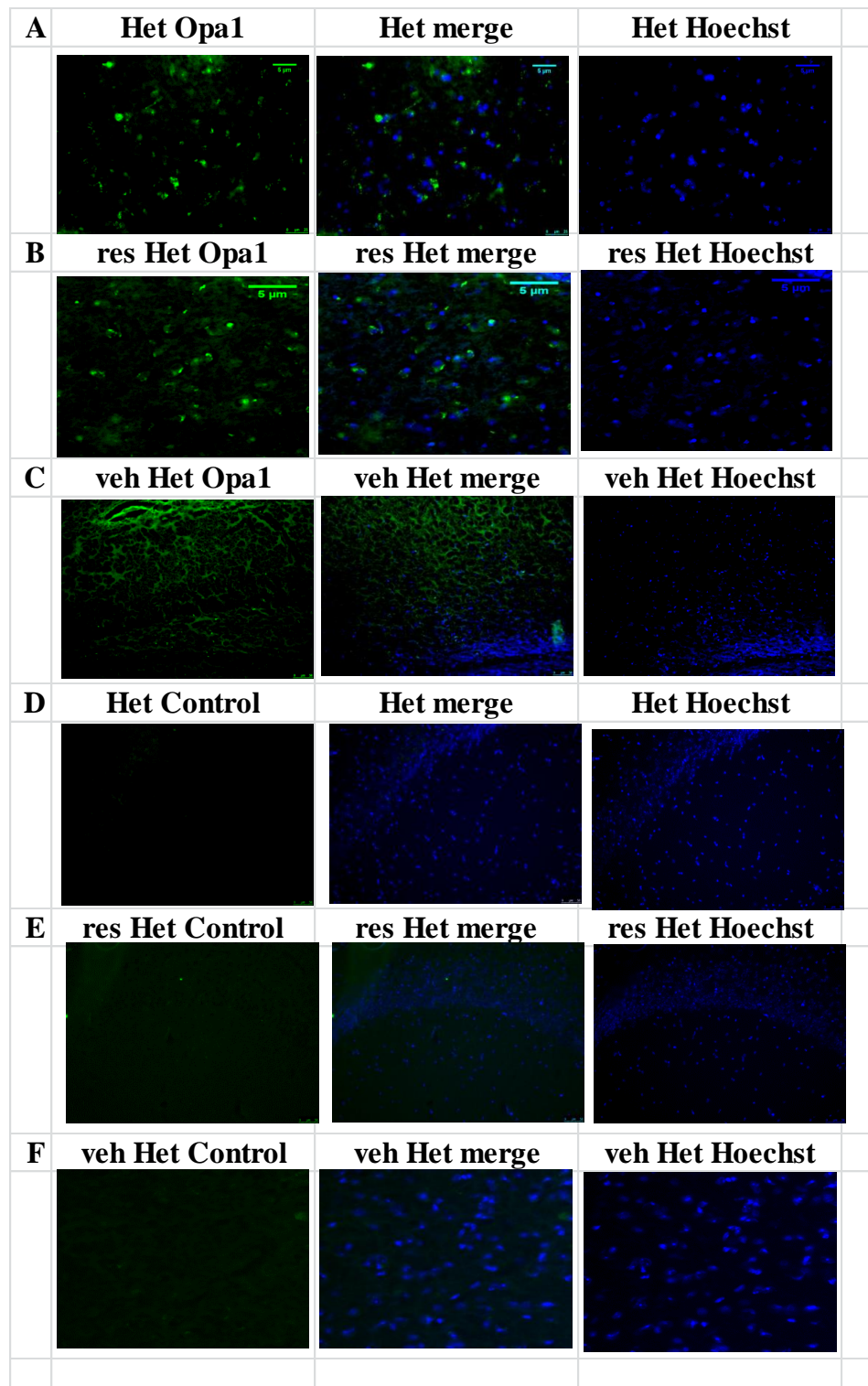


Figure 6.27 *Opa1* expression in brain of untreated res and veh Het

Representative images of Opa1 expression in (A) untreated Het (B) res Het and (C) veh Het brain. Control sections for (D) untreated Het (E) res Het and (F) veh Het were processed without primary antibody.

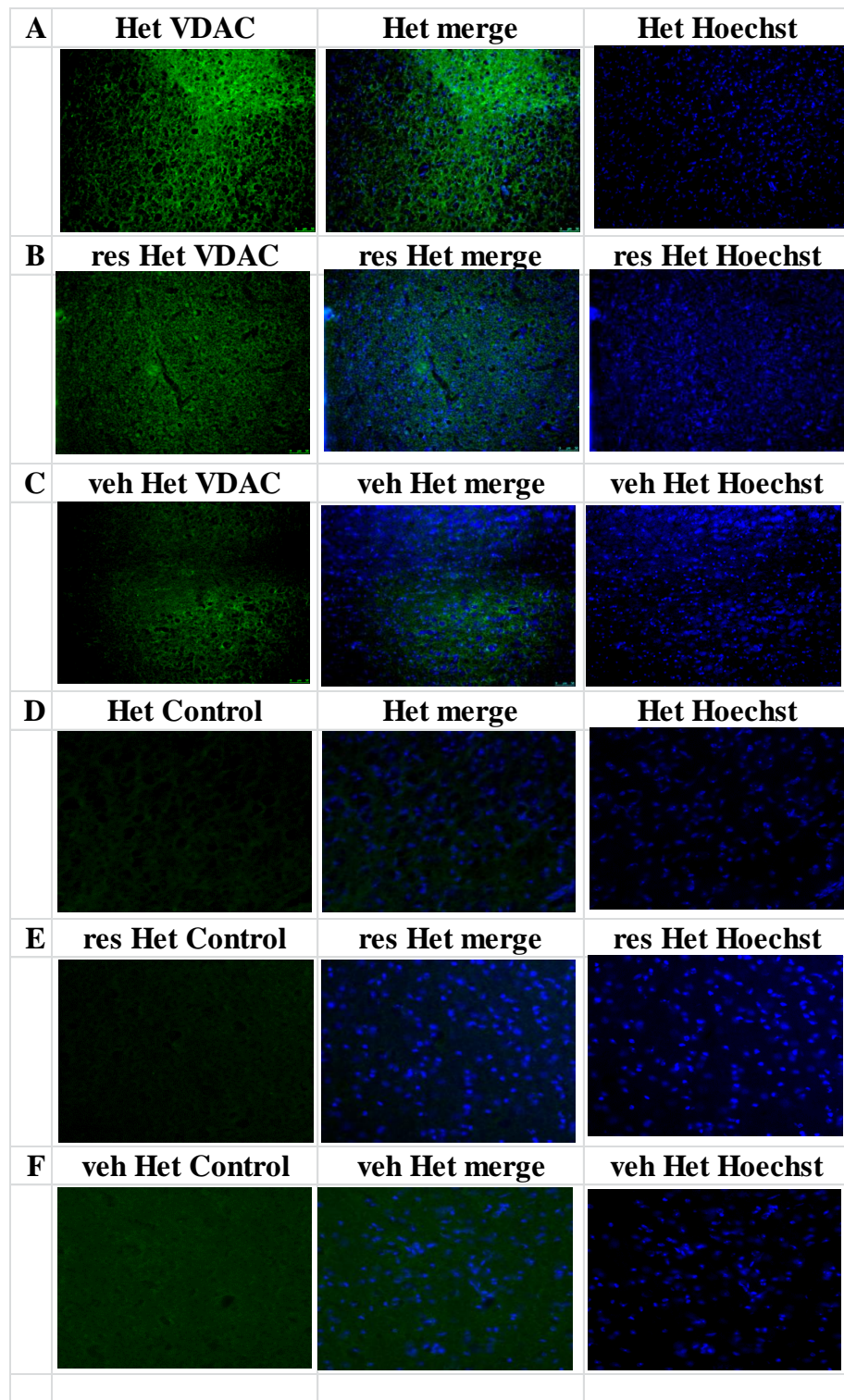


Figure 6.28 VDAC expression in brain of untreated res and veh Het

Representative images of VDAC expression in (A) untreated Het (B) res Het and (C) veh Het brain. Control sections for (D) untreated Het (E) res Het and (F) veh Het were processed without primary antibody.

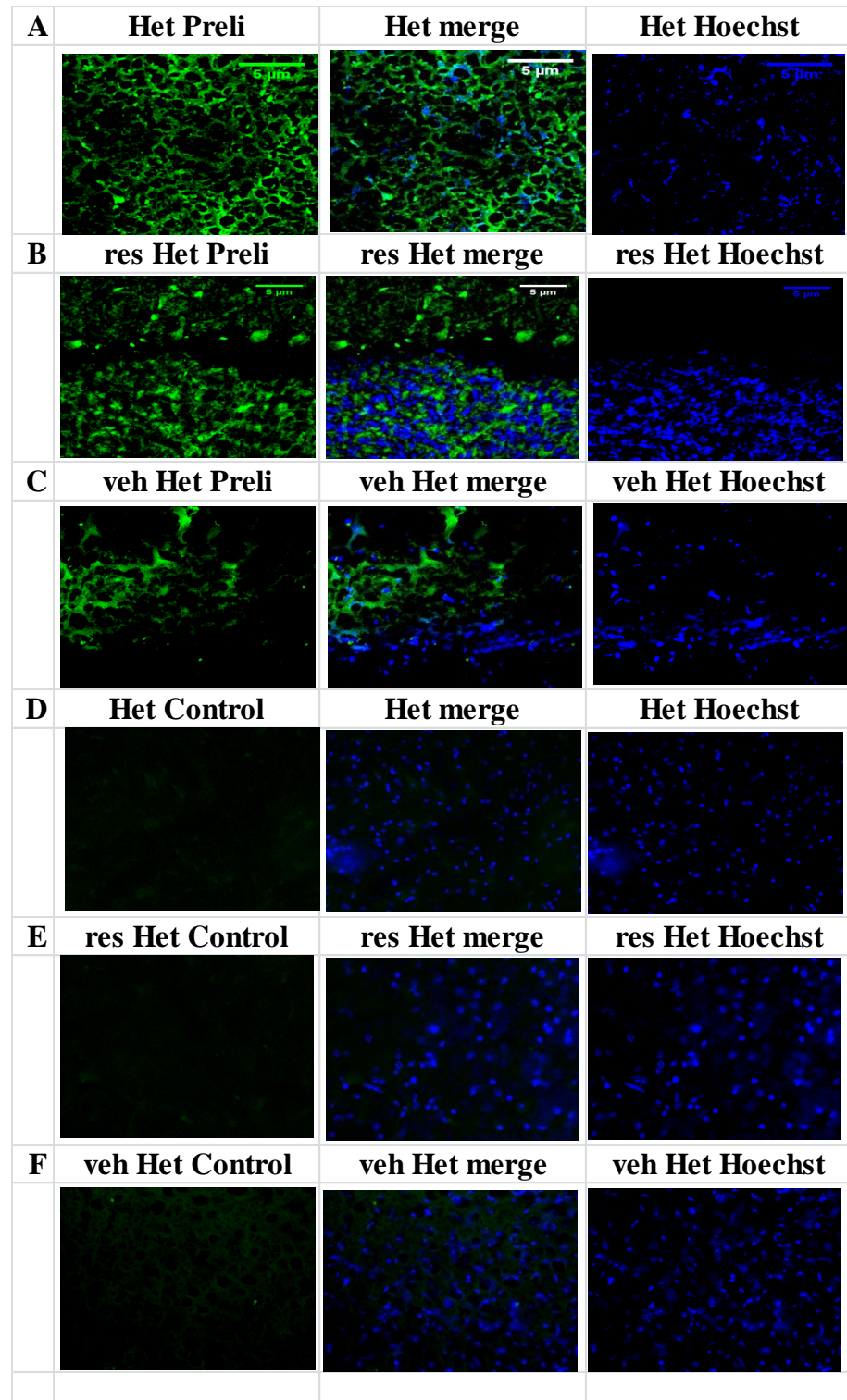


Figure 6.29 Preli expression in brain of untreated res and veh Het

Representative images of Preli expression in (A) untreated Het (B) res Het and (C) veh Het brain. Control sections for (D) untreated Het (E) res Het and (F) veh Het were processed without primary antibody.

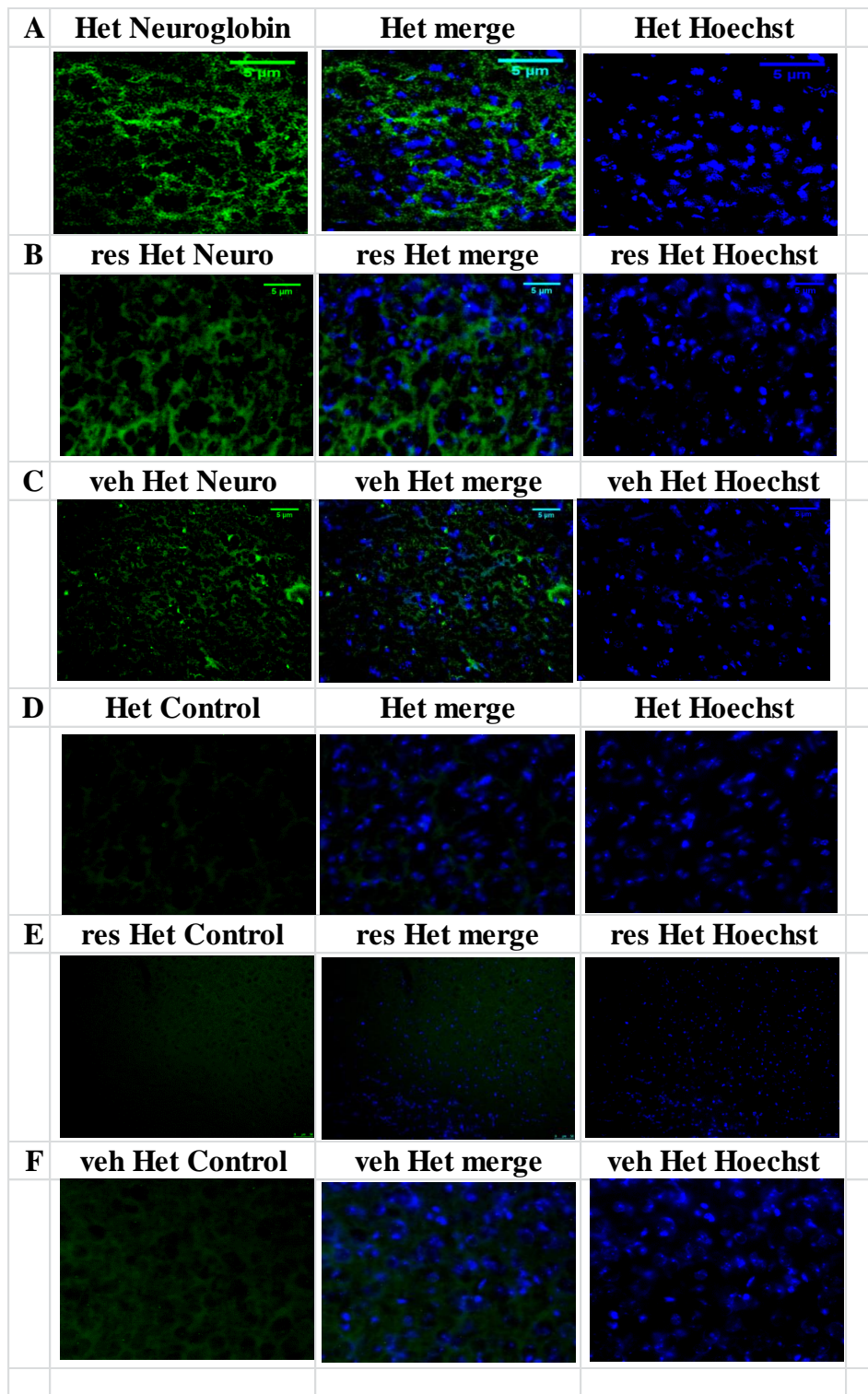


Figure 6.30 Neuroglobin expression in brain of untreated res and veh Het

Representative images of Neuroglobin expression in (A) untreated Het (B) res Het and (C) veh Het brain. Control sections for (D) untreated Het (E) res Het and (F) veh Het were processed without primary antibody.

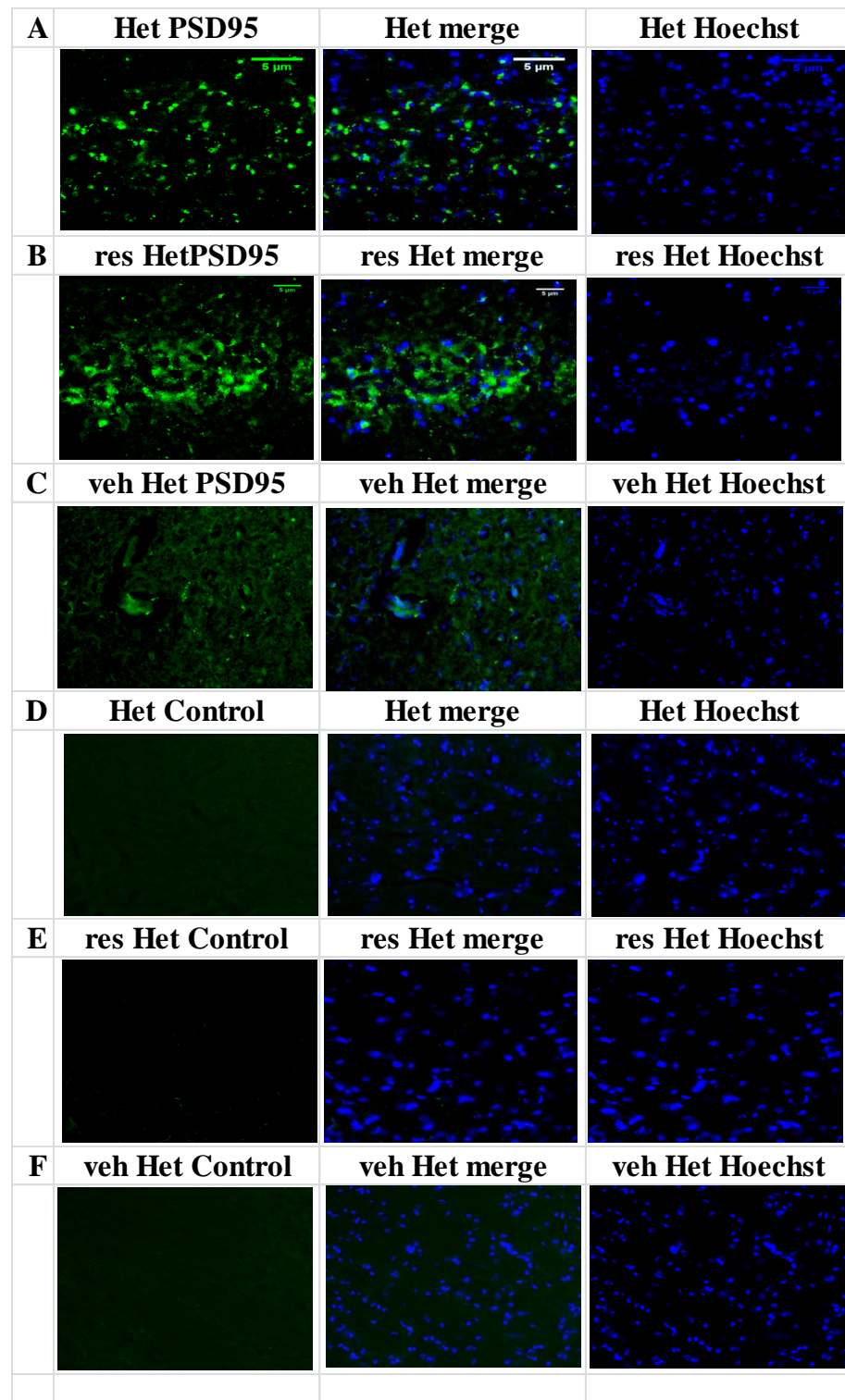


Figure 6.31 PSD95 expression in brain of untreated res and veh Het

Representative images of PSD95 expression in (A) untreated Het (B) res Het and (C) veh Het brain. Control sections for (D) untreated Het (E) res Het and (F) veh Het were processed without primary antibody.

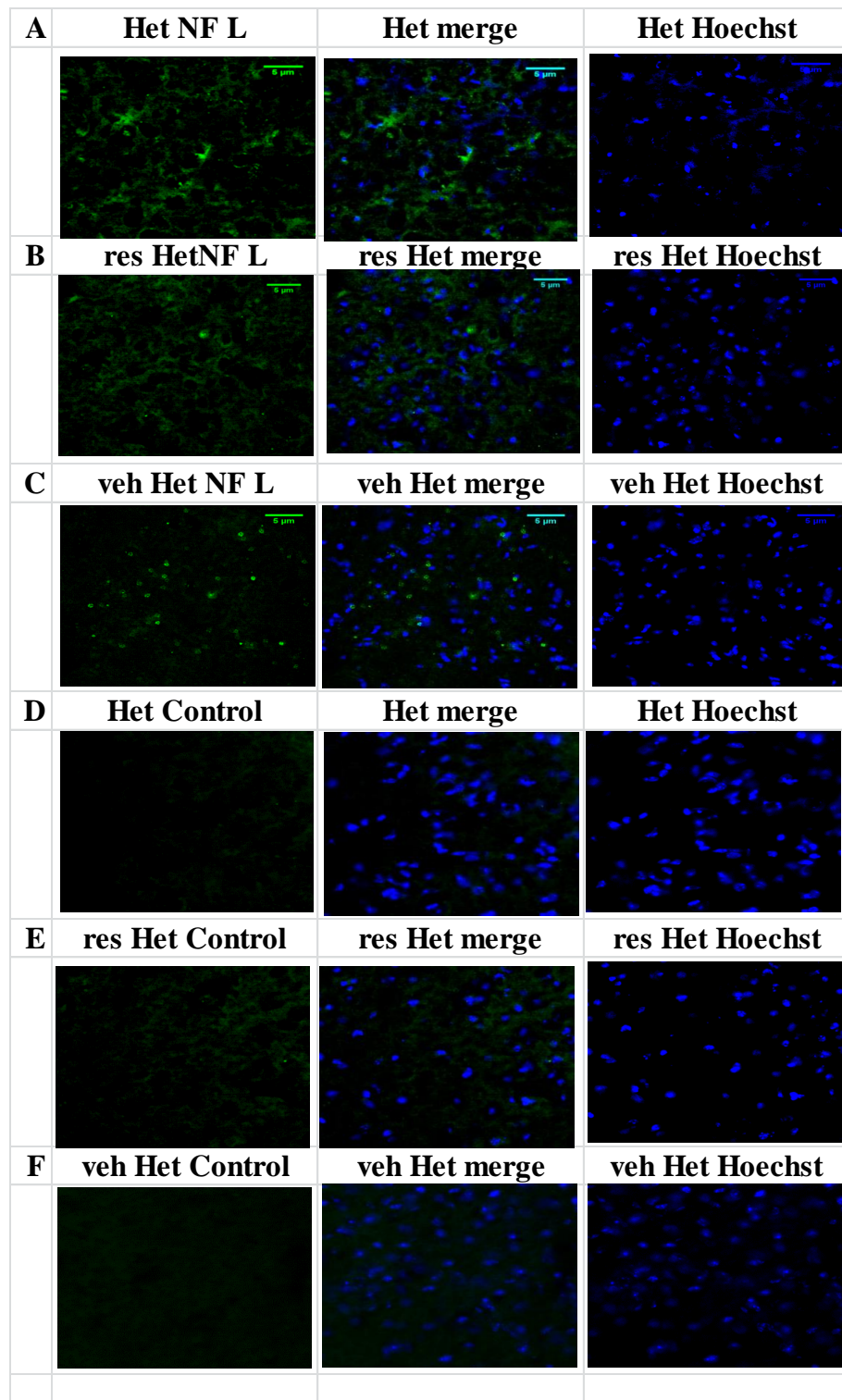


Figure 6.32 NF h expression in brain of untreated res and veh Het

Representative images of NF h expression in (A) untreated Het (B) res Het and (C) veh Het brain. Control sections for (D) untreated Het (E) res Het and (F) veh Het were processed without primary antibody.

6.7.9 Discussion of mitochondrial protein expression in res treated brain and retina

The percent difference observed in retinal layers was examined for each protein profile in res and veh Het sections. In order to determine the extent of change, all the data was compared to untreated WT as this was the standard to which any potential therapy aspired to. Table 6.18 shows a summary of the percentage difference in untreated res and veh Het retinal layers compared to untreated WT.

Table 6.18 Percentage change in retinal protein expression compared to WT

Het	PRL	ONL	OPL	INL	IPL	GCL	Ave
Mito	29	135	21	92	80	15	62
Comp	44	185	35	150	125	38	96
Dam	95	62	131	178	64	4.2	89
resHet	PRL	ONL	OPL	INL	IPL	GCL	Ave
Mito	49	25	-7	2	-7	-22	7
Comp	40	41	-10	14	8	-2	15
Dam	168	213	303	418	89	42	206
vehHet	PRL	ONL	OPL	INL	IPL	GCL	Ave
Mito	19	18	5	26	27	-7	14
Comp	12	43	6	37	62	11	29
Dam	94	86	119	428	24	-15	123
Brain	Mito	Comp	Dam	Ret	Mito	Comp	Dam
Het	46	118	119	Het	55	89	63
rHet	24	26	274	rHet	23	16	150
vHet	26	26	-35	vHet	14	26	65

Table shows the percentage change observed in retinal layers of protein expression in untreated res and veh Het retina. The percentage change in the whole retina and brain is included.

Compared to untreated WT, mitochondrial specific proteins of untreated Het had a 63% increase. The ONL had the highest increase with 135% and the GCL had the least with 15%. Compensation protein expression was increased by an average 96%. The ONL showed the highest increase with 185% and the OPL with the least of 35%. Damage mediated protein expression was increased by 89%. The INL had the highest percent increase with 178%. The GCL had the least damage with 4% increase.

Res Het had an average of 7% increase in mitochondrial proteins. This was observed in the PRL only. The GCL had the highest reduction of mitochondrial proteins with a 22% loss compared to untreated WT. Compensation protein expression in res Het has an average 15% increase. The ONL had the highest with 41% and the GCL had the least with a 2% reduction. Damage mediated protein expression was increased by 206% in res Het retina. The INL had the highest

Chapter 6 Trial of resveratrol in *Opa1^{Q285STOP}* mouse

increase with 418%. The GCL had the least increase in damage protein expression with a 42% increase.

Vehicle treated Het retina had an average 14% increase in mitochondrial protein expression compared to WT. The INL had the highest increase with 26%. The GCL had a reduction of 7%. Compensation protein expression in veh Het showed a 29% increase in expression with the IPL showing the highest increase with 62%. The OPL had the least percent change with 6% increase. Damage mediated protein expression in veh Het had a 123% increase in expression. The INL had the highest with 428% increase and the GCL showed a 15% reduction compared to untreated WT.

The mean percentage change in retina and brain is shown in Figure 6.33. It demonstrates that res treated Het had increased damage mediated protein expression with reduced compensation in both brain and retina. As vehicle treated Het protein profile showed, there was a substantial reduction in compensatory protein expression but without the increased damage protein expression suggesting that veh Het may have less oxidative stress.

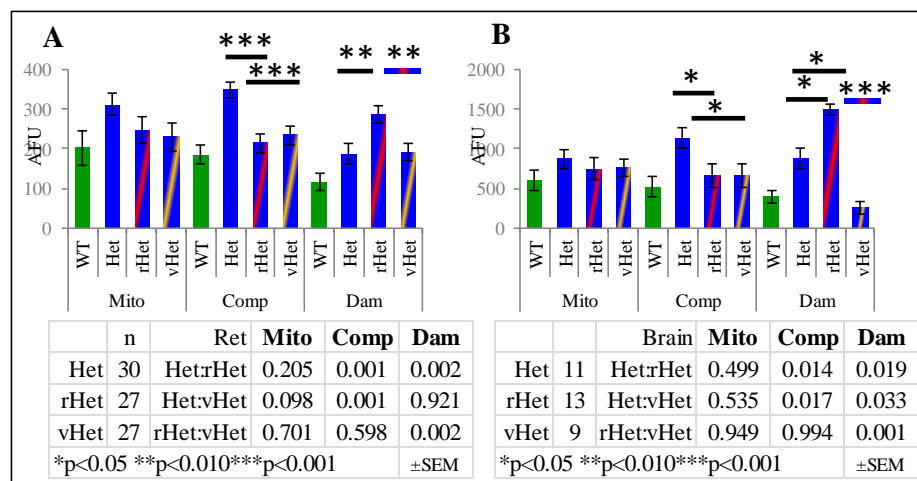


Figure 6.33 Protein profiles of untreated res and veh Het brain and retina

Graphs show the mean ± SEM AFU of mitochondrial, compensation and damage mediated protein expression in (A) retina and (B) brain of untreated, res and veh Het.

Chapter 6 Trial of resveratrol in $Opa1^{Q285STOP}$ mouse

The effects of resveratrol minus vehicle demonstrated that compared to untreated Het, mitochondrial protein in brain was unchanged, damage mediated proteins increased by 141% and compensation proteins reduced by 1%. Retinal mitochondrial protein in res Het showed a 7% increase in mitochondrial related protein expression with a 51% increase in damage proteins and a reduction of 6% in compensation proteins. The ratio of compensation to damage mediated proteins was lost in both tissues.

Cultured glioblastoma (glioma stem cell) in the presence of resveratrol increased the expression of neurofilament (Sato et al. 2013). There are reports of antioxidant activity and the reduction of neurofilament expression suggesting that protection was conferred on cultures cells following damage. Ladostigil was observed to confer protection in aged rats (Weinreb et al. 2007). Direct application of antioxidant therapy as an intravitreal injection attenuated retinal degeneration with respect to protein expression. Epigallocatechin gallate, the active ingredient of green tea reduced the expression of sodium nitroprusside induced neurofilament in photoreceptor (Zhang and Osborne 2006). Dietary supplementation in canine age related neurodegeneration reduced neurofilament expression (Opii et al. 2008).

PSD95 expression in Alzheimer's hippocampal neuronal cell culture reduced the expression of PSD95 which supports the findings reported Rege. Pre-treatment of rats with resveratrol protect them against morphine induced neuroinflammation with reduced PSD95 expression (Tsai et al. 2012). Treatment of a mouse model of Alzheimer's disease reduced the expression of PSD 95 (Porquet et al. 2013).

Resveratrol appeared to have specific adverse effects within the retina where there was a significant increase in damage mediated protein expression without the potentially protective effect of compensatory proteins. This was possibly due to the enhanced H_2O_2 mediated damage initiated by increased MnSOD activity.

6.8 Endogenous antioxidants in res treated *Opal*^{Q285STOP} mouse

6.8.1 Catalase activity in res treated *Het*

Catalase activity in untreated *Het* showed a reduction in spinal cord and retina of 40% and 30% respectively. Brain catalase was reduced by 8%. The effects of resveratrol on catalase activity in *Het* brain, spinal cord and retina were examined.

6.8.1.1 Results of catalase activity in res treated *Het*

For catalase analysis the assay was performed as described in Chapter C5 section 1.2.

Brain		SC		Retina	
Het	8	Het	7	Het	4
rHet	6	rHet	3	rHet	3
vHet	6	vHet	3	vHet	0

Table 6.19 Summary of test samples for catalase activity in untreated res and veh *Het*

The catalase activity in untreated *Het* brain homogenate had 3.50 ± 0.31 units/mg. Res *Het* brain homogenate had 4.60 ± 0.34 units/mg which was not significantly different to untreated *Het* ($p=0.077$). Catalase activity in veh *Het* brain homogenate had 1.70 ± 0.34 units/mg. which was statistically reduced compared to untreated *Het* brain ($F(5,31) 7.995$ $p=0.001$).

The catalase activity in spinal cord homogenate of untreated *Het* had 1.70 ± 0.25 units/mg. Res *Het* had 2.20 ± 0.40 units/mg which was not statistically different to untreated *Het* ($p=0.278$) and veh *Het* had 2.70 ± 0.12 units/mg which was significantly increased compared to untreated *Het* ($F(5,18) 10.902$ $p=0.043$).

The catalase activity in untreated *Het* retinal homogenate was 2.10 ± 0.35 units/mg and res *Het* ($n3$) had 1.0 ± 0.12 units/mg which was significantly reduced compared to untreated *Het* ($F(3,10) 9.156$ $p=0.007$).

The kinetic reactions of the catalase assay are shown in Figure 6.34 and a graphical representation of catalase activity in shown in Figure 6.35.

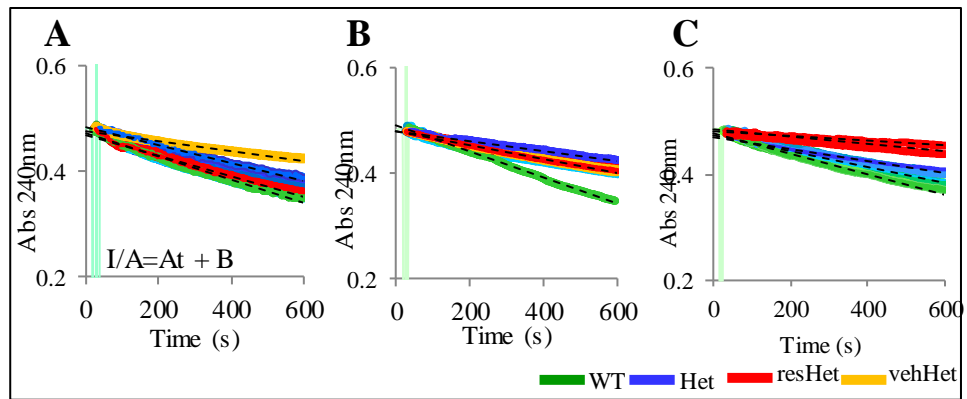


Figure 6.34 Kinetics of H₂O₂ decomposition in Het, res and veh treated Het

Representative kinetics of H₂O₂ decomposition in the presence of 80µg tissue homogenates from WT, Het, res Het and veh Het brain (A) Brain, spinal cord (B) and retina (C).

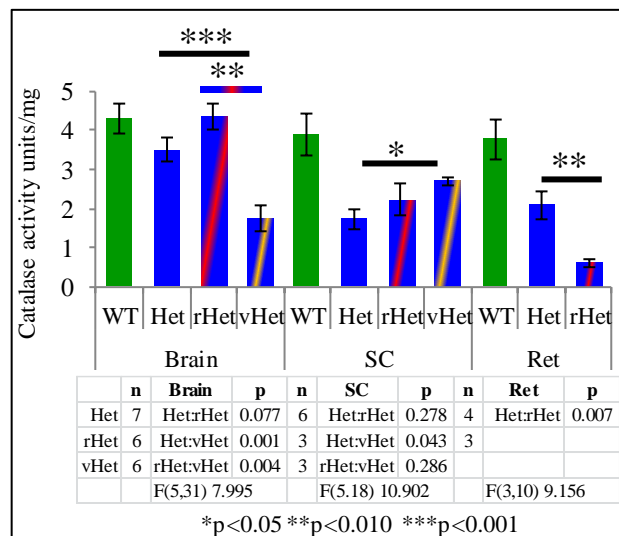


Figure 6.35 Catalase activity in tissue homogenate of untreated and treated Het.

Graph showing the mean ±SD catalase activity per mg tissue homogenate from Het, res Het and veh Het brain, spinal cord (SC) and retina (Ret).

6.8.1.2 Discussion of catalase activity in res treated Het

The catalase activity in res Het brain homogenate was enhanced by 23% compared to untreated Het. Res spinal cord homogenate was enhanced by 29% compared to untreated Het. Retinal catalase activity was reduced by 52% compared to untreated Het.

Catalase activity in veh Het brain homogenate showed a 74% reduction compared to untreated Het. Veh Het spinal cord homogenate had a 29% increase compared to untreated Het.

Catalase activity in retinal homogenate of res Het was reduced by 53% compared to untreated Het and 73% compared to untreated WT. Untreated Het retinal catalase activity was reduced by

Chapter 6 Trial of resveratrol in *Opal^{Q285STOP}* mouse

43% compared to WT, however the further 29% reduction in res Het treated retina would suggest that resveratrol has exerted a negative influence on H₂O₂ decomposition.

6.8.2 SOD activity in res treated *Opal^{Q285STOP}* mouse

6.8.2.1 Introduction to SOD assay in res treated Het

An increase in MnSOD activity with administration of resveratrol has been well publicised (Robb et al. 2008a; Robb et al. 2008b; Danz et al. 2009; Ryan et al. 2010; Mojica-Villegas et al. 2014; Robb and Stuart 2014) The SOD assay was performed as previously described.

6.8.2.2 Results of SOD assay in res treated Het

Brain		SC		Retina	
WT	6	WT	4	WT	6
Het	7	Het	4	Het	6
rHet	6	rHet	3	rHet	6
vHet	6	vHet	3	vHet	3

Table 6.20 Summary of test samples for SOD analysis in untreated, res and veh Het

Table 6.21 shows a summary of SOD activity in untreated Het, res and veh Het brain, spinal cord and retinal homogenate for total SOD, MnSOD and CuZnSOD. The kinetic reactions of the SOD assay are in Appendix N and the calculations for line fittings used are in Appendix O.

Figure 6.36 shows graphical representations of these data.

	Brain			SC			Ret		
	Het	rHet	vHet	Het	rHet	vHet	Het	rHet	vHet
Total SOD	10.34	22.66	14.12	0.63	30.71	31.41	1.59	1.23	0.76
	0.15	1.57	1.51	0.12	1.19	1.61	0.54	0.46	0.02
	Het:rHe 0.001			0.001			0.385		
	Het:vHet 0.001			0.001			0.108		
	rHet:vF 0.001			0.001			0.353		
	F(5,12) 32.430			F(5,12) 105.37			F(5,1) 8.912		
MnSOD	0.409	2.651	0.651	0.007	0.201	0.016	0.164	0.256	0.074
	0.049	0.533	0.125	0.001	0.017	0.002	0.097	0.108	0.004
	Het:rHe 0.001			0.001			0.340		
	Het:vHet 0.494			0.712			0.448		
	rHet:vF 0.001			0.001			0.131		
	F(5,12) 48.676			F(5,12) 22.619			F(5,1) 3.743		
CuZnSOD	1.645	1.788	1.466	0.132	0.792	0.162	0.247	0.069	0.082
	0.219	0.134	0.057	0.013	0.137	0.008	0.080	0.017	0.008
	Het:rHe 0.478			0.013			0.002		
	Het:vHet 0.377			0.771			0.029		
	rHet:vF 0.125			0.053			0.804		
	F(5,12) 257.825			F(5,12) 15.439			F(5,1) 10.892		

Table 6.21 Summary of SOD analysis in untreated, res and veh Het

Table shows a summary of total SOD, MnSOD and CuZnSOD activity in Het, res and veh Het brain, spinal cord (SC) and retinal (Ret) homogenate. The statistical difference (p value) between groups is shown with the percentage change compared to untreated Het.

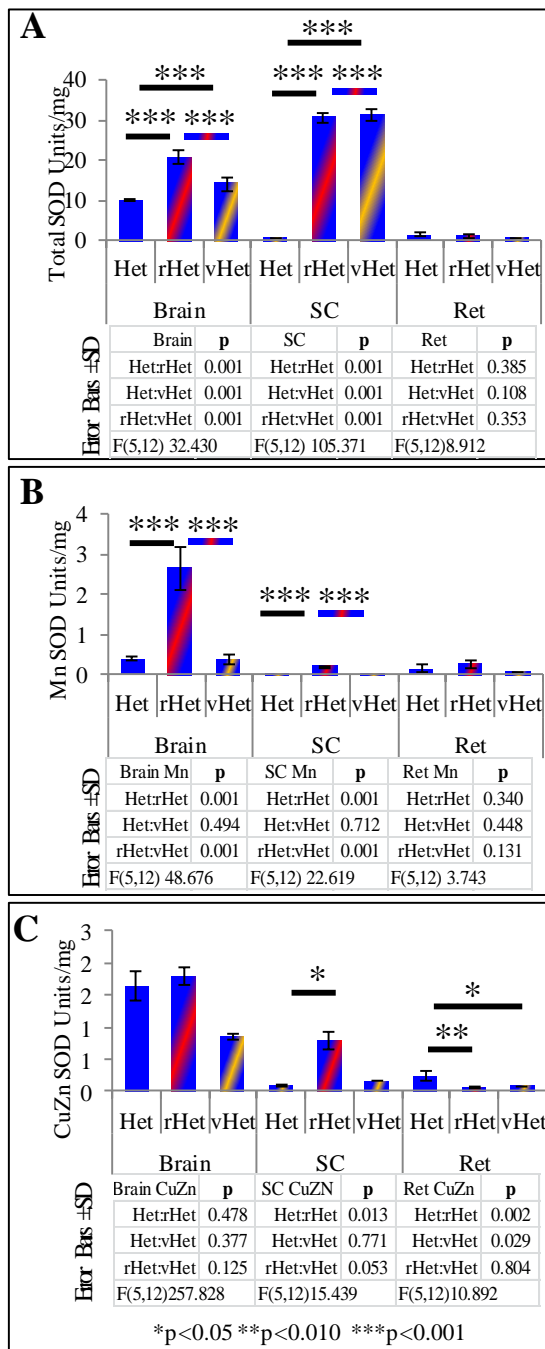


Figure 6.36 SOD units of activity in tissue homogenate of untreated and treated Het.

(A) Graph showing the mean \pm SD of total SOD activity of Het, res Het and veh Het in brain, spinal cord (SC) and retinal (Ret) homogenate.

(B) Graph showing the mean \pm SD of MnSOD activity in tissue homogenate brain, spinal cord (SC) and retina (Ret) in untreated Het, res Het and veh Het.

(C) Graph showing the mean \pm SD of CuZnSOD activity in untreated Het, res Het and veh Het brain, spinal cord (SC) and retina (Ret). ($p=0.004$).

6.8.2.3 Discussion of SOD activity in res treated Het

Due to the profound reduction in untreated Het spinal cord SOD activity, the average percent changes observed in res and veh Het were examined according to tissue type homogenate.

Compared to untreated Het, brain homogenate in res Het had a 225% increase in SOD activity. This was due to the 548% increase in MnSOD activity. Res Het spinal cord homogenate showed a 2681% increase in SOD activity compared to untreated Het. MnSOD activity was increased 2780% and CuZnSOD activity was increased 498%. Retinal homogenate in res Het showed a

Chapter 6 Trial of resveratrol in *Opa1^{Q285STOP}* mouse

reduction of 13% compared to untreated Het. CuZnSOD activity was reduced by 72%. MnSOD activity was increased by 56%.

Compared to untreated Het, veh Het brain homogenate had a 28% increase in SOD activity. Spinal cord homogenate had a 1674% increase in SOD activity compared to untreated Het. Retinal homogenate in veh Het had a 58% reduction in SOD activity compared to untreated Het.

On examining the original data where the inhibition of formazan formation results in a change in absorbance, the percentage inhibition with the combined MnSOD and CuZnSOD should have been equal to the percent inhibition obtained with total SOD. In untreated Het brain there was 23%±6 non-SOD activity. In res Het there was 7%±4 non-SOD which was significantly reduced compared to untreated Het (F(5,30) 25.624 p=0.001). Veh Het brain homogenate had 25%±5 non-SOD activity which was not significantly different compared to untreated Het (p=0.672). Spinal cord homogenate in untreated Het had 35%±2 non-SOD activity, res Het had 7%±2 non-SOD which was significantly reduced compared to untreated Het (F(5,20) 19.228 p=0.001). Veh Het had 49%±2 non SOD activity which was significantly increased compared to untreated Het (p=0.030). Retinal homogenate in untreated Het had 21%±2 non-SOD activity. Res Het had 23±5 which was not significantly different compared to untreated Het (p=0.536). Veh Het had 23%±1 which was not significantly different compared to untreated Het (p=0.603). Figure 6.37 summarises this observation.

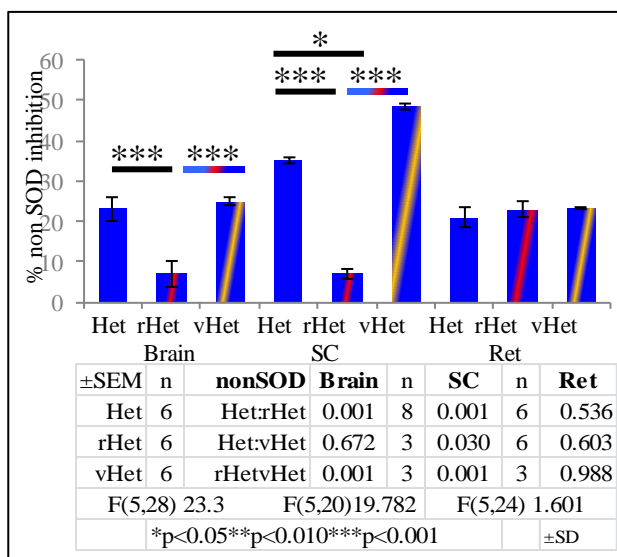


Figure 6.37 Non-SOD inhibition of formazan formation in Het homogenates

Graph showing the mean ±SEM of non-SOD activity in untreated, res and veh Het tissue homogenate. Res Het brain and spinal cord homogenate had significantly less non SOD activity compared to untreated Het. Veh Het spinal cord homogenate had a significantly higher percentage of non-SOD activity compared to untreated Het.

Chapter 6 Trial of resveratrol in *Opa1^{Q285STOP}* mouse

6.8.3 Antioxidant index in res treated *Opa1^{Q285STOP}* mouse

As discussed in Chapter 5 Section 5.1.3, the combined changes observed in catalase activity and SOD were used to establish an antioxidant profile specific for tissue type. In res treated Het brain AO index was 171. This was due to the increase in brain MnSOD. Spinal cord AO index in res Het was 1089. Retinal AO index in res Het was reduced to minus 23 due to a reduction in all but MnSOD activity. The tissue specific AO profile index in res Het was 715. Vehicle treated Het brain AO index was 5. Spinal cord AO index was 51 and retinal AO index was reduced to minus 61 due to the combined reduction of all AO activity observed. The tissue specific AO profile index in veh Het was minus 408.

The effect of vehicle treatment was obtained by subtracting the fold changes observed in veh Het antioxidant activity. The effects of resveratrol on the antioxidant status of Het showed a 7% reduction of catalase activity compared to untreated Het. CuZnSOD activity was increased by 163% and MnSOD activity increased 1066%. Res treated Het brain had an AO index of 145, spinal cord had an AO of 751 and retinal AO index was 21. The AO index of res Het was 306. Figure 6.38 shows a summary of this.

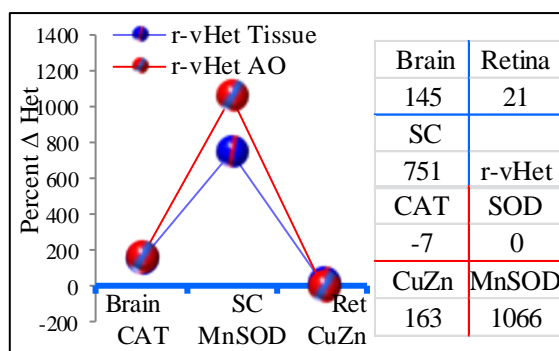


Figure 6.38 AO profile in res treated Het

Line graph representing the percent changes in res treated Het compared to untreated Het (represented by blue line). All res Het homogenates showed an increase in AO activity. Spinal cord had the highest increase of 751%. Antioxidant activity showed catalase activity was marginally reduced, CuZnSOD activity increased 163% and MnSOD activity was increased 10.85 fold compared to untreated Het.

6.8.4 MnSOD protein expression in res treated *Opa1^{Q285STOP}* mouse

6.8.4.1 Introduction

As described previously immunohistology was performed using MnSOD antibody on untreated Het (n4), res Het (n4) and veh Het (n4) retina and brain sections. Western blotting was performed on untreated Het (n4) and res Het (n4) retinal and brain homogenate.

6.8.5 Results of MnSOD protein expression in untreated res and veh Het retina

Table 6.22 shows a summary of the MnSOD expression in the retina of untreated Het res and veh Het. Figure 6.39 (A) shows the mean AFU for MnSOD expression in untreated, res and veh Het retina. Figure 6.39 (B) shows the mean AFU for MnSOD expression in untreated, res and veh Het brain.

Table 6.22 Summary of MnSOD protein expression in untreated and treated Het retina

MnSOD	PRL			ONL			OPL			INL			IPL			GCL		
	Het	rHet	vHet	Het	rHet	vHet	Het	rHet	vHet	Het	rHet	vHet	Het	rHet	vHet	Het	rHet	vHet
Ave	381.3	332.8	161.9	131.8	146.4	101.2	119.1	263.4	150.1	227.2	172.4	121.3	800	863.3	291.7	228.8	246.9	170.4
SEM	20.21	92.62	46.38	90.69	60.95	19.74	32.28	80.97	43.82	75.88	56.4	45.36	14.84	45.24	92.73	4.403	86.99	73.54
Het:rHet		0.772			0.193			0.074			0.540			0.393			0.211	
Het:vHet			0.003			0.193			0.112			0.026			0.006			0.169
F		F (5,16)	8.912		F (5,16)	11.416		F (5,16)	10.444		F (5,16)	4.028		F (5,16)	2.850		F (5,16)	8.476

Table shows the mean (\pm SEM) of retinal mitochondrial expression of MnSOD in untreated, res and veh treated Het. The statistical difference between groups is represented by p value.

IHC of brain in untreated Het had 558 \pm 92AFU. Res treated Het had 1806 \pm 351 which was significantly increased compared to Het (F(5,32) 6.913 p=0.006). Veh Het had 789 \pm 87 which was not significantly different to untreated Het. Figure 6.39 (B) shows this data.

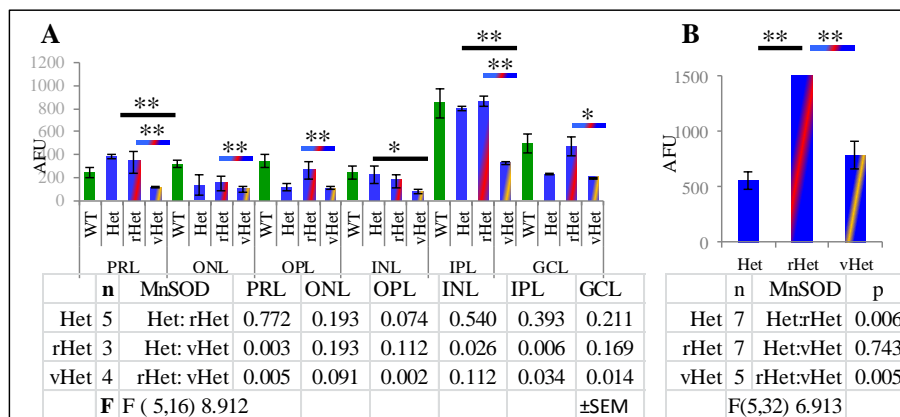


Figure 6.39 MnSOD expression in untreated, res and veh Het retina and brain

Graph shows the mean \pm SEM of MnSOD expression in Het, res Het and veh Het (A)retinal layers and (B) Brain.

Chapter 6 Trial of resveratrol in *Opa1^{Q285STOP}* mouse

Western blotting of brain homogenate in untreated Het had 0.86 ± 0.12 and res Het had 0.95 ± 0.21 ($p=0.229$). Retinal homogenate in untreated Het had 1.06 ± 0.09 and res Het had 1.60 ± 0.11 which was significantly increased compared to Het ($F(3,12) 1.591$ $p=0.003$). Figure 6.40 shows representative bands from Western blotting.

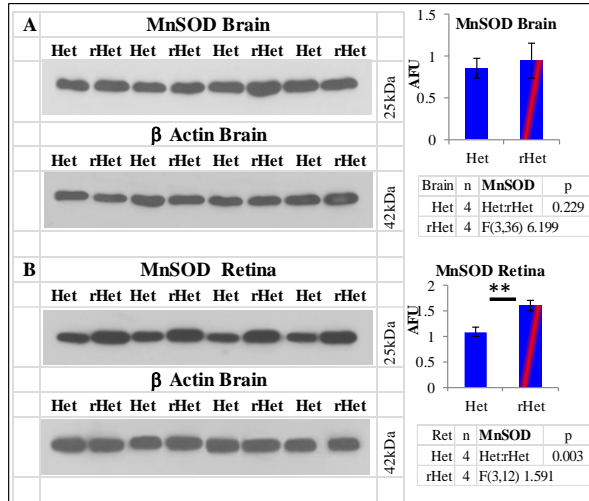


Figure 6.40 MnSOD protein in brain and retinal homogenate of untreated and res Het

Images show representative bands from Western blotting of (A) brain and (B) retinal homogenate from untreated Het (n4) and res treated Het (n4) for MnSOD. Lower bands show beta actin as a loading control.

Figures 6.41 and 6.42 show representative images of MnSOD expression in retina and brain from untreated res and veh Het.

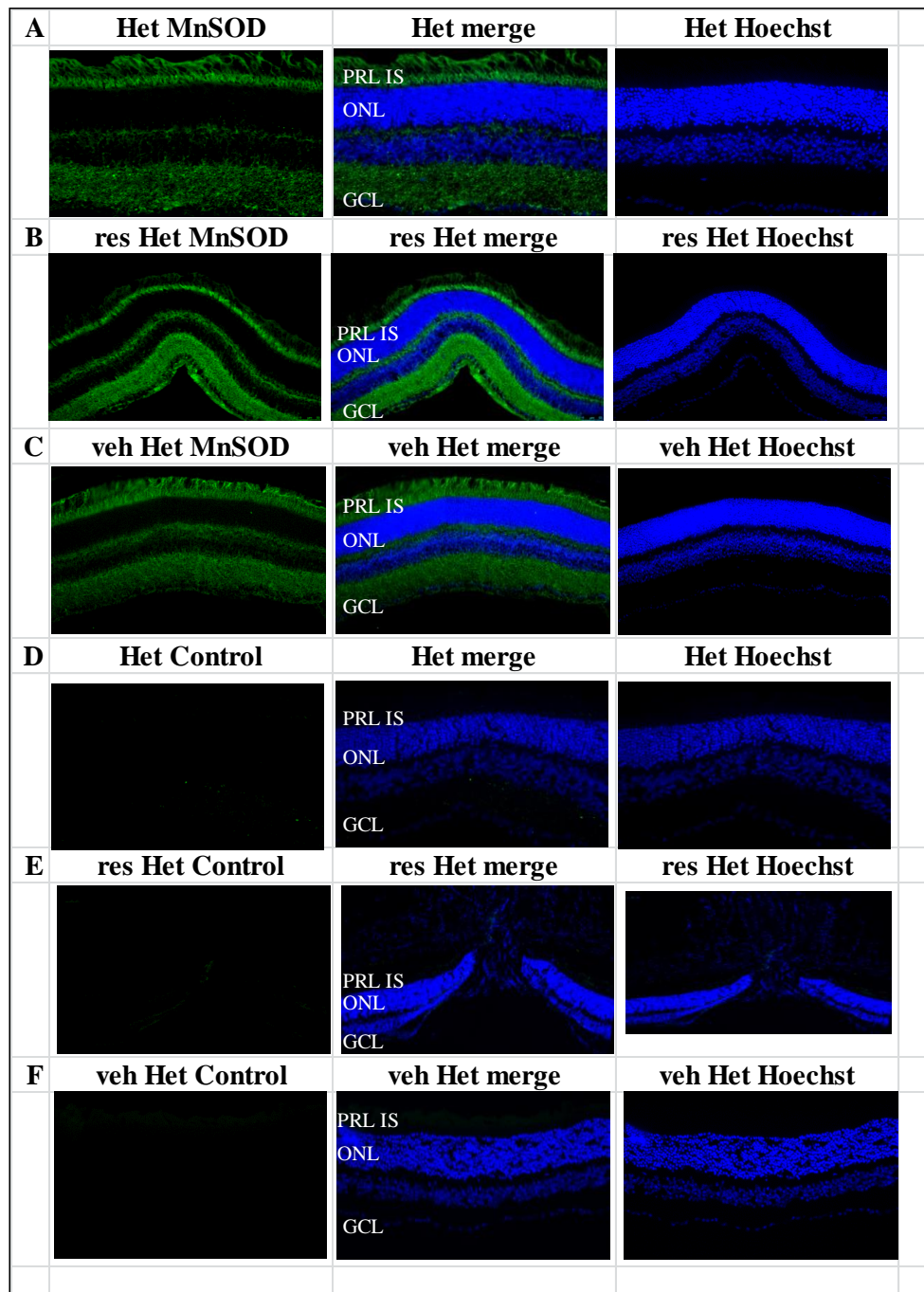


Figure 6.41 MnSOD expression in untreated res and veh treated retina

Representative images of MnSOD expression in Het (A), res Het (B) and veh Het (C) retinal sections. Negative control sections (omission of primary antibody) for Het (D), res Het (E) and veh Het (F) are shown.

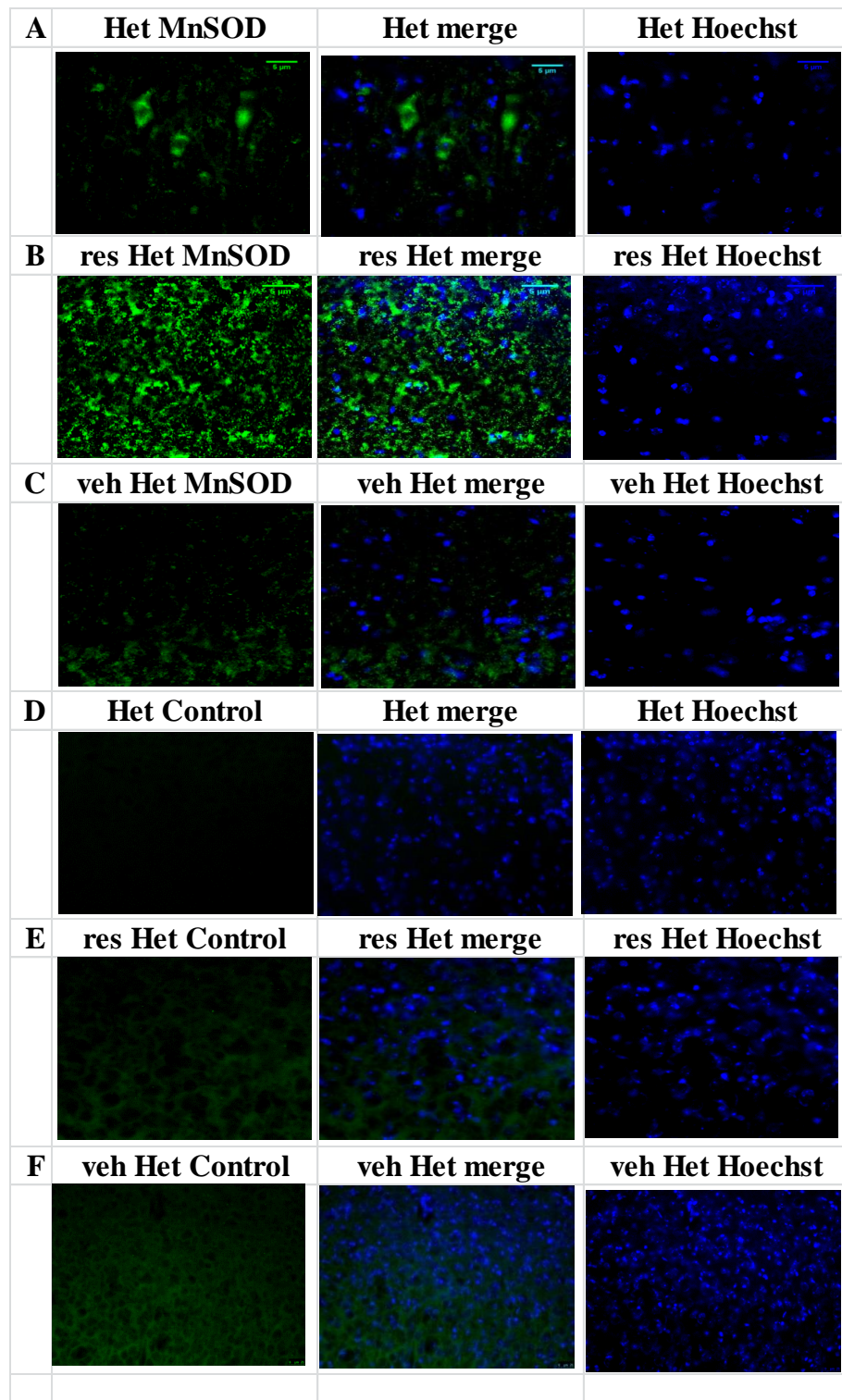


Figure 6.42 MnSOD expression in untreated res and veh treated brain

Representative images of MnSOD expression in (A) untreated Het (B) res Het and (C) veh Het brain. Control sections for (D) untreated Het (E) res Het and (F) veh Het were processed without primary antibody.

Chapter 6 Trial of resveratrol in $Opa1^{Q285STOP}$ mouse

6.8.5.1 Discussion of SOD activity in res treated Het

6.8.5.1.1 MnSOD expression in retina

Res Het retinal tissue showed a mean 35% increase in retinal layers. Western blotting showed a 48% increase compared to untreated Het. The res Het retinal homogenate MnSOD assay showed a 56% increase compared to untreated Het. This suggested that all the available MnSOD was functional. Veh Het retinal MnSOD expression was reduced by 47% compared to untreated Het. The MnSOD assay showed a reduction of 56% compared to untreated Het. This suggested that 9% of MnSOD in veh Het was non-functional.

6.8.5.1.2 MnSOD expression in brain

MnSOD activity was investigated by IHC and Western blotting where there was a significant increase in protein expression compared to untreated Het. Previously, MnSOD activity was examined in brain homogenate where it showed a 570% increase in activity. The increase in protein deposition combined with increased dismutation suggested that the surplus MnSOD was functional. Veh Het MnSOD expression was increased by 41% compared to untreated Het. MnSOD activity in the inhibition of formazan showed veh Het had 63% more activity compared to untreated Het. This suggested that the expressed MnSOD was functional.

6.8.6 3 Nitrotyrosine deposition in untreated res and veh Het retina

Table 6.23 shows a summary of 3 nitrotyrosine deposition in the retinal layers of untreated res and veh Het.

Table 6.23 3Nitrotyrosine deposition in retinal layers of untreated res and veh Het

	PRL			ONL			OPL			INL			IPL			GCL		
3 Nitro	Het	rHet	vHet	Het	rHet	vHet	Het	rHet	vHet	Het	rHet	vHet	Het	rHet	vHet	Het	rHet	vHet
Ave	360	407	400	45	330	253	220	262	457	175	143	292	338	243	533	320	120	178
SEM	38.1	29.1	93.1	16.4	17	63.7	20.6	14.3	180	25.7	21.4	63	54.8	6.62	130	2.05	17.4	35.5
Het:rHet		0.048			0.198			0.574			0.226			0.046			0.007	
Het:vHet			0.974			0.812			0.977			0.586			0.854			0.014
F	F (5,15) 2.210			F (5,15) 1.269			F (5,15) 0.624			F (5,15) 0.244			F (5,15) 1.252			F (5,15) 2.896		

Table shows the mean (\pm SEM) of 3 Nitrotyrosine deposition in retinal layers of untreated res and veh Het. Statistical difference between groups is represented by the p value.

3 nitrotyrosine deposition was examined in brain sections. Untreated Het had 1561 ± 275 AFU. Res Het had 477 ± 98 which was significantly reduced ($F(5,30) 7.919$ $p=0.001$). Veh Het had 286 ± 44 which was also significantly reduced ($p=0.001$). Figure 6.43 shows a summary of 3 nitrotyrosine deposition in retina (A) and brain (B) of untreated res and veh Het.

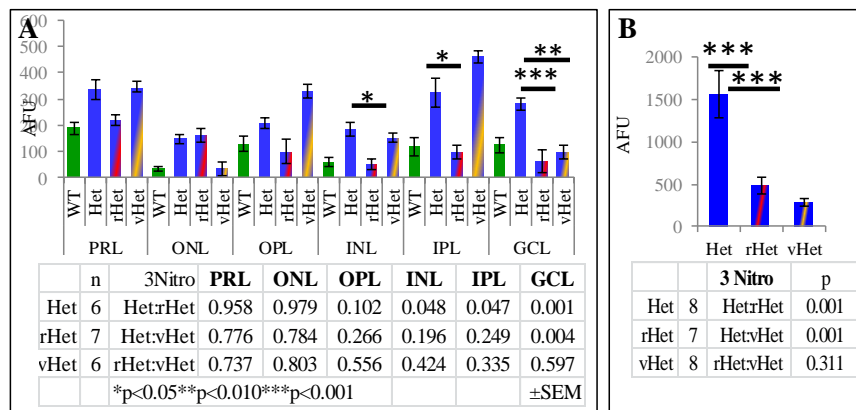


Figure 6.43 3 Nitrotyrosine deposition in untreated res and veh Het

Graph shows the mean \pm SEM of 3 nitrotyrosine deposition in Het, res Het and veh Het (A) retinal layers and (B) brain.

Figures 6.44 show representative images of 3 nitrotyrosine deposition in retinal I sections and Figure 6.45 shows same in brain sections expression in retina and brain from untreated res and veh Het.

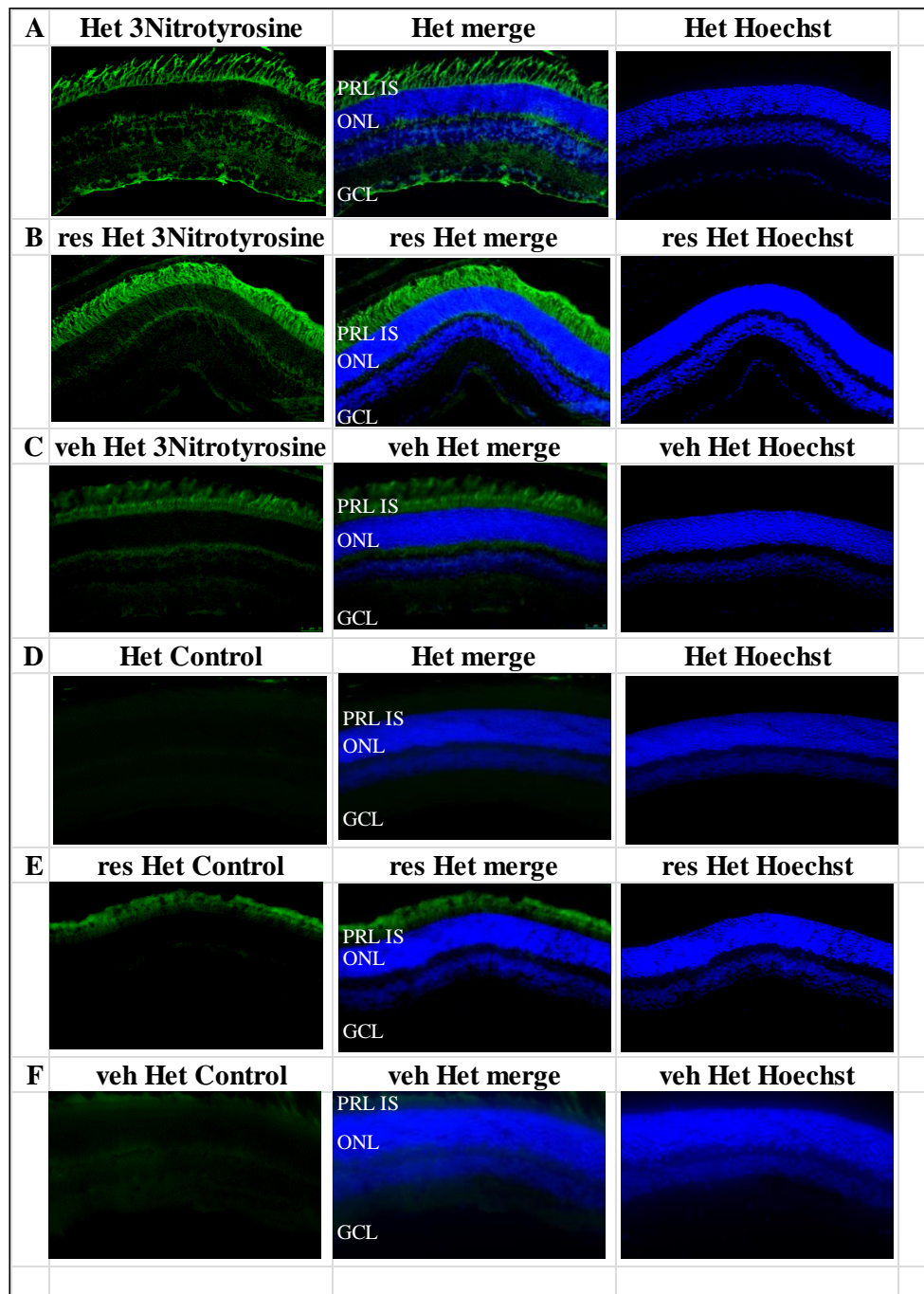


Figure 6.44 3 Nitrotyrosine deposition in untreated res and veh Het retina

Representative images of 3 nitrotyrosine deposition in Het (A), res Het (B) and veh Het (C) retinal sections. Negative control sections (omission of primary antibody) for Het (D), res Het (E) and veh Het (F) are shown.

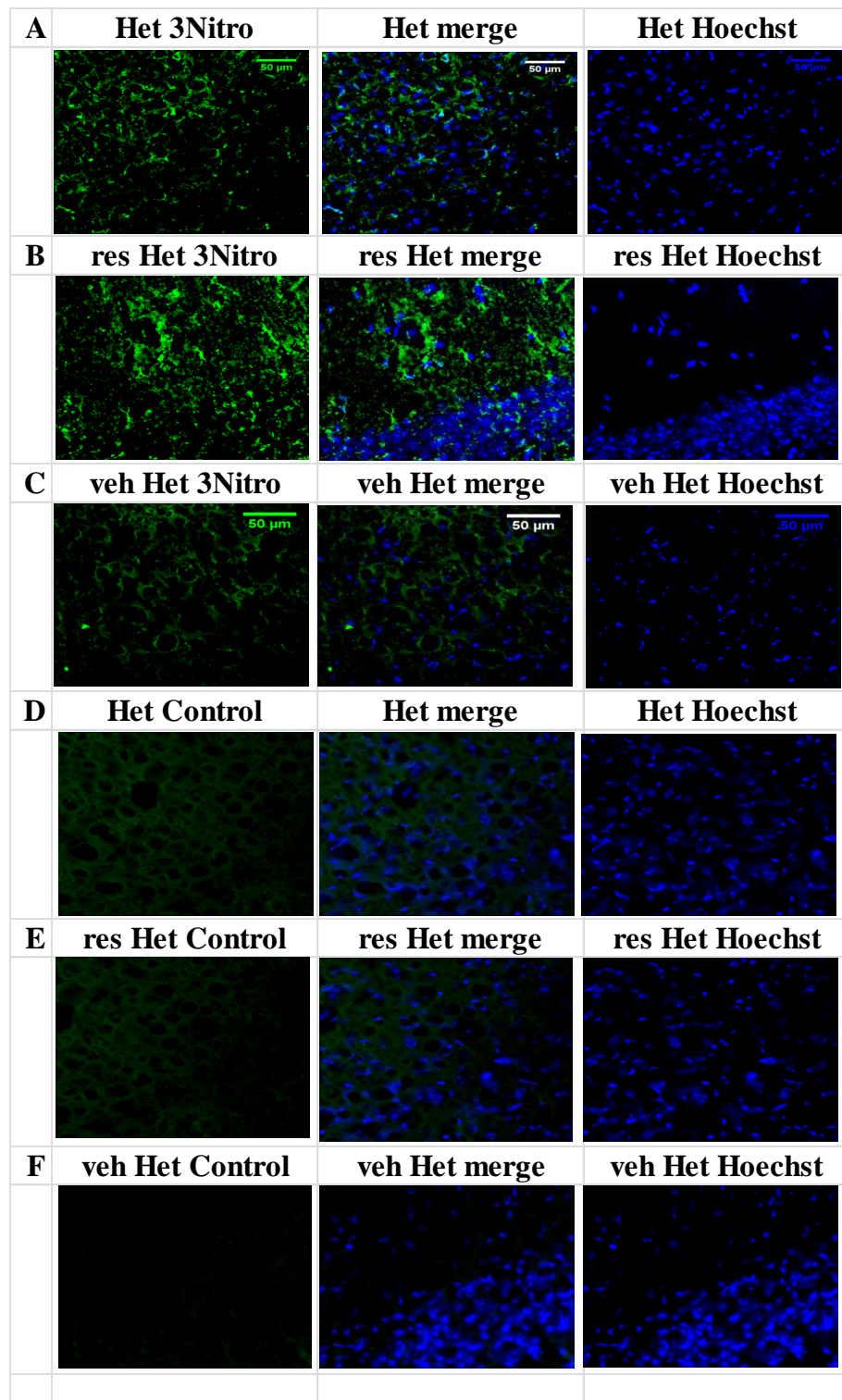


Figure 6.453 Nitrotyrosine deposition in untreated res and veh Het brain

Representative images of 3 nitrotyrosine deposition in (A) untreated Het (B) res Het and (C) veh Het brain. Control sections for (D) untreated Het (E) res Het and (F) veh Het were processed without primary antibody.

Chapter 6 Trial of resveratrol in *Opa1^{Q285STOP}* mouse

The presence of 3 Nitrotyrosine was significantly reduced in res Het compared to untreated Het. In the INL there was a significant 73% reduction (F(5,12) 1.415 p=0.048) which was not present in veh Het INL (p=0.196). Res Het IPL showed a 69% reduction of 3 Nitrotyrosine deposition which was also significant (F(5,12) 1.402 p=0.047) and was not present in the veh Het IPL (p=0.249). The GCL of res Het had a 77% reduction in the presence of nitrotyrosine (F(5,12) 4.201 p=0.001) . This was also present in veh Het with a 66% reduction (p=0.004).

3 Nitrotyrosine deposition was significantly reduced in brain of both res and veh Het. Res Het had a 70% reduction (F(5,30) 7.919 p=0.001) and veh Het had 81% less 3Nitrotyrosine compared to untreated Het.

The ratio of 3 Nitrotyrosine to MnSOD was examined in the retinal layers. The ratios obtained were compared to WT. The mean ratio in WT was 0.31. Untreated Het had a ratio of 1.03. Res Het ratio was 0.45 and veh Het ratio was 1.75. This meant that although the deposition of 3 Nitrotyrosine in veh Het may not have been significantly more compared to untreated Het, the combined reduction of MnSOD resulted in significantly more oxidative stress. The ratio in WT brain was 0.31. Untreated Het brain was 1.03. res Het ratio was 0.45 and veh Het 1.75. Figure 6.46 summarises these data.

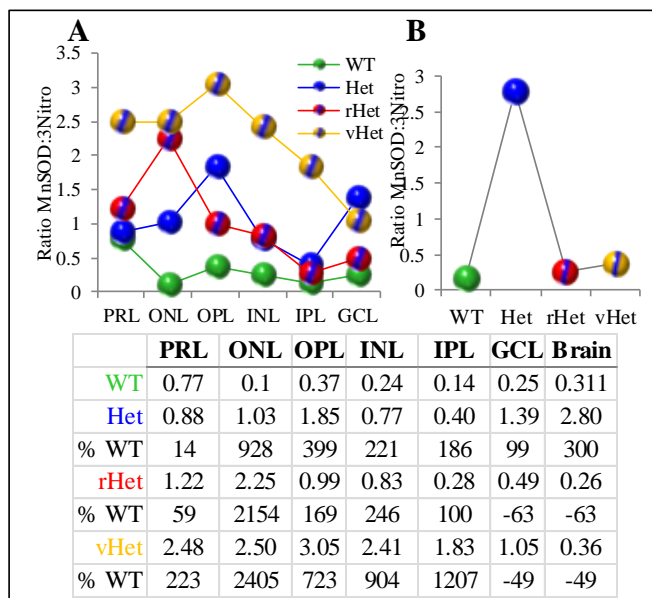


Figure 6.46 Ratio of MnSOD to 3 Nitrotyrosine in res retina and brain
Line graph showing the ratio of MnSOD to 3 nitrotyrosine in untreated, res and veh retinal layers and brain. The percentage difference compared to untreated WT is shown.

Chapter 6 Trial of resveratrol in $Opa1^{Q285STOP}$ mouse

6.8.7 Summary of Chapter 6: Trial of resveratrol in $Opa1^{Q285STOP}$ mouse

Brain weight was significantly reduced in res treated female Het mice. Cardiac weight ratio was also significantly reduced.

6.8.7.1 Neuromuscular anomalies in res treated $Opa1^{Q285STOP}$ mouse

There was a significant reduction in neuromuscular function as seen in rotarod testing. This was seen in female resveratrol and vehicle treated female Het mice. Resveratrol treated male Het showed no housing dependent change in rotarod performance. Resveratrol treated Het mice appeared to have reduced fear conditioning which was evident in rope and beam testing. There was no significant difference in learning skills in res treated Het mice.

6.8.7.2 Cognitive function in $Opa1^{Q285STOP}$ mouse

Spontaneous alternation testing of resveratrol treated Het demonstrated a significant increase in investigation and discrimination ratio which was not observed in vehicle treated Het. Novel object recognition testing did not reveal any significant difference between untreated and resveratrol treated Het mice.

6.8.7.3 Bioenergetic impairment in res treated $Opa1^{Q285STOP}$ mouse

Resveratrol treated Het showed a significant increase in complex I activity by 24% at the expense of complex II. Complex IV activity was increased by 40% compared to untreated Het. CNS specific effects were observed in all tissues examined with the brain showing the greatest reduction in ETC activity.

6.8.7.4 Antioxidant activity in res treated $Opa1^{Q285STOP}$ mouse

Resveratrol treated Het had a significant increase in MnSOD activity which had a potential negative influence on catalase activity. Res Het spinal cord showed the greatest enhancement to AO activity. The combined changes in antioxidant activity in a reduced catalase environment may be detrimental to mitochondrial survival.

6.8.7.5 Protein profile expression in $Opa1^{Q285STOP}$ mouse

Resveratrol treated tissues showed an increase in mitochondrial related protein expression in both brain and retina. Retina specifically showed enhanced damage mediated protein expression. Both brain and retina showed significantly reduced compensatory protein expression compared to untreated Het.

Chapter 6 Trial of resveratrol in $Opa1^{Q285STOP}$ mouse

The effects of resveratrol administration were compounded by the presence of ethanol which itself resulted in alterations of both *In Vivo* and *In Vitro* measured parameters. There were no significant improvement in neuromuscular function or cognitive performance save for an enhanced fear response. This would be considered disadvantageous to any mouse as it is likely to result in a reduced life span. Bioenergetic changes resulted in enhanced activity but the specific ratios of activity were significantly disturbed in the res Het mouse for complex II (retina) which was also observed in veh Het. The ratio for complex IV activity in Het spinal cord was significantly disturbed in the res treated but not the veh treated Het mice. This suggested that resveratrol was enhancing the electron transport function at a cost to the mitochondria of the spinal cord and resulting periphery. Enhanced MnSOD activity in the res Het mitochondria was possibly responsible for enhancing the concentration of H_2O_2 but in the presence of reduced catalase activity would prove detrimental to mitochondrial function.

Chapter 7 Paradoxical effects of resveratrol in WT C57BL/6

7.1 Introduction

The resveratrol study was a three-armed trial. The inclusion of wild type (WT) mouse was incorporated with vehicle treated WT to extend a comprehensive analysis of the effects of resveratrol. Resveratrol was given to a total of 26 WT mice (14 female and 12 male). For the vehicle arm of the trial, a total of 12 WT were treated (6 female and 6 male). The resveratrol treated and vehicle treated WT mice were housed with Het cage mates and testing conditions for all experiments were performed concurrent with Het treated. As all previous techniques have been described in the previous chapters, all that remains are the results of the data collected. All resveratrol treated WT are called res WT and vehicle treated WT as veh WT. Mice were given resveratrol at a concentration of 219.06mM in their drinking water. Vehicle treated mice were given ethanol at a concentration of 17mM. Mice were examined thoroughly for any adverse effects including gastro intestinal disturbances that might indicate the presence of emodin at greater than acceptable concentration. The bottled water containing resveratrol required replacement at 24 hour intervals which also provided an opportunity to examine the mice for signs of stress. The trial design is available in Appendix C.

7.2 Health monitoring in res treated WT

7.2.1 Introduction

The health and safety of all participants on the resveratrol trial was paramount. Monitoring of weight was considered an excellent indicator of general health. The weekly post weaned weights of res treated WT was discussed in Chapter 6 section 6.2.1.2. The monthly weight checks continued to 15 months.

7.2.1.1 Results of weight monitoring at 15 months

All female mice treated and untreated were housed in groups. Male untreated and treated were kept as group housed where possible. Individual housed males were either isolated for breeding purposes or because of in cage harassment. Where possible the assailants were removed to solitary quarters. Weights were analysed according to housing conditions in male mice only. Both untreated and res

Chapter 7 Paradoxical effects of resveratrol in C57Bl/6

treated males were both solitary and group housed. Veh treated male WT were housed in group cages only. Table 7.1 summarises the results showing the percentage difference between treated and untreated WT and the statistical p value.

		n	Body weight (g)	Brain weight (g)	Cardiac ratio
	FWT	25	27.7 ± 1.7	0.59 ± 0.18	0.62 ± 0.14
	rFWT	13	32.2 ± 5.9	0.42 ± 0.05	0.55 ± 0.08
	vFWT	6	28.7 ± 3.1	0.42 ± 0.03	0.71 ± 0.33
	FWT:rFWT		0.001	0.001	0.050
	FWT:vFWT		0.525	0.009	0.180
	rFWT:vFWT		0.057	0.421	0.006
	F(11,191)		9.866	2.725	1.935
S	sMWT	4	34.0 ± 2.6	0.490 ± 0.08	0.52 ± 0.08
O	srMWT	6	34.8 ± 1.5	0.438 ± 0.05	0.60 ± 0.05
H	L sMWT:srMWT		0.786	0.963	0.343
O	O sMWT:gMWT		0.624	0.909	0.012
U	srMWT:grMWT		0.251	0.015	0.129
S	G F(9,57)		1.043	1.037	2.565
I	R gMWT	7	32.5 ± 1.2	0.48 ± 0.04	0.66 ± 0.03
N	O grMWT	6	37.3 ± 1.5	0.43 ± 0.05	0.54 ± 0.03
G	U gvMWT	6	35.3 ± 1.5	0.40 ± 0.05	0.71 ± 0.05
	P gMWT:grMWT		0.017	0.288	0.046
	gMWT:gvMWT		0.163	0.257	0.336
	rgMWT:gvMWT		0.358	0.755	0.340
	F(9,57)		1.043	1.037	2.565
r=resveratrol v=vehicle s=solitary housed g=group housed					

Table 7.1 Body brain and cardiac weight ratio in untreated, res and veh WT

Table showing weights in untreated, res and veh treated female and male WT at 15 months. The statistical p value is shown between groups.

7.2.1.2 Discussion of weight at 15 months

In the WT population there was a significant 16% increase in res treated female WT weight compared to untreated females (F(15,150) 6.471 p=0.001). Veh treated female Het had a 3% increase which suggested resveratrol was responsible for 13% of this increase. Both res treated and veh treated females showed a significant reduction in brain weight of 29% in res WT (F(15,150) 2.400 (p=0.001) and 28% in veh WT (p=0.009) compared to untreated female WT. Res treated females had a significant 13% reduction in cardiac weight ratio (F(15,150) 1.805 (p=0.025) compared to untreated females. Veh treated females had a 13% increase in cardiac weight ratio compared to untreated female WT which was not statistically significant (p=0.180). There was no significant difference observed between the solitary housed untreated and solitary housed res treated male WT. Solitary housed untreated male WT and group housed untreated male WT differed significantly in cardiac weight ratio (F(15,150) 1.805 (p=0.012) with group housed male WT showing a 28% increase. Solitary housed res treated male WT differed significantly to group housed res treated male WT in brain weight (F(15,150) 2.400 (p=0.015) where solitary housed had a 11% increase compared to group housed. Group housed

Chapter 7 Paradoxical effects of resveratrol in C57Bl/6

male res treated weight was significantly increased by 15% compared to group housed male WT (F(15,150) 6.471(p=0.017). Veh treated group housed males showed a non-significant 9% increase in weight compared to untreated group housed male WT (p=0.163). Group housed male brain weight was reduced by a significant 19% (F(15,150) 2.400 p=0.049) compared to untreated male WT.

Resveratrol has been reported as showing no significant effect in body or organ weights mouse when administered at a concentration of 3g/kg in CD-1 mouse strain (Kyselova et al. 2003). Dietary induced increased body weight and abdominal fat volume have been reduced with the addition of resveratrol (Baek et al. 2014). Resveratrol offers resistance to high fat induced obesity and insulin resistance (Lagouge et al. 2006; Jeon et al. 2014). The current literature supports the anti-obesity effects of resveratrol in multiple species including primates (Jimenez-Gomez et al. 2013; Roberts et al. 2014), pig (Azorín-Ortuño et al. 2011), rat (Beaudoin et al. 2013; Nagao et al. 2013), mouse (Hogan et al. 2010; Kim et al. 2011) and even zebra fish (Pardal et al. 2014). The doses range from 3mg/kg to 200mg/kg. The only significant difference was the duration of therapy. Most studies ranged from two weeks to 16 weeks.

The average brain weight in mouse is reported as 450g but C57Bl/6 brain weight is heavier than other lab mice (Wahlsten et al. 2006). Any loss of weight can impact metabolic constraints and there exists functional correlates between brain weight and function (Williams et al. 1998).

The cardiovascular protection conferred by resveratrol is presumed to be by mechanism including reduced platelet aggregation, improved endothelial function, and the reduction of myocardial fibrosis (Petrovski et al. 2011; Magyar et al. 2012; Hao et al. 2013; Soner and Sahin 2014). The application of cardiac weight as an indirect function of left ventricular hypertrophy suggests that a bulky muscle mass doesn't equate to function. This would suggest that resveratrol provided cardio protection to the res treated WT where the presence of ethanol could have adverse effects.

7.3 Neuromuscular impairment in res treated WT

7.3.1 SHIRPA analysis in res treated WT

Chapter 7 Paradoxical effects of resveratrol in C57Bl/6

SHIRPA analysis was performed on six untreated WT and six res WT. There were three males and three females in each group. Observations were made in the viewing jar, above the arena and in the arena. The total number of observations for each mouse was lower motor function was 11, cerebrosplinal function 12, sensory 7, neuropsychiatric 8 and autonomic 17.

7.3.1.1 Results of SHIRPA in res treated WT

For lower motor function WT scored 0.06 ± 0.03 and res WT scored 0.03 ± 0.01 ($p=0.074$). Cerebrosplinal function in WT was 0.11 ± 0.05 and res WT was 0.08 ± 0.02 ($p=0.161$). Sensory function in WT was 0.04 ± 0.01 . res WT sensory function was 0.11 ± 0.02 ($p=0.053$). Neuropsychiatric function was 0.13 ± 0.03 in WT and 0.14 ± 0.04 in res WT ($p=0.074$). Autonomic function in WT was 0.06 ± 0.03 and in res WT was 0.03 ± 0.03 ($p=0.055$). (Appendix G contains raw data for SHIRPA analysis of res WT).

7.3.1.2 Discussion of SHIRPA in res treated WT

Analysis of lower motor function score showed a reduction of 52% compared to untreated WT. Cerebrosplinal function score was less than 25% compared to untreated WT. The score in sensory function was increased by 200%. The result from three different observational recordings (in the viewing jar, in the arena and above the arena) was not statistically significant. Neuropsychiatric function score was reduced by 14% and autonomic function score reduced by 42% compared to untreated WT.

7.3.1.3 Rotarod analysis in res treated WT

Analysis of motor function and coordination was performed in res WT and veh WT. The number of animals tested is summarised in Table 7.2.

7.3.1.4 Results of rotarod in res treated WT

Rotarod Analysis			
F WT	11	M WT	8
rFWT	6	rMWT	5
vFWT	3	vMWT	0
sMWT	4	gMWT	5
rsMWT	3	rgMWT	3
s:solitary g:group r:res v :veh			

Table 7.2 Summary of test numbers for rotarod in WT res and veh WT

Chapter 7 Paradoxical effects of resveratrol in C57Bl/6

Latency to fall in untreated female WT was 110±4 seconds. In res WT latency was 74±4 seconds which was significantly reduced compared to untreated WT (F(4,28) 6.098 p=0.002). Veh WT female latency was 87±7 seconds which was also significantly different to untreated WT F(4,28) 6.098 p=0.024). Male WT latency was 64±5 seconds. Res treated WT male latency was 60±3 seconds which was not significantly different to untreated WT (p=0.520). There was no significant difference in male res treated WT where housing conditions were previously seen to affect the performance of rotarod. Solitary housed male WT latency was 104±2 seconds and solitary housed res treated male WT latency was 58±5 seconds which was significantly reduced compared to untreated WT (F(3,12) 3.897 p=0.003). Untreated group housed male WT latency was 50±7 seconds and group housed res treated male WT latency was 60±3 seconds which was not significantly different to untreated male WT (p=0.488). Figure 7.1 shows a graphical representation of this data.

The effect of weight on latency to fall was considered. Untreated female WT who weighed less than 30g had a latency of 117±4 seconds. Res treated female WT who weighed less than 30g had a latency of 84±5 seconds which was significantly reduced compared to untreated female WT (F(7,262) 17.943 p=0.002). Latency in untreated male WT who weighed less than 34g was 76±5 seconds and latency in res treated male WT who weighed less than 34g was 58±5 seconds which was significantly reduced compared to untreated male WT (p=0.036).

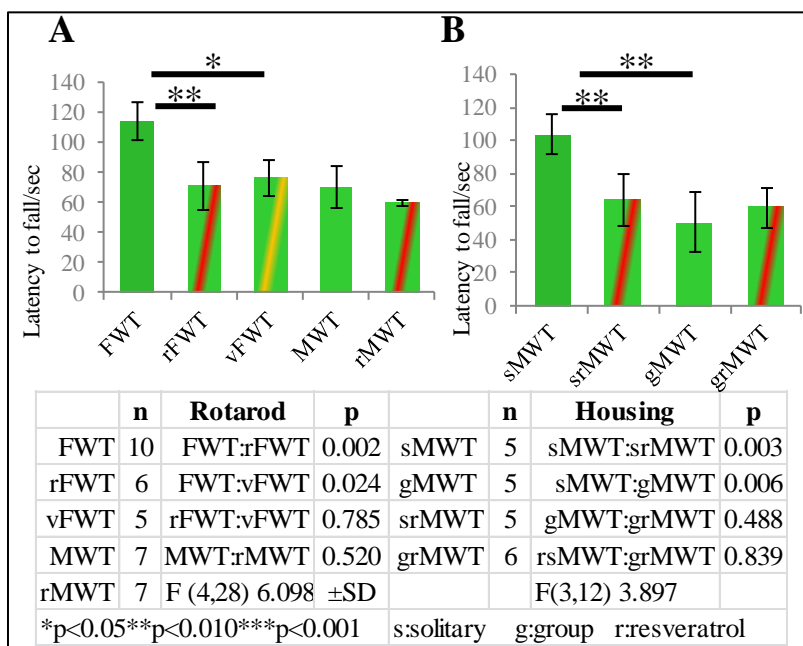


Figure 7.1 Latency to fall in untreated, res and veh WT

(A) Graphs show the mean ±SD of latency to fall from rotarod in female and male untreated res and veh treated WT. (B) Graph shows the mean ±SD of housing conditions and latency in untreated and res treated male WT.

Chapter 7 Paradoxical effects of resveratrol in C57Bl/6

7.3.1.5 Discussion of rotarod in res treated WT

In female res WT there was a reduction of 33% in latency compared to untreated WT. Veh treated female WT showed a 21% reduction compared to untreated WT. Solitary housed res treated male WT had a 45% reduction in latency to fall and group housed res treated male WT had an increase of 18% compared to group housed untreated male WT.

7.3.1.6 Results of narrow beam and in res treated WT

Rope/Beam			
F WT	5	M WT	5
rFWT	4	rMWT	4
vFWT	3	vMWT	0

Table 7.3 Summary of test numbers for beam and rope in WT

In untreated WT, beam initiation was 4.8±1.2 seconds. In res WT initiation was 25±6 seconds. There was a significant increase in initiation time between untreated WT and res WT (F(2,16) 7.966 p=0.004). Vehicle treated WT beam initiation was 12±3 seconds which was not significantly different compared to untreated WT (p=0.380). Figure 7.2 A shows these data.

7.3.1.7 Results of tight rope testing in res treated WT

In the tightrope test, the distance travelled by untreated WT was 8.4±1.1/cm. The distance travelled by res WT was 4.1±1.6/cm which was significantly reduced compared to untreated WT (F(2,16) 6.680 p=0.024). Veh WT travelled 4.3 ±0.3/cm which was significantly reduced compared to untreated WT (p=0.019). Figure 7.2B shows this data.

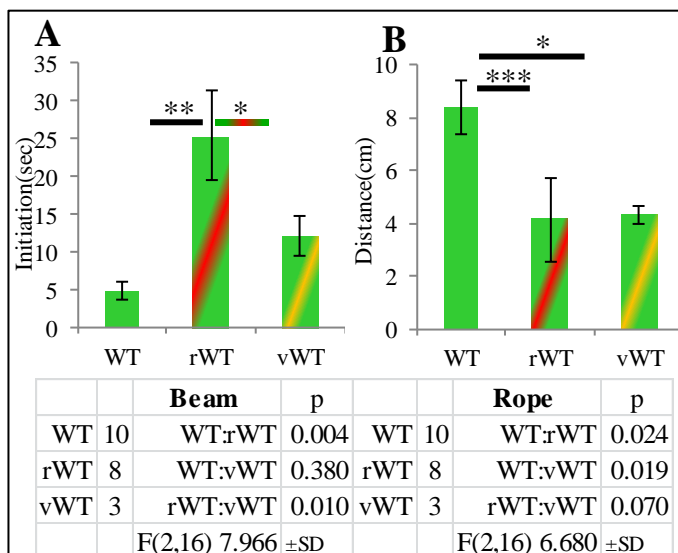


Figure 7.2 Beam initiation and tight rope distance in untreated res and veh WT

Graph showing mean ±SD of (A) narrow beam initiation to travel/seconds in untreated WT, res WT and veh WT. (B) Tightrope distance travelled/cm in untreated WT, res treated WT and veh WT.

7.3.1.8 Discussion of narrow beam and tight rope testing in res treated WT

In the narrow beam test the time to initiate travel down the beam was increased by 440% in the res WT population. The initiation time in res WT females was increased by 1680% compared to untreated female WT. Veh treated WT female initiation was increased by 488%. The male res treated WT initiation time was increased by 93% compared to untreated male WT.

In the tight rope test, the distance travelled by res female WT was reduced by 15% compared to untreated female WT and male res WT reduced by 79% compared to untreated male WT. Veh female had a 63% increase in distance travelled compared to untreated female WT.

7.3.1.9 Fear conditioning in res treated WT and Het

An increase in narrow beam initiation time was considered a symptom of anxiety in untreated Het mice. Res treated Het female initiation was 80% less than res treated female WT. Res treated Het male initiation was 26% less than res treated WT. This suggested that res treated WT mice were more disturbed by the narrow beam test compared to res treated Het. Res treated female WT initiation time was a mere 18% better than untreated female Het. Res treated male WT initiation time was 364% faster than untreated male Het.

Res treated female Het had a 192% increase in distance travelled compared to res treated WT. Res treated male Het had a 1162% increase in distance travelled compared to res treated male WT. This suggested that resveratrol had exerted significantly different effects in the functioning brain of WT and Het. A clear reduction in fear conditioning in the res Het mice was not evident in res treated WT.

7.3.1.10 Learning skills in res treated WT

Learning skills were calculated as previously described. Essentially the ability to learn over a three day time period, the skills required to retain a position on the rotarod. This was a combination of modified body positioning with the incremental revs per minute and maintaining a simultaneous forward gait movement with both hind and fore paws. Also concentration on the task as distraction resulted in losing the pace of the rotarod.

Chapter 7 Paradoxical effects of resveratrol in C57Bl/6

7.3.1.11 Results of learning skills in res treated WT

The learning skills in untreated female WT mice were 0.56 ± 0.15 . Resveratrol treated female WT learning score was 0.26 ± 0.1 which was not significantly different compared to untreated WT ($p=0.245$). Female Veh WT scored 0.10 ± 0.18 which was not significantly different compared to untreated WT ($p=0.166$). The learning score in untreated male WT was 0.34 ± 0.18 . Res treated male WT learning score was 0.20 ± 0.02 which was not statistically significant ($p=0.654$).

7.3.1.12 Discussion of learning skills in res treated WT

There was a 54% reduction in learning in female res treated WT compared to untreated female WT. Vehicle treated female WT had a 82% reduction in learning compared to untreated WT. Male res treated learning was reduced by 41% compared to untreated WT. Housing conditions did not influence learning abilities in res treated male WT. Solitary housed res WT were not significantly different compared to res treated group housed male WT ($p=0.327$).

7.4 Cognitive impairment in res treated WT

7.4.1 Introduction

Cognitive function was examined in res treated WT consecutively with untreated WT and vehicle treated WT to explore the activity of resveratrol on hippocampal dependent learning and memory. Investigations comprised of T maze spontaneous alternation and novel object recognition test. These tests were performed in mice at 15 months of age.

7.4.2 T Maze testing in res treated WT

For spontaneous alternation testing, T maze analysis in untreated, res treated and veh treated WT was performed. Spontaneous alternation in a two armed T maze was used to identify spatial anomalies in the res treated WT population. The time in seconds to locate the novel arm, time spent in the novel arm and time spent in the original arm were collated to generate the investigation (IR), and discrimination ratio (DR). The sample numbers are summarised in tables preceding the results.

Chapter 7 Paradoxical effects of resveratrol in C57Bl/6

7.4.2.1 Results of T maze testing in res treated WT

T Maze			
F WT	7	M WT	6
rFWT	4	rMWT	4
vFWT	4	vMWT	0

Table 7.4 Summary of test numbers for T maze in untreated res and veh WT

The time to explore the novel arm in untreated WT was 11 ±2 seconds and in res WT was 19 ±4 seconds which was significantly increased compared to untreated WT (F(2,22) 6.124 p=0.037). Veh treated WT took 7±2 seconds which was not statistically different to untreated WT (p=0.540).

The time spent in the novel arm in untreated WT was 29±3 seconds. In res treated WT it was 22±3 seconds which was statistically reduced compared to untreated WT (F(2,22)5.913 p=0.015). Vehicle treated WT spent 20±3 seconds in the novel arm which was also significantly reduced compared to untreated WT (p=0.015).

Time spent in the original arm in untreated WT was 12±2seconds and 18±3 seconds in res treated WT which was not significantly different to untreated WT (p=0.059). Vehicle WT spent 12±2 seconds in the original arm which was not significantly different to untreated WT (p=0.674).Figure 7.3 shows a summary of these findings.

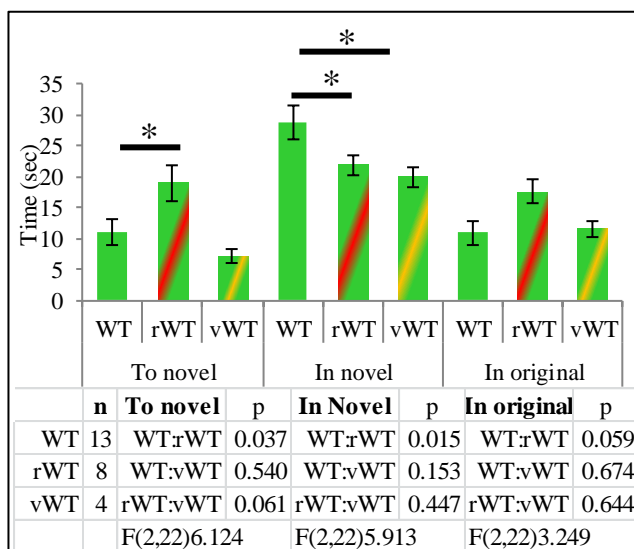


Figure 7.3 T Maze test parameters in untreated and treated WT

Graph showing the mean ±SD time in seconds of T maze testing parameters measured in untreated, res and veh treated WT. Time to novel arm, time spent in novel arm and time spent in original arm.

The IR in untreated WT was 0.66±0.05. In res WT the IR was 0.57±0.03 which was not significantly different to untreated WT (p=0.174). The IR in veh WT was 0.59±0.02 which was not significantly different to untreated WT (p=0.776).

Chapter 7 Paradoxical effects of resveratrol in C57Bl/6

The DR in untreated WT was 0.39±0.05. Res WT DR was 0.15±0.01 which was significantly reduced compared to untreated WT (F(2,22) 25.448 p=0.004). The DR of veh WT was 0.26 ±0.02 which was not significantly different compared to WT (p=0.268). Figure 7.4 shows the IR and DR of T maze testing.

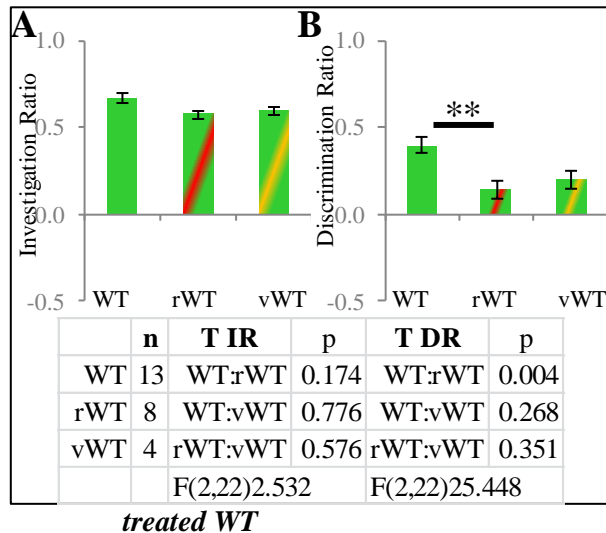


Figure 7.4 T maze IR and DR in untreated res and veh WT

Graph showing the mean ±SD (A) investigation and (B) discrimination ratio for T maze testing in untreated, res and veh treated WT.

7.4.2.2 Discussion of T maze testing in res

In T maze analysis, res WT took 72% longer to explore the novel arm compared to untreated WT which was considered statistically different (p0.037). Veh WT took 35% less time than untreated WT. The time spent in the novel arm was reduced in res WT mice by 23% (p=0.015) and by 30% in the veh treated group(p=0.015). The time spent in the original arm in res WT was increased by 49% compared to untreated WT. Veh WT time in original arm was the same as untreated WT. The IR of res WT was reduced by 21% compared to untreated WT. Veh WT IR was increased by 6%. The DR in res WT was reduced by 14% (p=0.004) whereas in veh WT it was reduced by 11% compared to untreated WT.

7.4.3 Novel object recognition testing in res treated WT

For novel object recognition testing untreated WT (n9), res WT (n6) and vehicle treated WT (n3) performed the object recognition task with a total of seven novel items. The same testing parameters were applied. The IR and DR were obtained as previously described.

7.4.3.1 Results of NOR testing in res treated WT

NOR			
F WT	6	M WT	5
rFWT	4	rMWT	4
vFWT	4	vMWT	0

Table 7.5 Summary of test numbers for NOR testing in WT

Chapter 7 Paradoxical effects of resveratrol in C57Bl/6

Time to novel object was significantly increased in res WT compared to untreated WT (F(2,20) 3.512 p=0.001). Time to novel in veh WT was also significantly increased (p=0.011). The time spent with the novel object was 22±2 seconds in untreated WT, 15±2 seconds in res WT which was significantly reduced compared to untreated WT (F(2,20) 6.454 p=0.001). Veh WT time with novel object was also significantly reduced to 12±1 seconds (p=0.024).

Time spent with the original object in untreated WT was 7±1 seconds. Res WT also spent 6.6±1.8 seconds which was not significantly different compared to untreated WT (p=0.960). Veh WT spent 3.2±0.9 seconds which was not statistically significant compare to untreated WT (p=0.418). Figure 7.5 shows a summary of these finding.

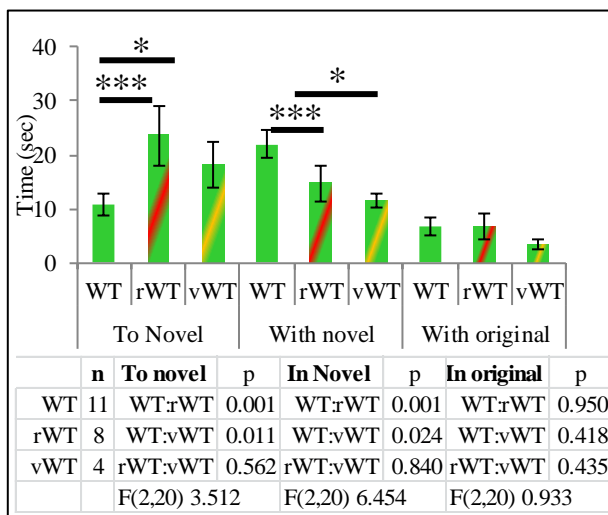


Figure 7.5 NOR test parameters untreated and treated WT

Graph showing the mean ±SD time in seconds for the testing parameters used in novel object recognition testing. The time to novel object, time with novel object and time with original object in untreated res and veh WT.

The IR in untreated WT was 0.71±0.05. IR in res WT was 0.57±0.1 which was not statistically different compared to untreated WT (p=0.144). The IR in veh WT was 0.72±0.07 which was not statistically different compared to untreated WT (p=0.706).

The DR in untreated WT was 0.51±0.09. In res treated WT the DR was 0.30±0.09 which was significantly reduced compared to untreated WT (F(2,20) 3.372 p=0.013). Veh WT DR was 0.53±0.11 which was not significantly different to untreated WT (p=0.942). Figure 7.6 shows the IR and DR of NOR in res treated WT.

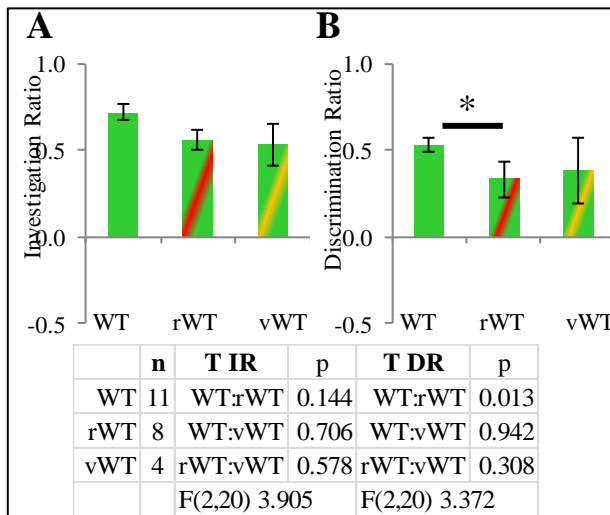


Figure 7.6 NOR IR and DR in untreated, res and veh WT

Graph showing the mean \pm SD of NOR (A) investigation ratio and (B) discrimination ratio in untreated WT, res WT and veh WT for NOR testing.

7.4.3.2 Discussion of NOR in res treated WT

In NOR, the time to novel object was increased by 120% in res WT which was significantly different compared to untreated WT ($p=0.001$) and by 69% in veh WT ($p=0.011$). The time with the novel object was reduced by 33% in res WT ($p=0.001$) and by 47% in veh WT. The time with the original item was unchanged in res WT but reduced by 51% in veh WT. The IR in res WT was reduced by 20% and in veh WT was unchanged compared to untreated WT. The DR in res WT was reduced by 41% and in veh WT was increased by 4%. The preference for particular objects was examined.

The time spent with individual items demonstrated preference which was considered noteworthy as untreated WT had shown particular behavioural traits in response to items that were considered normal exploratory behavioural traits. In the untreated WT, the time spent with silicone was 22 ± 5 /sec. Res WT spent 7 ± 4 /sec which was significantly reduced ($F(2,20)$ 2.677 $p=0.010$). Veh WT spent 8 ± 1 /sec which was also significantly reduced ($p=0.024$). Untreated WT spent 23 ± 5 /sec with wood. Res WT spent 10 ± 6 /sec which was significantly reduced ($F(2,20)$ 14.28 $p=0.008$). Veh WT spent 8 ± 0.8 /sec which was also significantly reduced ($p=0.011$). Untreated WT spent 31 ± 2 /sec with fabric. Veh treated WT spent 9 ± 0.8 /sec which was significantly reduced compared to untreated WT $F(2,20)$ 3.327 $p=0.024$). Untreated WT spent 15 ± 4 sec with glass. Res WT spent 6 ± 3 /sec which was significantly reduced compared to untreated WT ($F(2,20)$ 4.02 $p=0.044$). Figure 7.7 attempts to demonstrate these findings.

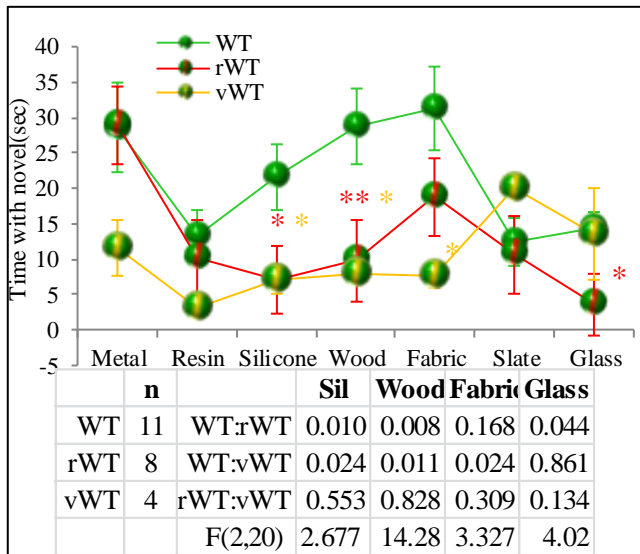


Figure 7.7 Preference in NOR testing

Line graph showing both the preference for specific objects (mean (\pm SD) time with novel/sec) and the trend in test participation in NOR testing. Compared to untreated WT, res WT spent a significantly less time with silicone ($p=0.010$), wood ($p=0.008$) and glass ($p=0.044$). Compared to untreated WT, veh WT spent a significantly less time with silicone ($p=0.024$), wood ($p=0.011$) and fabric ($p=0.024$).

While some items were less favourable (resin and slate), this did not deter untreated WT from continuing to investigate on each successive test. In res WT, the reduced IR can be seen as a significant reduction in time spent with novel objects. The trend showed a decline in test participation from the 2nd test. Vehicle treated WT followed a similar but more exaggerated trend in time spent with novel objects. The time spent with a less favourable object (slate) although not statistically significant ($p=0.249$) suggested the discrimination in veh WT was disturbed. The time spent with fabric which was increased in all tested mice was significantly reduced in veh WT.

7.5 Bioenergetic dysfunction in res treated WT

7.5.1 Introduction

The activity of the electron transport system was examined in the res WT population using mitochondrial extractions from brain, spinal cord, and retinal and gastrocnemius skeletal muscle. The number of tests performed for each complex is summarised in a table preceding each section. The methods used have been described elsewhere. The presence of residual succinate in complex I activity showed no significant effect. This is summarised in Appendix P. The kinetic reactions of ETC are shown in Appendix Q and the calculations for line fitting are shown in Appendix R.

Chapter 7 Paradoxical effects of resveratrol in C57Bl/6

7.5.1.1 Results of Bioenergetic assays in res treated WT

CI B		CI SC		CII B		CII SC		CIV B		CIV SC	
WT	8	WT	10	WT	8	WT	10	WT	9	WT	10
rWT	7	rWT	9	rWT	8	rWT	6	rWT	8	rWT	8
vWT	5	vWT	8	vWT	7	vWT	6	vWT	5	vWT	5
CI Ret		CI Mus		CII Ret		CII Mus		CIV Ret		CIV Mus	
WT	9	WT	4	WT	9	WT	4	WT	8	WT	4
rWT	6	rWT	3	rWT	6	rWT	4	rWT	6	rWT	3
vWT	6	vWT	3	vWT	6	vWT	3	vWT	6	vWT	3

Table 7.5 shows a summary of test numbers for bioenergetic assays.

Table 7.6 shows a summary of complex I, complex II and complex IV activity in brain, spinal cord retina and skeletal muscle of untreated WT, res and veh WT.

Table 7.6 Bioenergetics of WT, res and veh WT

	Brain			SC			Ret			Mus			
CI	WT	rWT	vWT	WT	rWT	vWT	WT	rWT	vWT	WT	rWT	vWT	
nMol/mg/ml	262±33	134±7	43±4	341±17	73±9	300±28	288±14	131±3	304±22	154±17	172±10	94±4	
WT:rWT		0.002			0.008			0.057			0.014		
WT:vWT			0.001			0.548			0.828			0.001	
rWT:vWT		0.001			0.054			0.025			0.153		
	F(2,17)9.987			F(2,24)65.876			F(2,18)7.790			F(2,9)9.987			
CII	WT	rWT	vWT	WT	rWT	vWT	WT	rWT	vWT	WT	rWT	vWT	
µMol/mg/min	50±4	32±2	60±3	54±2	14±1	33±2	128±9	61±2	117±6	39±6	28±5	17±2	
WT:rWT		0.012			0.023			0.001			0.146		
WT:vWT			0.001			0.527			0.001			0.148	
rWT:vWT		0.001			0.007			0.001			0.914		
	F(2,20)12.650			F(2,17)7.880			F(2,20)12.650			F(2,9)4.411			
CIV	WT	rWT	vWT	WT	rWT	vWT	WT	rWT	vWT	WT	rWT	vWT	
µMol/mg/min	3.6±0.1	1.9±0.1	1.8±0.0	2.5±0.1	0.9±0.1	1.8±0.0	1.4±0.0	2.3±0.1	3.0±0.2	2.5±0.0	1.4±0.0	1.3±0.1	
WT:rWT		0.001			0.001			0.001			0.172		
WT:vWT			0.001			0.001			0.010			0.007	
rWT:vWT		0.552			0.926			0.113			0.001		
	F(2,19)8.616			F(2,20)31.193			F(2,17)9.694			F(2,9)8.616			

Table shows a summary of bioenergetic analysis of complex I, complex II and complex IV activity in isolated mitochondria of untreated, res and veh WT brain spinal cord (SC) retina (Ret) and skeletal muscle (Mus). The statistical difference between groups is represented by p value.

Chapter 7 Paradoxical effects of resveratrol in C57Bl/6

Figures 7.8 A–C shows a graphical representation of the ETC activity in WT, res and veh treated mouse.

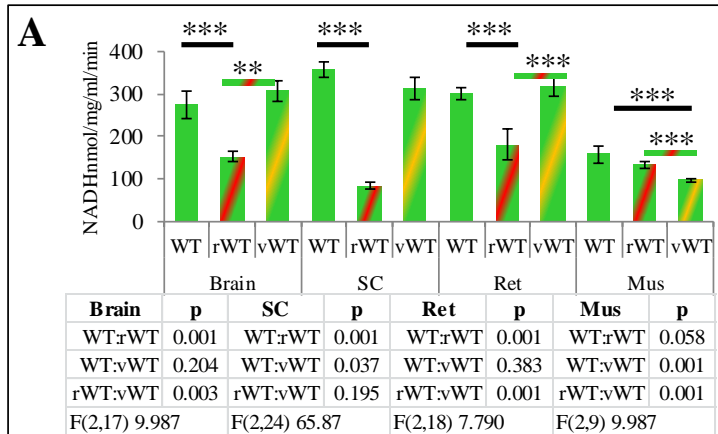
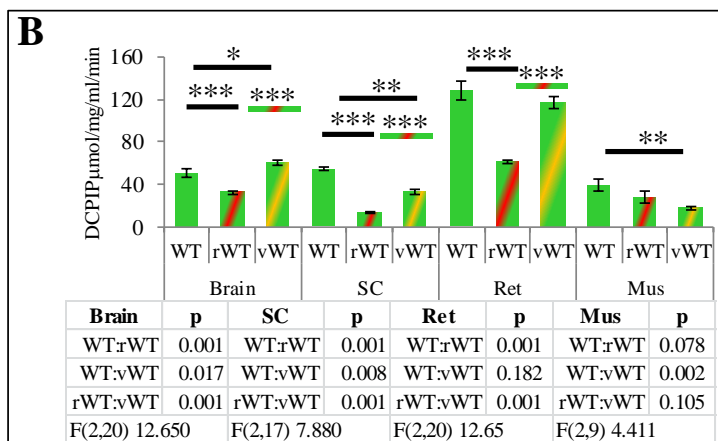
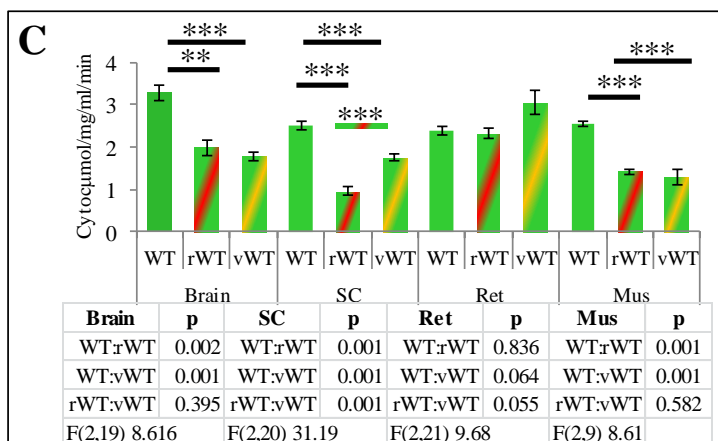


Figure 7.8 Complex 1 activity in res WT mouse

(A) Graphs of mean \pm SD complex I oxidation of NADH in isolated mitochondria from untreated, res and veh treated WT brain, spinal cord (SC), retina (Ret) and skeletal muscle (Mus).



(B) Graphs of mean \pm SD Complex II reduction of DCPIP in 50 μ g/ml isolated mitochondria from WT, res and veh WT brain, spinal cord (SC), retina (Ret) and skeletal muscle (Mus).



(C) Graphs of mean \pm SD Complex IV oxidation of reduced cytochrome c in isolated mitochondria from WT, res WT and veh WT in brain, spinal cord (SC), retina (Ret) and skeletal muscle (Mus).

The ratio of individual complex activity was examined in the mitochondrial from the CNS. As previously observed, untreated WT showed the highest ratio of activity for complex I in spinal cord, for complex II in retina and complex IV in brain. Table 7.7 shows the ratio for individual complexes in the CNS in untreated, res and veh treated WT.

	Brain			SC			Ret			Mus		
	WT	rWT	vWT	WT	rWT	vWT	WT	rWT	vWT	WT	rWT	vWT
CI Ave	29	43	33	38	22	33	33	35	34	25	25	33
SEM	8	5	5	7	5	8	7	6	4	1	2	2
WT:rWT		0.180			0.064			0.937			0.002	
WT:vWT			0.793			0.551			0.789			0.002
rWT:vWT		0.341			0.270			0.955			0.002	
	F(2,65)53.749											
CII Ave	21	30	30	23	14	16	56	56	54	2	25	33
SEM	3	5	3	5	2	2	10	3	2	4	4	4
WT:rWT		0.063			0.012			0.538			0.995	
WT:vWT			0.077			0.179			0.178			0.150
rWT:vWT		0.993			0.302			0.470			0.150	
	F(2,61)5.219											
CIV Ave	41	38	26	30	18	27	29	44	47	25	34	36
SEM	6	7	2	5	4	4	2	5	6	2	2	2
WT:rWT		0.257			0.001			0.001			0.002	
WT:vWT			0.001			0.200			0.001			0.001
rWT:vWT		0.009			0.044			0.587			0.123	
	F(2,62)16.734											

Table 7.7 Ratio of complex activity in untreated res and veh WT

The table shows the ratio of complex I, complex II and complex IV activity in brain, spinal cord and retinal mitochondria in untreated res and veh WT.

Untreated WT demonstrated that complex I activity was highest in spinal cord mitochondria, complex II activity was highest in retinal mitochondria and complex IV activity was highest in brain mitochondria. Res WT ratio in spinal cord mitochondria was not significantly different to untreated WT ($p=0.064$). The ratio of complex II activity in res WT retinal mitochondria was not significantly different to untreated WT ($p=0.538$). The ratio of complex IV activity in res WT brain was not significantly different to untreated WT ($p=0.257$). The ratio of complex I activity in veh treated WT spinal cord was not significantly different to untreated WT ($p=0.551$). The ratio of complex II activity in veh WT retinal mitochondria was not significantly different to untreated WT ($p=0.178$). The ratio of complex IV activity in veh WT brain mitochondria was significantly reduced compared to untreated WT ($F(2,62) 16.734 p=0.001$).

7.5.1.2 Discussion of ETC activity in res treated WT

Tissue specific reductions in ETC activity were examined in res and veh WT.

Res WT brain mitochondria had a reduction of 41% in ETC activity compared to untreated WT. All complexes tested were reduced: Complex I had a 49% reduction, complex II had a 36% reduction and complex IV showed a 39% reduction.

Chapter 7 Paradoxical effects of resveratrol in C57Bl/6

The bioenergetic activity in res WT SC mitochondria had a 72% reduction in ETC activity compared to untreated WT. Complex I activity was reduced by 78%, complex II reduced by 75% and complex IV reduced by 62% compared to untreated WT.

Res treated retinal mitochondria had a 38% reduction in electron transfer activity compared to untreated WT. Complex I was reduced by 60%, complex II was reduced by 52% and complex IV was reduced by 3%.

Skeletal muscle in res WT had a 20% reduction in bioenergetic activity compared to untreated WT. Complex I was enhanced by 11%, complex II was reduced by 48% and complex IV was reduced by 37%.

Veh treated WT brain mitochondria had a 4% reduction in electron transport. Complex I was enhanced by 12%, complex II was enhanced by 20% and complex IV was reduced by 45%. Veh WT spinal cord mitochondria had a 27% reduction in activity compared to untreated WT. Complex I was reduced by 12%, complex II was reduced by 40% and complex IV was reduced by 30%. Veh WT retinal mitochondria were enhanced by 8% compared to untreated WT. Complex I was increased by 6%, complex II was reduced by 9% and complex IV was increased by 28%. Skeletal muscle in veh WT had a 48% reduction in bioenergetic activity compared to untreated WT. Complex I was reduced by 40%, complex II reduced by 56% and complex IV reduced by 49%. Table 7.8 shows a summary of these findings.

rWT	Brain	SC	Ret	Mus	Ave ETC
CI	-49	-78	-60	11	-44
CII	-36	-75	-52	-28	-48
CIV	-39	-62	-3	-44	-37
Ave	-41	-72	-38	-20	
vWT	Brain	SC	Ret	Mus	Ave ETC
CI	12	-12	6	-40	-8
CII	20	-40	-9	-56	-21
CIV	-45	-30	28	-49	-24
Ave	-4	-27	8	-48	

Table 7.8 Percentage changes in res and veh treated WT mitochondria

Table showing the percentage change in bioenergetic activity in res and veh WT compared to untreated WT. Res WT had a 44% reduction in complex I activity, 48% reduction in complex II and 67% reduction in complex IV. Veh WT had a 8% reduction of complex I, 21% reduction in complex II and 24% reduction in complex IV.

Chapter 7 Paradoxical effects of resveratrol in C57Bl/6

The effects of 0.1% ethanol over a 15 month time period had a negative impact on electron transport compounded by the addition of resveratrol. The percent reduction in ETC activity seen in the vehicle treated brain, SC retina and skeletal muscle was subtracted from the percent change observed in res treated WT. This represented the effects of resveratrol only in WT mouse in this trial.

Tissue specific changes due to resveratrol were examined.

Brain mitochondria showed a 37% reduction in activity. This was observed in both complex I with a 61% and complex II with 56% reductions. Complex IV showed a marginal 6% increase. Res WT spinal cord mitochondria had 45% reduction in bioenergetic activity. Complex I was reduced by 67%, complex II reduced by 35% and complex IV was reduced by 32%. Retinal mitochondria in res WT showed a 46% reduction in electron transport compared to untreated WT. Complex I was reduced by 65%, complex II was reduced by 43% and complex IV was reduced by 30%. Skeletal muscle in res WT showed a 28% increase in bioenergetic activity compared to untreated WT. Complex I was reduced by 35%, complex II was reduced by 27% and complex IV reduced by 13%. Figure 7.9 shows a graphical representation of these data.

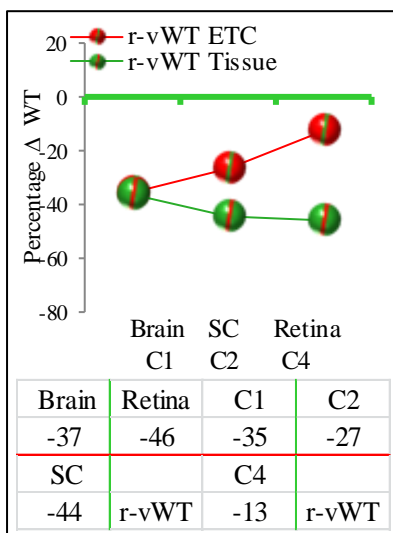


Figure 7.9 Resveratrol specific bioenergetic effects in WT mouse

Graph representing the tissue specific and complex specific changes in res treated WT compared to untreated WT (represented by green line). The mitochondrial tissue specific changes showed that all CNS mitochondria had reduced activity. Skeletal muscle showed a 28% increase in activity. Complex specific activities showed that complex I was reduced 35%, complex II reduced 45% and complex IV reduced by 46%.

Resveratrol may have had a positive impact on the bioenergetic function of skeletal muscle in res treated WT, unfortunately this was not evident during rotarod testing. Resveratrol appeared to have an adverse effect in the CNS on all complexes notably in the retinal and spinal cord mitochondria with a combined reduction of 46% activity.

Chapter 7 Paradoxical effects of resveratrol in C57Bl/6

7.5.2 Results of mitochondrial related protein expression

Table 7.9 shows a summary of mitochondrial Opa1, VDAC and Preli expression in retinal layers of untreated, res and veh WT. Figure 7.10 shows a graphical representation of this data. Table 7.10 summarises Neuroglobin, PSD95 and neurofilament expression and Figure 7.11 shows graphs representing this data.

Table 7.9 Mitochondrial protein expression in retina of untreated and treated WT

A	Opa1	PRL			ONL			OPL			INL			IPL			GCL		
		WT	rWT	vWT	WT	rWT	vWT	WT	rWT	vWT	WT	rWT	vWT	WT	rWT	vWT	WT	rWT	vWT
	Ave	192	302	203	256	330	199	258	487	336	224	255	243	281	298	255	187	203	142
	SEM	39.3	50.4	36.2	52.6	56.8	42.5	73	94.4	36.8	79.2	36.4	18	41.8	21.5	4.46	30.5	28	33.3
	WT:rWT	0.546			0.789			0.215			0.204			0.281			0.197		
	WT:vWT	0.213			0.780			0.840			0.974			0.070			0.251		
	F	F (5,16) 2.285			F (5,15) 4.390			F (5,15) 2.751			F (5,15) 5.463			F (5,15) 9.729			F (5,15) 15.05		
B	VDAC	PRL			ONL			OPL			INL			IPL			GCL		
		WT	rWT	vWT	WT	rWT	vWT	WT	rWT	vWT	WT	rWT	vWT	WT	rWT	vWT	WT	rWT	vWT
	Ave	91.9	185	144	273	466	130	184	245	102	215	429	179	181	366	108	404	435	224
	SEM	15.9	56.4	6.18	25.1	197	0.44	19.6	118	7.21	26.5	134	13.3	25.7	136	3.94	30.6	247	7.2
	WT:rWT	0.062			0.242			0.001			0.814			0.354			0.782		
	WT:vWT	0.001			0.425			0.006			0.746			0.309			0.648		
	F	F (5,15) 10.470			F (5,15) 1.380			F (5,15) 6.747			F (5,15) 1.028			F (5,15) 1.146			F (5,15) 0.441		
C	Preli	PRL			ONL			OPL			INL			IPL			GCL		
		WT	rWT	vWT	WT	rWT	vWT	WT	rWT	vWT	WT	rWT	vWT	WT	rWT	vWT	WT	rWT	vWT
	Ave	366	240	262	17	19	69	194	113	172	110	119	56	122	130	62	213	128	36
	SEM	120	84	73	4	1	12	63	14	48	16	9	8	37	44	20	61	29	15
	WT:rWT	0.282			0.001			0.016			0.102			0.219			0.614		
	WT:vWT	0.080			0.750			0.041			0.729			0.511			0.592		
	F	F (5,28) 1.900			F (5,28) 1.176			F (5,28) 4.913			F (5,28) 2.091			F (5,28) 2.78			F (5,28) 5.075		

Table shows the mean ±SEM of retinal mitochondrial expression of (A) Opa1 (B) VDAC (C) Preli in untreated, res and veh treated WT. The statistical difference between groups is represented by p value.

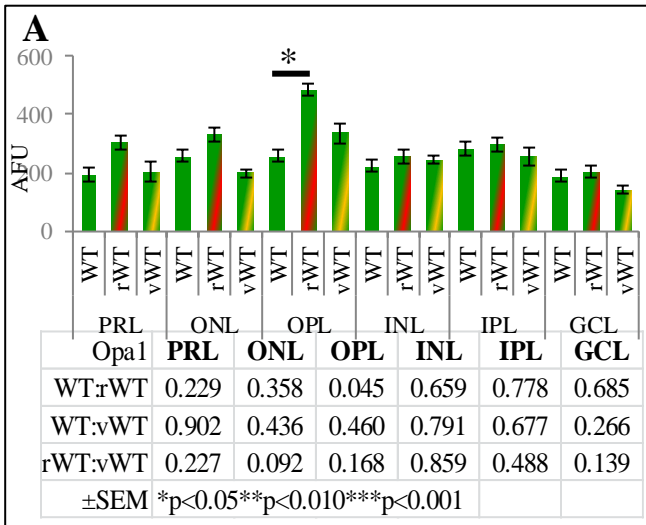
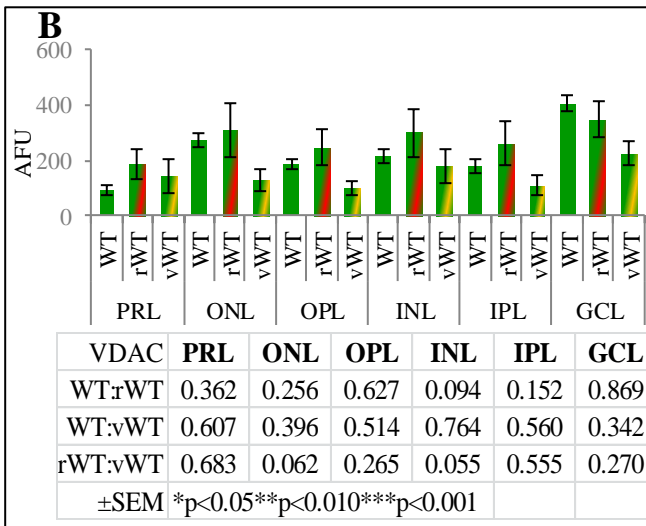
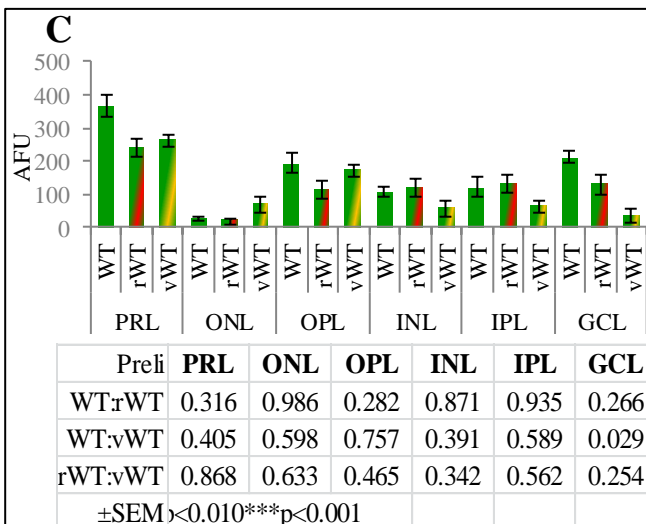


Figure 7.10 Mitochondrial related protein expression in untreated, res and veh WT retina

(A) Graph shows the mean \pm SEM of Opa1 expression in WT, res WT and veh WT retinal layers.



(B) Graph shows the mean \pm SEM of VDAC expression in WT, res WT and veh WT retinal layers.



(C) Graph shows the mean \pm SEM of VDAC expression in WT, res WT and veh WT retinal layers.

Table 7.10 Mitochondrial related proteins expression in untreated and treated WT

D	Neuro	PRL			ONL			OPL			INL			IPL			GCL			
		WT	rWT	vWT	WT	rWT	vWT	WT	rWT	vWT	WT	rWT	vWT	WT	rWT	vWT	WT	rWT	vWT	
	Ave	228.1	158.4	154.5	218.1	210.7	189.4	170.2	158.6	96.18	163.3	119	123	180.9	165.8	80.36	71.34	113.9	75.07	
	SEM	52.27	2.327	28.11	99.93	20.05	34.19	54.2	40.82	27.34	81.32	30.8	31.49	80.56	36.4	7.807	36.4	10.7	17.84	
	WT:rWT		0.408			0.817			0.562			0.962			0.405			0.452		
	WT:vWT			0.240			0.814			0.732			0.892			0.402			0.652	
	F		F (5,20) 1.530			F (5,20) 0.784			F (5,20) 0.969			F (5,20) 0.896			F (5,20) 1.654			F (5,20) 0.838		
E	PSD95	PRL			ONL			OPL			INL			IPL			GCL			
		WT	rWT	vWT	WT	rWT	vWT	WT	rWT	vWT	WT	rWT	vWT	WT	rWT	vWT	WT	rWT	vWT	
	Ave	90.5	189	156	37.8	269	66.9	84.4	237	105	24.5	209	50.3	40.3	228	58.8	34	189	25.4	
	SEM	10.2	3.57	48.8	10.3	66.7	28.8	24.6	65.7	58	11.3	53.3	22.4	18.1	59.1	31.8	26.4	67.9	11	
	WT:rWT		0.064			0.958			0.987			0.905			0.822			0.351		
	WT:vWT			0.028			0.847			0.558			0.574			0.043			0.809	
	F		F (5,15) 18.664			F (5,21) 1.843			F (5,15) 5.851			F (5,15) 4.645			F (5,15) 1.132			F (5,15) 3.626		
F	NF L	PRL			ONL			OPL			INL			IPL			GCL			
		WT	rWT	vWT	WT	rWT	vWT	WT	rWT	vWT	WT	rWT	vWT	WT	rWT	vWT	WT	rWT	vWT	
	Ave	112	67.6	153	165	77.1	196	99.2	102	257	57.1	72.4	162	195	94.7	358	443	####	424	
	SEM	13.2	6.61	23.8	87.1	2.09	47.8	3.55	34.2	34.9	11.7	22.9	17.7	28.3	32.3	53.8	37.6	67.6	113	
	WT:rWT		0.128			0.536			0.041			0.278			0.311			0.003		
	WT:vWT			0.001			0.745			0.036			0.149			0.001			0.299	
	F		F (5,23) 8.530			F (5,23) 1.280			F (5,23) 4.219			F (5,23) 3.493			F (5,23) 7.706			F (5,23) 2.512		

Table shows the mean ±SEM of (D) neuroglobin (E) PSD95 and (F) NF l expression in retinal layers of untreated, res and veh treated WT. The statistical difference between groups is represented by p value.

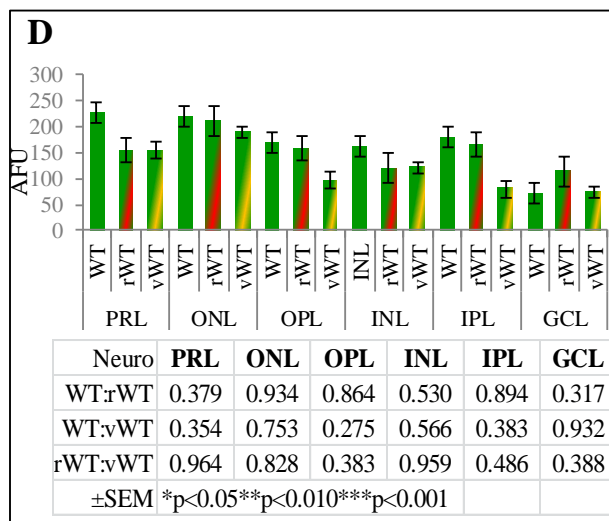
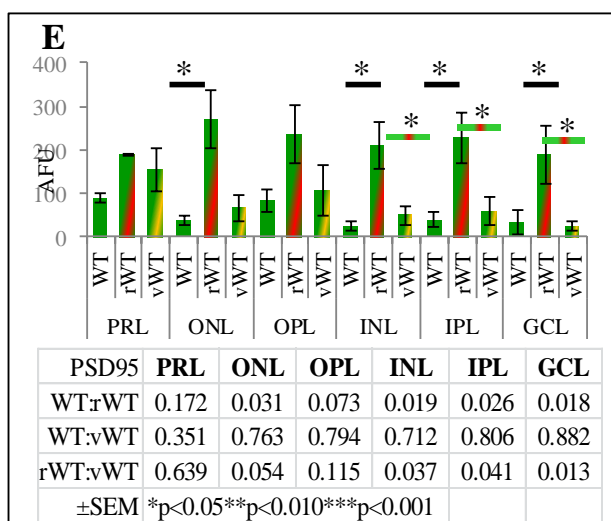


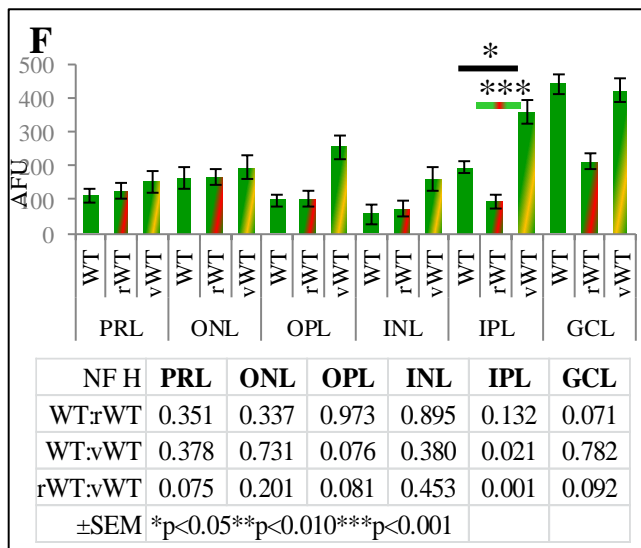
Figure 7.11 Mitochondrial related proteins expression in untreated and treated WT

(D) Graphs shows the mean ±SEM of Neuroglobin in WT, res WT and veh WT retinal layers.



(E) Graphs shows the mean ±SEM of PSD95 in WT, res WT and veh WT retinal layers.

Chapter 7 Paradoxical effects of resveratrol in C57Bl/6



(F) Graphs shows the mean ±SEM of NF1 A in WT, res WT and veh WT retinal layers.

Res treated WT had a significant 89% increase in Opa1 expression in the OPL (F (5,13) 3.085 p=0.045). Opa1 expression in all other res treated WT retinal layers was not significantly different compared to untreated WT. Veh WT Opa1 expression was unchanged compared to untreated WT. VDAC expression There was no significantly difference in protein expression of VDAC, Preli or Neuroglobin in res or veh treated WT compared to untreated WT.

Compared to untreated WT res WT had a significant increase in PSD95 expression in the ONL (F(5,12) 3.404 p=0.031), INL (F(5,12) 2.248 p=0.019) IPL (F(5,12) 2.214 p=0.026), and GCL (F(5,12) 2.431 p=0.018). These findings were not present in veh treated WT. Neurofilament expression in res treated WT was not significantly different compared to untreated WT. Veh WT had a significant 184% increase of NF 1 expression in the IPL (F5,12)5.823 p=0.021).

7.5.2.1 Western blotting of res treated retinal homogenate

Opa1 expression in retinal homogenate of untreated WT retinal homogenate had 1.04±0.11 RD. Opa1 expression in res treated WT retina had 0.57±0.16 which was statistically reduced compared to untreated WT (F(3,12) 11.110 p=0004). Retinal expression of neuroglobin showed untreated WT had 0.61±0.27RD. Res treated WT had 0.44±0.16RD which was not statistically significant compared to untreated (p=0.128). Preli expression in retinal homogenate of untreated WT had 0.91±0.21 RD. Res WT retinal homogenate had 0.52±0.07 RD which was significantly reduced compared to untreated WT (F(3,12) 5.115 p=0.009).Figure 7.12 shows representative bands from Western blot for this data.

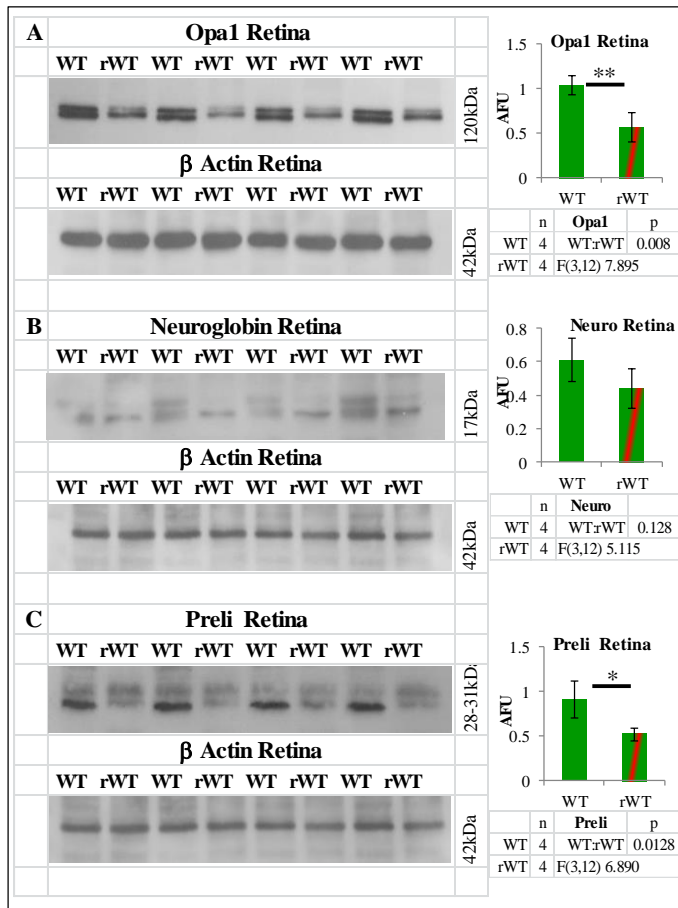


Figure 7.12 Western blotting of untreated and res treated WT retinal homogenate

Representative bands from Western blotting of retinal homogenate from untreated WT(n4) and res treated WT(n4) for (A)Opa1 (B), neuroglobin (C) and preli. Graphs show the mean ±SEM RD of proteins Lower bands show β actin as a loading control.

Figures 7.13-7.18 show representative images of protein expression in untreated, res and veh WT retinal sections. Control sections are shown are processed sections omitting the use of the primary antibody.

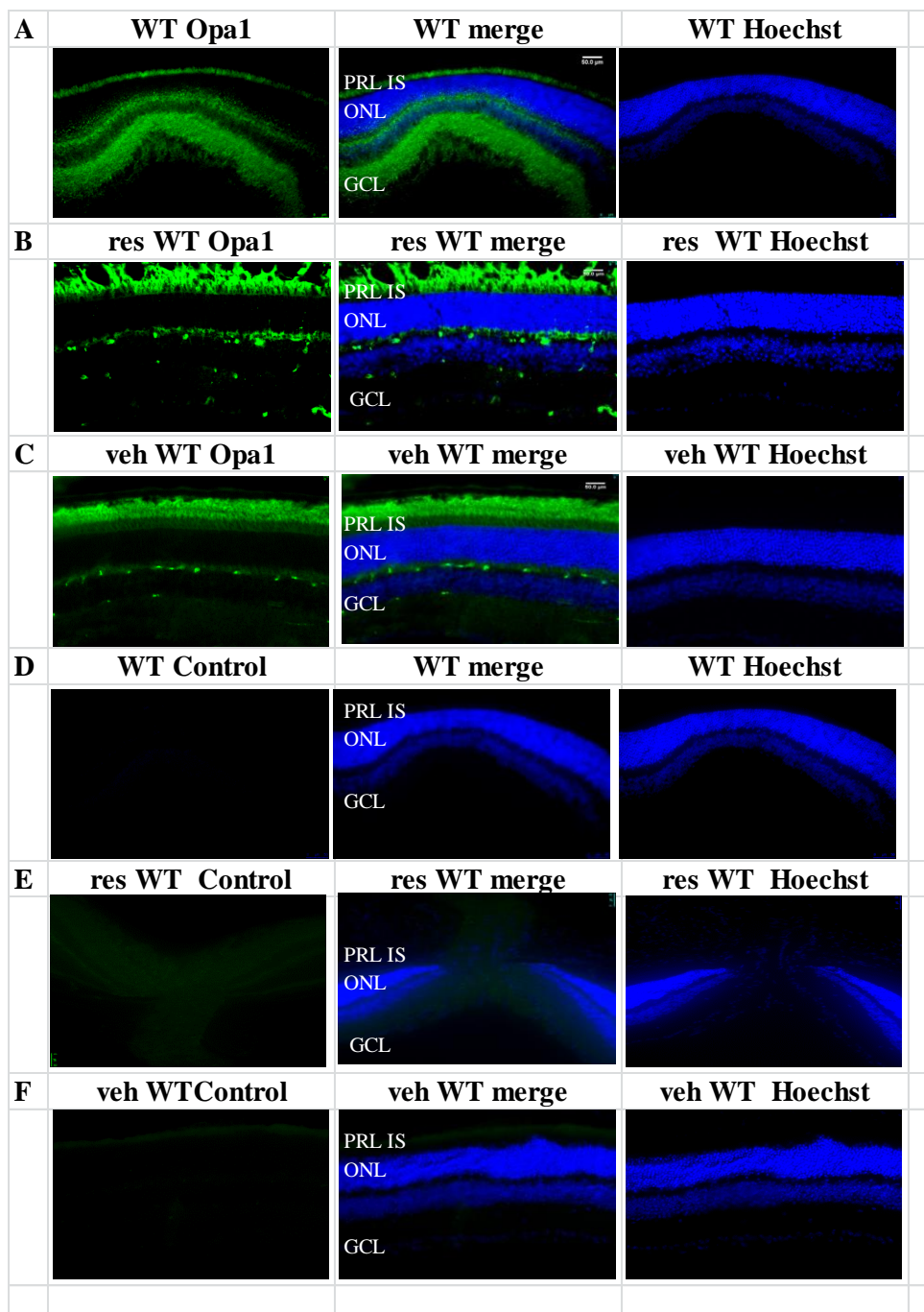


Figure 7.13 Opa1 expression in retina of untreated, res and veh treated WT

Representative images of Opa1 expression in WT (A), res WT (B) and veh WT (C) retinal sections. Negative control sections (omission of primary antibody) for WT (D), res WT (E) and veh WT (F) are shown.

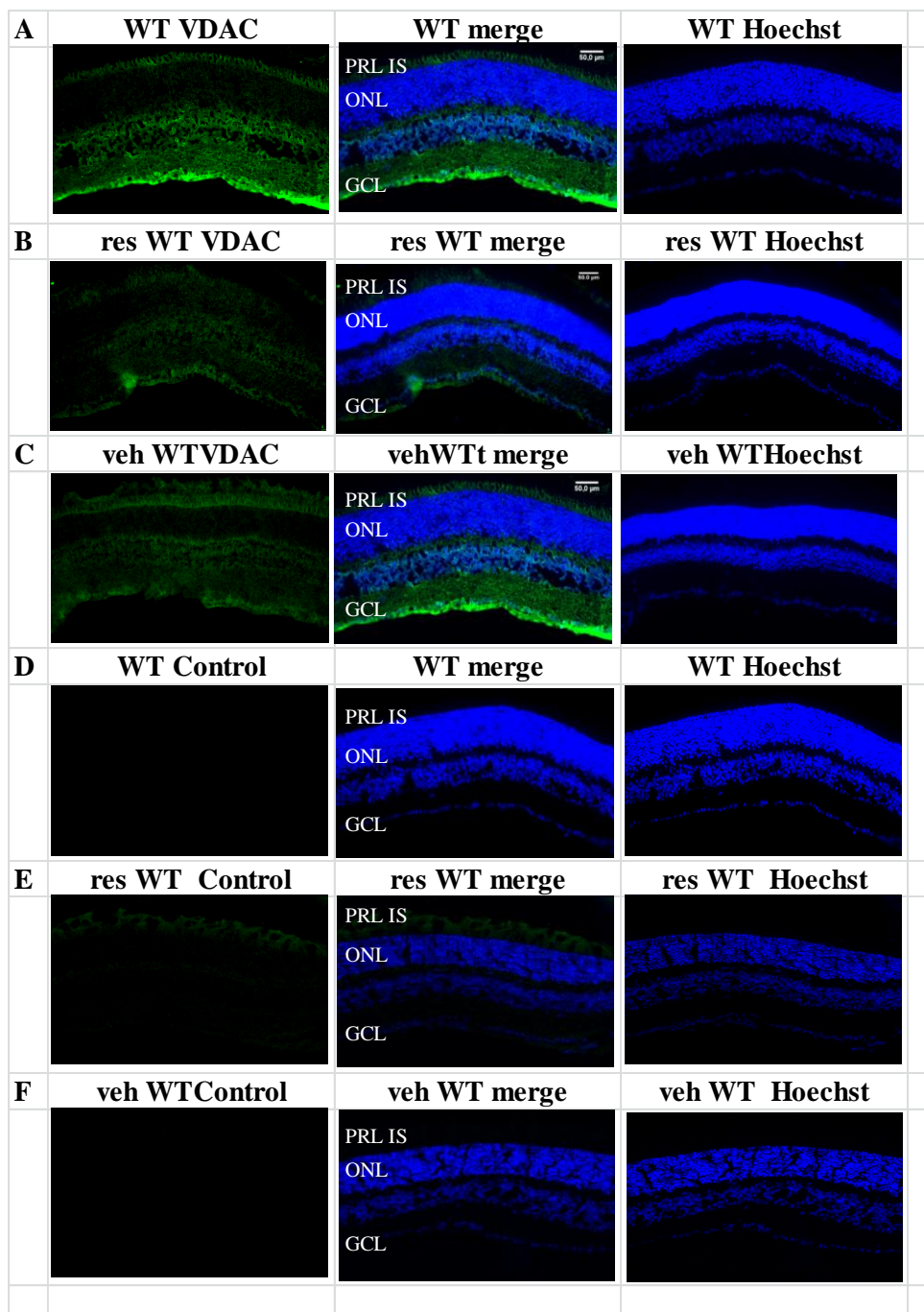


Figure 7.14 VDAC expression in retina of untreated, res and veh treated WT

Representative images of VDAC expression in WT (A), res WT (B) and veh WT (C) retinal sections. Negative control sections (omission of primary antibody) for WT (D), res WT (E) and veh WT (F) are shown.

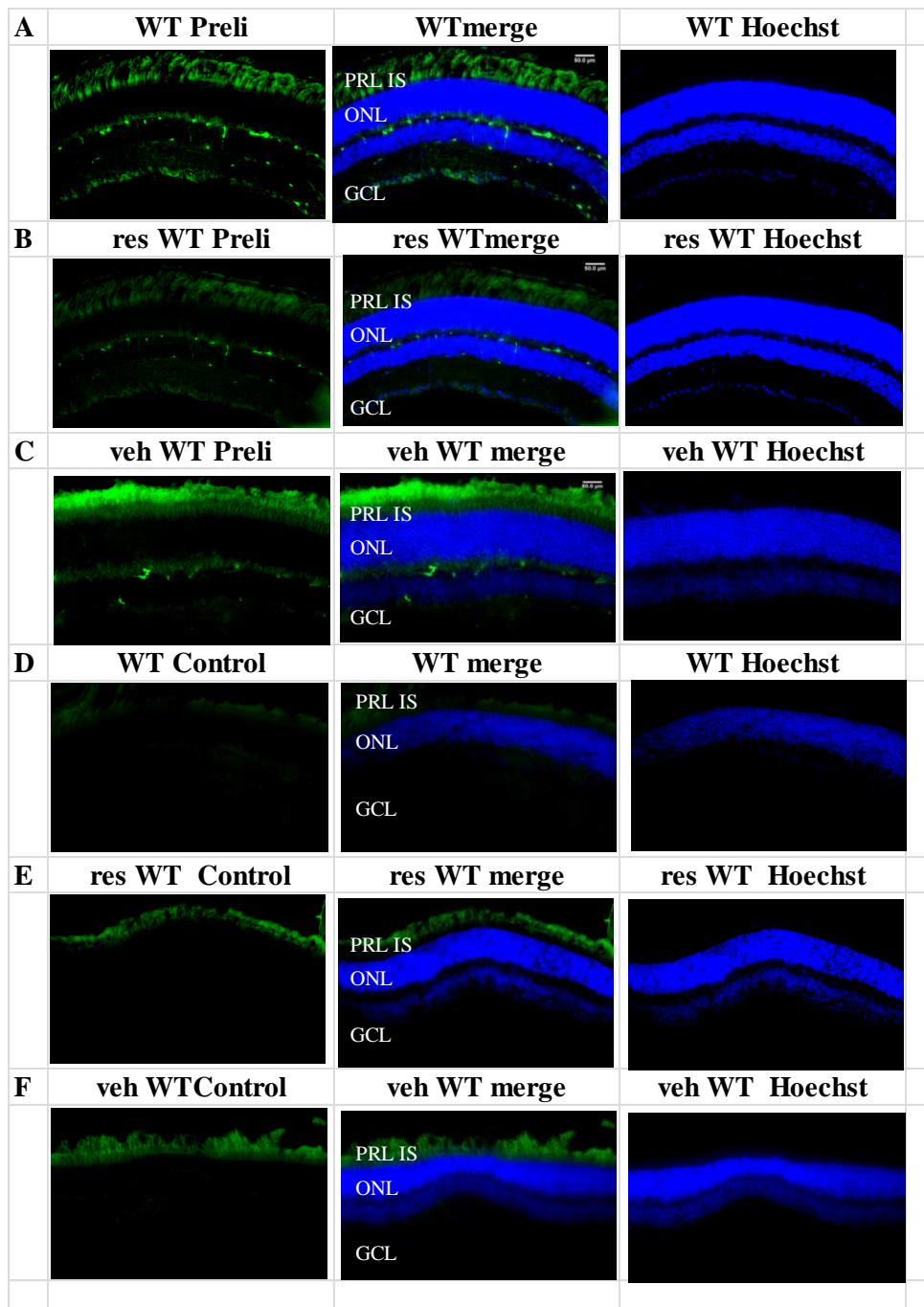


Figure 7.15 Preli expression in retina of untreated, res and veh treated WT

Representative images of Preli expression in WT (A), res WT (B) and veh WT (C) retinal sections. Negative control sections (omission of primary antibody) for WT (D), res WT (E) and veh WT (F) are shown.

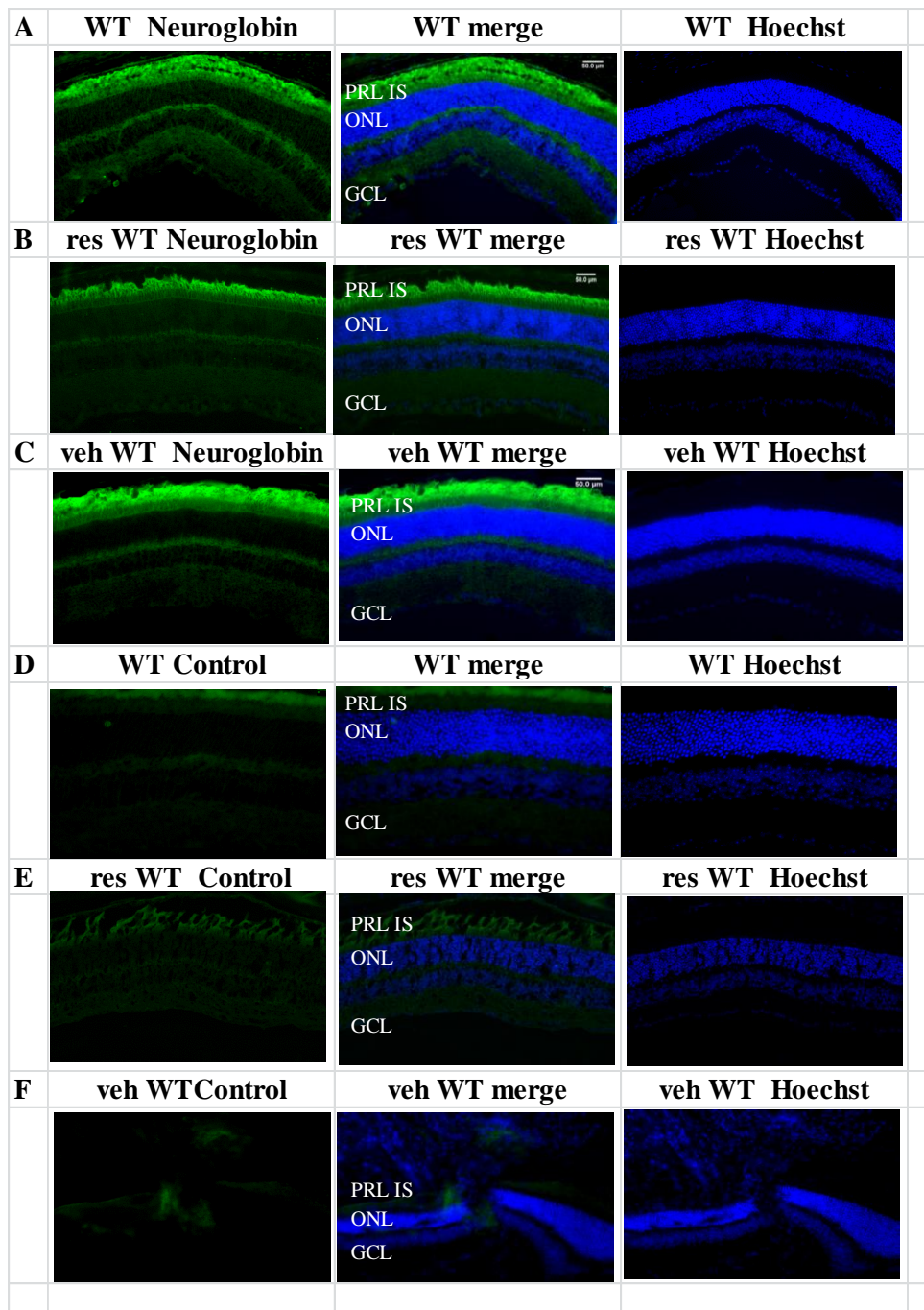


Figure 7.16 Neuroglobin expression in retina of untreated, res and veh treated WT

Representative images of Neuroglobin expression in WT (A), res WT (B) and veh WT (C) retinal sections. Negative control sections (omission of primary antibody) for WT (D), res WT (E) and veh WT (F) are shown.

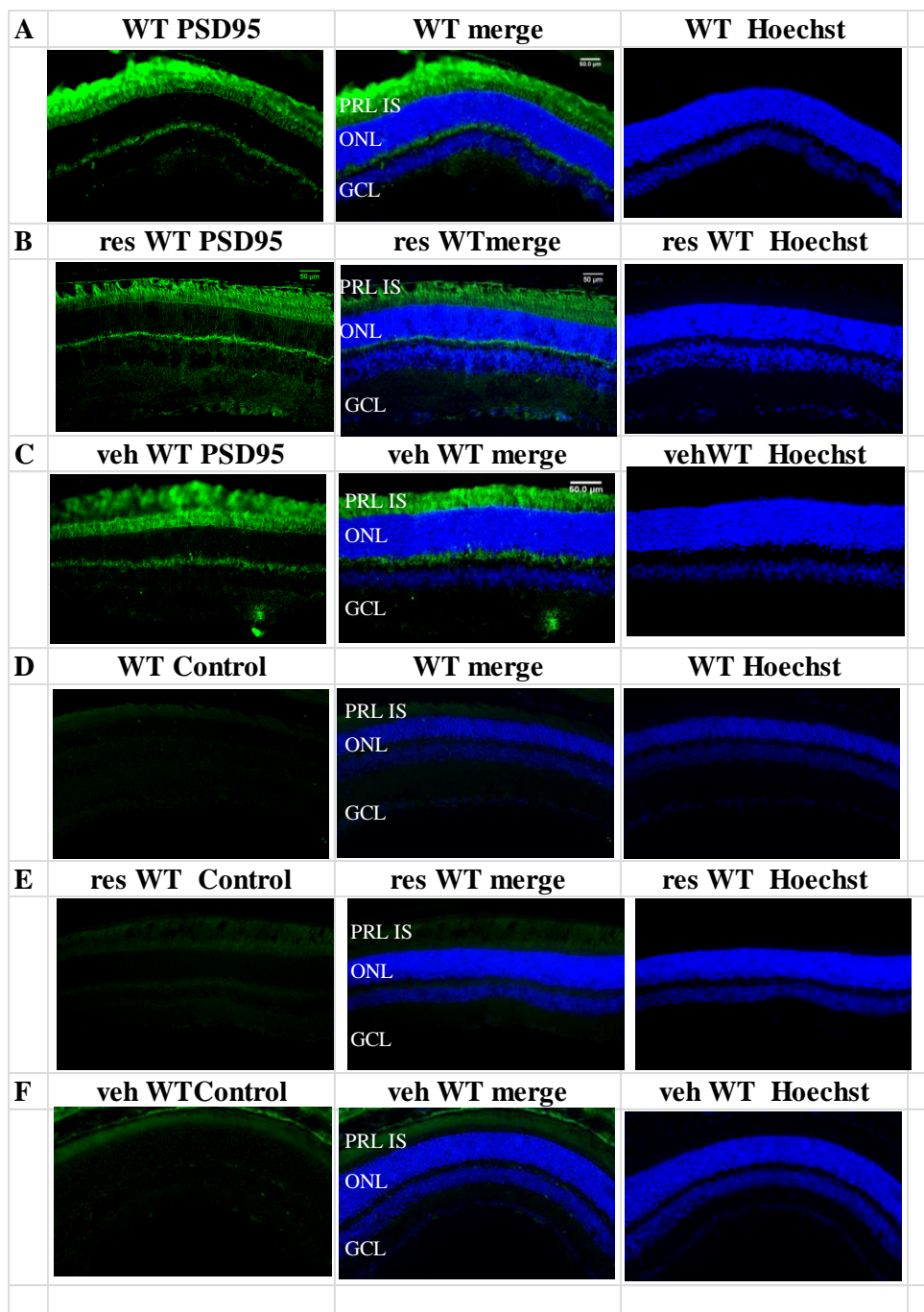


Figure 7.17 PSD 95 expression in retina of untreated, res and veh treated WT

Representative images of PSD95 expression in WT (A), res WT (B) and veh WT (C) retinal sections. Negative control sections (omission of primary antibody) for WT (D), res WT (E) and veh WT (F) are shown.

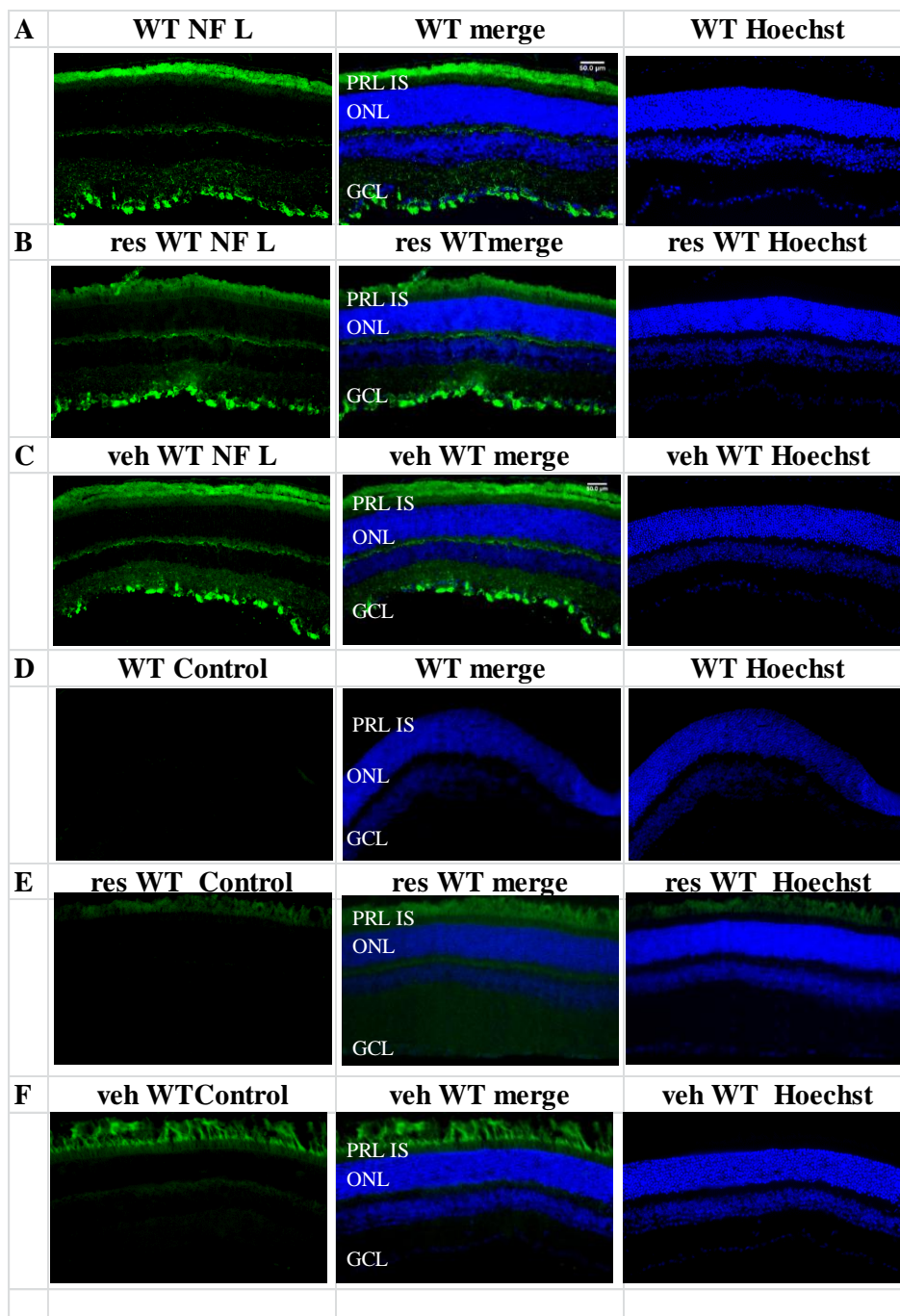


Figure 7.18 NF L expression in retina of untreated, res and veh treated WT

Representative images of Neurofilament L expression in WT (A), res WT (B) and veh WT (C) retinal sections. Negative control sections (omission of primary antibody) for WT (D), res WT (E) and veh WT (F) are shown.

The combined AFU from Opa1, VDAC and Preli expression generated the mitochondrial profile. Compensatory proteins were combined AFU of VDAC, and neuroglobin, and damage mediated

Chapter 7 Paradoxical effects of resveratrol in C57Bl/6

protein expression was the combined AFU of PSD95 and NF L. Table 7.11 summarises these findings and Figure 7.19 shows a graphical representation of the data.

Table 7.11 Summary of retinal protein profile in untreated and treated WT

		PRL			ONL			OPL			INL			IPL			GCL		
A	Mito	WT	rWT	vWT	WT	rWT	vWT	WT	rWT	vWT	WT	rWT	vWT	WT	rWT	vWT	WT	rWT	vWT
	Ave	176	215	167	246	335	176	201	297	178	197	268	181	211	277	148	206	251	147
	SEM	20.0	29.0	21.0	40.0	29.0	29.0	21.0	28.0	20.0	33.0	28.0	21.0	27.0	39.0	21.0	40.0	38.0	29.0
	WT(5):rWT(4)		0.546			0.355			0.194			0.438			0.446			0.664	
	WT(5):vWT(3)			0.883			0.448			0.759			0.865			0.466			0.568
	rWT(4):vWT(3)		0.466			0.104			0.119			0.357			0.506			0.238	
	F(5,15)			2.285			4.39			2.751			5.436			9.729			15.06
B	Comp	WT	rWT	vWT	WT	rWT	vWT	WT	rWT	vWT	WT	rWT	vWT	WT	rWT	vWT	WT	rWT	vWT
	Ave	232	242	203	166	272	133	210	281	203	175	268	159	187	265	142	263	256	134
	SEM	18.0	24.0	21.0	13.0	16.0	28.0	18.0	12.0	15.0	24.0	18.0	15.0	13.0	25.0	26.0	16.0	20.0	18.0
	WT(5):rWT(4)		0.888			0.340			0.329			0.337			0.350			0.944	
	WT(5):vWT(3)			0.677			0.765			0.723			0.867			0.586			0.202
	rWT(4):vWT(3)		0.697			0.765			0.923			0.273			0.152			0.239	
	F(5,15)			1.047			1.38			6.747			1.028			1.146			0.441
C	Damage	WT	rWT	vWT	WT	rWT	vWT	WT	rWT	vWT	WT	rWT	vWT	WT	rWT	vWT	WT	rWT	vWT
	Ave	101	128	155	102	173	131	92	169	181	41	141	106	117	161	209	238	202	225
	SEM	19.0	14.0	15.0	20.0	17.0	12.0	16.0	20.0	19.0	20.0	15	16	13	18	12.0	12.0	18.0	15.0
	WT(5):rWT(4)		0.559			0.315			0.025			0.005			0.529			0.775	
	WT(5):vWT(3)			0.253			0.670			0.019			0.015			0.195			0.915
	rWT(4):vWT(3)		0.570			0.558			0.865			0.608			0.495			0.858	
	F(5,21)			21.47			1.843			5.831			4.645			1.132			3.626

Table shows the mean (\pm SEM) of (A) mitochondrial (B) compensation and (C) damage mediated protein expression in retinal layers of untreated WT, res and veh WT. Statistical difference between groups is represented by the p value.

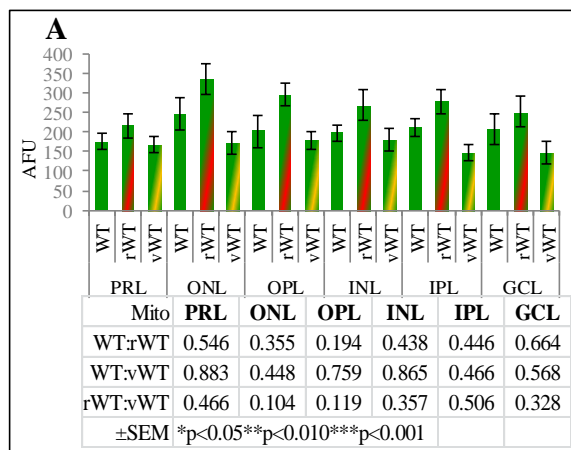
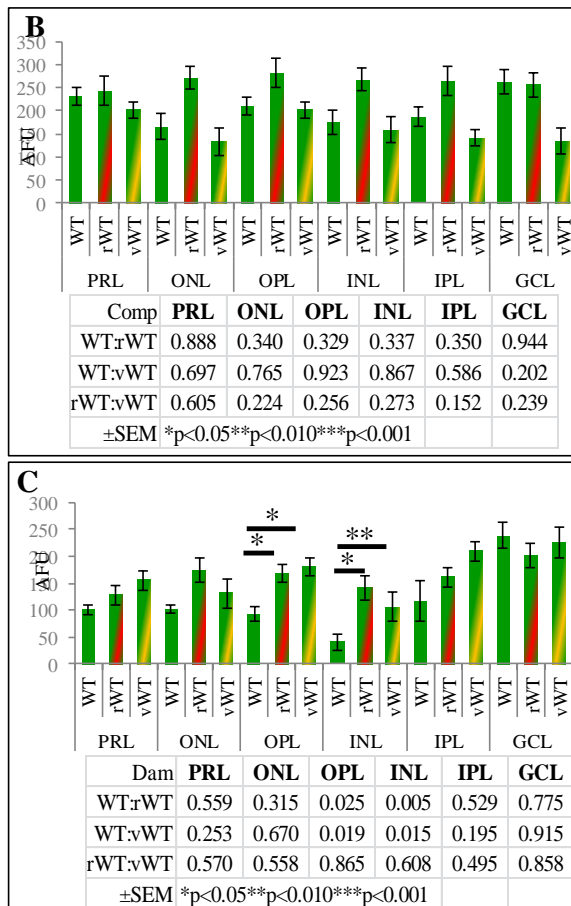


Figure 7.19 Protein profiles in untreated res and veh treated WT

Graphs showing the mean \pm SEM AFU of (A) mitochondrial related protein expression in retinal sections of untreated res and veh treated WT.



...Figure 7.19

(B) Graphs showing the mean ±SEM AFU of compensation mediated protein expression in retinal sections of untreated res and veh treated WT.

(C) Graphs showing the mean ±SEM AFU of damage mediated expression in retinal sections of untreated res and veh treated WT.

There was no significant difference observed in mitochondrial or compensatory protein expression between untreated WT and res or veh treated WT. Res treated WT had a significant 84% increase in damage mediated protein expression in the OPL (F(5,48) 3.380 p=0.025). Veh treated WT had a 19% increase in damage mediated protein expression in the OPL which was significantly increased compared to untreated WT (p=0.019). Res WT had a 244% increase in damage mediated protein expression the INL (F(5,45) 6.662 p=0.005). Veh WT had a 159% increase which was also significant compared to untreated WT (p=0.015).

7.5.3 Mitochondrial protein expression in brain of untreated and treated WT

Table 7.12 shows a summary of mitochondrial related protein expression in brain of untreated res and veh treated WT. Figure 7.20 shows graphs representing this data.

A Opa1				D Preli			
WT(n5)	rWT(n4)	vWT(n3)		WT(n5)	rWT(n4)	vWT(n3)	
Ave	619.9	1024	612.8	Ave	542.4	1308	1007
SEM	119.6	278.8	208.7	SEM	107.6	270.7	206.2
WT:rWT		0.223		WT:rWT		0.874	
WT:vWT			0.982	WT:vWT			
rWT:vWT		0.21		rWT:vWT		0.321	
	F(5,30)	4.527			F(5,30)	4.627	
B VDAC				E PSD95			
WT(n5)	rWT(n4)	vWT(n3)		WT(n5)	rWT(n4)	vWT(n3)	
Ave	542.4	1308	1007	Ave	623	2056	781.1
SEM	107.6	270.7	206.2	SEM	93.35	401.6	
WT:rWT		0.012		WT:rWT		0.267	
WT:vWT			0.112	WT:vWT			0.53
rWT:vWT		0.348		rWT:vWT		0.651	
	F(5,18)	2.870			F(5,39)	2.983	
C Neuro				F NF H			
WT(n5)	rWT(n4)	vWT(n3)		WT(n5)	rWT(n4)	vWT(n3)	
Ave	390	179.5	272.3	Ave	524.5	884.4	158.1
SEM	128.7	42.4	65.3	SEM	176	138.4	44.14
WT:rWT		0.001		WT:rWT		0.182	
WT:vWT			575	WT:vWT			0.301
rWT:vWT		0.001		rWT:vWT		0.774	
	F(5,17)	2.454			F(5,17)	7.832	

Table 7.12 Mitochondrial protein expression in brain of untreated and treated WT

Table shows the mean \pm SEM of mitochondrial (A) Opa1, (B)VDAC, (C)Preli, (D)Neuroglobin, (E)PSD95 and (F)NF H protein expression in brain of untreated, res and veh WT. The statistical difference between groups is represented by the p value.

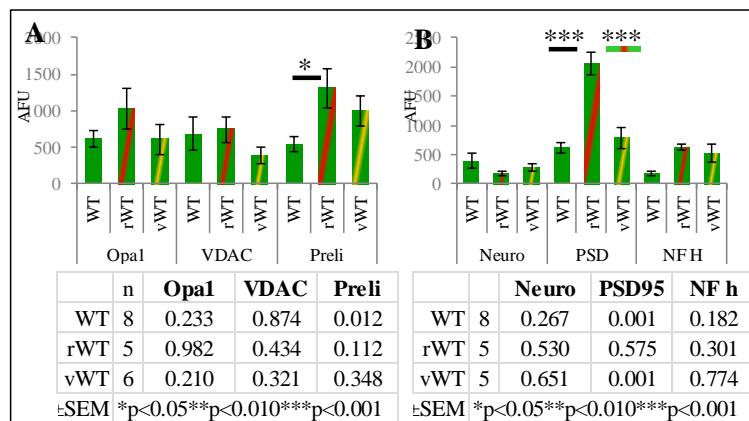


Figure 7.20 Protein expression in brain of untreated res and veh WT

Graphs show the mean \pm SEM AFU of (A) Opa1, VDAC and Preli (B) Neuroglobin, PSD95 and NF H in brain sections of untreated res and veh WT.

There was no statistical difference observed between untreated and res or veh treated WT for Opa1 or VDAC expression. Res treated WT brain had a significant increase in Preli expression compared to untreated WT (p=0.012) which was not observed in veh treated WT. PSD95 expression was increased by 230% in res treated WT which was significantly different

7.5.3.1 Western blotting of untreated and res WT brain homogenate

Brain homogenate was examined for Opa1, neuroglobin and VDAC expression in untreated and res treated WT. Western blotting of brain homogenate for Opa1 protein expression in untreated WT brain was 0.99 ± 0.1 RD. Res treated WT had 0.94 ± 0.10 which was not significantly different to WT (p=0.813). Western blotting for neuroglobin expression in untreated brain was 1.0 ± 0.16 RD. Res treated brain had 0.91 ± 0.12 RD which was not significantly different to untreated (p=0.693). Western blotting of brain homogenate for VDAC expression in untreated WT brain showed 0.88 ± 0.13 RD. Res

Chapter 7 Paradoxical effects of resveratrol in C57Bl/6

treated WT brain had 0.83 ± 0.23 which was not significantly different to untreated WT ($p=0.153$).

Figure 7.21 shows these data.

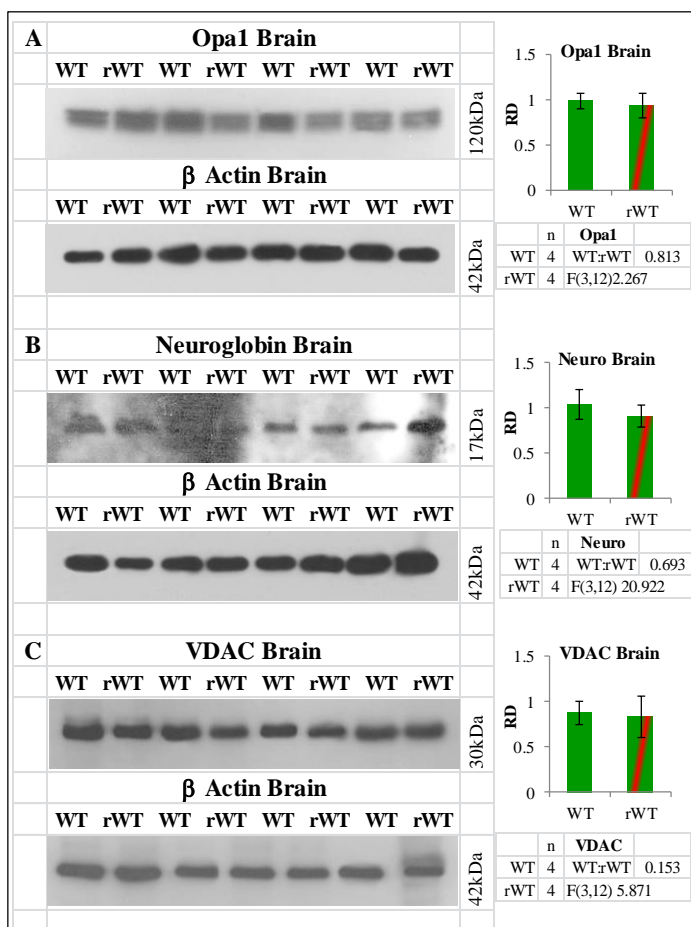


Figure 7.21 Western blotting of untreated and res treated WT brain homogenate

Figure shows representative bands from Western blotting of brain homogenate from untreated WT (n4) and res treated WT (n4) for (A) Opa1 (B) neuroglobin and (C) VDAC Lower bands show β actin as a loading control. Graphs represent the mean ± SEM of RD.

Figures 7.22-7.27 show representative images of protein expression in untreated, res and veh WT retinal sections. Control sections are shown are processed sections omitting the use of the primary antibody.

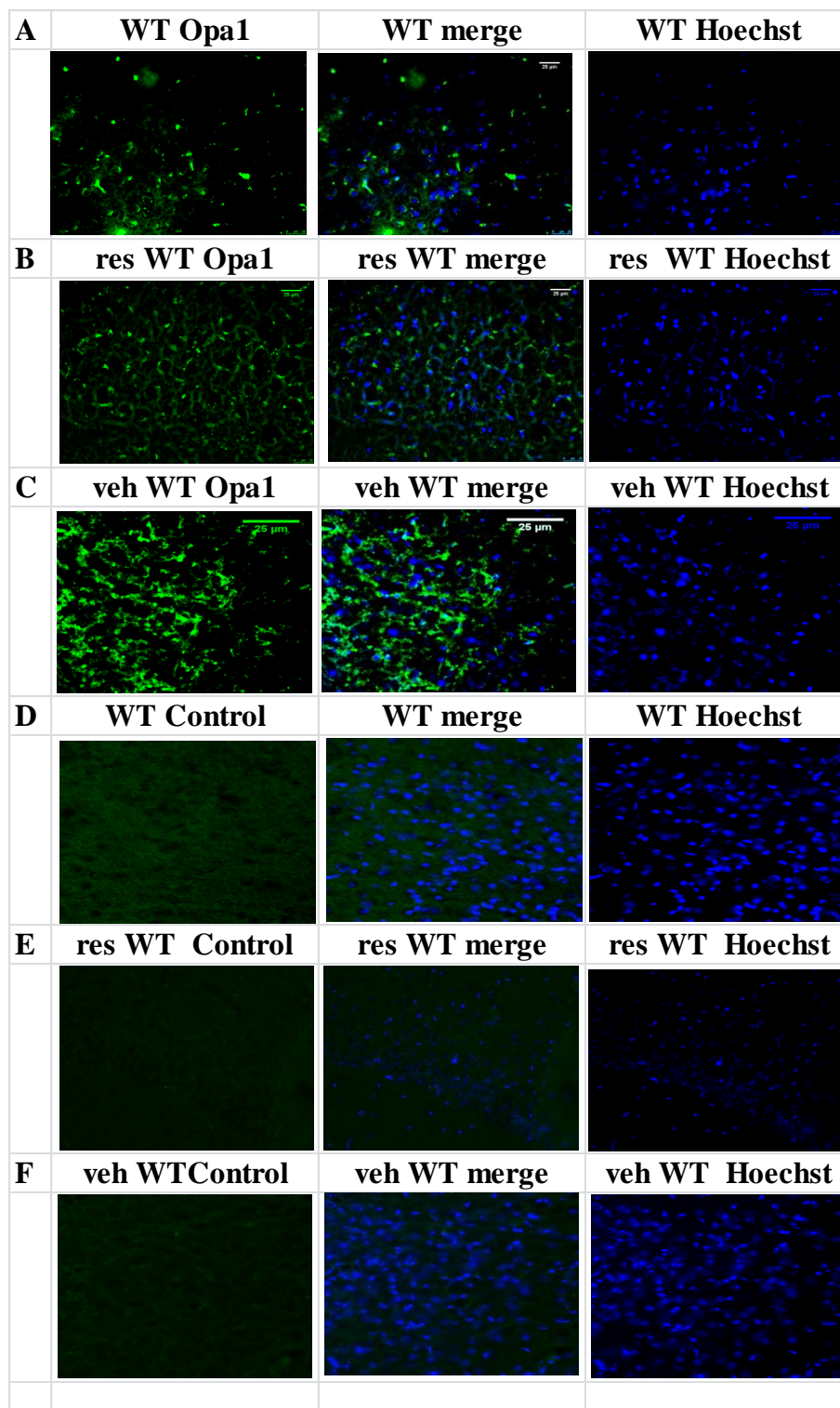


Figure 7.22 Opa1 expression in untreated res and veh WT brain

Representative images of Opa1 expression in (A) untreated WT (B) res WT and (C) veh WT brain. Control sections for (D) untreated WT (E) res WT and (F) veh WT were processed without primary antibody.

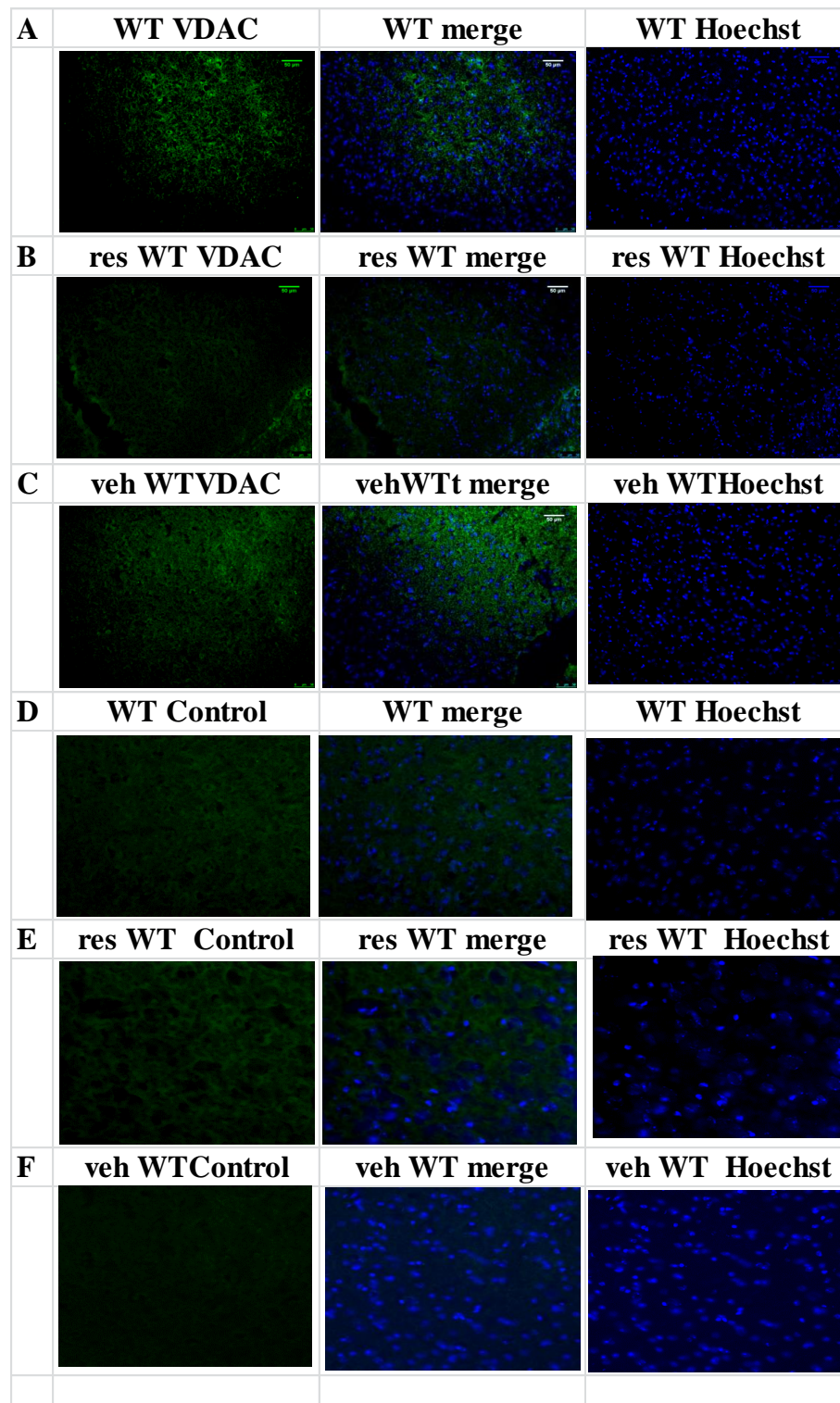


Figure 7.23 VDAC expression in untreated res and veh WT brain

Representative images of VDAC expression in (A) untreated WT (B) res WT and (C) veh WT brain. Control sections for (D) untreated WT (E) res WT and (F) veh WT were processed without primary antibody.

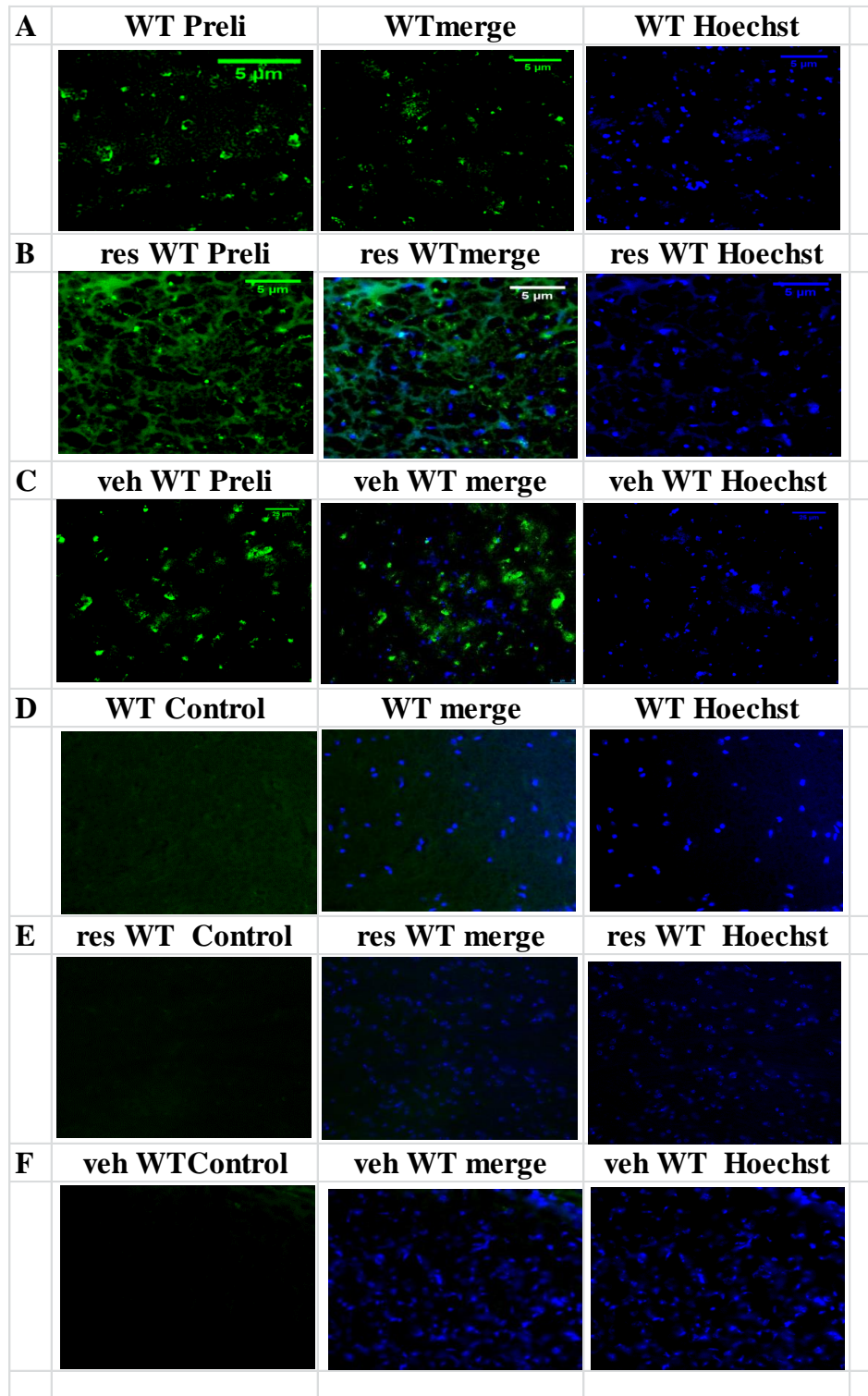


Figure 7.24Preli expression in untreated res and veh WT brain

Representative images of Preli expression in (A) untreated WT (B) res WT and (C) veh WT brain. Control sections for (D) untreated WT (E) res WT and (F) veh WT were processed without primary antibody.

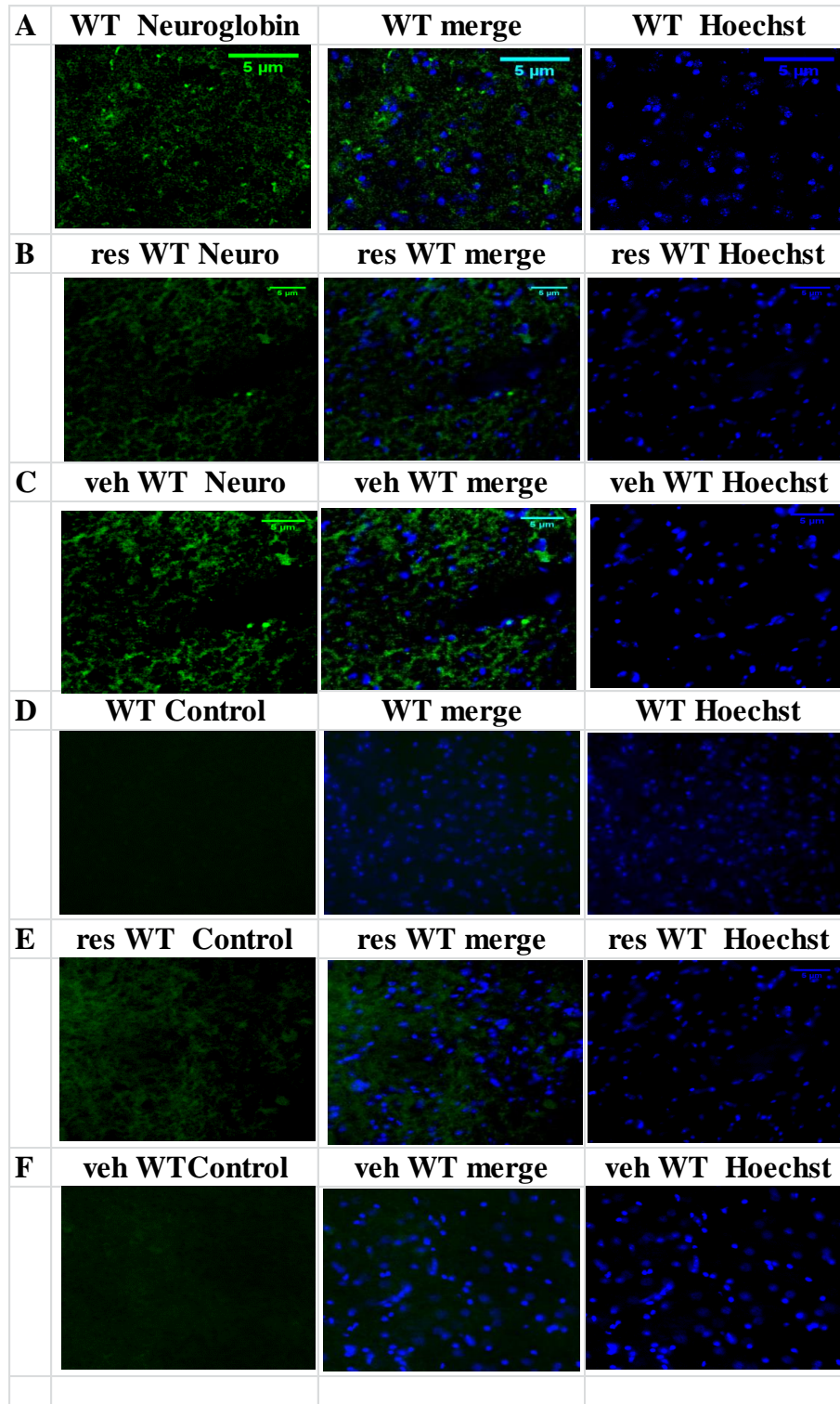


Figure 7.25 Neuroglobin expression in untreated res and veh WT brain

Representative images of Neuroglobin expression in (A) untreated WT (B) res WT and (C) veh WT brain. Control sections for (D) untreated WT (E) res WT and (F) veh WT were processed without primary antibody.

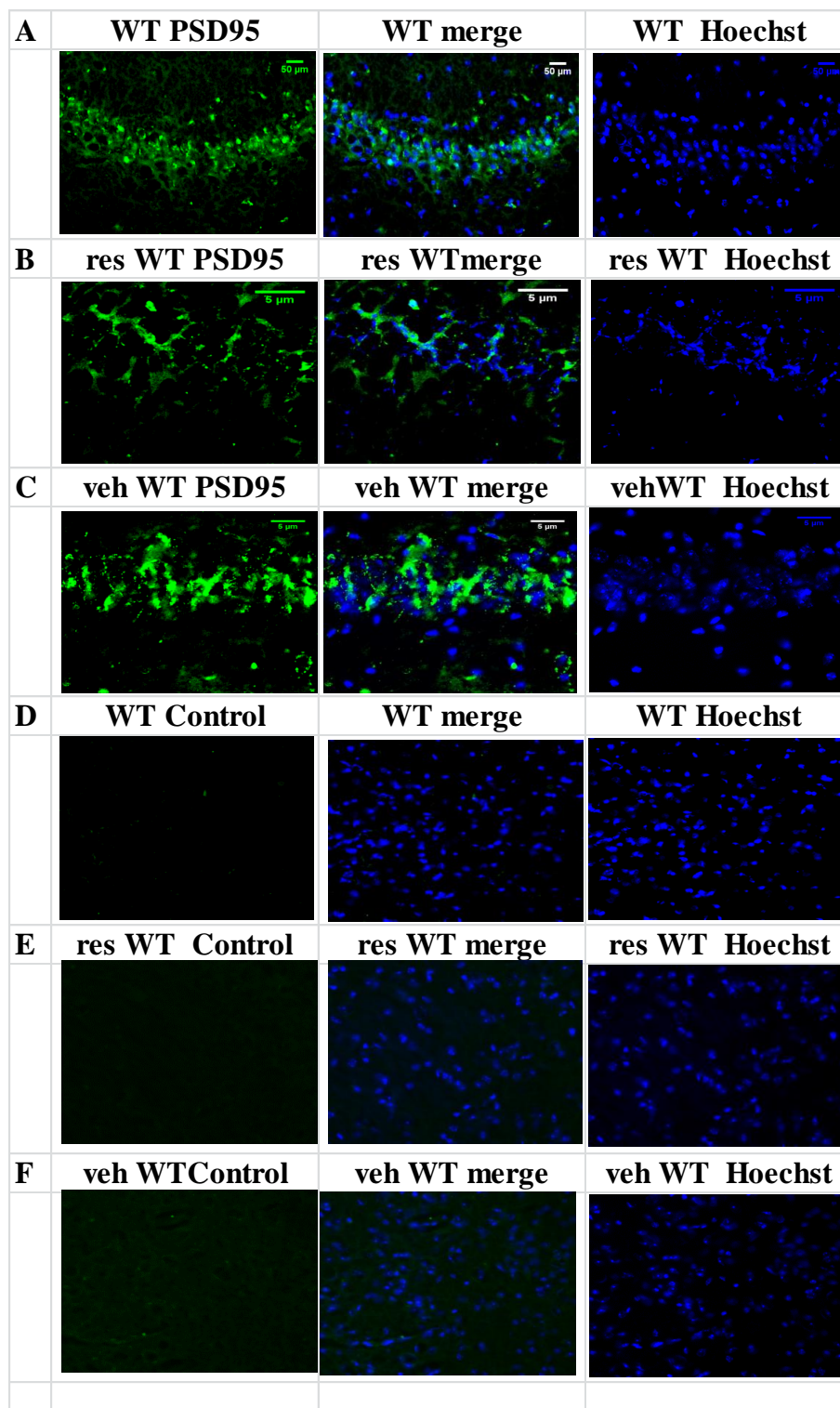


Figure 7.26 PSD95 expression in untreated res and veh WT brain

Representative images of PSD95 expression in (A) untreated WT (B) res WT and (C) veh WT brain. Control sections for (D) untreated WT (E) res WT and (F) veh WT were processed without primary antibody.

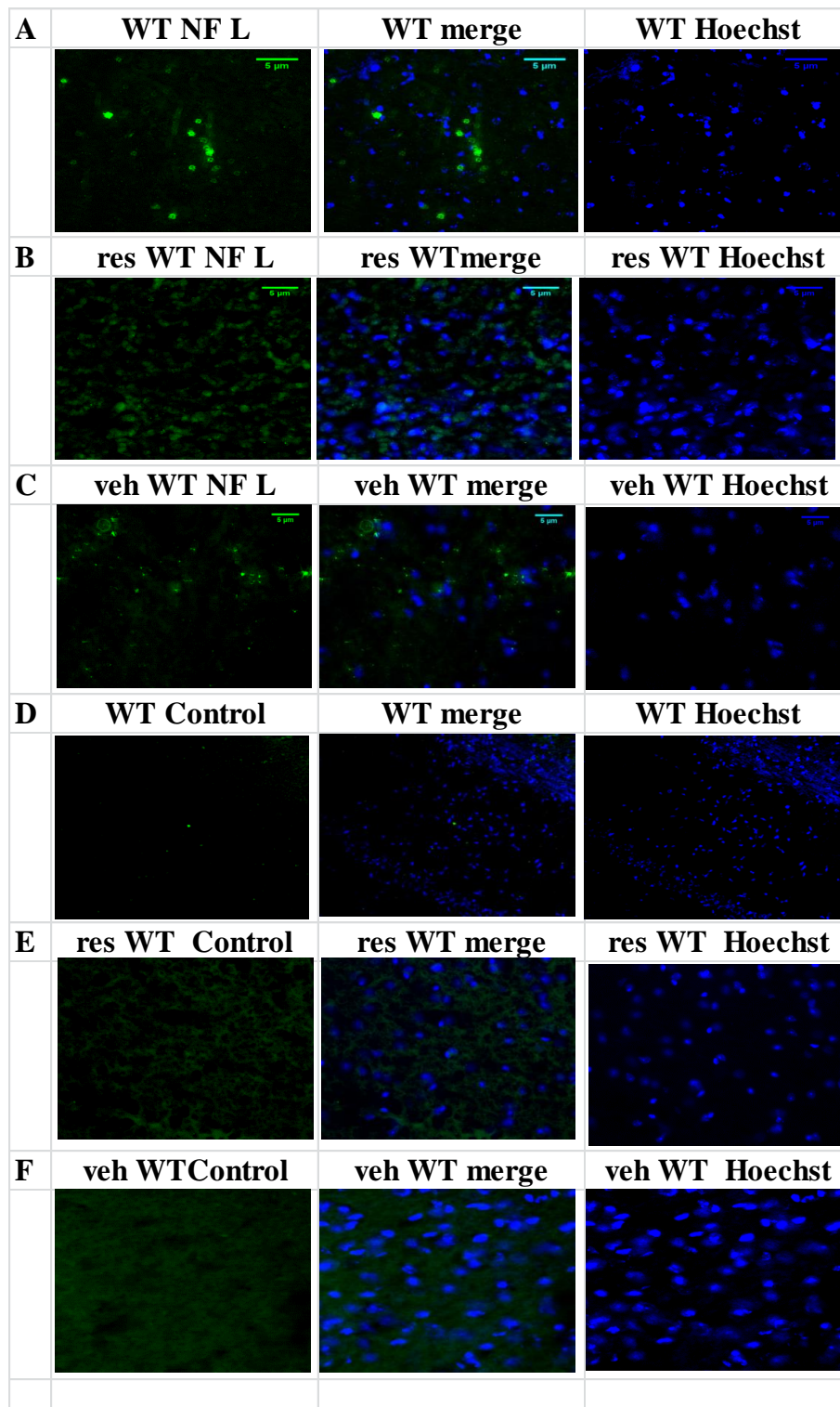


Figure 7.27 NF H expression in untreated res and veh WT brain

Representative images of NF H expression in (A) untreated WT (B) res WT and (C) veh WT brain. Control sections for (D) untreated WT (E) res WT and (F) veh WT were processed without primary antibody.

Chapter 7 Paradoxical effects of resveratrol in C57Bl/6

The combined AFU of mitochondrial, compensation and damage mediated proteins are summarised in Table 7.13. Figure 7.28 shows the summary of profiles in both retina and brain.

Retina	Mito			Comp			Dam		
	WT	rWT	vWT	WT	rWT	vWT	WT	rWT	vWT
Ave	303	319	225	158	211	125	129	178	191
SEM	28	28	22	23	25	24	20	19	20
WT:rWT		0.211			0.514			0.136	
WT:vWT			0.645			0.069			0.097
WT:vWT		0.096			0.016			0.867	
	F(5,369)7.522			F(5,414)2.399			F(5,425)5.581		
Brain	Mito			Comp			Dam		
	WT	rWT	vWT	WT	rWT	vWT	WT	rWT	vWT
Ave	600	107	663	523	785	575	400	1484	666
SEM	79	132	61	10	131	108	82	158	93
WT:rWT		0.033			0.165			0.001	
WT:vWT			0.745			0.781			0.340
WT:vWT		0.071			0.293			0.006	
	F(5,75)2.411			F(5,68)5.957			F(5,75)2.573		

Table 7.13 Summary of protein profile of retina and brain in untreated and treated WT

Table shows the mean \pm SEM of mitochondrial, compensatory and damage mediated protein expression in retina and brain of untreated res and veh treated WT. The statistical difference between groups is represented by the p value.

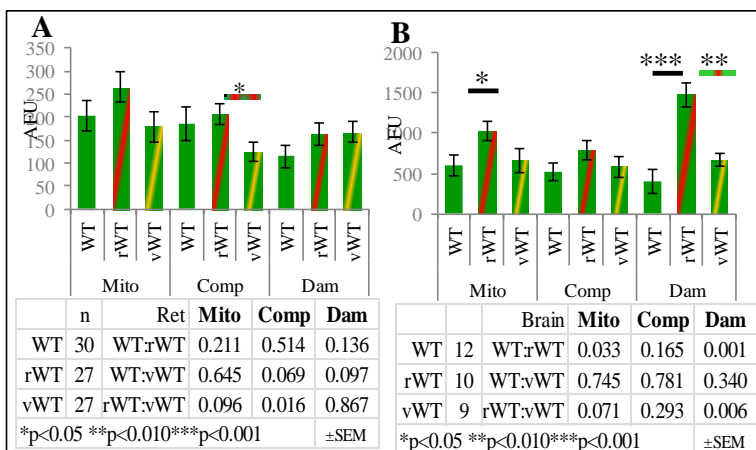


Figure 7.28 Protein profiles in retina and brain of untreated and treated WT

Graphs show the mean \pm SEM AFU of mitochondrial, compensatory and damage mediated protein expression of (A)retina and (B) brain of untreated, res and veh treated WT.

Although there was no significant difference seen in retinal compensatory protein expression, the ratio of compensatory to damage mediated expression was considered. Table 7.14 shows the ratios of compensation to damage protein expression.

Table 7.14 Ratio compensation: damage protein expression in untreated and treated WT

C:D 1:	PRL	ONL	OPL	INL	IPL	GCL	Brain
WT	0.44	0.61	0.44	0.23	0.63	0.90	0.76
rWT	0.53	0.64	0.60	0.53	0.61	0.79	1.89
% WT	22	5	38	125	-3	-13	147
vWT	0.76	0.98	0.89	0.67	1.47	1.68	1.15
% WT	75	62	104	185	135	86	51

Ratio of compensation to damage protein expression where a value of less than 1 indicates control of oxidative stress.

7.5.4 Discussion of mitochondrial related protein expression in res WT

Res treated retinal protein expression showed a 5% increase compared to untreated Wt. There was a 34% increase in compensatory protein expression and a 38% increase in damage mediated protein expression. The ratio of damage to compensation was 0.84, which suggested that oxidative stress was under control. Res treated brain showed a 71% increase in mitochondrial related protein expression. There was a 50% increase in compensatory proteins and a 271% increase in damage mediated proteins expression. Res WT brain had a damage to compensation ratio of 1.89 which suggested that the extent of damage was not under controlled.

Veh treated WT retina had a reduction of 11% mitochondrial protein expression compared to untreated WT. Compensation protein expression was reduced by 21% and damage mediated proteins expression increased by 48%. The ratio of damage to compensation proteins was 1.53, which suggested that the retinal environment was under considerable oxidative stress. Veh treated WT brain has 11% increase in mitochondrial proteins expression and a 10% increase in compensation proteins. There was a 67% increase in damage mediated protein expression. This meant the damage to compensation ratio was 1.16. Figure 7.29 summarises the effects of resveratrol minus ethanol on retinal and brain proteins.

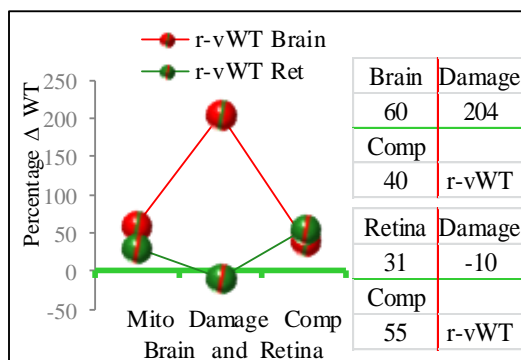


Figure 7.29 Effects of resveratrol on protein expression in retina and brain of WT

Line graph shows the percentage change in protein expression compared to untreated WT (represented by green line) in res minus ethanol WT retina and brain.

These findings suggested that resveratrol did not cause any change to the mitochondrial environment of WT retina. The ratio of damage to compensation proteins suggested that oxidative stress was controlled. Res WT brain showed that the mitochondria were under considerable stress with a significant increase in damage mediated proteins expression and inadequate compensation protein expression to control for this.

7.6 Endogenous antioxidants in res treated WT

7.6.1 Introduction to catalase activity in res treated WT

Catalase activity was examined as described in brain and spinal cord of res WT and veh WT mouse. For catalase activity in the retina, due to the homogenate requirement, veh WT mice were not analysed. Results are presented as units/mg homogenate protein.

7.6.1.1 Results of catalase activity in res treated WT

Brain		SC		Retina	
WT	6	WT	7	WT	4
rWT	6	rWT	3	rWT	3
vWT	6	vWT	3	vWT	0

Table 7.15 Test numbers for catalase activity in untreated res and veh WT homogenate

Catalase activity in brain homogenate of untreated WT, res WT and veh WT were analysed for the ability to decompose a known concentration of H₂O₂. The catalase activity in untreated WT brain homogenate had 4.30±0.38 units/mg. Res WT brain had 3.20±0.70 units/mg which was significantly reduced compared to untreated WT F(5,31) 7.995 p=0.042). Veh WT brain homogenate had 2.80±0.34 units/mg which was significantly reduced compared to untreated WT (p=0.006).

The catalase activity in spinal cord homogenate of untreated WT had 3.90±0.54 units/mg. Res WT had 4.0±0.18units/mg which was not significantly different compared to untreated WT (p=0.761), and veh WT had 3.60±0.18 units/mg which was not significantly different compared to untreated WT (p=0.499).

Catalase activity in retinal homogenate from untreated WT had 3.70±0.51 units/mg. Res WT had 2.60±0.10 units/mg which was not statistically different compared to untreated WT (p=0.055).

Figure 7.30 shows the kinetics of catalase activity and Figure 7.31 shows a graphical representation of the data.

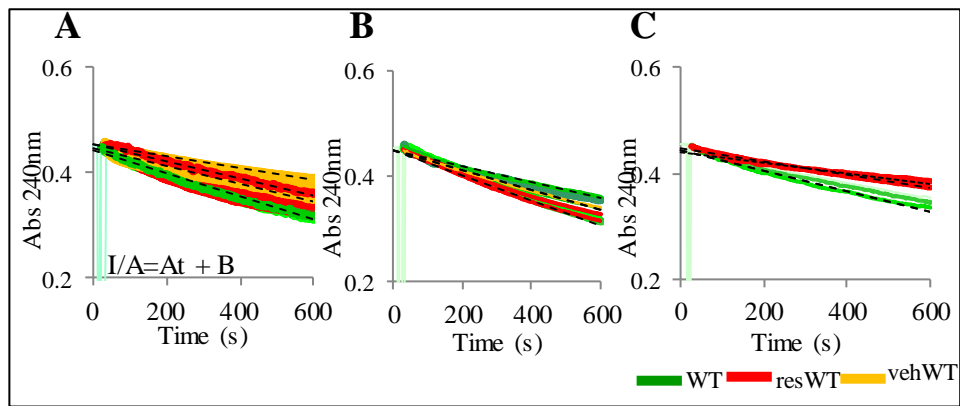


Figure 7.30 Kinetics of H₂O₂ decomposition in res treated WT mouse

Representative kinetics showing the decomposition of H₂O₂ in the presence of brain (A) spinal cord (B) and retinal (C) homogenate from untreated WT, res WT and veh WT.

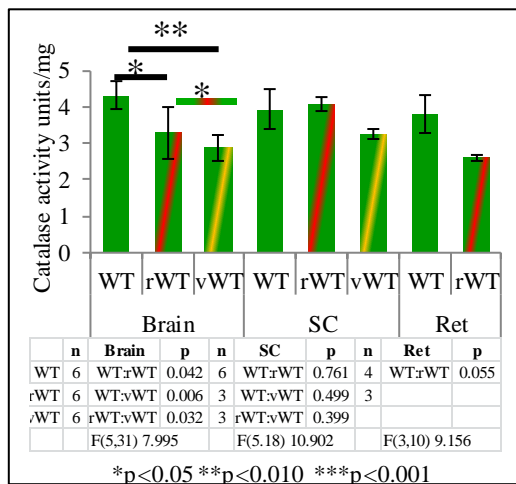


Figure 7.31 Catalase activity in res treated WT

Graph of mean \pm SD catalase activity units/mg in 80 μ g homogenate of untreated, res and veh treated WT brain, spinal cord (SC) and retina (Ret).

7.6.1.2 Discussion of catalase activity *n res WT*

Catalase activity in res treated WT showed a significant 26% reduction in brain homogenate compared to untreated WT. Catalase activity in res treated retinal homogenate was reduced by 30% compared to untreated WT. Res treated spinal cord was essentially unchanged compared to untreated WT.

Veh treated WT brain homogenate showed a significant 35% (p=0.006) reduction in catalase activity compared to untreated WT. Veh treated WT spinal cord homogenate was unchanged compared to untreated WT.

This suggested that resveratrol had enhanced the catalytic activity in brain homogenate by 9% despite the presence of 0.1% ethanol.

Chapter 7 Paradoxical effects of resveratrol in C57Bl/6

It would appear that in WT, resveratrol successfully combatted the adverse effects of ethanol on catalase function specifically in brain. Retinal catalase activity in res treated WT may have been reduced indirectly through the actions of MnSOD.

7.6.2 SOD analysis in res treated WT

SOD activity was analysed in res WT and veh WT mouse as previously described. Brain, spinal cord and retinal homogenate were analysed for total SOD activity, CuZn and MnSOD activity with the use of specific inhibitors for each sub type.

7.6.2.1 Results of SOD analysis in res treated WT

Brain		SC		Retina	
WT	6	WT	7	WT	6
rWT	6	rWT	3	rWT	6
vWT	6	vWT	3	vWT	3

Table 7.16 Test numbers for SOD analysis in untreated res and veh WT homogenate

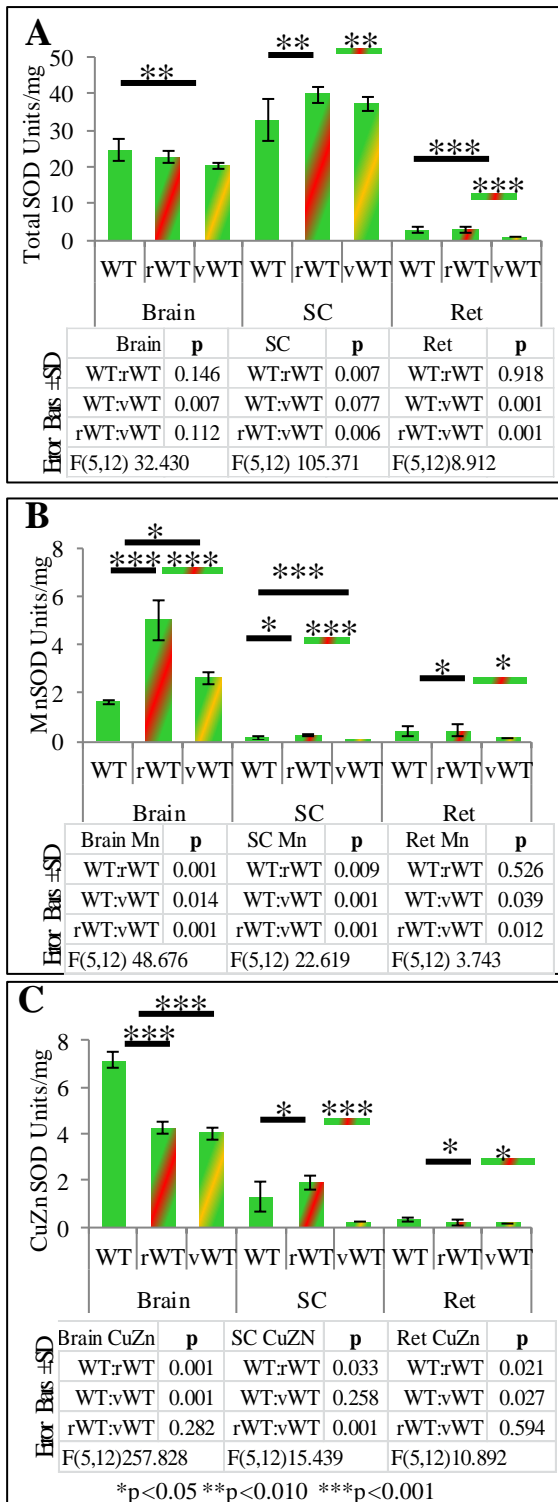
Table 7.17 shows a summary of SOD activity in untreated WT, res and veh WT brain, spinal cord and retinal homogenate for total SOD, MnSOD and CuZnSOD activity. The kinetic reactions of SOD are shown in Appendix S and the calculations for line fittings are shown in Appendix T. Figure 7.32 shows a graphical representation of the data.

Table 7.17 Summary of analysis of SOD activity in untreated res and veh WT

	Brain			SC			Ret		
	WT	rWT	vWT	WT	rWT	vWT	WT	rWT	vWT
Total SOD	24.77	22.66	20.32	32.87	39.87	37.19	2.93	2.89	0.96
	3.15	1.57	0.61	5.77	2.15	1.97	1.04	0.90	0.04
WT:rWT	0.146			0.007			0.981		
WT:vWT			0.007			0.077			0.001
rWT:vWT	0.112			0.006			0.001		
	F(5,12) 13.076			F(5,12)853.093			F(5,12) 78.006		
MnSOD	WT	rWT	vWT	WT	rWT	vWT	WT	rWT	vWT
	1.64	5.03	2.63	0.16	0.24	0.04	0.38	0.45	0.13
	0.06	0.82	0.27	0.08	0.01	0.01	0.21	0.25	0.01
WT:rWT	0.001			0.001			0.340		
WT:vWT			0.494			0.712			0.448
rWT:vWT	0.001			0.001			0.131		
	F(5,12) 13.076			F(5,12)853.093			F(5,12) 78.006		
CuZnSOD	WT	rWT	vWT	WT	rWT	vWT	WT	rWT	vWT
	7.15	4.25	4.03	1.29	1.88	0.24	0.33	0.19	0.17
	0.37	0.27	0.26	0.65	0.31	0.02	0.08	0.11	0.00
WT:rWT	0.001			0.033			0.021		
WT:vWT			0.001			0.258			0.027
rWT:vWT	0.282			0.001			0.594		
	F(5,12) 13.076			F(5,12)853.093			F(5,12) 78.006		

Table shows a summary of total SOD, MnSOD and CuZnSOD activity in WT, res and veh WT brain, spinal cord (SC) and retinal (Ret) homogenate. The statistical difference (p value) between groups is shown.

Figure 7.32 SOD activity in WT res and veh WT homogenate



(A) Graph showing the mean \pm SD of total SOD activity of homogenate in untreated WT, res and veh WT brain spinal cord (SC) and retina (Ret).

(B) Graph showing the mean \pm SD of MnSOD activity in untreated WT, res WT and veh WT brain spinal cord (SC) and retina (Ret) tissue homogenate.

(C) Graph showing the mean \pm SD of CuZnSOD activity units/mg in brain, spinal cord (SC) and retina (Ret) of untreated WT, res and veh WT.

7.6.2.2 Discussion of SOD analysis in res treated WT

Compared to untreated WT, the activity of CuZnSOD was reduced by 12% in res WT. Res WT brain homogenate had a 40% reduction and retinal homogenate had a 42% reduction compared to untreated

Chapter 7 Paradoxical effects of resveratrol in C57Bl/6

WT. CuZnSOD was increased by 46% in res WT spinal cord homogenate compared to untreated WT. MnSOD activity was increased by 84% compared to untreated WT. Res WT brain homogenate had a 208% increase, spinal cord had 55% increase and retinal homogenate a 16% increase.

Compared to untreated WT, veh WT showed a 59% reduction of CuZnSOD. Veh WT brain homogenate had a 44% reduction, spinal cord had 82% reduction and retinal homogenate had a 50% reduction. MnSOD activity in veh WT had a 27% reduction compared to untreated WT. Veh WT brain homogenate had a 60% increase, spinal cord had 74% reduction and retinal homogenate had 66% reduction.

In the assay of inhibition of formazan formation, the combined percentage inhibition of CuZnSOD and MnSOD should equal the total SOD inhibition. Any inhibition of formazan formation not directly due to either CuZnSOD or MnSOD was called non-SOD. WT brain homogenate had $1\% \pm 2.0$ non-SOD. Res WT had $-11\% \pm 8$ which was significantly different to untreated WT ($F(5,30) 25.624$ $p=0.006$). Veh WT had $3\% \pm 2$ which was not significantly different to untreated WT ($p=0.416$). Untreated WT spinal cord homogenate had $14\% \pm 4$ non-SOD. Res WT had 1 ± 0.94 non-SOD which was significantly different to untreated WT ($F(5,20) 19.228$ $p=0.013$). Veh WT had $37\% \pm 1$ non-SOD activity which was significantly more than untreated WT ($F(5,20) 19.228$ $p=0.001$). Retinal homogenate in untreated WT had $15\% \pm 6$ non-SOD. Res WT had $18\% \pm 5$ which was not significantly different compared to untreated WT ($p=0.372$). Veh WT had $16\% \pm 1$ non-SOD activity which was not significantly different to untreated WT ($p=0.842$). Figure 7.33 shows a summary of these data.

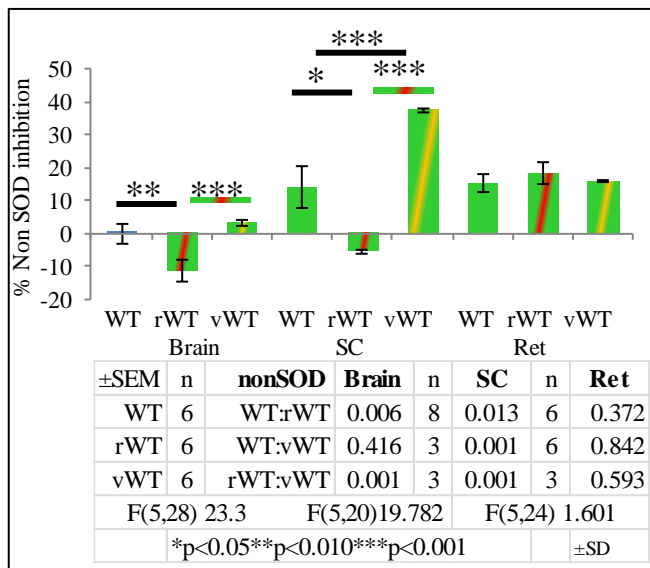


Figure 7.33 Inhibition of formazan formation by non-SOD activity.

Inhibition of formazan formation that was not due to MnSOD or CuZnSOD was called non-SOD. Non-SOD activity in veh treated WT was significantly increased in brain, spinal cord (SC) and retina (Ret) compared to untreated WT and res WT.

7.6.3 Antioxidant profile for res treated WT

The antioxidant ‘index’ (AO index) was obtained by taking the percentage increase or decrease in the combined SOD and catalase activity for each tissue. A negative value was considered indicative of oxidative stress.

In res WT the tissue specific AO profile was 23. Res WT brain homogenate profile was 53 which represented the combined percent reductions in catalase and CuZnSOD with the increased MnSOD activity. Res WT spinal cord profile was 36 which represented the percent increase in catalase, CuZn SOD and MnSOD. Retina had a profile of -17 due to the reduction of catalase and CuZnSOD.

The antioxidant activity in res WT compared to untreated WT had 9% reduction of catalase activity, 12% reduction of CuZnSOD and 93% increase in MnSOD.

Veh WT tissue specific AO profile was -34. Compared to untreated WT, veh WT brain had an antioxidant reduction of 4%. Spinal cord was reduced by 54% and retina was reduced by 58%. Catalase activity was reduced by 17%. CuZnSOD was reduced by 59% and MnSOD by 27%.

When res treated WT values were corrected for ethanol, the AO profile index for res WT increased to 63. Res WT brain AO activity was increased by 57% compared to untreated WT, res WT spinal cord was increased by 90% and res WT retinal homogenate was increased by 43%. Catalase activity was increased by 25%, CuZnSOD activity was increased by 46% and MnSOD activity increased by 119%.

Figure 7.34 shows a summary of this profile.

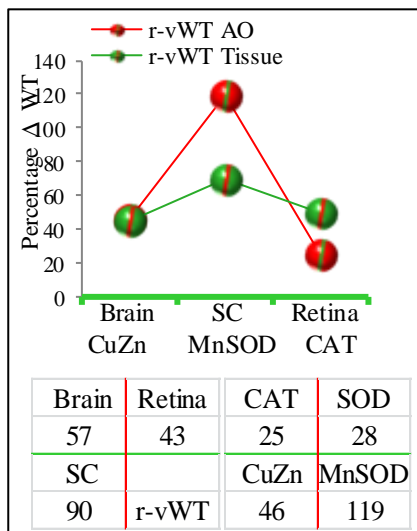


Figure 7.34 AO profile in res treated WT

Line graph representing the percentage changes in res treated WT compared to untreated WT (represented by green line). Compared to untreated WT, the AO activity in all tissues was increased. The AO activity of catalase increased by 25%, CuZnSOD activity was increased by 46% and MnSOD increased by 119%.

The enhanced MnSOD activity observed in all tissues possibly served to exhaust circulating catalase. The reduction of retinal catalase in res treated WT may have been induced by the excessive H₂O₂ production initiated by an excess MnSOD. The increase of MnSOD activity seen in both WT and Het resveratrol treated mice clearly had profound effects within the mitochondria. The strategy for coping with excess H₂O₂ was not challenged with an excess catalase response in either genotype suggesting that the duration of therapy exceeded any potentially useful benefit resveratrol may have conferred.

7.6.4 MnSOD protein expression in res treated WT

7.6.4.1 Introduction to MnSOD protein in res treated WT

IHC was performed on retinal and brain sections of untreated, res and veh WT as previously described.. A minimum of four independent WT, res treated WT and vehicle treated WT were used. Western blotting was performed on tissue homogenate of brain and retina from untreated WT and res WT only

7.6.5 Results of MnSOD expression in res treated WT

7.6.5.1 MnSOD expression in res treated WT retina and brain

Table 7.18 shows a summary of MnSOD expression in the retinal layers and brain of untreated res and veh WT. Figure 7.35 shows a graph of this data.

Table 7.18 MnSOD expression in untreated and treated WT retina and brain

MnSOD	PRL			ONL			OPL			INL			IPL			GCL			
	WT	rWT	vWT	WT	rWT	vWT	WT	rWT	vWT	WT	rWT	vWT	WT	rWT	vWT	WT	rWT	vWT	
Ave	245.4	506	118.4	318	710.8	174.3	344.9	643.1	271.1	244.9	427.9	122	847.5	1256	291.3	497.7	646.7	199.4	
SEM	47.57	18.49	6.053	31.72	97.28	48.47	41.43	95.82	49.16	56.74	38.32	15.09	224.9	318.5	21.02	85.14	112	21.17	
WT:rWT		0.002			0.001			0.016			0.152			0.746			0.827		
WT:vWT			0.232			0.168			0.689			0.300			0.244			0.039	
F		F (5,16) 8.912			F (5,16) 11.416			F (5,16) 10.444			F (5,16) 4.028			F (5,16) 2.850			F (5,16) 8.476		

Table shows the mean \pm SEM MnSOD expression in retinal layers of WT, res and veh WT. The statistical difference between groups is represented by the p value.

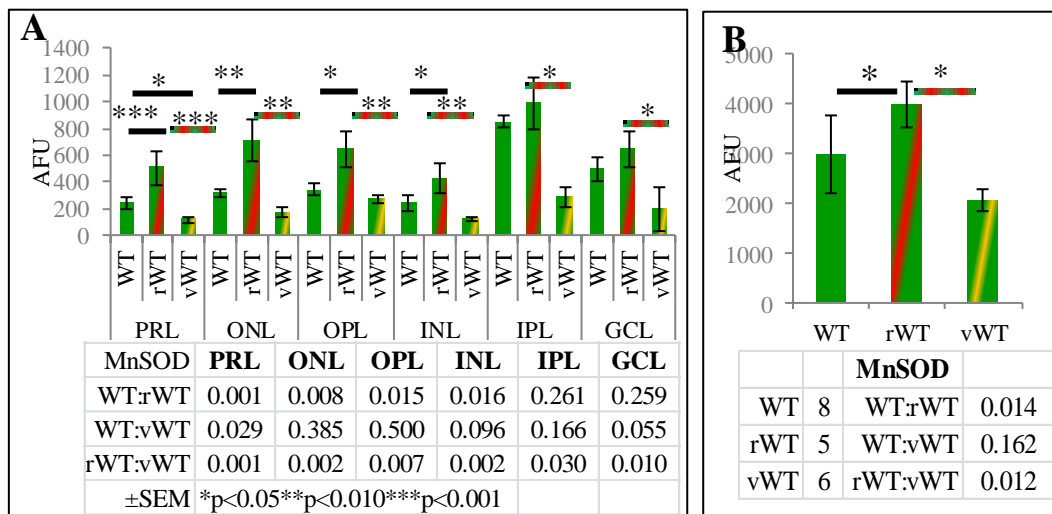


Figure 7.35 MnSOD expression in untreated and treated retinal layers and brain

Graph shows the mean \pm SEM of MnSOD expression in WT, res and veh WT (A) retinal layers and (B) brain.

7.6.5.2 Western blotting of retinal and brain homogenate in WT and res WT

MnSOD expression in untreated WT brain homogenate had 1.03 ± 0.25 RD. Res treated WT brain had 1.49 ± 0.130 which was significantly increased compared to untreated WT (F(3,18) 9.181 p=0.017).

MnSOD expression in retinal homogenate of untreated WT had 1.12 ± 0.04 RD and res treated WT retina had 1.20 ± 0.20 which was not significantly different compared to untreated WT (p=0.709).

Figure 7.36 shows a summary of these data.

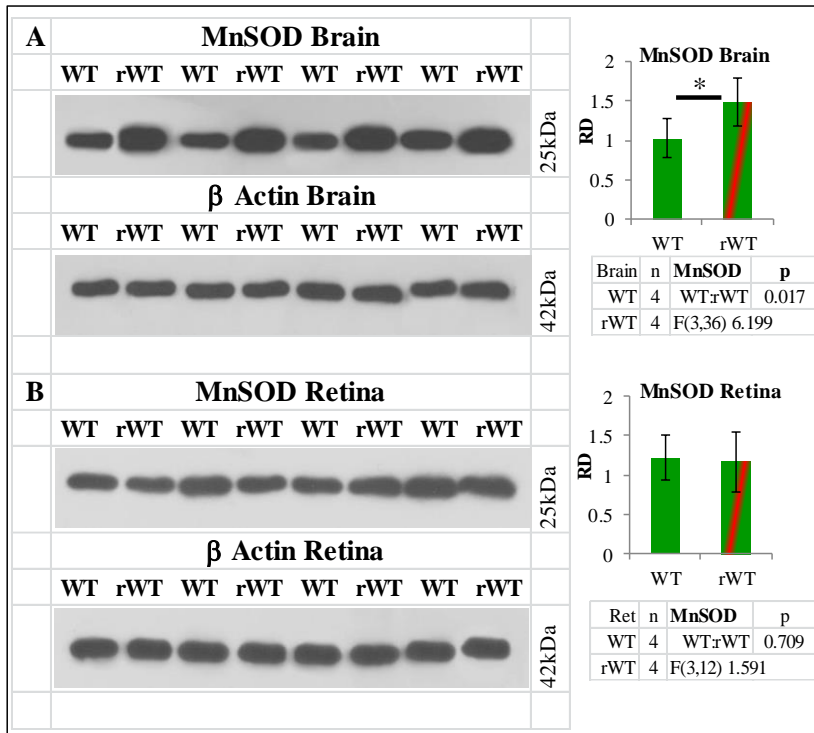


Figure 7.36 MnSOD expression in brain and retinal homogenate of WT and res WT

Representative bands from Western blotting of (A) brain and (B) retinal homogenate from untreated WT(n4) and res treated WT(n4) for MnSOD. Graphs show the mean \pm SEM RD of proteins. Lower bands show β actin as a loading control.

Figures 7.37 show representative images of MnSOD expression in untreated, res and veh WT retinal sections. Control sections are shown are processed sections omitting the use of the primary antibody. Figure 7.38 shows representative images of MnSOD expression in brain sections as above.

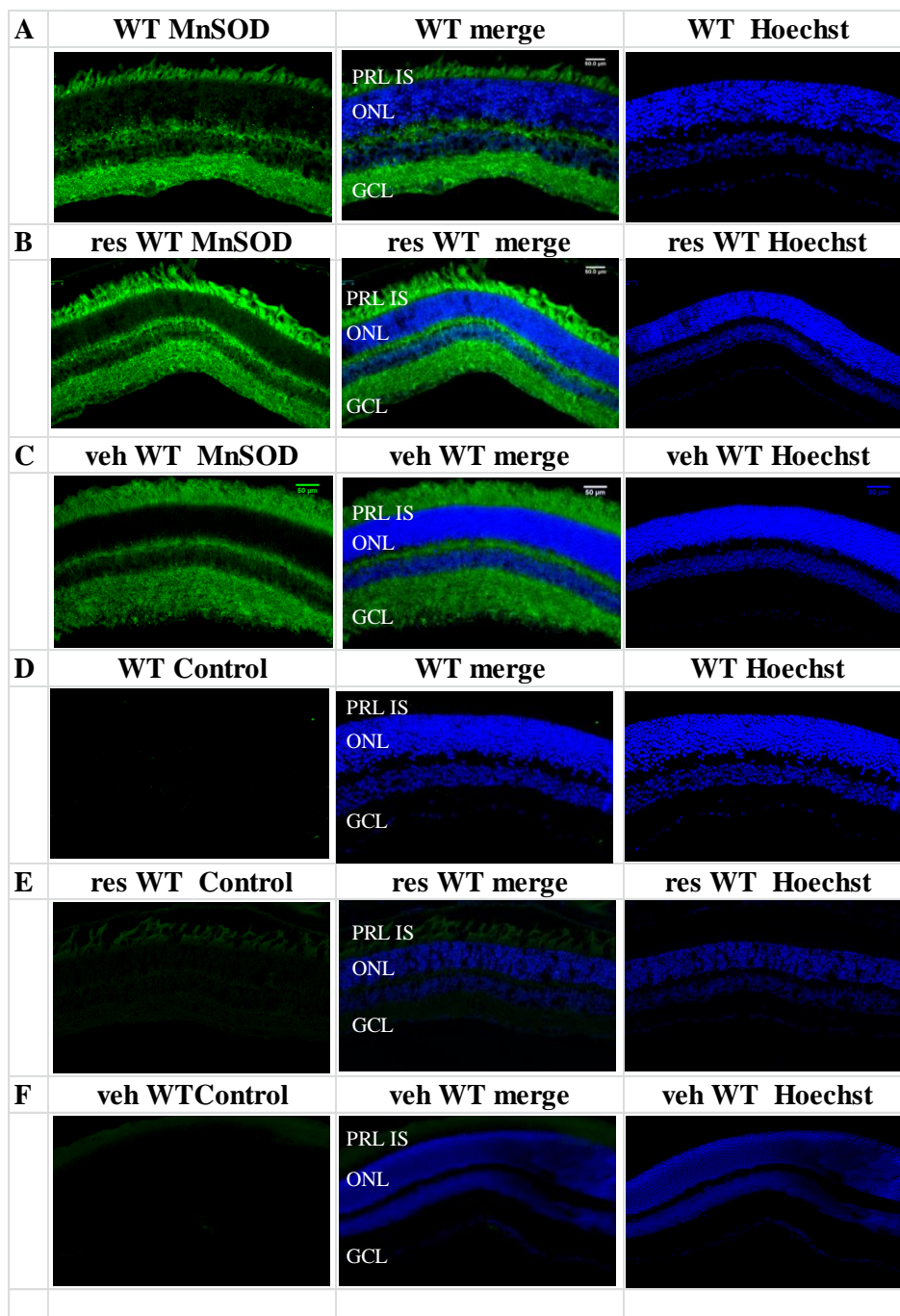


Figure 7.37 MnSOD expression in retina of untreated, res and veh treated WT

Representative images of MnSOD expression in WT (A), res WT (B) and veh WT (C) retinal sections. Negative control sections (omission of primary antibody) for WT (D), res WT (E) and veh WT (F) are shown.

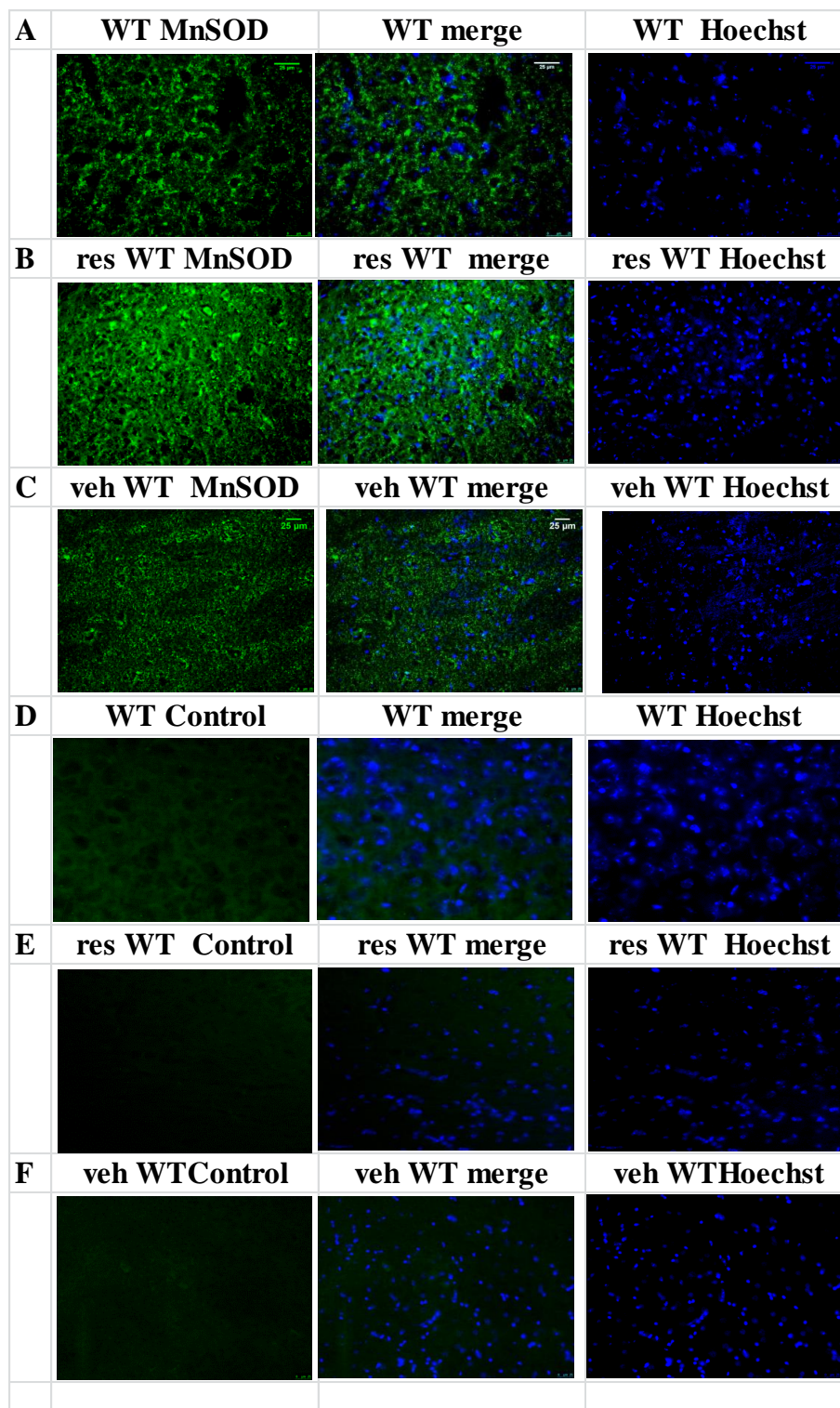


Figure 7.38 MnSOD expression in untreated res and veh WT brain

Representative images of MnSOD expression in (A) untreated WT (B) res WT and (C) veh WT brain. Control sections for (D) untreated WT (E) res WT and (F) veh WT were processed without primary antibody.

7.6.5.3 Discussion of mitochondrial related protein expression in res WT

7.6.5.3.1 MnSOD in retina of res and veh treated WT

MnSOD protein expression was examined in the retinal layers of untreated res and veh treated WT. Compared to untreated WT, res WT had a significant 107% increase in the PRL (F(5,17) 35.531 p=0.001), 124% increase in the ONL (F(5,17) 15.534 p=0.008), 85% increase in the OPL (F(5,17) 7.631 p=0.015), 75% increase in the INL (F(5,17) 11.515 p=0.016). There was no significant difference observed in the IPL (p=0.261) or GCL (p=0.259). The average increase of MnSOD expression in res WT was 73%.

Veh treated WT retina had a significant 52% reduction in the PRL (F(5,17) 35.531 p=0.029). All other retinal layers were not statistically different to untreated WT but showed a reduction in MnSOD expression. The mean percentage reduction was 49%.

The activity of MnSOD in retinal homogenate of res WT showed a 16% increase compared to untreated WT, which suggested that 57% of the mean increase in protein expression was not functional. Veh treated WT had a 66% reduction in MnSOD activity with a 49% reduction in protein expression which suggested that 17% of the expressed SOD was not active.

7.6.5.3.2 MnSOD activity in brain of res and veh WT

MnSOD protein expression in res WT brain was increased by a significant 68% (F(5,32) 6.913 p0.014. compared to untreated WT. Western blotting showed that res WT had a significant 45% increase in expression (p=0.017). The MnSOD activity in brain homogenate of res WT showed an increase in excess of 200% compared to untreated WT. This suggested that the quantification of protein expression by IHC has limitations.

MnSOD expression in Veh treated WT was not significantly different to untreated WT however did show a 31% reduction (p=0.162).

Chapter 7 Paradoxical effects of resveratrol in C57Bl/6

7.6.6 3 Nitrotyrosine deposition in retina and brain of res treated WT

The presence of 3 nitrotyrosine deposition in the retina and brain of untreated res and veh treated WT was examined using IHC. Table 7.19 shows a summary of 3 Nitrotyrosine deposition in the retinal layers and brain of untreated res and veh WT. Figure 7.39 (A) shows a graph of retinal data and Figure 7.39 (B) shows a graph of brain.

Table 7.19 3Nitrotyrosine deposition in res treated WT retina and brain

	PRL			ONL			OPL			INL			IPL			GCL			
3Nitro	WT	rWT	vWT	WT	rWT	vWT	WT	rWT	vWT	WT	rWT	vWT	WT	rWT	vWT	WT	rWT	vWT	
Ave	189	281	286	33.1	303	188	129	178	254	59	129	188	118	355	354	125	185	139	
SEM	23.6	32.6	59.9	7.25	45.5	54.7	26.8	16.8	48.5	18.5	37.8	30.5	36	51.8	63.8	58.2	11.2	8.5	
WT:rWT		0.629			0.260			0.552			0.841			0.729			0.029		
WT:vWT			0.152			0.265			0.733			0.746			0.696			0.861	
F		F (5,15) 2.210			F (5,15) 1.269			F (5,15) 0.624			F (5,15) 0.244			F (5,15) 1.252			F (5,15) 2.896		

Table shows the mean \pm SEM 3 nitrotyrosine deposition in retinal layers of WT, res and veh WT. The statistical difference between groups is represented by the p value.

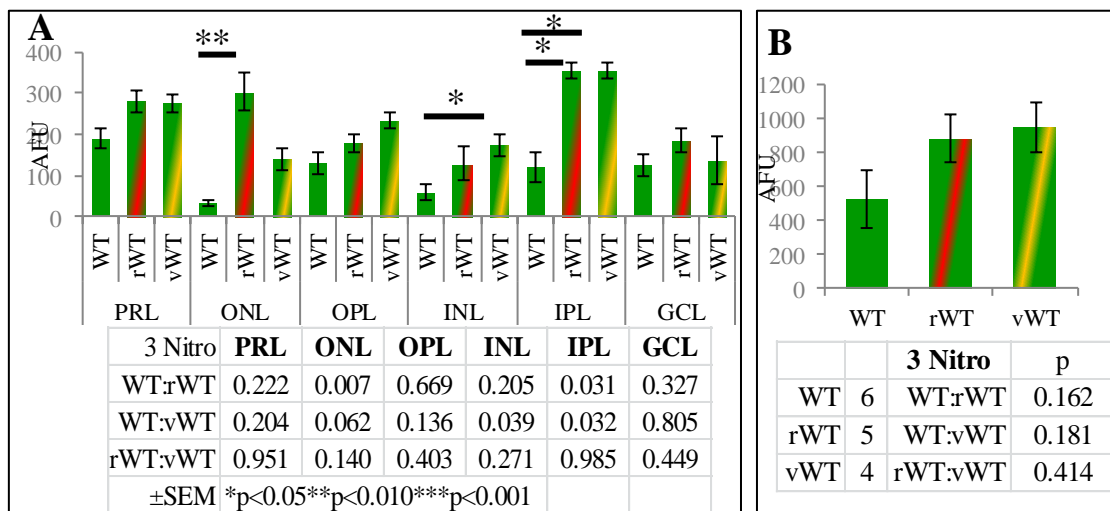


Figure 7.39 3 Nitrotyrosine deposition in untreated res and veh WT

Graph shows the mean \pm SEM of 3 Nitrotyrosine deposition in WT, res and veh WT (A) retinal layers and (B) brain.

Figures 7.40 shows representative images of 3 Nitrotyrosine in retina and Figure 7.41 show brain of untreated, res and veh treated WT.

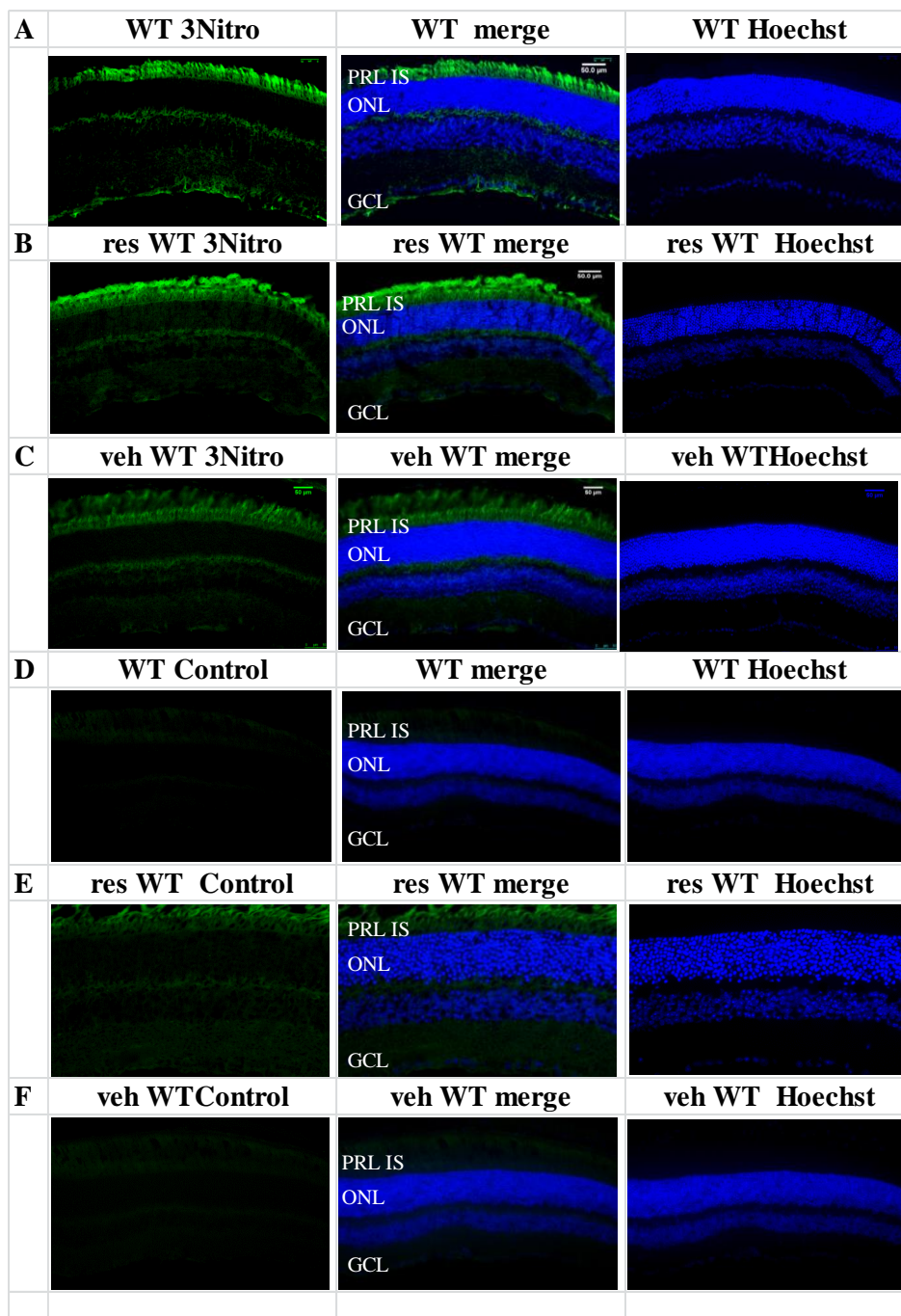


Figure 7.40 3 Nitrotyrosine deposition in retina of untreated, res and veh treated WT

Representative images of 3 Nitrotyrosine deposition in WT (A), res WT (B) and veh WT (C) retinal sections. Negative control sections (omission of primary antibody) for WT (D), res WT (E) and veh WT (F) are shown.

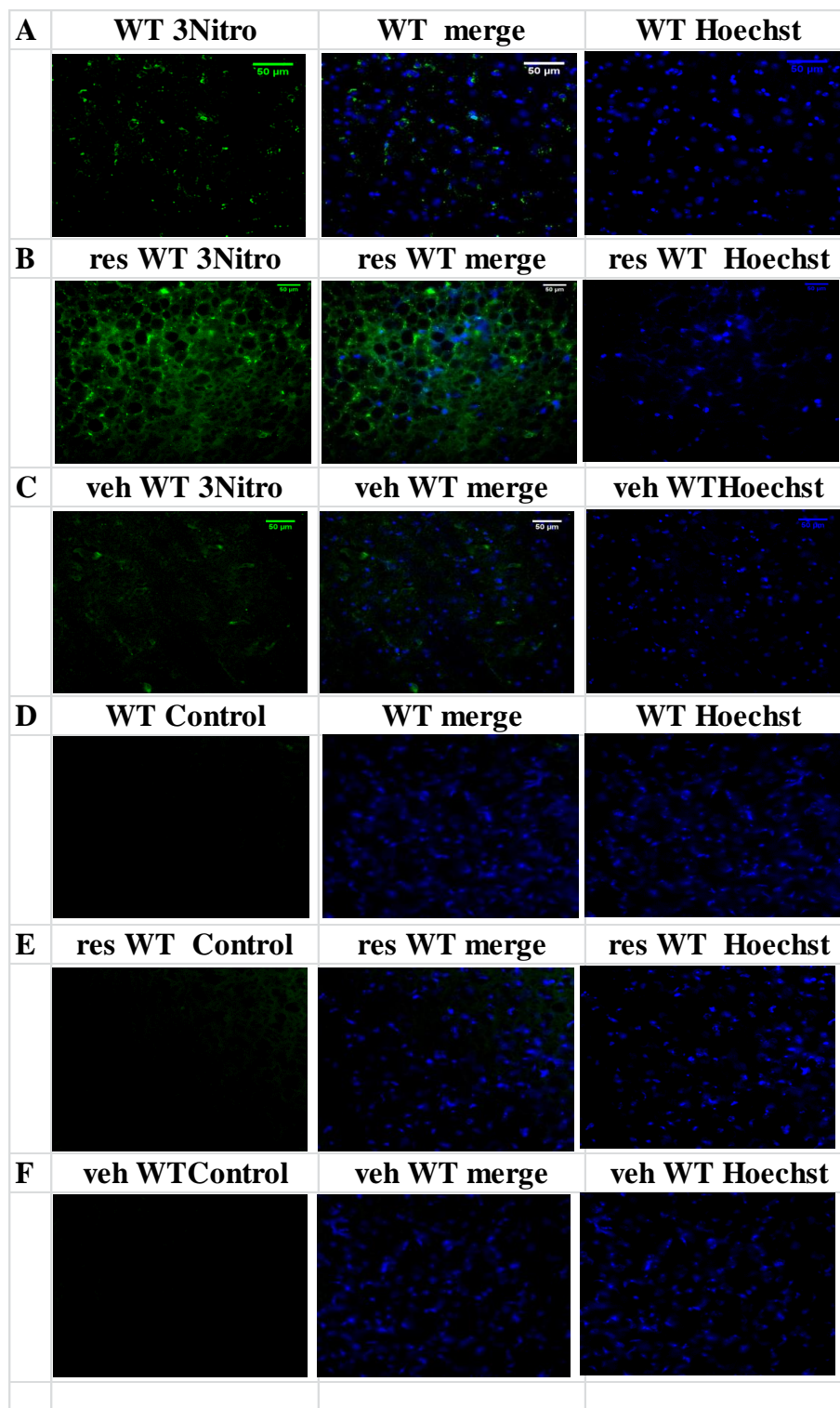


Figure 7.41 3 Nitrotyrosine deposition in untreated res and veh WT brain

Representative images of 3 Nitrotyrosine deposition in (A) untreated WT (B) res WT and (C) veh WT brain. Control sections for (D) untreated WT (E) res WT and (F) veh WT were processed without primary antibody.

Chapter 7 Paradoxical effects of resveratrol in C57Bl/6

Compared to untreated WT, res WT had a significant 818% increase of 3 nitrotyrosine in the ONL (F(5,12) 8.011 p=0.007) which was not observed in veh WT. There was a significant 200% increase in the IPL of res WT (F(5,12) 5.221 p=0.031). This was also observed in the IPL of veh treated WT (p=0.032). 3Nitrotyrosine deposition in brain of res and veh treated WT was not significantly different to untreated WT.

The ratio of 3 Nitrotyrosine deposition to MnSOD expression was examined. Res treated WT maintained a ratio where the score did not exceed a value of 1 indicating that the excess of MnSOD expression was keeping nitration reduced. Veh treated WT showed values in excess of 1 in the PRL, INL and IPL. This suggested that the reduction in MnSOD expression was influencing the nitration of retinal proteins .Figure 7.42 summarises these findings.

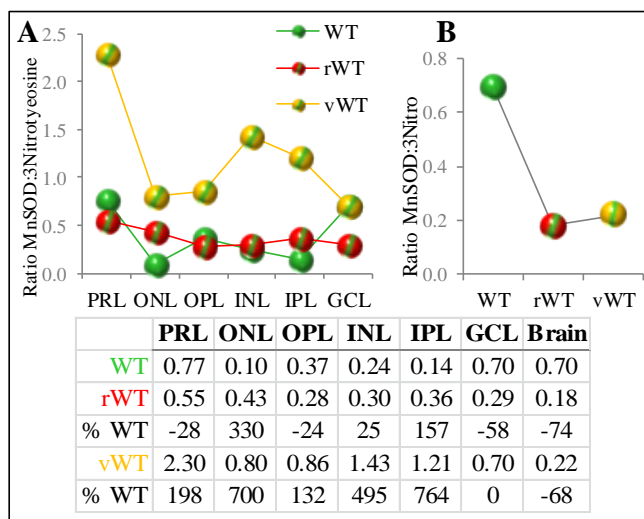


Figure 7.42 Ratio of MnSOD to 3 Nitrotyrosine expression in untreated res and veh WT

Line graph showing the ratio of MnSOD to 3 Nitrotyrosine expression in (A)retinal layers and (B)brain of untreated res and veh treated WT. The table insert shows the percentage difference between groups.

7.6.7 Discussion of 3 nitrotyrosine deposition in res treated WT

Res treated WT had a mean 212% increase in 3 nitrotyrosine deposition in the retina compared to untreated WT. Despite this the ratio of MnSOD to 3 nitrotyrosine was comparable to the values observed in untreated WT. This would suggest that resveratrol did not prevent the deposition of nitrotyrosine. Res treated brain had a 69% increase in nitrotyrosine compared to untreated WT.

Veh treated WT had an increase of 143% in 3 nitrotyrosine deposition compared to untreated WT. Because of the reduction in MnSOD expression, the ratio to nitrotyrosine exceeded untreated WT

Chapter 7 Paradoxical effects of resveratrol in C57Bl/6

values in the PRL, INL and IPL. Nitrotyrosine deposition in veh treated WT brain was reduced by 70% compared to untreated WT.

7.6.8 Summary of Chapter 7: Resveratrol administration in C57BL/6 mouse

7.6.8.1 Reduced organ weight and lower motor function in res WT

Compared to untreated female WT, female resveratrol treated WT mice had a significant increase in body weight, with a reduction in brain weight and cardiac weight ratio. Lower motor function was reduced in female WT.

7.6.8.2 Cognitive impairment in res treated WT

Compared to untreated WT, res WT cognitive function was impaired in T maze testing with a significant reduction in discrimination ratio. NOR demonstrated a reduced IR and DR in res WT not observed in veh WT. Despite their reduced fear response, discrimination was reduced.

7.6.8.3 Bioenergetic dysfunction in res treated WT

In resveratrol treated WT C57Bl/3 mouse, all complexes of the ETC tested were impaired. Complex I activity showed the greatest reduction of 63%. Tissue specific ETC impairment was highest in res WT spinal cord with 77% reduction in ETC activity. The ratio of complex activity was preserved in res WT.

7.6.8.4 Antioxidant activity in res treated WT

The antioxidant activity in res WT was enhanced by the administration of resveratrol. Despite the enhanced activity of MnSOD, the tissue specific reduction of both catalase and CuZnSOD resulted in oxidative stress most notably in the spinal cord.

7.6.8.5 Protein expression profile in res treated WT

Resveratrol treated mitochondrial related protein expression in WT brain was increased but was combined with increased damage mediated protein expression. There was an insufficient compensatory protein response to this damage. expression. Resveratrol treated retina showed an enhanced protein and compensatory protein expression.

Chapter 7 Paradoxical effects of resveratrol in C57Bl/6

The administration of resveratrol did not confer any identified advantage to C57Bl/6 mouse. The reduced neuromuscular activity seen on *In Vivo* testing was compounded by the increase in body weight. Bioenergetic activity in res treated WT was reduced to the level of untreated Het. The antioxidant status was unbalanced with the increase in MnSOD there was a reduction in spinal cord CuZn SOD and catalase activity. Despite the increase in mitochondrial related proteins, the ratio was unbalanced favouring damage mediated protein expression over compensatory in res WT brain.

Chapter 8 Discussion of *Opa1*^{Q285STOP} mouse model

8.1 Spectrum of phenotypic anomalies in *Opa1*^{Q285STOP} mouse

The physical abilities of *Opa1*^{Q285STOP} mouse were tested at 12 months of age. This was at the onset of ophthalmic deterioration. However, it would appear that *Opa1*^{Q285STOP} mouse had several impaired neuromuscular and cognitive mechanisms as determined by a variety of tests.

Other physical impairments not before associated with this mouse model were neuropsychiatric function associated with reduced exploratory behaviour, prolonged extended freeze in novel environments, extended latency to investigate – all of which are associated with depressive states. The *Opa1*^{Q285STOP} mouse model appeared to lack the adaptive stimuli specific response to his environment. Figure 8.1 shows some of the anomalies associated with Het neuromuscular function.



Figure 8.1 *Opa1*^{Q285STOP} mouse on the tightrope

Opa1^{Q285STOP} mouse on the tightrope demonstrating reduced lower motor function –note the lack of hind paw grip and nail use on front right paw. Reduced autonomic function – note the lack of prehensile tail.

Impaired cognitive function was identified which related to region specific impairment in Het brain. . T maze tested the functional activity of the hippocampus and specifically the dorsal hippocampus where spatial reference memory acquisition is located. (Bannerman et al. 1995). The anterior hippocampus is located in close proximity to the amygdala which controls behaviour in anxiogenic conditions. Anxiety as a tonic response to aversion depends on the anterior hippocampus but fear is controlled by the amygdala. Dorsal hippocampal spatial

Chapter 8 Discussion of $Opa1^{Q285STOP}$ mouse model

reference is influenced by the anterior hippocampal response. The anterior hippocampal response is modulated by stress (Kim et al. 2001). The IR of T maze demonstrated female Het mice specifically had enhanced anterior hippocampal dysfunction. Dorsal hippocampal discrimination in both male and female Het mice was impaired.

Novel object recognition examined the function of the perirhinal cortex (Murray et al. 2007; Kim et al. 2014). By employing objects made from different substrates, the false positive effect was avoided, (Kivisaari et al. 2013). The perirhinal cortex facilitates the recognition of objects through the combined inputs and outputs to other structures including the entorhinal cortex (Clark et al. 2000), involving olfactory association, insular cortex (Bermudez-Rattoni et al. 2005) via somatosensory inputs, the cingulate cortex (Aggleton et al. 1997; Ennaceur et al. 1997), which plays a role in attention and memory retrieval (Leech and Sharp 2014) and the para hippocampal gyrus responsible for environmental recognition including topographical cues (Epstein and Kanwisher 1998). Functional perirhinal activity was impaired specifically in male Het mice with a significant reduction in IR. Somatosensory deficit was also evident in male Het mice with a significantly reduced DR. Figure 8.2 shows a map of $Opa1^{Q285STOP}$ mouse brain with specific regions of impaired function in specific pathways identified in cognitive testing.

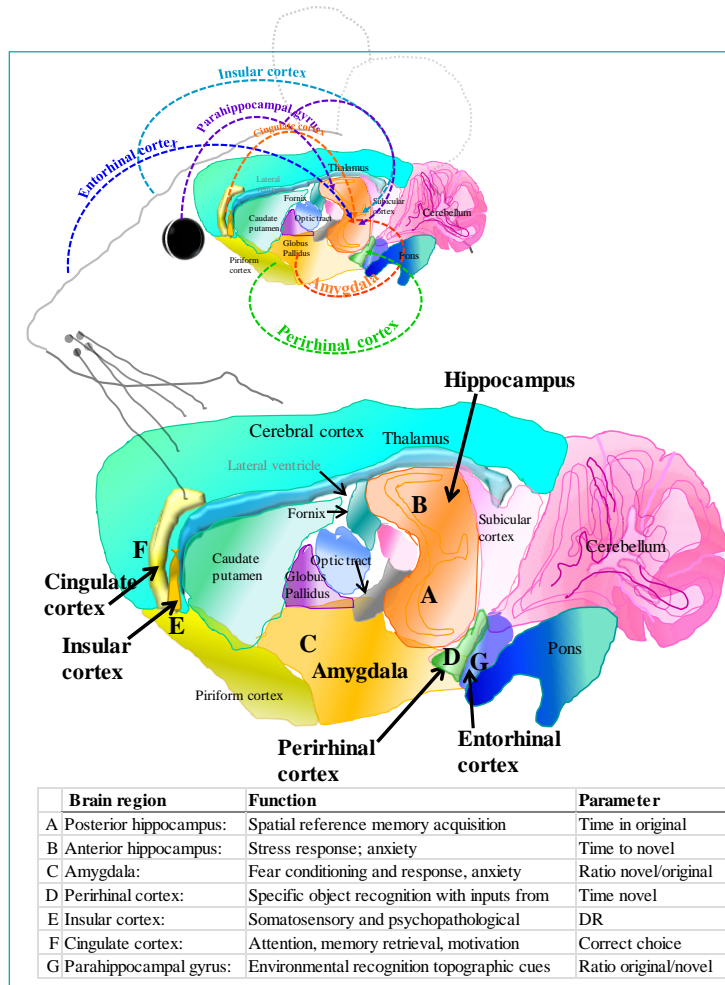


Figure 8.2 Impaired cognitive function in *Opa1*^{Q285STOP} mouse

Brain specific regions in *Opa1*^{Q285STOP} mouse brain showed impaired function as demonstrated by cognitive function analysis. The combined parameters of T maze and NOR are applied where applicable. Untreated Het response to novel showed heightened stress response (amygdala) influencing hippocampal spatial reference and acquisition. Perirhinal cortex activity dependent on combined cingulate, insular and entorhinal cortex inputs specific to NOR testing was impaired.

8.1.1 Spectrum of human phenotypic anomalies with ADOA Plus syndrome

ADOA Plus humans have neuromuscular and neurological involvement. The presence of MS like symptoms have been reported with cerebellar ataxia and spastic paraplegia (Verny et al. 2008; Milea et al. 2010; Yu-Wai-Man et al. 2010; Marelli et al. 2011; Pretegiani et al. 2011; Liskova et al. 2013). Symptoms can be indistinguishable from other degenerative diseases such as hereditary spastic paraplegia (Finsterer et al. 2012; Klebe et al. 2012; Kumar et al. 2013), multiple sclerosis (Verny et al. 2008; Yu-Wai-Man et al. 2010) and Alzheimer's disease (Wang et al. 2009).

Reduced neuronal plasticity in mitochondrial associated disorders can cause phenotypic behavioural patterns. Mood disorder like phenotypes may be associated with the accumulation of mitochondrial mutations (Kasahara et al. 2006). There is also the significant association

Chapter 8 Discussion of Opa1^{Q285STOP} mouse model

between neuron-specific mitochondrial mutations and mood disorder phenotypes (Kato 2001; Kasahara et al. 2006). Suboptimal mitochondrial function can be found in human depressive states (Morava and Kozicz 2013) which would agree with the SHIRPA neuropsychiatric functional assessment in Opa1^{Q285STOP} mouse.

8.2 Spectrum of bioenergetic anomalies in Opa1^{Q285STOP} mouse

The reduction in cognitive function may be due to a decline in the brain reserves of ATP when functioning under stressful conditions. Male Het mouse showed enhanced ATP levels compared to WT. Opa1^{Q285STOP} mouse showed a significant increase in the proportion of smaller sized mitochondria. This may indicate that the threshold for mitophagy onset differs in Het mouse. Mitophagy is initiated when small sized mitochondria with a reduced $\Delta\Psi_m$ present. The $\Delta\Psi_m$ of Het mitochondria did not differ to WT so despite the reduction in size, these mitochondria were functional. However the precise location of mitochondria within brain is significant for the limits of bioenergetic threshold. Non synaptic brain mitochondria can withstand a 72% reduction in complex I activity before there are significant changes in ATP or $\Delta\Psi_m$. In synaptic mitochondria, the threshold is reduced to 25% (Davey et al. 1997; Davey et al. 1998). As the ATP determination assays were performed on a complete half of brain, partial length spinal cord and whole retina, specific regional differences in ATP would not have been detected. The reduction of $\Delta\Psi_m$ in synaptic mitochondria may be a protective mechanism against the generation of ROS. ROS production requires a minimum mitochondrial membrane potential of -350mVm (Korshunov et al. 1997).

The bioenergetic deficits observed in Het mouse were 54% for complex I, complex II 32% and complex IV 5%. The tissue specificity of this dysfunction revealed that retinal mitochondria had the highest percentage reduction in activity with 77% reduction for complex I and 58% for complex IV. However on examination of the ratio of ETC, it was observed that complex II activity has the highest activity in the retinal mitochondria with 55%. Complex I activity has 38% activity in the spinal cord and complex IV has 40% activity in the brain. Het retained these ratios albeit at a reduced rate.

Chapter 8 Discussion of *Opa1*^{Q285STOP} mouse model

As complex I is the proximal component of the ETC, it is responsible for transfer of electrons to ubiquinone. By passing electrons from the mitochondrial matrix to the inner membrane space, it also maintains the mitochondrial electron gradient $\Delta\Psi_m$. A reduction in complex I activity should therefore result in reduced ATP synthesis and a reduced $\Delta\Psi_m$. As this was not so in Het, an alternate mechanism is proposed: As a Another preventative mechanism for ROS generation is the presence of intermembrane cytochrome c peroxide (Gilmour et al. 1994). Intermembrane cytochrome c can bypass the superoxide producing electron chain by the external NADH-cytochrome b5 reductase in the outer membrane and can oxidize superoxide to oxygen preventing the formation of H₂O₂ (Figure 8.3). When cytochrome c is released, electron transport in the complexes is inhibited due to limitations on cytochrome c oxygenase (Kuznetsov et al. 2004). Cytochrome c release into the cytosol forms a complex with Apaf-1, (Vaux 1997), which in turn triggers a cascade of apoptotic signals. If the imminent cession of electron transport can be by-passed through a cytosolic cytochrome c substrate, this will reduce complex I mediated ROS generation (La Piana et al. 1998; Skulachev 1998). It also gives complex 4 the task of maintaining the $\Delta\Psi_m$. This mechanism would appear to be operational in *Opa1*^{Q285STOP} mouse. It provides a rational for normal ATP levels and essentially normal $\Delta\Psi_m$ observed in brain and retinal mitochondrial isolates. Figure 8.3 shows a schematic of the proposed function of intermembrane cytochrome c.

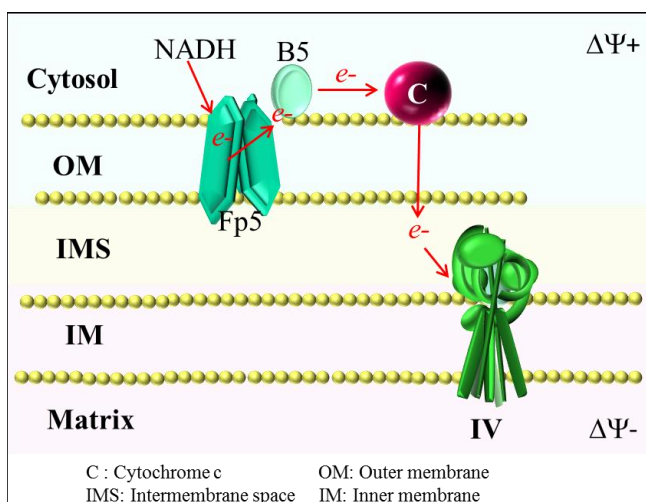


Figure 8.3 Mitochondria maintain function following cytochrome c release

Intermembrane cytochrome c can pass electrons directly to complex 4 thereby reducing complex 1 mediated ROS. Complex 4 becomes responsible for maintaining $\Delta\Psi_m$.

The activity of employing intermembrane cytochrome c to pass electrons directly to complex IV may have tissue specific restrictions. The retinal phenotype of *Opa1*^{Q285STOP} mouse is age related

with symptoms beginning from 12 months. As mouse maturation rate is 25 times faster (Flurkey et al. 2007b, a) than human at this age, the presentation of advanced pathologies may not be surprising. Figure 8.4 shows the mouse aging process in relation to human aging with maturation rate equivalents.

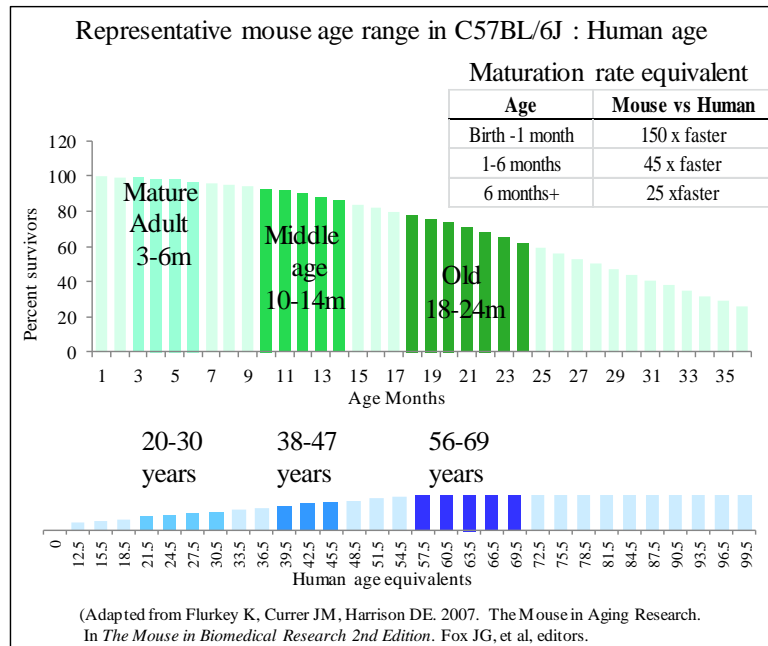


Figure 8.4 Representative mouse age range in C57BL/6 with human age equivalents

*Mouse age in months and its relation to human age in years. As mouse maturation is 25 times faster than human at 12 months, the accelerated pathology of *OPAI* mutation can be expected.*

The preservation of complex ratios in Het CNS might explain how faced with significant reductions in bioenergetic activity Het mouse remained in good health. The preservation of ratios in complexes II and IV might suggest that complex I mediated impairment acts as the trigger mechanism for altering the threshold of the other components in the chain. The provision of a voluntary running saucer may have provided a mitochondrial advantage to middle aged Het mouse (Iqbal et al. 2013; Fealy et al. 2014; Zhang et al. 2014). The modest fat content of mouse diet also conferred advantages to maintaining mitohormesis (Bosma 2014; Feillet-Coudray et al. 2014). Table 8.1 shows a summary of the ratios of individual complexes and the tissues they were associated with.

CI	B	SC	Ret
WT	29	38	33
Het	45	33	22
CII	B	SC	Ret
WT	21	23	56
Het	21	19	60
CIV	B	SC	Ret
WT	41	30	29
Het	43	42	15

Table 8.1 Ratios of complex activity and tissue association

Table shows a summary of the ratio of individual complexes in each tissue. Complex I activity was highest in spinal cord, complex II was highest in retina and complex IV was highest in brain.

8.2.1 Spectrum of human bioenergetic anomalies in ADOA Plus syndrome

Bioenergetic analysis in human ADOA has been performed on isolated lymphocytes where patients with normal vision showed an increased complex II and III activity with increased complex IV proteins. Reduced OPA1 impairs ETC efficiency, but compensation through increased distal complexes activity may preserve mitochondrial ATP production in patients who maintain normal vision (Van Bergen et al. 2011). Cell culture of human skeletal muscle biopsy showed a deficiency in complex I mediated bioenergetics (Lodi et al. 2004). This was in agreement with findings. Fibroblasts from ADOA individuals showed reduced complex I activity and demonstrated the association between Opa1 and complexes I, II and III but not IV (Zanna et al. 2008).

8.3 Resveratrol therapy in *Opa1*^{Q285STOP} mouse

The administration of resveratrol to *Opa1*^{Q285STOP} mouse from conception to 15 months revealed a reduction of brain and cardiac weight ratio in female Het. This further compounded neuromuscular testing as weight can have a significant impact on performance. SHIRPA analysis revealed that sensory function in res Het was significantly more impaired compared to untreated Het. Resveratrol treated Het mice demonstrated a reduced fear response and thus showed enhanced cognitive function through investigation and discrimination ratios compared to untreated Het mice.

Chapter 8 Discussion of Opa1^{Q285STOP} mouse model

8.3.1 Spectrum of bioenergetic dysfunction in res treated Opa1^{Q285STOP} compared to WT

The administration of resveratrol to Het mouse restored the activity of complex I to 20% higher than that of WT. Complex IV activity was 10% higher than that of untreated WT but complex II mediated activity was 47% less than WT. Untreated Het complex II activity was reduced by 59% therefore resveratrol did not confer any advantage. As previously discussed, untreated Het maintained the correct ratio of bioenergetic activity, notably the retinal mitochondria showed over 60% complex II specific activity. This was also observed in veh Het retinal mitochondria. Therefore the findings of SHIRPA in res Het were confirmed. The bioenergetic activity in retinal mitochondria of res Het favoured complex IV activity. This clearly did not confer any functional advantage as res Het sensory function was over 500% higher than untreated Het.

The antioxidant activity in res treated Het was examined. Mitochondrial MnSOD showed a significant 83% higher activity compared to untreated WT. Considering that untreated Het had a 76% reduction; this greatly enhanced activity can be expected to generate a significant amount of ROS. Figure 8.5 shows the mitochondrial environment of WT, Het and res Het demonstrating the significant ROS enhanced environment initiated by resveratrol.

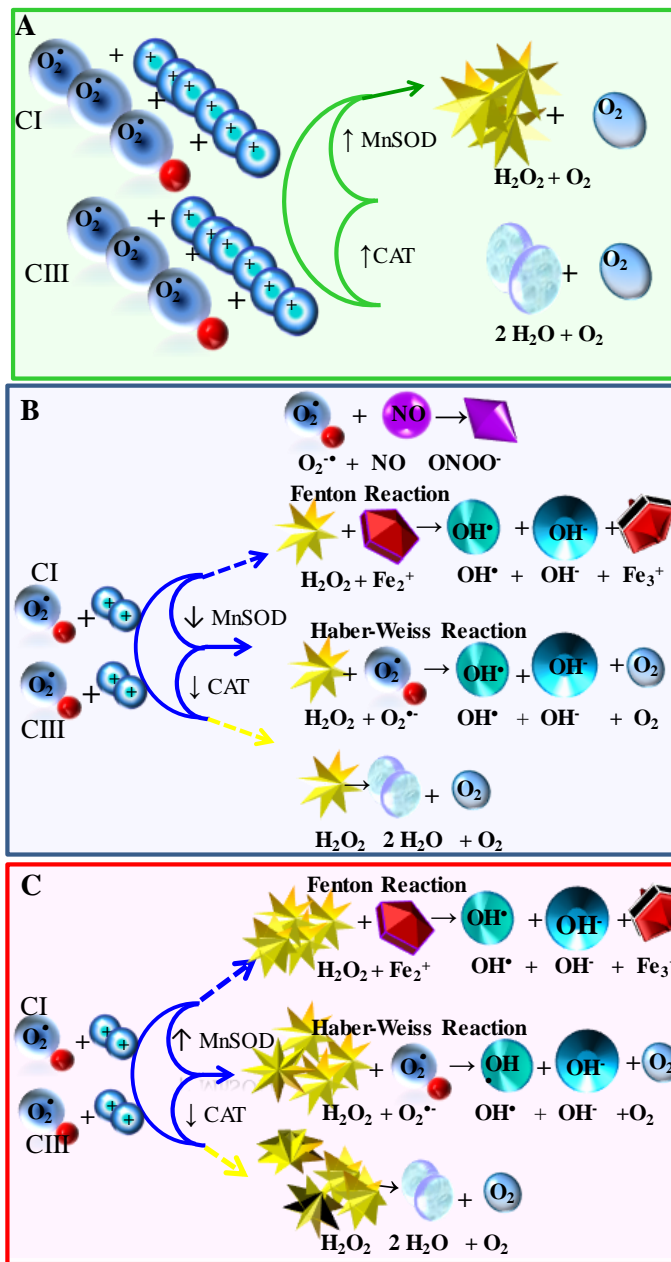


Figure 8.5 Schematic of the mitochondrial environment in WT and Het

WT (A) production of excess superoxide ($O_2^{\bullet -}$) from complexes I and III are dismutated by MnSOD. This results in the production of H_2O_2 and O_2 . Catalase decomposes H_2O_2 to H_2O and O_2 . Het (B) shows reduced superoxide production due to reduced activity of complex I (and potentially complex III). The reduced MnSOD can dismutate a modest amount of $O_2^{\bullet -}$ to H_2O_2 and O_2 . Reduced catalase decomposes some H_2O_2 but the remainder allows further generation of radicals with transition metals (Fenton reaction). (C) Res Het has excess MnSOD which dismutates $O_2^{\bullet -}$ rapidly producing an excess of H_2O_2 . Resveratrol did not enhance catalase activity, thus allowing a higher concentration of H_2O_2 in Het mitochondria that previously found to generate even more radicals.

8.3.1.1 Resveratrol induced mitochondrial alterations in res Het mouse

The dose dependency of resveratrol is critical. Specific dose response effects of resveratrol in isolated cell populations have been performed (Hofer et al. 2014). At concentrations of $75\mu\text{M}$ and less, resveratrol enhanced the production of complex I, complex II and complex VI. It also increased the concentration of VDAC and TIM22 import channel. At concentrations of $100\mu\text{M}$ and higher, the reverse effects were observed. In the presence of resveratrol at a concentration of $50\mu\text{M}$, neuronal cell response to stress resulted in increased mTOR phosphorylation and

Chapter 8 Discussion of Opa1^{Q285STOP} mouse model

increased AMPK activation. Resveratrol increased the electron transfer supercomplex rather than individual complexes (Hofer et al., 2014).

Cytochrome P450 is mono oxygenase that catalyses several reactions involved in drug metabolism. CYP3A4 is a member of the cytochrome P450 family. It localises to the ER and its expression is induced by glucocorticoids. Mitochondrial P450 employ adrenodoxin reductase to transfer electrons from NADPH to P450. Resveratrol inhibits CYP3A4 which could potentially increase the bioavailability and toxicity of other drugs (Piver et al. 2001; Regev-Shoshani et al. 2004). This may explain the effects of 0.1% ethanol content in resveratrol therapy.

Resveratrol has antioxidant properties which include the ability to scavenge O_2^{\bullet} and metal induced radicals (Martinez and Moreno 2000; Leonard et al. 2003; Losa 2003; Yen et al. 2003). Resveratrol also exhibits pro oxidant effects including lipoperoxidation (Martins et al. 2013), and DNA damage (Rahman et al. 1990). Resveratrol had been reported to reduce catalase activity in rats (Skrajnowska et al. 2013). In isolated cardiomyocytes, catalase activity was reduced in the presence of H_2O_2 (Movahed et al. 2012). This suggested that resveratrol was unable to initiate up regulation of catalase production in the face of increased H_2O_2 .

The resveratrol induced increase in MnSOD activity has been established (Robb et al. 2008a; Robb and Stuart 2014). More recently, the effects of resveratrol on the expression level of CuZnSOD mRNA and catalase mRNA demonstrated significant inhibitory activity (Yang et al. 2013).

The pathogenic effects of excess H_2O_2 can have further downstream effects. The transient receptor potential canonicals (TRPC) are cationic channels consisting of two subfamilies divided on their structure. The activation of TRPC5 is H_2O_2 dependent and modulated by catalase. Catalase provides a protective role in brain mitochondrial function (Nazıroğlu 2012). The presence of H_2O_2 activates TRPC which responds by opening a non-specific cation channel leading to increased calcium influx. The oxidative stress induced calcium stimulated mitochondrial uptake is modulated by catalase. TRPC5 is also implicated in hippocampal neurite outgrowth (Strübing et al. 2001) and the associated AHN (adult hippocampal

Chapter 8 Discussion of Opa1^{Q285STOP} mouse model

neurogenesis) (Greka et al. 2003). TRPC5 in the amygdala is also responsible for fear conditioning (Riccio et al. 2009) and regulates the inborn fear response behaviour. This behavioural response was noted to be reduced in resveratrol treated Het population who performed tight rope and narrow beam tests. Resveratrol has been identified as an inhibitor of TRPC5 which is independent of its antioxidant capabilities (Naylor et al. 2011). At concentrations of between 4-30µM, resveratrol inhibited TRPC5 in a sustained fashion. By either increasing catalase production or reducing H₂O₂, the detrimental effects observed in res treated Het physical phenotype began to explain themselves.

8.4 Spectrum of phenotypic anomalies in C57Bl/6 WT mouse

If a very brief summary of res WT mouse phenotype was required, it would be accurate to say that C57Bl/6 WT exhibited almost identical *In Vivo* and *In Vitro* pathologies. There were some significant differences in res WT which included a substantial increase in body weight combined with a significant reduction in brain weight and cardiac weight ratio. Their *In Vivo* neuromuscular performance was not significantly different compared to untreated Het with reduced latency on rotarod which allowing for body weight suggested impaired neuromuscular function. They also exhibited a reduced fear response but not to the extent as res Het as the percentage reduction compared to untreated WT was statistically higher than that of res Het.

8.4.1 Spectrum of bioenergetic dysfunction in C57Bl/6 WT

Res treated WT bioenergetic profile for complex I activity showed a 63% reduction in activity compared to untreated WT. Untreated Het had a 64% reduction. Complex II activity was reduced by 44% in res WT and 59% in untreated Het. Complex IV activity was reduced by 18% in res WT and 22% in untreated Het. The only important interpretation from this data that can be inferred is that res WT mitochondria were doing whatever was necessary to maintain function in a deleterious environment. As is happened to be identical to untreated Het was not a coincidence.

Clearly untreated Het are compensating for impaired fusion from the time of conception. Het mouse has a normal possibly extended lifespan (personal observation) despite their reduced

Chapter 8 Discussion of Opa1^{Q285STOP} mouse model

mitochondrial fusion abilities. As this is a congenital mutation, it is possible that compensatory changes are initiated as part of a postnatal adaptation mechanism (Escobar et al. 2013).

Despite the bioenergetic dysfunction observed in res WT, the ratio of complex II activity was preserved in retinal mitochondria. The ratio of complex I was not preserved for spinal cord but for brain. The ratio of complex IV was not preserved for brain but retina. This alteration in complex mediated tissue specific activity is possibly why their neuromuscular performances were impaired.

Resveratrol has been reported to have an adverse effect in hippocampal neurogenesis. Administration of resveratrol and adverse hippocampal neurogenesis was first reported in 2012 (Park et al. 2012). At a concentration of 10mg/kg, the activation of AMPK results in reduced proliferation and survival of neural progenitor cells in the dentate gyrus of the hippocampus. Reduced brain derived neurotrophic factor (BDNF) in the hippocampus of mice results in impaired neurogenesis (Lee et al. 2002; Duan et al. 2003). Resveratrol reduced BDNF in a dose dependent manner. Resveratrol down regulates phosphorylated cyclic AMP (cAMP) response element binding protein (pCREB) (Kim et al. 2010). The requirement of pCREB in spatial learning and memory is well established (Nagakura et al. 2002; Martel et al. 2006; Porte et al. 2008). Resveratrol activates SIRT1 whether directly or indirectly. Enhanced SIRT1 activity can impair and prevent adult neural precursors from differentiating into neurons (Saharan et al. 2013). This suggests SIRT1 is a negative regulator of neuronal differentiation. There are two regions in brain that are capable of generating new neurons – the subventricular zone and the dentate gyrus (Spalding et al. 2013). Many factors affect adult hippocampal neurogenesis (AHN) including environmental enrichment (Kempermann et al. 1997; van Praag et al. 1999). Aging, stress and anxiety all have detrimental effects (Prickaerts et al. 2004; Mirescu and Gould 2006). Given that the untreated Het population had identical bioenergetic dysfunction compared to res treated WT, it would appear the provision of a running saucer provided more beneficial support to Opa1^{Q285STOP} mouse than the administration of resveratrol (Nishijima et al. 2013). Figure 8.6 summarises the percentage difference observed in untreated Het, res Het and res WT when compared to untreated WT.

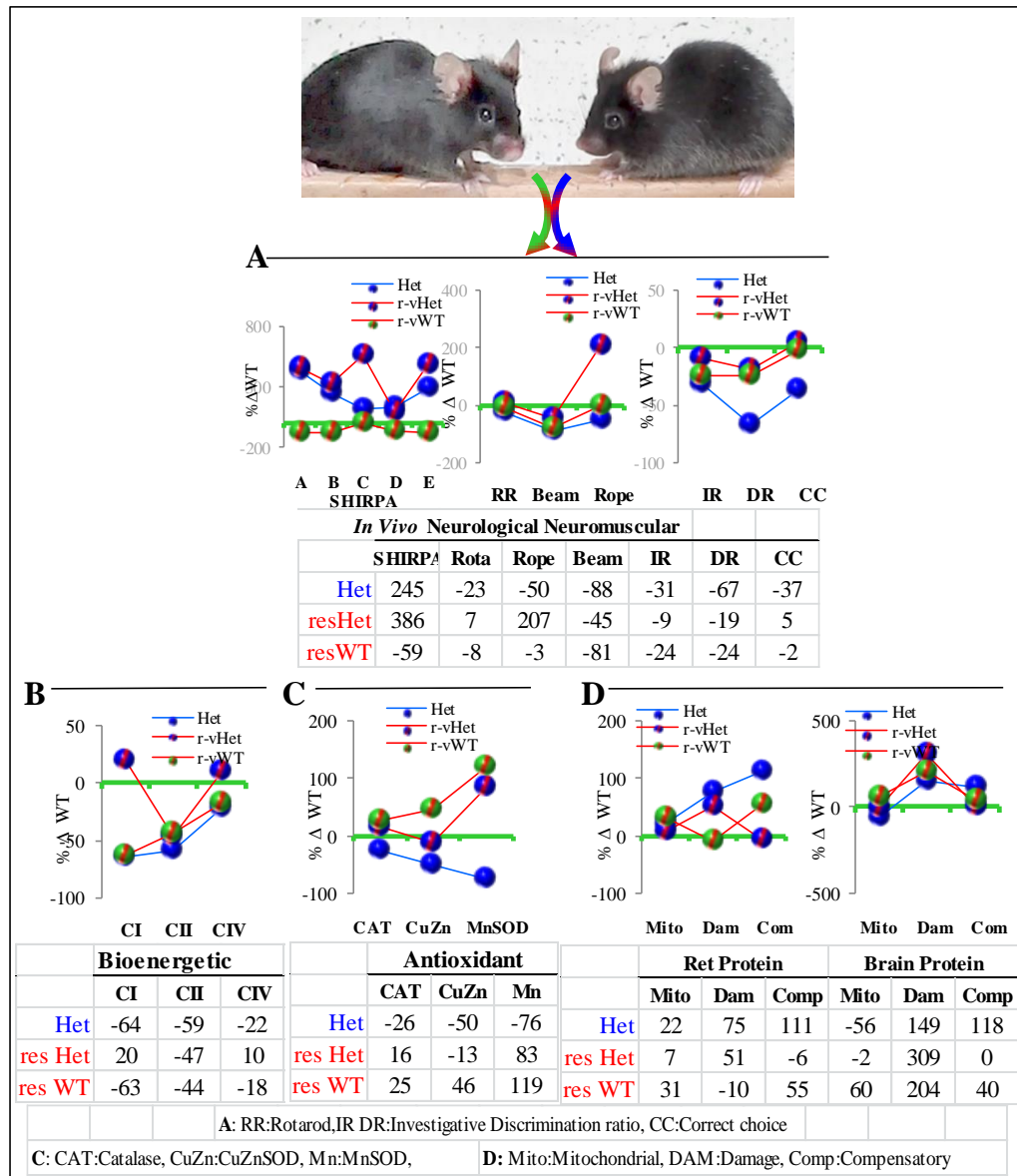


Figure 8.6 Summary of Untreated, res and WT treated mitochondrial profiles

This flow chart shows line graphs of the percentage difference observed in untreated Het, res Het & WT when compared to untreated WT. (A) shows the results of neuromuscular testing SHIRPA, rotarod, tight rope and narrow beam. (B) shows bioenergetic activity. (C) shows antioxidant activity. (D) shows the protein expression profiles in retina and brain.

8.5 Conclusions on resveratrol as a therapy for Opa1^{Q285STOP} mouse

With the benefit of hindsight, the potential to augment the effects of resveratrol delivered as an ethanol based therapy with P450 (CYP3A4) inhibition (Piver et al. 2001; Lu et al. 2013), would now appear perilous in the face of fusion deficiency. The bioavailability of resveratrol following ingestion is dependent on the availability of sulfatases. Resveratrol is metabolised into glucuronides and sulfates of resveratrol. Steroid sulfatases deconjugate resveratrol sulfates at the required time or location. Meanwhile, resveratrol can be transported as a stable sulfate conjugated complex in plasma (Patel et al. 2013). This now suggests that resveratrol may have a cumulative effect.

Administration from before the age of retinal phenotype onset (~10 months) may prove more instrumental in preservation of mitochondrial bioenergetics. However, resveratrol does not have a role in the therapy of any retinal disease. Complex II activity is highest in the retinal mitochondria. Resveratrol specifically reduced the activity of complex II in both WT and Het mice. Therefore it must be considered that it offers no advantage to Opa1^{Q285STOP} mouse.

8.6 Implications for novel therapy in Opa1^{Q285STOP} mouse

Opa1^{Q285STOP} mouse model of ADOA represents a late onset 'Plus' model of disease. From 12 months, mouse vision deteriorates with respect to retinal function. The reason for this deterioration must be found in the mitochondria that serve a more immediate purpose. A reduction in mitochondrial fusion would be expected to result in reduced $\Delta\Psi_m$. However if the population of mitochondria are physically small, the $\Delta\Psi_m$ threshold may be simultaneously reduced. This will influence mitophagy which targets mitochondria specifically with reduced $\Delta\Psi_m$. Reduced complex I activity may be a preventative measure against ROS induced mitochondrial damage. Utilizing intermembrane cytochrome c also reduces the potential for ROS. With advanced age the mechanisms maintaining Opa1^{Q285STOP} mitochondrial function becomes impaired.

Chapter 8 Discussion of Opa1^{Q285STOP} mouse model

In Opa1^{Q285STOP} mouse, the age related reduction of cytochrome c may occur prematurely. At 10 months, the reproductive life span of mouse is at an end and the natural cycle of events dictates that mouse has no more to contribute to the gene pool.

Therefore the pathology associated with Opa1 reduction might be targeted directly. Cardiolipin is responsible for holding the electron transport chain as a supercomplex (Zhang et al. 2002a; Mileykovskaya and Dowhan 2014). Cardiolipin is an anionic phospholipid found in micro domains of the IMM (Ardail et al. 1990). Preli provides the phosphatidic acid required for cardiolipin synthesis. It bonds non covalently to cytochrome c (Tyurin et al. 2007). The space between complexes III and IV is 6nm (Kurisu et al. 2001). Cardiolipin occupies the space between the supercomplexes to facilitate transfer of electrons. A reduction in cardiolipin results in alternations between the individual complex spacing and specifically results in complex 4 depletion (Ostrander et al. 2001; Bazán et al. 2013).

The Opa1: cardiolipin interaction enhances GTP hydrolysis (Ban et al. 2010). Lipid binding, GTP hydrolysis and membrane tubulation are key events in fusion. If the availability of Opa1 protein is reduced, the possibility exists that cardiolipin is reduced. Figure 8.7 shows a hypothetical schematic of Opa1 and cardiolipin interaction in WT and in Opa1^{Q285STOP} mouse. As Opa1^{Q285STOP} mouse ages, the number of available mitochondria with a WT copy of the OPA1 gene is reduced. Cardiolipin levels reach a threshold where complex IV formation becomes compromised and phenotypic changes become evident. If the complex IV subunit of the supercomplex is not present in sufficient quantity, then therapy designed to maximise its electron transfer ability may force it beyond a recoverable state.

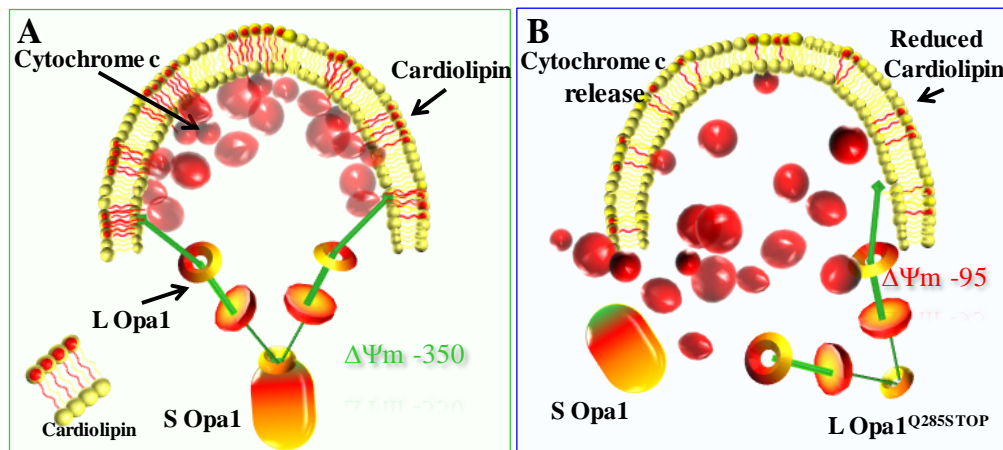


Figure 8.7 Opa1 Cardiolipin interaction

(A) Cardiolipin and Opa1 interact at the IMS enhancing GTP hydrolysis. Cardiolipin bonds non-covalently to cytochrome c assisting Opa1 in its segregation within cristae. Cardiolipin is responsible for complex IV assembly to a functional unit. (B) Reduced Opa1 combined with reduced cardiolipin resulting in poorly sequestered cytochrome c. Complex IV non assembly resulting in reduced membrane potential all trigger mitophagy in high ATP dependent cells.

8.6.1 A novel therapy for *Opa1^{Q285STOP}* mouse

Mitochondrial specific therapies designed at correcting a cardiolipin imbalance are available (Zhao et al. 2004). A peptide drug SS-31 is a Szeto-Schiller (SS) peptide that specifically targets the inner mitochondrial membrane. It selectively binds to cardiolipin through hydrophobic interaction and prevents the conversion of cytochrome c to peroxidase. SS-31 peptide has antioxidant properties in the form of a dimethyltyrosine residue (Szeto 2006). SS-31 has been used in ischemia-reperfusion injury (Cho et al. 2007), protection against neurodegeneration (Yang et al. 2009) and the prevention of insulin resistance. An improvement in the age related effects of skeletal muscle have been observed in 27 month old mouse following 1 injection (Siegel et al. 2013). Vehicle treated mice were given saline !

By considering the many functions of Opa1, addressing the possible cause of reduced ETC function in late onset ADOA may be more beneficial than targeting individual complexes. The generation of ROS in *Opa1^{Q285STOP}* mouse with a profound complex I reduction is a misconception (Ian Holt personal communication).

8.7 Conclusions on a mitochondrial profile of Opa1^{Q285STOP} mouse

This study attempted to address some of the unanswered questions regarding the disease profile in a mouse model of ADOA. It identified a range of disorders particular to the CNS whose effects were identified in the musculoskeletal, neurological, and neuropsychiatric systems. It examined aspects of the differences between the sexes. It also considered ‘environmental’ conditions, which affected the tolerance for Opa1 mutation. In view of this extended profile, Opa1^{Q285STOP} mouse model may be considered a ‘plus’ model of the disease.

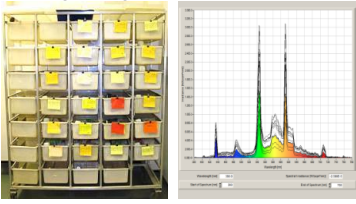
The findings supported a bioenergetic deficit as the likely cause of disease onset. The ATP content was not reduced. The ratio of complex II activity was highest in retinal mitochondria and complex II supports less equivalents of ATP production. Although there were deficits in the antioxidant system, these were homogenous across the range of tissues examined thus not indicative of a tissue-targeted disorder. The administration of resveratrol disrupted the in-built compensatory mechanisms that appear to be inherent in Opa1^{Q285STOP} mouse model. It altered the ratio of individual complex activity in specific tissues. Resveratrol did not appear to confer any mitochondrial advantage to Opa1^{Q285STOP} mouse when administered from conception to 15 months but more importantly resveratrol did not appear to damage Opa1^{Q285STOP} mouse. There was no change in the lifespan of treated Het compared to untreated Het. The retinal specific disruption of complex ratio activity indicates that resveratrol is not suitable therapy for retinal disorders.

Appendix A Lux readings from Redwood animal house

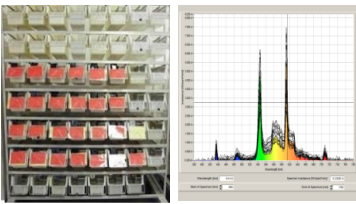
Lux readings Mouse room Redwood

		Equation $E_v = I_v D^2$, measuring distance D (m)									
		From Candela (I_v)					To Lux (E_v)				
OPTOM 2.61											
	Mouse bench	7.6	7.4	7.51		3.38	3.29	3.34			3.33
	Tissue bench	40.9	42.6	48.5		18.18	18.93	21.56			19.55
Redwood											
	Res Rack Row 1	56.5	49.7	54.4		Row 1	25.11	22.09	24.18		23.79
	Row 2	14.6	23.8	24.4		Row 2	6.49	10.58	10.84		9.3
	Row 3	7.2	8.5	18.5		Row 3	3.2	3.78	8.22		5.06
	Row 4	5.8	4.8	15.4		Row 4	2.58	2.13	6.84		3.85
	Row 5	6.8	4.8	13.5		Row 5	3.02	2.13	6		3.71
	Row 6	6.4	5.4	8		Row 6	2.84	2.4	3.56		2.93
	Row 7	6.2	4.8	8.3		Row 7	2.76	2.13	3.69		2.86
	Stock rack Row 1	39.4	17.4	31		Row 1	17.51	7.73	13.78		13
	Row 2	9.4	18.3	23		Row 2	4.13	8.13	10.22		7.49
	Row 3	8.5	6.3	7.6		Row 3	3.78	2.8	3.38		3.32
	Row 4	5.5	4.9	6.5		Row 4	2.44	2.18	2.89		2.5
	Row 5	6.3	3.6	9.6		Row 5	2.8	1.6	4.27		2.89
	Row 6	8.3	3.6	5		Row 6	3.69	1.6	2.22		2.5
	Row 7	7	2.3	6.11		Row 7	3.11	1.02	2.72		2.28
	Double rack Row 1	21.8	16.1			Row 1	9.69	7.16			8.42
	Row 2	17.4	6.8			Row 2	7.73	3.02			5.37
	Row 3	12.3	6.5			Row 3	5.47	2.89			4.18
	Row 4	11.25	9.3			Row 4	5	4.13			4.56
	Row 5	8.8	7.5			Row 5	3.91	3.33			3.62
	Row 6	7.8	6.8			Row 6	3.47	3.02			3.24
	Row 7	6.5	5.4			Row 7	2.89	2.4			2.64
	Room (door open)	78.9	30.7	44.6	118.4		35.07	13.64	19.82	52.62	30.28
	Room (door shut)	72.6	22.2	38.1	45.7		32.27	9.87	16.93	20.31	19.84
	Anteroom	149	163	163			66.0	72.2	72.4	29.3	59.98
	Rotarod Room	106.4	108.6	107.5			47.29	48.27	21.02		38.86

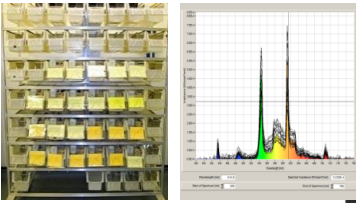
Large cages




Res cages



Stock cages





Lux readings converted from candela m^2 including wavelength spectrum of triphosphor tubes 3000k 18w warm white in place. All mouse cages were located in the same room. Top cages were not used due to the increase in lux. All other locations where mouse procedures were performed were also measured.



CERTIFICATE OF ANALYSIS 1419/11

RESVERATROL HP

Molecular Weight : 228.25
Molecular Formula : C₁₄H₁₂O₃

C.A.S.No. : 501-36-0

Batch No : 00101008

Description : slightly yellow - brownish powder

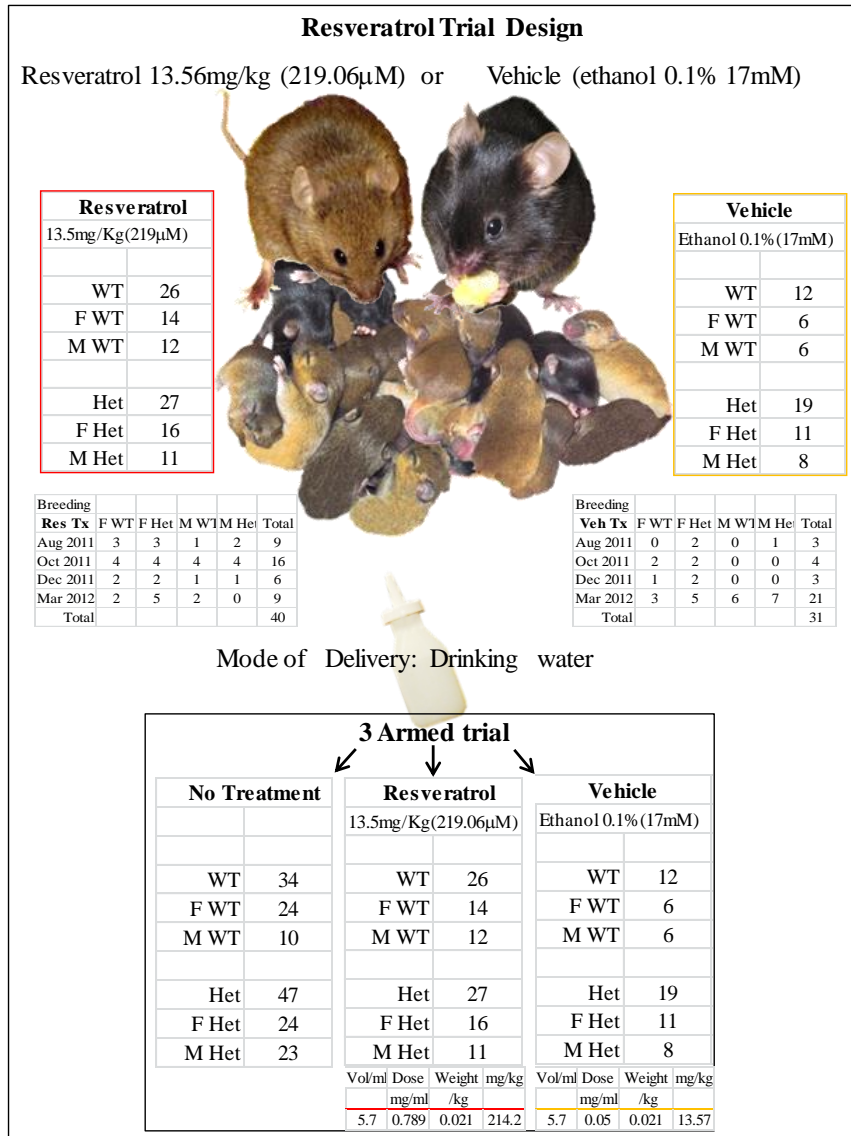
Testing :

	Actually found	Specification
trans-Resveratrol (HPLC purity)	98.8 % Area	min. 98.0 % Area
Total impurities (HPLC area %)	1.2 % Area	max. 2.0 % Area
cis-Resveratrol (HPLC)	0.1 % Area	max. 0.2 % Area
trans-Resveratrol-3-O-glucoside (HPLC)	0.1 % Area	max. 1.0 % Area
cis-Resveratrol-3-O-glucoside (HPLC)	<0.1 % Area	max. 0.2 % Area
Impurity A, unidentified RRT= 1.08 (HPLC)	0.1 % Area	max. 0.4 % Area
Impurity B, unidentified RRT= 1.11 (HPLC)	<0.1 % Area	max. 0.2 % Area
Impurity C, unidentified RRT=1.27 (HPLC)	<0.1 % Area	max. 0.2 % Area
Impurity D, unidentified RRT= 1.36 (HPLC)	<0.1 % Area	max. 0.3 % Area
Impurity E, unidentified RRT= 1.37 (HPLC)	<0.1 % Area	max. 0.5 % Area
Impurity F, unidentified RRT= 1.38 (HPLC)	0.2 % Area	max. 0.3 % Area
Impurity G, unidentified RRT= 1.47 (HPLC)	0.6 % Area	max. 1.0 % Area
Impurity H, unidentified RRT= 1.49 (HPLC)	<0.1 % Area	max. 0.2 % Area
Any other unidentified impurity (HPLC)	0.1 % Area	max. 0.1 % Area
trans-Resveratrol (HPLC assay, external calibration)	99.0 % (w/w)	96.0 - 104.0 % (w/w)
Emodin (LC-MS)	<0.01 %	max. 0.01 %
Emodin glucoside (LC-MS)	<0.01 %	max. 0.01 %
Ethanol (GC)	440 ppm	max. 5000 ppm
Loss on drying (105 °C)	0.3 %	max. 4.0 %
As	<2 ppm	max. 2 ppm
Pb	<2 ppm	max. 2 ppm
Cd	<1 ppm	max. 1 ppm
Hg	<1 ppm	max. 1 ppm

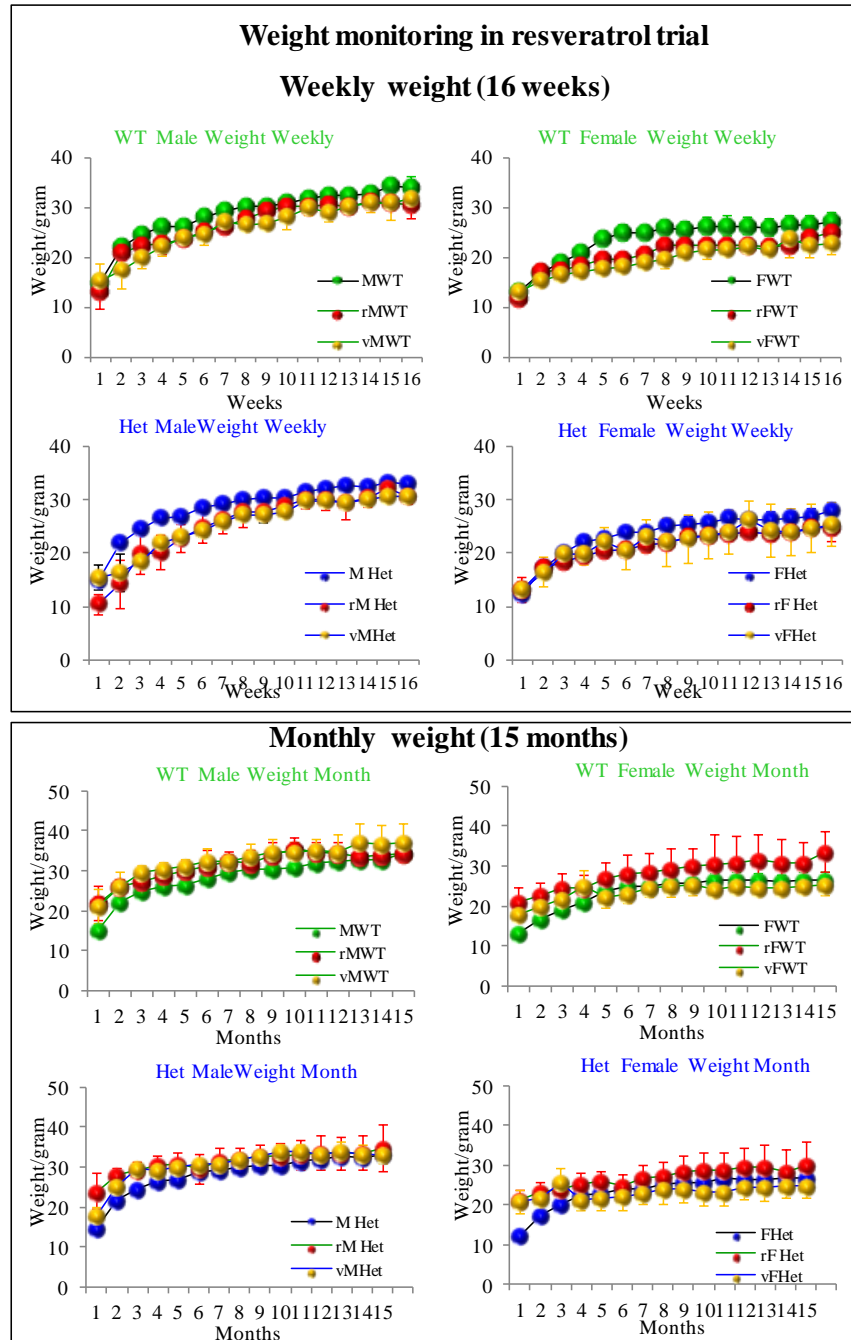
Interpharma Praha, a.s., Komofánská 955, 143 10 Praha 4 - Modřany, Czech Republic
Tel.: Secretariat: 00420-244 403 462, Switchboard: 241 773 214, Fax: 241 773 235
E-mail: interpharma@interpharma-praha.cz, www.interpharma-praha.com

A copy of the original specification number R05 for resveratrol HP (high purity)

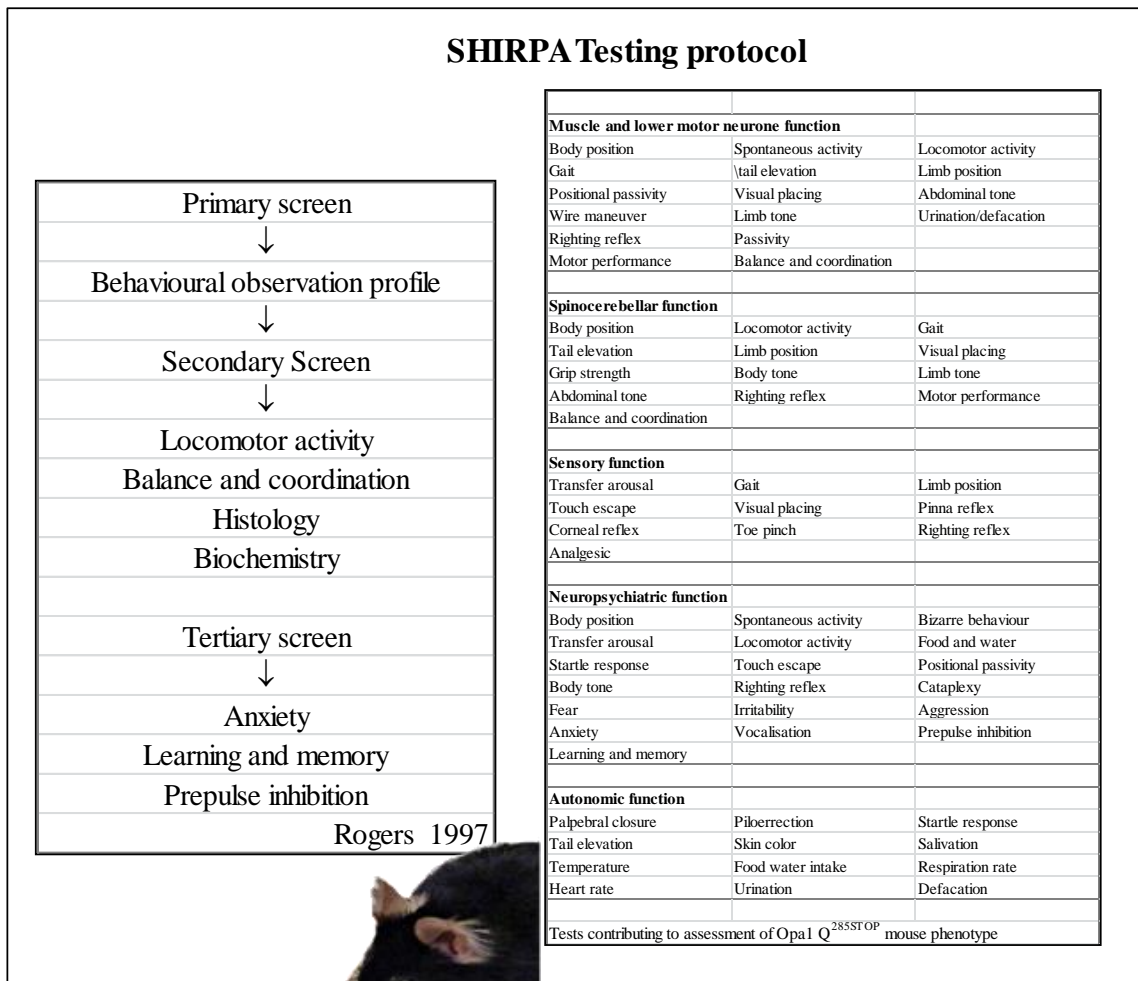
Appendix C Resveratrol Trial Design



Resveratrol three armed trial consisted of untreated WT and Het, resveratrol treated WT and Het and vehicle treated WT and Het. There was a total of 34 untreated WT and 47 untreated Het. There was 26 res treated WT and 27 res treated Het. There was 12 veh treated WT and 19 veh treated Het.



Health monitoring in trial mice. Mice were weighed weekly from time of weaning to 16 weeks. Weight monitoring continued from week 16 on a monthly basis until 15 months. Untreated WT and Het males and females were included for comparative data collection.



SHIRPA primary screening protocol where specific functional analysis pertained to multiple test observations throughout the testing procedure.

Appendix G SHIRPA res treated WT & Het 12 months

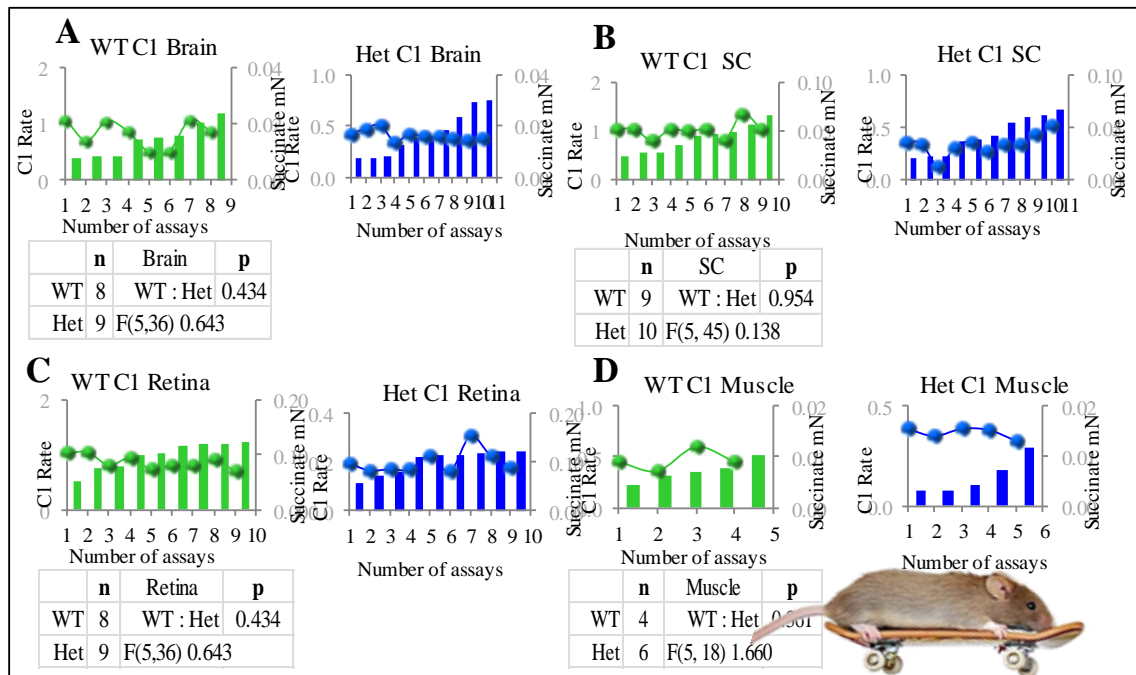
Raw data for resveratrol treated WT & Het

SHIRPA res WT & res Het 12 months															
Mouse ID	2085	2086	2072	2075	2076	2065	2083	2070	2073	2074	2072	2066			
Genotype	WT	WT	WT	WT	WT	WT	Het	Het	Het	Het	Het	Het			
DOB	22.10.11	22.09.11	21.09.11	21.09.11	19.09.11	21.09.11	21.09.11	19.09.11	21.09.11	21.10.11	19.09.11	21.10.11			
Sex	M	M	M	F	F	F	M	M	M	F	F	F			
Housing	G	G	G	G	G	G	G	G	G	G	G	G			
Weight	32g	42g	35g	26g	25g	32g	34g	32g	31g	32g	26g	24g			
Date	01.12.12	12.12.12	12.12.12	12.12.12	12.12.12	12.12.12	01.12.12	12.12.12	12.12.12	12.12.12	12.12.12	12.12.12			
Viewing Jar															
A B	Body positio	Inactive	0	0	0	0	0	0	0	0	0	0			
		Active						1		1	1	1			
		Hyperactive							2			2			
D E	Coat	Well groomed	0	0	0	0	0	0	0	0	0	0			
		Piloerection													
		Color	flecked	g	deep bl	Bl	Bl	Brown	flecked	gr	Bl	Br	deep bl	brown	Br
B D E	Defecation	Present	0		0	0	0	0							
		Absent		1					1	1	1	1	1	1	
B D E	Urination	Present	0	0	0	0	0	0		0					
		Absent							1		1	1	1		
A D E	Tremor	Present	0	0	0	0	0	0							
		Absent							1	1	1	1			
C E	Palpebral cl	Eyes open	0	0	0	0	0	0							
		Eyes closed										0			
C E	Lacrimation	Absent	0	0	0	0	0	0							
		Present													
Arena															
A B D	Transfer Ar	Extended freeze	0		0	0	0								
		Brief freeze		1				1				1			
		Immediate move							2	2		2			
A B	Gait	Fluid	0	0	0	0	0	0	1	Heel wear	legs	0	0		
		Other													
A B E	Tail elevatio	Dragging	0	0	0	0	0	0		0	0				
		Horizontal							1			1			
		Straub tail													
A B E	Pelvic eleva	Less than 5mm	0	0	0	0	0	0			0	0			
		more than 5mm							1	1		1			
C D E	Startle respi	None	0	0	0	0	0	0				0			
		(Backward Preyer flick							1	1	1	1			
C D E	Touch escap	No response	0		0	0	0	0				0			
		Response		1					1	1	1	1			
		Flees prior to													
Above Arena															
A B E	Position	Tail hold	0	0	0	0	0	0	0	0	0				
		Scruff hold													
		supine													
		no struggle													
A B E	Trunk curl	Absent	0	0	0	0	0	0	0	0		0			
		Present									1	1			
A B E	Limb graspi	Absent	0	0	0	0	0	0	0	0					
		Present									1	1			
C D E	Pinna reflex	Present	0	0	0	0	0	0	0	0	0	0			
		Absent													
C D E	Corneal refl	Present	0	0	0	0	0	0	0	0	0	0			
		Absent													
A B E	Contact right	Present	0	0	0	0	0	0	0	0	0	0			
		Absent													
C E	Evidence bi	None	0	0	0	0	0	0	0	0	0	0			
		Attempted													
C D	Vocalisator	None	0	0	0		0	0		0		0			
		Vocal				1			1		1	1			



Different observations of mouse behavior were categorized in one of five 'functions' designed to identify anomalous behavior in more than one category. In both res WT and res Het there were three males and three females. The individual SHIRPA scores of 6 resveratrol treated WT and 6 resveratrol treated Het mice are shown

Appendix H Succinate content in complex 1 assay WT and Het



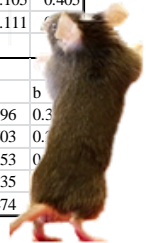
Individual histograms of succinate concentration with line graphs of rate of NADH oxidation in isolated mitochondria from WT and Het brain (A), spinal cord (B) retina (C) and skeletal muscle (D). Mitochondria were suspended in storage buffer for a maximum time of 30 minutes at 4°C prior to assay for complex I. These graphs showed that the succinate content did not adversely affect the assay of complex I activity

Appendix

Appendix I ETC substrate oxidation WT and Het

Calculation of substrate oxidation from line fittings

A: Complex I					B: Complex II					C: Complex IV							
Complex I Brain					Complex II Brain					Complex IV Brain							
Equation for linear regression I/A=A ₁ +B					Equation for linear regression I/A=A ₁ +B					Equation for exponential decay A ₅₅₀ (t)=A ₀ exp(-kt)+A∞							
WT	Slope	y I/c	Het	Slope y I/c	WT	Slope	y I/c	Het	Slope y I/c	WT	yo	a	b	Het	yo	a	b
1976	0.549	611.0	1970	0.360 607.5	2017	0.062	0.350	1956	0.022 0.359	1969	0.210	0.503	0.589	1977	0.367	0.408	1.000
1991	0.699	617.5	1977	0.387 598.0	1991	0.062	0.360	1977	0.031 0.366	1976	0.317	0.460	1.164	2001	0.365	0.408	1.000
1995	1.053	643.3	2001	0.360 605.2	2031	0.063	0.343	2001	0.023 0.361	1991	0.301	0.494	1.160	1970	0.288	0.484	1.161
2005	1.077	646.8	1990	0.424 604.6	1976	0.033	0.351	1955	0.028 0.361	1995	0.301	0.494	1.160	1990	0.364	0.408	0.998
2037	1.077	642.6	1993	0.512 613.6	2042	0.031	0.341	1956	0.033 0.357	2005	0.315	0.462	0.935	1993	0.365	0.434	0.998
1968	0.864	624.3	1999	0.481 615.3	1968	0.060	0.364	2040	0.018 0.352	2037	0.317	0.474	1.179	1999	0.360	0.408	0.998
2041	0.512	613.6	1955	0.392 610.6	2041	0.070	0.371	2039	0.011 0.353	1968	0.294	0.472	0.653	1955	0.354	0.408	0.989
2042	0.505	591.3	1956	0.425 605.9	2042	0.062	0.363	2039	0.018 0.353	2041	0.288	0.457	0.653	1956	0.311	0.484	0.933
			2040	0.401 606.7						2042	0.291	0.462	0.653	2040	0.361	0.408	1.000
Complex I SC					Complex II SC					Complex IV SC							
1991	1.035	662.7	1977	0.300 605.5	2024	0.060	0.340	2047	0.023 0.345	1976	0.277	0.506	0.735	1993	0.358	0.408	1.001
1976	1.000	643.9	2001	0.368 611.6	2019	0.059	0.356	2022	0.027 0.356	1969	0.359	0.383	0.696	1999	0.358	0.401	1.012
1969	1.000	642.9	1964	0.268 611.1	2026	0.063	0.365	2039	0.012 0.354	1991	0.268	0.519	0.737	2059	0.324	0.482	1.213
1995	1.049	351.3	1990	0.134 604.6	2029	0.064	0.357	2027	0.032 0.362	1995	0.361	0.383	0.696	1960	0.325	0.466	0.986
2005	1.036	631.4	1993	0.369 601.8	2031	0.060	0.342	1960	0.025 0.352	2005	0.269	0.499	0.517	1962	0.361	0.456	0.931
2037	0.852	622.8	1999	0.345 613.2	2008	0.054	0.365	1962	0.017 0.354	2037	0.291	0.494	0.734	2007	0.315	0.441	0.626
2024	0.814	622.4	2000	0.279 586.9				2059	0.012 0.356	2030	0.329	0.448	0.815	2001	0.341	0.456	0.931
2019	1.366	659.7	2022	0.343 618.8						2031	0.274	0.465	0.476	1964	0.321	0.446	0.755
2026	1.097	639.9	2047	0.334 618.9						2008	0.288	0.454	0.531	1977	0.264	0.475	0.426
2029	1.035	634.3	2039	0.426 605.3													
Complex I Retina					Complex II Retina					Complex IV Retina							
2003	1.050	653.2	1992	0.165 594.8	2003	0.061	0.349	1962	0.024 0.346	1969	0.097	0.613	0.178	1950	0.537	0.182	0.405
2018	1.035	633.0	1963	0.195 578.9	2018	0.097	0.361	1963	0.493 0.352	2023	-2.196	2.888	0.022	2022	0.490	0.232	0.276
2017	0.814	621.6	1964	0.170 596.4	2017	0.061	0.363	1964	0.493 0.352	1995	0.101	0.616	0.176	1990	0.458	0.277	0.379
1976	0.905	622.0	1977	0.305 605.2	1976	0.096	0.367	1977	0.035 0.344	2005	0.102	0.618	0.176	1993	0.537	0.195	0.365
1975	0.747	605.1	1970	0.161 582.9	1975	0.097	0.363	1970	0.034 0.334	2037	0.563	23.260	0.003	1999	0.458	0.277	0.379
1968	0.816	623.9	2007	0.169 600.6	1968	0.093	0.355	2007	0.049 0.352	1989	0.368	0.384	0.428	2000	0.604	0.112	0.402
1969	0.947	601.8	2002	0.182 606.8	1989	0.093	0.357	2000	0.039 0.352	2029	0.369	0.383	0.431	2001	0.606	0.105	0.405
2023	0.814	633.2	1981	0.226 606.2	2029	0.062	0.357	2001	0.029 0.358	2030	0.351	0.398	0.435	2002	0.602	0.111	
2036	0.707	620.3	1950	0.226 606.2	2030	0.102	0.375	2002	0.038 0.352								
Complex I Muscle					Complex II Muscle					Complex IV Muscle							
1969	0.457	598.9	1960	0.380 593.1	1969	0.037	0.361	1960	0.032 0.356	1976	0.391	0.356	0.820	1950	0.321	0.396	0.3
1976	0.599	608.2	1962	0.348 598.0	1976	0.065	0.367	1962	0.032 0.355	2008	0.361	0.390	0.653	1960	0.127	0.603	0
2008	0.362	594.7	2007	0.348 598.1	2008	0.029	0.353	2007	0.018 0.360	2018	0.379	0.362	0.734	1962	0.345	0.353	0
2018	0.905	622.0	2009	0.284 594.3	2018	0.041	0.358	2009	0.025 0.355	1969	0.411	0.348	0.836	2016	0.393	0.335	0
			1950	0.325 593.5				1950	0.031 0.358					2009	0.238	0.474	



Calculation of substrate oxidation in isolated mitochondria of WT and Het. From line fitting (A)Complex I oxidation of NADH using the absorption coefficient of NADH at 340nm 6200 M⁻¹ x cm⁻¹ at 460nm wavelength. (B) Complex II reduction of DCPIP using the absorption coefficient of 22 x 10³ M⁻¹- cm⁻¹ at 600nm wavelength. (C) Complex IV oxidation of reduced cytochrome c using the absorption coefficient of 21.1 x10³ M⁻¹ cm⁻¹ at 550nm wavelength.

Appendix J SOD inhibition of formazan formation WT and Het.

A: Brain						B: Spinal cord						C: Retina					
Total SOD Brain						Total SOD SC						Total SOD retina					
Equation for linear regression I/A=A ₁ +B						Equation for linear regression I/A=A ₁ +B						Equation for linear regression I/A=A ₁ +B					
WT	Slope y=	I/c	Het	Slope y=	I/c	WT	Slope y=	I/c	Het	Slope y=	I/c	WT	Slope y=	I/c	Het	Slope y=	I/c
2062	0.0074	0.0534	2016	0.0128	0.0681	1975	0.0015	0.0599	1962	0.0165	0.0487	2024	0.0141	0.0618	2110	0.0170	0.0628
2046	0.0058	0.0535	2011	0.0126	0.0707	1997	0.0015	0.0618	1955	0.0174	0.0469	2036	0.0144	0.0591	2111	0.0171	0.0619
2042	0.0065	0.0518	2012	0.0126	0.0666	2003	0.0014	0.0340	1964	0.0177	0.0429	2041	0.0145	0.0560	2112	0.0165	0.0879
2026	0.0060	0.0520	2028	0.0130	0.0808	2017	0.0221	0.0676	2009	0.0168	0.0667	1975	0.0146	0.0499	1964	0.0178	0.0598
2029	0.0074	0.0555	2032	0.0128	0.0783	2036	0.0230	0.0773	2010	0.0174	0.0532	2008	0.0138	0.0230	2000	0.0183	0.0597
2030	0.0083	0.0488	2033	0.0133	0.0823	2041	0.0220	0.0853	2011	0.0178	0.0414	2019	0.0152	0.0290	2009	0.0184	0.0509
						2042	0.0222	0.0373	2012	0.0176	0.0453						
Mn SOD Brain						Mn SOD SC						Mn SOD Retina					
WT	Slope y=	I/c	Het	Slope y=	I/c	WT	Slope y=	I/c	Het	Slope y=	I/c	WT	Slope y=	I/c	Het	Slope y=	I/c
2062	0.0105	0.0387	2016	0.0197	0.0555	1975	0.0221	0.0599	1962	0.0325	0.0782	2024	0.0161	0.0583	2110	0.0196	0.0672
2046	0.0132	0.0334	2011	0.0212	0.0417	1997	0.0216	0.0480	1955	0.0314	0.0721	2036	0.0168	0.0747	2111	0.0201	0.0659
2042	0.0108	0.0436	2012	0.0189	0.0474	2003	0.0215	0.0650	1964	0.0315	0.0576	2041	0.0168	0.0654	2112	0.0211	0.0878
2026	0.0134	0.0313	2028	0.0198	0.0324	2017	0.0237	0.0316	2009	0.0304	0.0420	1975	0.0222	0.0499	1964	0.0228	0.0755
2029	0.0134	0.0226	2032	0.0192	0.0367	2036	0.0222	0.0580	2010	0.0302	0.0503	2008	0.0205	0.0607	2000	0.0215	0.0630
2030	0.0132	0.0322	2033	0.0201	0.0339	2041	0.0238	0.0136	2011	0.0306	0.0420	2019	0.0205	0.0663	2009	0.0223	0.0711
						2042	0.0239	0.0102	2012	0.0301	0.0503						
CuZnSOD Brain						CuZnSOD SC						CuZnSOD Retina					
WT	Slope y=	I/c	Het	Slope y=	I/c	WT	Slope y=	I/c	Het	Slope y=	I/c	WT	Slope y=	I/c	Het	Slope y=	I/c
2062	0.0240	0.0392	2016	0.0307	0.0350	1975	0.0117	0.0490	1962	0.0149	0.0313	2024	0.0215	0.0340	2110	0.0224	0.0909
2046	0.0247	0.0323	2011	0.0297	0.0391	1997	0.0117	0.0254	1955	0.0132	0.0390	2036	0.0208	0.0597	2111	0.0221	0.0696
2042	0.0236	0.0397	2012	0.0294	0.0358	2003	0.0119	0.0401	1964	0.0149	0.0368	2041	0.0224	0.0729	2112	0.0224	0.0759
2026	0.0236	0.0397	2028	0.0278	0.0361	2017	0.0152	0.0429	2009	0.0184	0.0478	1975	0.0160	0.0475	1964	0.0196	0.0672
2029	0.0237	0.0277	2032	0.0277	0.0391	2036	0.0141	0.0732	2010	0.0185	0.0511	2008	0.0164	0.0517	2000	0.0203	0.0624
2030	0.0250	0.0393	2033	0.0297	0.0391	2041	0.0156	0.0211	2011	0.0188	0.0448	2019	0.0159	0.0379	2009	0.0200	0.0864
						2042	0.0154	0.0558	2012	0.0183	0.0477						

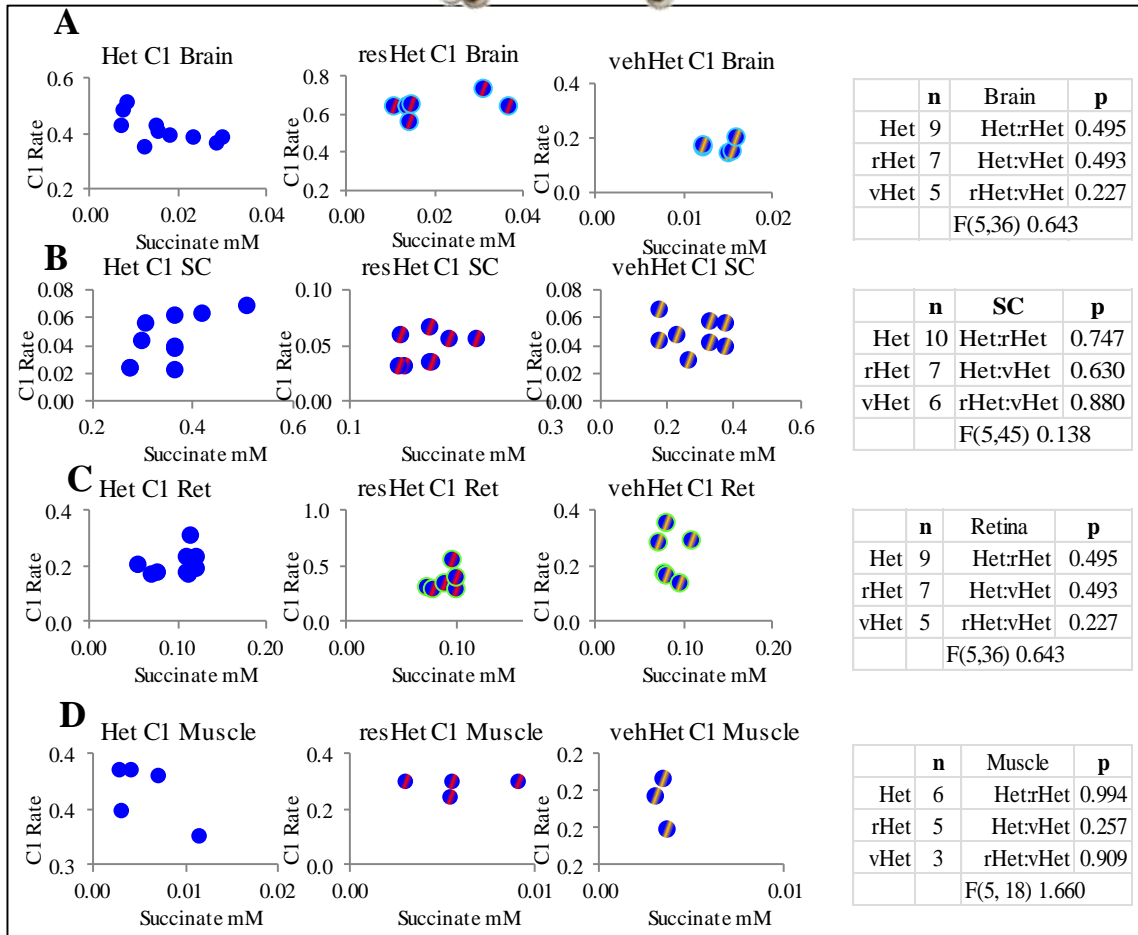


Percentage of inhibition of formazan formation were calculated from the calculation

where S1 was formazan formation with no inhibition, S2 was sample minus enzyme and S3 was diluent only with no enzyme. Specific inhibition of MnSOD or CuZnSOD allowed different subtypes to be examined in (A) Brain, (B) spinal cord and (C) retinal homogenate of WT and Het.

Appendix

Appendix K Succinate content in complex I assay Het res and veh Het

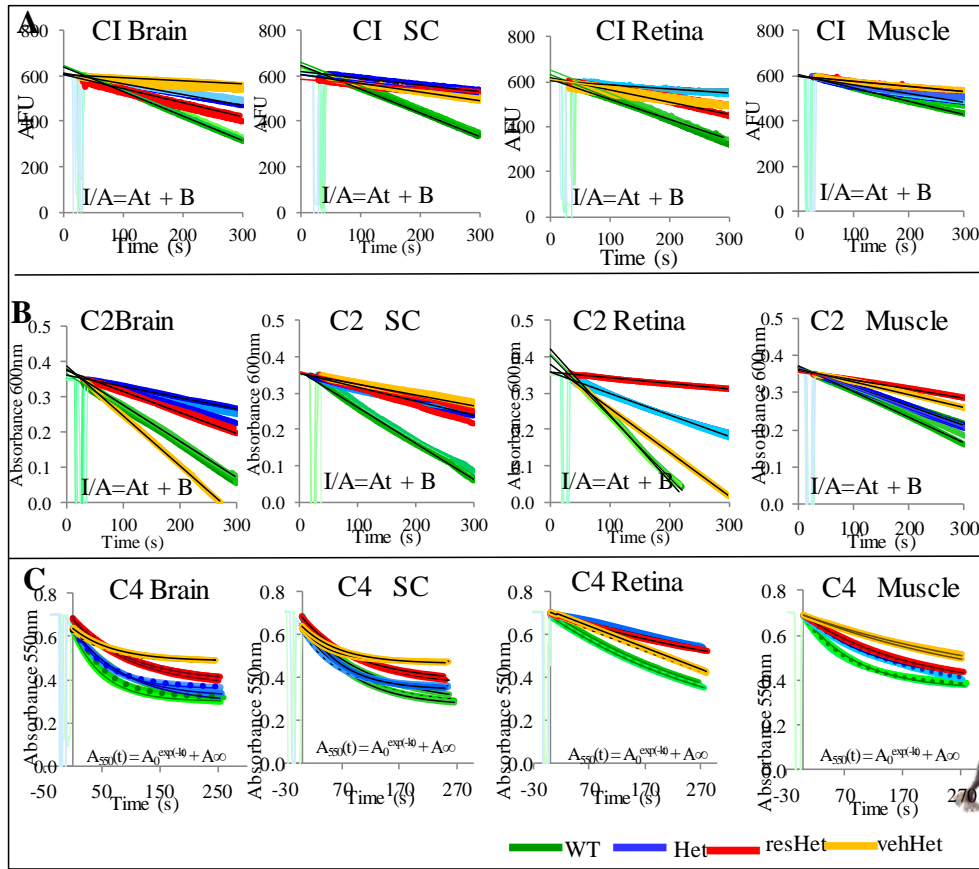


Individual histograms of succinate concentration with line graphs of rate of NADH oxidation in isolated mitochondria from Het, res Het and veh Het brain (A), spinal cord (B) retina (C) and skeletal muscle (D). Mitochondria were suspended in storage buffer for a maximum time of 30 minutes at 4°C prior to assay for complex I. These graphs showed that the succinate content did not adversely affect the assay of complex I activity

Appendix

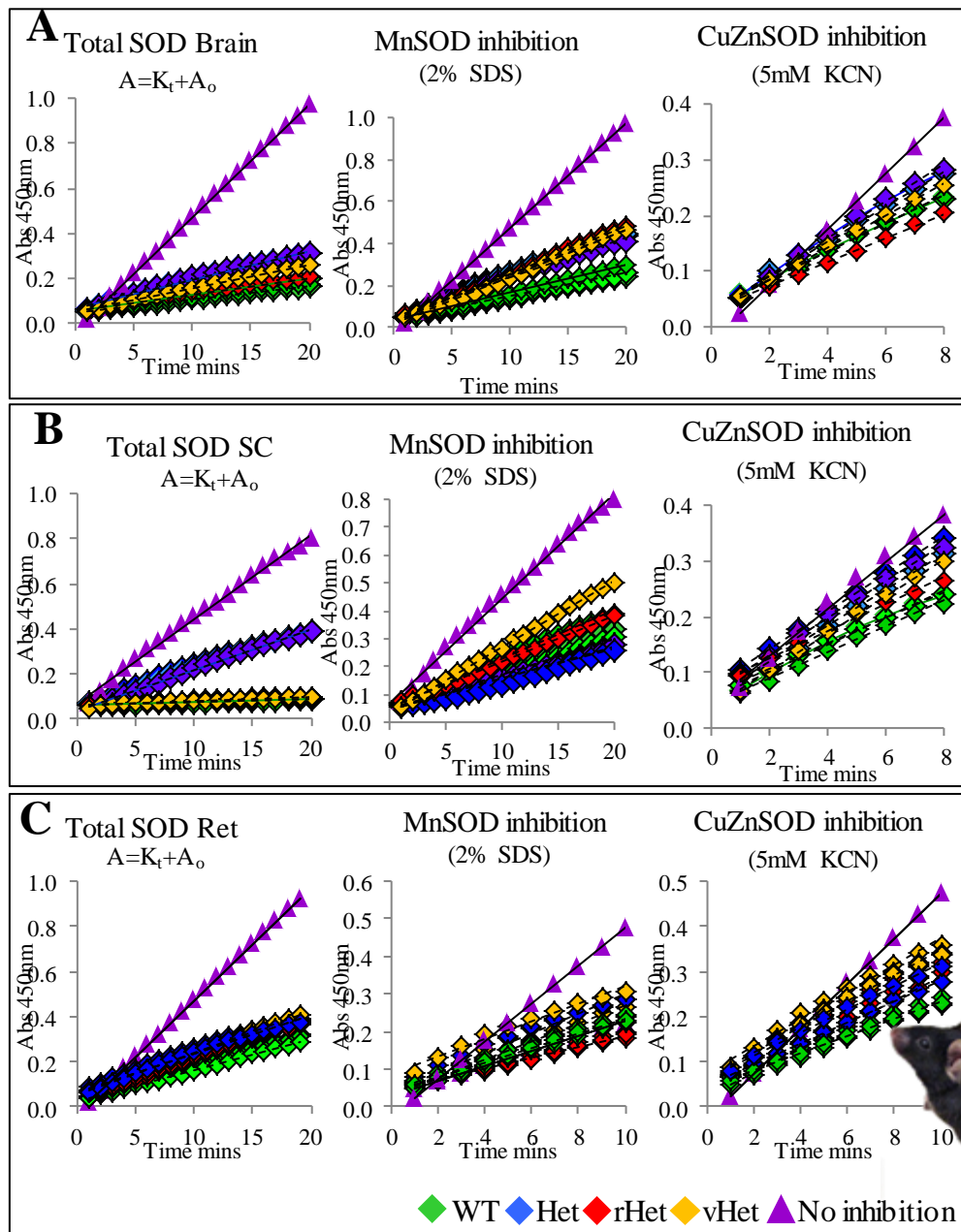
Appendix L

Kinetics of ET in isolated mitochondria of Het, res Het and veh Het



Representative kinetics of (A) complex I activity in isolated mitochondria of Het, res and veh Het at 460nm using fluorescence spectrophotometry in the presence of 30 μ g/ml mitochondria. (B) Complex II succinate dehydrogenase activity in Het, res and veh Het was followed at 600nm (C) Complex IV absorbance of reduced cytochrome c was followed at 550nm in the presence of 30 μ g mitochondrial protein.

Appendix N SOD kinetics in Het, res and veh Het tissue homogenate



Graphs show the kinetic inhibition of formazan formation in the presence of tissue homogenate from (A) brain (B) spinal cord and (C) retina of Het, res Het and veh Het. WT and control (no inhibition) is included for reference. SOD subtypes were examined using specific inhibitors for MnSOD (2% SDS) and CuZnSOD (5, M KCN)

Appendix

Appendix O SOD inhibition of formazan formation Het, res and veh Het



A: Brain

B: Spinal cord

C: Retina

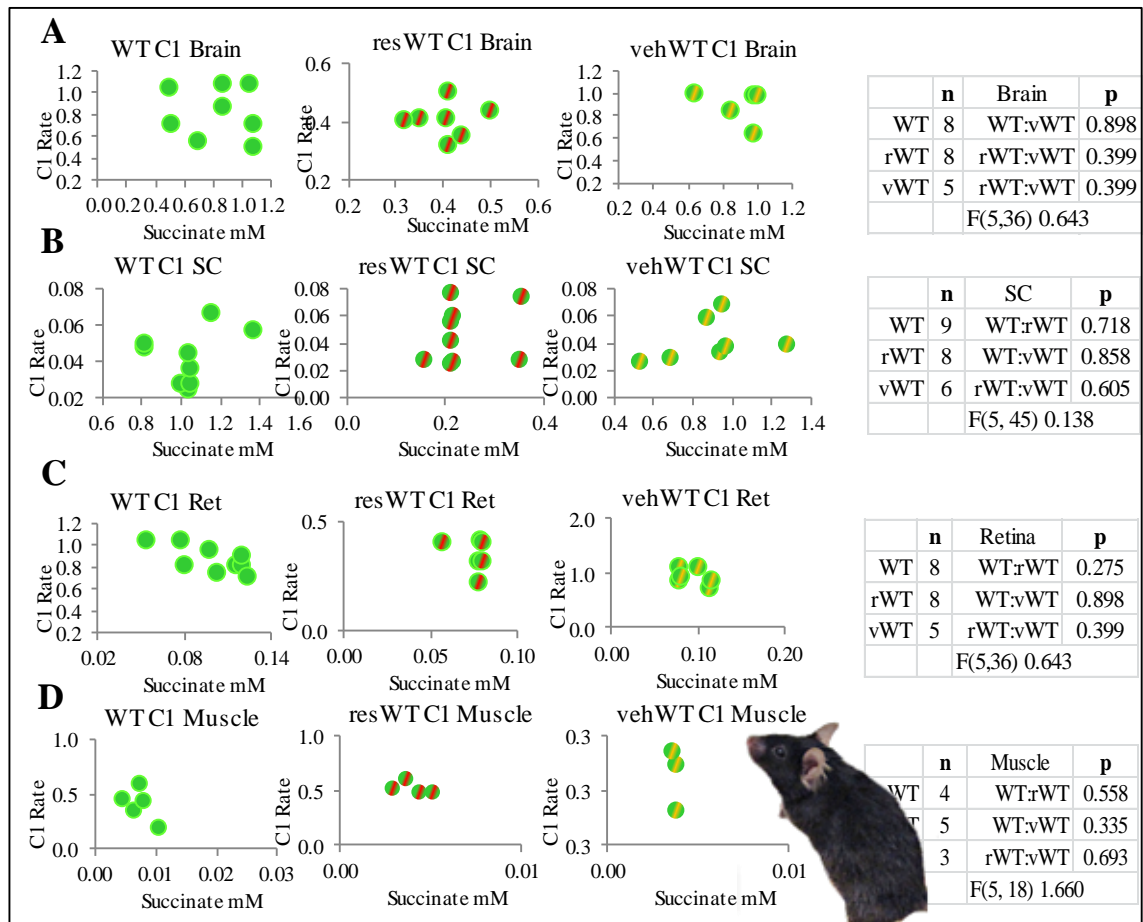
Total SOD Brain							Total SOD SC							Total SOD retina													
Equation for linear regression I/A=A ₁ +B							Equation for linear regression I/A=A ₁ +B							Equation for linear regression I/A=A ₁ +B													
Het	Slope y=I/c	rHet	Slope y=I/c	vHet	Slope y=I/c		Het	Slope y=I/c	rHet	Slope y=I/c	vHet	Slope y=I/c		Het	Slope y=I/c	rHet	Slope y=I/c	vHet	Slope y=I/c								
2016	0.0128	0.0681	2074	0.0080	0.0553	2120	0.0108	0.0489	1962	0.0165	0.0487	2073	0.0020	0.0764	2128	0.0021	0.0584	2110	0.0170	0.0628	2105	0.0185	0.0306	2128	0.0184	0.0419	
2011	0.0126	0.0707	2081	0.0077	0.0544	2121	0.0095	0.0520	1955	0.0174	0.0469	2105	0.0020	0.0842	2133	0.0023	0.0662	2111	0.0171	0.0619	2107	0.0181	0.0418	2133	0.0186	0.0547	
2012	0.0126	0.0666	2083	0.0072	0.0327	2128	0.0106	0.0710	1964	0.0177	0.0429	2107	0.0023	0.0780	2149	0.0019	0.0790	2112	0.0165	0.0879	2109	0.0170	0.0470	2149	0.0185	0.0457	
2028	0.0130	0.0808	2145	0.0080	0.0553	2138	0.0108	0.0489	2009	0.0168	0.0667							1964	0.0178	0.0598	2073	0.0188	0.0268				
2032	0.0128	0.0783	2147	0.0079	0.0522	2149	0.0102	0.0536	2010	0.0174	0.0532							2000	0.0183	0.0597	2104	0.0195	0.0659				
2033	0.0133	0.0823	2157	0.0067	0.0453	2150	0.0110	0.0534	2011	0.0178	0.0414							2009	0.0184	0.0509	2067	0.0193	0.0654				
									2012	0.0176	0.0453																
Mn SOD Brain							Mn SOD SC							Mn SOD Retina													
Equation for linear regression I/A=A ₁ +B							Equation for linear regression I/A=A ₁ +B							Equation for linear regression I/A=A ₁ +B													
Het	Slope y=I/c	rHet	Slope y=I/c	vHet	Slope y=I/c		Het	Slope y=I/c	rHet	Slope y=I/c	vHet	Slope y=I/c		Het	Slope y=I/c	rHet	Slope y=I/c	vHet	Slope y=I/c								
2016	0.0197	0.0555	2074	0.0216	0.0263	2120	0.0230	0.0150	1962	0.0325	0.0782	2073	0.0221	0.0844	2128	0.0316	0.0430	2110	0.0196	0.0672	2105	0.0134	0.0457	2128	0.0192	0.0920	
2011	0.0212	0.0417	2081	0.0230	0.0250	2121	0.0225	0.0153	1955	0.0314	0.0721	2105	0.0231	0.0558	2133	0.0322	0.0403	2111	0.0201	0.0659	2107	0.0143	0.0520	2133	0.0220	0.0859	
2012	0.0189	0.0474	2083	0.0220	0.0306	2128	0.0220	0.0156	1964	0.0315	0.0576	2107	0.0280	0.0309	2149	0.0333	0.0404	2112	0.0211	0.0878	2109	0.0137	0.0490	2149	0.0200	0.0719	
2028	0.0198	0.0324	2145	0.0222	0.0258	2138	0.0223	0.0145	2009	0.0304	0.0420							1964	0.0228	0.0755	2073	0.0152	0.0630				
2032	0.0192	0.0367	2147	0.0220	0.0308	2149	0.0220	0.0158	2010	0.0302	0.0503							2000	0.0215	0.0630	2104	0.0160	0.0520				
2033	0.0201	0.0339	2157	0.0229	0.0255	2150	0.0229	0.0155	2011	0.0306	0.0420							2009	0.0223	0.0711	2067	0.0151	0.0543				
									2012	0.0301	0.0503																
CuZnSOD Brain							CuZnSOD SC							CuZnSOD Retina													
Equation for linear regression I/A=A ₁ +B							Equation for linear regression I/A=A ₁ +B							Equation for linear regression I/A=A ₁ +B													
Het	Slope y=I/c	rHet	Slope y=I/c	vHet	Slope y=I/c		Het	Slope y=I/c	rHet	Slope y=I/c	vHet	Slope y=I/c		Het	Slope y=I/c	rHet	Slope y=I/c	vHet	Slope y=I/c								
2016	0.0307	0.0350	2074	0.0187	0.0312	2120	0.0278	0.0315	1962	0.0149	0.0313	2073	0.0151	0.0452	2128	0.0233	0.0361	2110	0.0224	0.0909	2105	0.0284	0.0554	2128	0.0278	0.0699	
2011	0.0297	0.0391	2081	0.0160	0.0306	2121	0.0279	0.0241	1955	0.0132	0.0390	2105	0.0164	0.0528	2133	0.0231	0.0524	2111	0.0221	0.0696	2107	0.0277	0.0183	2133	0.0286	0.0811	
2012	0.0294	0.0358	2083	0.0174	0.0319	2128	0.2930	0.0261	1964	0.0149	0.0368	2107	0.0158	0.0390	2149	0.0239	0.0673	2112	0.0224	0.0759	2109	0.0285	0.0318	2149	0.0285	0.0618	
2028	0.0278	0.0361	2145	0.0199	0.0404	2138	0.0307	0.0324	2009	0.0184	0.0478							1964	0.0196	0.0672	2073	0.0276	0.0587				
2032	0.0277	0.0391	2147	0.0178	0.0375	2149	0.0298	0.0305	2010	0.0185	0.0511							2000	0.0203	0.0624	2104	0.0280	0.0332				
2033	0.0297	0.0391	2157	0.0222	0.0424	2150	0.0310	0.0355	2011	0.0188	0.0448							2009	0.0200	0.0864	2067	0.0288	0.0687				
									2012	0.0183	0.0477																

Percentage of inhibition of formazan formation were calculated from the calculation

$$\{[(S1 - S3) - (SS - S2)] / (S1 - S3)\} \times 100.$$

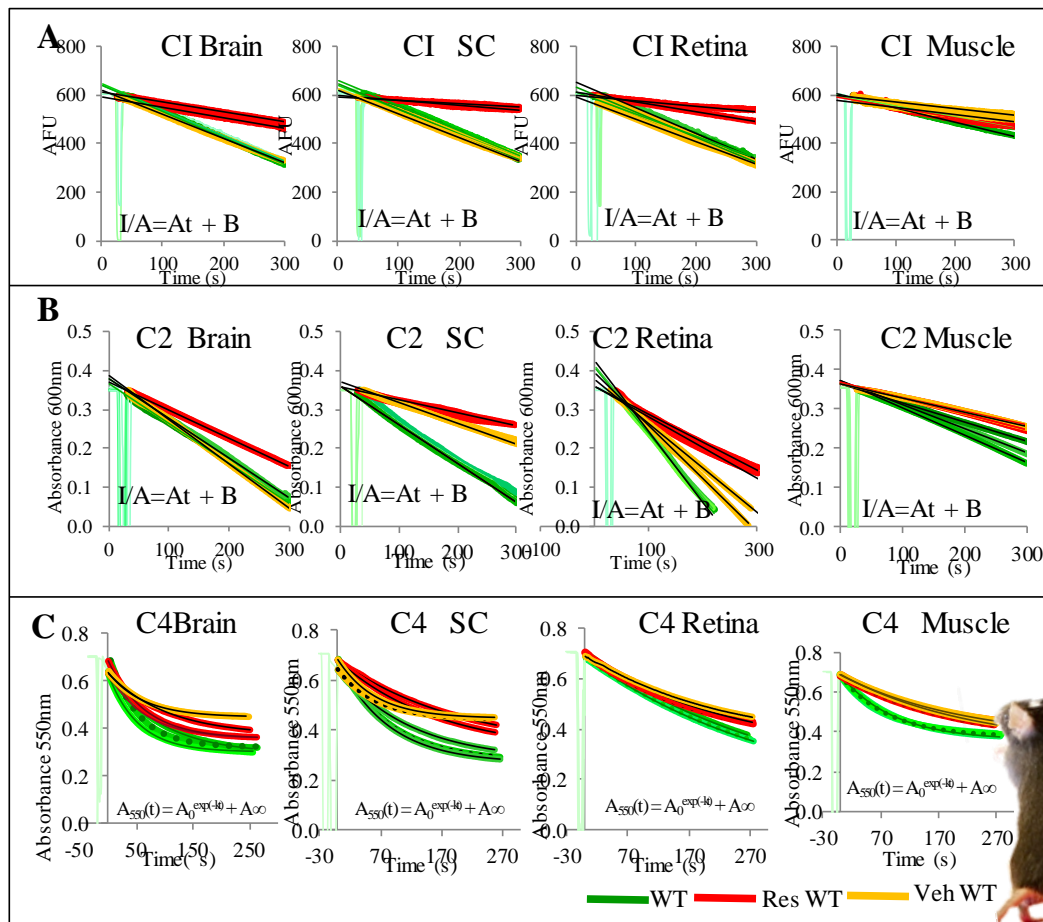
where S1 was formazan formation with no inhibition, S2 was sample minus enzyme and S3 was diluent only with no enzyme. Specific inhibition of MnSOD or CuZnSOD allowed different subtypes to be examined in (A) Brain, (B) spinal cord and (C) retinal homogenate of Het, res Het and veh Het

Appendix P Succinate content in complex I assay of WT, res and veh WT



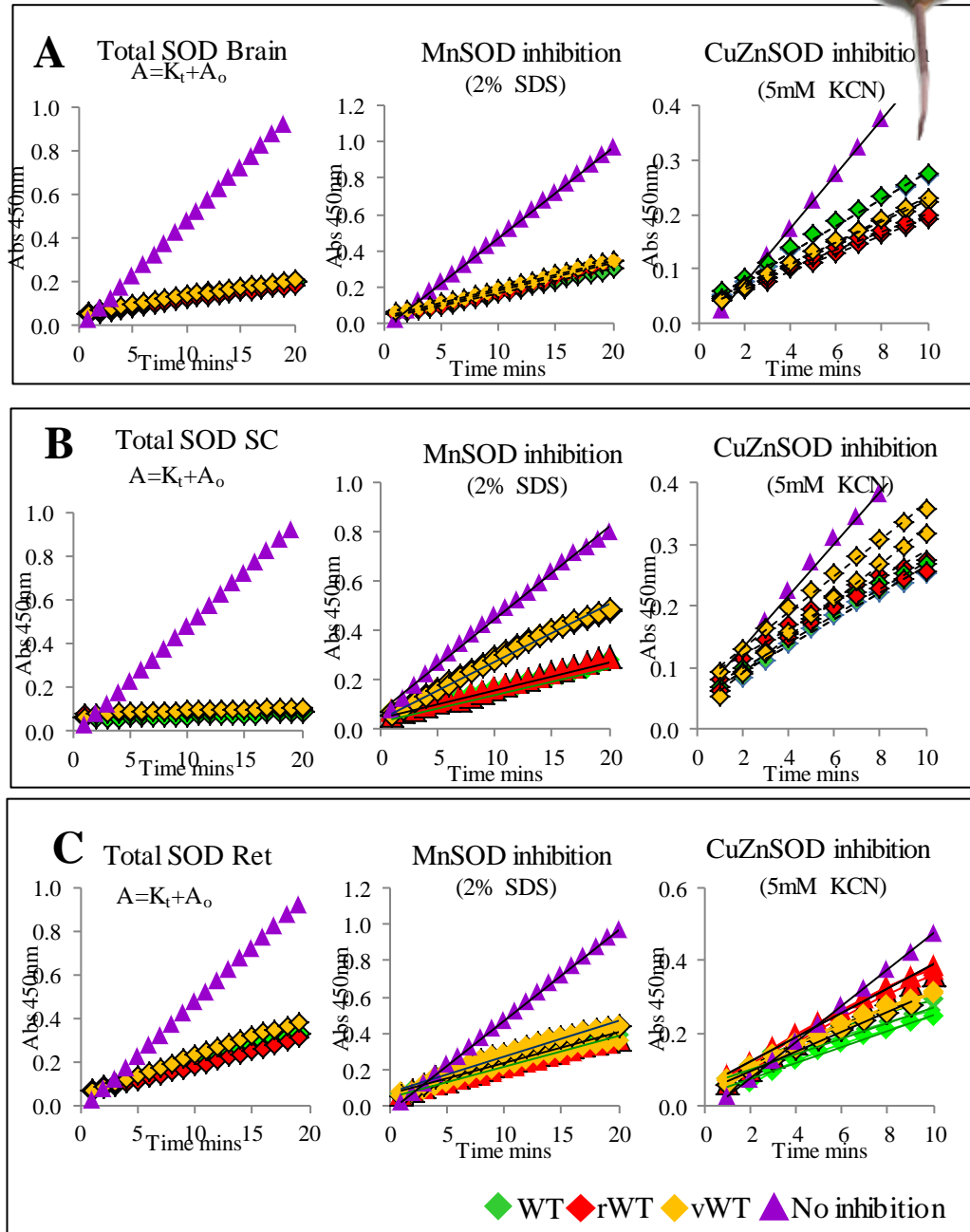
Individual histograms of succinate concentration with line graphs of rate of NADH oxidation in isolated mitochondria from WT, res WT and veh WT brain (A), spinal cord (B) retina (C) and skeletal muscle (D). Mitochondria were suspended in storage buffer for a maximum time of 30 minutes at 4°C prior to assay for complex I. These graphs showed that the succinate content did not adversely affect the assay of complex I activity

Appendix Q Kinetics of ET in isolated mitochondria of WT, res and veh WT



Representative kinetics of (A) complex I activity in isolated mitochondria of WT, res and veh WT at 460nm using fluorescence spectrophotometry in the presence of 30 μ g/ml mitochondria. (B) Complex II succinate dehydrogenase activity in Het, res and veh Het was followed at 600nm (C) Complex IV absorbance of reduced cytochrome c was followed at 550nm in the presence of 30 μ g mitochondrial protein.

Appendix S SOD kinetics in WT, res and veh WT tissue homogenate



Graphs show the kinetic inhibition of formazan formation in the presence of tissue homogenate from (A) brain (B) spinal cord and (C) retina of WT, res WT and veh WT. Control (no inhibition) is included for reference. SOD subtypes were examined using specific inhibitors for MnSOD (2% SDS) and CuZnSOD (5, M KCN)

Appendix T SOD inhibition of formazan formation in WT, res and veh WT



A: Brain									B: Spinal cord						C: Retina											
Total SOD Brain									Total SODSC						Total SOD Retina											
Equation for linear regression I/A=A ₁ +B									Equation for linear regression I/A=A ₁ +B						Equation for linear regression I/A=A ₁ +B											
WT	Slope y=	I/c	rWT	Slope y=	I/c	vWT	Slope y=	I/c	WT	Slope y=	I/c	rWT	Slope y=	I/c	vWT	Slope y=	I/c	WT	Slope y=	I/c	rWT	Slope y=	I/c	vWT	Slope y=	I/c
2062	0.0074	0.0534	2061	0.0074	0.0458	2130	0.0080	0.0540	1975	0.0015	0.0599	1988	0.0012	0.0656	2119	0.0017	0.0658	2024	0.0141	0.0618	2110	0.0145	0.0493	2144	0.0177	0.0494
2046	0.0058	0.0535	2065	0.0073	0.0566	2131	0.0076	0.0590	1997	0.0015	0.0618	2061	0.0015	0.0770	2152	0.0016	0.0750	2036	0.0144	0.0591	2114	0.0142	0.0432	2152	0.0173	0.0563
2042	0.0065	0.0518	2069	0.0066	0.0535	2139	0.0078	0.0565	2003	0.0014	0.0340	2065	0.0014	0.0731	2154	0.0016	0.0550	2041	0.0145	0.0560	2115	0.0132	0.0316	2154	0.0175	0.0566
2026	0.0060	0.0520	2146	0.0094	0.0555	2119	0.0080	0.0540	2017	0.0221	0.0676							1975	0.0146	0.0499	1986	0.0148	0.0886			
2029	0.0074	0.0555	2148	0.0082	0.0497	2125	0.0076	0.0590	2036	0.0230	0.0773							2008	0.0138	0.0230	1987	0.0148	0.0708			
2030	0.0083	0.0488	2155	0.0090	0.0525	2126	0.0090	0.0571	2041	0.0220	0.0853							2019	0.0152	0.0290	1988	0.0154	0.0493			
									2042	0.0222	0.0373															
Mn SOD Brain									Mn SODSC						Mn SOD Retina											
WT	Slope y=	I/c	rWT	Slope y=	I/c	vWT	Slope y=	I/c	WT	Slope y=	I/c	rWT	Slope y=	I/c	vWT	Slope y=	I/c	WT	Slope y=	I/c	rWT	Slope y=	I/c	vWT	Slope y=	I/c
2062	0.0105	0.0387	2061	0.0153	0.0231	2130	0.0153	0.0231	1975	0.0221	0.0599	1988	0.0215	0.0559	2119	0.0293	0.0339	2024	0.0161	0.0583	2110	0.0159	0.0529	2144	0.0164	0.0684
2046	0.0132	0.0334	2065	0.0154	0.0237	2131	0.0149	0.0218	1997	0.0216	0.0480	2061	0.0228	0.0323	2152	0.0280	0.0380	2036	0.0168	0.0747	2114	0.0160	0.0475	2152	0.0160	0.0516
2042	0.0108	0.0436	2069	0.0149	0.0218	2139	0.0154	0.0371	2003	0.0215	0.0650	2065	0.0215	0.0759	2154	0.0292	0.0739	2041	0.0168	0.0654	2115	0.0160	0.0633	2154	0.0188	0.0941
2026	0.0134	0.0313	2146	0.0149	0.0214	2119	0.0229	0.0155	2017	0.0237	0.0316							1975	0.0222	0.0499	1986	0.0143	0.0705			
2029	0.0134	0.0226	2148	0.0166	0.0245	2125	0.0217	0.0156	2036	0.0222	0.0580							2008	0.0205	0.0607	1987	0.0151	0.0520			
2030	0.0132	0.0322	2155	0.0145	0.0296	2126	0.0223	0.0125	2041	0.0238	0.0136							2019	0.0205	0.0663	1988	0.0146	0.0725			
									2042	0.0239	0.0102															
CuZnSOD Brain									CuZnSODSC						CuZnSOD Retina											
WT	Slope y=	I/c	rWT	Slope y=	I/c	vWT	Slope y=	I/c	WT	Slope y=	I/c	rWT	Slope y=	I/c	vWT	Slope y=	I/c	WT	Slope y=	I/c	rWT	Slope y=	I/c	vWT	Slope y=	I/c
2062	0.0240	0.0392	2061	0.0129	0.0318	2130	0.0207	0.0259	1975	0.0117	0.0490	1988	0.0117	0.0502	2119	0.0217	0.0578	2024	0.0215	0.0340	2110	0.0324	0.0582	2144	0.0251	0.0604
2046	0.0247	0.0323	2065	0.0168	0.0349	2131	0.0196	0.0312	1997	0.0117	0.0254	2061	0.0129	0.0373	2152	0.0214	0.0646	2036	0.0208	0.0597	2114	0.0326	0.0607	2152	0.0250	0.0654
2042	0.0236	0.0397	2069	0.0163	0.0309	2139	0.0185	0.0364	2003	0.0119	0.0401	2065	0.0116	0.0538	2154	0.0222	0.0520	2041	0.0224	0.0729	2115	0.0326	0.0392	2154	0.0252	0.0248
2026	0.0236	0.0397	2146	0.0192	0.0431	2119	0.0244	0.0113	2017	0.0152	0.0429							1975	0.0160	0.0475	1986	0.0296	0.0866			
2029	0.0237	0.0277	2148	0.0187	0.0312	2125	0.0228	0.0137	2036	0.0141	0.0732							2008	0.0164	0.0517	1987	0.0276	0.0747			
2030	0.0250	0.0393	2155	0.0192	0.0375	2126	0.0244	0.0073	2041	0.0156	0.0211							2019	0.0159	0.0379	1988	0.0254	0.0797			
									2042	0.0154	0.0558															

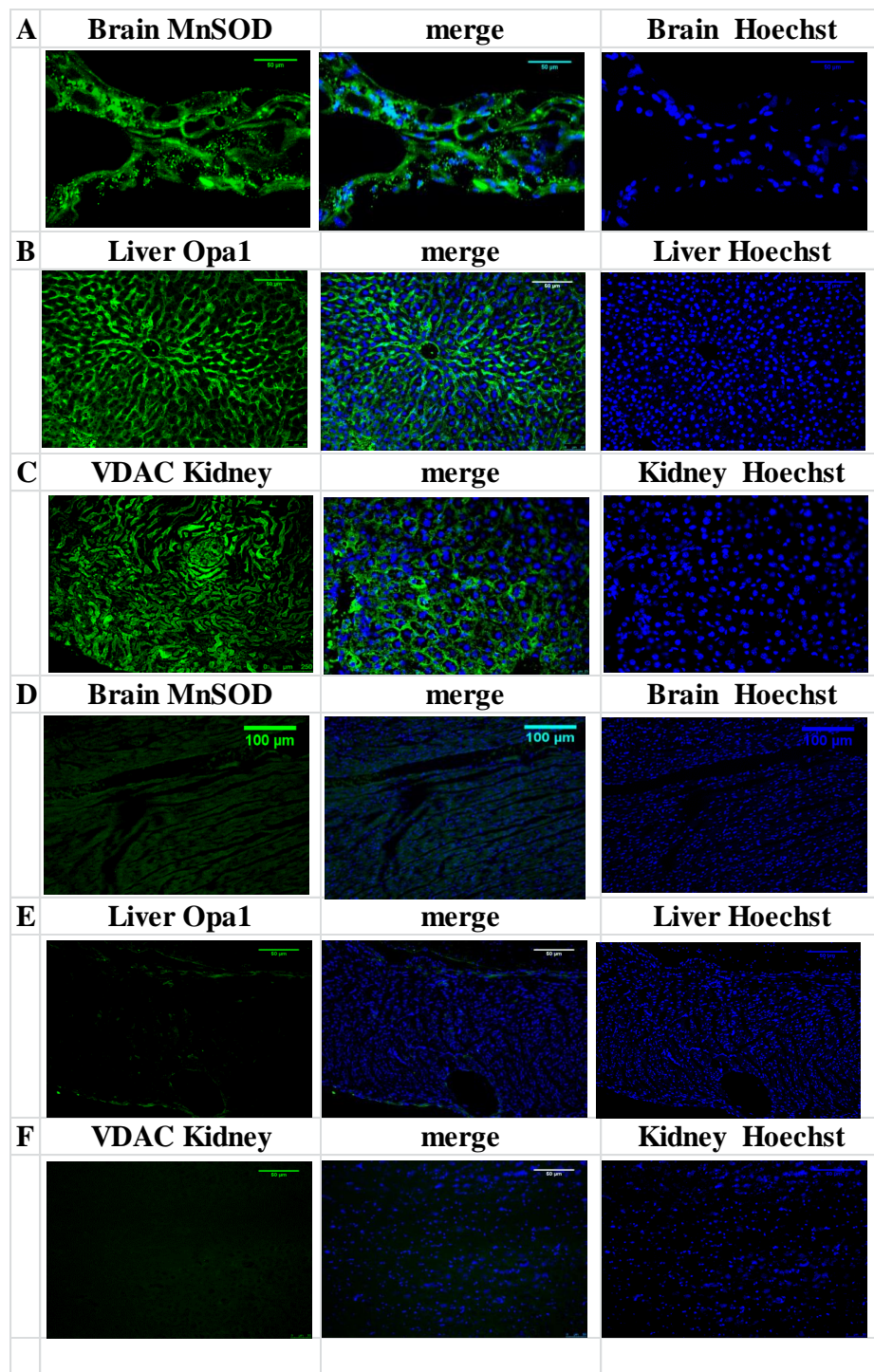
Percentage of inhibition of formazan formation were calculated from the calculation

$$\{[(S1 - S3) - (SS - S2)] / (S1 - S3)\} \times 100.$$

where S1 was formazan formation with no inhibition, S2 was sample minus enzyme and S3 was diluent only with no enzyme. Specific inhibition of MnSOD or CuZnSOD allowed different subtypes to be examined in (A) Brain, (B) spinal cord and (C) retinal homogenate of WT, res WT and veh WT

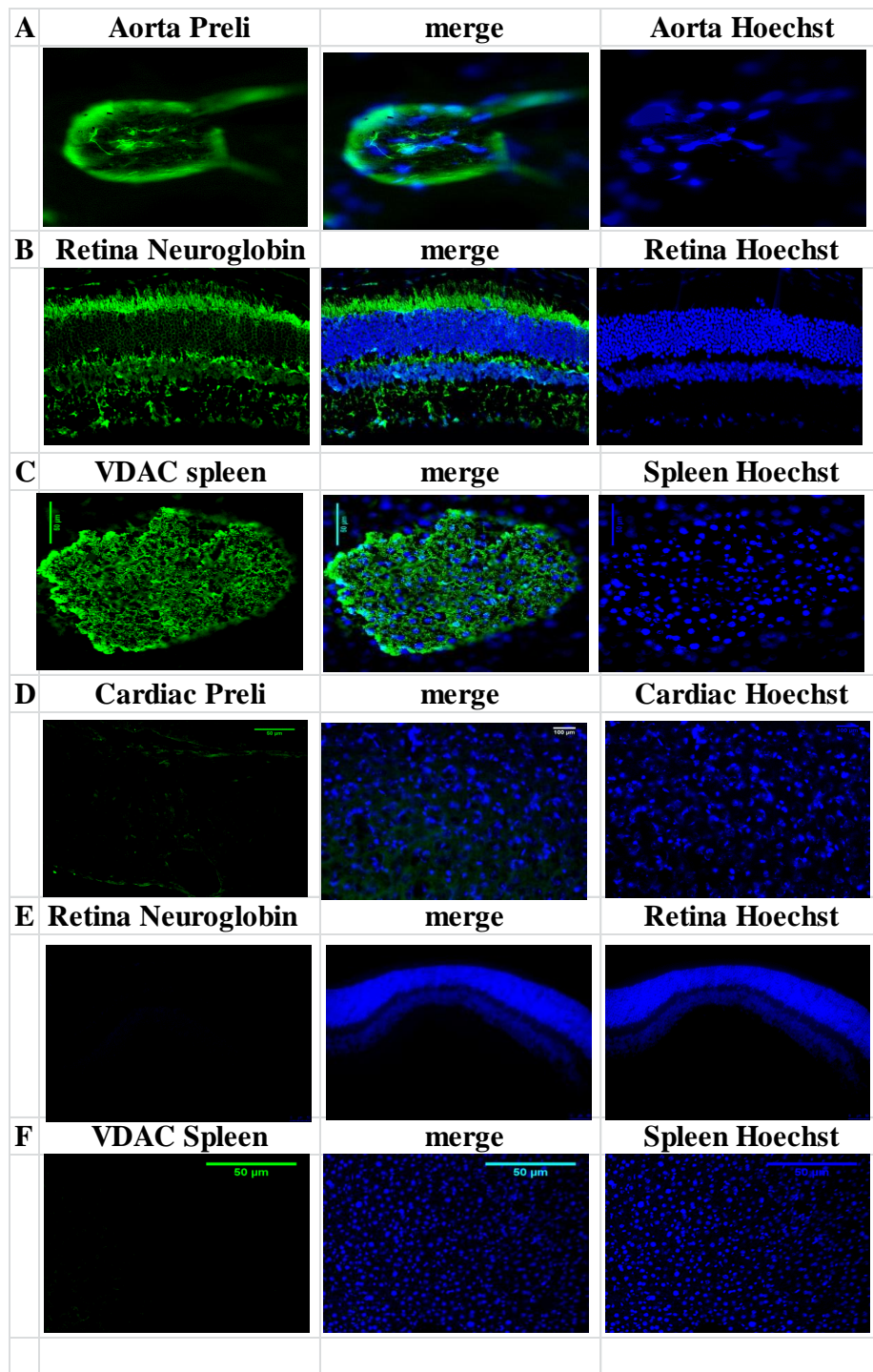
Appendix

Appendix U Positive Control sections for IHC



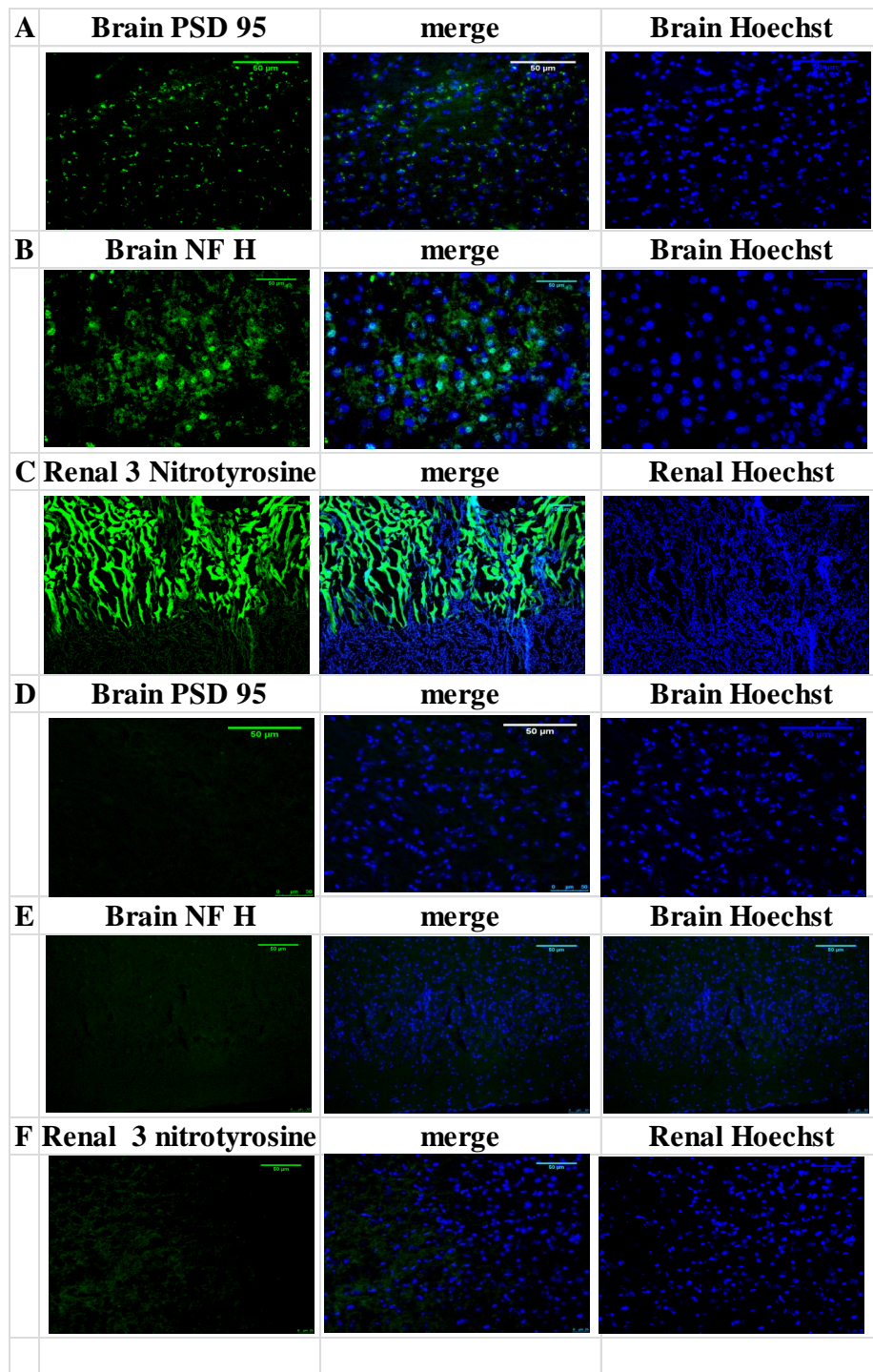
Control sections for mitochondrial specific protein expression in mouse tissue. Each positive control has a tissue matched negative control. (A): MnSOD expression in male C57Bl/6 brain at 3 months showing mitochondrial staining clustered around Hoechst stained nucleus. (B): Opa1 expression in hepatocytes showing high density staining. (C): VDAC staining in kidney nephron. Negative tissue controls (D)Brain (E)Liver(F) Kidney

Positive Control sections for IHC



Control sections for compensatory protein expression in mouse tissue. (A): Preli expression in aortic arch of C57Bl/6 at 3 months. mitochondria of mouse olfactory bulb. (B): Neuroglobin expression retinal section of C57Bl/6 3 months (C): VDAC expression in spleen *Opa1*^{Q285STOP} mouse at 3 months .Negative tissue controls (D)Cardiac (E)Retina (F) spleen

Positive Control sections for IHC



Control sections for damaged mediated protein expression. (A) PSD95 expression : expression in cerebellum of Python Het (Drp1) brain. (B): Neurofilament heavy chain expression in olfactory bulb of Python Het brain. (C): 3nitrotyrosine deposition in the glomerulus of 12 month C57Bl/6 WT. Negative control sections (D) Python Brain (E) Python Brain (F) Renal

Appendix

Appendix V Retinal IHC counts Het res & veh Het

Average counts in retinal layers Het, res and veh Het

IHC Retinal layers Het								IHC Retinal layers res Het								IHC Retinal layers veh Het							
Opal	Het	PRL	ONL	OPL	INL	IPL	GCL	rHet	PRL	ONL	OPL	INL	IPL	GCL	vHet	PRL	ONL	OPL	INL	IPL	GCL		
	Ave	96.4	98.8	130	71.1	89	77.7	Ave	235	131	185	93.4	101	52.6	Ave	188	164	217	160	162	146		
	SEM	26.8	37.6	26.3	11.9	29.2	10.3	SEM	72.3	24.7	61.6	36.1	23.7	12.4	SEM	84.6	53.6	75.8	50.3	72.1	23.5		
MnSOD	Het	PRL	ONL	OPL	INL	IPL	GCL	rHet	PRL	ONL	OPL	INL	IPL	GCL	vHet	PRL	ONL	OPL	INL	IPL	GCL		
	Ave	381.3	131.8	119.1	227.2	800	228.8	Ave	332.8	146.4	263.4	172.4	524.9	246.9	Ave	161.9	101.2	150.1	121.3	291.7	170.4		
	SEM	20.21	90.69	32.28	75.88	14.84	4.403	SEM	92.62	60.95	80.97	56.4	172.3	86.99	SEM	46.38	19.74	43.82	45.36	92.73	73.54		
VDAC	Het	PRL	ONL	OPL	INL	IPL	GCL	rHet	PRL	ONL	OPL	INL	IPL	GCL	vHet	PRL	ONL	OPL	INL	IPL	GCL		
	Ave	555	944	526	890	747	798	Ave	422	403	221	351	244	390	Ave	269	311	250	339	268	349		
	SEM	88	23.5	81.9	66.1	67.6	65.8	SEM	72.8	116	72.3	61.4	34.7	44.1	SEM	70.7	76	84.4	66.4	89.8	79.6		
Neuro	Het	PRL	ONL	OPL	INL	IPL	GCL	rHet	PRL	ONL	OPL	INL	IPL	GCL	vHet	PRL	ONL	OPL	INL	IPL	GCL		
	Ave	250.5	349.2	129.8	259.3	90.41	64.78	Ave	214.3	181.4	85.71	94.48	95.08	66.7	Ave	176.4	267.1	134.2	151.1	223.1	129.3		
	SEM	38.15	38.98	20.76	21.29	34.99	23.16	SEM	30.29	5.215	13.97	27.37	42.04	10.76	SEM	97.47	69.44	70.63	29.79	150.6	40.57		
Preli	Het	PRL	ONL	OPL	INL	IPL	GCL	rHet	PRL	ONL	OPL	INL	IPL	GCL	vHet	PRL	ONL	OPL	INL	IPL	GCL		
	Ave	255	186	144	120	215	99	Ave	380	88	182	96	178	171	Ave	368	109	196	162	284	236		
	SEM	71	113	58	43	106	30	SEM	52	85	34	33	31	16	SEM	73	66	53	94	131	104		
PSD95	Het	PRL	ONL	OPL	INL	IPL	GCL	rHet	PRL	ONL	OPL	INL	IPL	GCL	vHet	PRL	ONL	OPL	INL	IPL	GCL		
	Ave	267	162	239	82.8	211	92.9	Ave	252	352	230	174	125	75.7	Ave	250	256	215	131	167	63.9		
	SEM	24.2	32	2.26	11.2	15.8	15.6	SEM	58.5	115	71.5	70.7	75.4	36.5	SEM	62	18.7	13.7	42.5	38.8	11.7		
NFL	Het	PRL	ONL	OPL	INL	IPL	GCL	rHet	PRL	ONL	OPL	INL	IPL	GCL	vHet	PRL	ONL	OPL	INL	IPL	GCL		
	Ave	128	168	182	140	173	405	Ave	291	281	506	242	318	602	Ave	143	121	185	291	124	341		
	SEM	56.5	54.8	70.4	42	54.7	105	SEM	39.5	89	76.5	81.1	24.9	28.5	SEM	25.8	48.3	81.6	173	55.8	97.5		
3 Nitro	Het	PRL	ONL	OPL	INL	IPL	GCL	rHet	PRL	ONL	OPL	INL	IPL	GCL	vHet	PRL	ONL	OPL	INL	IPL	GCL		
	Ave	215	167	240	213	468	522	Ave	220	164	100	50.4	100	63.2	Ave	186	136	148	112	267	124		
	SEM	28.1	113	54.9	62.3	132	101	SEM	110	81.2	55.9	21.5	67.2	40.2	SEM	29.9	45.2	26.7	37.2	77.3	52.4		



The average of a minimum of three independent experiments for expression of proteins as listed for Het, res Het and veh Het. Average AUF in retinal layers of untreated Het, res and veh treated Het: Opa1, MnSOD, VDAC, Neuroglobin, Preli, PSD95, NFL and 3 Nitrotyrosine.

Appendix

Retinal IHC counts WT, res & veh WT

Average counts in retinal layers WT, res and veh WT

IHC Retinal layers WT								IHC Retinal layers res WT						IHC Retinal layers veh WT							
Opal1	WT	PRL	ONL	OPL	INL	IPL	GCL	rWT	PRL	ONL	OPL	INL	IPL	GCL	yWT	PRL	ONL	OPL	INL	IPL	GCL
	Ave	192	256	258	224	281	187	Ave	302	330	487	255	298	203	Ave	203	199	336	243	255	142
	SEM	39.3	52.6	73	79.2	41.8	30.5	SEM	50.4	56.8	94.4	36.4	21.5	28	SEM	36.2	42.5	36.8	18	4.46	33.3
MnSOD	WT	PRL	ONL	OPL	INL	IPL	GCL	rWT	PRL	ONL	OPL	INL	IPL	GCL	yWT	PRL	ONL	OPL	INL	IPL	GCL
	Ave	757.2	605.5	767.2	627.3	1745	939.4		316.8	324.2	274.8	215.7	388.7	268.8		306.6	219.1	262	228.2	537.2	470.2
	SEM	129.6	118.5	56.31	60.44	416.3	141.4		127.4	153.8	133.3	106.2	198.1	133.8		24.43	42.9	28.78	8.806	76.19	163.8
VDAC	WT	PRL	ONL	OPL	INL	IPL	GCL	rWT	PRL	ONL	OPL	INL	IPL	GCL	yWT	PRL	ONL	OPL	INL	IPL	GCL
	Ave	91.9	273	184	215	181	404	Ave	185	466	245	429	366	435	Ave	144	130	102	179	108	224
	SEM	15.9	25.1	19.6	26.5	25.7	30.6	SEM	56.4	197	118	134	136	247	SEM	6.18	0.44	7.21	13.3	3.94	7.2
Neuro	WT	PRL	ONL	OPL	INL	IPL	GCL	rWT	PRL	ONL	OPL	INL	IPL	GCL	yWT	PRL	ONL	OPL	INL	IPL	GCL
	Ave	228.1	218.1	170.2	163.3	180.9	71.34	Ave	158.4	210.7	158.6	119	165.8	113.9	Ave	154.5	189.4	96.18	123	80.36	75.07
	SEM	52.27	99.93	54.2	81.32	80.56	36.4	SEM	2.327	20.05	40.82	30.8	36.4	10.7	SEM	28.11	34.19	27.34	31.49	7.807	17.84
Preli	WT	PRL	ONL	OPL	INL	IPL	GCL	rWT	PRL	ONL	OPL	INL	IPL	GCL	yWT	PRL	ONL	OPL	INL	IPL	GCL
	Ave	366	17	194	110	122	213	Ave	240	19	113	119	130	128	Ave	262	69	172	56	62	36
	SEM	120	4	63	16	37	61	SEM	84	1	14	9	44	29	SEM	73	12	48	8	20	15
PSD95	WT	PRL	ONL	OPL	INL	IPL	GCL	rWT	PRL	ONL	OPL	INL	IPL	GCL	yWT	PRL	ONL	OPL	INL	IPL	GCL
	Ave	90.5	37.8	84.4	24.5	40.3	34	Ave	189	269	237	209	228	189	Ave	156	66.9	105	50.3	58.8	25.4
	SEM	10.2	10.3	24.6	11.3	18.1	26.4	SEM	3.57	66.7	65.7	53.3	59.1	67.9	SEM	48.8	28.8	58	22.4	31.8	11
NFL	WT	PRL	ONL	OPL	INL	IPL	GCL	rWT	PRL	ONL	OPL	INL	IPL	GCL	yWT	PRL	ONL	OPL	INL	IPL	GCL
	Ave	112	165	99.2	57.1	195	443	Ave	67.6	77.1	102	72.4	94.7	215	Ave	153	196	257	162	358	424
	SEM	13.2	87.1	3.55	11.7	28.3	37.6	SEM	6.61	2.09	34.2	22.9	32.3	67.6	SEM	23.8	47.8	34.9	17.7	53.8	113
3 Nitro	WT	PRL	ONL	OPL	INL	IPL	GCL	rWT	PRL	ONL	OPL	INL	IPL	GCL	yWT	PRL	ONL	OPL	INL	IPL	GCL
	Ave	82.6	157	99.2	174	210	220	Ave	280	257	156	84.6	338	155	Ave	275	140	235	175	435	172
	SEM	30.2	52.9	48.1	64.1	104	96	SEM	33.2	35.9	12.5	16.9	66.5	29.1	SEM	84.8	33.8	67.5	47.4	137	57.8

The average of a minimum of three independent experiments for expression of proteins as listed for WT, res WT and veh WT. Average AUF in retinal layers of untreated WT, res and veh WT: Opal1, MnSOD, VDAC, Neuroglobin, Preli, PSD95, NFL and 3 Nitrotyrosine.

Appendix

Brain IHC counts WT, res & veh WT, Het res Het & veh Het

Average counts in brain sections of WT, Het, res WT, res Het, veh WT, and veh Het

IHC Brain								
WT res & veh WT					Het, res & veh Het			
	Opal				Opal			
	WT	rWT	vWT		Het	rHet	vHet	
Ave	619.9	1024	612.8		Ave	419.1	589.4	471.4
SEM	119.6	278.8	208.7		SEM	80.2	211.4	126.7
MnSOD					MnSOD			
	WT	rWT	vWT		Het	rHet	vHet	
Ave	2983	4000	2055		Ave	557.8	1806	788.8
SEM	789	466	222		SEM	92	351	87.3
VDAC					VDAC			
	WT	rWT	vWT		Het	rHet	vHet	
Ave	542.4	1308	1007		Ave	1016	939.7	901.4
SEM	107.6	270.7	206.2		SEM	299.8	220	40.36
Neuroglobin					Neuroglobin			
	WT	rWT	vWT		Het	rHet	vHet	
Ave	390	179.5	272.3		Ave	969	159.9	542.5
SEM	128.7	42.4	65.3		SEM	195	51.9	177.8
Preli					Preli			
	WT	rWT	vWT		Het	rHet	vHet	
Ave	542.4	1308	1007		Ave	1016	939.7	901.4
SEM	107.6	270.7	206.2		SEM	299.8	220	40.36
PSD95					PSD95			
	WT	rWT	vWT		Het	rHet	vHet	
Ave	623	2056	781.1		Ave	164.4	1660	259.2
SEM	93.35	401.6	173.7		SEM	36.66	52.48	88.36
NF					NF			
	WT	rWT	vWT		Het	rHet	vHet	
Ave	177.8	624.9	521.5		Ave	1469	1135	265.5
SEM	37.8	57.19	153.9		SEM	305.9	295.2	126.9
3Nitro					3Nitro			
	WT	rWT	vWT		Het	rHet	vHet	
Ave	524.5	884.4	158.1		Ave	1561	476.7	286.2
SEM	176	138.4	44.14		SEM	275.4	98.04	43.55

The average of a minimum of three independent experiments for expression of proteins as listed for WT, res WT and veh WT, Het, res Het and veh Het . Average AUF in brain: Opal, MnSOD, VDAC, Neuroglobin, Preli, PSD95, NFL and 3 Nitrotyrosine.


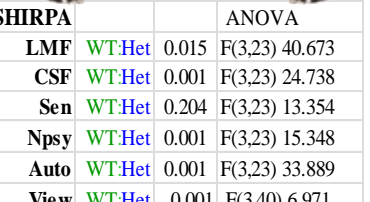
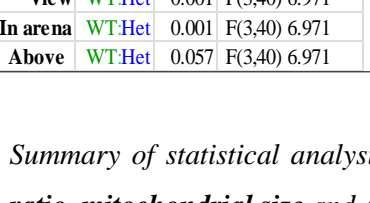
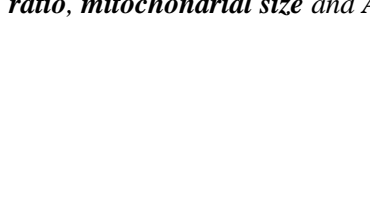
Statistical Testing Parameters				
1	Shapiro Wilk Normality of Distribution (sig. <0.05)			
2	Levene's parametric T Test Variance (Levene's sig. <0.05, 2 tailed sig. >0.05)			
3	ANOVA (parametric) means of more than 2 groups (with post hoc)			
4	Post hoc: Tukey (equal group size) Dunnett (unequal group size)			
5	Mann-Whitney U test (non parametric) Asymp.(2 tailed) <0.05*			
6	Kruskal-Wallis H test (non parametric)			
*Bonferroni Adjustment (sig.0.05/no. T tests performed)				
WT & Het : Rotarod Beam, Rope, T Maze, NOR				
Rotarod Latency to fall				
RM ANOVA (3,41) 3.168				
	M WT	F Het	M Het	
F WT	0.001	0.004	0.001	
M WT			0.948	
F Het			0.053	
M Het				
Rotarod Latency:housing				
RM ANOVA (3,20) 21.433				
	sMHet	gMWT	gMHet	
sMWT	0.934	0.013	0.001	
sMHet		0.001	0.020	
gMWT			0.989	
gMHet				
Narrowbeam Initiation				
ANOVA (3,22)6.361				
	M WT	F Het	M Het	
F WT	0.297	0.001	0.031	
M WT		0.001	0.001	
F Het			0.530	
M Het				
Tight rope Distance				
ANOVA (3,22)13.833				
	M WT	F Het	M Het	
F WT	0.369	0.106	0.519	
M WT		0.086	0.026	
F Het			0.867	
M Het				
T Maze To novel arm				
ANOVA (3,20) 1.145				
	M WT	F Het	M Het	
F WT	0.719	0.001	0.064	
M WT		0.001	0.020	
F Het			0.001	
M Het				
T Maze In novel arm				
ANOVA (3,20) 9.651				
	M WT	F Het	M Het	
F WT	0.019	0.001	0.001	
M WT		0.048	0.530	
F Het			0.087	
M Het				
T Maze in Original arm				
ANOVA (3,20) 1.279				
	M WT	F Het	M Het	
F WT	0.659	0.741	0.340	
M WT		0.878	0.221	
F Het			0.199	
M Het				
T Maze IR				
ANOVA (3,20) 1.592				
	M WT	F Het	M Het	
F WT	0.805	0.006	0.136	
M WT		0.144	0.144	
F Het			0.033	
M Het				
T Maze DR				
ANOVA (3,20) 4.744				
	M WT	F Het	M Het	
F WT	0.726	0.002	0.032	
M WT		0.130	0.096	
F Het			0.835	
M Het				
NOR To Novel object				
ANOVA (3,23) 7.443				
	M WT	F Het	M Het	
F WT	0.914	0.001	0.001	
M WT		0.001	0.001	
F Het			0.899	
M Het				
NOR with Novel object				
ANOVA (3,23) 4.094				
	M WT	F Het	M Het	
F WT	0.024	0.024	0.116	
M WT		0.001	0.004	
F Het			0.710	
M Het				
NOR with Originalobject				
ANOVA (3,23) 2.616				
	M WT	F Het	M Het	
F WT	0.880	0.883	0.012	
M WT		0.933	0.021	
F Het			0.002	
M Het				
NOR IR				
ANOVA (3,23) 5.033				
	M WT	F Het	M Het	
F WT	0.106	0.005	0.045	
M WT		0.090	0.004	
F Het			0.403	
M Het				
NOR DR				
ANOVA (3,23) 7.370				
	M WT	F Het	M Het	
F WT	0.352	0.004	0.001	
M WT		0.046	0.002	
F Het			0.015	
M Het				

Summary of statistical analysis performed on data from SHIRPA, rotarod, narrowbeam and tight rope testing in untreated and treated WT and Het.

Appendix

WT & Het : Thermal, Body, Brain, Cardiac weight ± enrichment											
Thermal Head				Weight/enrichment Body				Weight/Housing Body			
Head ANOVA (3,26)38.542				ANOVA (6,71) 12.283				ANOVA (6,71) 12.283			
	yHet	oWT	oHet		M WT	F Het	M Het		gM WT	sM Het	g MHet
yWT	0.001	0.321	0.001	eFHet	0.914	0.009	0.001	sMWT	0.624	0.634	
yHet		0.001	0.797	eM WT	0.001	0.001	0.001	sMHet		0.247	
oWT			0.004	eM Het			0.008	gMWT			0.317
oHet								g Mhet			
Thermal Flank				Weight/enrichment Brain				Weight/Housing Brain			
Flank ANOVA (3,26)2.077				ANOVA (6,71) 1.369				ANOVA (6,71) 12.283			
	yHet	oWT	oHet		M WT	F Het	M Het		gM WT	sM Het	g MHet
yWT	0.112	0.112	0.030	eFHet	0.001	0.020	0.001	sMWT	0.009	0.963	
yHet		0.009	0.130	eM WT	0.846	0.001	0.001	sMHet		0.015	
oWT			0.130	eM Het			0.534	gMWT			0.288
oHet								g MHet			
Thermal Tail				Weight/enrichment Cardiac				Weight/Housing Cardiac			
Tail ANOVA (3,26)2.502				ANOVA (6,71) 1.681				ANOVA (6,71) 12.283			
	yHet	oWT	oHet		M WT	F Het	M Het		gM WT	sM Het	g MHet
yWT	0.024	0.371	0.006	eFHet	0.001	0.009	0.001	sMWT	0.012	0.343	
yHet		0.005	0.439	eM WT	0.287	0.001	0.001	sMHet		0.129	
oWT			0.287	eM Het			0.004	gMWT		0.317	0.779
oHet								g MHet			

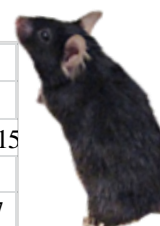
WT & Het : Mito size, ΔΨ, ATP

				Mito Size Brain				ATP Brain ANOVA (3,13) 1.869							
				ANOVA (5,12) 26.391				ANOVA (5,12) 26.391				ANOVA (5,12) 26.391			
					Min	Med	Max		M WT	F Het	M Het		M WT	F Het	M Het
				Het min	0.007			F WT	0.520	0.859		M WT			0.349
				Het med		0.007		F Het				M WT			0.279
Het max			0.855	M Het				F Het			0.375				
				Mito Size Retina				ATP SC ANOVA (3,14) 1.633							
				ANOVA (5,12) 26.391				ANOVA (5,12) 26.391				ANOVA (5,12) 26.391			
					Min	Med	Max		M WT	F Het	M Het		M WT	F Het	M Het
				Het min	0.009			F WT	0.464	0.218		M WT			0.737
				Het med		0.048		F Het				M WT			0.969
Het max			0.971	M Het				F Het			0.001				
				Mito ΔΨ Brain				ATP Ret ANOVA (3,14) 1.633							
				ANOVA (3,12) 26.391				ANOVA (3,12) 26.391				ANOVA (3,12) 26.391			
					WT	WT	WT		M WT	F Het	M Het		M WT	F Het	M Het
				Het	0.110			F WT	0.049	0.171		M WT			0.969
				Het		0.254		F Het				M WT			0.969
Het			0.226	F Het				F Het			0.001				
				Mito ΔΨ Retina				ATP All ANOVA (5,45) 7.036							
				ANOVA (3,12) 26.391				ANOVA (3,12) 26.391				ANOVA (3,12) 26.391			
					WT	WT	WT		B Het	SC Het	Ret Het		B WT	SC WT	Ret WT
				Het	0.120			B Het	0.335			B WT	0.335		
				Het		0.329		SC WT				SC WT		0.551	
Het			0.560	Ret WT				Ret WT			0.258				

Summary of statistical analysis of thermal function, body, brain and cardiac weight ratio, mitochondrial size and ATP in untreated and treated WT and Het.

WT & Het : ETC CI, CII, CIV Brain, SC, Retina & Muscle												
ETC: CI Brain			ETC: CII Brain			ETC: CIV Brain			ETC: Ratio CI			
ANOVA(7,55) 22.123			ANOVA(7,48) 55.804			ANOVA(7,53) 27.562			ANOVA(5,48) 2.144			
	WT	Het		WT	Het		WT	Het		Het	Het	Het
	WT	0.001		WT	0.001		WT	0.017	Brain	WT	0.017	
	Het			Het			Het		SC	WT		0.685
									Ret	WT		0.597
ETC: CI SC			ETC: CII SC			ETC: CIV SC			ETC: Ratio CII			
ANOVA(7,55) 89.435			ANOVA(7,48) 54.260			ANOVA(7,53) 42.356			ANOVA(5,40) 45.389			
	WT	Het		WT	Het		WT	Het		Het	Het	Het
	WT	0.001		WT	0.001		WT	0.203	Brain	WT	0.675	
	Het			Het			Het		SC	WT		0.626
									Ret	WT		0.779
ETC: CI Ret			ETC: CII Ret			ETC: CIV Ret			ETC: Ratio CIV			
ANOVA(7,55) 60.655			ANOVA(7,48) 45.570			ANOVA(7,53) 8.631			ANOVA(5,46) 38.685			
	WT	Het		WT	Het		WT	Het		Het	Het	Het
	WT	0.001		WT	0.001		WT	0.001	Brain	WT	0.278	
	Het			Het			Het		SC	WT		0.001
									Ret	WT		0.001
ETC: CI Muscle			ETC: CII Muscle			ETC: CIV Muscle			ETC: Ratio Skeletal Muscle			
ANOVA(7,55) 66.350			ANOVA(7,48) 4.374			ANOVA(7,53) 13.864			ANOVA(5,17) 11.87			
	WT	Het		WT	Het		WT	Het		Het	Het	Het
	WT	0.004		WT	0.025		WT	0.001	C I	WT	0.022	
	Het			Het			Het		C II	WT		0.036
									C IV	WT		0.255

WT & Het : SOD & Catalase Brain, SC Retina												
Total SOD						Non SOD						
Brain		SC		Ret		Brain		SC		Ret		
F(5,12)32.4		F(5,12)105.3		F(5,12)8.8		F(5,28)23.3		F(5,20)19.78		F(5,24)1.60		
	Het		Het		Het		Het		Het		Het	
	WT	0.001	WT	0.001	WT	0.003	WT	0.001	WT	0.001	WT	0.109
MnSOD												
Brain		SC		Ret								
F(5,12)48.7		F(5,12)22.6		F(5,12)3.74								
	Het		Het		Het							
	WT	0.001	WT	0.001	WT	0.029						
CuZnSOD						Catalase						
Brain		SC		Ret		Brain		SC		Ret		
F(5,12)3257.8		F(5,12)15.4		F(5,12)10.8		F(5,31) 7.995		F(5,18) 10.9		F(3,10) 9.15		
	Het		Het		Het		Het		Het		Het	
	WT	0.004	WT	0.001	WT	0.299	WT	0.099	WT	0.001	WT	0.007



Summary of statistical analysis of electron transfer in **complex I**, **complex II** and **complex IV**, and antioxidant **SOD** and **Catalase** in untreated and treated WT and Het.

WT & Het : IHC Retina & Brain

Opa1 Ret AFU						
ANOVA (5,15) 3.865 Post Hoc Tukey						
	PRL	OPL	ONL	NIL	IPL	GCL
Mito	Het	Het	Het	Het	Het	Het
WT	0.241	0.024	0.006	0.177	0.022	0.008
Het						
VDAC Ret AFU						
ANOVA (5,15) 2.751 Post Hoc Tukey						
	PRL	OPL	ONL	NIL	IPL	GCL
Mito	Het	Het	Het	Het	Het	Het
WT	0.005	0.769	0.023	0.008	0.010	0.031
Het						
Preli Ret AFU						
ANOVA (5,21) 21.466 Post Hoc Tukey						
	PRL	OPL	ONL	NIL	IPL	GCL
Mito	Het	Het	Het	Het	Het	Het
WT	0.386	0.520	0.004	0.898	0.027	0.003
Het						
Neuroglobin Ret AFU						
ANOVA (5,20) 1.530 Post Hoc Tukey						
	PRL	OPL	ONL	NIL	IPL	GCL
Mito	Het	Het	Het	Het	Het	Het
WT	0.384	0.722	0.701	0.634	0.846	0.503
Het						
PSD 95 Ret AFU						
ANOVA (5,28) 1.900 Post Hoc Tukey						
	PRL	OPL	ONL	NIL	IPL	GCL
Mito	Het	Het	Het	Het	Het	Het
WT	0.314	0.292	0.750	0.272	0.122	0.346
Het						
NFL Ret AFU						
ANOVA (5,23) 8.530 Post Hoc Tukey						
	PRL	OPL	ONL	NIL	IPL	GCL
Mito	Het	Het	Het	Het	Het	Het
WT	0.020	0.536	0.059	0.452	0.740	0.038
Het						
MnSOD Ret AFU						
ANOVA (5,16) 8.916 Post Hoc Tukey						
	PRL	OPL	ONL	NIL	IPL	GCL
Mito	Het	Het	Het	Het	Het	Het
WT	0.651	0.653	0.020	0.606	0.886	0.002
Het						
3Nitro Ret AFU						
ANOVA (5,20) 2.732 Post Hoc Tukey						
	PRL	OPL	ONL	NIL	IPL	GCL
Mito	Het	Het	Het	Het	Het	Het
WT	0.048	0.001	0.840	0.032	0.547	0.023
Het						



Brain A	Opa1	VDAC	Preli
F(5,30)	4.527	2.87	4.57
	Het	Het	Het
WT	0.008	0.005	0.008
	Het		
Brain A	MnSOD	3Nitro	
F(5,30)	6.91	7.919	
	Het	Het	
WT	0.001	0.001	
	Het		
Brain A	Neuro	Psd95	NF h
F(5,30)	4.527	2.454	2.983
	Het	Het	Het
WT	0.008	0.005	0.008
	Het		

Mito Ret AFU						
ANOVA (5,69) 5.364 Post Hoc Tukey						
	PRL	OPL	ONL	NIL	IPL	GCL
Mito	Het	Het	Het	Het	Het	Het
WT	0.366	0.044	0.531	0.090	0.067	0.683
Het						
Comp Ret AFU						
ANOVA (5,78) 2.133 Post Hoc Tukey						
	PRL	OPL	ONL	NIL	IPL	GCL
Mito	Het	Het	Het	Het	Het	Het
WT	0.074	0.002	0.250	0.005	0.014	0.376
Het						
Damage Ret AFU						
ANOVA (5,81) 1.741 Post Hoc Tukey						
	PRL	OPL	ONL	NIL	IPL	GCL
Mito	Het	Het	Het	Het	Het	Het
WT	0.046	0.370	0.006	0.001	0.110	0.485
Het						
Brain AFU			Retina AFU			
ANOVA (5,75) 2.411			ANOVA (5,369) 7.500			
	Mito			Mito		
WT	Het			WT	Het	
Het	0.134			Het	0.024	
Brain AFU			Retina AFU			
ANOVA (5,68) 5.957			ANOVA (5,414) 2.39			
Comp			Comp			
WT	Het			WT	Het	
Het	0.001			Het	0.001	
Brain AFU			Retina AFU			
ANOVA (5,75) 2.573			ANOVA (5,425) 5.581			
Dam			Dam			
WT	Het			WT	Het	
Het	0.007			Het	0.023	

Summary of statistical analysis antioxidant activity **IHC retina and brain** in untreated and treated WT and Het.

Het, res Het & veh Het : Weight Rotarod Beam, Rope, T Maze, NOR

Weight/Body		Rotarod Latency to fall			T Maze To novel arm			NOR To Novel object					
ANOVA (11,161) 9.8		RM ANOVA (9,70) 2.554			ANOVA (3,34) 4.639			ANOVA (3,36) 8.106					
	rHet	vF Het		rHet	vFHet	M Het		rHet	vHet				
F Het	0.165	0.401		F Het	0.001	0.003	0.040	Het	0.021	0.008	Het	0.638	0.910
rHet		0.656		rFHet		0.996	0.893	rHet		0.527	rHet		0.649
vF Het				vFHet			0.998	vHet			vHet		
Weight Brain		Rotarod Latency:housing			T Maze In novel arm			NOR with Novel object					
ANOVA (11,161) 2.722		RM ANOVA (3,32) 2.756			ANOVA (3,34) 3.939			ANOVA (3,36) 4.117					
	rHet	vF Het		rsMHet	gMHet	rgMHet		rHet	vHet		rHet	vHet	
F Het	0.025	0.263		sMHet	0.001	0.003	0.001	Het	0.030	0.137	Het	0.588	0.583
rFHet		0.458		rsMHet			0.126	rHet		0.767	rHet		0.378
vF Het				gMHet			0.989	vHet			vHet		
Weight/Cardiac		Narrowbeam Initiation			T Maze in Original arm			NOR with Originalobject					
ANOVA (11,161) 1.945		ANOVA (15,80)5.403			ANOVA (3,34) 1.864			ANOVA (3,36) 1.606					
	rHet	vF Het			rHet	vHet		rHet	vHet		rHet	vHet	
F Het	0.505	0.035		Het	0.001	0.019		Het	0.028	0.987	Het	0.085	0.112
rFHet		0.112		rHet		0.256		rHet		0.108	rHet		0.963
vF Het				vHet				vHet			vHet		
Weight/Housing Body		Tight rope Distance			T Maze IR			NOR IR					
ANOVA (6,71) 12.283		ANOVA (15,80)6.704			ANOVA (3,34) 2.418			ANOVA (3,36) 2.254					
	srMHet	grMHet			rHet	vHet		rHet	vHet		rHet	vHet	
sMHet	0.385	0.450		Het	0.001	0.294		Het	0.006	0.144	Het	0.067	0.069
srMHet		0.450		rHet		0.001		rHet		0.244	rHet		0.874
g MHet		0.308		vHet				vHet			vHet		
grMHet													
Weight/Housing Brain		SHIRPA			T Maze DR			NOR DR					
ANOVA (6,71) 12.283		ANOVA			ANOVA (3,34) 6.708			ANOVA (3,36) 2.254					
	srMHet	grMHet		LMF	Het:rHet	0.951	F(3,23) 40.673		rHet	vHet		rHet	vHet
sMHet	0.385			CSF	Het:rHet	0.109	F(3,23) 24.738	Het	0.002	0.096	Het	0.078	0.024
srMHet		0.829		Sen	Het:rHet	0.051	F(3,23) 13.354	rHet		0.494	rHet		0.564
g MHet		0.672		Npsy	Het:rHet	0.012	F(3,23) 15.348	vHet			vHet		
grMHet				Auto	Het:rHet	0.041	F(3,23) 33.889						
Weight/Housing Cardiac													
ANOVA (6,71) 12.283													
	srMHet	grMHet											
sMHet	0.820	0.450											
srMHet		0.962											
g MHet		0.275											
grMHet													




Summary of statistical analysis of Het. res and veh Het weight, rotarod, beam and rope, & cognitive T test and NOR

Het, res & veh Het : ETC CI, CII, CIV Brain, SC, Retina & Muscle

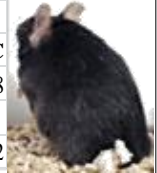
ETC: CI Brain			ETC: CII Brain			ETC: CIV Brain			ETC: Ratio CI			
ANOVA(5,38)25.123			ANOVA(5,48) 55.804			ANOVA(5,35) 27.562			ANOVA(5,48) 2.144			
	rHet	vHet		rHet	vHet		rHet	vHet		rHet	vHet	
Het	0.002	0.001	Het	0.012	0.001	Het	0.001	0.001	Brain	Het	0.909	0.001
rHet		0.001	rHet		0.001	rHet		0.552	SC	Het	0.001	0.775
vHet			vHet			vHet			Ret	Het	0.781	0.736
ETC: CI SC			ETC: CII SC			ETC: CIV SC			ETC: Ratio CII			
ANOVA(5,38)89.435			ANOVA(5,31) 54.260			ANOVA(5,38) 42.356			ANOVA(5,40) 45.389			
	rHet	vHet		rHet	vHet		rHet	vHet		rHet	vHet	
Het	0.008	0.548	Het	0.023	0.527	Het	0.001	0.001	Brain	Het	0.001	0.001
rHet		0.054	rHet		0.007	rHet		0.926	SC	Het	0.001	0.004
vHet			vHet			vHet			Ret	Het	0.001	0.011
ETC: CI Ret			ETC: CII Ret			ETC: CIV Ret			ETC: Ratio CIV			
ANOVA(5,36)69.424			ANOVA(5,36) 45.570			ANOVA(5,34) 8.631			ANOVA(5,46) 38.685			
	rHet	vHet		rHet	vHet		rHet	vHet		rHet	vHet	
Het	0.057	0.828	Het	0.001	0.001	Het	0.001	0.010	Brain	Het	0.001	0.001
rHet		0.025	rHet		0.001	rHet		0.113	SC	Het	0.001	0.052
vHet			vHet			vHet			Ret	Het	0.001	0.001
ETC: CI Muscle			ETC: CII Muscle			ETC: CIV Muscle			ETC: Ratio Skeletal Mus			
ANOVA(5,17)66.414			ANOVA(5,17)4.374			ANOVA(5,16) 13.864			ANOVA(5,17) 11.87			
	rHet	vHet		rHet	vHet		rHet	vHet		rHet	vHet	
Het	0.014	0.001	Het	0.146	0.148	Het	0.172	0.007	C I	Het	0.009	0.462
rHet		0.153	rHet		0.914	rHet		0.001	C II	Het	0.001	0.260
vHet			vHet			vHet			C IV	Het	0.001	0.001

Het, res & veh Het : SOD & Catalase

Total SOD							Non SOD						
Brain			SC		Ret		Brain			SC		Ret	
F(5,12)32.4			F(5,12)105.3		F(5,12)8.8		F(5,28)23.3			F(5,20)19.78		F(5,24)1.60	
	rHet	vHet	rHet	vHet	rHet	vHet		rHet	vHet	rHet	vHet	rHet	vHet
Het	0.001	0.001	0.001	0.001	0.385	0.108	Het	0.001	0.672	0.001	0.030	0.536	0.603
MnSOD													
Brain			SC		Ret								
F(5,12)48.7			F(5,12)22.6		F(5,12)3.74								
	rHet	vHet	rHet	vHet	rHet	vHet							
Het	0.001	0.494	0.001	0.712	0.340	0.448							
CuZnSOD							Catalase						
Brain			SC		Ret		Brain			SC		Ret	
F(5,12)3257.8			F(5,12)15.4		F(5,12)10.8		F(5,31) 7.995			F(5,18) 10.902		F(3,10) 9.156	
	rHet	vHet	rHet	vHet	rHet	vHet		rHet	vHet	rHet	vHet	rHet	vHet
Het	0.478	0.377	0.013	0.771	0.022	0.029	Het	0.077	0.001	0.278	0.043	0.007	

Summary of statistical analysis of Het, res and veh Het ETC, and antioxidant Catalase and SOD

Het, res & veh Het : IHC Retina & Brain												
Opal	Ret AFU					ANOVA (5,15) 3.865 Post Hoc Tukey						
	PRL		OPL		ONL		IPL		INL		GCL	
	rHet	vHet	rHet	vHet	rHet	vHet	rHet	vHet	rHet	vHet	rHet	vHet
Het	0.241	0.691	0.959	0.524	0.539	0.030	0.818	0.004	0.877	0.014	0.557	0.017
VDAC	Ret AFU					ANOVA (5,15) 10.47 Post Hoc Tukey						
	PRL		OPL		ONL		IPL		INL		GCL	
	rHet	vHet	rHet	vHet	rHet	vHet	rHet	vHet	rHet	vHet	rHet	vHet
Het	0.374	0.008	0.012	0.952	0.698	0.016	0.004	0.001	0.665	0.074	0.228	0.461
Preli	Ret AFU					ANOVA (5,21) 21.466 Post Hoc Tukey						
	PRL		OPL		ONL		IPL		INL		GCL	
	rHet	vHet	rHet	vHet	rHet	vHet	rHet	vHet	rHet	vHet	rHet	vHet
Het	0.252	0.447	0.780	0.075	0.723	0.875	0.228	0.152	0.342	0.461	0.591	0.943
Neuro	Ret AFU					ANOVA (5,20) 1.530 Post Hoc Tukey						
	PRL		OPL		ONL		IPL		INL		GCL	
Mito	rHet	vHet	rHet	vHet	rHet	vHet	rHet	vHet	rHet	vHet	rHet	vHet
Het	0.454	0.776	0.457	0.102	0.508	0.341	0.781	0.223	0.537	0.090	0.410	0.928
PSD 95	Ret AFU					ANOVA (5,28) 1.900 Post Hoc Tukey						
	PRL		OPL		ONL		IPL		INL		GCL	
	rHet	vHet	rHet	vHet	rHet	vHet	rHet	vHet	rHet	vHet	rHet	vHet
Het	0.654	0.041	0.347	0.050	0.347	0.049	0.850	0.113	0.293	0.028	0.446	0.115
NF1	Ret AFU					ANOVA (5,23) 8530 Post Hoc Tukey						
	PRL		OPL		ONL		IPL		INL		GCL	
	rHet	vHet	rHet	vHet	rHet	vHet	rHet	vHet	rHet	vHet	rHet	vHet
Het	0.029	0.938	0.023	0.369	0.011	0.556	0.002	0.040	0.001	0.820	0.890	0.263
MnSOD	Ret AFU					ANOVA (5,23) 8530 Post Hoc Tukey						
	PRL		OPL		ONL		IPL		INL		GCL	
	rHet	vHet	rHet	vHet	rHet	vHet	rHet	vHet	rHet	vHet	rHet	vHet
Het	0.727	0.003	0.193	0.193	0.074	0.112	0.540	0.026	0.393	0.006	0.211	0.169
3 Nitro	Ret AFU					ANOVA (5,23) 8530 Post Hoc Tukey						
	PRL		OPL		ONL		IPL		INL		GCL	
	rHet	vHet	rHet	vHet	rHet	vHet	rHet	vHet	rHet	vHet	rHet	vHet
Het	0.958	0.776	0.979	0.784	0.102	0.266	0.048	0.196	0.047	0.249	0.001	0.004
Mito	Ret AFU					ANOVA (5,16) 2.285						
	PRL		OPL		ONL		IPL		INL		GCL	
Mito	rHet	vHet	rHet	vHet	rHet	vHet	rHet	vHet	rHet	vHet	rHet	vHet
Het	0.514	0.765	0.108	0.086	0.423	0.461	0.109	0.230	0.054	0.233	0.331	0.556
Comp	Ret AFU					ANOVA (5,15) 10.47						
	PRL		OPL		ONL		IPL		INL		GCL	
Mito	rHet	vHet	rHet	vHet	rHet	vHet	rHet	vHet	rHet	vHet	rHet	vHet
Het	0.881	0.222	0.023	0.026	0.156	0.337	0.015	0.043	0.030	0.236	0.380	0.559
Damage	Ret AFU					ANOVA (5,21) 21.466						
	PRL		OPL		ONL		IPL		INL		GCL	
Mito	rHet	vHet	rHet	vHet	rHet	vHet	rHet	vHet	rHet	vHet	rHet	vHet
Het	0.117	0.098	0.038	0.741	0.027	0.877	0.166	0.152	0.375	0.501	0.489	0.717
Brain AFU												
Brain A	Opal	VDAC				Preli						
F(5,30)	4.527											
	rHet	vHet	rHet	vHet	rHet	vHet	rHet	vHet	rHet	vHet	rHet	vHet
Het	0.582	0.159	0.005	0.017	0.813	0.723						
MnSOD												
F(5,30)	6.910											
	rHet	vHet										
Het	0.006	0.745									0.001	0.001
Neuro												
F(5,30)	4.527											
	rHet	vHet	rHet	vHet	rHet	vHet	rHet	vHet	rHet	vHet	rHet	vHet
Het	0.001	0.054	0.001	0.761	0.635	0.001						
Western Blot Retina RD												
	Opal	Neuro	Preli									
F(3,12)	7.895	1.012	5.115									
Mito	rHet	rHet	rHet									
Het	0.005	0.484	0.032									
Western Blot Brain RD												
	Opal	Neuro	VDAC									
F(3,12)	2.267	20.92	1.968									
Mito	rHet	rHet	rHet									
Het	0.460	0.121	0.672									
Brain AFU												
F(5,75)	2.411											
Mito	rHet	vHet	Mito	rHet	vHet							
Het	0.499	0.535	Het	0.250	0.098							
Retina AFU												
F(8,68)	5.957											
Comp	rHet	vHet	Comp	rHet	vHet							
Het	0.014	0.017	Het	0.001	0.001							
Brain AFU												
F(5,75)	2.573											
Dam	rHet	vHet	Dam	rHet	vHet							
Het	0.019	0.033	Het	0.019	0.033							



Summary of statistical analysis of Het, res and veh Het IHC in retina & brain. Protein profiles for mitochondria, compensation and damage profile in retina and brain.

WT, res WT & veh WT: Weight Rotarod Beam, Rope, T Maze, NOR													
Rotarod Latency to fall			T Maze To novel arm			NOR To Novel object			Weight/Body				
RM ANOVA (9,70) 2.554			ANOVA (2,19) 4.639			ANOVA (2,22) 8.106			ANOVA (11,161) 9.8				
	rFWT	vFWT	rM WT		rWT	vWT		rWT	vWT		rFWT	vFWT	
F WT	0.002	0.024		WT	0.037	0.540		WT	0.001	0.011	F WT	0.001	0.525
rFWT		0.785		rWT		0.061		rWT		0.562	rFWT		0.057
vFWT				vWT				vWT			vFWT		
M WT			0.520	T Maze In novel arm			NOR with Novel object			Weight Brain			
rM WT				ANOVA (2,19) 3.339			ANOVA (2,22) 4.117			ANOVA (11,161) 2.722			
Rotarod Latency:housing			T Maze in Original arm			NOR with Originalobject			Weight/Cardiac				
RM ANOVA (3,32) 2.756			ANOVA (2,19) 1.864			ANOVA (2,22) 1.606			ANOVA (11,161) 1.945				
	srMWT	g MWT	grMWT		rWT	vWT		rWT	vWT		rFWT	vFWT	
sMWT	0.003	0.006		WT	0.015	0.153		WT	0.010	0.024	F WT	0.001	0.009
srMWT		0.002	0.839	rWT		0.447		rWT		0.840	rFWT		0.421
g MWT			0.488	vWT				vWT			vFWT		
grMWT				T Maze IR			NOR IR			Weight/Housing Body			
Narrowbeam Initiation			T Maze DR			NOR DR			ANOVA (11,161) 12.283				
ANOVA (15,80)5.403			ANOVA (2,19) 6.708			ANOVA (2,22) 2.254			ANOVA (6,71) 12.283				
	rWT	vWT			rWT	vWT		rWT	vWT		srMWT	grMWT	
WT	0.004	0.380		WT	0.174	0.776		WT	0.144	0.706	sMWT	0.786	
rWT		0.017		rWT		0.576		rWT		0.578	srMWT		0.251
vWT				vWT				vWT			g MWT		0.017
Tight rope Distance			SHIRPA			ANOVA			Weight/Housing Brain				
ANOVA (15,80)6.704			ANOVA (3,23) 40.673			ANOVA (3,23) 24.738			ANOVA (6,71) 12.283				
	rWT	vWT	LMF	WT:rWT	0.074	F(3,23) 40.673	Weight/Housing Cardiac						
WT	0.001	0.019	CSF	WT:rWT	0.161	F(3,23) 24.738	ANOVA (6,71) 12.283						
rWT		0.423	Sen	WT:rWT	0.053	F(3,23) 13.354	srMWT			grMWT			
vWT			Npsy	WT:rWT	0.074	F(3,23) 15.348	sMWT			0.343	0.450		
			Auto	WT:rWT	0.055	F(3,23) 33.889	srMWT				0.129		
									g MWT			0.336	
									grMWT				



Summary of statistical analysis of WT res and veh WT Rotarod, Beam, Rope T maze and NOR.

WT, res & veh WT : ETC CI, CII, CIV Brain, SC, Retina & Muscle

ETC: CI Brain			ETC: CII Brain			ETC: CIV Brain			ETC: Ratio CI				
ANOVA(5,38)25.123			ANOVA(5,48) 55.804			ANOVA(5,35) 27.562			ANOVA(5,48) 2.144				
	rWT	vWT		rWT	vWT		rWT	vWT		rWT	vWT		vWT
WT	0.002	0.001	WT	0.012	0.001	WT	0.001	0.001	Brain	WT	0.180	0.793	
rWT		0.001	rWT		0.001	rWT		0.522	SC	WT	0.064	0.551	
vWT			vWT			vWT			Ret	WT	0.937	0.789	
ETC: CI SC			ETC: CII SC			ETC: CIV SC			ETC: Ratio CII				
ANOVA(5,38)89.435			ANOVA(5,31) 54.260			ANOVA(5,38) 42.356			ANOVA(5,40) 45.389				
	rWT	vWT		rWT	vWT		rWT	vWT		rWT	vWT		vWT
WT	0.008	0.548	WT	0.030	0.527	WT	0.001	0.001	Brain	WT	0.077	0.077	
rWT		0.054	rWT		0.007	rWT		0.926	SC	WT	0.012	0.179	
vWT			vWT			vWT			Ret	WT	0.538	0.178	
ETC: CI Ret			ETC: CII Ret			ETC: CIV Ret			ETC: Ratio CIV				
ANOVA(5,36)69.424			ANOVA(5,36) 45.570			ANOVA(5,34) 8.631			ANOVA(5,46) 38.685				
	rWT	vWT		rWT	vWT		rWT	vWT		rWT	vWT		vWT
WT	0.057	0.828	WT	0.001	0.001	WT	0.001	0.010	Brain	WT	0.260	0.001	
rWT		0.025	rWT		0.001	rWT		0.113	SC	WT	0.001	0.200	
vWT			vWT			vWT			Ret	WT	0.001	0.001	
ETC: CI Muscle			ETC: CII Muscle			ETC: CIV Muscle			ETC: Ratio Skeletal Mus				
ANOVA(5,17)66.414			ANOVA(5,17)4.374			ANOVA(5,16) 13.864			ANOVA(5,17) 11.87				
	rWT	vWT		rWT	vWT		rWT	vWT		rWT	vWT		vWT
WT	0.014	0.001	WT	0.146	0.148	F WT	0.172	0.007	C I	WT	0.009	0.462	
rWT		0.153	rWT		0.914	rFWT		0.001	C II	WT	0.001	0.260	
vWT			vWT			vFWT			C IV	WT	0.001	0.001	

WT, res & veh WT : SOD & Catalase

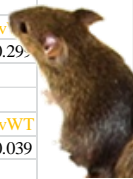
Total SOD							Non SOD						
Brain			SC		Ret		Brain			SC		Ret	
F(5,12)32.4			F(5,12)105.3		F(5,12)8.8		F(5,28)23.3			F(5,20)19.78		F(5,24)1.60	
	rWT	vWT	rWT	vWT	rWT	vWT		rWT	vWT	rWT	vWT	rWT	vWT
WT	0.146	0.007	0.007	0.077	0.981	0.004	WT	0.006	0.416	0.013	0.001	0.372	0.842
MnSOD							Catalase						
Brain			SC		Ret		Brain			SC		Ret	
F(5,12)48.7			F(5,12)22.6		F(5,12)3.74		F(5,31) 7.995			F(5,18) 10.902		F(3,10) 9.156	
	rWT	vWT	rWT	vWT	rWT	vWT		rWT	vWT	rWT	vWT	rWT	vWT
WT	0.001	0.494	0.001	0.712	0.340	0.448	WT	0.042	0.006	0.761	0.499	0.055	
CuZnSOD													
Brain			SC		Ret		Brain			SC		Ret	
F(5,12)3257.8			F(5,12)15.4		F(5,12)10.8		F(5,31) 7.995			F(5,18) 10.902		F(3,10) 9.156	
	rWT	vWT	rWT	vWT	rWT	vWT		rWT	vWT	rWT	vWT	rWT	vWT
WT	0.001	0.001	0.033	0.258	0.021	0.027	WT	0.042	0.006	0.761	0.499	0.055	



Summary of statistical analysis of ETC in WT, res and veh WT, Antioxidant Catalase and SOD.

Appendix

WT res WT & veh WT : IHC Retina & Brain															
Opa1	Ret AFU			ANOVA (5,15) 3.865 Post Hoc Tukey							Brain AFU				
	PRL	ONL	OPL	INL	IPL	GCL					Brain A	Opa1	VDAC	Preli	
	rWT	vWT	rWT	vWT	rWT	vWT	rWT	vWT	rWT	vWT	rWT	vWT	rWT	vWT	
WT	0.546	0.213	0.789	0.780	0.215	0.840	0.204	0.974	0.281	0.070	0.197	0.251			
VDAC	Ret AFU			ANOVA (5,15) 10.47 Post Hoc Tukey											
	PRL	ONL	OPL	INL	IPL	GCL					WT	0.223	0.982	0.012	0.112
	rWT	vWT	rWT	vWT	rWT	vWT	rWT	vWT	rWT	vWT	rWT	vWT			
WT	0.262	0.001	0.242	0.425	0.001	0.006	0.814	0.746	0.354	0.309	0.782	0.648			
Preli	Ret AFU			ANOVA (5,21) 21.466 Post Hoc Tukey											
	PRL	ONL	OPL	INL	IPL	GCL					WT	0.014	0.162		0.162
	rWT	vWT	rWT	vWT	rWT	vWT	rWT	vWT	rWT	vWT	rWT	vWT			
WT	0.282	0.080	0.001	0.750	0.016	0.041	0.102	0.119	0.219	0.511	0.614	0.592			
Neuro	Ret AFU			ANOVA (5,20) 1.530 Post Hoc Tukey											
	PRL	ONL	OPL	INL	IPL	GCL					WT	0.001	0.575	0.267	0.530
	rWT	vWT	rWT	vWT	rWT	vWT	rWT	vWT	rWT	vWT	rWT	vWT			
WT	0.408	0.240	0.817	0.814	0.562	0.732	0.962	0.732	0.405	0.402	0.452	0.652			
PSD 95	Ret AFU			ANOVA (5,28) 1.900 Post Hoc Tukey											
	PRL	ONL	OPL	INL	IPL	GCL									
	rWT	vWT	rWT	vWT	rWT	vWT	rWT	vWT	rWT	vWT	rWT	vWT			
WT	0.128	0.204	0.958	0.847	0.987	0.558	0.905	0.574	0.822	0.043	0.351	0.809			
NF1	Ret AFU			ANOVA (5,23) 8530 Post Hoc Tukey											
	PRL	ONL	OPL	INL	IPL	GCL									
	rWT	vWT	rWT	vWT	rWT	vWT	rWT	vWT	rWT	vWT	rWT	vWT			
WT	0.128	0.001	0.536	0.745	0.041	0.036	0.278	0.149	0.311	0.001	0.003	0.292			
MnSOD	Ret AFU			ANOVA (5,23) 8530 Post Hoc Tukey											
	PRL	ONL	OPL	INL	IPL	GCL									
	rWT	vWT	rWT	vWT	rWT	vWT	rWT	vWT	rWT	vWT	rWT	vWT			
WT	0.222	0.232	0.001	0.168	0.016	0.689	0.152	0.300	0.746	0.244	0.827	0.039			
3 Nitro	Ret AFU			ANOVA (5,23) 8530 Post Hoc Tukey											
	PRL	ONL	OPL	INL	IPL	GCL									
	rWT	vWT	rWT	vWT	rWT	vWT	rWT	vWT	rWT	vWT	rWT	vWT			
WT	0.222	0.204	0.007	0.062	0.669	0.136	0.205	0.039	0.031	0.032	0.327	0.449			
Mito	Ret AFU			ANOVA (5,16) 2.285											
	PRL	ONL	OPL	INL	IPL	GCL									
	rWT	vWT	rWT	vWT	rWT	vWT	rWT	vWT	rWT	vWT	rWT	vWT			
WT	0.546	0.883	0.355	0.448	0.194	0.759	0.438	0.865	0.446	0.466	0.664	0.568			
Comp	Ret AFU			ANOVA (5,15) 10.47											
	PRL	ONL	OPL	INL	IPL	GCL									
	rWT	vWT	rWT	vWT	rWT	vWT	rWT	vWT	rWT	vWT	rWT	vWT			
WT	0.888	0.697	0.340	0.765	0.329	0.723	0.337	0.867	0.350	0.586	0.944	0.202			
Damage	Ret AFU			ANOVA (5,21) 21.466											
	PRL	ONL	OPL	INL	IPL	GCL									
	rWT	vWT	rWT	vWT	rWT	vWT	rWT	vWT	rWT	vWT	rWT	vWT			
WT	0.559	0.253	0.315	0.670	0.025	0.019	0.005	0.015	0.529	0.195	0.775	0.915			
											Western Blot Retina RD				
											Opal Neuro Preli MnSO				
											F(3,12) 7.895 1.012 5.115 6.199				
											rWT rWT rWT rWT				
											WT 0.008 0.128 0.128 0.709				
											Western Blot Brain RD				
											Opal Neuro VDAC MnSO				
											F(3,12) 2.267 20.92 1.968 6.199				
											rWT rWT rWT rWT				
											WT 0.813 0.693 0.153 0.017				
											Brain AFU Retina AFU				
											F(5,75) 2.411 7.5				
											Mito rWT vWT Mito rWT vWT				
											WT 0.033 0.745 WT 0.211 0.645				
											Brain AFU Retina AFU				
											F (8,68) 5.957 2.39				
											Comp rWT vWT Comp rWT vWT				
											WT 0.165 0.781 WT 0.511 0.069				
											Brain AFU Retina AFU				
											F(5,75) 2.573 5.581				
											Dam rWT vWT Dam rWT vWT				
											WT 0.001 0.340 WT 0.163 0.097				



Summary of statistical analysis of WT, res and veh WT IHC in retina & brain. Protein profiles for mitochondria, compensation and damage profile in retina and brain.

Appendix X Copyright permission from Wiley

Chapter1: Figure 1.5 Copyright permission

JOHN WILEY AND SONS LICENSE TERMS AND CONDITIONS
May 15, 2014

This is a License Agreement between Caroline Waters ("You") and John Wiley and Sons ("John Wiley and Sons") provided by Copyright Clearance Center ("CCC"). The license consists of your order details, the terms and conditions provided by John Wiley and Sons, and the payment terms and conditions.

All payments must be made in full to CCC. For payment instructions, please see information listed at the bottom of this form.

License Number	3390221059124
License date	May 15, 2014
Licensed content publisher	John Wiley and Sons
Licensed content publication	Journal of Comparative Neurology
Licensed content title	Tracer coupling patterns of the ganglion cell subtypes in the mouse retina
Licensed copyright line	Copyright © 2008 Wiley-Liss, Inc.
Licensed content author	Béla Völgyi, Samir Chheda, Stewart A. Bloomfield
Licensed content date	Dec 2, 2008
Start page	664
End page	687
Type of use	Dissertation/Thesis
Requestor type	University/Academic
Format	Print
Portion	Figure/table
Number of figures/tables	1
Original Wiley figure/table number(s)	Figure 13 page 5
Will you be translating?	No
Title of your thesis / dissertation	Mitochondrial dysfunction in a mouse model of autosomal dominant optic atrophy 'plus'
Expected completion date	Jul 2014
Expected size (number of pages)	200
Total	0.00 GBP

Wiley Copyright Licence for use of Figure 1.5 Chapter 1 Page 10 'Mouse C57Bl/6 retinal ganglion cell subsets taken from 'Tracer Coupling Patterns of the Ganglion Cell Subtypes in the Mouse Retina' J Comp Neurol. Feb 10, 2009; 512(5): 664–687. Volgyi, Chheda Bloomfield

Appendix

Appendix Z Reagents

Bioenergetic Assays	(All buffers pretreated with Chelex overnight)			
Mitochondrial Isolation	Complex I (stock)	Complex II (stock)	Complex IV (stock)	Cytochrome c reduction
Extraction buffer A	PB 20mM pH7.4	PB 20mM pH 7.8	PB 10mM pH7.4	
50mM HEPES pH7.5	NADH 100mM	Succinate 1M	n-Dodecyl β -D-maltoside	10mMK ₂ HPO ₄
1M Mannitol	KCN 1M	Decylub 40mM		10mMKH ₂ PO ₄
350mM sucrose	CoenzymeQ ₁ 40mM	KCN 1M	Cytochrome c 2mM	Sephadex column
5mM EGTA		DCPIP 16mM	Ascorbate 100mM	Add 1ml 2mM Cyto c to
	Complex I assay	Complex II assay	Complex IV assay	:1ml 100mM Ascorbate
Extraction buffer B	in 499 μ l PB	in 492.5 μ l PB	in 540 μ l PB +0.005% nDoc	Incubate 5 mins RT
100mM MOPS pH 7.5	NADH 100 μ M: 5 μ l stock	Succinate 10 μ M:50 μ l stock	Cyto c 100 μ M:30 μ l stock	Add to Sephadex column
550mM KCl	KCN 1 μ M: 5 μ l stock	Decylub 100 μ M:12.5 μ l stock		Wash with PB
5mM EGTA	CQ ₁ 40 μ M: 1 μ l stock	KCN 2mM 10 μ l stock		Collect fractions (x4)
		DCPIP 16 μ M:5 μ l stock		Dilute ~1:20
Storage Buffer				Check absorbance
50mM HEPES pH 7.5				Store under Argon -80°C
1.25M sucrose				
5mM ATP	Complex I inhibition	Complex II inhibition	Complex IV inhibition	
0.4mM ADT	Rotenone 2mM stock	TTFA 100mM stock	KCN 200mM stock	
25mM sodium succinate	in 495 μ l PB	in 495 μ l PB	in 30 μ l mito	
10mM K ₂ HPO ₄	Rotenone 2 μ M:5 μ l stock	TTFE 100 μ M:5 μ l stock	KCN 20 μ M:3 μ l stock	
Reagents SIGMA	Reagents SIGMA	Reagents SIGMA	Reagents SIGMA	Reagents SIGMA
Chelex #95577	NADH #N8129	DCPIP #D1878	Cyto c #C2506	Ascorbate #95209
Dialysis tubing #D9277	KCN #31252	TTFA #T27006		SephadexG100 #S6147
EGTA #E3889	CoQ ₁ #7959	Decylub # D7911		
MOPS #M1254	Rotenone #R8875			
HEPES #H3375				
Mannitol #M4125				
Sucrose #S7903				
KCL #P9333				
ATP #A7699				
ADP # A2754				
Succinate #A5247				
Potassium Dibasic #P3786				
Potassium Monobasic #P5655				

Buffers reagents and concentrations used for isolation and analysis of mitochondrial bioenergetics

Appendix

Antioxidant assays		Protein assays	
CAT assay	SOD assay	Western Blotting	Immunohistochemistry
50mM KH ₂ PO ₄	WST1+ O ₂ [•] → formazan	RIPA buffer	PBS 1l pH 7.4
10.3mM H ₂ O ₂	O ₂ [•] xanthine	50mM TrisHCL pH8.0	137mM NaCl
	WST1+ O ₂ [•] + SOD = ↓ formazan	150mM NaCl	2.7mM KCl
9.4 M H ₂ O ₂ stock (30%) in 5ml PB	B1: formazan no inhibition	1% Igepal	10mM Na ₂ HPO ₄
H ₂ O ₂ 10.3mM: 5.47μl stock	B2: sample blank(no enzyme)	0.5% sodium deoxycholate	2mM KH ₂ PO ₄
ε43.6 M ⁻¹ cm ⁻¹	B3: reagent blank(no enzyme)	0.1% SDS	Sterilise by autoclave
Begin with	SOD standard		
H ₂ O ₂ 10.3mM: 5.4μl stock	5mM KCN(CuZn inhibition)	Running buffer 1l pH 8.3	PFA 4% pH 7.4 (hood)
Check absorbance 240nm	2% SDS(MnSOD inhibition)	125mM Tris	Heat to 56°C
A 240nm 0.449 = 10.30mM		1.25M glycine	Continual stirring
if req adjust H ₂ O ₂ content		0.5% SDS	Filter sterilise
Check absorbance 240nm		Transfer Buffer 1l	Blocking agent
		48mM Tris HcL	Goat serum 10%
Normal saline	DNA extraction buffer	39mM Glycine	Heat inactivate 56°C 30min
0.9% NaCL	50mM NaOH	0.037% SDS	Aliquot 100μl -20°C
1l MQ water	1M Tris HCL pH 6.0	20% Methanol	
Sterilise by autoclave			
		Gel reagents	Endogenous Peroxidase
Reagents SIGMA	Reagents SIGMA	1.5M Tris pH 8.0	(In safety hood)
Hydrogen peroxide #16911	SOD assay kit #19160	0.5M Tris pH 6.8	H ₂ O ₂ 3%
Catalase #C1345	Sodium hydroxide #306776	10% SDS	1.5ml of stock 30%
	Hydrochloric acid #H1758	10% APS	3.5ml PBS
	SDS #74255	TEMED	200μl/slide
		Reagents SIGMA	Reagents SIGMA
		Igepal # I8896	Paraformaldehyde #P6148
		Tris-Glycine #T4904	NGS #G9023
		Na deoxycholate # D6750	
		Methanol #322415	
		APS #A3678	
		TEMED #T9281	

Buffers reagents and concentrations used for analysis of antioxidant activity and protein chemistry

References

References for Mitochondrial profile of Opa1^{Q285STOP} mouse model of ADOA

Abe, A. et al. 2009. Neurofilament light chain polypeptide gene mutations in Charcot-Marie-Tooth disease: nonsense mutation probably causes a recessive phenotype. *J Hum Genet* 54(2), pp. 94-97.

Abramoff, M. and Magalhaes, P. 2004. Image Processing with ImageJ. *Biophotonics International* 11(7), pp. 36-42.

Abramoff, M. D. et al. 2010. Retinal imaging and image analysis. *IEEE Rev Biomed Eng* 3, pp. 169-208.

Abramov, U. et al. 2008. Different housing conditions alter the behavioural phenotype of CCK(2) receptor-deficient mice. *Behav Brain Res* 193(1), pp. 108-116.

Adachi, M. et al. 2004. Bax interacts with the voltage-dependent anion channel and mediates ethanol-induced apoptosis in rat hepatocytes. *Am J Physiol Gastrointest Liver Physiol* 287(3), pp. G695-705.

Aebi, H. 1984. Catalase in vitro. *Methods Enzymol* 105, pp. 121-126.

Aggleton, J. P. et al. 1997. Extensive cytotoxic lesions involving both the rhinal cortices and area TE impair recognition but spare spatial alternation in the rat. *Brain Res Bull* 43(3), pp. 279-287.

Ahsan, H. and Hadi, S. M. 1998. Strand scission in DNA induced by curcumin in the presence of Cu(II). *Cancer Lett* 124(1), pp. 23-30.

Akkerman, S. et al. 2012a. Object recognition testing: methodological considerations on exploration and discrimination measures. *Behav Brain Res* 232(2), pp. 335-347.

Akkerman, S. et al. 2012b. Object recognition testing: statistical considerations. *Behav Brain Res* 232(2), pp. 317-322.

Alavi, M. V. et al. 2007. A splice site mutation in the murine Opa1 gene features pathology of autosomal dominant optic atrophy. *Brain* 130(Pt 4), pp. 1029-1042.

Alemanly, M. 2012. Regulation of adipose tissue energy availability through blood flow control in the metabolic syndrome. *Free Radic Biol Med* 52(10), pp. 2108-2119.

Alexander, C. et al. 2000. OPA1, encoding a dynamin-related GTPase, is mutated in autosomal dominant optic atrophy linked to chromosome 3q28. *Nat Genet* 26(2), pp. 211-215.

Ali, S. S. et al. 2011. Initial evidence linking synaptic superoxide production with poor short-term memory in aged mice. *Brain Res* 1368, pp. 65-70.

References

- Allbutt, H. N. and Henderson, J. M. 2007. Use of the narrow beam test in the rat, 6-hydroxydopamine model of Parkinson's disease. *J Neurosci Methods* 159(2), pp. 195-202.
- Allen, D. L. et al. 2001. Cardiac and skeletal muscle adaptations to voluntary wheel running in the mouse. *J Appl Physiol (1985)* 90(5), pp. 1900-1908.
- Althoff, T. et al. 2011. Arrangement of electron transport chain components in bovine mitochondrial supercomplex I₁III₂IV₁. *EMBO J* 30(22), pp. 4652-4664.
- Altomare, R. E. et al. 1974. Deactivation of immobilized beef liver catalase by hydrogen peroxide. *Biotechnol Bioeng* 16(12), pp. 1659-1673.
- Amati-Bonneau, P. et al. 2005. OPA1 R445H mutation in optic atrophy associated with sensorineural deafness. *Ann Neurol* 58(6), pp. 958-963.
- Amati-Bonneau, P. et al. 2009. OPA1-associated disorders: phenotypes and pathophysiology. *Int J Biochem Cell Biol* 41(10), pp. 1855-1865.
- Ames, A. 2000. CNS energy metabolism as related to function. *Brain Res Brain Res Rev* 34(1-2), pp. 42-68.
- Anderson, E. J. et al. 2009. Mitochondrial H₂O₂ emission and cellular redox state link excess fat intake to insulin resistance in both rodents and humans. *J Clin Invest* 119(3), pp. 573-581.
- Anderson, E. J. et al. 2007. Induction of endogenous uncoupling protein 3 suppresses mitochondrial oxidant emission during fatty acid-supported respiration. *J Biol Chem* 282(43), pp. 31257-31266.
- Angebault, C. et al. 2011. Idebenone increases mitochondrial complex I activity in fibroblasts from LHON patients while producing contradictory effects on respiration. *BMC Res Notes* 4, p. 557.
- Ankarcrona, M. et al. 1995. Glutamate-induced neuronal death: a succession of necrosis or apoptosis depending on mitochondrial function. *Neuron* 15(4), pp. 961-973.
- Apostolova, I. et al. 2012. Brain perfusion SPECT in the mouse: normal pattern according to gender and age. *Neuroimage* 63(4), pp. 1807-1817.
- Araújo, G. W. et al. 2008. Oestrogen influences on mitochondrial gene expression and respiratory chain activity in cortical and mesencephalic astrocytes. *J Neuroendocrinol* 20(7), pp. 930-941.
- Ardail, D. et al. 1990. Mitochondrial contact sites. Lipid composition and dynamics. *J Biol Chem* 265(31), pp. 18797-18802.

References

Arnao, M. B. et al. 1990. A kinetic study on the suicide inactivation of peroxidase by hydrogen peroxide. *Biochim Biophys Acta* 1041(1), pp. 43-47.

Arqué, G. et al. 2008. Impaired spatial learning strategies and novel object recognition in mice haploinsufficient for the dual specificity tyrosine-regulated kinase-1A (Dyrk1A). *PLoS One* 3(7), p. e2575.

Arrigoni, O. and Singer, T. P. 1962. Limitations of the phenazine methosulphate assay for succinic and related dehydrogenases. *Nature* 193, pp. 1256-1258.

Aufradet, E. et al. 2012. In vivo cardiac anatomical and functional effects of wheel running in mice by magnetic resonance imaging. *Exp Biol Med (Maywood)* 237(3), pp. 263-270.

Azorín-Ortuño, M. et al. 2011. Metabolites and tissue distribution of resveratrol in the pig. *Mol Nutr Food Res* 55(8), pp. 1154-1168.

Bachmanov, A. A. et al. 2002. Food intake, water intake, and drinking spout side preference of 28 mouse strains. *Behav Genet* 32(6), pp. 435-443.

Baek, S. H. et al. 2014. Treatment of obesity with the resveratrol-enriched rice DJ-526. *Sci Rep* 4, p. 3879.

Baines, C. P. et al. 2007. Voltage-dependent anion channels are dispensable for mitochondrial-dependent cell death. *Nat Cell Biol* 9(5), pp. 550-555.

Bakhtiarova, A. et al. 2006. Resveratrol inhibits firefly luciferase. *Biochem Biophys Res Commun* 351(2), pp. 481-484.

Ban, T. et al. 2010. OPA1 disease alleles causing dominant optic atrophy have defects in cardiolipin-stimulated GTP hydrolysis and membrane tubulation. *Hum Mol Genet* 19(11), pp. 2113-2122.

Bannerman, D. M. et al. 1995. Distinct components of spatial learning revealed by prior training and NMDA receptor blockade. *Nature* 378(6553), pp. 182-186.

Barboni, P. et al. 2010. OPA1 mutations associated with dominant optic atrophy influence optic nerve head size. *Ophthalmology* 117(8), pp. 1547-1553.

Barboni, P. et al. 2013. Idebenone treatment in patients with OPA1-mutant dominant optic atrophy. *Brain*.

Barksdale, K. A. et al. 2010. Mitochondrial viability in mouse and human postmortem brain. *FASEB J* 24(9), pp. 3590-3599.

References

- Baroncelli, L. et al. 2010. Nurturing brain plasticity: impact of environmental enrichment. *Cell Death Differ* 17(7), pp. 1092-1103.
- Batandier, C. et al. 2004. Opening of the mitochondrial permeability transition pore induces reactive oxygen species production at the level of the respiratory chain complex I. *J Biol Chem* 279(17), pp. 17197-17204.
- Baud, O. et al. 2004. Glutathione peroxidase-catalase cooperativity is required for resistance to hydrogen peroxide by mature rat oligodendrocytes. *J Neurosci* 24(7), pp. 1531-1540.
- Baur, J. A. and Sinclair, D. A. 2006. Therapeutic potential of resveratrol: the in vivo evidence. *Nat Rev Drug Discov* 5(6), pp. 493-506.
- Bayir, H. et al. 2007. Neuronal NOS-mediated nitration and inactivation of manganese superoxide dismutase in brain after experimental and human brain injury. *J Neurochem* 101(1), pp. 168-181.
- Bazán, S. et al. 2013. Cardiolipin-dependent reconstitution of respiratory supercomplexes from purified *Saccharomyces cerevisiae* complexes III and IV. *J Biol Chem* 288(1), pp. 401-411.
- Beauchamp, M. H. et al. 2004. Redox-dependent effects of nitric oxide on microvascular integrity in oxygen-induced retinopathy. *Free Radic Biol Med* 37(11), pp. 1885-1894.
- Beaudoin, M. S. et al. 2013. Resveratrol supplementation improves white adipose tissue function in a depot-specific manner in Zucker diabetic fatty rats. *Am J Physiol Regul Integr Comp Physiol* 305(5), pp. R542-551.
- Beers and Sizer. 1952. A spectrophotometric method for measuring the breakdown of hydrogen peroxide by catalase. *J Biol Chem* 195(1), pp. 133-140.
- Bellaver, B. et al. 2014. Resveratrol increases antioxidant defenses and decreases proinflammatory cytokines in hippocampal astrocyte cultures from newborn, adult and aged Wistar rats. *Toxicol In Vitro* 28(4), pp. 479-484.
- Bermudez-Rattoni, F. et al. 2005. Insular cortex is involved in consolidation of object recognition memory. *Learn Mem* 12(5), pp. 447-449.
- Bernardi, P. 2013. The mitochondrial permeability transition pore: a mystery solved? *Front Physiol* 4, p. 95.
- Berski, S. et al. 2011. Electron localization function and electron localizability indicator applied to study the bonding in the peroxy-nitrous acid HOONO. *J Comput Chem* 32(8), pp. 1528-1540.
- Betzen, C. et al. 2009. Oxidative stress upregulates the NMDA receptor on cerebrovascular endothelium. *Free Radic Biol Med* 47(8), pp. 1212-1220.

References

- Bhattacharya, A. et al. 2011. Increased mitochondrial matrix-directed superoxide production by fatty acid hydroperoxides in skeletal muscle mitochondria. *Free Radic Biol Med* 50(5), pp. 592-601.
- Bicknell, I. R. et al. 2002. Alterations in retinal rod outer segment fatty acids and light-damage susceptibility in P23H rats. *Mol Vis* 8, pp. 333-340.
- Bolger, G. B. et al. 1996. Alternative splicing of cAMP-specific phosphodiesterase mRNA transcripts. Characterization of a novel tissue-specific isoform, RNPDE4A8. *J Biol Chem* 271(2), pp. 1065-1071.
- Borutaite, V. et al. 1999. Release of cytochrome c from heart mitochondria is induced by high Ca^{2+} and peroxynitrite and is responsible for Ca^{2+} -induced inhibition of substrate oxidation. *Biochim Biophys Acta* 1453(1), pp. 41-48.
- Bosma, M. 2014. Lipid homeostasis in exercise. *Drug Discov Today* 19(7), pp. 1019-1023.
- Boutbir, J. et al. 2012. Opposite effects of statins on mitochondria of cardiac and skeletal muscles: a 'mitohormesis' mechanism involving reactive oxygen species and PGC-1. *Eur Heart J* 33(11), pp. 1397-1407.
- Boveris, A. et al. 1972. The cellular production of hydrogen peroxide. *Biochem J* 128(3), pp. 617-630.
- Bradley, S. et al. 2010. Nitric oxide synthase regulates morphogenesis of zebrafish spinal cord motoneurons. *J Neurosci* 30(50), pp. 16818-16831.
- Branca, D. et al. 1988. The inhibition of calcium efflux from rat liver mitochondria by halogenated anesthetics. *Biochem Biophys Res Commun* 155(2), pp. 978-983.
- Bristow, E. A. et al. 2002. The distribution of mitochondrial activity in relation to optic nerve structure. *Arch Ophthalmol* 120(6), pp. 791-796.
- Brown, G. C. and Borutaite, V. 1999. Nitric oxide, cytochrome c and mitochondria. *Biochem Soc Symp* 66, pp. 17-25.
- Brown, G. C. and Borutaite, V. 2001. Nitric oxide, mitochondria, and cell death. *IUBMB Life* 52(3-5), pp. 189-195.
- Brown, M. R. et al. 2006. Synaptic mitochondria are more susceptible to Ca^{2+} -overload than nonsynaptic mitochondria. *J Biol Chem* 281(17), pp. 11658-11668.
- Bustos, F. J. et al. 2014. PSD95 suppresses dendritic arbor development in mature hippocampal neurons by occluding the clustering of NR2B-NMDA receptors. *PLoS One* 9(4), p. e94037.

References

- Cal, C. et al. 2003. Resveratrol and cancer: chemoprevention, apoptosis, and chemosensitizing activities. *Curr Med Chem Anticancer Agents* 3(2), pp. 77-93.
- Cancedda, L. et al. 2004. Acceleration of visual system development by environmental enrichment. *J Neurosci* 24(20), pp. 4840-4848.
- Carpéné, C. et al. 2014. Novel Strategies for preventing Diabetes and Obesity Complications with Natural Polyphenols. *Curr Med Chem*.
- Carroll, J. et al. 2006. Bovine complex I is a complex of 45 different subunits. *J Biol Chem* 281(43), pp. 32724-32727.
- Carter, R. J. et al. 2001. Motor coordination and balance in rodents. *Curr Protoc Neurosci* Chapter 8, p. Unit 8.12.
- Cartoni, R. and Martinou, J. C. 2009. Role of mitofusin 2 mutations in the physiopathology of Charcot-Marie-Tooth disease type 2A. *Exp Neurol* 218(2), pp. 268-273.
- Casado, B. et al. 2005. Human neuroglobin protein in cerebrospinal fluid. *Proteome Sci* 3(1), p. 2.
- Cassina, A. and Radi, R. 1996. Differential inhibitory action of nitric oxide and peroxynitrite on mitochondrial electron transport. *Arch Biochem Biophys* 328(2), pp. 309-316.
- Castro, L. et al. 2011. Mitochondrial protein tyrosine nitration. *Free Radic Res* 45(1), pp. 37-52.
- Celsi, F. et al. 2009. Mitochondria, calcium and cell death: a deadly triad in neurodegeneration. *Biochim Biophys Acta* 1787(5), pp. 335-344.
- Cereghetti, G. M. and Scorrano, L. 2006. The many shapes of mitochondrial death. *Oncogene* 25(34), pp. 4717-4724.
- Chacinska, A. et al. 2005. Mitochondrial presequence translocase: switching between TOM tethering and motor recruitment involves Tim21 and Tim17. *Cell* 120(6), pp. 817-829.
- Chakraborty, S. et al. 2013. Structural insights into Resveratrol's antagonist and partial agonist actions on estrogen receptor alpha. *BMC Struct Biol* 13, p. 27.
- Chan, E. Y. and McQuibban, G. A. 2012. Phosphatidylserine decarboxylase 1 (Psd1) promotes mitochondrial fusion by regulating the biophysical properties of the mitochondrial membrane and alternative topogenesis of mitochondrial genome maintenance protein 1 (Mgm1). *J Biol Chem* 287(48), pp. 40131-40139.

References

- Chance, B. et al. 1979. Hydroperoxide metabolism in mammalian organs. *Physiol Rev* 59(3), pp. 527-605.
- Chandor-Proust, A. et al. 2008. DNA repair and free radicals, new insights into the mechanism of spore photoproduct lyase revealed by single amino acid substitution. *J Biol Chem* 283(52), pp. 36361-36368.
- Chang, C. R. and Blackstone, C. 2007. Drp1 phosphorylation and mitochondrial regulation. *EMBO Rep* 8(12), pp. 1088-1089; author reply 1089-1090.
- Charych, E. I. et al. 2006. Activity-independent regulation of dendrite patterning by postsynaptic density protein PSD-95. *J Neurosci* 26(40), pp. 10164-10176.
- Cheek, D. B. and Holt, A. B. 1963. Growth and body composition of the mouse. *Am J Physiol* 205(5), pp. 913-918.
- Chen, H. et al. 2003. Mitofusins Mfn1 and Mfn2 coordinately regulate mitochondrial fusion and are essential for embryonic development. *J Cell Biol* 160(2), pp. 189-200.
- Chen, L. et al. 2012. OPA1 mutation and late-onset cardiomyopathy: mitochondrial dysfunction and mtDNA instability. *J Am Heart Assoc* 1(5), p. e003012.
- Chen, Y. P. and Chiao, C. C. 2014. Spatial distribution of excitatory synapses on the dendrites of ganglion cells in the mouse retina. *PLoS One* 9(1), p. e86159.
- Chevrollier, A. et al. 2008. Hereditary optic neuropathies share a common mitochondrial coupling defect. *Ann Neurol* 63(6), pp. 794-798.
- Cho, S. et al. 2007. A novel cell-permeable antioxidant peptide, SS31, attenuates ischemic brain injury by down-regulating CD36. *J Biol Chem* 282(7), pp. 4634-4642.
- Chung, S. et al. 2010. Regulation of SIRT1 in cellular functions: role of polyphenols. *Arch Biochem Biophys* 501(1), pp. 79-90.
- Cipolat, S. et al. 2006. Mitochondrial rhomboid PARL regulates cytochrome c release during apoptosis via OPA1-dependent cristae remodeling. *Cell* 126(1), pp. 163-175.
- Claiborne, A. et al. 1979. Purification and characterization of hydroperoxidase II of Escherichia coli B. *J Biol Chem* 254(22), pp. 11664-11668.
- Clark, R. E. et al. 2000. Impaired recognition memory in rats after damage to the hippocampus. *J Neurosci* 20(23), pp. 8853-8860.
- Cocco, T. et al. 2009. Control of OXPHOS efficiency by complex I in brain mitochondria. *Neurobiol Aging* 30(4), pp. 622-629.

References

- Cohn, A. C. et al. 2008. The natural history of OPA1-related autosomal dominant optic atrophy. *Br J Ophthalmol* 92(10), pp. 1333-1336.
- Colquhoun, A. 2010. Lipids, mitochondria and cell death: implications in neuro-oncology. *Mol Neurobiol* 42(1), pp. 76-88.
- Conde, A. et al. 2010. Transporters, channels, or simple diffusion? Dogmas, atypical roles and complexity in transport systems. *Int J Biochem Cell Biol* 42(6), pp. 857-868.
- Conti, B. et al. 2006. Transgenic mice with a reduced core body temperature have an increased life span. *Science* 314(5800), pp. 825-828.
- Cooper, K. D. et al. 1985. Phosphodiesterase inhibition by Ro 20-1724 reduces hyper-IgE synthesis by atopic dermatitis cells in vitro. *J Invest Dermatol* 84(6), pp. 477-482.
- Danz, E. D. et al. 2009. Resveratrol prevents doxorubicin cardiotoxicity through mitochondrial stabilization and the Sirt1 pathway. *Free Radic Biol Med* 46(12), pp. 1589-1597.
- Davey, G. P. et al. 1997. Threshold effects in synaptosomal and nonsynaptic mitochondria from hippocampal CA1 and paramedian neocortex brain regions. *J Neurochem* 69(6), pp. 2564-2570.
- Davey, G. P. and Clark, J. B. 1996. Threshold effects and control of oxidative phosphorylation in nonsynaptic rat brain mitochondria. *J Neurochem* 66(4), pp. 1617-1624.
- Davey, G. P. et al. 1998. Energy thresholds in brain mitochondria. Potential involvement in neurodegeneration. *J Biol Chem* 273(21), pp. 12753-12757.
- Davies, V. J. et al. 2007. Opa1 deficiency in a mouse model of autosomal dominant optic atrophy impairs mitochondrial morphology, optic nerve structure and visual function. *Hum Mol Genet* 16(11), pp. 1307-1318.
- Deeb, R. S. et al. 2013. Characterization of a cellular denitrase activity that reverses nitration of cyclooxygenase. *Am J Physiol Heart Circ Physiol* 305(5), pp. H687-698.
- Dekutovich, G. V. and Kargapolov, A. V. 1986. [Characteristic effect of local anesthetics on the phospholipid composition of mitochondria]. *Vopr Med Khim* 32(6), pp. 38-41.
- Delettre, C. et al. 2001. Mutation spectrum and splicing variants in the OPA1 gene. *Hum Genet* 109(6), pp. 584-591.
- Delettre, C. et al. 2000. Nuclear gene OPA1, encoding a mitochondrial dynamin-related protein, is mutated in dominant optic atrophy. *Nat Genet* 26(2), pp. 207-210.

References

- Demicheli, V. et al. 2007. Inactivation and nitration of human superoxide dismutase (SOD) by fluxes of nitric oxide and superoxide. *Free Radic Biol Med* 42(9), pp. 1359-1368.
- Devries, S. H. and Baylor, D. A. 1997. Mosaic arrangement of ganglion cell receptive fields in rabbit retina. *J Neurophysiol* 78(4), pp. 2048-2060.
- Diamond, M. E. et al. 2008. 'Where' and 'what' in the whisker sensorimotor system. *Nat Rev Neurosci* 9(8), pp. 601-612.
- Drögemüller, C. et al. 2011. An unusual splice defect in the mitofusin 2 gene (MFN2) is associated with degenerative axonopathy in Tyrolean Grey cattle. *PLoS One* 6(4), p. e18931.
- Duan, S. et al. 2003. Mitochondrial outer membrane permeability change and hypersensitivity to digitonin early in staurosporine-induced apoptosis. *J Biol Chem* 278(2), pp. 1346-1353.
- Dutta, R. and Trapp, B. D. 2011. Mechanisms of neuronal dysfunction and degeneration in multiple sclerosis. *Prog Neurobiol* 93(1), pp. 1-12.
- Duvezin-Caubet, S. et al. 2006. Proteolytic processing of OPA1 links mitochondrial dysfunction to alterations in mitochondrial morphology. *J Biol Chem* 281(49), pp. 37972-37979.
- Duvezin-Caubet, S. et al. 2007. OPA1 processing reconstituted in yeast depends on the subunit composition of the m-AAA protease in mitochondria. *Mol Biol Cell* 18(9), pp. 3582-3590.
- Earnhardt, J. N. et al. 2002. Induction of manganese superoxide dismutase in acute spinal cord injury. *J Neurotrauma* 19(9), pp. 1065-1079.
- Egger, A. et al. 2012. PGC-1 α determines light damage susceptibility of the murine retina. *PLoS One* 7(2), p. e31272.
- Ehse, S. et al. 2009. Regulation of OPA1 processing and mitochondrial fusion by m-AAA protease isoforms and OMA1. *J Cell Biol* 187(7), pp. 1023-1036.
- Eiberg, H. et al. 1994. Dominant optic atrophy (OPA1) mapped to chromosome 3q region. I. Linkage analysis. *Hum Mol Genet* 3(6), pp. 977-980.
- Eisen, E. J. 1976. Results of growth curve analyses in mice and rats. *J Anim Sci* 42(4), pp. 1008-1023.
- El Zein, N. et al. 2010. Crosstalks between the receptors tyrosine kinase EGFR and TrkA and the GPCR, FPR, in human monocytes are essential for receptors-mediated cell activation. *Cell Signal* 22(10), pp. 1437-1447.
- Elachouri, G. et al. 2011. OPA1 links human mitochondrial genome maintenance to mtDNA replication and distribution. *Genome Res* 21(1), pp. 12-20.

References

- Eldstrom, J. et al. 2002. N-terminal PDZ-binding domain in Kv1 potassium channels. *FEBS Lett* 531(3), pp. 529-537.
- Engmann, O. et al. 2011. Schizophrenia is associated with dysregulation of a Cdk5 activator that regulates synaptic protein expression and cognition. *Brain* 134(Pt 8), pp. 2408-2421.
- Ennaceur, A. and Delacour, J. 1988. A new one-trial test for neurobiological studies of memory in rats. 1: Behavioral data. *Behav Brain Res* 31(1), pp. 47-59.
- Ennaceur, A. et al. 1997. Spontaneous object recognition and object location memory in rats: the effects of lesions in the cingulate cortices, the medial prefrontal cortex, the cingulum bundle and the fornix. *Exp Brain Res* 113(3), pp. 509-519.
- Enns, G. M. et al. 2012. Initial experience in the treatment of inherited mitochondrial disease with EPI-743. *Mol Genet Metab* 105(1), pp. 91-102.
- Epstein, R. and Kanwisher, N. 1998. A cortical representation of the local visual environment. *Nature* 392(6676), pp. 598-601.
- Escobar, J. et al. 2013. Prolonging in utero-like oxygenation after birth diminishes oxidative stress in the lung and brain of mice pups. *Redox Biol* 1(1), pp. 297-303.
- Eyer, J. and Peterson, A. 1994. Neurofilament-deficient axons and perikaryal aggregates in viable transgenic mice expressing a neurofilament-beta-galactosidase fusion protein. *Neuron* 12(2), pp. 389-405.
- Faustin, B. et al. 2004. Mobilization of adenine nucleotide translocators as molecular bases of the biochemical threshold effect observed in mitochondrial diseases. *J Biol Chem* 279(19), pp. 20411-20421.
- Fealy, C. E. et al. 2014. Exercise training decreases activation of the mitochondrial fission protein dynamin-related protein-1 in insulin-resistant human skeletal muscle. *J Appl Physiol (1985)* 117(3), pp. 239-245.
- Feilchenfeld, Z. et al. 2008. Oxidative injury to blood vessels and glia of the pre-laminar optic nerve head in human glaucoma. *Exp Eye Res* 87(5), pp. 409-414.
- Feillet-Coudray, C. et al. 2014. Impact of high dietary lipid intake and related metabolic disorders on the abundance and acyl composition of the unique mitochondrial phospholipid, cardiolipin. *J Bioenerg Biomembr* 46(5), pp. 447-457.
- Ferezou, I. et al. 2006. Visualizing the cortical representation of whisker touch: voltage-sensitive dye imaging in freely moving mice. *Neuron* 50(4), pp. 617-629.

References

- Ferguson, G. D. et al. 2004. Altered hippocampal short-term plasticity and associative memory in synaptotagmin IV (-/-) mice. *Hippocampus* 14(8), pp. 964-974.
- Fernandes, N. D. et al. 2007. Activation of the kinase activity of ATM by retinoic acid is required for CREB-dependent differentiation of neuroblastoma cells. *J Biol Chem* 282(22), pp. 16577-16584.
- Ferré, M. et al. 2005. eOPA1: an online database for OPA1 mutations. *Hum Mutat* 25(5), pp. 423-428.
- Finsterer, J. et al. 2012. Hereditary spastic paraplegias with autosomal dominant, recessive, X-linked, or maternal trait of inheritance. *J Neurol Sci* 318(1-2), pp. 1-18.
- Fiocchetti, M. et al. 2013. Neuroglobin and neuronal cell survival. *Biochim Biophys Acta*.
- Fletcher, E. L. et al. 2000. Synaptic localization of NMDA receptor subunits in the rat retina. *J Comp Neurol* 420(1), pp. 98-112.
- Flurkey et al. 2007a. *The Mouse in Biomedical Research*. Burlington MA US: American College of Laboratory Animal Medicine (Elsevier), pp. 637-672.
- Flurkey et al. 2007b. *The Mouse in Biomedical Research*. Burlington MA US: American College of Laboratory Animal Medicine (Elsevier), pp. 637-672.
- Foncea, R. et al. 2000. Endothelial cell oxidative stress and signal transduction. *Biol Res* 33(2), pp. 89-96.
- Frank, S. et al. 2001. The role of dynamin-related protein 1, a mediator of mitochondrial fission, in apoptosis. *Dev Cell* 1(4), pp. 515-525.
- Franze, T. et al. 2004. Comparison of nitrotyrosine antibodies and development of immunoassays for the detection of nitrated proteins. *Analyst* 129(7), pp. 589-596.
- Frey, T. G. et al. 2006. Electron tomography of membrane-bound cellular organelles. *Annu Rev Biophys Biomol Struct* 35, pp. 199-224.
- Frick, K. M. and Gresack, J. E. 2003. Sex differences in the behavioral response to spatial and object novelty in adult C57BL/6 mice. *Behav Neurosci* 117(6), pp. 1283-1291.
- Fung, B. K. et al. 1981. Flow of information in the light-triggered cyclic nucleotide cascade of vision. *Proc Natl Acad Sci U S A* 78(1), pp. 152-156.
- Fyfe, J. C. et al. 2011. A novel mitofusin 2 mutation causes canine fetal-onset neuroaxonal dystrophy. *Neurogenetics* 12(3), pp. 223-232.

References

- Gadacha, W. et al. 2009. Resveratrol opposite effects on rat tissue lipoperoxidation: pro-oxidant during day-time and antioxidant at night. *Redox Rep* 14(4), pp. 154-158.
- Gadelha, F. R. et al. 1997. Ca²⁺-independent permeabilization of the inner mitochondrial membrane by peroxynitrite is mediated by membrane protein thiol cross-linking and lipid peroxidation. *Arch Biochem Biophys* 345(2), pp. 243-250.
- Gaiottino, J. et al. 2013. Increased neurofilament light chain blood levels in neurodegenerative neurological diseases. *PLoS One* 8(9), p. e75091.
- García-Ruiz, I. et al. 2010. Mitochondrial complex I subunits are decreased in murine nonalcoholic fatty liver disease: implication of peroxynitrite. *J Proteome Res* 9(5), pp. 2450-2459.
- Gaskill, B. N. et al. 2012. Heat or insulation: behavioral titration of mouse preference for warmth or access to a nest. *PLoS One* 7(3), p. e32799.
- Gassmann, M. et al. 2009. Quantifying Western blots: pitfalls of densitometry. *Electrophoresis* 30(11), pp. 1845-1855.
- Geller, B. L. and Winge, D. R. 1983. A method for distinguishing Cu,Zn- and Mn-containing superoxide dismutases. *Anal Biochem* 128(1), pp. 86-92.
- Genova, M. L. and Lenaz, G. 2013. A critical appraisal of the role of respiratory supercomplexes in mitochondria. *Biol Chem* 394(5), pp. 631-639.
- Gilkerson, R. W. et al. 2008. Mitochondrial nucleoids maintain genetic autonomy but allow for functional complementation. *J Cell Biol* 181(7), pp. 1117-1128.
- Gilmour, R. et al. 1994. The kinetics of the oxidation of cytochrome c by Paracoccus cytochrome c peroxidase. *Biochem J* 300 (Pt 3), pp. 907-914.
- Goecks, C. S. et al. 2012. Assessment of oxidative parameters in rat spinal cord after chronic constriction of the sciatic nerve. *Neurochem Res* 37(9), pp. 1952-1958.
- Goldberg, D. M. 1996. More on antioxidant activity of resveratrol in red wine. *Clin Chem* 42(1), pp. 113-114.
- Gomes, L. C. et al. 2011. During autophagy mitochondria elongate, are spared from degradation and sustain cell viability. *Nat Cell Biol* 13(5), pp. 589-598.
- Gonzales, P. and Rikke, B. A. 2010. Thermoregulation in mice exhibits genetic variability early in senescence. *Age (Dordr)* 32(1), pp. 31-37.

References

Goto, K. et al. 2010. Left-right asymmetry defect in the hippocampal circuitry impairs spatial learning and working memory in iv mice. *PLoS One* 5(11), p. e15468.

Gowrisankaran, S. et al. 2011. Structural and Functional Measures of Inner Retinal Integrity Following Visual Acuity Improvement in a Patient with Hereditary Motor and Sensory Neuropathy Type VI. *Ophthalmic Genet* 32(3), pp. 188-192.

Green, D. R. 2005. Apoptotic pathways: ten minutes to dead. *Cell* 121(5), pp. 671-674.

Greenacre, S. A. and Ischiropoulos, H. 2001. Tyrosine nitration: localisation, quantification, consequences for protein function and signal transduction. *Free Radic Res* 34(6), pp. 541-581.

Greka, A. et al. 2003. TRPC5 is a regulator of hippocampal neurite length and growth cone morphology. *Nat Neurosci* 6(8), pp. 837-845.

Griparic, L. et al. 2007. Regulation of the mitochondrial dynamin-like protein Opal by proteolytic cleavage. *J Cell Biol* 178(5), pp. 757-764.

Grivennikova, V. G. et al. 2010. What are the sources of hydrogen peroxide production by heart mitochondria? *Biochim Biophys Acta* 1797(6-7), pp. 939-944.

Gu, F. et al. 2013. Alterations in mitochondrial DNA copy number and the activities of electron transport chain complexes and pyruvate dehydrogenase in the frontal cortex from subjects with autism. *Transl Psychiatry* 3, p. e299.

Guo, J. et al. 2013. Motor neuron degeneration in a mouse model of seipinopathy. *Cell Death Dis* 4, p. e535.

Guo, X. D. et al. 2011. Phenolics content and antioxidant activity of tartary buckwheat from different locations. *Molecules* 16(12), pp. 9850-9867.

Gupta, A. A. et al. 2012. Spontaneous ocular and neurologic deficits in transgenic mouse models of multiple sclerosis and noninvasive investigative modalities: a review. *Invest Ophthalmol Vis Sci* 53(2), pp. 712-724.

Guy, J. et al. 1989. Antioxidant enzyme suppression of demyelination in experimental optic neuritis. *Curr Eye Res* 8(5), pp. 467-477.

Hagopian, K. et al. 2010. Complex I-associated hydrogen peroxide production is decreased and electron transport chain enzyme activities are altered in n-3 enriched fat-1 mice. *PLoS One* 5(9), p. e12696.

Hall, E. D. et al. 1987. Beneficial effects of the kappa opioid receptor agonist U-50488H in experimental acute brain and spinal cord injury. *Brain Res* 435(1-2), pp. 174-180.

References

- Hanley, P. J. et al. 2002. Halothane, isoflurane and sevoflurane inhibit NADH:ubiquinone oxidoreductase (complex I) of cardiac mitochondria. *J Physiol* 544(Pt 3), pp. 687-693.
- Hao, E. et al. 2013. Resveratrol alleviates endotoxin-induced myocardial toxicity via the Nrf2 transcription factor. *PLoS One* 8(7), p. e69452.
- Hattar, S. et al. 2002. Melanopsin-containing retinal ganglion cells: architecture, projections, and intrinsic photosensitivity. *Science* 295(5557), pp. 1065-1070.
- Heck, D. H. et al. 2008. Analysis of cerebellar function in Ube3a-deficient mice reveals novel genotype-specific behaviors. *Hum Mol Genet* 17(14), pp. 2181-2189.
- Heiduschka, P. et al. 2010. Electrophysiological and histologic assessment of retinal ganglion cell fate in a mouse model for OPA1-associated autosomal dominant optic atrophy. *Invest Ophthalmol Vis Sci* 51(3), pp. 1424-1431.
- Hervera, A. et al. 2010. The spinal cord expression of neuronal and inducible nitric oxide synthases and their contribution in the maintenance of neuropathic pain in mice. *PLoS One* 5(12), p. e14321.
- Hirrlinger, J. et al. 2002. Oligodendroglial cells in culture effectively dispose of exogenous hydrogen peroxide: comparison with cultured neurones, astroglial and microglial cells. *J Neurochem* 82(3), pp. 635-644.
- Ho, P. W. et al. 2012. Uncoupling protein-4 (UCP4) increases ATP supply by interacting with mitochondrial Complex II in neuroblastoma cells. *PLoS One* 7(2), p. e32810.
- Hochman, J. H. et al. 1982. Lateral mobility of cytochrome c on intact mitochondrial membranes as determined by fluorescence redistribution after photobleaching. *Proc Natl Acad Sci U S A* 79(22), pp. 6866-6870.
- Hofer, A. et al. 2014. Defining the action spectrum of potential PGC-1 α activators on a mitochondrial and cellular level in vivo. *Hum Mol Genet*.
- Hogan, S. et al. 2010. Effects of grape pomace antioxidant extract on oxidative stress and inflammation in diet induced obese mice. *J Agric Food Chem* 58(21), pp. 11250-11256.
- Holder, G. E. et al. 1998a. Electrophysiological findings in dominant optic atrophy (DOA) linking to the OPA1 locus on chromosome 3q 28-qter. *Doc Ophthalmol* 95(3-4), pp. 217-228.
- Holder, G. E. et al. 1998b. Electrophysiological findings in dominant optic atrophy (DOA) linking to the OPA1 locus on chromosome 3q 28-qter. *Doc Ophthalmol* 95(3-4), pp. 217-228.
- Hollyfield, J. G. et al. 1997. Hyaluronan localization in tissues of the mouse posterior eye wall: absence in the interphotoreceptor matrix. *Exp Eye Res* 65(5), pp. 603-608.

References

- Horgan, D. J. et al. 1968. Studies on the respiratory chain-linked reduced nicotinamide adenine dinucleotide dehydrogenase. XV. Interactions of piericidin with the mitochondrial respiratory chain. *J Biol Chem* 243(22), pp. 5967-5976.
- Horvath, R. et al. 2006. Phenotypic spectrum associated with mutations of the mitochondrial polymerase gamma gene. *Brain* 129(Pt 7), pp. 1674-1684.
- Hutson, K. A. and Masterton, R. B. 1986. The sensory contribution of a single vibrissa's cortical barrel. *J Neurophysiol* 56(4), pp. 1196-1223.
- Hwang, M. S. et al. 2014. Mitochondrial Ca(2+) influx targets cardiolipin to disintegrate respiratory chain complex II for cell death induction. *Cell Death Differ* 21(11), pp. 1733-1745.
- Iqbal, S. et al. 2013. Expression of mitochondrial fission and fusion regulatory proteins in skeletal muscle during chronic use and disuse. *Muscle Nerve* 48(6), pp. 963-970.
- Irie, Y. et al. 2003. Histone H1.2 is a substrate for denitrase, an activity that reduces nitrotyrosine immunoreactivity in proteins. *Proc Natl Acad Sci U S A* 100(10), pp. 5634-5639.
- Ischiropoulos, H. 2003. Biological selectivity and functional aspects of protein tyrosine nitration. *Biochem Biophys Res Commun* 305(3), pp. 776-783.
- Ischiropoulos, H. 2009. Protein tyrosine nitration--an update. *Arch Biochem Biophys* 484(2), pp. 117-121.
- Ishihara, N. et al. 2006. Regulation of mitochondrial morphology through proteolytic cleavage of OPA1. *EMBO J* 25(13), pp. 2966-2977.
- Jakobs, T. C. et al. 2008. The spatial distribution of glutamatergic inputs to dendrites of retinal ganglion cells. *J Comp Neurol* 510(2), pp. 221-236.
- Jaksch, M. et al. 2001. A mutation in mt tRNA^{Leu}(UUR) causing a neuropsychiatric syndrome with depression and cataract. *Neurology* 57(10), pp. 1930-1931.
- James, D. I. et al. 2003. hFis1, a novel component of the mammalian mitochondrial fission machinery. *J Biol Chem* 278(38), pp. 36373-36379.
- Jang, M. et al. 1997. Cancer chemopreventive activity of resveratrol, a natural product derived from grapes. *Science* 275(5297), pp. 218-220.
- Jang, Y. C. et al. 2012. Dietary restriction attenuates age-associated muscle atrophy by lowering oxidative stress in mice even in complete absence of CuZnSOD. *Aging Cell* 11(5), pp. 770-782.

References

- Jeon, C. J. et al. 1998. The major cell populations of the mouse retina. *J Neurosci* 18(21), pp. 8936-8946.
- Jeon, S. M. et al. 2014. Antiobesity and vasoprotective effects of resveratrol in apoE-deficient mice. *J Med Food* 17(3), pp. 310-316.
- Jeong, J. et al. 2010. Novel oxidative modifications in redox-active cysteine residues. *Mol Cell Proteomics* 2011 Mar;10(3):M110.000513. Epub 2010 Dec 10.
- Jia, Z. et al. 2012. Oxidative stress in spinal cord injury and antioxidant-based intervention. *Spinal Cord* 50(4), pp. 264-274.
- Jiang, F. et al. 2011. NADPH Oxidase-Mediated Redox Signaling: Roles in Cellular Stress Response, Stress Tolerance, and Tissue Repair. *Pharmacol Rev* Mar;63(1):218-42. Epub 2011 Jan 12.
- Jimenez-Gomez, Y. et al. 2013. Resveratrol improves adipose insulin signaling and reduces the inflammatory response in adipose tissue of rhesus monkeys on high-fat, high-sugar diet. *Cell Metab* 18(4), pp. 533-545.
- Kadiiska, M. B. et al. 2005. Biomarkers of oxidative stress study II: are oxidation products of lipids, proteins, and DNA markers of CCl4 poisoning? *Free Radic Biol Med* 38(6), pp. 698-710.
- Kaminsky, Y. G. and Kosenko, E. A. 2008. Effects of amyloid-beta peptides on hydrogen peroxide-metabolizing enzymes in rat brain in vivo. *Free Radic Res* 42(6), pp. 564-573.
- Kamisaki, Y. et al. 1998. An activity in rat tissues that modifies nitrotyrosine-containing proteins. *Proc Natl Acad Sci U S A* 95(20), pp. 11584-11589.
- Kanazawa, T. et al. 2008. The *C. elegans* Opa1 homologue EAT-3 is essential for resistance to free radicals. *PLoS Genet* 4(2), p. e1000022.
- Kanwar, M. et al. 2007. Oxidative damage in the retinal mitochondria of diabetic mice: possible protection by superoxide dismutase. *Invest Ophthalmol Vis Sci* 48(8), pp. 3805-3811.
- Kanwar, M. and Kowluru, R. A. 2009. Role of glyceraldehyde 3-phosphate dehydrogenase in the development and progression of diabetic retinopathy. *Diabetes* 58(1), pp. 227-234.
- Kasahara, T. et al. 2006. Mice with neuron-specific accumulation of mitochondrial DNA mutations show mood disorder-like phenotypes. *Mol Psychiatry* 11(6), pp. 577-593, 523.
- Kashiwabuchi, N. et al. 1995. Impairment of motor coordination, Purkinje cell synapse formation, and cerebellar long-term depression in GluR delta 2 mutant mice. *Cell* 81(2), pp. 245-252.

References

- Kato, T. 2001. DNA polymorphisms and bipolar disorder. *Am J Psychiatry* 158(7), pp. 1169-1170.
- Kempermann, G. et al. 1997. More hippocampal neurons in adult mice living in an enriched environment. *Nature* 386(6624), pp. 493-495.
- Khan, F. et al. 2006. Measurement and significance of 3-nitrotyrosine in systemic lupus erythematosus. *Scand J Immunol* 64(5), pp. 507-514.
- Khrapko, K. 2008. Two ways to make an mtDNA bottleneck. *Nat Genet* 40(2), pp. 134-135.
- Kiger, L. et al. 2011. Electron transfer function versus oxygen delivery: a comparative study for several hexacoordinated globins across the animal kingdom. *PLoS One* 6(6), p. e20478.
- Kim, D. H. et al. 2009. Genetic variants in the candidate genes of the apoptosis pathway and susceptibility to chronic myeloid leukemia. *Blood* 113(11), pp. 2517-2525.
- Kim, J. J. et al. 2001. Amygdala is critical for stress-induced modulation of hippocampal long-term potentiation and learning. *J Neurosci* 21(14), pp. 5222-5228.
- Kim, J. M. et al. 2014. Distinct roles of the hippocampus and perirhinal cortex in GABAA receptor blockade-induced enhancement of object recognition memory. *Brain Res* 1552, pp. 17-25.
- Kim, S. et al. 2011. Resveratrol exerts anti-obesity effects via mechanisms involving down-regulation of adipogenic and inflammatory processes in mice. *Biochem Pharmacol* 81(11), pp. 1343-1351.
- Kim, Y. H. et al. 2010. Resveratrol inhibits neuronal apoptosis and elevated Ca²⁺/calmodulin-dependent protein kinase II activity in diabetic mouse retina. *Diabetes* 59(7), pp. 1825-1835.
- Kivisaari, S. L. et al. 2013. False positives to confusable objects predict medial temporal lobe atrophy. *Hippocampus* 23(9), pp. 832-841.
- Klebe, S. et al. 2012. Spastic paraplegia gene 7 in patients with spasticity and/or optic neuropathy. *Brain* 135(Pt 10), pp. 2980-2993.
- Klopstock, T. et al. 2011. A randomized placebo-controlled trial of idebenone in Leber's hereditary optic neuropathy. *Brain* 134(Pt 9), pp. 2677-2686.
- Kma, L. 2013. Synergistic effect of resveratrol and radiotherapy in control of cancers. *Asian Pac J Cancer Prev* 14(11), pp. 6197-6208.

References

- Kohman, R. A. et al. 2012. Wheel running attenuates microglia proliferation and increases expression of a proneurogenic phenotype in the hippocampus of aged mice. *Brain Behav Immun* 26(5), pp. 803-810.
- Kong, Y. X. et al. 2012. Impact of aging and diet restriction on retinal function during and after acute intraocular pressure injury. *Neurobiol Aging* 33(6), pp. 1126.e1115-1125.
- Koopman, W. J. et al. 2010. Mammalian mitochondrial complex I: biogenesis, regulation, and reactive oxygen species generation. *Antioxid Redox Signal* 12(12), pp. 1431-1470.
- Koopman, W. J. et al. 2006. Simultaneous quantitative measurement and automated analysis of mitochondrial morphology, mass, potential, and motility in living human skin fibroblasts. *Cytometry A* 69(1), pp. 1-12.
- Korshunov, S. S. et al. 1997. High protonic potential actuates a mechanism of production of reactive oxygen species in mitochondria. *FEBS Lett* 416(1), pp. 15-18.
- Kortuem, K. et al. 2000. Differential susceptibility of retinal ganglion cells to reactive oxygen species. *Invest Ophthalmol Vis Sci* 41(10), pp. 3176-3182.
- Kowluru, A. 2003. Defective protein histidine phosphorylation in islets from the Goto-Kakizaki diabetic rat. *Am J Physiol Endocrinol Metab* 285(3), pp. E498-503.
- Kristl, J. et al. 2009. Improvements of cellular stress response on resveratrol in liposomes. *Eur J Pharm Biopharm* 73(2), pp. 253-259.
- Kroemer, G. and Blomgren, K. 2007. Mitochondrial cell death control in familial Parkinson disease. *PLoS Biol* 5(7), p. e206.
- Krätzer, C. et al. 2011. Methanoferrodoxin represents a new class of superoxide reductase containing an iron-sulfur cluster. *FEBS J* 278(3), pp. 442-451.
- Kubota, S. et al. 2010. Resveratrol prevents light-induced retinal degeneration via suppressing activator protein-1 activation. *Am J Pathol* 177(4), pp. 1725-1731.
- Kubota, S. et al. 2009. Prevention of ocular inflammation in endotoxin-induced uveitis with resveratrol by inhibiting oxidative damage and nuclear factor-kappaB activation. *Invest Ophthalmol Vis Sci* 50(7), pp. 3512-3519.
- Kumar, K. R. et al. 2013. Targeted next generation sequencing in SPAST-negative hereditary spastic paraplegia. *J Neurol* 260(10), pp. 2516-2522.
- Kurisu, G. et al. 2001. Structure of the electron transfer complex between ferredoxin and ferredoxin-NADP(+) reductase. *Nat Struct Biol* 8(2), pp. 117-121.

References

- Kuznetsov, A. V. et al. 2004. Mitochondrial defects and heterogeneous cytochrome c release after cardiac cold ischemia and reperfusion. *Am J Physiol Heart Circ Physiol* 286(5), pp. H1633-1641.
- Kyselova, V. et al. 2003. Effects of p-nonylphenol and resveratrol on body and organ weight and in vivo fertility of outbred CD-1 mice. *Reprod Biol Endocrinol* 1, p. 30.
- La Piana, G. et al. 1998. Mitochondrial membrane potential supported by exogenous cytochrome c oxidation mimics the early stages of apoptosis. *Biochem Biophys Res Commun* 246(2), pp. 556-561.
- Lagouge, M. et al. 2006. Resveratrol improves mitochondrial function and protects against metabolic disease by activating SIRT1 and PGC-1alpha. *Cell* 127(6), pp. 1109-1122.
- Landi, S. et al. 2007. Retinal functional development is sensitive to environmental enrichment: a role for BDNF. *FASEB J* 21(1), pp. 130-139.
- Lane, M. A. et al. 1996. Calorie restriction lowers body temperature in rhesus monkeys, consistent with a postulated anti-aging mechanism in rodents. *Proc Natl Acad Sci U S A* 93(9), pp. 4159-4164.
- Lapiente-Brun, E. et al. 2013. Supercomplex assembly determines electron flux in the mitochondrial electron transport chain. *Science* 340(6140), pp. 1567-1570.
- Lardinois, O. M. 1995. Reactions of bovine liver catalase with superoxide radicals and hydrogen peroxide. *Free Radic Res* 22(3), pp. 251-274.
- Lazarou, M. et al. 2007. Analysis of the assembly profiles for mitochondrial- and nuclear-DNA-encoded subunits into complex I. *Mol Cell Biol* 27(12), pp. 4228-4237.
- Lechauve, C. et al. 2012. Neuroglobin involvement in respiratory chain function and retinal ganglion cell integrity. *Biochim Biophys Acta* 1823(12), pp. 2261-2273.
- Lechauve, C. et al. 2014. Neuroglobin gene therapy prevents optic atrophy and preserves durably visual function in Harlequin mice. *Mol Ther* 22(6), pp. 1096-1109.
- Lee, H. C. and Wei, Y. H. 2012. Mitochondria and aging. *Adv Exp Med Biol* 942, pp. 311-327.
- Lee, J. et al. 2002. Evidence that brain-derived neurotrophic factor is required for basal neurogenesis and mediates, in part, the enhancement of neurogenesis by dietary restriction in the hippocampus of adult mice. *J Neurochem* 82(6), pp. 1367-1375.
- Lee, M. et al. 2011. Mg²⁺ ions reduce microglial and THP-1 cell neurotoxicity by inhibiting Ca²⁺ entry through purinergic channels. *Brain Res* 1369, pp. 21-35.

References

- Lee, Y. H. et al. 2007. Transforming growth factor-beta1 effects on endothelial monolayer permeability involve focal adhesion kinase/Src. *Am J Respir Cell Mol Biol* 37(4), pp. 485-493.
- Leech, R. and Sharp, D. J. 2014. The role of the posterior cingulate cortex in cognition and disease. *Brain* 137(Pt 1), pp. 12-32.
- Lemasters, J. J. and Holmuhamedov, E. 2006. Voltage-dependent anion channel (VDAC) as mitochondrial governor--thinking outside the box. *Biochim Biophys Acta* 1762(2), pp. 181-190.
- Leonard, S. S. et al. 2003. Resveratrol scavenges reactive oxygen species and effects radical-induced cellular responses. *Biochem Biophys Res Commun* 309(4), pp. 1017-1026.
- Letellier, T. et al. 1994. The kinetic basis of threshold effects observed in mitochondrial diseases: a systemic approach. *Biochem J* 302 (Pt 1), pp. 171-174.
- Li, L. et al. 2013. Neuroglobin Promotes Neurite Outgrowth via Differential Binding to PTEN and Akt. *Mol Neurobiol*.
- Li, Z. et al. 2004. The importance of dendritic mitochondria in the morphogenesis and plasticity of spines and synapses. *Cell* 119(6), pp. 873-887.
- Liang, H. and Ward, W. F. 2006. PGC-1alpha: a key regulator of energy metabolism. *Adv Physiol Educ* 30(4), pp. 145-151.
- Liesa, M. et al. 2009. Mitochondrial dynamics in mammalian health and disease. *Physiol Rev* 89(3), pp. 799-845.
- Lindholm, D. et al. 2004. Mitochondrial proteins in neuronal degeneration. *Biochem Biophys Res Commun* 321(4), pp. 753-758.
- Lipina, T. V. and Roder, J. C. 2012. Co-learning facilitates memory in mice: A new avenue in social neuroscience. *Neuropharmacology*.
- Liskova, P. et al. 2013. Novel OPA1 missense mutation in a family with optic atrophy and severe widespread neurological disorder. *Acta Ophthalmol* 91(3), pp. e225-231.
- Liu, H. et al. 2011. Smn deficiency causes neuritogenesis and neurogenesis defects in the retinal neurons of a mouse model of spinal muscular atrophy. *Dev Neurobiol* 71(2), pp. 153-169.
- Liu, J. et al. 2009a. Effects of neuroglobin overexpression on mitochondrial function and oxidative stress following hypoxia/reoxygenation in cultured neurons. *J Neurosci Res* 87(1), pp. 164-170.

References

- Liu, L. L. et al. 2014. Resveratrol induces antioxidant and heat shock protein mRNA expression in response to heat stress in black-boned chickens. *Poult Sci* 93(1), pp. 54-62.
- Liu, X. et al. 2009b. Mitochondrial 'kiss-and-run': interplay between mitochondrial motility and fusion-fission dynamics. *EMBO J* 28(20), pp. 3074-3089.
- Lorenz, P. et al. 2003. Oxyresveratrol and resveratrol are potent antioxidants and free radical scavengers: effect on nitrosative and oxidative stress derived from microglial cells. *Nitric Oxide* 9(2), pp. 64-76.
- Losa, G. A. 2003. Resveratrol modulates apoptosis and oxidation in human blood mononuclear cells. *Eur J Clin Invest* 33(9), pp. 818-823.
- Lu, Y. et al. 2013. [Advance of studies on effect of resveratrol on activity of cytochrome P450]. *Zhongguo Zhong Yao Za Zhi* 38(5), pp. 653-656.
- MacMillan-Crow, L. A. and Thompson, J. A. 1999. Tyrosine modifications and inactivation of active site manganese superoxide dismutase mutant (Y34F) by peroxynitrite. *Arch Biochem Biophys* 366(1), pp. 82-88.
- MacVicar, T. D. and Lane, J. D. 2014. Impaired OMA1-dependent cleavage of OPA1 and reduced DRP1 fission activity combine to prevent mitophagy in cells that are dependent on oxidative phosphorylation. *J Cell Sci* 127(Pt 10), pp. 2313-2325.
- Madrigal, J. L. et al. 2001. Inducible nitric oxide synthase expression in brain cortex after acute restraint stress is regulated by nuclear factor kappaB-mediated mechanisms. *J Neurochem* 76(2), pp. 532-538.
- Magyar, K. et al. 2012. Cardioprotection by resveratrol: A human clinical trial in patients with stable coronary artery disease. *Clin Hemorheol Microcirc* 50(3), pp. 179-187.
- Maldonado, E. N. and Lemasters, J. J. 2014. ATP/ADP ratio, the missed connection between mitochondria and the Warburg effect. *Mitochondrion*.
- Mancuso, M. et al. 2004. POLG mutations causing ophthalmoplegia, sensorimotor polyneuropathy, ataxia, and deafness. *Neurology* 62(2), pp. 316-318.
- Manczak, M. et al. 2011. Impaired mitochondrial dynamics and abnormal interaction of amyloid beta with mitochondrial protein Drp1 in neurons from patients with Alzheimer's disease: implications for neuronal damage. *Hum Mol Genet* 20(13), pp. 2495-2509.
- Mannella, C. A. 2006. Structure and dynamics of the mitochondrial inner membrane cristae. *Biochim Biophys Acta* 1763(5-6), pp. 542-548.
- Mannella, C. A. and Kinnally, K. W. 2008. Reflections on VDAC as a voltage-gated channel and a mitochondrial regulator. *J Bioenerg Biomembr* 40(3), pp. 149-155.

References

- Margoliash, E. and Frohwirt, N. 1959. Spectrum of horse-heart cytochrome c. *Biochem J* 71(3), pp. 570-572.
- Marin, R. et al. 2007. Voltage-dependent anion channel (VDAC) participates in amyloid beta-induced toxicity and interacts with plasma membrane estrogen receptor alpha in septal and hippocampal neurons. *Mol Membr Biol* 24(2), pp. 148-160.
- Martel, G. et al. 2006. Stimulation of hippocampal adenylyl cyclase activity dissociates memory consolidation processes for response and place learning. *Learn Mem* 13(3), pp. 342-348.
- Martin, L. J. et al. 2011. The mitochondrial permeability transition pore regulates nitric oxide-mediated apoptosis of neurons induced by target deprivation. *J Neurosci* 31(1), pp. 359-370.
- Martinez, J. and Moreno, J. J. 2000. Effect of resveratrol, a natural polyphenolic compound, on reactive oxygen species and prostaglandin production. *Biochem Pharmacol* 59(7), pp. 865-870.
- Martins, L. A. et al. 2013. Resveratrol Induces Pro-oxidant Effects and Time-Dependent Resistance to Cytotoxicity in Activated Hepatic Stellate Cells. *Cell Biochem Biophys*.
- Martins, L. A. et al. 2014. Resveratrol induces pro-oxidant effects and time-dependent resistance to cytotoxicity in activated hepatic stellate cells. *Cell Biochem Biophys* 68(2), pp. 247-257.
- Martínez-Salgado, C. et al. 2005. Gentamicin induces Jun-AP1 expression and JNK activation in renal glomeruli and cultured mesangial cells. *Life Sci* 77(18), pp. 2285-2298.
- Maruoka, T. et al. 2009. Maternal enrichment affects prenatal hippocampal proliferation and open-field behaviors in female offspring mice. *Neurosci Lett* 454(1), pp. 28-32.
- Mattenberger, Y. et al. 2003. Fusion of mitochondria in mammalian cells is dependent on the mitochondrial inner membrane potential and independent of microtubules or actin. *FEBS Lett* 538(1-3), pp. 53-59.
- Mazarakis, N. K. et al. 2014. 'Super-Enrichment' Reveals Dose-Dependent Therapeutic Effects of Environmental Stimulation in a Transgenic Mouse Model of Huntington's Disease. *J Huntingtons Dis* 3(3), pp. 299-309.
- McComb, R. B. et al. 1976. Determination of the molar absorptivity of NADH. *Clin Chem* 22(2), pp. 141-150.
- McKeller, M. R. et al. 2010. Vital function of PRELI and essential requirement of its LEA motif. *Cell Death Dis* 1, p. e21.
- McNiven, M. A. et al. 2000. Regulated interactions between dynamin and the actin-binding protein cortactin modulate cell shape. *J Cell Biol* 151(1), pp. 187-198.

References

- Meek, T. H. et al. 2014. Effects of early-life exposure to Western diet and wheel access on metabolic syndrome profiles in mice bred for high voluntary exercise. *Genes Brain Behav* 13(3), pp. 322-332.
- Meira Martins, L. A. et al. 2014. The Interplay Between Apoptosis, Mitophagy and Mitochondrial Biogenesis Induced by Resveratrol Can Determine Activated Hepatic Stellate Cells Death or Survival. *Cell Biochem Biophys*.
- Merkwirth, C. et al. 2008. Prohibitins control cell proliferation and apoptosis by regulating OPA1-dependent cristae morphogenesis in mitochondria. *Genes Dev* 22(4), pp. 476-488.
- Merry, B. J. 2004. Oxidative stress and mitochondrial function with aging--the effects of calorie restriction. *Aging Cell* 3(1), pp. 7-12.
- Meyer, D. et al. 2014. Balance and stability of synaptic structures during synaptic plasticity. *Neuron* 82(2), pp. 430-443.
- Mileykovskaya, E. and Dowhan, W. 2014. Cardiolipin-dependent formation of mitochondrial respiratory supercomplexes. *Chem Phys Lipids* 179, pp. 42-48.
- Milone, M. et al. 2009. Mitochondrial disorder with OPA1 mutation lacking optic atrophy. *Mitochondrion* 9(4), pp. 279-281.
- Mirescu, C. and Gould, E. 2006. Stress and adult neurogenesis. *Hippocampus* 16(3), pp. 233-238.
- Miyamoto, K. et al. 2014. PACAP38 Suppresses Cortical Damage in Mice with Traumatic Brain Injury by Enhancing Antioxidant Activity. *J Mol Neurosci* 54(3), pp. 370-379.
- Mojica-Villegas, M. A. et al. 2014. Protective effect of resveratrol on biomarkers of oxidative stress induced by iron/ascorbate in mouse spermatozoa. *Nutrients* 6(2), pp. 489-503.
- Mokni, M. et al. 2013. Resveratrol Provides Cardioprotection after Ischemia/reperfusion Injury via Modulation of Antioxidant Enzyme Activities. *Iran J Pharm Res* 12(4), pp. 867-875.
- Moore, B. A. et al. 2010. Mitochondrial retention of Opa1 is required for mouse embryogenesis. *Mamm Genome* 21(7-8), pp. 350-360.
- Morais, V. A. et al. 2009. Parkinson's disease mutations in PINK1 result in decreased Complex I activity and deficient synaptic function. *EMBO Mol Med* 1(2), pp. 99-111.
- Morava, E. and Kozicz, T. 2013. Mitochondria and the economy of stress (mal)adaptation. *Neurosci Biobehav Rev* 37(4), pp. 668-680.

References

- Moreno, A. J. et al. 2013. Mechanism of inhibition of mitochondrial ATP synthase by 17 β -estradiol. *J Bioenerg Biomembr* 45(3), pp. 261-270.
- Moreno, D. M. et al. 2011. Exploring the molecular basis of human manganese superoxide dismutase inactivation mediated by tyrosine 34 nitration. *Arch Biochem Biophys* 507(2), pp. 304-309.
- Morota, S. et al. 2007. Spinal cord mitochondria display lower calcium retention capacity compared with brain mitochondria without inherent differences in sensitivity to cyclophilin D inhibition. *J Neurochem* 103(5), pp. 2066-2076.
- Movahed, A. et al. 2012. Resveratrol protects adult cardiomyocytes against oxidative stress mediated cell injury. *Arch Biochem Biophys* 527(2), pp. 74-80.
- Munn. 1974. *The structure of Mitochondria*. London: Academic Press, p. 447.
- Murray, E. A. et al. 2007. Visual perception and memory: a new view of medial temporal lobe function in primates and rodents. *Annu Rev Neurosci* 30, pp. 99-122.
- Mérino, D. et al. 2009. The role of BH3-only protein Bim extends beyond inhibiting Bcl-2-like prosurvival proteins. *J Cell Biol* 186(3), pp. 355-362.
- Mòdol, T. et al. 2011. Apoptosis of hepatic stellate cells mediated by specific protein nitration. *Biochem Pharmacol* 81(3), pp. 451-458.
- Müller, M. and Holländer, H. 1988. A small population of retinal ganglion cells projecting to the retina of the other eye. An experimental study in the rat and the rabbit. *Exp Brain Res* 71(3), pp. 611-617.
- Nagakura, A. et al. 2002. Impairment of cerebral cAMP-mediated signal transduction system and of spatial memory function after microsphere embolism in rats. *Neuroscience* 113(3), pp. 519-528.
- Nagao, K. et al. 2013. Effect of dietary resveratrol on the metabolic profile of nutrients in obese OLETF rats. *Lipids Health Dis* 12, p. 8.
- Natali, A. J. et al. 2002. Different regional effects of voluntary exercise on the mechanical and electrical properties of rat ventricular myocytes. *J Physiol* 541(Pt 3), pp. 863-875.
- Naylor, J. et al. 2011. TRPC5 channel sensitivities to antioxidants and hydroxylated stilbenes. *J Biol Chem* 286(7), pp. 5078-5086.
- Nazıroğlu, M. 2012. Molecular role of catalase on oxidative stress-induced Ca²⁺ signaling and TRP cation channel activation in nervous system. *J Recept Signal Transduct Res* 32(3), pp. 134-141.

References

- Nishijima, T. et al. 2013. Cessation of voluntary wheel running increases anxiety-like behavior and impairs adult hippocampal neurogenesis in mice. *Behav Brain Res* 245, pp. 34-41.
- Nochez, Y. et al. 2009. Acute and late-onset optic atrophy due to a novel OPA1 mutation leading to a mitochondrial coupling defect. *Mol Vis* 15, pp. 598-608.
- Obinu, M. C. et al. 2002. Brain-selective stimulation of nicotinic receptors by TC-1734 enhances ACh transmission from frontoparietal cortex and memory in rodents. *Prog Neuropsychopharmacol Biol Psychiatry* 26(5), pp. 913-918.
- Olas, B. et al. 2004. Resveratrol protects against peroxynitrite-induced thiol oxidation in blood platelets. *Cell Mol Biol Lett* 9(4A), pp. 577-587.
- Olichon, A. et al. 2002. The human dynamin-related protein OPA1 is anchored to the mitochondrial inner membrane facing the inter-membrane space. *FEBS Lett* 523(1-3), pp. 171-176.
- Onishi, A. et al. 2010. The orphan nuclear hormone receptor ERRbeta controls rod photoreceptor survival. *Proc Natl Acad Sci U S A* 107(25), pp. 11579-11584.
- Organisciak, D. T. et al. 1996. Retinal light damage in rats with altered levels of rod outer segment docosahexaenoate. *Invest Ophthalmol Vis Sci* 37(11), pp. 2243-2257.
- Osborne, N. N. 2008. Pathogenesis of ganglion "cell death" in glaucoma and neuroprotection: focus on ganglion cell axonal mitochondria. *Prog Brain Res* 173, pp. 339-352.
- Osborne, N. N. 2010. Mitochondria: Their role in ganglion cell death and survival in primary open angle glaucoma. *Exp Eye Res* 90(6), pp. 750-757.
- Ostrander, D. B. et al. 2001. Lack of mitochondrial anionic phospholipids causes an inhibition of translation of protein components of the electron transport chain. A yeast genetic model system for the study of anionic phospholipid function in mitochondria. *J Biol Chem* 276(27), pp. 25262-25272.
- Otera, H. et al. 2010. Mff is an essential factor for mitochondrial recruitment of Drp1 during mitochondrial fission in mammalian cells. *J Cell Biol* 191(6), pp. 1141-1158.
- Pacholec, M. et al. 2010. SRT1720, SRT2183, SRT1460, and resveratrol are not direct activators of SIRT1. *J Biol Chem* 285(11), pp. 8340-8351.
- Packer, M. A. and Murphy, M. P. 1994. Peroxynitrite causes calcium efflux from mitochondria which is prevented by Cyclosporin A. *FEBS Lett* 345(2-3), pp. 237-240.
- Palchykova, S. et al. 2006. Sleep deprivation impairs object recognition in mice. *Neurobiol Learn Mem* 85(3), pp. 263-271.

References

- Paradies, G. et al. 2014. Functional role of cardiolipin in mitochondrial bioenergetics. *Biochim Biophys Acta* 1837(4), pp. 408-417.
- Pardal, D. et al. 2014. Resveratrol and piceid metabolites and their fat-reduction effects in zebrafish larvae. *Zebrafish* 11(1), pp. 32-40.
- Park, S. J. et al. 2012. Resveratrol ameliorates aging-related metabolic phenotypes by inhibiting cAMP phosphodiesterases. *Cell* 148(3), pp. 421-433.
- Parone, P. A. et al. 2008. Preventing mitochondrial fission impairs mitochondrial function and leads to loss of mitochondrial DNA. *PLoS One* 3(9), p. e3257.
- Passos, J. F. et al. 2010. Feedback between p21 and reactive oxygen production is necessary for cell senescence. *Mol Syst Biol* 6, p. 347.
- Patel, K. R. et al. 2013. Sulfate metabolites provide an intracellular pool for resveratrol generation and induce autophagy with senescence. *Sci Transl Med* 5(205), p. 205ra133.
- Patten, D. A. et al. 2014. OPA1-dependent cristae modulation is essential for cellular adaptation to metabolic demand. *EMBO J* 33(22), pp. 2676-2691.
- Pavlica, S. and Gebhardt, R. 2010. Protective effects of flavonoids and two metabolites against oxidative stress in neuronal PC12 cells. *Life Sci* 86(3-4), pp. 79-86.
- Peled-Kamar, M. et al. 1997. Oxidative stress mediates impairment of muscle function in transgenic mice with elevated level of wild-type Cu/Zn superoxide dismutase. *Proc Natl Acad Sci U S A* 94(8), pp. 3883-3887.
- Perez-Pinzon, M. A. et al. 2012. Novel mitochondrial targets for neuroprotection. *J Cereb Blood Flow Metab* 32(7), pp. 1362-1376.
- Perrot, R. and Eyer, J. 2009. Neuronal intermediate filaments and neurodegenerative disorders. *Brain Res Bull* 80(4-5), pp. 282-295.
- Perry, G. et al. 2002. The role of iron and copper in the aetiology of neurodegenerative disorders: therapeutic implications. *CNS Drugs* 16(5), pp. 339-352.
- Perry, J. J. et al. 2009. Contribution of human manganese superoxide dismutase tyrosine 34 to structure and catalysis. *Biochemistry* 48(15), pp. 3417-3424.
- Petrovski, G. et al. 2011. Resveratrol in cardiovascular health and disease. *Ann N Y Acad Sci* 1215, pp. 22-33.

References

- Pierce, G. B. et al. 1991. Hydrogen peroxide as a mediator of programmed cell death in the blastocyst. *Differentiation* 46(3), pp. 181-186.
- Pinto, M. C. et al. 1999. Resveratrol is a potent inhibitor of the dioxygenase activity of lipoxygenase. *J Agric Food Chem* 47(12), pp. 4842-4846.
- Piver, B. et al. 2001. Inhibition of CYP3A, CYP1A and CYP2E1 activities by resveratrol and other non volatile red wine components. *Toxicol Lett* 125(1-3), pp. 83-91.
- Porta, J. et al. 2010. Structural analysis of peroxide-soaked MnSOD crystals reveals side-on binding of peroxide to active-site manganese. *J Mol Biol* 399(3), pp. 377-384.
- Porte, Y. et al. 2008. Spatial memory in the Morris water maze and activation of cyclic AMP response element-binding (CREB) protein within the mouse hippocampus. *Learn Mem* 15(12), pp. 885-894.
- Potting, C. et al. 2010. Regulation of mitochondrial phospholipids by Ups1/PRELI-like proteins depends on proteolysis and Mdm35. *EMBO J* 29(17), pp. 2888-2898.
- Powell, S. B. et al. 2004. The balance between approach and avoidance behaviors in a novel object exploration paradigm in mice. *Behav Brain Res* 152(2), pp. 341-349.
- Preta, G. et al. 2010. MAP kinase-signaling controls nuclear translocation of tripeptidyl-peptidase II in response to DNA damage and oxidative stress. *Biochem Biophys Res Commun* 399(3), pp. 324-330.
- Prickaerts, J. et al. 2004. Learning and adult neurogenesis: survival with or without proliferation? *Neurobiol Learn Mem* 81(1), pp. 1-11.
- Profyris, C. et al. 2004. Degenerative and regenerative mechanisms governing spinal cord injury. *Neurobiol Dis* 15(3), pp. 415-436.
- Prokai-Tatrai, K. et al. 2013. 17 β -estradiol eye drops protect the retinal ganglion cell layer and preserve visual function in an in vivo model of glaucoma. *Mol Pharm* 10(8), pp. 3253-3261.
- Provis, J. M. and van Driel, D. 1985. Retinal development in humans: the roles of differential growth rates, cell migration and naturally occurring cell death. *Aust N Z J Ophthalmol* 13(2), pp. 125-133.
- Quirós, P. M. et al. 2012. Loss of mitochondrial protease OMA1 alters processing of the GTPase OPA1 and causes obesity and defective thermogenesis in mice. *EMBO J* 31(9), pp. 2117-2133.
- Rahman, A. et al. 1990. Complexes involving quercetin, DNA and Cu(II). *Carcinogenesis* 11(11), pp. 2001-2003.

References

Ramonet, D. et al. 2013. Optic atrophy 1 mediates mitochondria remodeling and dopaminergic neurodegeneration linked to complex I deficiency. *Cell Death Differ* 20(1), pp. 77-85.

Ramsden, D. B. et al. 2012. Human neuronal uncoupling proteins 4 and 5 (UCP4 and UCP5): structural properties, regulation, and physiological role in protection against oxidative stress and mitochondrial dysfunction. *Brain Behav* 2(4), pp. 468-478.

Ran, Q. et al. 2007. Reduction in glutathione peroxidase 4 increases life span through increased sensitivity to apoptosis. *J Gerontol A Biol Sci Med Sci* 62(9), pp. 932-942.

Rasband, W. S. 2014. Image J Image processing and analysis in Java. [Online]. Available at.

Rehcgil, M. and Heston, W. E. 1963. Tissue catalase activity in several C57BL substrains and in other strains of inbred mice. *J Natl Cancer Inst* 30, pp. 855-864.

Rehcgil, M. and Heston, W. E. 1967. Genetic regulation of enzyme activity in mammalian system by the alteration of the rates of enzyme degradation. *Biochem Biophys Res Commun* 27(2), pp. 119-124.

Reddehase, S. et al. 2009. The disulfide relay system of mitochondria is required for the biogenesis of mitochondrial Ccs1 and Sod1. *J Mol Biol* 385(2), pp. 331-338.

Regev-Shoshani, G. et al. 2004. Influence of lipophilicity on the interactions of hydroxy stilbenes with cytochrome P450 3A4. *Biochem Biophys Res Commun* 323(2), pp. 668-673.

Renner, L. D. and Weibel, D. B. 2011. Cardiolipin microdomains localize to negatively curved regions of Escherichia coli membranes. *Proc Natl Acad Sci U S A* 108(15), pp. 6264-6269.

Riccio, A. et al. 2009. Essential role for TRPC5 in amygdala function and fear-related behavior. *Cell* 137(4), pp. 761-772.

Ristow, M. 2014. Unraveling the truth about antioxidants: mitohormesis explains ROS-induced health benefits. *Nat Med* 20(7), pp. 709-711.

Ristow, M. and Zarse, K. 2010. How increased oxidative stress promotes longevity and metabolic health: The concept of mitochondrial hormesis (mitohormesis). *Exp Gerontol* 45(6), pp. 410-418.

Robb, E. L. et al. 2008a. Molecular mechanisms of oxidative stress resistance induced by resveratrol: Specific and progressive induction of MnSOD. *Biochem Biophys Res Commun* 367(2), pp. 406-412.

Robb, E. L. and Stuart, J. A. 2014. Multiple phytoestrogens inhibit cell growth and confer cytoprotection by inducing manganese superoxide dismutase expression. *Phytother Res* 28(1), pp. 120-131.

References

- Robb, E. L. et al. 2008b. Dietary resveratrol administration increases MnSOD expression and activity in mouse brain. *Biochem Biophys Res Commun* 372(1), pp. 254-259.
- Roberts, V. H. et al. 2014. Beneficial and cautionary outcomes of resveratrol supplementation in pregnant nonhuman primates. *FASEB J* 28(6), pp. 2466-2477.
- Rocher, C. et al. 2008. Influence of mitochondrial DNA level on cellular energy metabolism: implications for mitochondrial diseases. *J Bioenerg Biomembr* 40(2), pp. 59-67.
- Rodrigo, R. et al. 2011. The role of oxidative stress in the pathophysiology of hypertension. *Hypertens Res* Jun 1;50(11):1461-70. Epub 2011 Feb 2.
- Rogers, D. C. et al. 1997. Behavioral and functional analysis of mouse phenotype: SHIRPA, a proposed protocol for comprehensive phenotype assessment. *Mamm Genome* 8(10), pp. 711-713.
- Rojo, M. et al. 2002. Membrane topology and mitochondrial targeting of mitofusins, ubiquitous mammalian homologs of the transmembrane GTPase Fzo. *J Cell Sci* 115(Pt 8), pp. 1663-1674.
- Rolland, S. G. et al. 2013. Impaired complex IV activity in response to loss of LRPPRC function can be compensated by mitochondrial hyperfusion. *Proc Natl Acad Sci U S A* 110(32), pp. E2967-2976.
- Rosenfeld, M. et al. 2011. Perturbation in mitochondrial network dynamics and in complex I dependent cellular respiration in schizophrenia. *Biol Psychiatry* 69(10), pp. 980-988.
- Rossignol, R. et al. 1999. Threshold effect and tissue specificity. Implication for mitochondrial cytopathies. *J Biol Chem* 274(47), pp. 33426-33432.
- Rotondo, S. et al. 1996. Red wine, aspirin and platelet function. *Thromb Haemost* 76(5), pp. 818-819.
- Roux, A. et al. 2006. GTP-dependent twisting of dynamin implicates constriction and tension in membrane fission. *Nature* 441(7092), pp. 528-531.
- Ruiz-Ederra, J. et al. 2004. Comparative study of the three neurofilament subunits within pig and human retinal ganglion cells. *Mol Vis* 10, pp. 83-92.
- Russo, G. J. et al. 2009. Drosophila Miro is required for both anterograde and retrograde axonal mitochondrial transport. *J Neurosci* 29(17), pp. 5443-5455.
- Ryan, M. J. et al. 2010. Suppression of oxidative stress by resveratrol after isometric contractions in gastrocnemius muscles of aged mice. *J Gerontol A Biol Sci Med Sci* 65(8), pp. 815-831.

References

Saccà, S. C. et al. 2013. Environmental light and endogenous antioxidants as the main determinants of non-cancer ocular diseases. *Mutat Res* 752(2), pp. 153-171.

Sadowska-Bartos, I. et al. 2014. Posttranslational protein modifications by reactive nitrogen and chlorine species and strategies for their prevention and elimination. *Free Radic Res* 48(11), pp. 1267-1284.

Sadun, A. A. et al. 2012. Effect of EPI-743 on the clinical course of the mitochondrial disease Leber hereditary optic neuropathy. *Arch Neurol* 69(3), pp. 331-338.

Saharan, S. et al. 2013. SIRT1 regulates the neurogenic potential of neural precursors in the adult subventricular zone and hippocampus. *J Neurosci Res* 91(5), pp. 642-659.

Sale, A. et al. 2007. Maternal enrichment during pregnancy accelerates retinal development of the fetus. *PLoS One* 2(11), p. e1160.

Sale, A. et al. 2004. Enriched environment and acceleration of visual system development. *Neuropharmacology* 47(5), pp. 649-660.

Sanes, J. R. and Zipursky, S. L. 2010. Design principles of insect and vertebrate visual systems. *Neuron* 66(1), pp. 15-36.

Sarzi, E. et al. 2012. The human OPA1delTTAG mutation induces premature age-related systemic neurodegeneration in mouse. *Brain* 135(Pt 12), pp. 3599-3613.

Sasaki, S. et al. 2000. iNOS and nitrotyrosine immunoreactivity in amyotrophic lateral sclerosis. *Neurosci Lett* 291(1), pp. 44-48.

Sassi, N. et al. 2014. Cytotoxicity of mitochondria-targeted resveratrol derivatives: Interactions with respiratory chain complexes and ATP synthase. *Biochim Biophys Acta* 1837(10), pp. 1781-1789.

Sastre, J. et al. 1998. A Ginkgo biloba extract (EGb 761) prevents mitochondrial aging by protecting against oxidative stress. *Free Radic Biol Med* 24(2), pp. 298-304.

Satoh, M. et al. 2003. Differential sublocalization of the dynamin-related protein OPA1 isoforms in mitochondria. *Biochem Biophys Res Commun* 300(2), pp. 482-493.

Schaaf, C. P. et al. 2011. Early-onset severe neuromuscular phenotype associated with compound heterozygosity for OPA1 mutations. *Mol Genet Metab* 103(4), pp. 383-387.

Schapira, A. H. et al. 1990. Mitochondrial complex I deficiency in Parkinson's disease. *J Neurochem* 54(3), pp. 823-827.

References

Scharstuhl, A. et al. 2009. Involvement of VDAC, Bax and ceramides in the efflux of AIF from mitochondria during curcumin-induced apoptosis. *PLoS One* 4(8), p. e6688.

Scheffler. 2007. *Mitochondria*. 2nd Edition ed. New York: John Wiley & Sons, p. 462.

Schenkman, K. A. and Yan, S. 2000. Propofol impairment of mitochondrial respiration in isolated perfused guinea pig hearts determined by reflectance spectroscopy. *Crit Care Med* 28(1), pp. 172-177.

Schiapparelli, L. et al. 2006. Opposing effects of AMPA and 5-HT1A receptor blockade on passive avoidance and object recognition performance: correlation with AMPA receptor subunit expression in rat hippocampus. *Neuropharmacology* 50(7), pp. 897-907.

Schmidt, M. et al. 2003. How does the eye breathe? Evidence for neuroglobin-mediated oxygen supply in the mammalian retina. *J Biol Chem* 278(3), pp. 1932-1935.

Schwerzmann, K. et al. 1986. Molecular architecture of the inner membrane of mitochondria from rat liver: a combined biochemical and stereological study. *J Cell Biol* 102(1), pp. 97-103.

Schäfer, E. et al. 2006. Architecture of active mammalian respiratory chain supercomplexes. *J Biol Chem* 281(22), pp. 15370-15375.

Scorrano, L. et al. 2002. A distinct pathway remodels mitochondrial cristae and mobilizes cytochrome c during apoptosis. *Dev Cell* 2(1), pp. 55-67.

Sellayah, D. and Sikder, D. 2014. Orexin restores aging-related brown adipose tissue dysfunction in male mice. *Endocrinology* 155(2), pp. 485-501.

Sesaki, H. et al. 2006. Ups1p, a conserved intermembrane space protein, regulates mitochondrial shape and alternative topogenesis of Mgm1p. *J Cell Biol* 173(5), pp. 651-658.

Sgarbi, G. et al. 2014. Mitochondria hyperfusion and elevated autophagic activity are key mechanisms for cellular bioenergetic preservation in centenarians. *Aging (Albany NY)* 6(4), pp. 296-310.

Shah, M. D. and Iqbal, M. 2010. Diazinon-induced oxidative stress and renal dysfunction in rats. *Food Chem Toxicol* 48(12), pp. 3345-3353.

Shahrestani, P. et al. 2009. Heterozygous mutation of *Drosophila* Opa1 causes the development of multiple organ abnormalities in an age-dependent and organ-specific manner. *PLoS One* 4(8), p. e6867.

Shea, T. B. and Beermann, M. L. 1993. Evidence that the monoclonal antibodies SMI-31 and SMI-34 recognize different phosphorylation-dependent epitopes of the murine high molecular mass neurofilament subunit. *J Neuroimmunol* 44(1), pp. 117-121.

References

- Shi, Y. et al. 2014. The lack of CuZnSOD leads to impaired neurotransmitter release, neuromuscular junction destabilization and reduced muscle strength in mice. *PLoS One* 9(6), p. e100834.
- Shin, T. S. et al. 2010. Role of inducible nitric oxide synthase on the development of virus-associated asthma exacerbation which is dependent on Th1 and Th17 cell responses. *Exp Mol Med* 42(10), pp. 721-730.
- Shoshan-Barmatz, V. et al. 2010. VDAC, a multi-functional mitochondrial protein regulating cell life and death. *Mol Aspects Med* 31(3), pp. 227-285.
- Siegel, M. P. et al. 2013. Mitochondrial-targeted peptide rapidly improves mitochondrial energetics and skeletal muscle performance in aged mice. *Aging Cell* 12(5), pp. 763-771.
- Skrajnowska, D. et al. 2013. Copper and resveratrol attenuates serum catalase, glutathione peroxidase, and element values in rats with DMBA-induced mammary carcinogenesis. *Biol Trace Elem Res* 156(1-3), pp. 271-278.
- Skulachev, V. P. 1998. Cytochrome c in the apoptotic and antioxidant cascades. *FEBS Lett* 423(3), pp. 275-280.
- Smirnova, E. et al. 1998. A human dynamin-related protein controls the distribution of mitochondria. *J Cell Biol* 143(2), pp. 351-358.
- Smorodchenko, A. et al. 2009. Comparative analysis of uncoupling protein 4 distribution in various tissues under physiological conditions and during development. *Biochim Biophys Acta* 1788(10), pp. 2309-2319.
- Soner, B. C. and Sahin, A. S. 2014. Cardiovascular effects of resveratrol and atorvastatin treatments in an H₂O₂-induced stress model. *Exp Ther Med* 8(5), pp. 1660-1664.
- Song, R. et al. 2013. [Resveratrol reduces inflammatory cytokines via inhibiting nuclear factor- κ B and mitogen-activated protein kinase signal pathway in a rabbit atherosclerosis model]. *Zhonghua Xin Xue Guan Bing Za Zhi* 41(10), pp. 866-869.
- Song, W. et al. 2011. Mutant huntingtin binds the mitochondrial fission GTPase dynamin-related protein-1 and increases its enzymatic activity. *Nat Med* 17(3), pp. 377-382.
- Song, Z. et al. 2007. OPA1 processing controls mitochondrial fusion and is regulated by mRNA splicing, membrane potential, and Yme1L. *J Cell Biol* 178(5), pp. 749-755.
- Sorgato, M. C. et al. 1987. Patch-clamping of the inner mitochondrial membrane reveals a voltage-dependent ion channel. *Nature* 330(6147), pp. 498-500.

References

- Spalding, K. L. et al. 2013. Dynamics of hippocampal neurogenesis in adult humans. *Cell* 153(6), pp. 1219-1227.
- Spanevello, R. et al. 2009. Effect of vitamin E on ectonucleotidase activities in synaptosomes and platelets and parameters of oxidative stress in rats experimentally demyelinated. *Brain Res Bull* 80(1-2), pp. 45-51.
- Sparling, J. E. et al. 2010. The effects of gestational and postpartum environmental enrichment on the mother rat: A preliminary investigation. *Behav Brain Res* 208(1), pp. 213-223.
- St-Pierre, J. et al. 2002. Topology of superoxide production from different sites in the mitochondrial electron transport chain. *J Biol Chem* 277(47), pp. 44784-44790.
- St-Pierre, J. et al. 2006. Suppression of reactive oxygen species and neurodegeneration by the PGC-1 transcriptional coactivators. *Cell* 127(2), pp. 397-408.
- Staal, J. et al. 2004. Ridge-based vessel segmentation in color images of the retina. *IEEE Trans Med Imaging* 23(4), pp. 501-509.
- Starkov, A. A. et al. 2004. Mitochondrial alpha-ketoglutarate dehydrogenase complex generates reactive oxygen species. *J Neurosci* 24(36), pp. 7779-7788.
- Stones, R. et al. 2009. The role of transient outward K⁺ current in electrical remodelling induced by voluntary exercise in female rat hearts. *Basic Res Cardiol* 104(6), pp. 643-652.
- Strübing, C. et al. 2001. TRPC1 and TRPC5 form a novel cation channel in mammalian brain. *Neuron* 29(3), pp. 645-655.
- Sultanova, T. 2010. [Structural reaction of cardiomyocytes in response to loading on voluntary running wheel]. *Georgian Med News* (189), pp. 63-69.
- Sun, H. et al. 2011. The protective role of hydrogen-rich saline in experimental liver injury in mice. *J Hepatol* 54(3), pp. 471-480.
- Sun, Y. et al. 2012. Voltage-dependent anion channels (VDACs) recruit Parkin to defective mitochondria to promote mitochondrial autophagy. *J Biol Chem* 287(48), pp. 40652-40660.
- Surmeli, N. B. et al. 2010. Peroxynitrite mediates active site tyrosine nitration in manganese superoxide dismutase. Evidence of a role for the carbonate radical anion. *J Am Chem Soc* 132(48), pp. 17174-17185.
- Suzuki, Y. J. et al. 1997. Oxidants as stimulators of signal transduction. *Free Radic Biol Med* 22(1-2), pp. 269-285.

References

- Sweet, E. S. et al. 2011a. PSD-95 alters microtubule dynamics via an association with EB3. *J Neurosci* 31(3), pp. 1038-1047.
- Sweet, E. S. et al. 2011b. To branch or not to branch: How PSD-95 regulates dendrites and spines. *Bioarchitecture* 1(2), pp. 69-73.
- Szaro, B. G. and Strong, M. J. 2010. Post-transcriptional control of neurofilaments: New roles in development, regeneration and neurodegenerative disease. *Trends Neurosci* 33(1), pp. 27-37.
- Szeto, H. H. 2006. Cell-permeable, mitochondrial-targeted, peptide antioxidants. *AAPS J* 8(2), pp. E277-283.
- Sánchez, I. et al. 1996. Oligodendroglia regulate the regional expansion of axon caliber and local accumulation of neurofilaments during development independently of myelin formation. *J Neurosci* 16(16), pp. 5095-5105.
- Tang, S. et al. 2009. Heterozygous mutation of Opa1 in *Drosophila* shortens lifespan mediated through increased reactive oxygen species production. *PLoS One* 4(2), p. e4492.
- Tanito, M. et al. 2009. High levels of retinal membrane docosahexaenoic acid increase susceptibility to stress-induced degeneration. *J Lipid Res* 50(5), pp. 807-819.
- Tapel, A. L. 1960. Inhibition of electron transport by antimycin A, alkyl hydroxy naphthoquinones and metal coordination compounds. *Biochem Pharmacol* 3, pp. 289-296.
- Tapia, P. C. 2006. Sublethal mitochondrial stress with an attendant stoichiometric augmentation of reactive oxygen species may precipitate many of the beneficial alterations in cellular physiology produced by caloric restriction, intermittent fasting, exercise and dietary phytonutrients: "Mitohormesis" for health and vitality. *Med Hypotheses* 66(4), pp. 832-843.
- Tatsuta, T. and Langer, T. 2008. Quality control of mitochondria: protection against neurodegeneration and ageing. *EMBO J* 27(2), pp. 306-314.
- Tatsuta, T. et al. 2014. Mitochondrial lipid trafficking. *Trends Cell Biol* 24(1), pp. 44-52.
- Taylor, S. C. et al. 2013. A defined methodology for reliable quantification of Western blot data. *Mol Biotechnol* 55(3), pp. 217-226.
- Tezel, G. 2006. Oxidative stress in glaucomatous neurodegeneration: mechanisms and consequences. *Prog Retin Eye Res* 25(5), pp. 490-513.
- Thiselton, D. L. et al. 2002. A comprehensive survey of mutations in the OPA1 gene in patients with autosomal dominant optic atrophy. *Invest Ophthalmol Vis Sci* 43(6), pp. 1715-1724.

References

- Tretyakova, N. Y. et al. 2000. Peroxynitrite-induced DNA damage in the supF gene: correlation with the mutational spectrum. *Mutat Res* 447(2), pp. 287-303.
- Tyurin, V. A. et al. 2007. Interactions of cardiolipin and lyso-cardiolipins with cytochrome c and tBid: conflict or assistance in apoptosis. *Cell Death Differ* 14(4), pp. 872-875.
- Um, J. H. et al. 2010. AMP-activated protein kinase-deficient mice are resistant to the metabolic effects of resveratrol. *Diabetes* 59(3), pp. 554-563.
- Unsay, J. D. et al. 2013. Cardiolipin effects on membrane structure and dynamics. *Langmuir* 29(51), pp. 15878-15887.
- Utsunomiya, H. et al. 1991. Exact ultrastructural localization of glutathione peroxidase in normal rat hepatocytes: advantages of microwave fixation. *J Histochem Cytochem* 39(9), pp. 1167-1174.
- Uttara, B. et al. 2009. Oxidative stress and neurodegenerative diseases: a review of upstream and downstream antioxidant therapeutic options. *Curr Neuropharmacol* 7(1), pp. 65-74.
- Van Bergen, N. J. et al. 2011. Mitochondrial oxidative phosphorylation compensation may preserve vision in patients with OPA1-linked autosomal dominant optic atrophy. *PLoS One* 6(6), p. e21347.
- van den Elsen, L. W. et al. 2013. n-3 Long-chain PUFA reduce allergy-related mediator release by human mast cells in vitro via inhibition of reactive oxygen species. *Br J Nutr* 109(10), pp. 1821-1831.
- Van Gelder, B. and Slater, E. C. 1962. The extinction coefficient of cytochrome c. *Biochim Biophys Acta* 58, pp. 593-595.
- Van Goethem, G. et al. 2001. Mutation of POLG is associated with progressive external ophthalmoplegia characterized by mtDNA deletions. *Nat Genet* 28(3), pp. 211-212.
- Van Goethem, G. et al. 2003. Digenic progressive external ophthalmoplegia in a sporadic patient: recessive mutations in POLG and C10orf2/Twinkle. *Hum Mutat* 22(2), pp. 175-176.
- van Goethem, N. P. et al. 2012. Object recognition testing: rodent species, strains, housing conditions, and estrous cycle. *Behav Brain Res* 232(2), pp. 323-334.
- van Praag, H. et al. 1999. Running increases cell proliferation and neurogenesis in the adult mouse dentate gyrus. *Nat Neurosci* 2(3), pp. 266-270.
- Vaux, D. L. 1997. CED-4--the third horseman of apoptosis. *Cell* 90(3), pp. 389-390.

References

- Verny, C. et al. 2008. Multiple sclerosis-like disorder in OPA1-related autosomal dominant optic atrophy. *Neurology* 70(13 Pt 2), pp. 1152-1153.
- Verstraeten, S. V. et al. 2005. Relevance of lipid polar headgroups on boron-mediated changes in membrane physical properties. *Arch Biochem Biophys* 438(1), pp. 103-110.
- Vetrano, A. M. et al. 2005. Characterization of the oxidase activity in mammalian catalase. *J Biol Chem* 280(42), pp. 35372-35381.
- Votruba, M. et al. 1998. Clinical features, molecular genetics, and pathophysiology of dominant optic atrophy. *J Med Genet* 35(10), pp. 793-800.
- Võikar, V. et al. 2005. Long-term individual housing in C57BL/6J and DBA/2 mice: assessment of behavioral consequences. *Genes Brain Behav* 4(4), pp. 240-252.
- Völgyi, B. et al. 2009. Tracer coupling patterns of the ganglion cell subtypes in the mouse retina. *J Comp Neurol* 512(5), pp. 664-687.
- Wahlsten, D. et al. 2006. Stability of inbred mouse strain differences in behavior and brain size between laboratories and across decades. *Proc Natl Acad Sci U S A* 103(44), pp. 16364-16369.
- Wallace, D. C. et al. 1988. Mitochondrial DNA mutation associated with Leber's hereditary optic neuropathy. *Science* 242(4884), pp. 1427-1430.
- Wang, H. et al. 2011. Parkin ubiquitinates Drp1 for proteasome-dependent degradation: implication of dysregulated mitochondrial dynamics in Parkinson disease. *J Biol Chem* 286(13), pp. 11649-11658.
- Wang, X. et al. 2009. Impaired balance of mitochondrial fission and fusion in Alzheimer's disease. *J Neurosci* 29(28), pp. 9090-9103.
- Wang, Y. et al. 2014. 17 β -estradiol mediates upregulation of stromal cell-derived factor-1 in the retina through activation of estrogen receptor in an ischemia-reperfusion injury model. *Graefes Arch Clin Exp Ophthalmol*.
- Watanabe, T. et al. 2004. In vivo 3D MRI staining of the mouse hippocampal system using intracerebral injection of MnCl₂. *Neuroimage* 22(2), pp. 860-867.
- Waterham, H. R. et al. 2007. A lethal defect of mitochondrial and peroxisomal fission. *N Engl J Med* 356(17), pp. 1736-1741.
- Waters, R. P. et al. 2013. Selection for increased voluntary wheel-running affects behavior and brain monoamines in mice. *Brain Res* 1508, pp. 9-22.

References

- Weindruch, R. et al. 1988. Influences of aging and dietary restriction on serum thymosin alpha 1 levels in mice. *J Gerontol* 43(2), pp. B40-42.
- Whishaw, I. Q. and Tomie, J. 1996. Of mice and mazes: similarities between mice and rats on dry land but not water mazes. *Physiol Behav* 60(5), pp. 1191-1197.
- White, K. E. et al. 2009. OPA1 deficiency associated with increased autophagy in retinal ganglion cells in a murine model of dominant optic atrophy. *Invest Ophthalmol Vis Sci* 50(6), pp. 2567-2571.
- Williams, R. W. et al. 1998. Natural variation in neuron number in mice is linked to a major quantitative trait locus on Chr 11. *J Neurosci* 18(1), pp. 138-146.
- Williams, R. W. et al. 1996. Genetic and environmental control of variation in retinal ganglion cell number in mice. *J Neurosci* 16(22), pp. 7193-7205.
- Wisor, J. P. et al. 2011. Cerebral microglia mediate sleep/wake and neuroinflammatory effects of methamphetamine. *Brain Behav Immun* Cerebral microglia mediate sleep/wake and neuroinflammatory effects of methamphetamine.
- Witte, M. E. et al. 2013. Reduced expression of PGC-1 α partly underlies mitochondrial changes and correlates with neuronal loss in multiple sclerosis cortex. *Acta Neuropathol* 125(2), pp. 231-243.
- Wolfer, D. P. et al. 1998. Spatial Memory and Learning in Transgenic Mice: Fact or Artifact? *News Physiol Sci* 13, pp. 118-123.
- Wood, J. P. et al. 2008. The influence of visible light exposure on cultured RGC-5 cells. *Mol Vis* 14, pp. 334-344.
- Wu, C. S. et al. 2011. What can we get from 'barrels': the rodent barrel cortex as a model for studying the establishment of neural circuits. *Eur J Neurosci* 34(10), pp. 1663-1676.
- Wu, H. P. et al. 2013. Novel, whisker-dependent texture discrimination task for mice. *Behav Brain Res* 237, pp. 238-242.
- Wässle, H. 2004. Parallel processing in the mammalian retina. *Nat Rev Neurosci* 5(10), pp. 747-757.
- Yan, L. J. and Sohal, R. S. 1998. Mitochondrial adenine nucleotide translocase is modified oxidatively during aging. *Proc Natl Acad Sci U S A* 95(22), pp. 12896-12901.
- Yang, J. et al. 2013. Changes in expression of manganese superoxide dismutase, copper and zinc superoxide dismutase and catalase in *Brachionus calyciflorus* during the aging process. *PLoS One* 8(2), p. e57186.

References

- Yang, L. et al. 2009. Mitochondria targeted peptides protect against 1-methyl-4-phenyl-1,2,3,6-tetrahydropyridine neurotoxicity. *Antioxid Redox Signal* 11(9), pp. 2095-2104.
- Yang, W. and Hekimi, S. 2010. A mitochondrial superoxide signal triggers increased longevity in *Caenorhabditis elegans*. *PLoS Biol* 8(12), p. e1000556.
- Yao, R. et al. 2011. Polyphenols in alcoholic beverages activating constitutive androstane receptor CAR. *Biosci Biotechnol Biochem* 75(8), pp. 1635-1637.
- Yarosh, W. et al. 2008. The molecular mechanisms of OPA1-mediated optic atrophy in *Drosophila* model and prospects for antioxidant treatment. *PLoS Genet* 4(1), p. e6.
- Yen, G. C. et al. 2003. Effects of resveratrol and 4-hexylresorcinol on hydrogen peroxide-induced oxidative DNA damage in human lymphocytes. *Free Radic Res* 37(5), pp. 509-514.
- Yen, M. Y. et al. 1996. Compensatory elevation of complex II activity in Leber's hereditary optic neuropathy. *Br J Ophthalmol* 80(1), pp. 78-81.
- Youle, R. J. and van der Bliek, A. M. 2012. Mitochondrial fission, fusion, and stress. *Science* 337(6098), pp. 1062-1065.
- Youn, J. et al. 2012. Finding the right motivation: genotype-dependent differences in effective reinforcements for spatial learning. *Behav Brain Res* 226(2), pp. 397-403.
- Yu, X. X. et al. 2000. Characterization of novel UCP5/BMCP1 isoforms and differential regulation of UCP4 and UCP5 expression through dietary or temperature manipulation. *FASEB J* 14(11), pp. 1611-1618.
- Yu, Y. F. et al. 2011. The relationship between age-related hearing loss and synaptic changes in the hippocampus of C57BL/6J mice. *Exp Gerontol* 46(9), pp. 716-722.
- Yu, Z. et al. 2013. Neuroglobin overexpression inhibits oxygen-glucose deprivation-induced mitochondrial permeability transition pore opening in primary cultured mouse cortical neurons. *Neurobiol Dis* 56, pp. 95-103.
- Yu-Wai-Man P and al, e. 2010. The prevalence and natural history of dominant optic atrophy due to OPA1 mutations. *Ophthalmology*. Aug;117(8), pp. 1538-1546.
- Yu-Wai-Man, P. and Chinnery, P. F. 2013. Dominant optic atrophy: novel OPA1 mutations and revised prevalence estimates. *Ophthalmology* 120(8), pp. 1712-1712.e1711.
- Yu-Wai-Man, P. et al. 2010. Multi-system neurological disease is common in patients with OPA1 mutations. *Brain* 133(Pt 3), pp. 771-786.

References

Yum, S. W. et al. 2009. A novel recessive Nefl mutation causes a severe, early-onset axonal neuropathy. *Ann Neurol* 66(6), pp. 759-770.

Yuyama, K. et al. 2003. Caspase-independent cell death by low concentrations of nitric oxide in PC12 cells: involvement of cytochrome C oxidase inhibition and the production of reactive oxygen species in mitochondria. *J Neurosci Res* 73(3), pp. 351-363.

Zager, R. A. and Burkhart, K. 1997. Decreased expression of mitochondrial-derived H₂O₂ and hydroxyl radical in cytoresistant proximal tubules. *Kidney Int* 52(4), pp. 942-952.

Zeviani, M. 2008. OPA1 mutations and mitochondrial DNA damage: keeping the magic circle in shape. *Brain* 131(Pt 2), pp. 314-317.

Zhang, L. et al. 2014. Exercise pretreatment promotes mitochondrial dynamic protein OPA1 expression after cerebral ischemia in rats. *Int J Mol Sci* 15(3), pp. 4453-4463.

Zhang, M. et al. 2002a. Gluing the respiratory chain together. Cardiolipin is required for supercomplex formation in the inner mitochondrial membrane. *J Biol Chem* 277(46), pp. 43553-43556.

Zhang, Z. et al. 2002b. Normal dendritic arborization in spinal motoneurons requires neurofilament subunit L. *J Comp Neurol* 450(2), pp. 144-152.

Zhao, B. et al. 2012. Photooxidation of Amplex Red to resorufin: implications of exposing the Amplex Red assay to light. *Free Radic Biol Med* 53(5), pp. 1080-1087.

Zhao, K. et al. 2010. Induction of inducible nitric oxide synthase increases the production of reactive oxygen species in RAW264.7 macrophages. *Biosci Rep* 30(4), pp. 233-241.

Zhao, K. et al. 2004. Cell-permeable peptide antioxidants targeted to inner mitochondrial membrane inhibit mitochondrial swelling, oxidative cell death, and reperfusion injury. *J Biol Chem* 279(33), pp. 34682-34690.

Zheng, J. et al. 2010a. N-Acetylcysteine interacts with copper to generate hydrogen peroxide and selectively induce cancer cell death. *Cancer Lett* 298(2), pp. 186-194.

Zheng, L. and Kern, T. S. 2009. Role of nitric oxide, superoxide, peroxynitrite and PARP in diabetic retinopathy. *Front Biosci* 14, pp. 3974-3987.

Zheng, W. et al. 2009. Oxidative stress response of *Inonotus obliquus* induced by hydrogen peroxide. *Med Mycol* 47(8), pp. 814-823.

Zheng, Y. et al. 2010b. Resveratrol protects human lens epithelial cells against H₂O₂-induced oxidative stress by increasing catalase, SOD-1, and HO-1 expression. *Mol Vis* 16, pp. 1467-1474.

References

Zhou, T. et al. 2010. The pathogenic role of the canonical Wnt pathway in age-related macular degeneration. *Invest Ophthalmol Vis Sci* 51(9), pp. 4371-4379.

